Experimental and kinetic modelling studies of methanol conversion to hydrocarbons over zeolite catalysts

Omojola, Oluwatoyin

Award date:
2019

Awarding institution:
University of Bath

Experimental and kinetic modelling studies of methanol conversion to hydrocarbons over zeolite catalysts

Omojola, Oluwatoyin

Award date:
2019

Awarding institution:
University of Bath

Experimental and Kinetic Modelling Studies of Methanol Conversion to Hydrocarbons over Zeolite Catalysts

Oluwatoyin Omojola

A thesis submitted for the degree of Doctor of Philosophy

Department of Chemical Engineering

University of Bath

February 2019

To Katherina, Samuel and Jacob

Abstract

Methanol conversion to hydrocarbons (MTH) over zeolite catalysts is investigated using transient and steady-state kinetic experiments, FTIR spectroscopy and kinetic modelling to: (a) describe the formation of the first C-C bond during the induction period, (b) investigate factors governing steady-state product distribution and (c) improve product yields.

ZSM-5 catalysts with Si/Al ratios of 11.5, 25, 36 and 135 were characterised by SEM, XRD, TGA, nitrogen sorption, EDX and FTIR. Temperature programmed adsorption and desorption studies were conducted in a temporal analysis of products (TAP) reactor to study the preferential adsorption of methanol or dimethyl ether (DME). Desorption profiles were deconvoluted into two adsorption sites over ZSM-5 (Si/Al=135) and three adsorption sites over ZSM-5 (Si/Al=25 and 36). Molecular adsorption on the low temperature sites and dissociative adsorption on the medium and high temperature sites were observed. Higher activation energies of desorption were observed for DME (121 kJ mol^{-1}) compared to methanol (112 kJ mol^{-1}) over high temperature sites as validated by a transient kinetic model that shows that DME is the key oxygenate.

The transformation of DME to primary olefins is studied using a novel step-response methodology in the TAP reactor. Overshoots depicted by methanol and water, S-shaped propylene profiles and a rapid DME rise followed by a slower rise occur during a 44 min induction period in a first step response cycle at 300 °C. With temperature increase to 450 °C, methanol, water and DME increasingly exhibit monotonic profiles while ethylene and propylene retain their S-shaped behaviour. Precursors such as dimethoxymethane, carbon monoxide and hydrogen reduce the induction period and increase the autocatalytic rate of propylene formation according to a proposed crystal nucleation model. The transformation of the first C-C bond is rate-limiting according to a transient kinetic model. On subsequent step response cycles, the induction period is eliminated.

Several reaction families describe the complex steady-state product distribution from methanol. The olefin cycle (methylation, oligomerisation and cracking) controls product distribution with DME being 3.5 and 2.5 times more effective than methanol for olefin methylation and aromatic methylation chemistries respectively. A novel form of a structured reactor called zeolite minilith improves gasoline yields compared to zeolite powder while keeping pressure drop low.

The formation of the first C-C bond from methanol has been debated for over 40 years. This thesis provides evidence for the direct formation of primary olefins from methanol in which DME is the key oxygenate and the transformation of the first C-C bond is the major bottleneck during the induction period. At steady-state, the olefin cycle regulates product distribution and DME is the key methylating agent. Substantial operating cost reduction can be obtained using structured reactors such as zeolite miniliths while improving gasoline yield.

Acknowledgments

I have worked with many great mentors. I would like to thank my supervisor, Dr Dmitry B. Lukyanov, who helped immeasurably in all aspects of this work. His patience and careful attention to details has been a model for my work. Sincere gratitude to my PhD co-supervisor, Professor Semali P. Perera, for providing valuable advice on my thesis as well as providing resources for testing ZSM-5 miniliths for MTG conversion. I am grateful to Professor Evgeny V. Rebrov for valuable time on his fixed bed reactor, being a springboard for the steady-state end-of-pipe kinetic experiments and discussions on mass and heat transfer. I would like to appreciate Professor Dr Andre C. van Veen who allowed me to conduct transient experiments on his TAP reactor and for varied scientific discussions.

Much thanks to Dr Andrew McNab and Professor James Anderson at the University of Aberdeen for providing pyridine FTIR data on samples used for TPD experiments in the TAP reactor. Thanks to Dr Vladimir Zholobenko at Keele University for allowing me to conduct transmission FTIR experiments used to consolidate ideas developed during step response data analysis. I am grateful to Dr Nikolay Cherkasov for generating hydrocarbon-occluded ZSM-5 samples used for TPD experiments in the TAP reactor. Much thanks to Dr Dmitry Lukyanov for providing steady-state data used for kinetic modelling.

I would also like to thank my financial sponsors, *viz*. Petroleum Technology Development Fund of Nigeria (PTDF/ED/PHD/OO/766/15), Armourers and Brasiers Gauntlet Trust, Society of Chemical Industry, Royal Society of Chemistry, the Department of Chemical Engineering at the University of Bath and the Alumni Travel Fund of the University of Bath. In addition, funding received from the European Commission in the Scope of the 7th Framework BIOGO project (grant number: 604296) is gratefully acknowledged. I am very grateful to my supervisors for supporting my applications to these funding bodies.

I am wholeheartedly grateful to my parents (Dr Moses and Mrs Martina Omojola) and to Kayode, Kunle and Yemisi for their unending and unwavering support over my education and life. Their continued emphasis on discipline, hard work and patience will always be cherished. I am very grateful to my in-laws for their support for me and my family and particularly for their words of encouragement throughout my study at Bath. Much appreciation to Dr James Kariuki, Dr Maximilian Bock and Dr Tega Boro Edo for many interesting science related discussions.

Finally, I would like to thank my wife, Katherina Polig, for her patience, support, kindness and love and for keeping our home during my various research stays at the University of Warwick, Queen's University Belfast and Keele University as well as during my time away at national and international conferences. Also, to our sons, Samuel and Jacob, who infuse us daily with joy and have induced us into parenthood. I thank them for the many early mornings, evenings and weekends that they patiently allowed me to work on the chapters in this thesis and the resulting journal articles. I dedicate this work to them.

Bath, February 2019 Oluwatoyin Omojola

Declaration of any previous submission of the work

The material presented here for examination for the award of a higher degree by research has not been incorporated into a submission for another degree.

Signature …….

Declaration of authorship

The experimental and modelling work described in this thesis was carried out between 13th April 2015 and 12th December 2018. This thesis contains approximately 77,000 words, 58 figures and 28 tables.

I am the author of this thesis and the work described therein was carried out by myself personally except for the FTIR experiments presented in chapter 4, which were conducted by Dr Andrew McNab and Professor James Anderson at the University of Aberdeen and hydrocarbon-occluded zeolites which were generated by Dr Nikolay Cherkasov at the University of Warwick. In chapter 5, FTIR experiments were conducted by Dr Vladimir Zholobenko at Keele University and steady-state kinetic data, used in chapter 7, was provided by Dr Dmitry Lukyanov at the University of Bath.

Signature …….

Oluwatoyin Omojola
Department of Chemical Engineering
University of Bath
February 2019

Contents

List of Figures

Chapter 1

Chapter 2

Chapter 3

Chapter 4

Chapter 5

Chapter 6

Chapter 7

Chapter 8

List of Tables

Chapter 3

Chapter 4

Chapter 5

Chapter 6

Chapter 7

Chapter 8

Publications

The work presented in this thesis is also based on the following publications disseminated during my PhD study at the University of Bath:

P1. **Toyin Omojola**, Nikolay Cherkasov, Andrew I McNab, Dmitry B. Lukyanov, James A. Anderson, Evgeny V. Rebrov. Andre C. van Veen. Mechanistic insights into the desorption of methanol and dimethyl ether over ZSM-5 catalysts. 2018. *Catalysis Letters*. 148. 1. 474 – 488.

P2. **Toyin Omojola**, Nikolay Cherkasov, Evgeny Rebrov, Dmitry B. Lukyanov, Semali P. Perera. Zeolite minilith: A unique structured catalyst for the methanol to gasoline process. 2018. *Chemical Engineering and Processing: Process Intensification.* 131. 137 – 143

P3. **Toyin Omojola**, Dmitry B. Lukyanov, Andre C. van Veen. Transient kinetic studies and microkinetic modeling of primary olefin formation from dimethyl ether over ZSM-5 catalysts. 2019. *International Journal of Chemical Kinetics.* 51. 7. 528 – 537.

P4. **Toyin Omojola**, Dmitry B. Lukyanov, Nikolay Cherkasov, Vladimir L. Zholobenko, Andre C. van Veen. The influence of precursors on the induction and transition-regime of dimethyl ether conversion to hydrocarbons. 2019. Under review.

Conferences – Oral presentations

The work presented in this thesis has also been disseminated at the following conferences (* = presenter):

C1. **Toyin Omojola***. Invited Seminar at the Fritz Haber Institute of the Max Planck Society. Berlin. Germany. 04/2019. *Transient and steady-state kinetics of the conversion of methanol to hydrocarbons over ZSM-5 catalysts*

C2. **Toyin Omojola***. International Conference on Mathematics in (bio)Chemical Kinetics and Engineering (MaCKiE). Ghent. Belgium. 11/2018. On the induction period of the conversion of methanol over ZSM-5 catalysts: Transient studies using a TAP reactor

C3. **Toyin Omojola***, Nikolay Cherkasov, Evgeny V. Rebrov, Dmitry B. Lukyanov. ISCRE25, Florence, Italy. 05/2018. *Towards understanding primary olefin formation from methanol over ZSM-5 catalysts*

C4. **Toyin Omojola***, Nikolay Cherkasov, Dmitry B. Lukyanov, Evgeny V. Rebrov, Andre C. van Veen. UK Catalysis Conference. Loughborough, UK. 01/2018. *Towards understanding the nature of the hydrocarbon pool generated during primary olefin formation from methanol and DME: Influence of carbon monoxide and hydrogen*

C5. **Toyin Omojola***, Nikolay Cherkasov, Andre C. van Veen, Evgeny V. Rebrov, Dmitry B. Lukyanov. 13th European Congress on Catalysis (EUROPACAT), Florence, Italy. 08/2017. *Investigations into the mechanisms for the formation of primary olefins from methanol over ZSM-5 zeolite catalysts*

C6. **Toyin Omojola**, André C. van Veen*. 25th North American Catalysis Society Meeting. Denver. Colorado. USA. 06/2017. *Studies on the formation of primary olefins from methanol: Decoupling adsorption, desorption and activity using a TAP reactor*

C7. **Toyin Omojola***, Andre C. van Veen. IChemE Catalysis and Reaction Engineering Symposium, University of Sheffield. Sheffield. UK. 05/2017. *Comparing the desorption of methanol to DME over ZSM-5 catalysts*

C8. **Toyin Omojola***. ChemEngDayUK 2017, University of Birmingham. Birmingham. UK. 03/2017. *Effect of Si/Al ratios and mass transfer during the adsorption, desorption and activity of methanol and DME over ZSM-5 catalysts*

Conferences – Poster presentations

C9. **Toyin Omojola***, Dmitry B. Lukyanov, Semali P. Perera. ISCRE25, Florence, Italy. 05/2018. *Studies on primary olefin formation from methanol using short-contact-time reactors*

C10. **Toyin Omojola***. ChemEngDayUK 2017, University of Birmingham. Birmingham. UK. 03/2017. *Effect of Si/Al ratios and mass transfer during the adsorption, desorption and activity of methanol and DME over ZSM-5 catalysts*

C11. **Toyin Omojola***, Nikolay Cherkasov, Evgeny V. Rebrov, Andre C. van Veen, Dmitry B. Lukyanov. 18th International Zeolite Conference, Rio de Janeiro, Brazil. 06/2016. *Initial C-C formation during the conversion of methanol to hydrocarbons over ZSM-5 and ZSM-22 catalysts*

C12. **Toyin Omojola***, Nikolay Cherkasov, Evgeny V. Rebrov, Dmitry B. Lukyanov. ChemEngDayUK 2016, University of Bath, UK. 04/2016. *The primary products formed during the conversion of methanol to hydrocarbons over zeolite catalysts*

C13. **Toyin Omojola***, Nikolay Cherkasov, Andre C. van Veen, Evgeny V. Rebrov, Dmitry B. Lukyanov. 39th Annual Meeting of the British Zeolite Association, University of Bath, UK. 03/2016. *On the initial steps of the conversion of methanol to hydrocarbons over zeolite catalysts*

C14. **Toyin Omojola***, Dmitry B. Lukyanov. 38th Annual Meeting of the British Zeolite Association, University of Chester, UK. 07/2015. *Do primary olefins form directly from methanol over zeolite catalysts?*

Conference attendance

C15. 20th Anniversary of the EUROKIN Meeting. Vaals. Netherlands. 10/2018

Chapter 1

1. Introduction

1.1. Challenges in fuel and chemical production

Fuels and chemicals are increasingly used for transport, construction and packaging and as building blocks for other high-value chemical feedstock. Their production and utilisation should follow clean and sustainable methods that allow for habitable conditions for future generations. The increasingly affluent population of developing countries in Asia and Africa has led to a rise in demand for fuels and chemicals. In these countries, abundant conventional fossil fuels such as coal and natural gas are used to meet this demand. On the other hand, developed countries in Europe and the Americas are motivated by a need to secure new and stable resources with a very low carbon footprint. Increasingly, demand, security and sustainability are current global drivers to produce fuels and chemicals.

The recent rise in demand for light olefins and the upward trend in oil prices dating from the 1970s have led to rapid innovation in the chemical industry and the search for alternative production routes other than oil (1). Ethylene and propylene are the most demanded light olefins. The methanol to olefin process (MTO) is an alternative production route which represents a paradigm shift as the feedstock, methanol, is different from conventional feedstock (naphtha, liquefied petroleum gas or ethane) used to produce olefins (2). Ethylene is obtained majorly from steam crackers and from refinery off-gases while propylene is derived as a by-product of the ethylene production process. However, in recent years, the amount of propylene produced from steam crackers has been decreasing (3) and the demand for propylene has been growing faster than that of ethylene because its consumption is driven by higher-value chemical feedstock such as poly-propylene (4).

The demand for petrochemicals are expected to continually increase in accordance with the Gross Domestic Product (GDP) of developed countries and exceed the rate of GDP increase for developing countries while the demand for gasoline, diesel and jet-fuel would continue to increase and reach a plateau in the mid-2030s (5). With time, the progressively lower demand for conventional transport fuels would stem from a rise in investment made in the development of new fuel sources such as solar, hydrogen and biofuel. In the long-run, the demand for petrochemicals will exceed the demand for conventional fuels.

One way to meet the increasing demand for secure and sustainable sources of fuels and chemicals is to use non-conventional resources such as waste biomass, municipal waste, organic process waste (bark and fibre residues and fibre sludge) and recycled plastics. These non-conventional resources can be obtained cheaply from developed and developing countries where the conventional living standards lead to their production. Fuel and chemicals

production then lie within the framework of a circular economy. Solid bio-feedstock such as waste biomass, municipal waste and organic process waste, can be gasified to syngas ($CO/CO_2/H_2$ mixture) which can be liquefied to methanol. Methanol can be further converted to fuels and chemicals over zeolite or zeo-type catalysts in a chemical reactor. The conversion of methanol to fuels i.e. gasoline (MTG) and to chemicals i.e. olefins (MTO) are part of a generalised process called the methanol to hydrocarbons (MTH) conversion which is the primary focus of this thesis.

1.2. Catalyst and reactor design and development

The optimum design and development of fit-for-purpose catalysts to produce valuable products is of high industrial significance. Fuels and chemicals should be adaptable to various market demands, industrial processes should be flexible to various renewable feedstock and production and usage of these commodities should meet stringent environmental requirements. Current practices, however, adopt a trial and error approach towards catalyst development thereby leading to high time-to-market processes (6) and long catalyst development cycles (7). This slow approach is due to a lack in fundamental understanding of the nature and behaviour of catalysts.

The design and development of catalysts to meet the increasing demand for the secure and sustainable production of fuels and high value chemicals through industrial processes is one of the ultimate challenges. Factors affecting catalyst design include the structure sensitivity, surface energy and support-surface interaction of catalyst surfaces, transport within pores, catalyst impregnation profiles and catalyst particle shapes (8). Once designed, development ensues. Optimum catalyst development requires a good understanding of how the catalyst design is linked to product distribution. This linkage requires kinetic and structure characterisation (7). A comprehensive description of reaction mechanisms occurring at the active site, catalyst structural properties and their relationship are needed. Kinetic parameters that describe these surface reactions can be obtained from comparing adequate kinetic characterisation data to fundamental theory governing adsorption, desorption, diffusion and reaction in a reactor.

The knowledge of the rate of reaction is a prerequisite to the design of a new reactor (9, 10). Design equations for batch and flow reactors require the integration of the rate equation. The material and energy balance equations require specification of the rate of reactant loss or generated due to chemical reactions. Kinetic parameters that specify the rate of different underlying processes as specified in the rate equation can give an understanding into the reactor design.

Ultimately, these kinetic parameters are used for process design, optimisation and control of product distribution as well as catalyst design, optimisation and determination of catalyst structure-performance relations (11).

In this thesis, a comprehensive description of the reaction mechanism occurring at the active site and its relationship to the catalyst properties is provided for MTH conversion.

1.3. Methanol to hydrocarbons: Mechanistic implications

Zeolite catalysts convert methanol to hydrocarbons in three different phases. At the early phase of the reaction, the catalyst is conditioned until full mechanisms are developed. Then, steady state is achieved where these mechanisms regulate product distribution. Here, steady state regime may be properly defined as quasi-steady state as species accumulate during this phase that could block the active sites. The final phase involves catalyst deactivation where site blocking species control the rate of conversion of initial feed. This PhD thesis deals with the initial transient phase and the steady-state phase over ZSM-5 catalysts which have superior catalyst lifetime in comparison to other conventional zeolite and zeo-type catalysts for MTH conversion.

During steady-state MTH conversion, it is widely accepted that a hydrocarbon pool mechanism takes places over zeolite catalysts (12-14) where two catalytic cycles (an olefin cycle and an aromatic cycle) operate (Fig. 1.1). Over ZSM-5 catalysts, the hydrocarbon pool mechanism is known as the dual-cycle mechanism. Briefly, in the olefin cycle, primary olefins are methylated or oligomerised onto higher homologues which subsequently undergo catalytic cracking to complete the cycle. Higher olefin homologues (C_{6+}) undergo hydrogen transfer and cyclisation reactions to form the first aromatic building block. These initial aromatics undergo methylation to higher homologues and subsequently undergo dealkylation (a form of cracking) to give lower aromatics and small olefins. These small olefins re-propagate the alkene cycle.

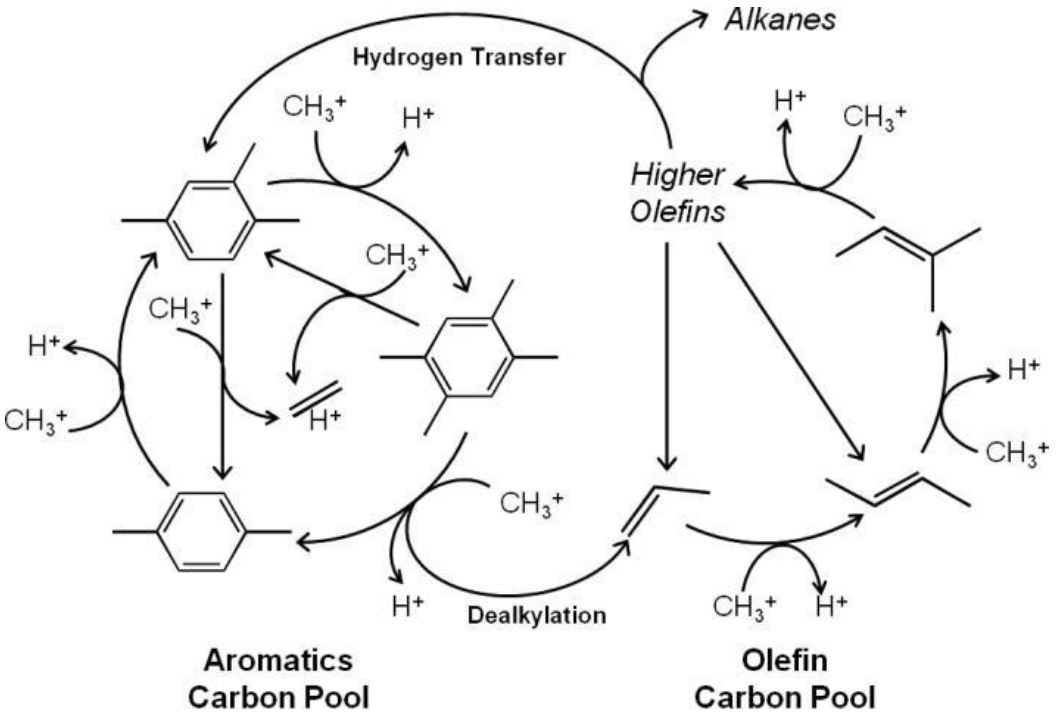

Fig. 1.1: Dual-cycle during the conversion of methanol to hydrocarbons over zeolite catalysts. Adapted from ref. (12). CH_3^+ groups are formed from methanol and/or DME.

In addition to ZSM-5, three major zeolite and zeo-type catalysts are used for MTH conversion (15). These include SAPO-34, ZSM-22 and Beta catalysts. The dominant cycle and nature of the hydrocarbon pool depends on zeolite or zeo-type topology and process conditions. Over ZSM-5 catalysts, lower methylbenzenes (toluene, xylene and trimethylbenzenes) and over Beta catalysts, higher methylbenzenes (tetra-, penta-, and hexamethylbenzenes) are the main hydrocarbon pool species (16, 17) under atmospheric conditions. Over SAPO-34 zeo-type catalysts, hexa- and hepta-methylbenzenes have been observed as the main hydrocarbon pool species (18-20) . However, over ZSM-22 catalysts, no aromatics have been observed in the gas phase at low contact times during MTH conversion (21) as these process conditions are effective in limiting side reactions (22-24). At higher contact times, trimethylbenzenes, ethylbenzene and ethyl toluene as well as other aromatics are occluded in the pores of the ZSM-22 catalyst showing an operative hydrocarbon pool mechanism (24).

The aromatic cycle controls product distribution over SAPO-34 and the olefin cycle controls product distribution over ZSM-22 (15). Over SAPO-34, pore cages are much wider than pore windows such that hydrocarbon pool species do not easily move out of the pores (hexa- and hepta-methylbenzenes) but dealkylate (or crack) to give gaseous light olefins through the aromatic cycle. Over ZSM-22, pore windows and intersections are too small to allow entry of large aromatic species leading to olefin release through the olefin cycle.

However, the control of product distribution over ZSM-5 and Beta catalysts is tunable as both catalysts have pore windows and intersections which are accessible to olefins and

aromatics. ZSM-5 was studied in this thesis due to its superior catalyst lifetime allowing focus on true transient and steady-state behaviour. Also, the tunability of both cycles over ZSM-5 catalysts allow investigations into kinetic effects and not steric hindrance. Over ZSM-5 catalysts during the steady-state phase, the major challenge is that there exists a clear lack of quantitative information that is necessary for insight into the relative propagation of both cycles. As the ZSM-5 topology allows for access of both olefins and aromatics through its pore windows, an understanding of the relative propagation of both cycles leads to an elucidation of the kinetic factors that regulate product distribution.

Although the hydrocarbon pool mechanism that occurs during steady-state MTH conversion is widely accepted (12-14), the formation of primary products during the early stages has been extensively debated. The dehydration of methanol to form dimethyl ether (DME) and water is the fastest reaction during MTH conversion (25). In understanding the early stages of the reaction, three key challenges are involved. Methanol, DME and water compete initially for active sites on the zeolite catalyst. Although methanol and DME can be used for methylating olefins or aromatics (Fig. 1.1), the source of the methylating agent has not been identified. The first challenge deals with identifying the source of methylating agent and the key oxygenate (methanol or DME) during MTH conversion.

The second challenge deals with identifying the nature of the first C-C bond and the formation of primary olefins as well as the conditions under which they are formed. Spectroscopic studies identify the first C-C bond by monitoring species occluded in the zeolite either during the reaction (*operando*) or after the reaction (*ex-situ*) while kinetic studies observe the primary gaseous olefin(s) through a gas chromatograph. Much debate was centred on whether ethylene or propylene or ethylene and propylene are the primary products (26-28). In these earlier kinetic studies, the structure of the zeolite catalyst was not adequately considered. Studies did not describe if experiments were conducted under intrinsic kinetic conditions, mass transport or heat transport limitations. Such considerations are necessary as the release of ethylene has recently been mechanistically linked to the formation and propagation of the aromatic cycle (29) as shown in Fig. 1.1. Heavy aromatics could cause zeolite pore clogging in which the release of other hydrocarbons is severely constrained. It should be considered if ethylene is produced under such mass transport limitations as earlier proposed by Haag and co-workers (30). The second challenge involves identifying the nature of the first C-C bond and primary olefin(s) and the conditions under which they are formed.

The last major challenge during MTH conversion relates to the exact pathway between the key reactant and the primary olefin(s). Although various mechanisms have been proposed, there is no consensus. The specie with the first C-C bond may be formed and occluded in the pores of the zeolite before the gaseous primary olefin(s) is released. The debate on the exact pathway and primary olefin formation centres essentially on whether primary olefins are

formed before or after constituents of the hydrocarbon pool are generated. Two major routes are suggested: (1) a direct mechanism where olefins are generated directly from the methanol/DME feed and (2) an indirect mechanism where impurities in the methanol or DME feed (such as ethanol and acetone) are precursors to the hydrocarbon pool which subsequently lead to primary olefin formation. In the direct mechanism, a further differentiation can be established: Olefins could form through a direct pathway from the feed involving no intermediate and in one step or an indirect pathway involving several intermediates and steps.

In addition to the three challenges listed above, the possibility that the zeolite could be altered during the induction period has not been comprehensively considered. This modification, particularly during MTH conversion under industrial conditions where large quantities of steam are generated for a long time at high temperatures, could alter the acidic properties of the zeolite leading to formation of extra-framework alumina (EFA) sites (31) and enhanced Brønsted acid (EBA) sites (32). These EFA and EBA sites could change product distribution and propagation of competing mechanisms during the induction period and later during steady state operation. Over laboratory-scale experiments, efforts are made to reduce the reaction time of the zeolite catalyst to prevent such acid site modification.

In many catalytic systems, in addition to adsorption, desorption and surface reactions, diffusion of species in the porous solid is important and should be considered (33, 34). The evolution and modification of active sites during the transient, steady-state and deactivation phases as species adsorb, desorb, diffuse and react makes the quantitative description of MTH conversion complex. Experiments should be conducted under intrinsic conditions to understand the behaviour of the zeolite catalyst under each isolated phenomenon and for each specie. Thereafter, a microkinetic model (35) describing catalyst behaviour can be constructed. This microkinetic model of the adsorption, desorption and reaction of species can be co-joined with a diffusion model to emulate industrial catalysts. The microkinetic model and diffusion model can then be placed in an energy, momentum and mass balance of a reactor model which can be combined with a fluid dynamics model and then scaled up to optimum industrial conditions and further used in the design of process plants used for MTH conversion.

In summary, a mechanistic approach towards understanding the product distributions obtained during MTH conversion can only come from validating the reaction mechanisms that take place and obtaining accurate kinetic parameters that describe the process (15, 36-41). Ultimately, the understanding of the initial transient stage and steady state process can give further clarification of the relation between catalyst structure (design) and product distribution and lead to the synthesis of superior catalysts. An understanding of the kinetic parameters that govern the MTH process can be used to tailor and optimise maximum throughput, selectivities and reactor design.

1.4. Reactors used for kinetic study

Equipment selection ultimately determines the success or failure of a kinetic study (9). A packed bed of catalysts is used in this study for the transient experiments and steady-state experiments. Conventionally, the temporal analysis of products (TAP) reactor is suited for studying the induction period as it allows for decoupling of adsorption, desorption, reaction and diffusion through a series of single pulse, multi-pulse and pump-probe experiments (7, 42, 43). Interpretation of TAP reactor data have led to mechanistic and kinetic insights. However, the TAP reactor is operated under vacuum conditions and extrapolation of experimental data to industrial conditions should be carefully considered. In this PhD study, the TAP reactor was used unconventionally i.e. without the use of pulses. The continuous flow panel of the TAP reactor was used to implement temperature programmed adsorption, desorption and step response experiments. For the first time, the TAP reactor framework was used to conduct transient experiments over a shallow bed under convective flow. Under these conditions, MTH conversion is investigated in a fixed-bed reactor under low-pressure conditions (<1000 Pa). Plug flow was initially assumed in the TAP reactor for transient experiments. Thereafter, a non-ideal plug flow model was used to simulate the TAP reactor. The influence of dispersion on step response experiments was analysed. Further justification of this methodology and assumption is given in chapters 3 and 4.

An atmospheric fixed bed reactor was used for obtaining experimental data on steady-state MTH conversion. Using a dilute feed, inert particles and adequate catalyst and inert packing, isothermality and plug flow behaviour are justifiably assumed. The ongoing trend in the chemical industry aims at increasing resource efficiency i.e. reducing material and energy consumption leading to more economic and sustainable processes (44). Enhancement of transport processes in chemical reactors can play a key role in process intensification leading to a reduced number of process steps. Structured catalysts such as monoliths can be used to meet such process intensification needs. Additive manufacturing is increasingly used to create tailored structured catalysts. Optimising product selectivity and yields in a complex reaction network can be obtained using structured reactors (45). Here, a novel structured reactor called ZSM-5 minilith was housed in a quartz cylindrical tube and compared to ZSM-5 powder for gasoline yields from methanol at close to atmospheric pressure.

1.5. Thesis structure

This thesis is divided into 9 chapters. MTH conversion over ZSM-5 catalysts is introduced in the 1st chapter. The key challenges, aims and objectives are stated.

In the 2nd chapter, a comprehensive literature review aimed at describing the key chemistries underlying MTH conversion is presented. The review covers chemistries pertaining to the transient and steady-state phase of MTH conversion. Chemistries and mechanisms over SAPO-34, ZSM-5, ZSM-22 and Beta catalysts are reviewed. Kinetic modelling techniques and results are also reviewed.

Methods used for catalyst characterisation and for conducting the TPD experiments are described in chapter 3. Additionally, the novel methodology for carrying out step response is detailed and the procedures for conducting the steady-state experiments are described. Data analysis method for transient and steady-state data is described. Finally, microkinetic modelling methods and approaches are described.

Chapter 4 describes experimental and kinetic modelling studies aimed at tackling the first challenge attributed to the induction period. A combination of experimental (temperature programmed desorption and adsorption) and microkinetic modelling is used to obtain key insights into the source of surface methoxy groups and the key oxygenate involved. Kinetic parameters were obtained from comparing experimental data to model.

Chapter 5 describes experimental studies of the induction period using step response experiments and transmission FTIR. The conversion of DME to primary olefin(s) is studied as the catalyst evolves onto its working state where the hydrocarbon pool dominates steady-state conversion. The influence of precursors such as dimethoxymethane, carbon monoxide and hydrogen are studied on the induction period. A reaction mechanism is also proposed for the conversion of DME to primary olefin(s) over ZSM-5 catalysts. This chapter aims at tackling the second and third challenge of the induction period.

Chapter 6 involves the transient kinetic modelling of the induction period observed from the step response experiments conducted in chapter 5. Here, a reduced reaction scheme based on recent evidence from density functional theory studies was used to validate the experimental data. Kinetic parameters were obtained by comparing experimental data to model. The bottle neck (rate limiting step) attributed to the formation of primary olefins from DME was identified. This chapter delves deeper by providing mechanistic insights on the challenges of the induction period.

Chapter 7 involves steady-state kinetic modelling studies of methanol conversion to hydrocarbons over ZSM-5 catalysts. A reduced lumped kinetic model is used to describe MTH conversion at 370 °C. Kinetic parameters were obtained by comparing experiment to model. This chapter aims at understanding the factors governing the relative propagation of both cycles. Validation of the key surface methylating specie was obtained. It is shown that complex

product distribution observed industrially consisting of C1-C10 compounds formed from a C1 molecule (methanol) can be explained by families of chemical reactions namely: olefin methylation, oligomerisation and cracking, aromatic methylation and dealkylation, paraffin cracking and alkylation. The key regulating cycle in the dual-cycle mechanism is established.

Chapter 8 describes comparative experimental studies during steady state MTH conversion over zeolite powder and miniliths. It considers the industrial practice of MTH conversion. A novel structured reactor is fabricated using a co-extrusion technique and characterised and compared to zeolite powder for hydrocarbon (in particular gasoline) yields from methanol.

Chapter 9 gives conclusions and outlook on chemical reaction engineering, chemical kinetics, modelling and heterogeneous catalysis following this PhD study. Each of these chapters are self-standing and together advance the current state of knowledge on MTH conversion.

This thesis has been presented according to the alternative thesis format permitted by the University of Bath. This format is chosen to allow presentation of the most important contributions which have been subjected to peer review in international journals. Additional experiments not submitted for publication have also been included in this thesis. At the time of submission, three chapters (4, 6 and 8) are published and elements of chapter 5 are under review.

In this alternative thesis format, the introduction, literature review, methodology, general conclusions and future work are presented as in a traditional thesis format in chapters 1, 2, 3 and 9, respectively. In the published chapters (4, 6 and 8), the accepted manuscript and supplementary information have been placed following each other. In chapter 4, additional unpublished results have been included and discussed after presentation of the supplementary information. Induction period data used for modelling in chapter 6 has been presented in the thesis appendix. Chapters 5 and 7 follow a more traditional thesis format. Transient and steady-state kinetic code, developed in MATLAB, used for parameter estimation and optimisation have been included in the thesis appendix.

1.6. References

1. Nesterenko N, Aguilhon J, Bodart P, Minoux D, Dath JP, Sels BF, et al. Chapter 5 - Methanol to Olefins: An Insight Into Reaction Pathways and Products Formation. Zeolites and Zeolite-Like Materials. Amsterdam: Elsevier; 2016. p. 189-263.
2. Vermeiren W, Gilson JP. Impact of zeolites on the petroleum and petrochemical industry. Top Catal. 2009;52(9):1131-61.
3. Ding J, Hua W. Game Changers of the C3 Value Chain: Gas, Coal, and Biotechnologies. Chem Eng Technol. 2013;36(1):83-90.
4. Chemical Market Associates I. World light olefins analysis. Houston, Texas.2012.
5. BP. BP Energy Outlook. 2018.
6. Pérez-Ramírez J, Kondratenko EV. Evolution, achievements, and perspectives of the TAP technique. Catal Today. 2007;121(3):160-9.
7. Gleaves JT, Yablonsky G, Zheng X, Fushimi R, Mills PL. Temporal analysis of products (TAP)—Recent advances in technology for kinetic analysis of multi-component catalysts. J Mol Catal A: Chem. 2010;315(2):108-34.
8. Hegedus LL, Colton CK. 12 Catalyst Design. Advances in Chemical Engineering. 16: Academic Press; 1991. p. 237-52.
9. Froment GF, Bischoff KB. Chemical Reactor Analysis and Design: John Wiley & Sons; 1979.
10. Levenspiel O. Chemical Reaction Engineering. 3rd ed: John Wiley & Sons; 1999. 668 p.
11. Bennett CO. Experiments and Processes in the Transient Regime for Heterogeneous Catalysis. In: Haag WO, Gates BC, Knözinger H, editors. Advances in Catalysis. 44: Academic Press; 1999. p. 329-416.
12. Arstad B, Kolboe S. Methanol-to-hydrocarbons reaction over SAPO-34. Molecules confined in the catalyst cavities at short time on stream. Catal Lett. 2001;71(3-4):209-12.
13. Goguen PW, Xu T, Barich DH, Skloss TW, Song W, Wang Z, et al. Pulse-quench catalytic reactor studies reveal a carbon-pool mechanism in methanol-to-gasoline chemistry on zeolite HZSM-5. J Am Chem Soc. 1998;120(11):2650-1.
14. Song W, Haw JF, Nicholas JB, Heneghan CS. Methylbenzenes are the organic reaction centers for methanol-to-olefin catalysis on HSAPO-34. J Am Chem Soc. 2000;122(43):10726-7.
15. Ilias S, Bhan A. Mechanism of the catalytic conversion of methanol to hydrocarbons. ACS Catalysis. 2013;3:18-31.
16. Bjørgen M, Olsbye U, Svelle S, Kolboe S. Conversion of methanol to hydrocarbons: The reactions of the heptamethylbenzenium cation over zeolite H-beta. Catal Lett. 2004;93(1-2):37-40.
17. Bjørgen M, Bonino F, Kolboe S, Lillerud KP, Zecchina A, Bordiga S. Spectroscopic Evidence for a Persistent Benzenium Cation in Zeolite H-Beta. J Am Chem Soc. 2003;125(51):15863-8.
18. Bjørgen M, Joensen F, Lillerud KP, Olsbye U, Svelle S. The mechanisms of ethene and propene formation from methanol over high silica H-ZSM-5 and H-beta. Catal Today. 2009;142(1-2):90-7.
19. Svelle S, Olsbye U, Joensen F, Bjørgen M. Conversion of methanol to alkenes over medium- and large-pore acidic zeolites: Steric manipulation of the reaction intermediates governs the ethene/propene product selectivity. Journal of Physical Chemistry C. 2007;111(49):17981-4.
20. Teketel S, Olsbye U, Lillerud KP, Beato P, Svelle S. Selectivity control through fundamental mechanistic insight in the conversion of methanol to hydrocarbons over zeolites. Microporous Mesoporous Mater. 2010;136(1-3):33-41.
21. Teketel S, Olsbye U, Lillerud KP, Beato P, Svelle S. Co-conversion of methanol and light alkenes over acidic zeolite catalyst H-ZSM-22: Simulated recycle of non-gasoline range products. Applied Catalysis A: General. 2015;494:68-76.

22. Cui ZM, Liu Q, Song WG, Wan LJ. Insights into the mechanism of methanol-to-olefin conversion at zeolites with systematically selected framework structures. Angewandte Chemie - International Edition. 2006;45(39):6512-5.
23. Cui ZM, Liu Q, Ma Z, Bian SW, Song WG. Direct observation of olefin homologations on zeolite ZSM-22 and its implications to methanol to olefin conversion. J Catal. 2008;258(1):83-6.
24. Teketel S, Svelle S, Lillerud KP, Olsbye U. Shape-selective conversion of methanol to hydrocarbons over 10-ring unidirectional-channel acidic H-ZSM-22. ChemCatChem. 2009;1(1):78-81.
25. Svelle S, Kolboe S, Swang O, Olsbye U. Methylation of Alkenes and Methylbenzenes by Dimethyl Ether or Methanol on Acidic Zeolites. The Journal of Physical Chemistry B. 2005;109(26):12874-8.
26. Kaeding WW, Butter SA. Production of chemicals from methanol. I. Low molecular weight olefins. J Catal. 1980;61(1):155-64.
27. Derouane EG, Nagy JB, Dejaifve P, van Hooff JHC, Spekman BP, Védrine JC, et al. Elucidation of the mechanism of conversion of methanol and ethanol to hydrocarbons on a new type of synthetic zeolite. J Catal. 1978;53(1):40-55.
28. Hutchings GJ, Gottschalk F, Hall MVM, Hunter R. Hydrocarbon formation from methylating agents over the zeolite catalyst ZSM-5. Comments on the mechanism of carbon-carbon bond and methane formation. Journal of the Chemical Society, Faraday Transactios 1: Physical Chemistry in Condensed Phases. 1987;83(3):571-83.
29. Bjørgen M, Svelle S, Joensen F, Nerlov J, Kolboe S, Bonino F, et al. Conversion of methanol to hydrocarbons over zeolite H-ZSM-5: On the origin of the olefinic species. J Catal. 2007;249(2):195-207.
30. Haag WO, Lago RM, Rodewald PG. Aromatics, light olefins and gasoline from methanol: Mechanistic pathways with ZSM-5 zeolite catalyst. J Mol Catal. 1982;17(2-3):161-9.
31. Sazama P, Wichterlova B, Dedecek J, Tvaruzkova Z, Musilova Z, Palumbo L, et al. FTIR and 27Al MAS NMR analysis of the effect of framework Al- and Si-defects in micro- and micro-mesoporous H-ZSM-5 on conversion of methanol to hydrocarbons. Microporous Mesoporous Mater. 2011;143(1):87-96.
32. Lukyanov DB. On the extremely high ability of enhanced activity sites in HZSM-5 to generate carbenium ions. Zeolites. 1994;14(3):233-4.
33. Conrad H, Ertl G, Latta EE. Adsorption of hydrogen on palladium single crystal surfaces. Surf Sci. 1974;41(2):435-46.
34. Rehren C, Isaac G, Schlögl R, Ertl G. Surface and subsurface products of the interaction of O2 with Ag under catalytic conditions. Catal Lett. 1991;11(3-6):253-65.
35. Dumesic JA, Rudd DF, Aparicio LM, Rekoske JE, Trevino AA. The Microkinetics of Heterogeneous Catalysis. Washington D.C: American Chemical Society; 1993.
36. Park TY, Froment GF. Kinetic modeling of the methanol to olefins process. 1. Model formulation. Ind Eng Chem Res. 2001;40(20):4172-86.
37. Park TY, Froment GF. Kinetic modeling of the methanol to olefins process. 2. Experimental results, model discrimination, and parameter estimation. Ind Eng Chem Res. 2001;40(20):4187-96.
38. Mihail R, Straja S, Maria G, Musca G, Pop G. A kinetic model for methanol conversion to hydrocarbons. Chem Eng Sci. 1983;38(9):1581-91.
39. Kumar P, Thybaut JW, Svelle S, Olsbye U, Marin GB. Single-event microkinetics for methanol to olefins on H-ZSM-5. Ind Eng Chem Res. 2013;52(4):1491-507.
40. Kumar P, Thybaut JW, Teketel S, Svelle S, Beato P, Olsbye U, et al. Single-Event MicroKinetics (SEMK) for Methanol to Hydrocarbons (MTH) on H-ZSM-23. Catal Today. 2013;215:224-32.
41. Alwahabi SM, Froment GF. Single event kinetic modeling of the methanol-to-olefins process on SAPO-34. Ind Eng Chem Res. 2004;43(17):5098-111.

42. Gleaves JT, Ebner JR, Kuechler TC. Temporal Analysis of Products (TAP) — A Unique Catalyst Evaluation System with Submillisecond Time Resolution. Catalysis Reviews. 1988;30(1):49-116.
43. Morgan K, Maguire N, Fushimi R, Gleaves JT, Goguet A, Harold MP, et al. Forty years of temporal analysis of products. Catalysis Science and Technology. 2017;7.
44. Perathoner S, Centi G. Science and Technology Roadmap on Catalysis for Europe: A path to create a sustainable future. 2015. p. 1-128.
45. Thomas S, Hamel C, Seidel-Morgenstern A. Basic Problems of Chemical Reaction Engineering and Potential of Membrane Reactors. Membrane Reactors. 2010.

Chapter 2

2. Literature review

2.1. Review background

This chapter reviews the current state of knowledge of the different chemistries occurring during the induction period and steady-state MTH conversion over zeolite and zeo-type catalysts with the aim of identifying the key gaps in knowledge.

2.2. Catalysts used for MTH conversion

An important intermediate in the conversion of renewable feedstock to liquid fuels and chemicals is methanol. Methanol can be produced from syngas which is obtained from the gasification of solid fuels. The gasification process is particularly advantageous for a landfill operator or a paper mill as profits can be increased from the utilisation of bio-waste products. Methanol can further be converted to other hydrocarbons over zeolite catalysts (1-6). Direct routes to methanol production via partial oxidation of methane are currently under development. A major challenge is the activation of the C-H bond in methane (7).

Zeolites and other zeo-type structures have been useful heterogeneous catalysts for MTH conversion due to their pore architecture, thermal stability, and their ability to donate protons via Brønsted sites and accept electrons via Lewis sites (8). The framework structure of zeolites consisting of corner-sharing silicate and alumina tetrahedra leads to various topologies and imparts a negative charge on the framework that has to be balanced by positively charged extra-framework cations (8, 9). For acidic zeolites, the bridging hydroxyl protons act as catalytic active sites. The general formula of a zeolite is (8):

$$M_{x/n}^{n+} Al_x Si_{1-x} O_2 . yY \qquad (2.1)$$

where M is the extra-framework charge-balancing cation and Y represents species such as water included or adsorbed within the pores. The ratio of silicon to aluminium in the framework can vary between infinity and 1. The lower limit of 1 arises due to Lowenstein's aluminium avoidance principle. Below this limit, it becomes impossible to avoid Al-O-Al linkages, which are electrostatically unfavourable due to the close distance between the negative charges associated with aluminium substitution for silicon in the lattice (8).

MTH conversion has been studied for *ca.* 40 years. Two widely studied microporous materials are ZSM-5 and SAPO-34. Ever since MTH process discovery with ZSM-5 catalysts in 1976 (1, 2), new processes using alternative zeolite catalysts have led to the production of other hydrocarbons. Among these are the generation of light olefins over SAPO-34 zeo-type

catalysts (MTO process). These zeo-type catalysts are substituted aluminophosphates. The direct replacement of isolated phosphorus atoms by silicon atoms results in a negatively charged framework and an acid site upon calcination (8). These catalysts have a 3D cage structure with small window sizes of 3.8 Å × 3.8 Å (Fig. 2.1a). The generation of light olefins during the steady state MTH conversion is rationalised due to the small pore windows which only allow for the exit of hydrocarbons of small molecular sizes (10, 11). In 2010, MTO conversion was commercialised on an industrial scale in China with SAPO-34 catalysts in a turbulent fluidised bed (12).

Gasoline range hydrocarbons (C_{5+} aliphatics and aromatics) have been produced over ZSM-5 catalysts in a methanol-to-gasoline (MTG) process (13). The ZSM-5 catalysts have a three-dimensional (3D) pore structure with 10 ring pore windows of size 5.1 × 5.5 Å and 5.3 × 5.6 Å (Fig. 2.1b). The basic building units of ZSM-5 are 5-5-1 units which link together to form chains. This in turn link to give silicalite sheets, which contain ten membered ring (10MR) openings, and these can be connected across inversion centres (8). Under operating conditions of high temperatures and low pressure, the product selectivity over ZSM-5 catalysts can be tuned towards propylene formation in a methanol-to-propylene (MTP) process (14). Aromatics can be generated in a methanol-to-aromatics (MTA) process over metal substituted ZSM-5 catalysts (15, 16).

At 370 °C, C_{5+} aliphatics can be generated over ZSM-22 catalysts, a 1D pore structure with 10-ring pore windows of size 5.7 × 4.6 Å (Fig. 2.1c). This is due to the narrow pore sizes and the alkenes residing at the pore windows which allow for olefin homologation reactions (17-21). The silicalite sheets of ZSM-22 are connected either by translation or by mirror planes (“unit cell twinning”) (8).

Of academic relevance is the wide pore Beta catalyst, a 3D pore structure with 12 membered ring (12MR) pore windows of size 6.6 × 6.7 and 5.6 × 5.6 Å (Fig. 2.1d), which also leads to the formation of aromatics, C_4 and C_{5+} aliphatics (22, 23). The intergrowths of the A- and B- polymorphs of zeolite Beta are made with silicalite sheets stacked layer to layer *via* one of four possible translations and with a high degree of disorder (8).

The diverse zeolite and zeo-type topologies mentioned above and process conditions give rise to different methanol conversions and product selectivities.

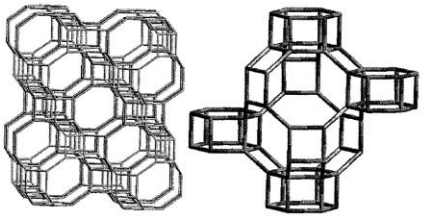

a). SAPO-34 pore structure (CHA Framework Type). [Left] Extended structure emphasising 6MR windows of sizes of *ca*. 0.38 nm and [Right] Expanded structure emphasising a cage of *ca*. 1 nm × 0.7 nm (24)

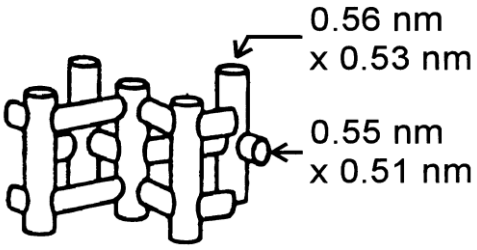

b). The channel structure in ZSM-5 (MFI Framework Type) (25)

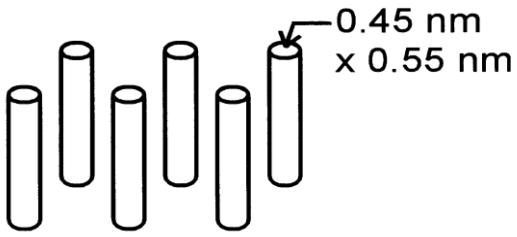

c). The channel structure of ZSM-22 (TON Framework Type) (25)

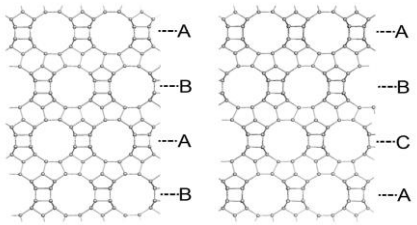

d). Beta pore structure (BEA Framework). [Left] Polymorph A emphasising an AB stacking sequence. [Right] Polymorph B emphasising an ABC stacking sequence (26)

Fig. 2.1: Channel and pore structures of (a) SAPO-34, (b) ZSM-5, (c) ZSM-22 and (d) Beta catalysts

2.3. Approaches used to study MTH conversion

Most conventional studies of the conversion of methanol to hydrocarbons fall into three categories: kinetic studies, spectroscopic studies and density functional theory (DFT) calculations (27). Steady state kinetic studies have been previously conducted to generate general parameters such as reaction order (by changing partial pressure) and rate constant (by changing temperature) in simple power law relationships. Phenomenological descriptions could also be applied to transient kinetic studies. Alternatively, reactions have been tuned for example using process variables such as weight hourly space velocities (contact time) to overcome competing side reactions to obtain suitable parameters for use in mechanistic considerations.

The induction period during which the primary C-C bonds are formed has been studied by carrying out steady state experiments at low temperatures (28), with water co-feeding (29) and at high weight hourly flow velocities (WHSV) (30, 31). In these steady-state studies, the induction period is not truly investigated as the hydrocarbon pool is formed *a priori*. Accurate description of the events that occur during the induction period should be studied as the catalyst evolves from its fresh state to its working state. The MTH reaction can be subjected to transient kinetic studies such as step responses, pulse responses and temperature

programmed methods i.e. temperature programmed adsorption, desorption and surface reaction. The overarching aim of these transient experiments is to constrain MTH reaction to low conversions and study the ZSM-5 catalysts as they evolve from their fresh state to working state. Further quantitative and mechanistic information (rate constants, activation energies) can be obtained *via* parameter estimation and optimisation by comparing experimental data with model.

Fourier Transform Infrared Spectroscopy (FTIR) and other modern spectroscopy techniques such as the solid-state Magic Angle Spinning Nuclear Magnetic Resonance Spectroscopy (MAS NMR) methods are used for the *in-situ* study of the behaviour of zeolite catalysts during MTH conversion. Particularly, they have been used for probing reaction intermediates formed during MTH conversion. Here, the assumption is that the results obtained during spectroscopic experiments are comparable to continuous flow conditions in a fixed bed reactor. Similar operating conditions are necessary to fulfil this criterion. The diffuse reflectance infrared transform spectroscopy (DRIFTS) mode of operation meets this recommendation (27). However, in comparing reactor and spectroscopic IR cells, there is important issue of heat loss through IR windows and this can lead to a significant difference in reaction rates (32) which could affect product distribution particularly in autocatalytic reactions as MTH conversion. These IR reaction rates may be incomparable to the rate at which primary olefins are formed. Moreover, thermal losses could lead to significant differences in conversions across the wafer. Nonetheless, rate measurement data obtained from standard fixed bed reactors can be used to obtain calibration curves which could overcome this problem. *Operando* surface science techniques applied to a fixed bed reactor can help study surface species during real-time operation.

Theoretical density functional theory (DFT) calculations are currently carried out at three levels, namely: 1) cluster level, 2) embedded cluster level and 3) periodic level. Cluster level calculations, which are carried out over 1-5 T atoms (T=Al atoms) allow for only a limited number of atoms in the zeolite to be accounted for and the dangling bonds of these atoms are saturated with hydrogen which has been shown to affect the acidity of the cluster (33). When a charged intermediate is encountered during calculations, the activation barriers could be inaccurate, and a larger model could be required (34, 35). Embedded clusters (ONIOM calculations) allow for a much larger set of atoms (30T, 46T) to be accounted for. They account for a relatively small acid site at high quantum-mechanical level and the larger surrounding framework at lower quantum mechanical levels (35). Although more computationally costly, only periodic density functional theory calculations can account for the entire unit cell of zeolite crystals (36). Periodic DFT results can be significantly different from cluster models when long range electrostatic forces are significant. The SAPO-34 topology (CHA framework) has been subjected to periodic density functional theory calculations by Shah and co-workers (37-39)

as it contains 108 atoms/unit cell. The ZSM-22 (TON framework) and Beta (BEA framework) have 72 and 192 atoms/unit cell respectively. However, no periodic level studies has been conducted for ZSM-5 (MFI framework) for MTH conversion as it has 288 atoms within a purely siliceous unit cell (39). It should be noted that theoretical calculations are very good at obtaining qualitative information about mechanisms of the MTH reaction. Cluster models could be very ineffective at providing quantitative data on MTH conversion due to the overestimation of barrier heights coupled with the limited description of the electrostatic field present within the zeolite pores and the poor ability to model weak dispersion forces which lead to destabilisation of charged species and transition states with charge separation relative to neutral molecules physisorbed onto the cluster (40). The extended cluster and periodic DFT calculations provide a better representation of the zeolite structure, specie stability as well as likelihood of the corresponding reactions occurring. The DFT calculations can yield rate parameters (activation energies, pre-exponential factors) through a microkinetic model based on modelling matter at the molecular level. Rate parameters can also be estimated based on a microkinetic model in which the laws of conservation are applied at a microscale level.

The results generated by these three approaches (kinetics, spectroscopy, microkinetic modelling) can be used in describing the various steps of the MTH process. Thus, two elucidating methods of analysis can be defined: the use of kinetic experiments with microscale level kinetic modelling and spectroscopy or the use of kinetic experiments with DFT calculations at a molecular scale and spectroscopy. The former method of combining kinetic experiments and modelling on the microscale level with complementary infrared spectroscopic data is the approach used in this thesis.

Of prime consideration is the active site distribution on the ZSM-5 catalysts and their evolution during the MTH process. The control over the active site distribution with respect to zeolite morphology and topology is a major parameter in understanding the product distribution during MTH conversion over zeolite powder or as a structured reactor.

2.4. Aluminium distribution and nature of acid sites in ZSM-5 catalysts

Distribution of aluminium in the zeolite varies with Si/Al ratio (41, 42). Two schools of thought exist: Dedecek and co-workers (43) observed that Al atoms are distributed in the pore channels and intersections as single Al atoms or Al pairs. This distribution has been found to depend principally on the methodology of hydrothermal synthesis. With a higher Al content, zeolites have a higher predominance of Al pairs which sit at pore intersections. Single Al atoms mostly sit on pore channels and windows.

The other school of thought is largely based on adsorption of molecules such as pyridine, carbon monoxide, and other amines to investigate the location of Al atoms (44, 45). ZSM-5 is

known to have bridging hydroxyl groups, silanol groups as well as coordinated unsaturated Al^{3+} ions present in its structure. The bridging hydroxyl groups are located within the internal zeolite channels while the silanol groups and the unsaturated Al^{3+} are located on the external surface of the zeolite which could exist as extra-framework cations (46). It is widely recognised that the bridging hydroxyl groups act as Brønsted acid sites while the weakly acidic coordinated Al^{3+} ions as well as the extra-framework Al atoms act as Lewis sites. Extra-framework material is composed of small particles mostly containing Al cations complexed by OH groups but sometimes also involving silicate species, likely interacting with framework walls, located in the cavities or on the external surface. The detection of octahedral Al ions in ^{27}Al NMR is the evidence of extra-framework material. Al ions in Brønsted acid positions are most likely in tetrahedral coordination (47).

In comparison with any non-zeolitic material based on silica and alumina, the bridging OH groups signify the presence of internal pore channels. Protonic zeolites are strong because, under normal conditions, the Al-O bond is weak. Interaction of protonic zeolites with a base strengthens the bond subsequently allowing for the solvation of the cation. This three-dimensional solvation occurs in the zeolite cages by the Van der Waals interactions with the walls of the pore channels. The strength of the Brønsted acid site is higher, the more the negative charge on the conjugate base is stabilised (46).

The internal acidic hydroxy groups of HZSM-5 interact with alkanes, alkenes and aromatics at low temperatures through hydrogen bonding. The hydrogen bonds follow the strength trend: olefins>aromatics>paraffins (44, 48). Olefins undergo an important vibrational perturbation upon H-bonding, showing that the interaction certainly involves C=C π-type orbitals. For aromatics, π-type electronic clouds are involved, but partial steric hinderance weakens this interaction. The interaction with the localized π-type orbitals of olefins (bond order 2) is stronger than that of the delocalised π-type orbitals of aromatics (bond order 1.5). The strength of interaction increases with carbon chain length of the aromatic i.e. p-xylene > toluene > benzene. The same occurs for olefins where the strength of interaction decreases in the following order: butenes > propylene > ethylene. Furthermore, Busca and co-workers showed that hydrogen bonds with alkanes involve C-C σ-type orbitals predominantly (48). The strength of the interaction increases with carbon chain length.

Knowledge of the distribution of Al atoms in ZSM-5 catalysts is necessary for the comprehension of the location of active sites in its porous matrix. The distribution has been shown to be a complex phenomenon (49). For instance, water is produced in significant amounts during methylation reactions over ZSM-5 catalysts under industrial conditions. The steam generated at high temperatures can progressively alter the nature of the sites leading to enhanced Brønsted acid sites (50) and re-distribution of Al atoms in the ZSM-5 catalyst (49).

2.5. Chemistries of MTH conversion

The chemistries involved during steady-state MTH conversion have been briefly described by Ilias and Bhan (4). These include: olefin methylation, olefin cracking, hydrogen transfer, cyclisation, aromatic methylation and aromatic dealkylation (cracking). This list is not exhaustive. Carbon monoxide, methane, hydrogen, formic acid and formaldehyde can be formed during reactions of methanol or DME (51, 52). At higher temperatures when methanol transformation is tuned towards olefin formation, paraffin cracking and hydrogen transfer between paraffins and olefins can also be important (53-55).

2.5.1. The formation of formaldehyde, carbon monoxide, methane, hydrogen and carbon dioxide

Methanol and DME have been shown to decompose to carbon monoxide, methane, hydrogen and carbon dioxide over acidic zeolites (56-58). There has been a debate on whether these products are formed from oxygenate (methanol, DME) decomposition. Mihail and co-workers used a kinetic model that takes into consideration the decomposition of methanol into hydrogen and carbon monoxide in modelling MTH conversion (59). To account for methane formation, they modelled the co-reaction of carbene and hydrogen generated from thermal cracking of alkanes. However, thermal cracking of alkanes is only dominant at high conversions and their model could not explain significant methane formation at low conversions. Hutchings et al. (60) refuted their claim due to low quantities of hydrogen observed from methanol decomposition and the water gas shift reaction at low conversions. Recently, Liu et al. (52) postulated the formation of major components such as carbon monoxide and formaldehyde from methanol over ZSM-5 catalysts. However, it is important to note that this postulation was suggested based on experiments conducted on inert surfaces such as silicalite, Na-ZSM-5 or ɣ-Al_2O_3. In earlier studies by Chu and Chang (58), carbon monoxide, carbon dioxide, hydrogen and methane were observed during steady-state MTH conversion, albeit in small quantities.

2.5.2. Equilibration between methanol, DME and water

In the first step during MTH conversion, methanol is rapidly equilibrated with DME and water (40). Methanol, DME and water compete initially for active sites. Over acidic catalysts, it is well established that hydrocarbon conversions occur through carbenium ions (61, 62). During MTH conversion over zeolite catalysts, carbenium ions could be initiated by the addition of the proton of zeolite to an olefin, abstraction of a hydride ion from a hydrocarbon by the Lewis acid sites of the catalyst or the addition of acids to methanol (61). The initial step during the addition of protons to the oxygenates (methanol or DME) is the formation of a

relatively stable oxonium salt (61). It is important to investigate which oxonium salt, formed from methanol or DME is more stable and how this contributes to the initial C-C bond.

DME and water are initially formed at high rates of methanol reaction over ZSM-5 (63). The dehydration of two methanol molecules into DME and water is the fastest reaction during MTH conversion, and methanol and DME are present simultaneously at less than 100% methanol conversion (40). By using an in-situ stopped flow (cross-polarisation) CP/MAS NMR spectroscopy method, Hunger and co-workers (64) observed surface methoxy species and proposed a route to DME formation *via* these surface methoxy species. An adsorbed methanol molecule converts to methoxy species which subsequently reacts with another methanol molecule to form DME (65, 66). These surface methoxy species could act as precursors for carbene and ylide intermediates for direct methanol conversion at temperatures (T) ≥ 493 K because the C-H bonds in the surface methoxy groups are weakened and hydrogen can be readily abstracted by the basic oxygen atoms of the framework. They react with water to form methanol and with methanol to form DME (64, 67). At very low temperatures, signals corresponding to Brønsted acid sites, methoxy groups, adsorbed methanol and DME have been obtained from ^{1}H MAS NMR and ^{13}C MAS NMR studies (68).

In contrast, Blaszkowski and van Santen (69) concluded that a concerted, single step mechanism of two methanol molecules is highly favoured over the mechanism involving a surface methoxy group as an intermediate using cluster methods. They obtained an activation barrier for DME formation of 145 kJ mol^{-1} for the case when two methanol molecules adsorbed simultaneously on a Brønsted acid site (70). Extended cluster models have produced lower activation barriers of 132 kJ mol^{-1}(40). Nonlocal periodic density functional calculations over chabazite give activation barriers of 119 kJ mol^{-1} for this mechanism (39).

However, surface methoxy groups are readily observed during MTH conversion and are also important in the mechanisms of direct olefin formation from methanol (10, 64, 67). For the mechanism involving surface methoxy intermediates, the rate limiting step was found to be the dehydration of the first methanol molecule (70). Here, methoxonium ion formally proposed (71, 72) to be an intermediate was found to be a transition state (73-76).

2.5.3. The debate on primary olefin formation

The mechanism for the primary formation of olefins during the induction period has been widely debated (34, 35, 60, 64, 67, 68, 77-91). Two schools of thought exist for the formation of primary olefins.

2.5.3.1. Indirect mechanism

The indirect mechanism was originally proposed by Dahl and Kolboe (92-95) over SAPO-34 catalysts and was further described as the formation of scaffolds, which are composed of well-defined organic species (polymethylbenzenes) on one or more inorganic acid sites that preserves the organic components and regulates selectivity through steric constraints (77). Earlier research showed that the hydrocarbon pool operates through aromatic methylation and dealkylation chemistries. These chemistries lead to the release of light olefins during MTH conversion over SAPO-34 catalysts (95).

Although two different dealkylation chemistries have been proposed for the indirect mechanism namely: (1) a side chain methylation mechanism (96-99) and (2) a paring mechanism (100) (Fig. 2.2), the dominating mechanism for the aromatic dealkylation chemistry during MTH conversion is still currently debated (101). Both mechanisms are initiated by the geminal methylation of a methylbenzene and the activation energy for gem-methylation decreases as the number of methyl groups on the benzene ring increases (102). In the side chain methylation mechanism, this leads to formation of an exocyclic double bond after elimination of a methyl hydrogen. This double bond can undergo side chain methylation which further cracks to form ethylene or propylene (4, 79, 103). During the paring mechanism, gem-methylation of a methylbenzene results in ring contraction, thereby leading to the formation and release of propylene (4, 103) or isobutene (80) (Fig. 2.2).

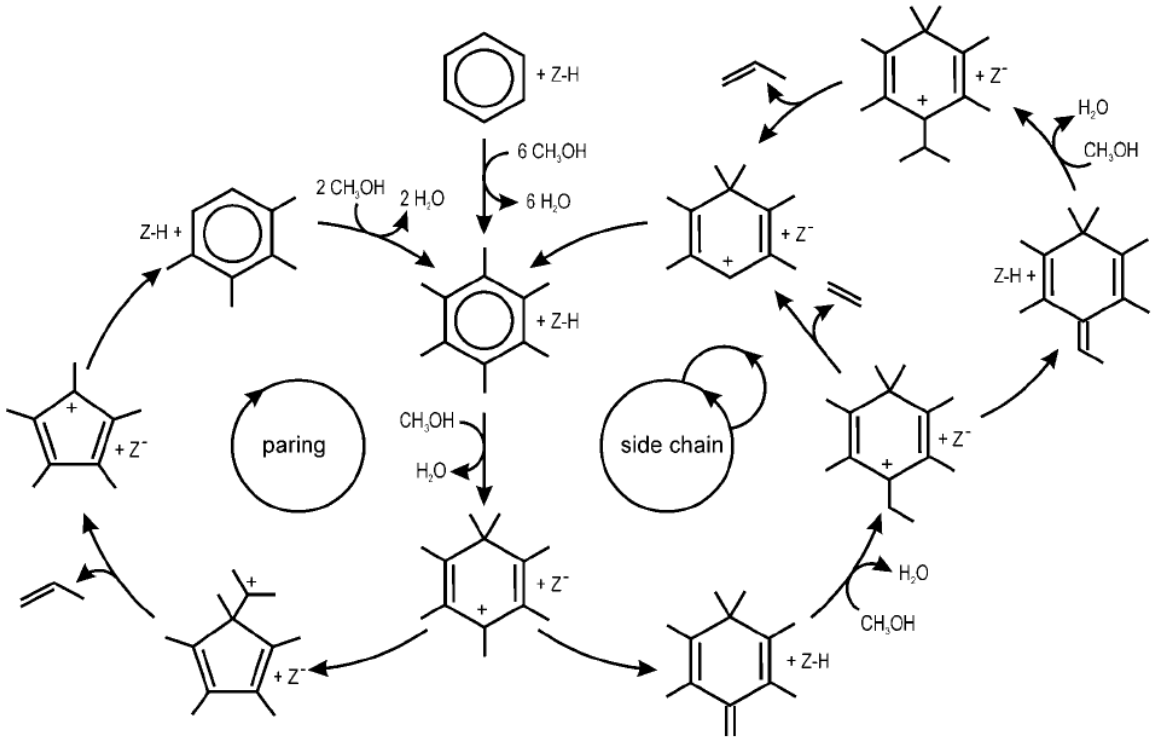

Fig. 2.2: Schematic representation of the paring and side-chain reaction concepts in MTO catalysis (104).

Haw and co-workers (77) reported the formation of methylbenzenes after 4 seconds reaction time during MTH conversion over SAPO-34 catalysts using ^{13}C NMR spectroscopy at 673 K. They observed that polymethylbenzenes are trapped in zeolite cages and are formed from impurities in the methanol feed, trace impurities in the carrier gas, incomplete combustion of organics on the catalysts and other sources of contamination (78). Surface methoxy groups were found from the studies of Haw and co-workers (77) and their concentration decreased during the reaction showing their role as reactive intermediates. These surface methoxy groups are shown to be reactive at temperatures lower than the starting temperature of the MTO process. If any organic impurities were present on solid acid catalysts, they should react with the surface methoxy groups at low temperatures. However, investigations by Hunger and co-workers (67, 104) do not show any reactivity of surface methoxy groups at temperatures (T) ≤ 473 K thereby raising doubts on the impurity route leading to aromatics that produce olefins through the dealkylation chemistry.

Moreover, the quantity of impurities (1 ppm ethanol and 11 ppm organic compounds) (78) may be too small for the initial formation of polymethylbenzenes. This can be observed from the results of Haw and co-workers (78). According to their work, pulses of 12.5 µL of methanol was passed over 300 mg of H-ZSM-5 (Si/Al=15) at 375 °C. 2 ppm of volatile hydrocarbons were formed from 1 ppm of ethanol impurity in the methanol feed and 650 ppm of volatile hydrocarbons were formed from 36 ppm of ethanol impurity. To verify the source of volatile hydrocarbons, the following calculations can be made:

1. 12.5×10^{-3} mL of methanol (32 g/mol) at 375 °C (ρ_{vap} = 0.602 mg/mL) gives 2.348×10^{-4} mol.
2. ZSM-5 (Si/Al=15) catalyst has 96/16 active sites per unit of ZSM-5 of 9.958×10^{19} units/gram. 9.958×10^{19} units/gram of ZSM-5 was obtained from its molecular weight (6048 g/mol) and the Avogadro number (6.0225×10^{23} units/mol). For 300 mg of ZSM-5, 1.7925×10^{20} active sites are available.
3. Consequently, a methanol coverage of 0.7866 methanol molecules/active site is obtained.
4. Haw and co-workers (78) used 1 ppm of ethanol impurity which gives 7.866×10^{-6} molecules per bridging OH while 36 ppm of ethanol impurity gives 2.83176×10^{-5} molecules per bridging OH.
5. However, if 1 ppm ethanol impurity (7.866×10^{-6} molecules per bridging OH) gives 2 ppm of volatile hydrocarbons, then, proportionally, 2.561×10^{-3} molecules per bridging OH should give 650 ppm of volatile hydrocarbons
6. The calculated 2.561×10^{-3} molecules per bridging OH is 2 orders of magnitude higher than the reagent quantity used by Haw and co-workers (78) which is 36 ppm of ethanol impurity - 2.83176×10^{-5} molecules per bridging OH

This shows that impurities are not solely responsible for the formation of the first hydrocarbons over ZSM-5 catalyst. Coverage is a function of adsorption, desorption and surface reaction. In the calculations above, it is assumed that the adsorption and desorption factors are not affected by the changes in ethanol impurity and that coverage has a linear dependence with surface reaction presumably from the dehydration of ethanol to ethylene. Nonetheless, the calculations above are in agreement with the work of Hunger and co-workers (104) who also observed that the conversion of methanol over SAPO-34 with loadings of 0.10 ethanol molecules per OH group or 0.05 acetone molecules per OH group are necessary to obtain aromatics and carbenium ions of similar concentrations to those obtained by the conversion of surface methoxy groups. Hunger and co-workers (104) observed that the concentration of ethanol and acetone impurities in reagent methanol feed are at least two orders of magnitude lower than that required to form aromatics and carbenium ions over SAPO-34 which is in agreement with the calculations above.

Haw and co-workers (80) also combined theoretical studies using extended cluster models with experimental clues of the existence of a 5-membered ring cation (1,3-dimethylcyclopentadienyl) (105) and a 6-membered ring cation (1,1,2,4,6-pentamethylbenzenium) (106) to show the co-conversion of toluene with methanol to give isobutene through a paring mechanism over ZSM-5 catalysts. The paring mechanism used by Haw and co-workers (80) to explain the co-conversion of toluene with methanol for the initial carbon-carbon formation presents one major challenge. The pre-existence of toluene in the methanol feed makes kinetic modelling for verifying reaction scheme very challenging.

Polymethylbenzenes over SAPO-34 catalysts and alkyl substituted cyclopentyl carbenium ions over ZSM-5 catalysts have been observed at relatively low contact times during MTH conversion (77, 105). Polymethylbenzenes form olefins, also observed at low contact times and conversions, through the aromatic dealkylation steps (77, 87).

Conversely, using in-situ ^{13}C NMR spectroscopy and gas chromatography during MTH conversion on ZSM-5 catalysts, Goguen et al. (91) observed ethylene traces at reaction times of 1 s. Kaeding and Butter observed ethylene at low conversions (86). Ethylene also forms alkyl substituted cyclopentyl carbenium ions at a reaction time of 4 s (105, 107). These cyclopentenyl carbenium ions are intermediates for toluene formation (another postulated hydrocarbon pool specie) over ZSM-5 catalysts. Derouane and co-workers (85) observed ethylene at low conversions although not with ^{13}C NMR and concluded that the high reactivity of ethylene with Brønsted acid sites readily lead to carbenium ions.

In summary, olefins and aromatics have been observed as initial C-C bond formed from oxygenates (methanol, DME). Where aromatics are formed initially from impurities in the feed, olefins are formed indirectly through an aromatic dealkylation chemistry. On the contrary, olefins could form directly from the methanol feed.

2.5.3.2. Direct mechanisms

The direct formation of olefins from oxygenates was initially proposed through various mechanisms (3). These mechanisms are identified by their key intermediate. Among these are the oxonium ylide, carbene, methane-formaldehyde, surface methoxy groups and carbon monoxide.

IR and ^{13}C MAS NMR investigations of the conversion of surface methoxy species over acidic zeolite support the view that the initial C-C bond forms *via* the direct mechanism (66, 67, 104, 108). Isolated surface methoxy groups can be rigidly bound on the catalyst surface and have a high thermal stability (64, 89). Using infrared and MAS NMR spectroscopy, surface methoxy species are present and directly coordinated to the aluminosilicate framework prior to the onset of hydrocarbon formation (65, 66, 109-111). Surface methoxy groups show high thermal stability below 200 °C. The conversion of pure methoxy species directly to olefins and other hydrocarbons have been observed using ^{13}C MAS NMR over H-Y, ZSM-5 and SAPO-34 catalysts at temperatures between 200 – 400 °C (67). They can act as precursors for carbene and ylide formation (89). Other direct mechanisms include:

A. Oxonium ylide mechanism

Mole and co-workers (112, 113) proposed the formation of oxonium-ylide species during MTH conversion at low temperatures (300 °C). Recent studies by Lesthaeghe and co-workers (34, 35, 82) using extended cluster DFT modelling showed that the primary formation of ethylene over ZSM-5 catalysts could occur through three routes (scheme 2.1).

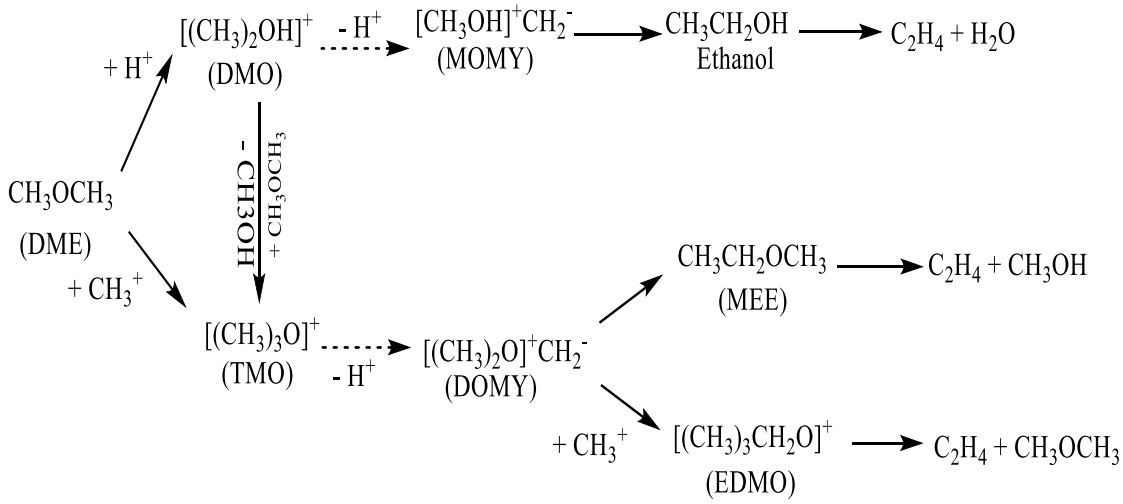

Scheme 2.1: Oxonium ylide mechanism

Following the equilibration of methanol, DME and water, dimethyl oxonium ion (DMO) could be formed directly from adsorbed DME. DMO could be deprotonated to obtain methyl oxonium methylide (MOMY) which further undergoes a Stevens-type intramolecular rearrangement leading to ethanol and the first C-C bond. Alternatively, trimethyl oxonium ion

(TMO) could be formed from the co-reaction of DME and methanol, co-reaction of two adsorbed DME molecules or reaction of a framework bound methoxy species with DME (82). Using periodic DFT studies, TMO has been shown to be stabilised by the zeolite framework (34, 39) and DMO can also react with DME to yield TMO. TMO could further undergo proton abstraction to yield dimethyl oxonium methylide (DOMY) which could undergo a Stevens-type intramolecular rearrangement, forming the first carbon-carbon bond, giving rise to methylethyl ether (86) or an intermolecular methylation forming ethyldimethyl oxonium ion (EDMO). EDMO could undergo β-elimination to form ethylene and dimethyl ether.

Using extended cluster DFT models, Lesthaeghe and co-workers obtained that the deprotonation steps from DMO to MOMY and from TMO to DOMY to be non-existent (34, 35, 39). The formation of TMO and EDMO are stable on ZSM-5 catalysts. However, due to steric constraints, Lesthaeghe and co-workers have shown the improbability of proton abstraction from TMO (34). Tajima et al. (114) and Lesthaeghe et al. (34) showed, using cluster and extended cluster models, DOMY to be a highly unstable specie. Periodic DFT calculations considering the whole unit cell of the zeolite could give confirmatory conclusions on stability of species and feasibility of the direct route. Also, framework aluminium might not possess the energy necessary for hydrogen abstraction from the oxonium ion (115). These studies (34, 39) show EDMO and TMO as stable species, however, their direct interconversion by insertion of a carbene groups has not been investigated either experimentally or theoretically (34).

B. Carbene mechanism

Carbene was suggested as the dominant intermediate in the methanol to gasoline reaction following a decrease of iso-butane to n-butane ratio (116). There are two proposed routes for the carbene mechanism (scheme 2.2). The first route involves the formation of carbenes via surface methoxy groups (scheme 2.2a). The formation of the surface methoxy groups has been studied theoretically from one methanol molecule (74, 117) and DME (70, 118) and from two methanol molecules (119). The conjugate base oxygen of the methylated acid site is the basic site used in the deprotonation of the surface methoxy species leading to carbene formation (119). Through the second route, carbenes could be formed from α-elimination of water molecules from methanol. Here, the formation of carbene species is based on the proximity of two acid sites (one in conjugate base form). They can further undergo subsequent oligomerisation to form olefins or by sp^3 insertion of the carbene into the methanol or DME in a free carbene mechanism (1, 3, 120).

i. From DME (via surface methoxy groups) (119)

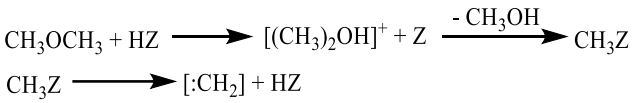

ii. From methanol (120)

$Z + CH_3OH + HZ \rightarrow Z + [: CH_2] + H_2O + HZ$

Scheme 2.2: Carbene mechanism

Both routes fail to account for methyl ethyl ether observed in the conversion of methanol over ZSM-5 catalysts (85). The conjugate base of the zeolite may not be strongly basic to abstract hydrogen from methanol (60). Using extended cluster approximations, the activation energy for carbene formation is high (215 – 232 kJ mol^{-1}) (35, 119). The desorption of carbenes involve high activation barriers of similar magnitude to the formation of the carbene itself (119) suggesting that ethylene formation via carbene polymerisation is unlikely (119, 121).

Hutchings and co-workers found the carbene proposal to be inconsistent with their observations of decreased methane/alkene ratios as conversion increased with contact times (60, 121). Mihail and co-workers (122) suggested that high methane concentrations observed at low conversions is due to the known reaction of carbene with hydrogen. However, Mihail and co-workers (122) suggested that a source of hydrogen could be from the water gas shift reaction or methanol decomposition although no experimental evidence was given. Hutchings and co-workers (60) checked for hydrogen formation through the water gas shift reaction over ZSM-5 catalysts at temperatures between 350 – 400 °C and found no evidence of this reaction. Here, methanol decomposition was studied over Na-ZSM-5 to avoid the complication of hydrocarbon formation (60) and found no evidence for methanol decomposition at 250 °C for a wide range of methanol feed rates. Methanol decomposition was only observed to a limited extent at higher temperatures (350 – 400 °C). The experiments demonstrate that methanol decomposition and water gas shift reaction are not viable sources of hydrogen for the formation of methane at low temperatures. Nonetheless, Kondo and co-workers (123), using IR spectroscopy, provided evidence for carbene-like intermediates on reaction between methoxy species and light alkenes.

C. Methane-formaldehyde mechanism

Methane and formaldehyde have been observed in similar amounts above 357 °C and low conversions under vacuum conditions in a TAP reactor (124). Less formaldehyde is detected with increasing temperature and methanol conversion (124, 125). Theoretically, there are multiple routes (scheme 2.3) towards methane and formaldehyde formation starting from two methanol molecules, or surface methoxy species and methanol, or from TMO adsorbed with methanol (35, 82, 114). Once formed, the adsorbed methane and formaldehyde

molecules react to form ethanol which subsequently dehydrates to form ethylene. Extended cluster models have shown this direct route to be improbable (35). They suggest that the conversion of methane or formaldehyde proceeds too slowly for this to be a suitable mechanism. However, recent studies using periodic DFT calculations suggest that the methane-formaldehyde mechanism is probable with methane formation having an activation energy of 149.6 kJ mol^{-1} and ethanol formation to be 124.5 kJ mol^{-1}(88). This mechanism cannot be faster than ethylene formation from ethanol impurities in methanol feed through the indirect mechanism.

$$CH_3OH + CH_3 \cdot Z \rightarrow CH_4 + CH_2O \cdot HZ \quad (2.3.1)$$

$$CH_4 + CH_2O \cdot HZ \rightleftharpoons CH_3CH_2OH \cdot HZ \quad (2.3.2)$$

$$CH_3CH_2OH \cdot HZ \rightleftharpoons CH_3CH_2 \cdot Z + H_2O \quad (2.3.3)$$

$$CH_3CH_2 \cdot Z + H_2O \rightleftharpoons C_2H_4 + H_2O \cdot HZ \quad (2.3.4)$$

Scheme 2.3: Methane-formaldehyde mechanism

D. Methoxymethyl cation mechanism

Fan and co-workers (88) provided spectroscopic and theoretical evidence for the direct mechanism for initial C-C bond formed from methanol over SAPO-34. They identified a methoxymethyl cation ($CH_3OCH_2^+$) using IR spectroscopy and verified its stability in the CHA cage of SAPO-34 using DFT calculations. $CH_3OCH_2^+$ forms from the reaction of DME and surface methoxy groups. $CH_3OCH_2^+$ combines with another DME or methanol molecule to give 1,2-dimethoxyethane or 2-methoxyethanol respectively (scheme 2.4). The latter components are methylated by methoxy species and decomposed in a series of reactions to give propylene as the primary olefin. Chowdhury et al. (126), using solid-state NMR spectroscopy with uV/Vis diffuse reflectance spectroscopy, provided evidence for intermediates such as surface acetate, methyl acetate and dimethoxymethane during MTO conversion over SAPO-34. Fan and co-workers (127) also proposed a route which involves methanol and surface methoxy groups leading to formaldehyde and methane, which subsequently leads to the formation of the first C-C bond. They showed that the methanol pathway for initial C-C bond is less favourable thermodynamically and kinetically than the DME pathway (involving the formation of $CH_3OCH_2^+$). These studies highlight a new direction in MTO chemistry involving the role of secondary oxygenates. The evidence (DFT and spectroscopy) suggests that primary oxygenates (methanol, DME) lead to secondary oxygenates (1,2-dimethoxyethane, dimethoxymethane, 2-methoxyethanol), which subsequently lead to primary olefins (ethylene and/or propylene).

$$CH_3 \cdot Z + CH_3OCH_3 \rightarrow CH_3OCH_2 \cdot Z + CH_4 \quad (2.4.1)$$

$$CH_3OCH_2 \cdot Z + CH_3 \cdot R \rightarrow CH_3OCH_2CH_2R + HZ \quad (2.4.2)$$

$$R = H, OH, OCH_3$$

Scheme 2.4: Methoxymethyl cation mechanism

E. Carbocation mechanism

This mechanism, originally proposed by Olah and co-workers (128) and modified by Kagi (129) involves methanol protonation in an acidic medium resulting in carbenium ion formation. The carbenium species react on vacant zeolite sites to form methyl ethyl ether which react with methyl carbenium ion supplied by protonated DME. The resultant methyl isopropyl ether could react with a methyl carbenium ion or eliminate methanol to form propylene (scheme 2.5). Another carbocation route involves the formation of carbenium ions which reacts with methanol to produce higher ethers which decompose to give propylene (66, 85).

$$2CH_3OH \rightleftharpoons CH_3OCH_3 + H_2O \quad (2.5.1)$$

$$CH_3OCH_3 \cdot HZ \rightleftharpoons [CH_3OCH_3 - H]^+ \cdot Z \quad (2.5.2)$$

$$[CH_3OCH_3 - H]^+ \cdot Z + CH_3OCH_3 \rightleftharpoons [(CH_3)_2OCH_3 - H]^+ \cdot Z + CH_3OH \quad (2.5.3)$$

$$[(CH_3)_2OCH_3 - H]^+ \cdot Z \rightleftharpoons CH_3CH_2OCH_3 \cdot HZ \quad (2.5.4)$$

$$CH_3CH_2OCH_3 + [CH_3OCH_3 - H]^+ \cdot Z \rightleftharpoons [(CH_3)_3OCH_3 - H]^+ \cdot Z + CH_3OH \quad (2.5.5)$$

$$[(CH_3)_3OCH_3 - H]^+ \cdot Z \rightleftharpoons (CH_3)_3OCH \cdot HZ \quad (2.5.6)$$

$$(CH_3)_3OCH \cdot HZ \rightarrow CH_3OH \cdot HZ + C_3H_6 \quad (2.5.7)$$

Scheme 2.5: Direct carbocation mechanism

F. Carbon monoxide mechanism

The carbonylation of methoxy groups by carbon monoxide originally proposed by Jackson and Bertsch (130) in 1990, has regained prominence (52, 126). Recently, it was shown that carbon monoxide forms slowly during the induction period and reacts with surface methoxy species leading to methyl acetate and acetic acid as intermediates (52, 130). Liu et al. (52) postulated that these intermediates undergo a series of acid-catalysed reaction such as acetylation, decarboxylation, aldol condensation, and cracking to obtain surface bound hydrocarbons, the hydrocarbon pool and the first olefin. The carbon monoxide mechanism is increasingly accepted as DFT calculations show that the carbonylation step has an activation energy as low as 80 kJ mol^{-1} (52). Other acid catalysed steps could involve prohibitively high activation energies. The intermediates observed here are similar to those involved with the indirect mechanism involving acetone impurities leading to primary C-C bond formation (131).

Over SAPO-34 zeo-type catalysts, Chowdhury et al. (126) provided evidence of the formation of surface acetate and methyl acetate as well as dimethoxymethane during the MTO process using a combination of solid-state NMR spectroscopy with UV/Vis diffuse reflectance spectroscopy and mass spectroscopy. Chowdhury et al. (132) further investigated the conversion of methyl acetate to olefinic and aromatic hydrocarbons using the same combination of solid-state NMR spectroscopy with UV/Vis diffuse reflectance and mass spectroscopy. Their separate pieces of work (126, 132) provide spectroscopic proof of the carbon monoxide carbonylation mechanism leading to methyl acetate and later to olefins and aromatics. The major challenge lies in bridging real kinetics with spectroscopic studies. Also, the pathway over ZSM-5 catalyst may be different from SAPO-34 due to their different pore architectures. Following the work of Dedecek and co-workers (41, 43, 133), the siting of single Al atoms and Al pairs are different for pore channels, intersections and cages. Due to the different architectures of ZSM-5 and SAPO-34, the siting and thus varied distribution of single Al atoms and Al pairs could affect the MTH chemistry differently.

G. Radical mechanism

Free radicals were observed during the conversion of DME to hydrocarbons at temperatures above 171 °C using electron spin and electron paramagnetic resonance. Radicals were associated with solid-state defects in the ZSM-5 catalyst (134). A mechanism was proposed by Clarke et al. (134) for the formation of the initial C-C bond involving either direct coupling of (methoxymethyl) radical species or C-H bond insertion by methylene, generated by methoxy radical scission. These mechanisms were disputed by Hunter et al. (121, 135) who observed no effect of adding 1-3% NO, a known radical scavenger, during methanol/DME conversion over Na-ZSM-5 at 250 °C. Na-ZSM-5 was chosen because it is essentially inactive towards DME under these conditions. However, Chang et al. (136) studied the effect of NO concentration (0, 450 and 5000 ppm) on zeolites with SiO_2/Al_2O_3 ratios of 1800 and 70 at 450 °C, 1 atm in a packed bed reactor. With lower acidity, addition of 5000 ppm NO completely suppressed hydrocarbon formation within 30 min. At 450 ppm, NO suppression required a 2 h induction period. Similar behaviour was observed at higher acidity albeit with a longer methanol breakthrough. They concluded that the catalyst was poisoned by a process involving radicals (136). The results of Chang et al. (136) are in agreement with Clarke et al. (134) but in contrast to Hunter et al. (121, 135), thus rendering this mechanism inconclusive.

2.5.3.3. Summary on primary olefin formation

Given the primary reactant (methanol and/or DME) and the primary olefin (ethylene and/or propylene), various mechanisms (direct or indirect) have been investigated. DFT calculations have shown the improbability of many direct pathways due to activation energies exceeding 200 kJ mol^{-1}. Major results from Lesthaeghe and co-workers (34, 35, 82) suggest that the direct formation of the first C-C bond from methanol or DME involve prohibitively high activation energies. They also cite the instability of intermediates such as oxonium ylides as key reasons for the failure of direct C-C coupling. Although, DFT calculations have refuted selected routes towards primary olefin formation, the direct mechanism could still possible.

Kinetic modelling techniques are indispensable tools used to discriminate between direct and indirect mechanisms of primary olefin formation. Parameter estimation and optimisation leads to adequate descriptions of the reaction chemistry at low conversions. Industrial processes can later be simulated by checking the effect of pressure, temperature and contact time. The olefins may be formed directly or indirectly through the aromatic dealkylation chemistry. If the polymethylbenzenes are initially formed and lead to olefins through the indirect mechanism, it is important to investigate how bulky polymethylbenzes of 8 to 9 carbons are formed in an initial single step or sequence of steps from methanol or DME which contain 1 and 2 carbons respectively.

After the primary products (decomposition products and primary olefins) are formed during the induction period, a working catalyst operates by regulating the product distribution *via* a hydrocarbon pool mechanism.

2.5.4. Hydrocarbon pool

From the studies on the direct and indirect mechanism, kinetic experiments aiming to investigate the early stages of MTH process lead to observation of primary olefins and decomposition products. However, spectroscopic experiments designed to probe the early stages of MTH conversion have led to the observation of certain surface intermediates including aromatics and acetates preceding primary olefins.

Over SAPO-34, the data on the appearance of intermediates (acetates, aromatics) and gaseous primary olefins are conclusive as the intermediates are too large to escape the cages of the zeo-type catalyst. The aromatic cycle controls product distribution due to steric constraints of internal cages.

For ZSM-5 catalysts where the pore size is comparable to the size of light polymethylbenzenes and olefins, it is important to investigate why aromatic species do not escape the pore channels during the early stages of the reaction. One reason for this could be that aromatics have higher desorption energies than olefins and so would not appear in the

gaseous product spectrum. However, aromatics appear at higher contact times. Over ZSM-5 catalysts, general steric constraints do not apply but kinetic constraints may occur.

The hydrocarbon pool regulates product distribution at steady state (Fig. 2.3). During kinetic experiments, at high flowrates (i.e. low contact times), where gaseous primary olefins are observed, it is likely that the catalytic cycles rotate or propagate with olefins as termination products. At low flowrates (i.e. high contact times), the dual-cycle is truncated such that both olefins and aromatics are observed simultaneously. At steady-state, product distribution is regulated by the propagation of both cycles of the hydrocarbon pool.

The hydrocarbon pool consists of the olefin cycle and the aromatic cycle over ZSM-5 catalysts. The hydrocarbon pool can be initiated depending on the initial availability of olefins (as observed in kinetic studies) or aromatics (as observed in spectroscopy). The olefin cycle involves chemistries such as olefin methylation, oligomerisation, and cracking. The aromatic cycle involves methylation and dealkylation. Hydrogen transfer and cyclisation steps link the olefin to aromatic cycle. Paraffins are termination products but their distribution at high temperatures is also regulated by cracking and alkylation with olefins.

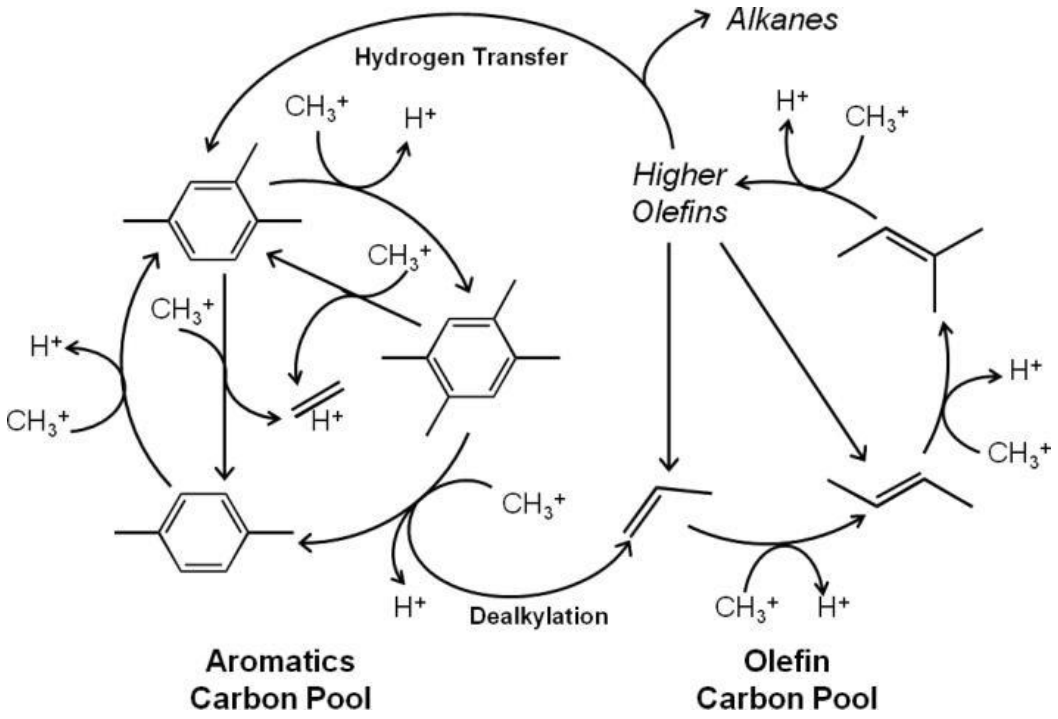

Fig. 2.3: Dual-cycle during the conversion of methanol to hydrocarbons over zeolite catalysts. Adapted from ref. (4).

2.5.4.1. Olefin methylation, oligomerisation and cracking

Once primary olefins are formed, they can undergo methylation to higher olefins in an autocatalytic cycle. Olefins are methylated by methyl groups generated from methanol and/or DME. Svelle and co-workers (40) observed that DME is a more reactive methylating agent

than methanol and that DME reacts faster with olefins than with aromatics. The reaction of methanol with butene is faster than methylation with propylene and ethylene. This is due to the formation of tertiary carbenium ion intermediates in case of butenes which are more stable than the secondary carbenium ion intermediates with propylene and primary carbenium ion intermediates with ethylene (66). Wu et al. (137) observed methylation rates to decrease in the following way: C5>C4>C6>C3>C2. Olefin methylation has been found to be zero order with respect to the methylating agent. The DME methylation rate of olefins is greater than methanol, with a factor close to 2.5 (40) at 350 °C.

Dahl and Kolboe (93, 94) observed the co-catalytic effects of the reaction of olefins with methanol at equivalent contact times greater than 10 s. In addition, Ono and Mori (66) showed that the induction period for MTH conversion is greatly reduced in the co-reaction of methanol and olefins over ZSM-5 catalysts. This is possibly due to the autocatalytic effect which is present at short contact times. Svelle and co-workers (30, 31) conducted kinetic studies of the co-reaction of methanol with olefins and extrapolated to zero olefin concentrations to extract information about methylation steps involved in MTH conversion. These studies were conducted at relatively high WHSV i.e. low contact times of 0.0042 – 0.042 h over 2.5 mg of ZSM-5 (Si/Al=45) catalysts at 350°C. Extrapolating to a zero contact time, an n-butene selectivity of about 70% was obtained as well as 15% C_5, 8% isobutene and 7% C_{6+} when co-feeding propylene and methanol. This shows that methylation of propylene was not the only reaction occurring as n-butene selectivities are less than 100%. When co-feeding ethylene with methanol, a contact time of 0.0034 – 0.034 h was used. A maximum conversion of about 7.5% and an autocatalytic effect was observed. Nevertheless, propylene selectivity of about 90% was obtained showing that other side reactions are occurring. The apparent activation energy for ethylene, propylene and butene methylation by methanol was obtained as 109, 110 and 90 kJ mol^{-1}. It is important to note that these are apparent activation energies where transport could affect intrinsic kinetics. The activation energy for gas-phase reactions is normally rather high (80 – 240 kJ mol^{-1}), while that for diffusion is small (about 5 kJ mol^{-1} at room temperature or 15 kJ mol^{-1} at 1000 °C). For reactions influenced by strong pore resistance, the observed activation energy is approximately half the true activation energy (138). Intrinsic kinetic parameters are always preferable in kinetic studies because they are scale-independent.

The conversion of primary olefins to hydrocarbons is well described by the carbenium ion mechanism. Alkenes can undergo true polymerisation involving the formation of oligomers from alkenes only (61). Rapid olefin double bond and skeletal isomerisation occur simultaneously with oligomerisation (61, 139). Subsequent oligomers could be cracked in a reversible reaction to give smaller olefins. Acidic oxides such as zeolites can catalyse various oligomerisation reactions. This include pure oligomerisation reactions and conjunct

oligomerisation reactions. Pure oligomerisation can either occur as simple polymerisation where one structural monomer is involved or co-polymerisation where two structurally different monomers react. Of the gaseous olefins, isobutylene is the most readily polymerised and ethylene is the least reactive. The rate of polymerisation is related to the ease with which a cation is formed through the interaction of the catalyst with alkenes (61). Carbenium ion mechanism is the accepted mechanism for olefin oligomerisation. Pure oligomerisation could occur with and without isomerisation. On the other hand, conjunct polymerisation occurs *via* polymerisation, isomerisation, cyclisation and hydrogen transfer chemistries. It leads to the formation of two layers on the catalyst; an upper hydrocarbon layer consisting of saturated hydrocarbons and a lower acid layer consisting of sludge hydrocarbons i.e. cyclic unsaturated hydrocarbons consisting of five-membered mono- or polycyclic rings and having an average of two or three double bonds per molecule (61).

Cracking also proceeds through carbenium ion intermediates (62). They occur at the bond located β to the carbon atom bearing the positive charge. In addition, any two alkenes may react to disproportionate, through a carbenium ion intermediate, to two olefins of different carbon numbers. The rates of oligomerisation, cracking and disproportionation determine the olefin product distribution (139). Catalytic cracking takes place by a heterolytic split of the C-C bond or ionic rupture of the bond in which a carbenium ion mechanism is involved (61). Olefins crack at a much higher rate than paraffins. Also, alkyl aromatics with propyl or larger substituents crack at a higher rate than paraffins. Alkyl aromatics crack preferentially close to the ring. For paraffins, the rate of cracking increases with the length of the carbon chain (61).

Olefin interconversion includes isomerisation, oligomerisation, cracking and methylation steps (140, 141). The chemistry of olefin oligomerisation can be greatly simplified by assuming that the isomers for a given carbon number are at equilibrium. They can be lumped and subject to further modelling studies (139, 142, 143).

2.5.4.2. Hydrogen transfer and cyclisation

Following the formation of C_{6+} olefins, the generation of olefinic carbenium ions (dienes adsorbed on protonic acid sites *via* hydrogen transfer reactions between olefins) is the first step in the sequence of reaction steps leading to aromatic formation. Through cyclisation, olefinic carbenium ions are transformed into cyclic olefins and hydrogen transfer steps between the cyclic olefins and diolefins and between cyclic olefins and carbenium ions result in aromatic formation (143). The formation of dienes, cyclic diolefins and aromatics is balanced by the formation of paraffins (61, 139, 144). With no coking, the alkane/aromatic ratio is three, however if there is coking, this ration is higher than three (23). Hydrogen transfer reactions between olefins can lead to aromatics via cycloalkanes. Muller et al. (145) and Martinez-Espin

et al. (146) recently investigated hydrogen transfer reactions between methanol and olefins and found this route to be faster than between olefins during MTH conversion.

2.5.4.3. Aromatic methylation and dealkylation

Studies of co-reaction of aromatics with methanol show that aromatics are mechanistically connected with ethylene production over ZSM-5 catalysts *via* the aromatic cycle (96, 147). Higher olefins except ethylene are formed as a result of olefin oligomerisation, methylation and cracking *via* the olefin cycle while aromatics formed from hydrogen transfer and cyclisation chemistries undergo an aromatic cycle through aromatic methylation and dealkylation chemistries (4). Co-feeding experiments (^{12}C p-xylene and ^{13}C methanol) conducted at high flowrates over ZSM-5 catalysts show that the aromatic cycle produces ethylene and propylene at similar rates (83, 148). The propagation of the olefin and aromatic cycles are tunable depending on the operating conditions (4). Recently, Lercher and co-workers showed qualitatively that the aromatic cycle dominates at low conversions while the olefin cycle is dominant at higher conversions (149) over ZSM-5 catalysts. While co-feeding aromatics free of diffusional constraints with methanol, the aromatic cycle is highly favoured over the olefin cycle. Conversely co-feeding olefins do not have significant effects on the olefin or aromatic cycle. They favour hydrogen transfer and the cyclisation step leading to the formation of aromatics (150).

The dominance of the chemistries of the dual-cycle during MTH conversion is different for SAPO-34. Methanol conversion over SAPO-34 leads to the production of light olefins. The aromatic cycle is propagated faster and dominant over the olefin cycle in SAPO-34 due to large cages that allow for their formation. Large polymethylbenzenes (hexa- and hepta-methylbenzenes) present in the cages of the zeolite are too bulky to escape and hinder the movement of small reactants and products. These large polymethylbenzenes through the aromatic cycle undergo dealkylation in the cages leading to the release of light olefins (151). Hunger and co-workers recently showed that the olefin cycle is dominant during the early stages of the reaction while the aromatic cycle is dominant at longer times on stream over SAPO-34 catalysts (68).

Aromatic dealkylation is a certain type of cracking reaction that proceeds through a carbenium ion mechanism. The dealkylation of alkyl aromatics lead to lower aromatics and olefins. They could also lead to the formation of an aromatic with olefinic side chain and a paraffin. The dealkylation of polymethylbenzenes occurs through either paring or side chain mechanisms (103) as previously mentioned.

^{1}H MAS NMR and ^{13}C MAS NMR spectroscopy have been used to study the species present on the zeolite catalysts. This has been used in confirming the presence of carbenium ions on zeolite and zeo-type catalysts such as ZSM-5 and SAPO-34 respectively (68, 84).

Specifically, ^{13}C MAS NMR techniques have also been used for observing the formation of surface methoxy groups and their conversion (65, 109, 111). Also, with probe molecules such as acetone, the ^{13}C MAS NMR technique has been used to study the proximity and synergy of Brønsted/Lewis acid sites on zeolite catalysed reactions (152). A recent review by Olsbye and co-workers (153) showed that three-membered ring compounds, dienes, polymethylcyclohexenyl, polymethylcyclopentenyl and polymethylbenzenium carbenium ions are active hydrocarbon pool species obtained during MTH conversion over SAPO-34. Several similar carbenium ions (polymethylbenzenium and polymethylcyclopentenyl) were identified over ZSM-5 catalysts.

In summary, MTH conversion over zeolite catalysts is autocatalytic in nature and is accelerated by the presence of olefins or aromatics in the feed. A typical S-shaped curve showing autocatalytic reaction is observed for the conversion of methanol with contact time (150) or temperature (68). Over SAPO-34 and ZSM-22 catalysts, product distribution at steady-state is regulated by steric constraints. Over ZSM-5 and Beta catalysts, kinetic constraints apply, and the product distribution is tunable depending on process conditions.

2.6. Product distribution in fixed bed reactors

MTH conversion, product selectivity and catalyst stability vary with bed dimensions and reaction time. In the absence of symmetric and radial contributions in a fixed bed, the axial length (z) is the prominent independent variable among the bed dimensions. The axial length can succinctly be represented as contact times. Accordingly, as the reaction progresses, conversion would also vary with catalyst lifetime. Catalyst lifetime is mostly recorded as time on stream (TOS). This dependence of product selectivity on axial length and catalyst lifetime can be quantified according to coupled partial differential equations given by the specie balance (154).

Most kinetic experiments investigate the changes in conversion with contact time while assuming conversion over time on stream stays constant (steady-state studies) or the changes in conversion with time on stream while its variation with contact time stays constant (pulse, step response, temperature-programmed studies). The contact time experiments are a measure of the catalyst activity and product selectivity. Time on stream experiments on the other hand give information on the catalyst lifetime. Also, studies conducted with time on stream at a specific contact time can give information on evolution of the reactant feed onto products. For instance, during MTH conversion, the adsorption, desorption, diffusion and reaction of methanol to form hydrocarbons can be decoupled when it is fed over fresh ZSM-5 catalysts using time on stream experiments. Kinetic studies on the primary formation of olefins from methanol should ideally provide contact times at which time on stream experiments are carried out and catalyst lifetimes (represented by time on streams) at which contact time

experiments are conducted. The evolution of primary olefins is best studied when both independent variables (contact time and reaction time) are varied accordingly.

With negligible contributions of axial and radial dispersion, the partial differential equation representing the variation of mole fraction with contact time, τ and time on stream (t) in a fixed bed of zeolite particles is given by:

$$-\frac{\partial y_i}{\partial \tau} - (-R_i)_s MW_i = \frac{w_T}{Q_f(1-\varphi)\rho_{cat}}\frac{\partial y_i}{\partial t} \qquad (2.6.1)$$

where y_i is the mole fraction of specie i (-), τ is the contact time (g_{cat} g_{feed}^{-1} h) , $(-R_i)_s$is the rate of consumption of specie i at the surface (mol g_{cat}^{-1} h^{-1}) , MW_i is the molecular weight of specie I (g_{feed} mol^{-1}), w_T is the total mass flowrate (g_{feed} h^{-1}), Q_f is the volumetric flowrate (m^3 h^{-1}), ρ_{cat} is the catalyst density (g_{cat} m^{-3}), $(1-\varphi)$ is the fraction of bed occupied by solid and t is the time on stream (h).This equation is derived later in chapter 3 (section 3.3.2.2).

Equation 2.6.1 holds for transient and steady state reactors. For experiments conducted in a TAP reactor at pressures less than 1000 Pa, the concentrations observed in the TAP are a hundred times less than those observed under kinetic experiments conducted under atmospheric conditions. Equation 2.6.1 for the TAP reactor then becomes close to the lower limit of the mole balance equation. Bimolecular reactions require adsorbed reactants on two adjacent sites (in a Langmuir-Hinshelwood mechanism) for product formation. The Langmuir-Hinshelwood mechanism occurs more frequently than the Eley-Rideal mechanism (155). There is a minimum coverage in each surface reaction that guarantees the proximity required for the Langmuir-Hinshelwood mechanism. The threshold of this minimum coverage is dependent on the specific reaction. In vacuum pressure conditions such as in the TAP reactor, the threshold might never be reached, thus leading to a “pressure gap” between vacuum studies and industrial conditions where full coverage is achieved. During MTH conversion, methanol with one carbon atom (C1) can be transformed to hydrocarbons (C1 – C10). The initial stages of this transformation could be monomolecular where methanol or dimethyl ether forms its primary products. Thus, the pressure gap should have little influence on the formation of the primary products at the early stages. Moreover, on continuous flow in the TAP reactor, this threshold should be easily met as there is constant feed supply. Experiments conducted in this thesis were under continuous flow in the TAP reactor over a shallow bed configuration.

2.7. Structured reactors for MTH conversion

Methanol has been converted to hydrocarbons over various structured reactors. Patil and Lachman (156) wash-coated silicalite over a cordierite honeycomb with increasing binder content in the wash-coat to determine the effect of blocking the zeolite active sites during MTH conversion. They observed that 20 – 30% binder in the wash-coat was suitable for excellent adhesion, high catalyst loading and catalytic activity. Anita and Govind (157) employed a

zeolite-coated monolithic reactor for MTG conversion. Similar yields were obtained over the zeolite-coated monoliths compared to fixed and fluidised bed reactors although product distribution varied. MTO conversion was studied by ZSM-5 zeolite membranes to achieve uniform contacting time of molecules with active sites (158). By adjusting the diffusion and chemical reaction rates of the molecules within the ZSM-5 zeolite layer of the membrane, a high olefin selectivity of up to 90% is achieved with conversions ranging from 80 – 90%. However, there were cracks in the membranes used due to severe thermal and mechanical shocks during MTO conversion. Zeolite coated ceramic foams have also been used (159) to allow for variation of catalyst bulk thickness to maintain control over the quantity of catalytic species required for MTO conversion. Ivanova et al. (160) observed substantial activity, selectivity and lifetime improvements with ZSM-5 coatings on *β*-SiC monoliths compared to conventional zeolite packings. In all these systems, however, catalyst inventory remains an important obstacle. This challenge can be circumvented using co-extrusion of a catalyst substrate and a binder (161). Recent simulations by Guo et al. (162) on comparing methanol to propylene conversion over a packed bed of ZSM-5 particles and a co-extruded monolith show a higher reactor efficiency and propylene selectivity for monoliths. However, there are no experimental results to validate these numerical simulations.

2.8. Kinetic models for MTH conversion

2.8.1. Steady-state kinetic models

Various lumped and single-event methodologies (163-169) have been used separately for the kinetic modelling of MTH conversion over zeolite catalysts. Chen and Reagan (163) used a four lump model in establishing the autocatalytic reaction between methanol/DME and olefins over ZSM-5 catalysts. Propylene was observed as the major olefin at conversions lower than 15%. The rate of higher olefin formation is about 50 times higher than the rate of the direct ethylene formation from methanol/DME. Chang (170) predicted the steady-state conversion and product selectivity during MTH conversion over ZSM-5 catalysts using a 4-lump model that assumes the direct formation of olefins over a wide range of pressures from 0.04 atm to 50 atm. Mihail et al. (59) explained MTH conversion through the generation of carbenes for primary olefin formation. However, the agreement between experiment and model was based on one data point for each specie and thus lacked sufficient rigour. Schoenfelder and co-workers (164) used a seven lump model in describing the MTH reaction over ZSM-5 in a fluidised bed reactor on the basis of kinetic studies conducted in a standard fixed bed reactor while Bos and co-workers (165) used a model system of 12 reactions involving 6 lumps and coke. Aguayo and co-workers (171-173) modelled the transformation of oxygenates to hydrocarbons assuming the direct olefin formation. Adsorption constants

were obtained from regression. They used a lumped model and assumed ideal plug flow reactor behaviour.

Park and Froment (166, 167) explained MTH product distribution over a ZSM-5 catalyst with Si/Al = 200 between 360 – 480 °C and space times of 0.1 – 7 g_{cat} h mol^{-1} with an oxonium methylide specie leading directly to ethylene and propylene as primary products using a Single Event Microkinetic (SEMK) methodology. Conversely, Kumar et al. (168) used the SEMK methodology over ZSM-5 with Si/Al = 200 between 370 – 480 °C and space times of 0.5 and 6.5 kg_{cat} s mol^{-1} (0.14 – 1.81 g_{cat} h mol^{-1}) and accounted for primary olefin formation using the indirect mechanism (aromatic hydrocarbon pool). The studies using the SEMK methodology highlights that different mechanisms could explain steady-state primary olefin formation. Steady-state data can be explained by several different models, but the results of transient experiments such as step or pulse responses are usually so rich that only a detailed complex model will come close to explaining the results (174).

2.8.2. Transient-state kinetic models

Currently, to the best of my knowledge, there are no transient kinetic models describing, on a microscale level, the early stages of MTH conversion except those explored in this thesis.

2.9. Gaps in the Literature

The review carried out above as well as the mechanistic implications described in the introduction (chapter 1) suggest the following gaps in understanding MTH conversion:

a. Evidence for the key oxygenate and source of methylating agents
b. Clarity on the exact pathway leading to primary olefin formation
c. Nature of primary olefins and conditions under which they are formed
d. General lack of microscale modelling techniques that can link modelling parameters obtained on a molecular level using DFT calculations and process level simulations
e. Lack of a transient kinetic model that can verify the pathway leading to primary olefins as steady-state models have been shown to be indiscriminate
f. Link between behaviour observed during the induction period and steady-state
g. Lack of consensus on the state and nature of the active site during MTH conversion.
h. Quantitative description of mechanisms that govern steady-state product distribution over ZSM-5 catalysts where propagation of olefin and aromatic cycles are tunable
i. Evidence for a structured reactor that can verify recent simulations and improve product yields

2.10. Thesis aims

The aims of this PhD project were to plug these gaps in literature by: (a) advancing understanding of the induction period during which primary olefins are formed, (b) quantitatively describing the mechanism that regulate product distribution during MTH conversion at steady-state over ZSM-5 catalysts and (c) to developing a novel structured catalyst that can reduce pressure drop and optimise desired product yield from methanol. These objectives were reached using a combined experimental (transient kinetics, steady-state kinetics, FTIR spectroscopy) and kinetic modelling approach on a microscale level.

ZSM-5 was chosen due to its superior lifetime, thus limiting this study to the induction period and steady-state behaviour.

2.11. Objectives

The physical properties of the ZSM-5 catalysts were obtained by field emission scanning electron microscopy, X-ray diffraction, nitrogen physisorption, energy dispersive X-ray analysis and thermogravimetric analysis. Their chemical nature was assessed by transmission pyridine FTIR studies. During the transient studies, the specific objectives were to:

a. Investigate the competitive adsorption and desorption of methanol and DME over ZSM-5 catalysts of different Si/Al ratios in a TAP reactor, estimate parameters governing the adsorption and desorption of methanol and DME with a transient kinetic model and obtain qualitative dependence of the competitive adsorption and desorption of methanol and DME with coverage.
b. Investigate the evolution of the key oxygenate to primary olefin(s) at various temperatures using an independently developed novel step response methodology in the TAP reactor and observe the influence of precursors such as dimethoxymethane, carbon monoxide and hydrogen on the induction period and the establishment of the hydrocarbon pool.
c. Propose a reaction mechanism through which primary olefins are formed from DME during the induction period from step response experiments, develop a transient kinetic code in MATLAB that can describe the step response data at low temperatures where primary olefins are limited and identify the rate-limiting step.

Thereafter, during the steady-state studies, the specific aims were to:

d. Develop a steady-state kinetic model in MATLAB to describe experimental data and quantitatively describe MTH conversion over ZSM-5 catalyst pellets at 370 °C.
e. Develop, characterise and compare a novel structured ZSM-5 reactor called ZSM-5 miniliths to ZSM-5 catalyst powder for hydrocarbon (specifically gasoline) yields

2.12. References

1. Chang CD, Silvestri AJ. The conversion of methanol and other O-compounds to hydrocarbons over zeolite catalysts. J Catal. 1977;47(2):249-59.
2. Chang CD, Lang WH, Smith RL. The conversion of methanol and other O-compounds to hydrocarbons over zeolite catalysts. II. Pressure effects. J Catal. 1979;56(2):169-73.
3. Stöcker M. Methanol-to-hydrocarbons: Catalytic materials and their behavior. Microporous Mesoporous Mater. 1999;29(1-2):3-48.
4. Ilias S, Bhan A. Mechanism of the catalytic conversion of methanol to hydrocarbons. ACS Catalysis. 2013;3:18-31.
5. White JL. Methanol-to-hydrocarbon chemistry: The carbon pool (r)evolution. Catalysis Science and Technology. 2011;1(9):1630-5.
6. Olsbye U, Svelle S, Bjrgen M, Beato P, Janssens TVW, Joensen F, et al. Conversion of methanol to hydrocarbons: How zeolite cavity and pore size controls product selectivity. Angewandte Chemie - International Edition. 2012;51(24):5810-31.
7. Perathoner S, Centi G. Science and Technology Roadmap on Catalysis for Europe: A path to create a sustainable future. 2015. p. 1-128.
8. Wright PA. Microporous framework solids. Cambridge: RSC; 2008.
9. Payra P, Dutta PK. Zeolites: A primer In: Auerbach SM, Carrado KA, Dutta PK, editors. Handbook of Zeolite Science and Technology United States of America: Marcel Dekker, Inc; 2003.
10. Wang W, Jiang Y, Hunger M. Mechanistic investigations of the methanol-to-olefin (MTO) process on acidic zeolite catalysts by in situ solid-state NMR spectroscopy. Catal Today. 2006;113(1–2):102-14.
11. Chen JQ, Bozzano A, Glover B, Fuglerud T, Kvisle S. Recent advancements in ethylene and propylene production using the UOP/Hydro MTO process. Catal Today. 2005;106(1-4):103-7.
12. Tian P, Wei Y, Ye M, Liu Z. Methanol to olefins (MTO): From fundamentals to commercialization. ACS Catalysis. 2015;5(3):1922-38.
13. Cobb J. New Zealand Synfuel: The Story of the World's First Natural Gas to Gasoline Plant Connell G, editor. Auckland, New Zealand: Cobb/Horwood Publications; 1995.
14. Koempel H, Liebner W. Lurgi's Methanol To Propylene (MTP®) Report on a successful commercialisation. Stud Surf Sci Catal2007. p. 261-7.
15. Wang T, Tang X, Huang X, Qian W, Cui Y, Hui X, et al. Conversion of methanol to aromatics in fluidized bed reactor. Catal Today. 2014;233:8-13.
16. Zhang JG, Qian WZ, Tang XP, Shen K, Wang T, Huang XF, et al. Influence of catalyst acidity on dealkylation, isomerization and alkylation in MTA process. Wuli Huaxue Xuebao/ Acta Physico - Chimica Sinica. 2013;29(6):1281-8.
17. Cui ZM, Liu Q, Song WG, Wan LJ. Insights into the mechanism of methanol-to-olefin conversion at zeolites with systematically selected framework structures. Angewandte Chemie - International Edition. 2006;45(39):6512-5.
18. Teketel S, Svelle S, Lillerud KP, Olsbye U. Shape-selective conversion of methanol to hydrocarbons over 10-ring unidirectional-channel acidic H-ZSM-22. ChemCatChem. 2009;1(1):78-81.
19. Cui ZM, Liu Q, Ma Z, Bian SW, Song WG. Direct observation of olefin homologations on zeolite ZSM-22 and its implications to methanol to olefin conversion. J Catal. 2008;258(1):83-6.
20. Li J, Wei Y, Liu G, Qi Y, Tian P, Li B, et al. Comparative study of MTO conversion over SAPO-34, H-ZSM-5 and H-ZSM-22: Correlating catalytic performance and reaction mechanism to zeolite topology. Catal Today. 2011;171(1):221-8.
21. Teketel S, Skistad W, Benard S, Olsbye U, Lillerud KP, Beato P, et al. Shape selectivity in the conversion of methanol to hydrocarbons: The catalytic performance of one-dimensional 10-ring zeolites: ZSM-22, ZSM-23, ZSM-48, and EU-1. ACS Catalysis. 2012;2(1):26-37.

22. Bjørgen M, Akyalcin S, Olsbye U, Benard S, Kolboe S, Svelle S. Methanol to hydrocarbons over large cavity zeolites: Toward a unified description of catalyst deactivation and the reaction mechanism. J Catal. 2010;275(1):170-80.
23. Mikkelsen O, Kolboe S. The conversion of methanol to hydrocarbons over zeolite H-beta. Microporous Mesoporous Mater. 1999;29(1-2):173-84.
24. Haw JF, Song W, inventorsShip in a bottle catalysts. United States2006.
25. Weitkamp J. Zeolites and catalysis. Solid State Ionics. 2000;131(1–2):175-88.
26. Tong M, Zhang D, Fan W, Xu J, Zhu L, Guo W, et al. Synthesis of chiral polymorph A-enriched zeolite Beta with an extremely concentrated fluoride route. Scientific Reports. 2015;5:11521.
27. Svelle S, Visur M, Olsbye U, Saepurahman, Bjørgen M. Mechanistic aspects of the zeolite catalyzed methylation of alkenes and aromatics with methanol: A review. Top Catal. 2011;54(13-15):897-906.
28. Qi L, Wei Y, Xu L, Liu Z. Reaction Behaviors and Kinetics during Induction Period of Methanol Conversion on HZSM-5 Zeolite. ACS Catalysis. 2015;5(7):3973-82.
29. De Wispelaere K, Wondergem CS, Ensing B, Hemelsoet K, Meijer EJ, Weckhuysen BM, et al. Insight into the Effect of Water on the Methanol-to-Olefins Conversion in H-SAPO-34 from Molecular Simulations and in Situ Microspectroscopy. ACS Catalysis. 2016;6(3):1991-2002.
30. Svelle S, Rønning PO, Kolboe S. Kinetic studies of zeolite-catalyzed methylation reactions: 1. Coreaction of [12C]ethene and [13C]methanol. J Catal. 2004;224(1):115-23.
31. Svelle S, Rønning PO, Olsbye U, Kolboe S. Kinetic studies of zeolite-catalyzed methylation reactions. Part 2. Co-reaction of [12C]propene or [12C]n-butene and [13C]methanol. J Catal. 2005;234(2):385-400.
32. Li H, Rivallan M, Thibault-Starzyk F, Travert A, Meunier FC. Effective bulk and surface temperatures of the catalyst bed of FT-IR cells used for in situ and operando studies. PCCP. 2013;15(19):7321-7.
33. Kramer GJ, Van Santen RA, Emeis CA, Nowak AK. Understanding the acid behaviour of zeolites from theory and experiment. Nature. 1993;363(6429):529-31.
34. Lesthaeghe D, Van Speybroeck V, Marin GB, Waroquier M. What role do oxonium ions and oxonium ylides play in the ZSM-5 catalysed methanol-to-olefin process? Chem Phys Lett. 2006;417(4-6):309-15.
35. Lesthaeghe D, Van Speybroeck V, Marin GB, Waroquier M. The rise and fall of direct mechanisms in methanol-to-olefin catalysis: An overview of theoretical contributions. Ind Eng Chem Res. 2007;46(26):8832-8.
36. Van Der Mynsbrugge J, Visur M, Olsbye U, Beato P, Bjorgen M, Van Speybroeck V, et al. Methylation of benzene by methanol: Single-site kinetics over H-ZSM-5 and H-beta zeolite catalysts. J Catal. 2012;292:201-12.
37. Shah R, Gale JD, Payne MC. Methanol adsorption in zeolites - A first-principles study. J Phys Chem. 1996;100(28):11688-97.
38. Shah R, Payne MC, Lee MH, Gale JD. Understanding the catalytic behavior of zeolites: A first-principles study of the adsorption of methanol. Science. 1996;271(5254):1395-7.
39. Shah R, Gale JD, Payne MC. In situ study of reactive intermediates of methanol in zeolites from first principles calculations. J Phys Chem B. 1997;101(24):4787-97.
40. Svelle S, Kolboe S, Swang O, Olsbye U. Methylation of Alkenes and Methylbenzenes by Dimethyl Ether or Methanol on Acidic Zeolites. The Journal of Physical Chemistry B. 2005;109(26):12874-8.
41. Dedecek J, Balgová V, Pashkova V, Klein P, Wichterlová B. Synthesis of ZSM-5 zeolites with defined distribution of Al atoms in the framework and multinuclear MAS NMR analysis of the control of Al distribution. Chemistry of Materials. 2012;24(16):3231-9.
42. Haag WO, Lago RM, Weisz PB. The active site of acidic aluminosilicate catalysts. Nature. 1984;309(5969):589-91.

43. Bernauer M, Tabor E, Pashkova V, Kaucký D, Sobalík Z, Wichterlová B, et al. Proton proximity – New key parameter controlling adsorption, desorption and activity in propene oligomerization over H-ZSM-5 zeolites. J Catal. 2016;344:157-72.
44. Trombetta M, Armaroli T, Gutièrrez Alejandre Ad, Ramirez Solis J, Busca G. An FT-IR study of the internal and external surfaces of HZSM5 zeolite. Applied Catalysis A: General. 2000;192(1):125-36.
45. Armaroli T, Simon LJ, Digne M, Montanari T, Bevilacqua M, Valtchev V, et al. Effects of crystal size and Si/Al ratio on the surface properties of H-ZSM-5 zeolites. Applied Catalysis A: General. 2006;306:78-84.
46. Phung TK, Busca G. On the Lewis acidity of protonic zeolites. Applied Catalysis A: General. 2015;504:151-7.
47. Milina M, Mitchell S, Trinidad ZD, Verboekend D, Pérez-Ramírez J. Decoupling porosity and compositional effects on desilicated ZSM-5 zeolites for optimal alkylation performance. Catalysis Science and Technology. 2012;2(4):759-66.
48. Trombetta M, Gutièrrez Alejandre A, Ramirez Solis J, Busca G. An FT-IR study of the reactivity of hydrocarbons on the acid sites of HZSM5 zeolite. Applied Catalysis A: General. 2000;198(1-2):81-93.
49. Perea DE, Arslan I, Liu J, Ristanović Z, Kovarik L, Arey BW, et al. Determining the location and nearest neighbours of aluminium in zeolites with atom probe tomography. Nature Communications. 2015;6.
50. Lukyanov DB. On the extremely high ability of enhanced activity sites in HZSM-5 to generate carbenium ions. Zeolites. 1994;14(3):233-4.
51. Comas-Vives A, Valla M, Copéret C, Sautet P. Cooperativity between al sites promotes hydrogen transfer and carbon-carbon bond formation upon dimethyl ether activation on alumina. ACS Central Science. 2015;1(6):313-9.
52. Liu Y, Müller S, Berger D, Jelic J, Reuter K, Tonigold M, et al. Formation Mechanism of the First Carbon-Carbon Bond and the First Olefin in the Methanol Conversion into Hydrocarbons. Angewandte Chemie - International Edition. 2016;55(19):5723-6.
53. Wielers AFH, Vaarkamp M, Post MFM. Relation between properties and performance of zeolites in paraffin cracking. J Catal. 1991;127(1):51-66.
54. Haag WO, Lago RM, Weisz PB. Transport and reactivity of hydrocarbon molecules in a shape-selective zeolite. Faraday Discussions of the Chemical Society. 1981;72:317-30.
55. Buchanan JS, Santiesteban JG, Haag WO. Mechanistic considerations in acid-catalyzed cracking of olefins. J Catal. 1996;158(1):279-87.
56. Cheung P, Bhan A, Sunley GJ, Law DJ, Iglesia E. Site requirements and elementary steps in dimethyl ether carbonylation catalyzed by acidic zeolites. J Catal. 2007;245(1):110-23.
57. Gay PF, Travers MW. On the thermal decomposition of dimethyl ether. Transactions of the Faraday Society. 1937;33:756-70.
58. Chu CTW, Chang CD. Methanol conversion to olefins over ZSM-5. II. Olefin distribution. J Catal. 1984;86(2):297-300.
59. Mihail R, Straja S, Maria G, Musca G, Pop G. A kinetic model for methanol conversion to hydrocarbons. Chem Eng Sci. 1983;38(9):1581-91.
60. Hutchings GJ, Gottschalk F, Hall MVM, Hunter R. Hydrocarbon formation from methylating agents over the zeolite catalyst ZSM-5. Comments on the mechanism of carbon-carbon bond and methane formation. Journal of the Chemical Society, Faraday Transactios 1: Physical Chemistry in Condensed Phases. 1987;83(3):571-83.
61. Pines H. Acid-Catalyzed Reactions The Chemistry of Catalytic Hydrocarbon Conversions. United Kingdom: Academic Press; 1981.
62. Gates BC, Katzer JR, Schuit GCA. Cracking. Chemistry of Catalytic Processes. United States of America: McGraw-Hill; 1979.
63. Butter SA, Kaeding WW, Jurewicz AT, inventors. U.S. 1975.

64. Wang W, Seiler M, Hunger M. Role of surface methoxy species in the conversion of methanol to dimethyl ether on acidic zeolites investigated by in situ stopped-flow MAS NMR spectroscopy. J Phys Chem B. 2001;105(50):12553-8.
65. Forester TR, Howe RF. In situ FTIR studies of methanol and dimethyl ether in ZSM-5. J Am Chem Soc. 1987;109(17):5076-82.
66. Ono Y, Mori T. Mechanism of methanol conversion into hydrocarbons over ZSM-5 zeolite. Journal of the Chemical Society, Faraday Transactions 1: Physical Chemistry in Condensed Phases. 1981;77(9):2209-21.
67. Wang W, Buchholz A, Seiler M, Hunger M. Evidence for an Initiation of the Methanol-to-Olefin Process by Reactive Surface Methoxy Groups on Acidic Zeolite Catalysts. J Am Chem Soc. 2003;125(49):15260-7.
68. Dai W, Wang C, Dyballa M, Wu G, Guan N, Li L, et al. Understanding the Early Stages of the Methanol-to-Olefin Conversion on H-SAPO-34. ACS Catalysis. 2015;5(1):317-26.
69. Blaszkowski SR, Van Santen RA. Theoretical study of the mechanism of surface methoxy and dimethyl ether formation from methanol catalyzed by zeolitic protons. J Phys Chem B. 1997;101(13):2292-305.
70. Blaszkowski SR, Van Santen RA. The mechanism of dimethyl ether formation from methanol catalyzed by zeolitic protons. J Am Chem Soc. 1996;118(21):5152-3.
71. Mirth G, Lercher JA, Anderson MW, Klinowski J. Adsorption complexes of methanol on zeolite ZSM-5. J Chem Soc, Faraday Trans. 1990;86(17):3039-44.
72. Kubelková L, Nováková J, Nedomová K. Reactivity of surface species on zeolites in methanol conversion. J Catal. 1990;124(2):441-50.
73. Blaszkowski SR, Van Santen RA. Density functional theory calculations of the activation of methanol by a Brønsted zeolitic proton. J Phys Chem. 1995;99(30):11728-38.
74. Zicovich-Wilson CM, Viruela P, Corma A. Formation of surface methoxy groups on H-zeolites from methanol. A quantum chemical study. J Phys Chem. 1995;99(35):13224-31.
75. Sauer J, Ugliengo P, Garrone E, Saunders VR. Theoretical study of van der Waals complexes at surface sites in comparison with the experiment. Chem Rev. 1994;94(7):2095-160.
76. Haase F, Sauer J. Ab initio molecular dynamics simulation of methanol interacting with acidic zeolites of different framework structure. Microporous Mesoporous Mater. 2000;35-36:379-85.
77. Song W, Haw JF, Nicholas JB, Heneghan CS. Methylbenzenes are the organic reaction centers for methanol-to-olefin catalysis on HSAPO-34. J Am Chem Soc. 2000;122(43):10726-7.
78. Song W, Marcus DM, Fu H, Ehresmann JO, Haw JF. An oft-studied reaction that may never have been: Direct catalytic conversion of methanol or dimethyl ether to hydrocarbons on the solid acids HZSM-5 or HSAPO-34. J Am Chem Soc. 2002;124(15):3844-5.
79. Haw JF, Song W, Marcus DM, Nicholas JB. The Mechanism of Methanol to Hydrocarbon Catalysis. Acc Chem Res. 2003;36:317-26.
80. McCann DM, Lesthaeghe D, Kletnieks PW, Guenther DR, Hayman MJ, Van Speybroeck V, et al. A complete catalytic cycle for supramolecular methanol-to-olefins conversion by linking theory with experiment. Angewandte Chemie - International Edition. 2008;47(28):5179-82.
81. Marcus DM, McLachlan KA, Wildman MA, Ehresmann JO, Kletnieks PW, Haw JF. Experimental evidence from H/D exchange studies for the failure of direct C-C coupling mechanisms in the methanol-to-olefin process catalyzed by HSAPO-34. Angewandte Chemie - International Edition. 2006;45(19):3133-6.
82. Lesthaeghe D, Van Speybroeck V, Marin GB, Waroquier M. Understanding the failure of direct C-C coupling in the zeolite-catalyzed methanol-to-olefin process. Angewandte Chemie - International Edition. 2006;45(11):1714-9.

83. Bjørgen M, Svelle S, Joensen F, Nerlov J, Kolboe S, Bonino F, et al. Conversion of methanol to hydrocarbons over zeolite H-ZSM-5: On the origin of the olefinic species. J Catal. 2007;249(2):195-207.
84. Song W, Nicholas JB, Haw JF. A persistent carbenium ion on the methanol-to-olefin catalyst HSAPO-34: Acetone shows the way. J Phys Chem B. 2001;105(19):4317-23.
85. Derouane EG, Nagy JB, Dejaifve P, van Hooff JHC, Spekman BP, Védrine JC, et al. Elucidation of the mechanism of conversion of methanol and ethanol to hydrocarbons on a new type of synthetic zeolite. J Catal. 1978;53(1):40-55.
86. Kaeding WW, Butter SA. Production of chemicals from methanol. I. Low molecular weight olefins. J Catal. 1980;61(1):155-64.
87. Fu H, Song W, Haw JF. Polycyclic aromatics formation in HSAPO-34 during methanol-to-olefin catalysis: Ex situ characterization after cryogenic grinding. Catal Lett. 2001;76(1-2):89-94.
88. Li J, Wei Z, Chen Y, Jing B, He Y, Dong M, et al. A route to form initial hydrocarbon pool species in methanol conversion to olefins over zeolites. J Catal. 2014;317(0):277-83.
89. Wang W, Hunger M. Reactivity of surface alkoxy species on acidic zeolite catalysts. Acc Chem Res. 2008;41(8):895-904.
90. Yamazaki H, Shima H, Imai H, Yokoi T, Tatsumi T, Kondo JN. Direct production of propene from methoxy species and dimethyl ether over H-ZSM-5. Journal of Physical Chemistry C. 2012;116(45):24091-7.
91. Goguen PW, Xu T, Barich DH, Skloss TW, Song W, Wang Z, et al. Pulse-quench catalytic reactor studies reveal a carbon-pool mechanism in methanol-to-gasoline chemistry on zeolite HZSM-5. J Am Chem Soc. 1998;120(11):2650-1.
92. Dahl IM, Kolboe S. On the reaction mechanism for propene formation in the MTO reaction over SAPO-34. Catal Lett. 1993;20(3-4):329-36.
93. Dahl IM, Kolboe S. On the Reaction Mechanism for Hydrocarbon Formation from Methanol over SAPO-34. I. Isotopic Labeling Studies of the Co-Reaction of Ethene and Methanol. J Catal. 1994;149(2):458-64.
94. Dahl IM, Kolboe S. On the reaction mechanism for hydrocarbon formation from methanol over SAPO-34: 2. Isotopic labeling studies of the Co-reaction of propene and methanol. J Catal. 1996;161(1):304-9.
95. Arstad B, Kolboe S. Methanol-to-hydrocarbons reaction over SAPO-34. Molecules confined in the catalyst cavities at short time on stream. Catal Lett. 2001;71(3-4):209-12.
96. Mole T, Bett G, Seddon D. Conversion of methanol to hydrocarbons over ZSM-5 zeolite: An examination of the role of aromatic hydrocarbons using 13carbon- and deuterium-labeled feeds. J Catal. 1983;84(2):435-45.
97. Mole T, Whiteside JA, Seddon D. Aromatic co-catalysis of methanol conversion over zeolite catalysts. J Catal. 1983;82(2):261-6.
98. Arstad B, Nicholas JB, Haw JF. Theoretical Study of the Methylbenzene Side-Chain Hydrocarbon Pool Mechanism in Methanol to Olefin Catalysis. J Am Chem Soc. 2004;126(9):2991-3001.
99. Sassi A, Wildman MA, Ahn HJ, Prasad P, Nicholas JB, Haw JF. Methylbenzene chemistry on zeolite HBeta: Multiple insights into methanol-to-olefin catalysis. J Phys Chem B. 2002;106(9):2294-303.
100. Sullivan RF, Sieg RP, Langlois GE, Egan CJ. A new reaction that occurs in hydrocracking of certain aromatic hydrocarbons. J Am Chem Soc. 1961;83(5):1156-&.
101. Bjørgen M, Olsbye U, Svelle S, Kolboe S. Conversion of methanol to hydrocarbons: The reactions of the heptamethylbenzenium cation over zeolite H-beta. Catal Lett. 2004;93(1-2):37-40.

102. Lesthaeghe D, De Sterck B, Van Speybroeck V, Marin GB, Waroquier M. Zeolite shape-selectivity in the gem-methylation of aromatic hydrocarbons. Angewandte Chemie - International Edition. 2007;46(8):1311-4.
103. Lesthaeghe D, Horré A, Waroquier M, Marin GB, Van Speybroeck V. Theoretical insights on methylbenzene side-chain growth in zsm-5 zeolites for methanol-to-olefin conversion. Chemistry - A European Journal. 2009;15(41):10803-8.
104. Jiang Y, Wang W, Marthala VRR, Huang J, Sulikowski B, Hunger M. Effect of organic impurities on the hydrocarbon formation via the decomposition of surface methoxy groups on acidic zeolite catalysts. J Catal. 2006;238(1):21-7.
105. Haw JF, Nicholas JB, Song W, Deng F, Wang Z, Xu T, et al. Roles for cyclopentenyl cations in the synthesis of hydrocarbons from methanol on zeolite catalyst HZSM-5. J Am Chem Soc. 2000;122(19):4763-75.
106. Xu T, Barich DH, Goguen PW, Song W, Wang Z, Nicholas JB, et al. Synthesis of a benzenium ion in a zeolite with use of a catalytic flow reactor. J Am Chem Soc. 1998;120(16):4025-6.
107. Oliver FG, Munson EJ, Haw JF. High-temperature in situ magic angle spinning NMR studies of chemical reactions on catalysts. J Phys Chem. 1992;96(20):8106-11.
108. Jiang Y, Wang W, Reddy Marthala VR, Huang J, Sulikowski B, Hunger M. Response to comments on the paper: "Effect of organic impurities on the hydrocarbon formation via the decomposition of surface methoxy groups on acidic zeolite catalysts" by Y. Jiang, W. Wang, V.R.R. Marthala, J. Huang, B. Sulikowski, M. Hunger. J Catal. 2006;244(1):134-6.
109. Bosáček V. Formation of surface-bonded methoxy groups in the sorption of methanol and methyl iodide on zeolites studied by 13C MAS NMR spectroscopy. J Phys Chem. 1993;97(41):10732-7.
110. Nováková J, Kubelková L, Dolejšek Z. Deuterium-labeled methanol in reactions with HZSM-5 zeolite. J Catal. 1986;97(1):277-9.
111. Derouane EG, Gilson JP, Nagy JB. Zeolites. 1982(2):42.
112. Mole T, Whiteside JA. Conversion of methanol to ethylene over ZSM-5 zeolite in the presence of deuterated water. J Catal. 1982;75(2):284-90.
113. Mole T. Conversion of methanol to ethylene over ZSM-5 zeolite: A reexamination of the oxonium-ylide hypothesis, using 13carbon- and deuterium-labeled feeds. J Catal. 1983;84(2):423-34.
114. Tajima N, Tsuneda T, Toyama F, Hirao K. A new mechanism for the first carbon-carbon bond formation in the MTG process: A theoretical study. J Am Chem Soc. 1998;120(32):8222-9.
115. Khadzhiev SN, Magomedova MV, Peresypkina EG. Mechanism of olefin synthesis from methanol and dimethyl ether over zeolite catalysts: A review. Petroleum Chemistry. 2014;54(4):245-69.
116. Dass DV, Martin RW, Odell AL, Quinn GW. A Re-Examination of Evidence for Carbene (CH2:) As An Intermediate in the Conversion of Methanol to Gasoline. The Effect of Added Propane. In: Bibby DM, Chang CD, Howe RF, Yurchak S, editors. Stud Surf Sci Catal. 36: Elsevier; 1988. p. 177-81.
117. Blaszkowski SR, Nascimento MAC, Van Santen RA. Activation of C-H and C-C bonds by an acidic zeolite: A density functional study. J Phys Chem. 1996;100(9):3463-72.
118. Chang CD. A reply to Kagi: Mechanism of conversion of methanol over ZSM-5 catalyst. J Catal. 1981;69(1):244-5.
119. Sinclair PE, Catlow CRA. Generation of carbenes during methanol conversion over Bronsted acidic aluminosilicates. A computational study. J Phys Chem B. 1997;101(3):295-8.
120. Swabb EA, Gates BC. Diffusion, reaction, and fouling in H-mordenite crystallites. The catalytic dehydration of methanol. Ind Eng Chem Fundam. 1972;11(4):540-5.

121. Hunter R, Hutchings GJ. Hydrocarbon formation from methanol using WO3/Al 2O3 and zeolite H-ZSM-5 catalysts: Further evidence on the reaction mechanism. J Chem Soc, Chem Commun. 1987(5):377-9.
122. Mihail R, Straja S, Marla G, Musca G, Pop G. Kinetic model for Methanol Conversion to Olefins. Ind Eng Chem Proc Des Dev. 1983(22):532-8.
123. Yamazaki H, Shima H, Imai H, Yokoi T, Tatsumi T, Kondo JN. Evidence for a "carbene-like" intermediate during the reaction of methoxy species with light alkenes on H-ZSM-5. Angewandte Chemie - International Edition. 2011;50(8):1853-6.
124. Nováková J, Kubelková L, Habersberger K, Dolejšek Z. Catalytic activity of dealuminated Y and HZSM-5 zeolites measured by the temperature-programmed desorption of small amounts of preadsorbed methanol and by the low-pressure flow reaction of methanol. Journal of the Chemical Society, Faraday Transactions 1: Physical Chemistry in Condensed Phases. 1984;80(6):1457-65.
125. Dewaele O, Geers VL, Froment GF, Marin GB. The conversion of methanol to olefins: A transient kinetic study. Chem Eng Sci. 1999;54(20):4385-95.
126. Chowdhury AD, Houben K, Whiting GT, Mokhtar M, Asiri AM, Al-Thabaiti SA, et al. Initial Carbon–Carbon Bond Formation during the Early Stages of the Methanol-to-Olefin Process Proven by Zeolite-Trapped Acetate and Methyl Acetate. Angewandte Chemie - International Edition. 2016;55(51):15840-5.
127. Wei Z, Chen YY, Li J, Guo W, Wang S, Dong M, et al. Stability and Reactivity of Intermediates of Methanol Related Reactions and C-C Bond Formation over H-ZSM-5 Acidic Catalyst: A Computational Analysis. Journal of Physical Chemistry C. 2016;120(11):6075-87.
128. Olah GA, Sommer J, Namanworth E. Stable carbonium ions. XLI. Protonated aliphatic alcohols and their cleavage to carbonium ions. J Am Chem Soc. 1967;89(14):3576-81.
129. Kagi D. In re: Mechanism of conversion of methanol over ZSM-5 catalyst. J Catal. 1981;69(1):242-3.
130. Jackson JE, Bertsch FM, Bertsch FM. Conversion of Methanol to Gasoline: A New Mechanism for Formation of the First Carbon-Carbon Bond. J Am Chem Soc. 1990;112(25):9085-92.
131. Tago T, Konno H, Sakamoto M, Nakasaka Y, Masuda T. Selective synthesis for light olefins from acetone over ZSM-5 zeolites with nano- and macro-crystal sizes. Applied Catalysis A: General. 2011;403(1-2):183-91.
132. Chowdhury AD, Paioni AL, Houben K, Whiting GT, Baldus M, Weckhuysen BM. Bridging the Gap between the Direct and Hydrocarbon Pool Mechanisms of the Methanol-to-Hydrocarbons Process. Angewandte Chemie - International Edition. 2018.
133. Dědeček J, Sobalík Z, Wichterlová B. Siting and Distribution of Framework Aluminium Atoms in Silicon-Rich Zeolites and Impact on Catalysis. Catalysis Reviews - Science and Engineering. 2012;54(2):135-223.
134. Clarke JKA, Darcy R, Hegarty BF, O'Donoghue E, Amir-Ebrahimi V, Rooney JR. Free Radicals in Dimethyl Ether on H-ZSM-5 Zeolite. A Novel Dimension of Heterogeneous Catalysis. J Chem Soc, Chem Commun. 1986(5):425-6.
135. Hunter R, Hutchings GJ, Pickl W. Mechanistic studies on initial C-C bond formation in the zeolite ZSM-5 catalysed methanol conversion reaction: Evidence against a radical pathway. J Chem Soc, Chem Commun. 1987(11):843-4.
136. Chang CD, Hellring SD, Pearson JA. On the existence and role of free radicals in methanol conversion to hydrocarbons over HZSM-5. I. Inhibition by NO. J Catal. 1989;115(1):282-5.
137. Wu W, Guo W, Xiao W, Luo M. Dominant reaction pathway for methanol conversion to propene over high silicon H-ZSM-5. Chem Eng Sci. 2011;66(20):4722-32.
138. Levenspiel O. Chemical Reaction Engineering. 3rd ed: John Wiley & Sons; 1999. 668 p.

139. Quann RJ, Green LA, Tabak SA, Krambeck FJ. Chemistry of olefin oligomerization over ZSM-5 Catalyst. Ind Eng Chem Res. 1988;27(4):565-70.
140. Garwood WE. Conversion of C_2 - C_{10} to Higher Olefins over Synthetic Zeolite ZSM-5. ACS Symp Ser. 1983;218:383.
141. Huang X, Aihemaitijiang D, Xiao W-D. Co-reaction of methanol and olefins on the high silicon HZSM-5 catalyst: A kinetic study. Chem Eng J. 2016;286:150-64.
142. Smith BD. AIChE J. 1959;5:26.
143. Lukyanov DB, Gnep NS, Guisnet MR. Kinetic modeling of ethene and propene aromatization over HZSM-5 and GaHZSM-5. Ind Eng Chem Res. 1994;33(2):223-34.
144. Poutsma ML. Mechanistic considerations of Hydrocarbon Transformations Catalyzed by Zeolites ACS Monograph. 1976;171:437.
145. Müller S, Liu Y, Kirchberger FM, Tonigold M, Sanchez-Sanchez M, Lercher JA. Hydrogen Transfer Pathways during Zeolite Catalyzed Methanol Conversion to Hydrocarbons. J Am Chem Soc. 2016;138(49):15994-6003.
146. Martinez-Espin JS, De Wispelaere K, Janssens TVW, Svelle S, Lillerud KP, Beato P, et al. Hydrogen Transfer versus Methylation: On the Genesis of Aromatics Formation in the Methanol-To-Hydrocarbons Reaction over H-ZSM-5. ACS Catalysis. 2017(7):5773-80.
147. Svelle S, Joensen F, Nerlov J, Olsbye U, Lillerud KP, Kolboe S, et al. Conversion of methanol into hydrocarbons over zeolite H-ZSM-5: Ethene formation is mechanistically separated from the formation of higher alkenes. J Am Chem Soc. 2006;128(46):14770-1.
148. Bjørgen M, Joensen F, Lillerud KP, Olsbye U, Svelle S. The mechanisms of ethene and propene formation from methanol over high silica H-ZSM-5 and H-beta. Catal Today. 2009;142(1-2):90-7.
149. Sun X, Mueller S, Liu Y, Shi H, Haller GL, Sanchez-Sanchez M, et al. On reaction pathways in the conversion of methanol to hydrocarbons on HZSM-5. J Catal. 2014;317:185-97.
150. Sun X, Mueller S, Shi H, Haller GL, Sanchez-Sanchez M, Van Veen AC, et al. On the impact of co-feeding aromatics and olefins for the methanol-to-olefins reaction on HZSM-5. J Catal. 2014;314:21-31.
151. Hereijgers BPC, Bleken F, Nilsen MH, Svelle S, Lillerud KP, Bjørgen M, et al. Product shape selectivity dominates the Methanol-to-Olefins (MTO) reaction over H-SAPO-34 catalysts. J Catal. 2009;264(1):77-87.
152. Li S, Zheng A, Su Y, Zhang H, Chen L, Yang J, et al. Brønsted/lewis acid synergy in dealuminated HY zeolite: A combined solid-state NMR and theoretical calculation study. J Am Chem Soc. 2007;129(36):11161-71.
153. Olsbye U, Svelle S, Lillerud KP, Wei ZH, Chen YY, Li JF, et al. The formation and degradation of active species during methanol conversion over protonated zeotype catalysts. Chem Soc Rev. 2015;44(20):7155-76.
154. Bird BR, Stewart WE, Lightfoot EN. Transport Phenomena Revised 2nd ed: John Wiley & Sons, Inc.; 2007.
155. Thomas JM, Thomas WJ. Principles and Practice of Heterogeneous Catalysis 2nd ed. Weinheim, Germany: Wiley-VCH; 2015. 744 p.
156. Patil MD, Lachman IM. Methanol Conversion on Ceramic Honeycombs Coated with Silicalite. In: Flank WH, editor. Perspectives in Molecular Sieve Science. Washington D.C: American Chemical Society; 1988. p. 492-9.
157. Anita JE, Govind R. Conversion of Methanol to Gasoline-Range Hydrocarbons in a ZSM-5 Coated Monolithic Reactor. Industrial Engineering and Chemistry Research. 1995;34:140-7.
158. Masuda T, Asanuma T, Shouji M, Mukai SR, Kawase M, Hashimoto K. Methanol to olefins using ZSM-5 zeolite catalyst membrane reactor. Chem Eng Sci. 2003;58(3-6):649-56.

159. Patcas FC. The methanol-to-olefins conversion over zeolite-coated ceramic foams. J Catal. 2005;231:194-200.
160. Ivanova S, Louis B, Madani B, Tessonnier JP, Ledoux MJ, Pham-Huu C. ZSM-5 Coatings on β-SiC Monoliths: Possible New Structured Catalyst for the Methanol-to-Olefins Process. The Journal of Physical Chemistry C. 2007;111(11):4368-74.
161. Cybulski A, Moulin J. Monoliths in Heterogeneous Catalysis. Catalysis Reviews. 1994;36(2):179-270.
162. Guo W, Xiao W, Luo M. Comparison among monolithic and randomly packed reactors for the methanol-to-propylene process. Chem Eng J. 2012;207-208:734-45.
163. Chen NY, Reagan WJ. Evidence of autocatalysis in methanol to hydrocarbon reactions over zeolite catalysts. J Catal. 1979;59(1):123-9.
164. Schoenfelder H, Hinderer J, Werther J, Keil FJ. Methanol to olefins-prediction of the performance of a circulating fluidized-bed reactor on the basis of kinetic experiments in a fixed-bed reactor. Chem Eng Sci. 1994;49(24):5377-90.
165. Bos ANR, Tromp PJJ, Akse HN. Conversion of methanol to lower olefins. Kinetic modeling, reactor simulation, and selection. Ind Eng Chem Res. 1995;34(11):3808-16.
166. Park TY, Froment GF. Kinetic modeling of the methanol to olefins process. 1. Model formulation. Ind Eng Chem Res. 2001;40(20):4172-86.
167. Park TY, Froment GF. Kinetic modeling of the methanol to olefins process. 2. Experimental results, model discrimination, and parameter estimation. Ind Eng Chem Res. 2001;40(20):4187-96.
168. Kumar P, Thybaut JW, Svelle S, Olsbye U, Marin GB. Single-event microkinetics for methanol to olefins on H-ZSM-5. Ind Eng Chem Res. 2013;52(4):1491-507.
169. Kumar P, Thybaut JW, Teketel S, Svelle S, Beato P, Olsbye U, et al. Single-Event MicroKinetics (SEMK) for Methanol to Hydrocarbons (MTH) on H-ZSM-23. Catal Today. 2013;215:224-32.
170. Chang CD. A kinetic model for methanol conversion to hydrocarbons. Chem Eng Sci. 1980;35(3):619-22.
171. Aguayo AT, Mier D, Gayubo AG, Gamero M, Bilbao J. Kinetics of methanol transformation into hydrocarbons on a HZSM-5 zeolite catalyst at high temperature (400-550 °c). Ind Eng Chem Res. 2010;49(24):12371-8.
172. Pérez-Uriarte P, Ateka A, Aguayo AT, Gayubo AG, Bilbao J. Kinetic model for the reaction of DME to olefins over a HZSM-5 zeolite catalyst. Chem Eng J. 2016;302:801-10.
173. Pérez-Uriarte P, Ateka A, Gamero M, Aguayo AT, Bilbao J. Effect of the Operating Conditions in the Transformation of DME to olefins over a HZSM-5 Zeolite Catalyst. Ind Eng Chem Res. 2016;55(23):6569-78.
174. Bennett CO. Understanding Heterogeneous Catalysis Through the Transient Method. Catalysis Under Transient Conditions. ACS Symposium Series. 178: American Chemical Society; 1982. p. 1-32.

Chapter 3

3. Methodology

3.1. Strategy of kinetic analysis

The PhD aims and objectives were met using a combination of transient and steady-state kinetic experiments, transmission FTIR studies and kinetic modelling. MTH conversion over ZSM-5 catalyst was investigated from a kinetic perspective with kinetic modelling for added depth and FTIR for added breadth and perspective.

The catalysts and miniliths were initially characterised by nitrogen physisorption, thermogravimetric analysis, powder X-ray diffraction, field emission scanning electron microscopy, imaging, energy-dispersive X-ray analysis and transmission Fourier transform infrared spectroscopy.

Transient kinetic studies such as temperature programmed desorption (TPD) and temperature programmed adsorption (TPA) have been used to provide detailed mechanistic information about the binding and release of species from active sites. Although pulse experiments have been conducted in MTH in conjunction with spectroscopic studies, a study of the continuous evolution of the dominant reactant to the primary olefin(s) has not been conducted before this work. A step response transient kinetic study can provide information on the evolution of the hydrocarbon pool and the formation of primary olefins. Through these transient kinetic studies, the adsorption, desorption and surface reaction of species can be described on the catalyst surface. Transmission FTIR data supports the transient kinetic studies as it provides detailed information on the nature of the active sites (Brønsted and Lewis acid site by pyridine FTIR study). Such information can be tied into the amount of desorbing species on the surface of the zeolite catalyst during TPD studies. Transmission FTIR is also used to describe the nature of adsorbed intermediates formed during the step response experiments.

The transient kinetic data is useful for accurate description of steady state kinetic data. TPD data gives site-specific information on the key reactant during MTH conversion. Step response data coupled with FTIR could provide knowledge on the primary olefin and the exact pathway leading to their formation. The transient kinetic data was used to investigate elementary steps and adsorbed intermediates. The characterisation and transient data were combined with steady-state kinetic studies to describe the early stages of MTH conversion. The mechanisms that regulate product distribution during steady state MTH conversion can be determined over zeolite pellets and structured reactors. During the transient and steady-state kinetic studies, microkinetic modelling was used as a tool to determine kinetic

parameters of reaction steps that control olefin formation during the induction period and product distribution under steady-state respectively.

A combined experimental (i.e. TPD, TPA, step response, steady-state over powder, pellets and structured reactors) and kinetic modelling approach (based on microscale level) can yield key parameters and information that can be used to optimise selectivity of desired products, increase catalyst activity and ultimately be used for the design of chemical reactors used for MTH conversion. The reaction mechanisms are elucidated by transient experiments at constant temperatures (step response, pulse response, steady-state) while the nature of the active sites is understood using temperature programmed methods (temperature programmed adsorption and desorption). To the best of my knowledge on published data, this approach has not yet been applied to MTH conversion over ZSM-5 catalysts.

3.2. Experimental

3.2.1. Catalyst samples

ZSM-5 samples with Si/Al ratios of 11.5 and 25, purchased from Zeolyst International, and of 36 and 135, obtained from BP chemicals, are here referred to as ZSM-5 (11.5), ZSM-5 (25), ZSM-5 (36) and ZSM-5 (135). The ZSM-5 particles are of a micro-porous and meso-porous nature. Pressing them together creates a system of macro-pores that are in fact the interstices of the powder particles and whose dimensions span the entire size of the particles. This leads to a tri-modal pore structure (1).

3.2.2. Characterisation

3.2.2.1. Nitrogen physisorption

Brunauer, Emmett and Teller proposed a method of evaluating catalyst surface area based on a description of multilayer adsorption of weakly adsorbed molecules (2). They reasoned molecules like nitrogen begin to form multilayers before completion of a full monolayer. This had four underlying assumptions (3): (a) layers are densely packed, (b) heat of adsorption for the first layer is greater than the second (and higher) layers, (c) heat of adsorption is constant for all molecules in the first layer and (d) heat of adsorption for the second (and higher) layers is the same as the heat of liquefaction. The most commonly used linearised version of the adsorption isotherm is the BET equation:

$$\frac{P}{V_{ads}(P_o - P)} = \frac{1}{cV_m} + \left(\frac{c-1}{cV_m}\right)\frac{P}{P_O} \tag{3.1}$$

where P is the equilibrium pressure of the gas with the surface, P_o is the saturation vapor pressure, V_{ads} is the volume of gas (STP) adsorbed by the sampled, V_m is the volume of gas

(STP) corresponding to the formation of a monolayer, and c is a fitted constant. A plot of the left-hand side of equation (3.1) against P/P_o gives a slope equal to $\left(\frac{c-1}{cV_m}\right)$ and intercept equal to $1/cV_m$. The slope and intercept lead to an evaluation of V_m. The best fits to experimental data for mesoporous solids are typically obtained within an experimental range of 0.05 to 0.3. Thus, to arrive at a surface area, the number of molecules adsorbed in a monolayer is multiplied by the cross-sectional area of the adsorbing gas:

$$S_{BET} = \frac{V_m N s}{V a} \tag{3.2}$$

where N is Avogadro's number (mol^{-1}), s is the cross-sectional area of adsorbing gas (nm^2), V is the molar volume of adsorbing gas ($m^3\ mol^{-1}$) and a is the mass of the solid sample (g).

Nitrogen physisorption studies were carried out either on a Micromeritics ASAP 2020 unit or a 3Flex unit. The micrometrics unit is used for measuring BET surface areas as well as pore volumes. Generally, the samples were degassed by heating to 300 °C under vacuum (10^{-6} mbar) for 8 h. After degassing, the dried sample weight was determined. Prior testing showed that heating at 300 °C under vacuum for 8 h is adequate for moisture removal and acid site and catalyst preservation. Subsequently, the sample was cooled to -196 °C and liquid nitrogen was adsorbed at increasing partial pressures. BET surface areas ($m^2\ g^{-1}$) and pore volumes ($cm^3\ g^{-1}$) were obtained. A Rouquerol adjusted BET surface area (4) which considers the microporous range of adsorption was calculated using the 3Flex software. The BET equation (3.1) applies to the straight part of the BET plot but the choice of the parts of the plot that look linear is very subjective. The Rouquerol adjusted BET surface area accounts for this. The Rouquerol adjusted BET surface area allows for the selection of an appropriate pressure range for microporous solids. The adjustment is made such that a positive value of the "c" constant is obtained and pressure range selection where $n_a \cdot (P_O\text{-}P)$ increases linearly with P/P_O in accordance with Rouquerol et al. (4) is used. Rouquerol adjusted BET surface areas of specific samples are given in chapters 4, 5 and 8.

3.2.2.2. Thermogravimetric analysis

Thermogravimetric analysis (TGA) relies on the principle of measuring the change in catalyst weight as sample is heated or cooled at a controlled rate (5). Volatile coke species and H/C ratios have been determined by a combination of TGA and GC, MS or IR (6). TGA of the ZSM-5 (25) zeolite and the bentonite used in minilith (micromonolith) fabrication was carried out in the Setsys Evolution TGA 16/18 instrument from SETARAM. Before each experiment, 12 mg of sample was placed into an alumina crucible held in a TGA chamber that was continuously purged at 20 °C at 200 mL min^{-1} for 8 min. The experiments were performed under air at 20 mL min^{-1} and programmed such that the temperature is held at 20°C for 2 min,

ramped to 600 °C at 5 °C min^{-1}, cooled to 20 °C at 20 °C min^{-1} and held at 20 °C for 20 min. Prior experiments showed that 5 °C min^{-1} ramp rate was adequate enough to allow for specie desorption from ZSM-5 catalysts. The outlet gas was monitored by a mass spectrometer. The experiments were conducted and analysed in chapter 8.

3.2.2.3. Powder X-ray Diffraction

Powder X-ray diffraction (XRD) is used to obtain structural information on the zeolite samples. XRD provides information about the Bragg angle (θ) of the reflection of an incident monochromatic x-ray beam on crystal planes, according to Bragg's equation:

$$n\lambda = 2d\ sin\theta \quad (3.3)$$

where n represents the order of reflection, λ the wavelength of the incident X-ray beam and d the spacing between reflecting crystal planes. Information is also provided about the intensities of the reflected X-rays. Each crystalline phase gives a typical XRD pattern which may be regarded as the fingerprint of the respective material (7).

The zeolite samples were investigated using a Bruker D5005 diffractometer using Cu K_α radiation equipped with standard Bragg-Brentano geometry and a diffracted beam graphite monochromator and analysed in chapters 4, 5 and 8.

3.2.2.4. Field Emission Scanning Electron Microscopy

Scanning electron microscopy gives quick information on the shape and distribution of the size of the crystals and also of the presence of amorphous material (5). In the scanning electron technique, a fine beam of electrons is scanned over the surface of the sample using a system of deflecting coils. The various signals produced by the interaction of the electron with the surface, such as secondary electrons, back scattered electrons, or X-rays can be used to form an image. Magnifications in the range of 20 – 50,000 are available with a resolution of about 100 Å. Non-metallic samples such as zeolites are coated to ensure a sufficient electric conductivity to prevent a surface charge which leads to distorted pictures (5).

The morphological features of the ZSM-5 catalysts were characterised using a Carl Zeiss sigma series Field Emission Scanning Electron Microscope and were analysed in chapters 4, 5 and 8 using an image processing software (ImageJ).

3.2.2.5. Fourier-Transform Infrared Spectroscopy

Infrared spectroscopy is used in catalysis to identify adsorbed species and to study the way in which these species are chemisorbed onto the catalyst's surface (8). The type of probe molecule would influence the obtained characteristics of the probed solids as well as the

structure-activity relationship. Pyridine is a frequently used probe molecule for the quantitative assessment of the nature of acid sites (9).

The pyridine FTIR procedure and experiments (chapter 4) were designed and conducted by Andrew. I McNab and Professor J.A Anderson at the School of Engineering of the University of Aberdeen. The procedure used is stated below:

Catalyst samples were calcined in air (50 mL min^{-1}) *ex-situ* at 450 °C for 2 h. The catalyst powders were then pressed into self-supporting discs, sufficient for the transmission of an IR beam and loaded into a custom-made thermogravimetric infrared cell with a CI Precision MK2-M5 LM 2-01 microbalance and a Bruker Vertex 70 FTIR spectrometer. The catalyst discs were heated to 215 °C in nitrogen flow (10 mL min^{-1}) for 2 h to dehydrate the sample before being cooled to an initial adsorption temperature of 100 °C where a spectrum was collected. Absorption coefficients were determined by pyridine uptake by the catalysts at two different temperatures. Samples were subjected to the flow of nitrogen over a schlenk flask containing pyridine. Once the amount of pyridine adsorbed had reached equilibrium, the source of pyridine was isolated and a further spectrum was collected. The cell temperature was then increased to *ca.* 130°C and the mass was allowed to equilibrate again after desorption of pyridine and a final spectrum was collected. The values of the absorption coefficients were calculated by simultaneous equations using data from the two temperatures according to:

$$n_T = \frac{A_B . C_d}{\varepsilon_B . m} + \frac{A_L . C_d}{\varepsilon_L . m} \qquad (3.4)$$

where n_T is the total uptake of pyridine (µmol g^{-1}) determined from the microbalance (i.e. mass difference between point before adsorption of pyridine and equilibrated mass at either temperature), C_d is the area of the disc used (cm^2), determined using imaging software, *ImageJ,* which calculates an area based on a user-defined section of a photograph, with known dimensions (in pixels), m is the initial mass (g) of the disc prior to adsorption, A_x is the integrated absorbance for the Brønsted (1540 cm^{-1}) or Lewis (1450 cm^{-1}) band, and ε_x are the absorption coefficients (cm μmol^{-1}) which are solved. Once the absorption coefficients for both Brønsted and Lewis sites have been solved (separate values determined for each catalyst), the coefficients are fed back into equation (3.4), and the individual numbers of Brønsted and Lewis sites were determined.

Transmission FTIR of adsorbed species on the working catalyst and of dimethoxymethane and 1,5-hexadiene on fresh catalysts are detailed in chapter 5. They were conducted by Dr Vladimir Zholobenko at Keele University and the raw data was analysed by the author using an OMNIC 9 software.

3.2.3. Transient studies

3.2.3.1. Temporal Analysis of Products reactor

Transient experiments are a powerful tool in determining key mechanistic information about elementary steps of a chemical reaction. The requirement, however, is that the duration of the transient is essentially longer than the time resolution of the monitoring equipment. The temporal analysis of products (TAP) reactor is conventionally used for measuring the evolution of short pulses with a sub-millisecond time resolution; a factor that cannot be afforded when conducting pulse experiments under atmospheric conditions. The TAP reactor offers a very low detection limit and the direct placement of the measuring probe and mass spectrometer into the vacuum chamber leads to undiluted shape of transient profiles obtained during temperature programmed desorption (TPD), adsorption (TPA), surface reaction (TPSR), step response and pulse response experiments.

Originally developed by John Gleaves and co-workers (10) at Monsanto company in 1977 using ideas from molecular beam and relaxation methodology, the TAP-1 reactor was designed for catalyst characterisation, revelations of “composition-activity” and “structure-activity” as well as deciphering the mechanisms of chemical reactions such as selective oxidation of propylene to acrolein, adsorption and desorption on metal oxides and selective oxidation and ammoxidation of methanol (11). The TAP reactor has gone through several variations into TAP-2 and TAP-3 models. Recent investigations include toluene oxidation, methane partial oxidation and methane dry reforming (10). TAP experiments can be regarded as a connecting link between conventional kinetic experiments with a packed bed of catalyst particles performed at atmospheric pressure and molecular beam studies with a catalytically active surface conducted under high-vacuum conditions. Although molecular beam techniques may provide detailed mechanistic insights into a catalytic reaction by identifying desorbing intermediates, it suffers from the small number of collisions between the reactant molecules and the catalytic surface, which restricts its application to highly reactive surfaces. In contrast, kinetic experiments at atmospheric pressure can be performed with catalysts exposing surfaces with low reactivity. Unfortunately, these studies rarely provide information about reactive intermediates as the large number of intermolecular collusions in the gas phase often reduces their concentration to undetectably small amounts (12).

The present work made use of the TAP-1 system (Fig. 3.1) stationed at the University of Warwick. In the following discussions, the TAP-1 reactor will be referred to as TAP reactor. The TAP reactor consists of three chambers in series: the reactor chamber, differential chamber and the detector chamber. The reactor chamber consists of a small reactor, 6 mm O.D, 4 mm I.D and 40 mm long. Gases are metered through two continuous feed valves or two pulse valves into the reactor inlet through a small volume. A gate valve separates the

reactor chamber from the differential chamber and allows for sample exchange while vacuum is maintained in the reactor. The pressure at the exit of the reactor chamber is maintained at 10^{-5} Pa while the pressure at the end of the differential chamber and inlet into the quadrupole mass spectrometer (QMS) is at 10^{-6} and 10^{-7} Pa respectively. Avoiding interactions and reactions with the oxidized steel of the reactor requires special care. Special modifications are made such that the catalyst particles are housed in a thin-zone packing configuration in a quartz tube which is then inserted in the steel reactor (13). The QMS can be run either in scan mode or multiple ion detection (MID) mode. To view the whole spectrum of species (m/z = 1 – 200) available, the scan mode is used. The MID mode allows the observation of 10 key species. In this mode, a spectrum of intensity against time on stream (TOS) is obtained.

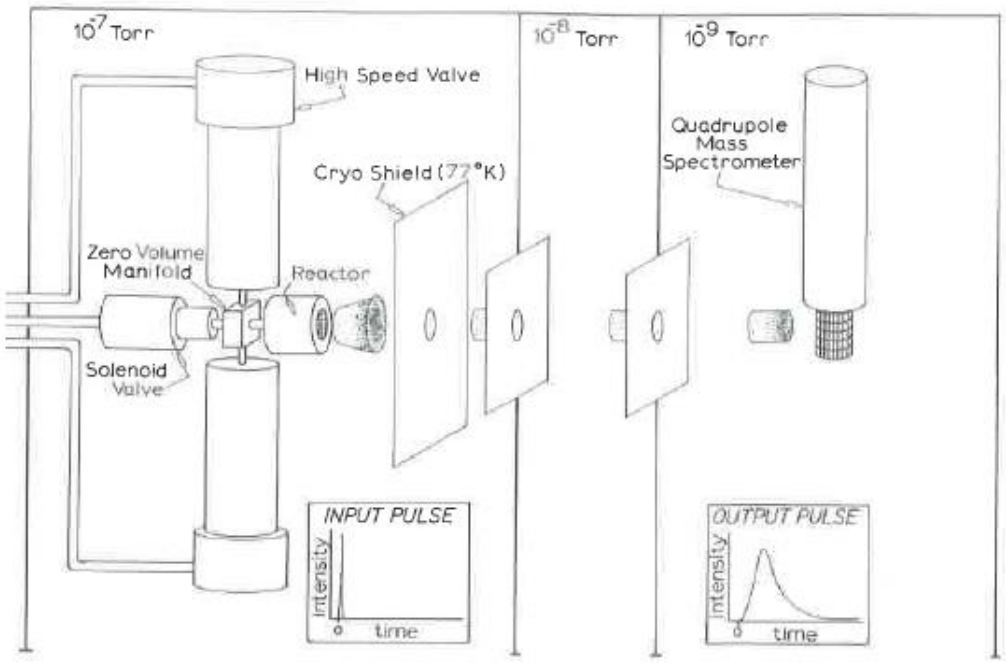

Fig. 3.1: Schematic diagram of the TAP reactor system. Reproduced from ref. (10)

The TAP method can be used for elucidation of complex catalytic processes such as the distinction between parallel, consecutive and multiple reaction pathways through pulse and step transients, determination of the nature of the active catalyst during reaction by means of transient response studies (temperature-programmed experiments) as well as fundamental modelling studies aiming at a mechanistic understanding in terms of microkinetic models (12).

The transient response experiments in this study have been carried out under continuous gas flow at low inlet pressure (< 1000 Pa) over ZSM-5 catalysts in a shallow bed packing configuration. Experiments conducted with a continuous gas feed allow the use of larger amounts of reactants. Therefore more pronounced changes in the catalyst state occur and can be traced by virtue of the high time resolution and comparably low reaction rate under

reduced pressure conditions by recording the changes in product spectra as a function of reaction time (12). Axial dispersion is negligible for the transient studies as convection is the main flow driver and gas expansion into vacuum leads to an increase in flow velocities. Conventionally, step response is achieved in the TAP reactor by using high frequency pulses. In this thesis, an alternative and novel approach was used that allowed the simultaneous switching of the feed stream and the active mixture stream using the continuous flow panel. Doing this allows for convective flow over ZSM-5 catalysts arranged in a shallow bed packing configuration in the TAP reactor. Nonetheless, the influence of dispersion was investigated.

The data analysis method detailing the conversion of ion current intensity to molar flow by accounting for recursive deconvolution of fragments, sensitivity factors obtained from calibrations and signal/noise ratios are detailed in the supplementary section of chapter 5. Experiments were conducted and analysed in chapters 4, 5 and 6.

3.2.4. Steady-state studies

3.2.4.1. Fixed bed reactor set-up and catalyst testing

Steady-state experiments were conducted by Dr Dmitry Lukyanov. Interpretation and modelling of the steady-state data was conducted by the author and detailed in chapter 7.

3.2.5. Steady-state minilith studies

3.2.5.1. Minilith fabrication

A different batch of a ZSM-5 (25) purchased from Zeolyst International was used in the zeolite fabrication, characterisation and testing studies. The free-flowing powder form ($d_{p,ave}$ = 60 µm) was mixed with 20 – 50 wt% sodium bentonite (RS minerals Ltd) of free-flowing powder form ($d_{p,ave}$ = 60 µm) to form a solid mixture. Distilled water was added to the solid mixture and the mixture was mixed manually. The optimum water content varied according to the solid binder weight (0.9 to 1.2 times the solid mixture weight). The wet paste was stirred in a high shear mixture for 2 min to form a homogenous mixture. In one batch, 10 wt% carbon was added to the solid mixture to investigate the influence of mesoporosity on the reaction. In another batch, the water content was varied to study its influence on pore volume, surface area and consequently on primary olefin formation. The wet homogenous paste was kneaded and extruded manually using a bench mounted press. Kneading was required to remove the excess air present in the paste. The minilith extrudates were then dried in a cold room (5°C) for a minimum of 24 h. The drying time varied according to solid binder weight. The dried minilith extrudates were heated in a kiln (Rohde) at 5 °C min^{-1} up to 450 °C and held for 0.5 h. This temperature was observed to preserve the strength of the zeolitic minilith while

maintaining the distribution of acid sites between Brønsted and Lewis acid sites. The fabricated extrudates (Table 3.1) were subjected to characterisation by XRD, nitrogen physisorption, SEM and TGA. All miniliths were fabricated and tested by the author and presented in chapter 8.

Table 3.1: Fabrication of zeolite miniliths

Sample Code	ZSM-5 (25) (g)	Sodium bentonite (g)	Carbon (g)	Water (g)
A	50	50	-	121
B	60	40	-	111
C	70	30	-	91
D	80	20	-	91
A2	50	50	10	137
B2	60	40	-	82

3.2.5.2. Minilith catalytic testing

The minilith was placed between two pieces of lightly compressed quartz wool, which acted as distributors and housed in a quartz tube. The protonated form of the ZSM-5 minilith was obtained by calcination in oxygen at 10 mL min^{-1} and 5 °C min^{-1} up to 450 °C. Thereafter the ZSM-5 minilith was held at 450 °C for 30 min before being brought down to 370 °C. At the start of the reaction, nitrogen was passed through the reactor for 10 min to remove any remaining oxygen still present in the bed. Thereafter, nitrogen was bubbled through methanol which was suppressed in a saturator (Lauda Eco Silver RE420 S) maintained at 4.2 °C to give 1.68 vol% of methanol at an inlet reactor pressure of 3 bar. The flow was maintained for 10 min time-on-stream before samples were taken from the off-gas. The off-gas was insulated at 110 °C and sampled through an online gas chromatograph equipped with a flame ionisation detector and a mass spectrometer. The gas chromatograph was of Shimadzu GC-10 plus equipped with an Equity™ – 1 fused silica capillary column with dimensions of 90m × 0.53 mm × 3.0µm film thickness and an FID detector. The effluent products were also analysed by an OMNI$^{STAR\ ™}$ MS.

3.3. Kinetic modelling

3.3.1. Transient kinetic model

A transient kinetic model was developed to simulate the TPD and step response data obtained in the TAP reactor.

3.3.1.1. Development of the structure of the kinetic model

The mathematical framework for modelling TAP experiments is based on the solution of the time-dependent mass, energy, and momentum balance equations with the knowledge of the estimated kinetic parameters in the model (e.g. rate constants, which could be further split up into the activation energy, E, and the pre-exponential factor A using the Arrhenius law). The modelling procedure comprises the following steps (12):

1. Formulation of the mass, energy, and momentum balance equations using an appropriate reactor transport model.
2. Choosing initial and boundary conditions to describe the underlying experimental conditions (e.g. step function experiments, temperature-programmed).
3. Implementing a model that adequately describes the reaction mechanism and the surface chemistry (e.g. mass-action law, Arrhenius law, Langmuir-Hinshelwood mechanism, kinetic Monte Carlo simulation).
4. Performing a calculation for the model based on the reaction conditions.
5. Optimisation routine (advanced mode, optional).

3.3.1.2. Temperature Programmed Desorption

A microkinetic model for simulating the temperature programmed desorption profiles was developed in collaboration with Professor Andre van Veen at the University of Warwick. A transient microkinetic model allowing for the solution of a system of coupled non-linear partial differential equations using a PDASAC routine developed by Caracotsios and Stewart (14) in the FORTRAN environment was used for the solution of the TPD profiles.

The TPD profile was simulated using a plug flow reactor model with coupled adsorption, desorption and convection. As shown later (see chapter 4), the model allowed for simulation and comparison of different desorption behaviours on up to three adsorption sites.

3.3.1.3. Step response

A transient kinetic model was initially written by the author for a thought experiment. It was applied to a simple “Langmuir system” given by:

$$A + * \longrightarrow A* \qquad k_a$$

$$A* \longrightarrow A + * \qquad k_d$$

For the reaction scheme depicted in chapter 6, the reactor was modelled as a plug flow reactor with coupled convection, adsorption, desorption and reaction steps.

$$\varepsilon_b \frac{\partial C_i}{\partial t} = -u \frac{\partial C_i}{\partial z} - \Gamma_t S_v (1 - \varepsilon_b)(k_a c_i - k_d \theta_{iZ}) \tag{3.5}$$

$$\frac{\partial \theta_i}{\partial t} = k_a c_i - k_d \theta_{iZ} \quad (3.6)$$

where k_a is the adsorption coefficient (m^3 mol^{-1} s^{-1}), c_i is the concentration of gas phase component, i (mol m^{-3}), ε_b is bed porosity; u is the superficial velocity, m s^{-1}; z is the bed length, m; t is time, s; Γ_t is the concentration of active sites per unit surface area of catalyst (mol m_{cat}^{-2}) and S_v is the catalyst surface area per unit volume (m_{cat}^{-1}), k_d is the desorption rate coefficient (s^{-1}) and θ_i is the fractional surface coverage of the adsorbed specie.

The initial conditions (at t = 0): C_i (z,0) = 0, θ_{iz} (z,0) = 0 and boundary conditions (at z=0): C_i (0, t) = forcing function f(t). The forcing function was introduced using an "IF, ELSE" statement in MATLAB. The plug flow model assumes that adsorbed species do not migrate along the axial dimension of the reactor and axial dispersion is negligible.

Multiplying (3.5) by dv = CSA.dz where CSA is the cross-sectional area, dv is change in volume and dz is the change in axial length across a control volume

$$\varepsilon_b dv \frac{\partial C_i}{\partial t} = -u.dv \frac{\partial C_i}{\partial z} - \Gamma_t S_v (1 - \varepsilon_b) \cdot dv \cdot r_i \quad (3.7)$$

$$\varepsilon_b \frac{\partial n_i}{\partial t} = -u \frac{\partial n_i}{\partial z} - \Gamma_t S_v (1 - \varepsilon_b) \cdot dv \cdot r_i \quad (3.8)$$

Equations 3.6 and 3.8 were used to model the step response of the conversion of dimethyl ether to primary olefins over ZSM-5 (25) catalysts in chapter 6. Model construction of the transient kinetic model used for the simulation of the step response data was carried out by the author.

3.3.1.4. Parameter estimation

Parameters were estimated by comparing experiment to model by progressively changing parameters until a suitable fit was established. In the simulation of temperature programmed desorption experiments, a sum of squares error (SSE) was calculated to obtain the closeness of fit. Furthermore, sensitivity analysis was carried out to obtain the effect of each parameter of desorption molar flow rates. All parameter estimation and optimisation from the use of the transient kinetic model was carried out by the author and presented in chapters 4 and 6.

3.3.2. Steady-state kinetic model

A steady-state kinetic model was used to simulate the product distribution obtained from methanol over ZSM-5 catalysts at 370 °C in chapter 7.

3.3.2.1. Development of the structure of the kinetic model

During MTH conversion over ZSM-5 catalysts, species up to C10 appear in the product mixture. To simplify modelling, the reduction of the number of species was conducted by lumping all isomers of the same carbon number into a single component. It has been shown previously (15, 16) that such lumping techniques can be used successfully in the design and development of industrial processes over ZSM-5 catalysts. For the derivation of the rate equations, it is assumed in the steady state model that the rates of hydrocarbon adsorption and desorption are much faster than the rates of hydrocarbon transformation such that adsorption equilibrium is established. Also, since the lumping methodology has been applied, it is further assumed that adsorption constants are independent of the hydrocarbon molecular weight. Rate equations are written according to the law of mass action. Then, the rates of transformation for each component involved in the reaction step are written and placed in a plug flow reactor model. This set of coupled non-linear ordinary differential equations were solved using MATLAB (2017 version).

It is assumed that molar expansion is negligible and that axial dispersion effects are minimal. According to Dr Dmitry Lukyanov, who obtained the steady-state experimental data, the ratio between the diameter of the reactor to that of catalyst particles (d_r/d_p) was more than 50. This is high enough to minimize the effect of channelling at the reactor wall (17-19). According to Satterfield (17), axial dispersion of gas-solid reactions is usually not important except for high conversions at low flow rates and short catalyst beds. A ratio between the length of catalyst bed and particle diameter (L/d_p) around or above 50 is usually recommended to achieve the plug flow. In the experiments conducted over ZSM-5 powder in chapter 8, this ratio was in the range between 66 in accordance to the above recommendation.

3.3.2.2. Steady state fixed bed reactor model

The design equation for a fixed bed reactor is given as follows:

$$F_A|_z - F_A|_{z+\Delta z} - \eta(-R_A)_s . m_s = \frac{dC_A}{dt}\Delta V \qquad (3.9)$$

$$F_A|_z - F_A|_{z+\Delta z} - \eta(-R_A)_s(1-\phi)\rho_{cat}\Delta V = \frac{dC_A}{dt}\Delta V$$

$$\Delta V = A_c \Delta z$$

Dividing all through $A_c \delta z$ and taking limits as $\Delta z \rightarrow 0$

$$-\frac{1}{A_c}\frac{dF_A}{dz} - \eta(-R_A)_s(1-\phi)\rho_{cat} = \frac{dC_A}{dt}$$

$$C_A = \frac{F_A}{Q_f} \qquad dC_A = \frac{1}{Q_f} dF_A$$

$$-\frac{1}{A_c}\frac{\partial F_A}{\partial z} - \eta(-R_A)_s(1-\phi)\rho_{cat} = \frac{1}{Q_f}\frac{\partial F_A}{\partial t} \qquad (3.10)$$

$$w_A = F_A MW_A$$

$$-\frac{1}{MW_A A_c}\frac{\partial w_A}{\partial z} - \eta(-R_A)_s(1-\phi)\rho_{cat} = \frac{1}{Q_f MW_A}\frac{\partial w_A}{\partial t}$$

$$-\frac{1}{A_c}\frac{\partial w_A}{\partial z} - \eta(-R_A)_s(1-\phi)\rho_{cat} MW_A = \frac{1}{Q_f}\frac{\partial w_A}{\partial t}$$

$$w_A = y_A w_T$$

$$-\frac{w_T}{A_c}\frac{\partial y_A}{\partial z} - \eta(-R_A)_s(1-\phi)\rho_{cat} MW_A = \frac{w_T}{Q_f}\frac{\partial y_A}{\partial t} \quad (3.11)$$

Assuming intrinsic kinetics for this analysis i.e. $\eta = 1$ and steady-state:

$$\frac{w_T}{A_c}\frac{\partial y_A}{\partial z} = -(-R_A)_s(1-\phi)\rho_{cat} MW_A \quad (3.12)$$

where F_A = molar flowrate (mol s^{-1}), C_A = concentration (mol m^{-3}), ρ_{cat} = density of catalyst, Q_f = volumetric flow rate (m^3 s^{-1}), MW_A = molecular weight of A, y_A = mass fraction (-), φ = bed voidage, A_c = flow area (m^2), w_T = total mass flowrate of the fluid (g s^{-1}).

Contact time: $\tau = \frac{m_s}{w_T} = \frac{(1-\phi)\rho_{cat}\Delta V}{w_T} = \frac{(1-\phi)\rho_{cat}A_c z}{w_T}$

$$\partial\tau = \frac{(1-\phi)\rho_{cat}A_c \partial z}{w_T}$$

Substituting the above equation gives:

$$\frac{dy_A}{d\tau} = -(-R_A)_s MW_A \quad (3.13a)$$

Thus, the reactions are substituted in the above equation. This equation is for decomposing species. For forming species, the corresponding equation is used:

$$\frac{dy_A}{d\tau} = (R_A)_s MW_A \quad (3.13b)$$

The full kinetic scheme is derived and discussed in chapter 7 of this thesis.

During desorption from porous catalysts in a packed bed, Demmin and Gorte (20, 21) identified various parameters for analysing the significance of convective lag, diffusive lag, particle concentration gradients, bed concentration gradients, re-adsorption at infinite flow rate and re-adsorption at low flow rate. The criteria for negligible particle concentration gradients $\left(\frac{Q\rho_P r^2}{3WD_K}\right)$ must be less than 0.05 for negligible gradients. Here, Q is the volumetric flow rate (cm^3 s^{-1}), ρ_P is the particle density (g cm^{-3}), r is the particle radius (cm), W is the catalyst mass (g), D_k is the Knudsen diffusion coefficient.

Furthermore, for accurate measurement of intrinsic reaction rates, negligible extra-particle heat and mass transfer and intra-particle heat and mass transport must be observed. The following equations give the criterion for measurement of intrinsic reaction rates (22):

a. To neglect extra-particle mass transfer limitation:

$$Ca = \frac{r_{v,obs}}{a' k_f C_b} < \frac{0.05}{|n|} \quad (3.14)$$

b. To neglect extra-particle heat transfer limitation:

$$\gamma\beta_e Ca = \left(\frac{E}{RT_b}\right)\left|\frac{(-\Delta H_r)k_f C_b}{hT_b}\right|\left(\frac{r_{v,obs}}{a' k_f C_b}\right) < 0.05 \quad (3.15)$$

c. To neglect intra-particle diffusion limitation:

$$\Phi = \eta\phi^2 = \left(\frac{r_{v,obs}L^2}{D_{eff}C_s}\right)\left(\frac{n+1}{2}\right) < 0.15 \quad (3.16)$$

d. To neglect intra-particle heat transport limitation:

$$\gamma\beta_i(\eta\phi^2) = \left(\frac{E}{RT_b}\right)\left|\frac{(-\Delta H_r)D_{eff}C_s}{\lambda_{eff,b}T_b}\right|\left(\frac{r_{v,obs}L^2}{D_{eff}C_s}\right) < 0.1 \quad (3.17)$$

Where Ca is the Carberry number, $r_{v,obs}$ is the observed reaction rate per unit particle volume (mol s^{-1} m_p^{-3}), a ' is the specific external surface area of the catalyst particle (a' = $6/d_p$ for spherical particles) (m^2 m^{-3}), d_p is the particle diameter (m), k_f is the mass transfer coefficient (m s^{-1}), C_b is bulk phase concentration (mol m^{-3}), n is the reaction order (-), ΔH_r is the heat of reaction (J mol^{-1}), E is the activation energy (J mol^{-1}), R is the universal gas constant (J mol^{-1} K^{-1}), T_b is the bulk phase temperature (K), h is the gas-solid heat transfer coefficient (J m^{-2} s^{-1} K^{-1}), Φ is the Wheeler-Weisz modulus ($\eta\phi^2$) with η being the effectiveness factor (-) and ϕ is the Thiele modulus) $\phi = L/\sqrt{k_v/D_{eff}}$ *where* k_v is the rate constant per unit volume expressed in s^{-1}, L is the characteristic catalyst dimension ($L=d_p/6$ for spherical particles (m), D_{eff} is the effective diffusivity in particle (m^2 s^{-1}), C_s is the concentration at the external particle surface (mol m^{-3}) and λ_{eff} is the effective thermal conductivity (J m^{-1} s^{-1} K^{-1}).

3.3.2.3. Parameter estimation

The model allowed for the solution of a system of coupled non-linear ordinary differential equations using a stiff ode solver (ode15s) in MATLAB. Kinetic parameters were estimated by comparing experimental data to model at 370 °C. Model construction, parameter estimation and optimisation were carried out by the author in chapter 7 of this thesis.

3.4. References

1. Keil FJ. Modeling Reactions in Porous Media. In: Deutschmann O, editor. Modeling and Simulation of Heterogeneous Catalytic Reactions Wiley-VCH; 2012. 149-79.
2. Brunauer S, Emmett PH, Teller E. Adsorption of Gases in Multimolecular Layers. J Am Chem Soc. 1938;60(2).
3. Davis ME, Davis RJ. Fundamentals of Chemical Reaction Engineering New York: McGraw-Hill; 2003. 368.
4. Rouquerol J, Llewellyn P, Rouquerol F. Is the BET equation application to microporous adsorbents? In: Llewellyn P, Rodriquez-Reinoso F, Rouquerol J, Seaton N, editors. Stud Surf Sci Catal. 160: Elsevier; 2007. 49-56.
5. Lechert H. The Physical Characterization of Zeolites. In: Riberia FR, Rodrigues AE, Rollmann AD, Naccache C, editors. Zeolite Science and Technology. The Hague: Martinus Nijhoff; 1984.
6. Bauer F, Karge HG. Characterization of Coke on Zeolites. In: Karge HG, Weitkamp J, editors. Characterization II. Molecular Sieves. 52007. 249 - 364.

7. Karge HG, Hunger M, Beyer HK. Characterization of Zeolites - Infrared and Nuclear Magnetic Resonance Spectroscopy and X-Ray Diffraction. In: Weitkamp J, Puppe L, editors. Catalysis and Zeolites: Fundamentals and Applications: Springer-Verlag GmbH; 1999.
8. Niemantsverdriet JW. Spectroscopy in catalysis : an introduction. 2nd ed. ed. Weinheim ; Chichester: Weinheim ; Chichester : Wiley-VCH; 2000.
9. Ryczkowski J. IR spectroscopy in catalysis. Catal Today. 2001;68.
10. Morgan K, Maguire N, Fushimi R, Gleaves JT, Goguet A, Harold MP, Kondratenko EV, Menon U, Schuurman Y, Yablonsky GS. Forty years of temporal analysis of products. Catalysis Science and Technology. 2017;7.
11. Gleaves JT, Ebner JR, Kuechler TC. Temporal Analysis of Products (TAP) — A Unique Catalyst Evaluation System with Submillisecond Time Resolution. Catalysis Reviews. 1988;30(1):49-116.
12. Hinrischen O, van Veen AC, Zanthoff HW, Muhler M. TAP Reactor Studies. In: Haw JF, editor. In-Situ Spectroscopy in Heterogeneous Catalysis. WeinHeim: Wiley-VCH; 2002.
13. Van Veen AC, Zanthoff HW, Hinrichsen O, Muhler M. Fixed-bed microreactor for transient kinetic experiments with strongly adsorbing gases under high vacuum conditions. Journal of Vacuum Science and Technology, Part A: Vacuum, Surfaces and Films. 2001;19(2):651-5.
14. Caracotsios M, Stewart WE. Sensitivity analysis of initial-boundary-value problems with mixed pdes and algebraic equations. Computers & Chemical Engineering. 1995;19(9):1019-30.
15. Lukyanov DB, Gnep NS, Guisnet MR. Kinetic modeling of ethene and propene aromatization over HZSM-5 and GaHZSM-5. Ind Eng Chem Res. 1994;33(2):223-34.
16. Quann RJ, Kerambeck FJ. Olefin oligomerization kinetics over ZSM-5 Chemical Reactions in Complex Mixtures; The Mobil Workshop, van Nostrand Reinhold, New York 1991. p. 143-62.
17. Satterfield CN. Heterogeneous Catalysis in Practice. New York: McGraw-Hill; 1980.
18. Richardson JT. Principles of Catalyst Development. New York: Plenum Press; 1989.
19. Rase HF. Chemical Reactor Design for Process Plant, Vol. 1: Principles and Techniques. New York: Wiley; 1977.
20. Gorte RJ. Design parameters for temperature programmed desorption from porous catalysts. J Catal. 1982;75(1):164-74.
21. Demmin RA, Gorte RJ. Design parameters for temperature-programmed desorption from a packed bed. J Catal. 1984;90(1):32-9.
22. Pérez-Ramírez J, Berger RJ, Mul G, Kapteijn F, Moulijn JA. Six-flow reactor technology a review on fast catalyst screening and kinetic studies. Catal Today. 2000;60(1):93-109.

Chapter 4

4. Mechanistic Insights into the Desorption of Methanol and Dimethyl Ether over ZSM-5 Catalysts

The following published work compares the adsorption and desorption of methanol to DME in a temporal analysis of products reactor using experimental data obtained from temperature programmed desorption experiments and microkinetic simulations. The rationale for this work was to identify the source of surface methoxy groups and the key oxygenate during the early stages of the MTH reaction. This is an open access publication and the accepted manuscript has been adjusted to fit this thesis format.

This declaration concerns the article entitled:									
Mechanistic Insights into the Desorption of Methanol and Dimethyl Ether over ZSM-5 Catalysts									
Publication status (tick one)									
draft manuscript		**Submitted**		**In review**		**Accepted**		**Published**	✓
Publication details (reference)	Toyin Omojola, Nikolay Cherkasov, Andrew I. McNab, Dmitry B. Lukyanov, James A. Anderson, Evgeny V. Rebrov, Andre C. van Veen. Mechanistic insights into the desorption of methanol and dimethyl ether over ZSM-5 catalysts. 2018. *Catalysis Letters*. 148. 1. 474 – 488.								
Candidate's contribution to the paper (detailed, and also given as a percentage).	The candidate predominantly executed the… Formulation of ideas: Oluwatoyin Omojola (50%) and Andre C. van Veen – Oluwatoyin Omojola developed the idea and designed the method for the effect of coverage on desorption experiments in the TAP reactor. Oluwatoyin Omojola initiated and developed the idea for temperature programmed adsorption in the TAP reactor. Design of methodology: Oluwatoyin Omojola (50%) and Andre C. van Veen Experimental work (80%): Oluwatoyin Omojola conducted all TPD and TPA experiments in the TAP reactor. Andrew I. McNab and James A. Anderson conducted FTIR experiments Simulations (80%): Oluwatoyin Omojola conducted all simulations using the microkinetic model and the Redhead method. Andre C. van Veen constructed the code for the microkinetic model. Presentation of data in journal format (80%): Oluwatoyin Omojola collated all data, interpreted the results and wrote the paper with suggestions and supervision from co-authors								
Statement from Candidate	This paper reports on original research I conducted during the period of my Higher Degree by Research candidature.								
Signed						**Date**	08/02/2019		

Abstract

The desorption of methanol and dimethyl ether has been studied over fresh and hydrocarbon-occluded ZSM-5 catalysts with Si/Al ratios of 25, 36 and 135 using a Temporal Analysis of Products (TAP) reactor. The catalysts were characterised by XRD, SEM, N_2 physisorption and pyridine FT-IR. The crystal size increases with Si/Al ratio from 0.10 to 0.78 µm. The kinetic parameters were obtained using the Redhead method and a plug flow reactor model with coupled convection, adsorption and desorption steps. ZSM-5 catalysts with Si/Al ratios of 25 and 36 exhibit three adsorption sites (low, medium, and high temperature sites), while there is no difference between medium and high temperature sites at a Si/Al ratio of 135. Molecular adsorption on the low temperature site and dissociative adsorption on the medium and high temperature sites give a good match between experiment and the plug flow reactor model. The DME desorption activation energy was systematically higher than that of methanol. Adsorption stoichiometry shows that methanol and DME form clusters onto the binding sites. When non-activated re-adsorption is accounted for, a local equilibrium is reached only on the low and medium temperature binding sites. No differences were observed, other than in site densities, when extracting the kinetic parameters for fresh and hydrocarbon-occluded ZSM-5 catalysts at full coverage.

Keywords: methanol-to-hydrocarbons, ZSM-5, TPD, DME, methanol, Redhead, Polanyi-Wigner, activation energies of desorption

4.1. Introduction

Alternative carbon sources such as biomass are vital for the secure and sustainable production of fuels and chemicals in the 21st century. Methanol can be produced *via* syngas obtained from such renewable feedstock and transformed into hydrocarbons (MTH) over zeolite catalysts (1). ZSM-5 zeolite catalysts, typically used for MTH conversion, have a three-dimensional (3D) pore structure with 10-membered-ring pores consisting of sinusoidal channels (0.51 nm × 0.55 nm) intersecting with straight channels (0.53 nm × 0.56 nm) (2). The channel intersections have a critical diameter of 0.9 nm (3). This 3D pore structure is responsible for its high selectivity and catalyst stability.

During the MTH process over ZSM-5 catalysts, methanol initially undergoes a rapid equilibration reaction leading to the formation of dimethyl ether (DME) and H_2O. Readily available oxygenates (methanol and DME) compete for active sites (4). Several pieces of theoretical work (5-7) have considered the adsorption energies of initial species over ZSM-5 catalysts. Density functional theory (DFT) calculations of the adsorption of one methanol molecule onto an active site give activation energies in the range of 104–139 kJ mol^{-1} (5, 8, 9). Blaszkowski and van Santen (10-12) showed that the simultaneous adsorption and activation of two methanol molecules towards the formation of DME and H_2O excluding surface methoxy group formation is the preferred pathway. However, surface methoxy groups have been readily observed with stopped flow NMR studies over ZSM-5 catalysts (13). These surface methoxy groups can be formed by the adsorption of methanol or DME. The presence or absence of surface methoxy groups, necessary to validate the computational studies, can be linked to the dissociative or associative adsorption behaviour of oxygenates respectively.

During steady state MTH conversion, the operation of a hydrocarbon pool mechanism which regulates product distribution over zeolite catalysts is dominant (14, 15). Within this hydrocarbon pool framework, two catalytic cycles have been readily distinguished: an alkene cycle and an aromatic cycle. Over ZSM-5 catalysts, the transformation of methanol can be tuned towards light olefin production (MTO) at high temperatures and low pressures (16-19). The underlying chemistry involves chain growth and cracking where larger molecules obtained through methylation by surface methoxy groups ($CH_3^+Z^-$) crack to give a product distribution rich in light olefins (20). To obtain a detailed understanding of this reaction mechanism, it is important to confirm the origin of these surface methylating species.

A current lack of knowledge on the primary surface reactant, the source of the surface methylating group, has led to the lumping of methanol and DME in previous experimental and modelling kinetic studies (20-22). This lumping methodology is fraught in its usage as it eludes the fact that both species have different interactions with the sites of the ZSM-5 catalysts and avoids mechanistic descriptions necessary for a microkinetic model. Detailed understanding

on the adsorption, desorption, and reactivity of initial oxygenates is necessary to provide site-specific comprehension of the nature and behaviour of ZSM-5 catalysts.

To verify the source of the methylating species, this paper provides a site-specific description of the behaviour of the desorption of methanol and DME. Using a temporal analysis of products (TAP) reactor, temperature programmed desorption (TPD) experiments of pre-adsorbed methanol or DME were carried out over various ZSM-5 samples in a shallow bed configuration under close to vacuum conditions. Key parameters such as site densities, pre-exponential factors and activation energies were obtained using a detailed elementary step model i.e. a plug flow reactor model with coupled convection, adsorption and desorption steps, which was used to simulate experimental desorption profiles.

4.2. Experimental Section

All experiments were carried out with 10 mg of ZSM-5 catalysts of different Si/Al ratios (25, 36 and 135), here referred to as ZSM-5 (25), ZSM-5 (36) and ZSM5 (135) respectively. ZSM-5 (25) was purchased from Zeolyst International while ZSM-5 (36) and ZSM-5 (135) catalysts were obtained from BP chemicals. The ammonium form of these zeolites was pressed, crushed, and sieved to obtain particle sizes in the range of 250–500 µm. The active catalyst was tightly packed between two quartz wool plugs, with the active catalyst zone of length 2 mm, in a bed length of 25 mm. In this arrangement, the thin-zone TAP reactor configuration was approached. The inert quartz tube used to house the fixed bed, as adapted by van Veen and co-workers (23), was placed in the metallic body to suppress adsorption and further reaction on the walls as well as provide mechanical stability. Anhydrous DME (99.999%) and argon (99.999%) were obtained from CK special gases Ltd. Ultra-high purity water-free methanol (99.8%) was purchased from Aldrich.

The experimental set up allowed for the formation of active H-form of the zeolite catalyst by decomposition of the ammonium form under vacuum conditions. Probe molecules (5 vol% DME or 5 vol% methanol in Ar) were fed to the TAP system using continuous feeding valves. The concentrations of probe molecules were calibrated against signal intensity by passing streams of gas in argon over an inert quartz bed catalyst of similar dimensions. From the mass spectra data, sensitivity coefficients were obtained and further used to obtain the molar flow rates during TPD experiments. Argon was monitored at m/e = 40, CH_3OH at m/e = 31, DME at m/e = 45, H_2O at m/e = 18, CO at m/e = 28, CO_2 at m/e = 44, H_2 at m/e = 2, CH_4 at m/e = 16, C_2H_4 at m/e = 27, and C_3H_6 at m/e = 41. Over ZSM-5 (36) and ZSM-5 (135) only DME or methanol was observed individually in the desorption profile. However, over ZSM-5 (25), following DME desorption, there was some release of methanol. Subsequent deconvolution allowed for the subtraction of minor fragments of other species from the main species.

4.2.1. Characterisation

The zeolite samples were studied by X-ray diffraction (XRD) with a Bruker D5005 diffractometer using Cu K_α radiation equipped with standard Bragg-Brentano geometry and a diffracted beam graphite monochromator. The morphology was characterised using a Carl Zeiss sigma series Field Emission Scanning Electron Microscope (FE-SEM) at an accelerated voltage of 20 kV. The crystal size distribution was obtained from an image analysis software. Nitrogen physisorption studies were carried out on a Micromeritics 2020 unit. The samples were degassed by heating to 400 °C under vacuum (10^{-6} mbar) for 12 h prior to measurements.

4.2.2. Acid site density determination

Zeolite catalyst samples were calcined in air (50 mL min^{-1}) *ex-situ* at 450 °C for 2 h. The catalyst powders were then pressed into self-supporting discs and loaded into a custom-made thermogravimetric infrared cell with a CI Precision MK2-M5 LM 2-01 microbalance and a Bruker Vertex 70 FTIR spectrometer. The catalyst discs were heated to 215 °C in nitrogen (10 mL min^{-1}) for 2 h to dehydrate the sample before being cooled to an initial adsorption temperature of 100°C where a spectrum was collected. Pyridine was then introduced to the samples by the flow of nitrogen gas over a schlenk flask containing pyridine. Sample temperature was then raised to 128 ^oC. Spectra and the total mass due to pyridine adsorption were recorded at both temperatures which then permits absorption coefficients for bands due to two independent modes of vibration for Lewis and Brønsted bound pyridine to be determined. The values of the absorption coefficients then permits the individual numbers of Brønsted and Lewis acid sites to be determined (24). Although signal to noise ratio in some samples was lower than ideal, determination of molar absorption coefficients using the above methodology permitted a cross-check that these were consistent with published values (24) and thus a degree of confidence in the values obtained for the densities of the Brønsted and Lewis acid sites was afforded.

4.2.3. TPD experiments

Before the start of each TPD experimental series, the catalysts were pre-heated at 15 °C min^{-1} under vacuum conditions up until 450 °C and held for 30 min before subsequently cooled down at 25 °C min^{-1} to room temperature. TPD experiments were carried out firstly by pre-adsorbing the pre-treated catalyst with a continuous flow of 5 vol% methanol or 5 vol% DME in Ar until saturation. Thereafter, weakly adsorbed species were removed from the surface by argon flowing at ca. 10^{-7} mol s^{-1}. Thereafter, the catalyst was subjected to a linear temperature ramp at three different heating rates of (β = 5, 15 or 30 °C min^{-1}) until a final set

point of 450 °C. The released gas was analysed using a quadrupole mass spectrometer (QMS) operating in a multiple ion detector (MID) mode. The low base pressure (10^{-7} Pa) in the analysis chamber allowed for high detection sensitivity necessary for quantitative analysis. The effect of initial coverage of DME (or methanol) was studied separately on ZSM-5 (36) at a heating rate of 15°C min^{-1}. The initial coverages were obtained by an integration of desorption profile.

4.2.4. Steady state experiments

The ZSM-5 catalyst was calcined in a 20 mL min^{-1} flow of 30 vol.% O_2/N_2 in a fixed bed reactor at 450°C and held for 30 min before cooling down at 25°C min^{-1} to 370 °C. Afterwards, the catalyst was subjected to a flow of 1.3 vol% methanol in nitrogen at 10 mL min^{-1} for 2 h to generate the hydrocarbon pool species in the zeolite micropores. The off-gas was analysed with an online gas chromatograph (Shimadzu GC-2010) equipped with an Equity-1 column (90m × 0.53mm × 3.0µm) and a flame ionization detector followed by a quadrupole mass spectrometer. The samples with the hydrocarbon species occluded in the zeolite pores will be referred to as “active samples” hereafter.

4.2.5. Desorption profile model

Two approaches were used to simulate TPD profiles: (i) the Redhead method (25) and (ii) the detailed elementary step model. The desorption profile was firstly deconvoluted and analysed using the Redhead method. Originally developed for the desorption of species over metal surfaces, the Redhead method gives a quick indication of the nature of the active sites as well as the maximum temperatures of desorption, number of binding sites and number of molecules adsorbed onto each binding site. However, there are a few limitations as discussed in section 4.3.2.3 below.

To overcome these limitations, the detailed elementary step model was also used as described in section 4.3.2.5 using data obtained from the Redhead method as initial guess values for estimation of desorption parameters. The model was implemented with a FORTRAN code and used to extract desorption parameters (site densities, frequency factors and activation energies) over the ZSM-5 catalysts. The code uses a PDASAC routine to solve the stiff, nonlinear initial-boundary-value problem obtained from the desorption profiles (26). A similar method has been used by Rebrov and co-workers (27, 28).

4.3. Results

4.3.1. Characterisation

Catalytic active sites can be present inside the zeolite micropores, the pore mouth, and onto the external surface of the crystals (29). Characteristic SEM images of three zeolite samples with Si/Al ratio of 25, 36 and 135 are shown in Figure 4.1 with the mean crystal size presented in Table 4.1.

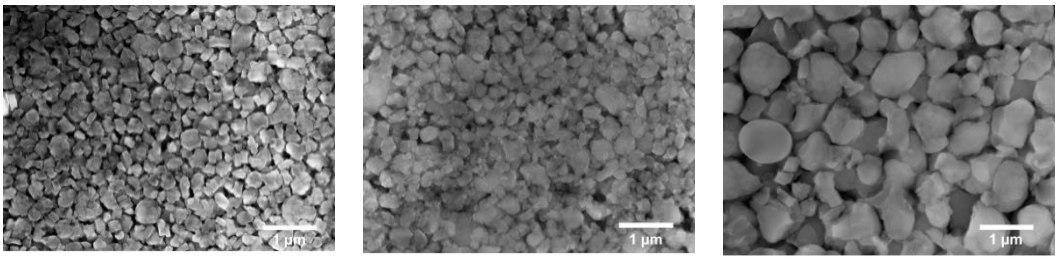

(a) ZSM-5 (25) **(b) ZSM-5 (36)** **(c) ZSM-5 (135)**

Fig. 4.1: FE-SEM of (a) ZSM-5 (25), (b) ZSM-5 (36) and (c) ZSM-5 (135) catalysts

The XRD patterns of the three ZSM-5 samples and a reference ZSM-5 patterns are shown in Figure 4.2. All three samples are highly crystalline zeolites with the MFI structure. The higher intensity of the XRD pattern of ZSM-5 (135) compared to the ZSM-5 (25) and ZSM-5 (36) shows its higher crystallinity. The lower intensities of ZSM-5 (25) and ZSM-5 (36) are probably due to their small crystal sizes which lead to a higher proportion of framework and structure defects. In Figure 4.2, relative intensities have been plotted to show the similar zeolite characteristics.

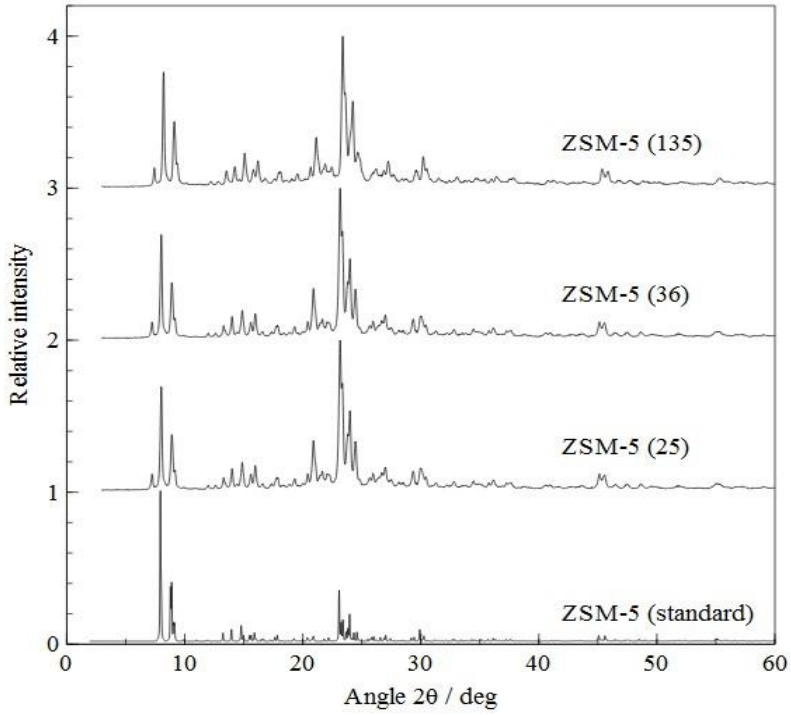

Fig. 4.2: XRD patterns of the ZSM-5 samples and a reference highly crystalline ZSM-5 sample (standard) obtained from the database of the International Zeolite Association (30).

ZSM-5 (25, 36 and 135) catalysts show a distribution of micropores and mesopores (see section 4B for isotherms). The BET surface areas and the micropore volumes of the ZSM-5 samples are given in Table 4.1.

Table 4.1: Physical properties and acidity of H-ZSM-5 catalysts

Sample	BET surface area ($m^2 g^{-1}$)	HK Pore volume* ($cm^3 g^{-1}$)	Crystal size (SEM, µm)	Nominal acidity (µmol g^{-1})	Total acidity$^+$ (µmol g^{-1})	Amount of Lewis acid sites (µmol g^{-1})	Amount of Brønsted acid sites (µmol g^{-1})
ZSM-5 (25)	413	0.154	0.10 ± 0.02	610	496	140	356
ZSM-5 (36)	410	0.147	0.33 ± 0.05	429	197	80	117
ZSM-5 (135)	358	0.141	0.78 ± 0.07	116	108	30	78

***** HK = Horvath-Kawazoe micropore volume

\+ = Total acidity based on pyridine adsorption at 100°C

The IR spectra of pyridine adsorbed on the H-form of ZSM-5 (25), ZSM-5 (36) and ZSM-5 (135) show features due to pyridinium ions formed via the protonation of pyridine on Brønsted acid sites as well as molecular pyridine on strong Lewis acid sites (Figure. 4.3). The most evident band distinguishing molecular pyridine on strong Lewis acid sites is at 1450 cm^{-1} similar to alumina and silica-alumina (31, 32) while pyridinium ions give rise to the characteristic band at 1545 cm^{-1} with both forms of adsorption contributing to the intensity at

1490 cm^{-1} (33). In addition to this qualitative assessment, coupling to a gravimetric balance permitted the total acidity to be assessed (Table 1) along with the individual contributions due to adsorption on the different acid sites when coupling balance and FTIR data. Total acidity follows the trend ZSM-5 (25) > (36) > (135) which is consistent with the trend for nominal acidity. The major contribution to base adsorption in all cases was due to uptake by Brønsted acid sites (Table 1) with the relative percentages of this mode of adsorption being 72, 59 and 72% for ZSM-5 (25), (36) and (135), respectively. At 128°C, the relative percentages are 88, 77% for ZSM-5 (25) and (36) respectively.

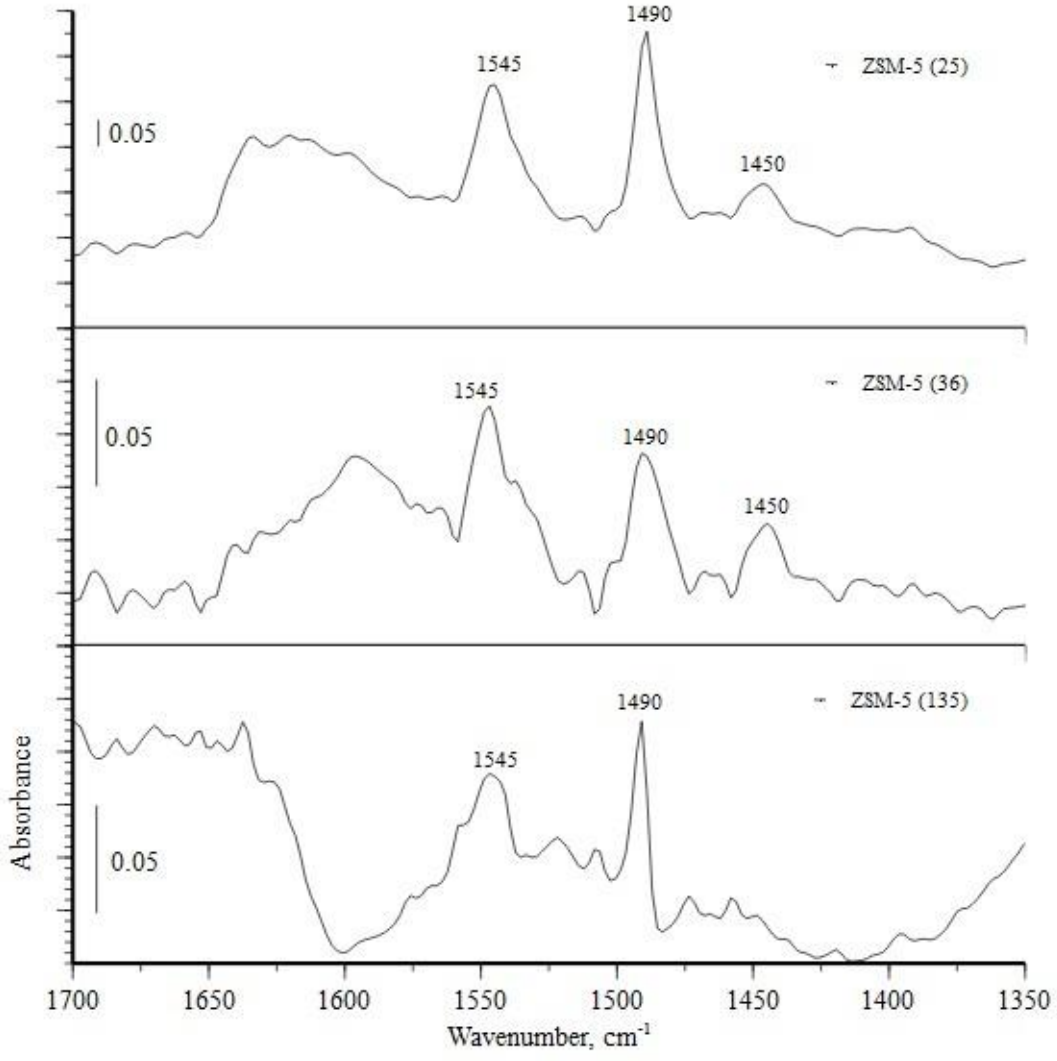

Fig. 4.3: FT-IR spectra of ZSM-5 (25), ZSM-5 (36) and ZSM-5 (135) zeolite samples (previously activated by outgassing at 450 °C), and then exposed to pyridine vapour at 100°C and subsequent outgassing at 128°C.

4.3.2. Methanol and DME TPD

4.3.2.1. Desorption

The rate of desorption, which describes the desorption profile in the absence of activated re-adsorption, is described by equation (4.1).

$$r_{des} = -\frac{d\theta}{dt} = k_d\theta^n = \theta^n A_d \exp(-E_d/RT) \qquad (4.1)$$

Where θ is the surface density of adsorbed molecules (mol m^{-3}), *n* is the order of desorption, *T* is the temperature (K), A_d is the pre-exponential factor (s^{-1}), E_d is the activation energy for desorption (J mol^{-1}). At a constant heating rate, β (K min^{-1}) = *dT/dt*, the rate of desorption can be rearranged as follows:

$$r_{des} = -\frac{d\theta}{dT} = \frac{\theta^n A_d}{\beta}\exp(-E_d/RT) \qquad (4.2)$$

Desorption profiles of methanol to DME over the ZSM-5 (25) catalyst are compared in Figure 4.4. Several features are observed. Firstly, the rate of desorption of methanol is higher than that of DME, demonstrating that a larger amount of methanol molecules occupies the sites and desorbs at any time. Secondly, the DME desorption profile shifts to the higher temperatures as compared to that of methanol. This suggests that DME adsorption is much stronger. Thirdly, there are several desorption sites as evidenced by the presence of shoulders in the desorption profiles. This is a common feature of all TPD profiles over fresh and activated ZSM-5 catalysts at full initial coverage.

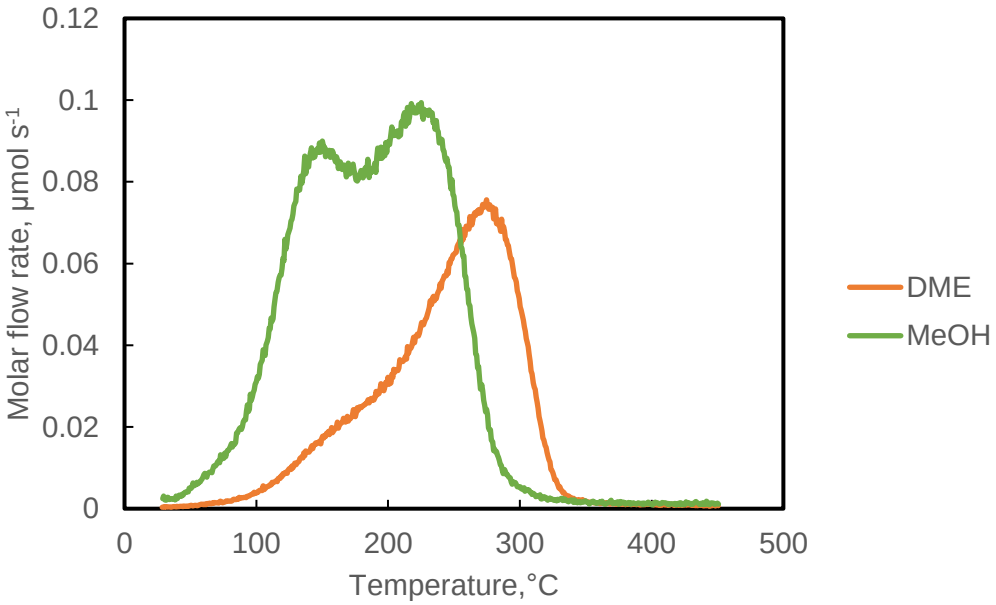

Fig. 4.4: Desorption profiles of methanol and DME over fresh ZSM-5 (25) at 15 °C min^{-1}

4.3.2.2. Effect of variation of initial coverage

The initial coverage of the pre-adsorbed oxygenates onto the fresh ZSM-5 (36) catalyst was varied by altering the adsorption duration. The initial coverage was obtained by integration of desorption curves and the total number of acid sites as determined from FTIR/microbalance data of pyridine adsorption at 128°C. It was observed that oxygenates are adsorbed onto different acid sites in the order of decreasing strength, with highest energy sites filling up first. Their desorption occurred in the reverse order with the lowest energy sites being emptied first. The integration of equation 4.2 at maximum temperature leads to a temperature independence of the peak position on initial coverage for a first order desorption process and a temperature dependence for a second order desorption process (34, 35). Our results suggest that methanol desorption follows a first order kinetics (Figure 4.5a) while DME desorption follows a second order kinetics (Figure 4.5b) as the position of the DME desorption peak decreases at higher initial coverages.

The discussion above does not consider the fact that the overall profile can be deconvoluted into different individual peaks and each desorption peak can have its own desorption kinetics. While the order of desorption kinetics may vary for each site, their contributions could still lead to the behaviour exhibited by the overall desorption profile. Also, it dismisses the effect of re-adsorption which results in peak broadening of the desorption profile. Under vacuum conditions in the TAP reactor, methanol has a maximum saturation coverage of 0.43 and DME has a maximum saturation coverage of 0.28. Increasing the dosing pressure has been shown to raise the saturation coverage of adsorbents in similar TPD studies (36). Finally, the lower temperature binding sites are only observed at high coverages.

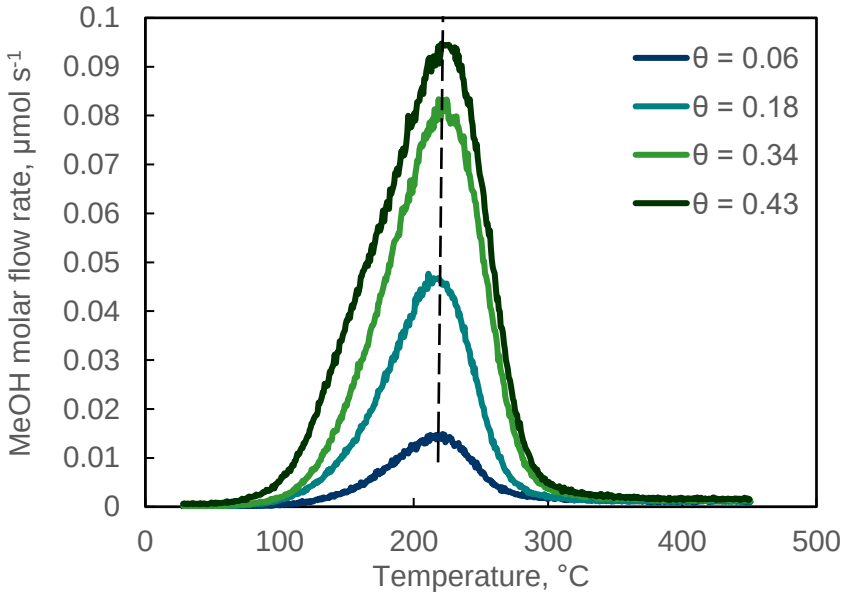

(a)

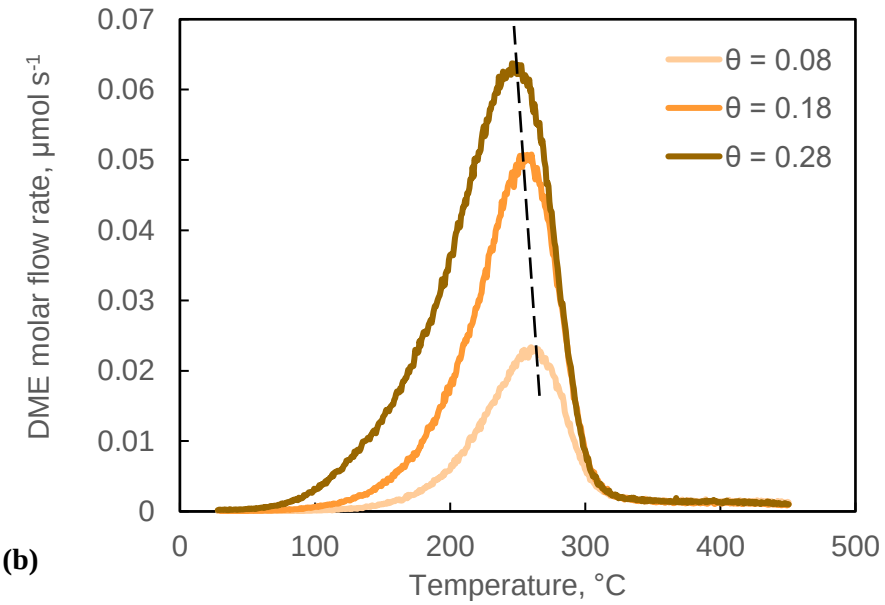

Fig. 4.5: The effect of initial coverage on (a) methanol and (b) DME desorption over fresh ZSM-5 (36) catalyst at a heating rate of 15 °C min^{-1}

4.3.2.3. Effect of heating rate

Redhead (25) proposed a method for desorption profile analysis based on the analysis of maximum temperatures. An assumption of the order of desorption must be made first. It is well established that the addition of acids to alcohols leads to the formation of a relatively stable oxonium salt which could decompose under suitable conditions (37, 38). The same can be observed for DME. Here, the products are methanol and methoxy groups (39). This behaviour supports dissociative (i.e. second order) adsorption. According to Redhead (25), second order desorption is characterised by a surface coverage which is half the initial surface coverage at maximum temperature. This is evidenced by fitting symmetrical Gaussian curves over the TPD profiles for each site. In this case, a plot of $(2\ln T_{p,\,max} - \ln \beta)$ vs $1/T_{p,\,max}$ gives the activation energies of desorption and the desorption rate constant in the absence of re-adsorption ($T_{p,\,max}$ is the temperature of maximum desorption at each site). In this method, across heating rates (5, 15 and 30 °C min^{-1}), the width as well as ratio of the areas across site were kept constant for each desorbing specie. Starting with an approximation of second order desorption where methanol dissociates on the active sites, three desorption sites were observed over ZSM-5 (25) and ZSM-5 (36) and two desorption sites over ZSM-5 (135) for both methanol and DME. The three desorption sites – sites 1, 2 and 3 – are here referred to as low temperature (LT), medium temperature (MT) and high temperature (HT) sites. A representative example of a DME desorption profile is presented in Figure 4.6.

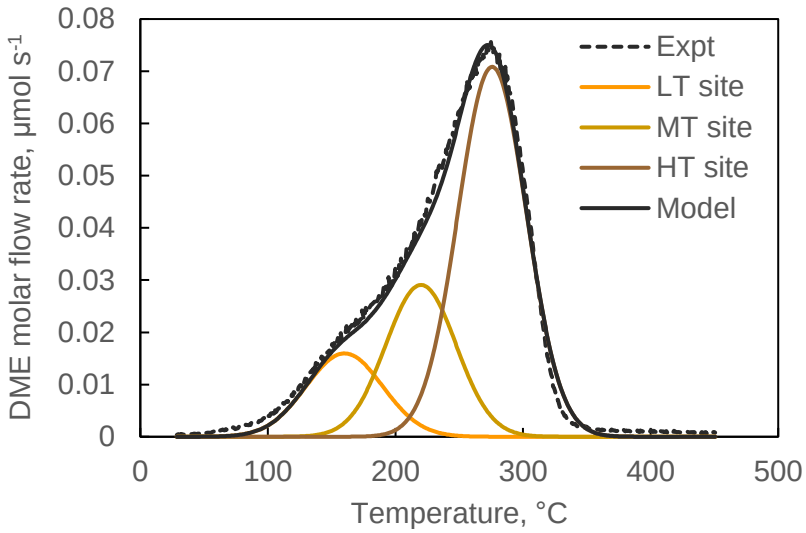

Fig. 4.6: Desorption profile of DME from a fresh ZSM-5 (25) catalyst at a heating rate of 15 °C min^{-1} with its fitting to 3 sites using the Redhead method.

In the absence of re-adsorption, Figure 4.7 gives the desorption activation energy obtained with the Redhead method. A common trend can be observed over all ZSM-5 catalysts studied: the activation energy of desorption of DME is greater than that of methanol over fresh ZSM-5 catalysts. For example, an activation energy of DME desorption of 42.0 kJ mol^{-1} is higher compared to 31.6 kJ mol^{-1} for methanol over ZSM-5 (36). Over activated ZSM-5 (36) and ZSM-5 (135) catalysts, the activation energy of desorption of DME is greater than that of methanol. However, over activated ZSM-5 (25), the activation energy of desorption of DME is less than that of methanol. For completion, other parameters (desorption frequency factors) for fresh and activated catalysts are given in S4.1 and S4.2 of the supplementary information respectively.

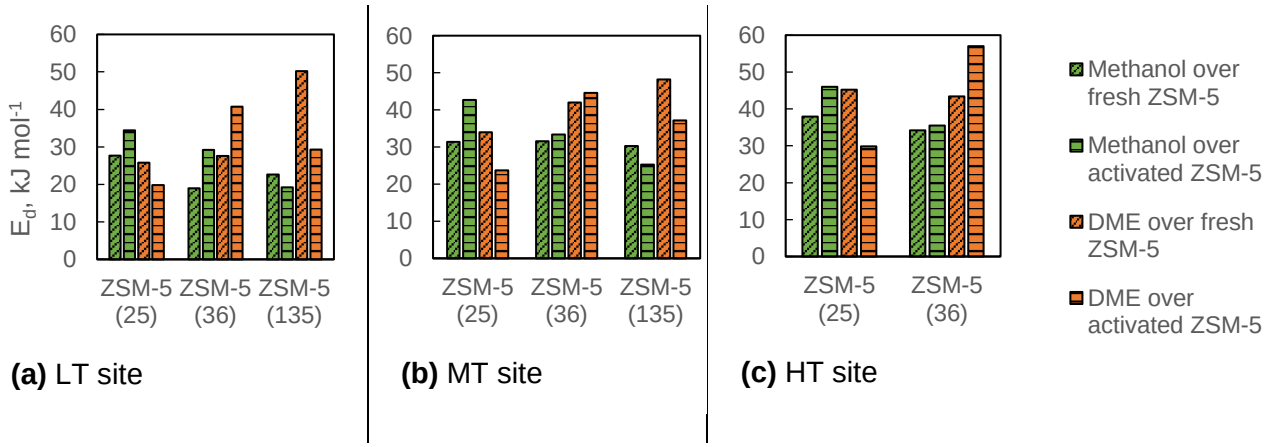

Fig. 4.7: A comparison of activation energy of desorption of methanol and DME over fresh and activated ZSM-5 catalysts over low (LT), medium (MT) and high (HT) temperature sites.

4.3.2.4. Amount of species adsorbed onto each site

Further analysis of the desorption profiles was carried out over the zeolite samples to obtain the amount of specie accessible to each site. The areas under each Gaussian curve give the amount of species adsorbed onto each site. Analysis was carried out on desorption profiles obtained at 15 °C min^{-1} as the ratio of each site was kept constant at all heating rates during data analysis. Thus, the results obtained are tenable at 5 °C min^{-1} and at 30 °C min^{-1}. The number of molecules per active sites was derived using nominal acidity (active sites/gram) obtained from Si/Al ratios. The total amounts of methanol and DME adsorbed on each site of the fresh ZSM-5 catalysts are given in Tables 4.2 and 4.3.

Table 4.2: Adsorption stoichiometry over different adsorption sites onto fresh ZSM-5 catalysts

Sample	**MEOH**			**DME**		
	Molecules/ active site – LT site	Molecules/ active site – MT site	Molecules/ active site – HT site	Molecules/ active site – LT site	Molecules/ active site – MT site	Molecules/ active site – HT site
ZSM-5 (25)	2.7	2.5	3.6	0.8	1.3	3.1
ZSM-5 (36)	3.4	2.8	6.1	0.9	1.3	2.5
ZSM-5 (135)	2.9	6.9	0	2.3	4.1	0

Table 4.2 shows that more methanol molecules were adsorbed on each adsorbed site than DME. A clustering effect has been mentioned previously to account for multiple molecules on the adsorption site (40).

Table 4.3: Adsorption stoichiometry over different adsorption sites onto active ZSM-5 catalysts

Sample	**MEOH**			**DME**		
	Molecules/ active site – LT site	Molecules/ active site –MT site	Molecules/ active site – HT site	Molecules/ active site – LT site	Molecules/ active site – MT site	Molecules/ active site – HT site
ZSM-5 (25)	2.8	2.3	3.9	0.6	1.8	2.3
ZSM-5 (36)	2.1	2.1	4.1	0.6	1.5	3.3
ZSM-5 (135)	7.9	11.8	0	2.3	3.3	0

Tables 4.2 and 4.3 show that a lower amount of DME species is adsorbed compared to methanol. Given the limited amount of deactivation (Figure 4.8) on the ZSM-5 catalysts after 2 h on stream, the number of molecules adsorbed per active site is indicative of the occupancy of non-deactivating species, possibly the adsorbed hydrocarbon pool, present in the porous

network of the zeolite. It can be readily observed that the amount of DME species adsorbed stays roughly constant over fresh and activated ZSM-5 catalysts. A similar behaviour exists for methanol adsorption over ZSM-5 (25) and ZSM-5 (36). However, a notable difference in adsorption amount is observed between fresh and activated ZSM-5 (135) catalysts.

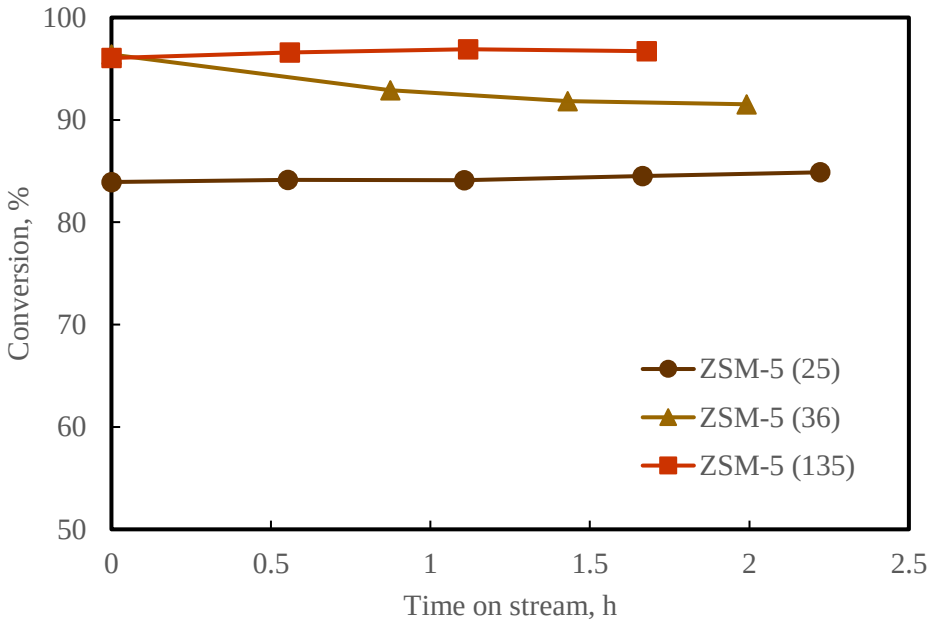

Fig. 4.8: Pre-activation of ZSM-5 samples at 370°C, 2 h time on stream (TOS), 10 mL min-1 of 1.3 vol% methanol in nitrogen. Pressure = 1 bar.

4.3.2.5. Effect of re-adsorption

A detailed elementary step model that accounts for re-adsorption and desorption was used to describe the desorption profiles. The following stoichiometry was used:

Site 1: $CH_3OH + * \rightleftharpoons CH_3OH*$ $\quad CH_3OCH_3 + * \rightleftharpoons CH_3OCH_3*$

Site 2: $CH_3OH + 2* \rightleftharpoons CH_3* + OH*$ $\quad CH_3OCH_3 + 2* \rightleftharpoons CH_3* + CH_3O*$

Site 3: $CH_3OH + 2* \rightleftharpoons CH_3* + OH*$ $\quad CH_3OCH_3 + 2* \rightleftharpoons CH_3* + CH_3O*$

where * denotes an adsorption site.

Using initial estimates from the Redhead method (25), the model allowed for three adsorption sites on ZSM-5 (25) and ZSM-5 (36) and two adsorption sites on ZSM-5 (135). The adsorption profiles on three sites over ZSM-5 (25) and ZSM-5 (36) were modelled using a plug flow reactor with coupled convection, adsorption and desorption steps (see S4.3 in supplementary information). The model was adjusted appropriately for ZSM-5 (135) where two desorption sites were observed. A comparison of 5 desorption models (Table 4.4) to experimental data was made. The comparison of these models was based on a sum of squares error (SSE):

$$\sum_{i}^{n}\left(Y_{expt} - Y_{model}\right)^2 \rightarrow min \qquad (4.3)$$

where Y_{expt} is the experimental desorption profile and Y_{model} is the simulated desorption profile. The best description (minimum SSE) allowed for a very good match between dissociative adsorption on MT and HT sites and molecular adsorption on the LT sites.

Table 4.4: A comparison of different models for methanol desorption over ZSM-5 (36) using sum of square error.

Model	LT (site 1)	MT (site 2)	HT (site 3)	SSE
A	Molecular adsorption	Molecular adsorption	Molecular adsorption	3.019
B	Dissociative adsorption	Dissociative adsorption	Dissociative adsorption	2.575
C	Molecular adsorption	Dissociative adsorption	Dissociative adsorption	0.016
D	Molecular adsorption	Molecular adsorption	Dissociative adsorption	3.018
	Single site			
E	Molecular adsorption			2.485

As shown in Figure 4.7, the Redhead model gives different values of activation energies of desorption for fresh and activated ZSM-5 catalysts. With the detailed elementary step model, such specificity between fresh and active catalyst was hardly seen albeit in the difference in site densities. However, major differences arise between methanol and DME desorption. A sample desorption profile is given at a heating rate of 30 °C min^{-1} (Figure 4.9). Activation energies of desorption obtained are presented in Figure 4.10. For completion, other parameters (adsorption and desorption frequency factors) for all catalysts studied are given in S4.4 of the supplementary information.

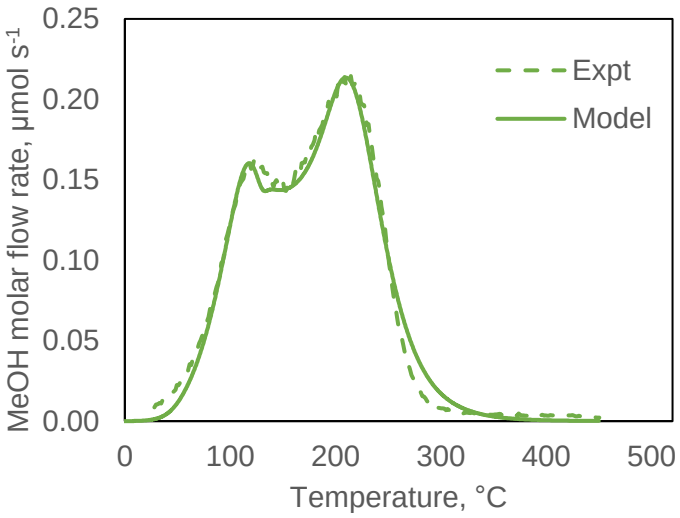

Fig. 4.9: Methanol desorption profile over fresh ZSM-5 (36) at 30 °C min^{-1}

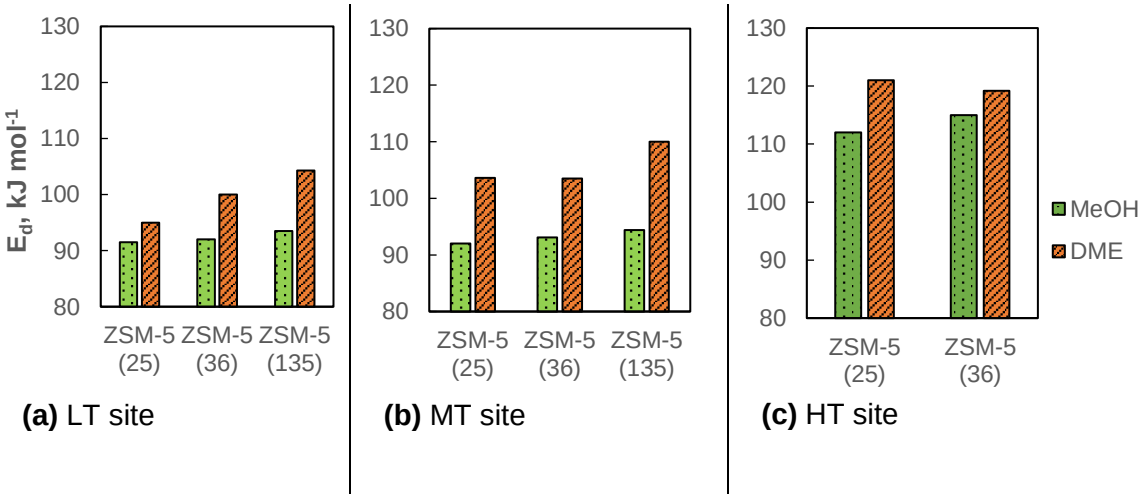

Fig. 4.10: Comparison of the activation energy of desorption of methanol and DME over ZSM-5 catalysts derived using the detailed elementary step model

As can be observed above, the activation energies of desorption are higher over ZSM-5 catalysts when re-adsorption is considered. In all cases, as observed with the Redhead method, the activation energies of desorption of DME over the various ZSM-5 catalysts are greater than that of methanol.

Given that the plug flow reactor model with coupled convection, adsorption and desorption steps involving molecular adsorption on LT sites and dissociative adsorption on MT and HT sites gives the best match to experimental data, the sensitivity coefficients of the rate constant of each elementary step were calculated. To assess the sensitivity coefficient, each rate constant was multiplied by perturbation factors of 5 or 0.2 while other rate constants were kept constant. The relative changes in desorption profiles were obtained with or without

the perturbation factor. Subsequently, the sensitivity coefficient was obtained as presented in equation 4.4 (41) :

$$K_s = \frac{\ln(Y_P/Y_O)}{\ln(F)} \tag{4.4}$$

where Y_p and Y_o are the rates with and without perturbation and F is the perturbation factor. Figure 4.11 shows the sensitivity coefficients of each parameter.

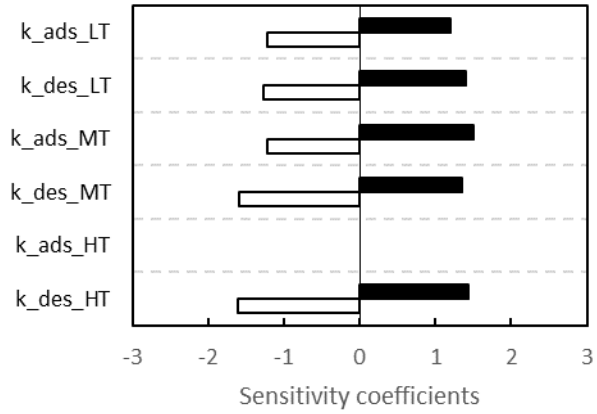

Fig. 4.11: Sensitivity coefficients for the desorption rates over fresh ZSM-5 (36) at a heating rate of 30 °C min^{-1}. k_ads_LT is the rate constant for adsorption over the low temperature site, k_des_LT is the rate constant for desorption over the low temperature

4.4. Discussion

4.4.1. Limiting factors

The TAP reactor developed by Gleaves and co-workers (42) is conventionally used for pulse response experiments due to its sub-millisecond time resolution. Here, it has been exploited for TPD experiments as its operation under vacuum is necessary to reduce the influence of re-adsorption.

Two methods have been used to quantify desorption: the Redhead model and the detailed elementary step model, both based on a fundamental Polanyi-Wigner desorption kinetics. The Redhead model only considers the kinetics of desorption, while the detailed elementary step model, based on species balance, also considers possible re-adsorption effects and fluid flow through the packed bed.

Mass transport effects accompanying desorption have been discussed in depth in the literature (43-45). As the pressures used were much lower than 1 mbar, external mass transfer to the particle is negligible due to low gas densities which allow for the absence of a stagnant film around the particle in the TAP reactor. They are suppressed due to negligible intramolecular collisions under vacuum conditions (23). Local temperature spikes are insignificant due to the very dilute oxygenate mixtures and the presence of fewer molecules

in comparison with the thermal mass of the bed. In the absence of reaction, the thin-zone configuration of the TAP reactor allows for decoupling of diffusion from desorption with or without re-adsorption and eliminates the concentration gradients along the bed (46). In the TPD profiles obtained, intra-particle diffusion does not limit the desorption/re-adsorption process according to the criteria given in refs. (43, 45, 47). See S4.5 in supplementary information.

The TAP reactor has high detection capabilities due to its low detection limit and offers for an unperturbed shape of the desorption profiles caused by a direct placement of the measuring probe and mass spectrometer into the detection chamber. It is well known that the desorption profile for strongly adsorbing molecules such as methanol can be significantly altered by the adsorption phenomena in the conventional mass spectrometer equipment which use an inlet capillary tube (48). The removal of extra-particle mass transfer and decrease in the contribution of re-adsorption phenomena under vacuum conditions in the TAP reactor shows its immense benefit.

The conventional TAP method of time evolution of short pulses was originally initiated to be used to decouple adsorption and desorption of oxygenates (methanol, DME) over ZSM-5 catalyst following the methodology of Nijhuis and co-workers (49). However, the lack of an outlet response of methanol following an inlet short pulse subjected our experimental methods to non-conventional methods in TAP of obtaining adsorption and desorption parameters under convective flow (see S4.6 in supplementary information). S4.6 shows full uptake of CH_3OH regardless of temperature during pulse experiments and partial uptake of DME with an increasing response with temperature.

A comparison of experimental data and the detailed elementary step model leads to the observation of intrinsic activation energies of desorption. The model considers convection, adsorption and desorption parameters. This means adsorption and desorption occur at a certain location in the reactor. However, this is not the case in zeolites as adsorption and desorption occur in the pore and the released substance can only move towards the free gas space once it leaves the pore. In essence, diffusion does not limit adsorption and desorption.

4.4.2. Comparing Redhead method to the detailed elementary step model

Over the MT and HT sites, both the Redhead method and the detailed elementary step model allow for dissociative adsorption (second order desorption). Over the LT sites, while the Redhead method allowed for dissociative desorption, molecular desorption was indicative on the LT sites with the detailed elementary step model (Figure 4.8). This disagreement between both methods was resolved by conducting TPD experiments at different initial coverages over the ZSM-5 (36) catalyst.

As mentioned previously, experiments conducted at different initial coverages showed that molecules fill up the sites in order of decreasing energies and desorb in order of increasing energies. At very high coverages, when low energy sites fill up, the temperatures at which maximum desorption occurs stay constant with the coverage over the LT site. Moreover, alternative models on the LT site assuming second order desorption gave a poor match between experiment and model. This provided further confidence in the detailed elementary step model showing that desorption is first order on the LT sites and second order on MT and HT sites. In the detailed elementary step model, re-adsorption leads to broadening on the LT and MT sites. This broadening effect gave an overlap between desorption temperatures in the LT and MT sites of ZSM-5 catalyst during methanol and DME desorption allowing for their direct comparison. In the TAP reactor, it has been shown that such re-adsorption can hardly be neglected over porous catalysts (42). The higher activation energies of desorption obtained using the detailed elementary step model is due to re-adsorption effects which the Redhead method failed to account for.

4.4.3. Comparing desorption of methanol to DME

Methanol readily desorbs from the catalyst before DME does. The higher activation energy of desorption can also be rationalised through proton-transfer chemisorption occurring through localized oxonium ion/framework anion pairs (Scheme 4.1). The binding energies of these oxonium ions are related to gas phase proton affinities of the adsorbing species (50). The adsorption of methanol leads to the formation of a methoxonium ($CH_3OH_2^+$) intermediate on Brønsted acid sites. On the other hand, the adsorption of DME leads to the formation of a dimethyloxonium ion (DMO^+) intermediate (39). The higher activation energies of desorption of DME compared to methanol over ZSM-5 catalysts suggests that DME has a higher proton affinity than methanol over Brønsted acid sites. Here, further dehydration of the oxonium ion intermediates formed to surface methoxy groups when heated in the TPD experiment occurs with equal propensity due to equal stability of the methoxy group formation with DME or methanol adsorption. Also, the probability for DME protonation is about 2 times higher than methanol suggesting higher tendencies towards larger activation energies of desorption for DME (51).

$CH_3OH + HZ \rightleftharpoons CH_3OH_2^+ + Z^-$	$CH_3OCH_3 + HZ \rightleftharpoons (CH_3)_2OH^+ + Z^-$
$CH_3OH_2^+ + Z^- \rightleftharpoons CH_3^+ + H_2O$	$(CH_3)_2OH^+ \rightleftharpoons CH_3^+ + CH_3OH$

Scheme 4.1: Oxygenate dehydration over H-ZSM-5 catalysts

Higher values of activation energies of desorption of DME than methanol are generally in accordance with previous studies (40, 52-55) but in contrast to values obtained by Pope (56) through calorimetric methods (Table 4.5).

Table 4.5: Heats of desorption of species from ZSM-5 catalysts obtained from literature

Sample	Si/Al ratio	Molecules/ unit cell	Molecules/active site	E_d (kJ mol^{-1})	Method	Source
Methanol	36	1 – 2.5 2.5 - 16	0.39 – 0.97 0.97 – 6.18	74 - 107 47 - 74	Calorimetric	(56)
Methanol	15	0 – 6 6 – 15	0 – 1 1 – 2.5	65 – 85 50 – 65	TPD	(53)
DME	36	1 – 2.5 2.5 – 10	0.39 – 0.97 0.97 – 3.86	20 - 94 20	Calorimetric	(56)

Both models show that a higher number of methanol molecules is adsorbed per active site compared to DME. Clusters of adsorbed methanol molecules have been proposed in the cages of zeolite catalysts (40, 55, 57, 58). Blaszkowski and van Santen(59) observed the end-on configuration where the hydroxyl groups of the methanol are directed towards the basic oxygen of the zeolite as a favourable geometry for methanol adsorption using density functional theory (DFT) calculations.

In summary, more methanol clusters are adsorbed on the zeolite catalyst than DME, although it takes lower temperatures to desorb them from the catalyst surface.

4.4.4. Effect of Si/Al ratio on the desorption kinetics in ZSM-5 catalysts

With the Redhead method, over fresh catalysts, DME has a higher activation energy of desorption than methanol. After catalyst activation during MTH conversion, DME still maintains a higher activation energy of desorption over ZSM-5 (36) and ZSM-5 (135). However, on the ZSM-5 (25) catalyst, DME has a lower activation energy of desorption compared to methanol. Firstly, it is important to state that the data obtained from ZSM-5 (25) should be treated cautiously as during TPD experiments of methanol, minor amounts of other species were desorbed suggesting a possible interaction between species.

The high acid site density of ZSM-5 (25) leads to a different product distribution (Figure 4.12) as compared to ZSM-5 (36) and ZSM-5 (135) catalysts. The product distribution is representative of the well-established hydrocarbon pool mechanism which is propagated to various proportions due to dissimilar acid densities of the various ZSM-5 catalysts. As shown in Figure 4.12, ZSM-5 (25) has a lower selectivity of lower olefins and a higher selectivity of aromatics showing a prevalence of the aromatic cycle after 2 h time on stream (TOS). The occupancy of sites with prevalent species from the aromatic cycle over ZSM-5 (25) would lead to a larger constraint on the mobility of DME than methanol. Site blockage due to a dominant aromatic cycle on ZSM-5 (25) means that larger molecules such as DME are easily removed

from the zeolite in comparison to methanol. The occupancy of sites with prevalent olefin species on ZSM-5 (36) and (135) leads to a lower constraint on the mobility of DME giving the expected behaviour as observed in Figure 4.7. These effects of site occupancy are pronounced when adspecies move on the surface of the catalyst. When re-adsorption is accounted for as with the plug flow model with coupled convection, adsorption and desorption steps, these effects are largely removed.

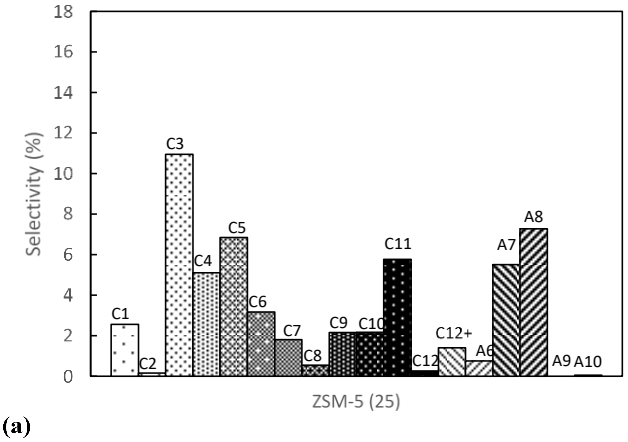

(a)

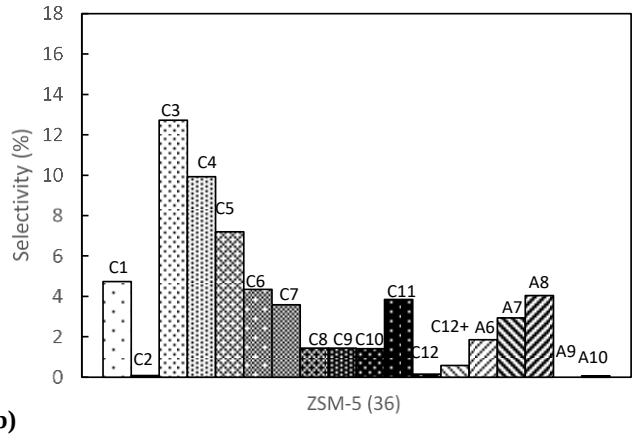

(b)

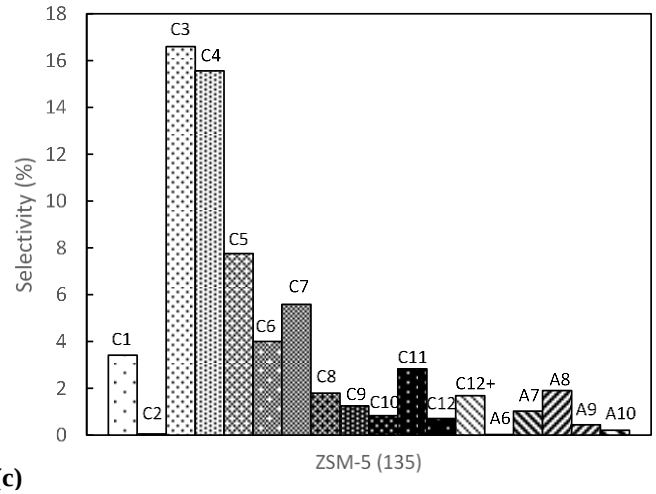

(c)

Fig. 4.12: Hydrocarbon pool distribution over (a) ZSM-5 (25), (b) ZSM-5 (36) and (c) ZSM-5 (135) catalysts at 370°C, 2 h TOS, 10 mL/min of 1.3 vol% methanol in nitrogen. Pressure = 1 bar. A6 = Benzene, A7 = Toluene, A8 = Xylene, A9 = TriMB, A10 = TetraMB

4.4.5. Nature of binding sites

The desorption behaviour of oxygenates and the zeolite's pore architecture should be considered in understanding the nature of the binding sites. Two desorption sites were observed with ZSM-5 (135) and three desorption sites over ZSM-5 (25) and (36). A combination of the detailed elementary step model and experimental data showed that molecular adsorption occurs on the LT site while dissociative adsorption occurs on the MT and HT sites. Furthermore, re-adsorption occurs on the LT and MT sites only (S4.4 in supplementary information). The pore architecture shows higher space constraints in the pore channels (0.53 nm × 0.56 nm and 0.51 nm × 0.55 nm) than at the pore intersections (0.9 nm).

The plug flow reactor model accounts for differences between the desorption profiles of methanol and DME due to any associated re-adsorption and convective effects. Methanol binds weakly to sites in comparison to DME as it has lower activation energy of desorption and hence lower adsorption enthalpy. However, re-adsorption is much faster with methanol (see S4.4 in supplementary information). This means that methanol can move in the pore system without much restriction, but it re-binds very easily such that the recurrent adsorption-desorption process finally becomes limiting to the motion of the molecule. The higher recurrent interaction (re-adsorption) of methanol with the active sites give rise to lower desorption energies compared to DME.

The presence of re-adsorption over the LT and MT sites suggests a local equilibrium with the gas phase at these sites. Since the LT site is first order, observed desorption pre-exponential factors lower than 10^{13} s^{-1} suggests that ,the activated complex, just above the binding site, has a lower degree of freedom compared to its adsorbed state (34). The limited

degree of freedom of the transition state in comparison to the adsorbed state is probably due to the clustering effect of oxygenates at each binding state which further hinders free movement. Dissociation which occurs in the zeolite pores allows for a higher partial molar entropy of the adsorbed oxygenate compared to the gas phase (60). As mentioned previously, gases desorb from site in order of increasing energies. As gases move from the HT sites to the LT sites, the surface concentration starts to increase leading to increasing probability of re-adsorption along the dimensions of the ZSM-5 zeolite.

Consideration of the adsorption stoichiometry (Table 4.2) shows that the MT and HT sites over ZSM-5 (25) and ZSM-5 (36) merge to give a MT site on ZSM-5 (135). In fact, the addition of the number of molecules/active site on MT and HT sites on ZSM-5 (25) and (36) gives the molecules/active site on MT sites on ZSM-5(135). This nullifies the conception that sites disappear over highly siliceous zeolites. TAP reactor data at low coverages show that over ZSM-5 (25), sites are relatively populated with active sites distributed within the zeolite. On increasing the Si/Al ratio, merging of the sites occurs, leading to isolated sites preferentially located on the straight channels of the ZSM-5 catalyst (61).

In addition, there is high convergence between the percentage of sites from MT and HT (69, 72 and 70% for ZSM-5 (25), (36) and (135) respectively) to Brønsted acid site density at 100 °C (See Table 1 and S4.7 in supplementary information). Thus, this simplified microkinetic model along with pyridine FTIR data would suggest the MT and HT sites to be of a Brønsted acid nature and the LT site to be of a Lewis acid nature. The agreement between the nature of the sites and their desorption behaviour solidifies this relationship. Accessibility to binding sites and site density using pyridine FT-IR data is different from oxygenate adsorption. This is due to the different molecular kinetic diameters, different temperatures of adsorption and different basicity. Clearly, the clustering effect on the ZSM-5 catalyst gives a far higher number of molecules adsorbed (as obtained from the detailed elementary step model) compared to the density of active sites obtained through pyridine FTIR.

4.5. Conclusions

The desorption of methanol and dimethyl ether (DME) has been studied over ZSM-5 catalysts with different Si/Al ratios. Three desorption sites were observed over ZSM-5 catalysts, while two of them cannot be distinguished in the sample with a Si/Al ratio of 135 and were observed as a single peak. Based on the shape of desorption peaks, it can be concluded that molecular adsorption takes place on the low temperature binding sites while dissociative adsorption occurs on the medium and high temperature binding sites. A comparison of pyridine FTIR data and microkinetic modelling suggests the medium and high temperatures sites are of Brønsted acid nature due to their dissociative nature. The low temperature sites correspond to a Lewis acid nature due to their molecular adsorption properties. For both

oxygenates, re-adsorption occurs on the low and medium temperature binding sites but does not occur on the high temperature binding sites. Overall, methanol desorbs easily in comparison to DME, showing that adsorbed DME is the primary oxygenate and key methylating agent in surface reactions during MTH conversion.

4.6. Notes

All data supporting this study is provided as supplementary information accompanying this paper.

4.7. References

1. Chang CD, Silvestri AJ. The conversion of methanol and other O-compounds to hydrocarbons over zeolite catalysts. Journal of Catalysis. 1977;47(2):249-59.
2. Weitkamp J. Zeolites and catalysis. Solid State Ionics. 2000;131(1–2):175-88.
3. Babu GP, Hegde SG, Kulkarni SB, Ratnasamy P. Active centres over HZSM5 zeolites. Journal of Catalysis. 1983;81(2):471-7.
4. Svelle S, Kolboe S, Swang O, Olsbye U. Methylation of Alkenes and Methylbenzenes by Dimethyl Ether or Methanol on Acidic Zeolites. The Journal of Physical Chemistry B. 2005;109(26):12874-8.
5. Haase F, Sauer J. Ab initio molecular dynamics simulation of methanol interacting with acidic zeolites of different framework structure. Microporous and Mesoporous Materials. 2000;35-36:379-85.
6. Štich I, Gale JD, Terakura K, Payne MC. Role of the zeolitic environment in catalytic activation of methanol. Journal of the American Chemical Society. 1999;121(14):3292-302.
7. Hytha M, Štich I, Gale JD, Terakura K, Payne MC. Thermodynamics of catalytic formation of dimethyl ether from methanol in acidic zeolites. Chemistry - A European Journal. 2001;7(12):2521-7.
8. Greatbanks SP, Hillier IH, Burton NA, Sherwood P. Adsorption of water and methanol on zeolite Brønsted acid sites: An ab initio, embedded cluster study including electron correlation. Journal of Chemical Physics. 1996;105(9):3770-6.
9. O'Malley AJ, Logsdail AJ, Sokol AA, Catlow CRA. Modelling metal centres, acid sites and reaction mechanisms in microporous catalysts. Faraday Discussions. 2016;188(0):235-55.
10. Blaszkowski SR, Van Santen RA. The mechanism of dimethyl ether formation from methanol catalyzed by zeolitic protons. Journal of the American Chemical Society. 1996;118(21):5152-3.
11. Blaszkowski SR, Van Santen RA. Theoretical study of C-C bond formation in the methanol-to- gasoline process. Journal of the American Chemical Society. 1997;119(21):5020-7.
12. Blaszkowski SR, Van Santen RA. Theoretical study of the mechanism of surface methoxy and dimethyl ether formation from methanol catalyzed by zeolitic protons. Journal of Physical Chemistry B. 1997;101(13):2292-305.
13. Wang W, Seiler M, Hunger M. Role of surface methoxy species in the conversion of methanol to dimethyl ether on acidic zeolites investigated by in situ stopped-flow MAS NMR spectroscopy. Journal of Physical Chemistry B. 2001;105(50):12553-8.
14. Bjørgen M, Joensen F, Lillerud KP, Olsbye U, Svelle S. The mechanisms of ethene and propene formation from methanol over high silica H-ZSM-5 and H-beta. Catalysis Today. 2009;142(1-2):90-7.

15. Bjørgen M, Svelle S, Joensen F, Nerlov J, Kolboe S, Bonino F, Palumbo L, Bordiga S, Olsbye U. Conversion of methanol to hydrocarbons over zeolite H-ZSM-5: On the origin of the olefinic species. Journal of Catalysis. 2007;249(2):195-207.
16. Liang J, Li H, Zhao S, Guo W, Wang R, Ying M. Characteristics and performance of SAPO-34 catalyst for methanol-to-olefin conversion. Applied Catalysis. 1990;64:31-40.
17. Vora BV, Marker TL, Barger PT, Nilsen HR, Kvisle S, Fuglerud T. Economic route for natural gas conversion to ethylene and propylene. In: Pontes Md, Espinoza RL, Nicolaides CP, Scholtz JH, Scurrell MS, editors. Studies in Surface Science and Catalysis. Volume 107: Elsevier; 1997. p. 87-98.
18. Koempel H, Liebner W. Lurgi's Methanol To Propylene (MTP®) Report on a successful commercialisation. Studies in Surface Science and Catalysis2007. p. 261-7.
19. Chang CD, Lang WH, Smith RL. The conversion of methanol and other O-compounds to hydrocarbons over zeolite catalysts. II. Pressure effects. Journal of Catalysis. 1979;56(2):169-73.
20. Ilias S, Bhan A. Mechanism of the catalytic conversion of methanol to hydrocarbons. ACS Catalysis. 2013;3:18-31.
21. Chang CD. A kinetic model for methanol conversion to hydrocarbons. Chemical Engineering Science. 1980;35(3):619-22.
22. Chen NY, Reagan WJ. Evidence of autocatalysis in methanol to hydrocarbon reactions over zeolite catalysts. Journal of Catalysis. 1979;59(1):123-9.
23. Van Veen AC, Zanthoff HW, Hinrichsen O, Muhler M. Fixed-bed microreactor for transient kinetic experiments with strongly adsorbing gases under high vacuum conditions. Journal of Vacuum Science and Technology, Part A: Vacuum, Surfaces and Films. 2001;19(2):651-5.
24. McCue AJ, Mutch GA, McNab AI, Campbell S, Anderson JA. Quantitative determination of surface species and adsorption sites using Infrared spectroscopy. Catalysis Today. 2016;259:19-26.
25. Redhead PA. Thermal desorption of gases. Vacuum. 1962;12(4):203-11.
26. Caracotsios M, Stewart WE. Sensitivity analysis of initial-boundary-value problems with mixed pdes and algebraic equations. Computers & Chemical Engineering. 1995;19(9):1019-30.
27. Rebrov EV, Simakov AV, Sazonova NN, Rogov VA, Barannik GB. Propane and oxygen action on NOx adspecies on low-exchanged Cu-ZSM-5. Catalysis Letters. 1998;51(3-4):27-40.
28. Rebrov EV, Simakov AV, Sazonova NN, Stoyanov ES. Dinitrogen formation over low-exchanged Cu-ZSM-5 in the selective reduction of NO by propane. Catalysis Letters. 1999;58(2-3):107-18.
29. Busca G. The surface acidity of solid oxides and its characterization by IR spectroscopic methods. An attempt at systematization. Physical Chemistry Chemical Physics. 1999;1(5):723-36.
30. Baerlocher C, McCusker LB. Database of Zeolite Structures http://www.iza-structure.org/databases/
31. Phung TK, Lagazzo A, Rivero Crespo MÁ, Sánchez Escribano V, Busca G. A study of commercial transition aluminas and of their catalytic activity in the dehydration of ethanol. Journal of Catalysis. 2014;311:102-13.
32. Kassab E, Castellà-Ventura M. Theoretical study of pyridine and 4,4′-bipyridine adsorption on the Lewis acid sites of alumina surfaces based on ab initio and density functional cluster calculations. Journal of Physical Chemistry B. 2005;109(28):13716-28.
33. Castellà-Ventura M, Akacem Y, Kassab E. Vibrational analysis of pyridine adsorption on the brønsted acid sites of zeolites based on density functional cluster calculations. Journal of Physical Chemistry C. 2008;112(48):19045-54.
34. Madix RJ, editor The Kinetics of Elementary Reactions on Crystal Surfaces. AIP Conference, The Physics of Surfaces: Aspects of the Kinetics and Dynamics of Surface Reactions 1979; La Jolla Institute.

35. Boudart M, Djega-Mariadassou G. Kinetics of heterogeneous catalytic reactions Princeton: Princeton University Press; 1984.
36. Genger T, Hinrichsen O, Muhler M. The temperature-programmed desorption of hydrogen from copper surfaces. Catalysis Letters. 1999;59(2-4):137-41.
37. Pines H. Acid-Catalyzed Reactions The Chemistry of Catalytic Hydrocarbon Conversions. United Kingdom: Academic Press; 1981.
38. Gates BC. Catalytic Chemistry John Wiley 1991.
39. Park TY, Froment GF. Kinetic modeling of the methanol to olefins process. 1. Model formulation. Industrial and Engineering Chemistry Research. 2001;40(20):4172-86.
40. Mirth G, Lercher JA, Anderson MW, Klinowski J. Adsorption complexes of methanol on zeolite ZSM-5. Journal of the Chemical Society, Faraday Transactions. 1990;86(17):3039-44.
41. Caracotsios M, Stewart WE. Sensitivity analysis of initial value problems with mixed odes and algebraic equations. Computers and Chemical Engineering. 1985;9(4):359-65.
42. Gleaves JT, Ebner JR, Kuechler TC. Temporal Analysis of Products (TAP) — A Unique Catalyst Evaluation System with Submillisecond Time Resolution. Catalysis Reviews. 1988;30(1):49-116.
43. Demmin RA, Gorte RJ. Design parameters for temperature-programmed desorption from a packed bed. Journal of Catalysis. 1984;90(1):32-9.
44. Tronconi E, Forzatti P. Modelling and experimental verification of TPD from porous catalysts. Chemical Engineering Science. 1986;41(10):2541-5.
45. Rieck JS, Bell AT. Influence of adsorption and mass transfer effects on temperature-programmed desorption from porous catalysts. Journal of Catalysis. 1984;85(1):143-53.
46. Shekhtman SO, Yablonsky GS, Chen S, Gleaves JT. Thin-zone TAP-reactor - theory and application. Chemical Engineering Science. 1999;54(20):4371-8.
47. Gorte RJ. Design parameters for temperature programmed desorption from porous catalysts. Journal of Catalysis. 1982;75(1):164-74.
48. Kanervo JM, Kouva S, Kanervo KJ, Kolvenbach R, Jentys A, Lercher JA. Prerequisites for kinetic modeling of TPD data of porous catalysts-Exemplified by toluene/H-ZSM-5 system. Chemical Engineering Science. 2015;137:807-15.
49. Nijhuis TA, Van Den Broeke LJP, Linders MJG, Van De Graaf JM, Kapteijn F, Makkee M, Moulijn JA. Measurement and modeling of the transient adsorption, desorption and diffusion processes in microporous materials. Chemical Engineering Science. 1999;54(20):4423-36.
50. Aronson MT, Gorte RJ, Farneth WE. The influence of oxonium ion and carbenium ion stabilities on the Alcohol/H-ZSM-5 interaction. Journal of Catalysis. 1986;98(2):434-43.
51. Martinez-Espin JS, De Wispelaere K, Westgård Erichsen M, Svelle S, Janssens TVW, Van Speybroeck V, Beato P, Olsbye U. Benzene co-reaction with methanol and dimethyl ether over zeolite and zeotype catalysts: Evidence of parallel reaction paths to toluene and diphenylmethane. Journal of Catalysis. 2017;349:136-48.
52. Zecchina A, Bordiga S, Spoto G, Scarano D, Spanò G, Geobaldo F. IR spectroscopy of neutral and ionic hydrogen-bonded complexes formed upon interaction of CH3OH, C2H5OH, (CH3)2O, (C2H5)2O and C4H8O with H-Y, H-ZSM-5 and H-mordenite: Comparison with analogous adducts formed on the H-Nafion superacidic membrane. Journal of the Chemical Society - Faraday Transactions. 1996(23):4863-75.
53. Hunger B, Matysik S, Heuchel M, Einicke WD. Adsorption of methanol on ZSM-5 zeolites. Langmuir. 1997;13(23):6249-54.
54. Fujino T, Kashitani M, Kondo JN, Domen K, Hirose C, Ishida M, Goto F, Wakabayashi F. T-IR and quantum chemical studies of the interaction between dimethyl ether and IZSM-5 zeolite. Journal of Physical Chemistry. 1996;100(28):11649-53.
55. Lee CC, Gorte RJ, Farneth WE. Calorimetric study of alcohol and nitrile adsorption complexes in H-ZSM-5. Journal of Physical Chemistry B. 1997;101(19):3811-7.

56. Pope CG. Adsorption of methanol and related molecules on zeolite H-ZSM-5 and silicalite. Journal of the Chemical Society, Faraday Transactions. 1993;89(7):1139-41.
57. Shah R, Gale JD, Payne MC. Methanol adsorption in zeolites - A first-principles study. Journal of Physical Chemistry. 1996;100(28):11688-97.
58. Sinclair PE, Catlow CRA. Computational studies of the reaction of methanol at aluminosilicate Brønsted acid sites. Journal of the Chemical Society - Faraday Transactions. 1996;92(12):2099-105.
59. Blaszkowski SR, Van Santen RA. Density functional theory calculations of the activation of methanol by a Brønsted zeolitic proton. Journal of Physical Chemistry. 1995;99(30):11728-38.
60. Riekert L. Sorption, Diffusion, and Catalytic Reaction in Zeolites. Advances in Catalysis. 1970;21:281-322.
61. Titiloye JO, Parker SC, Stone FS, Catlow CRA. Simulation studies of the structure and energetics of sorbed molecules in high-silica zeolites. 1. Hydrocarbons. Journal of Physical Chemistry. 1991;95(10):4038-44.

S4. Supplementary Information

Mechanistic insights into the desorption of methanol and dimethyl ether over ZSM-5 catalysts

S4.1: Kinetic parameters of the LT, MT, and HT sites on fresh ZSM-5 (25), (36) and (135) with the Redhead method

Methanol on LT site				DME on LT site			
	A_des (s^{-1})		E_des (kJ/mol)	A_des (s^{-1})		E_des (kJ/mol)
ZSM-5 (25)	2.46	× 10^7	27.7	6.40	× 10^7	25.8
ZSM-5 (36)	2.33	× 10^8	19.0	4.38	× 10^7	27.6
ZSM-5 (135)	6.80	× 10^7	22.6	2.67	× 10^5	50.2

Methanol on MT site				DME on MT site			
	A_des (s^{-1})		E_des (kJ/mol)	A_des (s^{-1})		E_des (kJ/mol)
ZSM-5 (25)	2.85	× 10^7	31.4	3.69	× 10^7	34.0
ZSM-5 (36)	2.68	× 10^8	31.6	5.65	× 10^7	42.0
ZSM-5 (135)	4.81	× 10^7	30.3	2.50	× 10^5	48.2

Methanol on HT site				DME on HT site			
	A_des (s^{-1})		E_des (kJ/mol)	A_des (s^{-1})		E_des (kJ/mol)
ZSM-5 (25)	1.91	× 10^7	37.9	1.15	× 10^7	45.2
ZSM-5 (36)	4.51	× 10^7	34.2	1.17	× 10^7	43.4
ZSM-5 (135)						

S4.2: Kinetic parameters of the LT, MT, and HT sites on activated ZSM-5 (25), (36) and (135) with the Redhead method

Methanol on LT site			DME on LT site	
	A_des (s^{-1})	E_des (kJ/mol)	A_des (s^{-1})	E_des (kJ/mol)
ZSM-5 (25)	3.35×10^6	34.4	1.65×10^8	19.8
ZSM-5 (36)	1.64×10^7	29.2	1.15×10^6	40.7
ZSM-5 (135)	1.81×10^8	19.2	6.87×10^7	29.3

Methanol on MT site			DME on MT site	
	A_des (s^{-1})	E_des (kJ/mol)	A_des (s^{-1})	E_des (kJ/mol)
ZSM-5 (25)	1.32×10^6	42.7	2.42×10^8	23.7
ZSM-5 (36)	1.77×10^7	33.4	2.33×10^6	44.6
ZSM-5 (135)	1.83×10^8	25.3	3.71×10^7	37.2

Methanol on HT site			DME on HT site	
	A_des (s^{-1})	E_des (kJ/mol)	A_des (s^{-1})	E_des (kJ/mol)
ZSM-5 (25)	2.27×10^6	46.0	1.74×10^8	29.9
ZSM-5 (36)	3.25×10^7	35.5	5.95×10^5	57.0
ZSM-5 (135)				

S4.3: Plug flow model with coupled convection and adsorption and desorption steps

$$\frac{\partial n_i}{\partial t} = -u\frac{\partial n_i}{\partial z} - \eta_1 . A_b . u . \left(A_{ads,1} . exp\left(\frac{-E_{ads,1}}{RT}\right) . P_i . (1-\theta_1) - A_{des,1} . \exp\left(\frac{-E_{des,1}}{RT}\right) . \theta_1\right)$$
$$- \eta_2 . A_b . u . \left(A_{ads,2} . exp\left(\frac{-E_{ads,2}}{RT}\right) . P_i . (1-\theta_2) . (1-\theta_2) - A_{des,2} . \exp\left(\frac{-E_{des,2}}{RT}\right) . \theta_2 . \theta_2\right)$$
$$- \eta_3 . A_b . u . \left(A_{ads,3} . exp . \left(\frac{-E_{ads,3}}{RT}\right) . P_i . (1-\theta_3) . (1-\theta_3)\right.$$
$$\left. - A_{des,3} . exp\left(\frac{-E_{des,3}}{RT}\right) . \theta_3 . \theta_3\right) \qquad (S4.3.1)$$

$$\frac{\partial \theta_1}{\partial t} = A_{ads,1} . exp\left(\frac{-E_{ads,1}}{RT}\right) . P_i . (1-\theta_1) - A_{des,1} . exp\left(\frac{-E_{des,1}}{RT}\right) . \theta_1 \qquad (S4.3.2)$$

$$\frac{\partial \theta_2}{\partial t} = A_{ads,2} . exp\left(\frac{-E_{ads,2}}{RT}\right) . P_i . (1-\theta_2) . (1-\theta_2) - A_{des,2} . exp\left(\frac{-E_{des,2}}{RT}\right) . \theta_2 . \theta_2 \qquad (S4.3.3)$$

$$\frac{\partial \theta_3}{\partial t} = A_{ads,3} . exp\left(\frac{-E_{ads,3}}{RT}\right) . P_i . (1-\theta_3) . (1-\theta_3) - A_{des,3} . exp\left(\frac{-E_{des,3}}{RT}\right) . \theta_3 . \theta_3 \qquad (S4.3.4)$$

where p_i is the partial pressure of specie i (Pa), t is the desorption time (s), z is the axial length of the bed (m), u is the velocity (m s^{-1}), η_i is the site density (mol m^{-3}), A_b is the area of bed (m^2), θ_i is the coverage of specie i, R is the molar gas constant (J mol^{-1} K^{-1}), T is the temperature (K), A_{ads} is the adsorption frequency factor (Pa^{-1} s^{-1}).

S4.4: Kinetic parameters of the LT, MT, and HT sites on ZSM-5 (25), (36) and (135) with the plug flow model with coupled convection and adsorption and desorption steps

	Methanol on LT site				DME on LT site			
	A_ads $(Pa.s)^{-1}$	E_ads (kJ/mol)	A_des (s^{-1})	E_des (kJ/mol)	A_ads $(Pa.s)^{-1}$	E_ads (kJ/mol)	A_des (s^{-1})	E_des (kJ/mol)
ZSM-5 (25)	6.9×10^{-2}	0	9.0×10^{11}	91.5	2.51×10^{-1}	0	6.0×10^{11}	95.0
ZSM-5 (36)	6.9×10^{-2}	0	9.0×10^{11}	92.0	8.9×10^{-2}	0	5.0×10^{11}	100.0
ZSM-5 (135)	1.35×10^{-1}	0	9.0×10^{11}	93.5	4.00×10^{-1}	0	5.0×10^{11}	104.3

	Methanol on MT site				DME on MT site			
	A_ads $(Pa.s)^{-1}$	E_ads (kJ/mol)	A_des (s^{-1})	E_des (kJ/mol)	A_ads $(Pa.s)^{-1}$	E_ads (kJ/mol)	A_des (s^{-1})	E_des (kJ/mol)
ZSM-5 (25)	2.8×10^{-2}	0	1.5×10^{10}	92.0	2.5×10^{-2}	0	1.4×10^{10}	103.6
ZSM-5 (36)	3.0×10^{-2}	0	1.5×10^{10}	93.1	1.8×10^{-2}	0	1.4×10^{10}	103.5
ZSM-5 (135)	4.95×10^{-2}	0	9.3×10^{9}	94.4	2.0×10^{-4}	0	1.4×10^{10}	110.0

	Methanol on HT site				DME on HT site			
	A_ads $(Pa.s)^{-1}$	E_ads (kJ/mol)	A_des (s^{-1})	E_des (kJ/mol)	A_ads $(Pa.s)^{-1}$	E_ads (kJ/mol)	A_des (s^{-1})	E_des (kJ/mol)
ZSM-5 (25)	0	0	1.8×10^{11}	112.0	0	0	7.5×10^{10}	121.0
ZSM-5 (36)	0	0	1.8×10^{11}	115.0	0	0	8.0×10^{10}	119.2
ZSM-5 (135)	0	0	0	0	0	0	0	0

S4.5: Parameter values used to compute particle concentration gradients

Parameter	**Values**
Pore diameter (d_{pore})	5.5×10^{-10} m
Particle density (ρ_P)	1.1 g cm^{-3}
Temperature (T)	723 K
Molar gas constant (R)	8.314 J mol^{-1} K^{-1}
Catalyst Mass (W)	0.01 g
Particle porosity (ϵ_p)	0.5
Molar flowrate	10^{-7} mol s^{-1}
Volumetric flowrate (Q)	1.20×10^{-1} cm^3 s^{-1}
Particle Radius (r)	0.0015 cm
Knudsen diffusion coefficient, D_{kn} (methanol)	0.00228 cm^2 s^{-1}
Particle concentration gradient (methanol)	0.00435
Knudsen diffusion coefficient, D_{kn} (DME)	0.00226 cm^2 s^{-1}
Particle concentration gradient (DME)	0.00439

Particle concentration gradients were obtained from (1):

$$\frac{Q\rho_P r^2}{3WD_K} < 0.05 \qquad (S4.5.1)$$

Diffusion in zeolites takes place in the Knudsen diffusion regime or in the configurational diffusion regime. Transition from Knudsen diffusion to configurational diffusion depends on the properties of the molecules and zeolites. For ZSM-5, this transition may occur for roughly spherical molecules when the ratio of molecular diameter to channel diameter, λ, is greater than approximately 0.6 – 0.8 (2). Channel diameter in ZSM-5 is ca. 0.55 nm.

Specie	Molecular diameter (nm)*	Knudsen or configurational?
Methanol	0.297	0.539, thus Knudsen
Dimethyl ether	0.313	0.569, thus Knudsen

* The molecular diameter was obtained from the Van der Waals “b” constant, the Avogadro number ($6.02214086 \times 10^{23}$ mol^{-1}) and the volume of a spherical molecule.

S4.6: Methanol and DME pulse experiments over hydrocarbon-occluded ZSM-5 (25)

Pulse experiments were conducted by Prof. Andre C. van Veen at the University of Warwick.

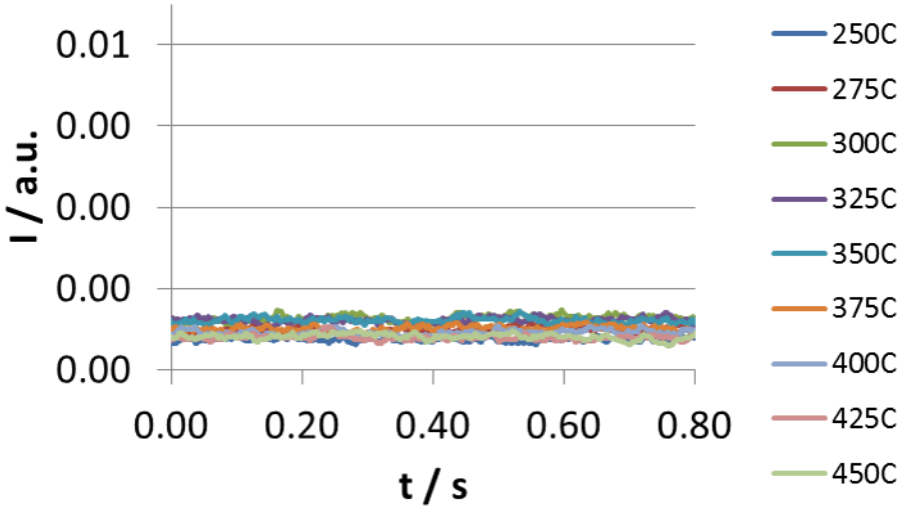

(a) Outlet methanol (m/e=31) pulse response following inlet pulses of 10 vol% CH_3OH/Ar over ZSM-5 (25)

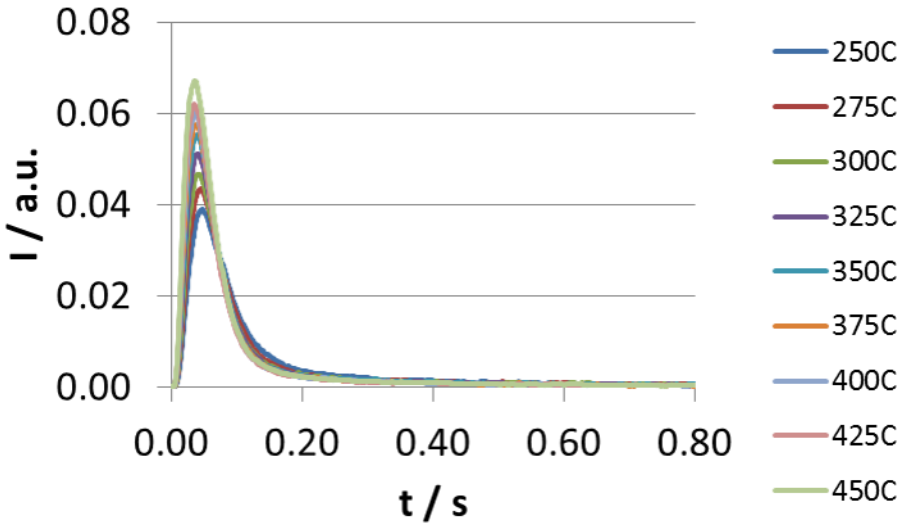

(b) Outlet DME (m/e=45) pulse response following inlet pulses of 10 vol% DME/Ar over ZSM-5 (25)

S4.7: Acid site density determination

Sample	Total acidity^ (µmol g^{-1})	Amount of Lewis acid sites (µmol g^{-1})	Amount of Brønsted acid sites (µmol g^{-1})
ZSM-5 (25)	384	47	337
ZSM-5 (36)	150	35	115
ZSM-5 (135)*	108	30	78

^ = Total acidity based on pyridine adsorption at 128°C

* = Total acidity based on pyridine adsorption at 100°C

References

1. Demmin RA, Gorte RJ. Design parameters for temperature-programmed desorption from a packed bed. J Catal. 1984;90(1):32-9.
2. Xiao J, Wei J. Diffusion mechanism of hydrocarbons in zeolites—I. Theory. Chem Eng Sci. 1992;47(5):1123-41.

4A. Additional studies on the adsorption and desorption of methanol and DME

Further experiments were conducted on the preferential adsorption of methanol and DME on ZSM-5 catalysts after publication of initial studies reported in chapter 4.

4.1. Methodology

A ZSM-5 catalyst with Si/Al ratio of 11.5, obtained from Zeolyst International was used in the following temperature programmed adsorption (TPA) experiments. In a first series of experiments, ZSM-5 (11.5) was saturated with methanol in a TAP reactor at room temperature. Then, the catalyst was purged with argon for 2 h to remove weakly bound species. Thereafter, the argon flow was switched to dimethyl ether (DME) which was passed through the reactor chamber while the catalyst was heated at 15 K min^{-1}. In a second series of experiments, ZSM-5 (11.5) was saturated with DME in a TAP reactor at room temperature. Then, the catalyst was purged with argon for 1 h to remove weakly bound species. Subsequently, the argon flow was switched to a flow of methanol which was passed through the reactor chamber while the catalyst was heated at 15 K min^{-1}. In both experiments, the effluent was monitored using the quadrupole mass spectrometer housed in the detector chamber of the TAP reactor.

4.2. Results and discussion

The temperature programmed adsorption (TPA) of DME over adsorbed methanol and TPA of methanol over adsorbed DME over ZSM-5 (11.5) catalyst are given in Figs. 4A.1 and 4A.2 respectively. Fig. 4A.1 shows that DME displaces methanol when it is adsorbed *a priori* on the ZSM-5 catalyst. Water is formed during this process as this displacement occurs over a highly reactive zeolite catalyst with a Si/Al ratio of 11.5. The desorption profile of DME is shifted to the right of y-axis indicating a higher temperature is required for its desorption.

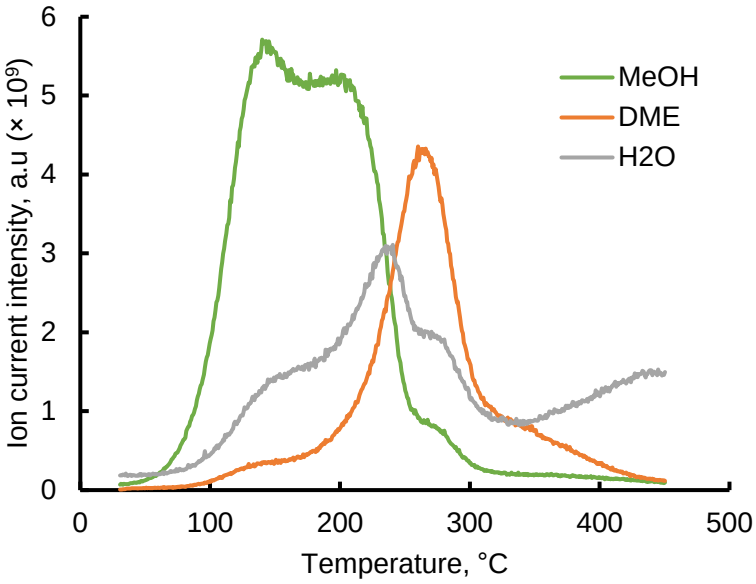

Fig. 4A.1: Temperature programmed adsorption of DME over pre-adsorbed methanol

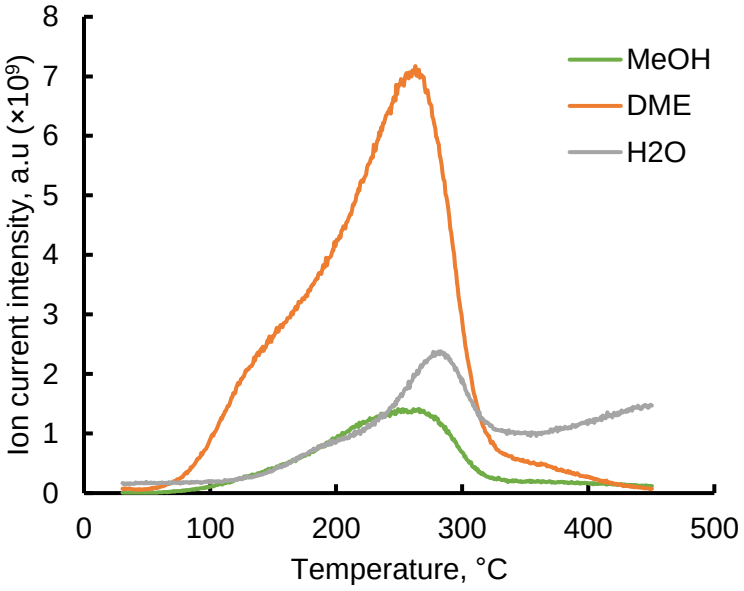

Fig. 4A.2: Temperature programmed adsorption of methanol over pre-adsorbed DME

Conversely, methanol cannot displace DME from the surface of the zeolite catalyst when DME is adsorbed *a priori*. This is shown in Fig. 4A.2 where the desorption profile of methanol is still within the desorption profile of DME.

4B. Nitrogen isotherms for ZSM-5 (11.5), (25), (36) and (135) used in temperature programmed studies

1. ZSM-5 (11.5)

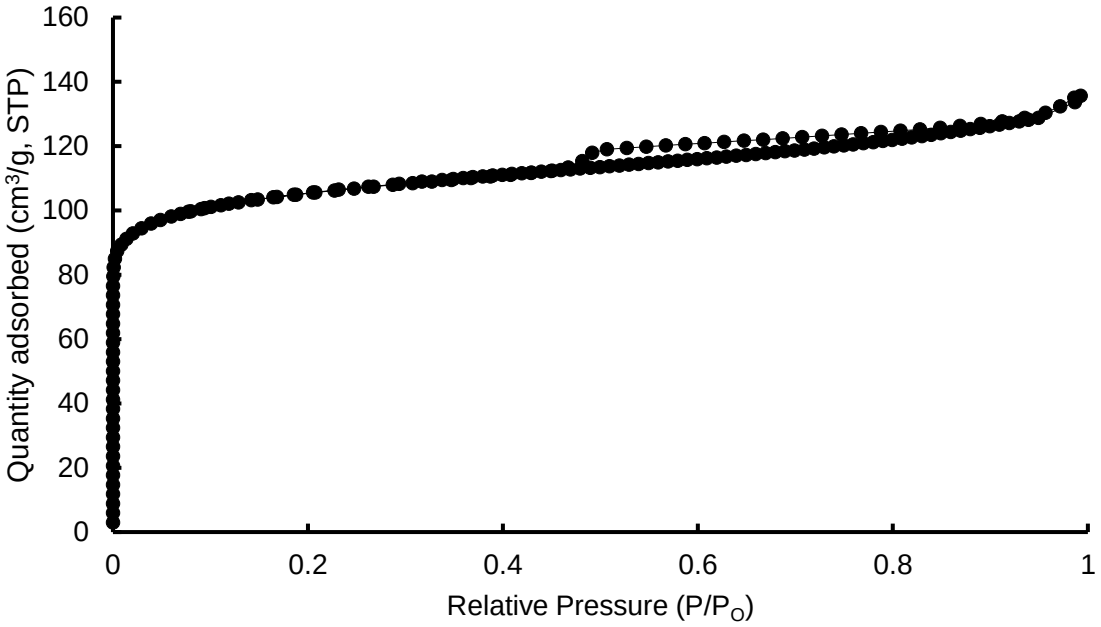

Fig 4B.1: Nitrogen sorption isotherm for ZSM-5 (11.5)

2. ZSM-5 (25)

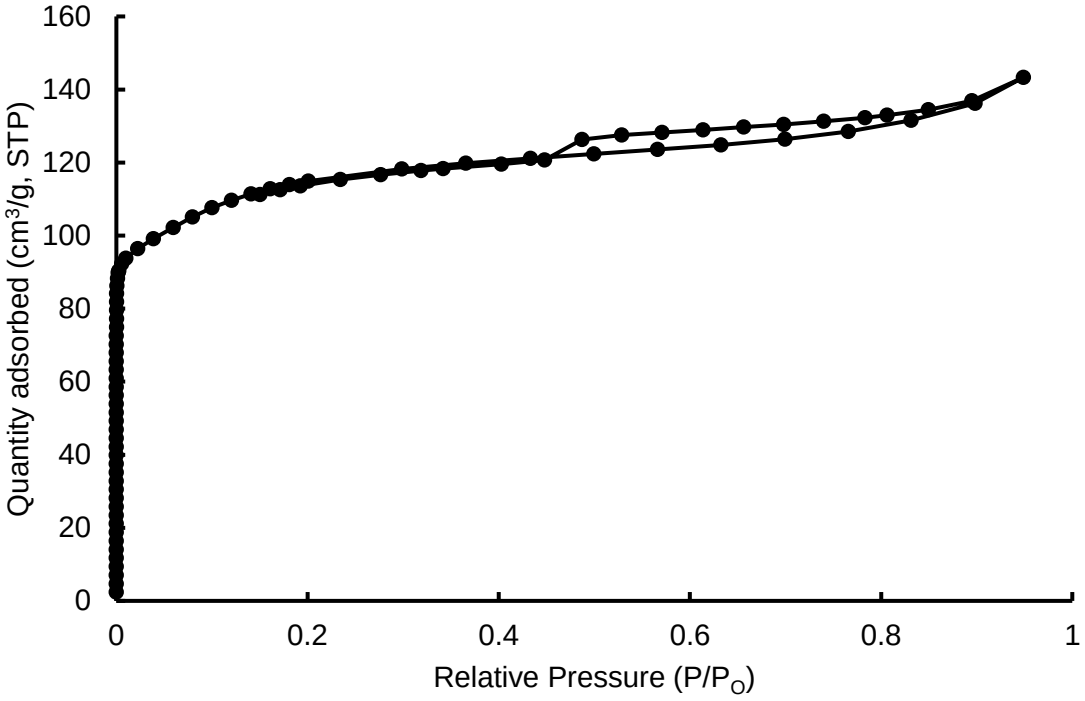

Fig 4B.2: Nitrogen sorption isotherm for ZSM-5 (25)

3. ZSM-5 (36)

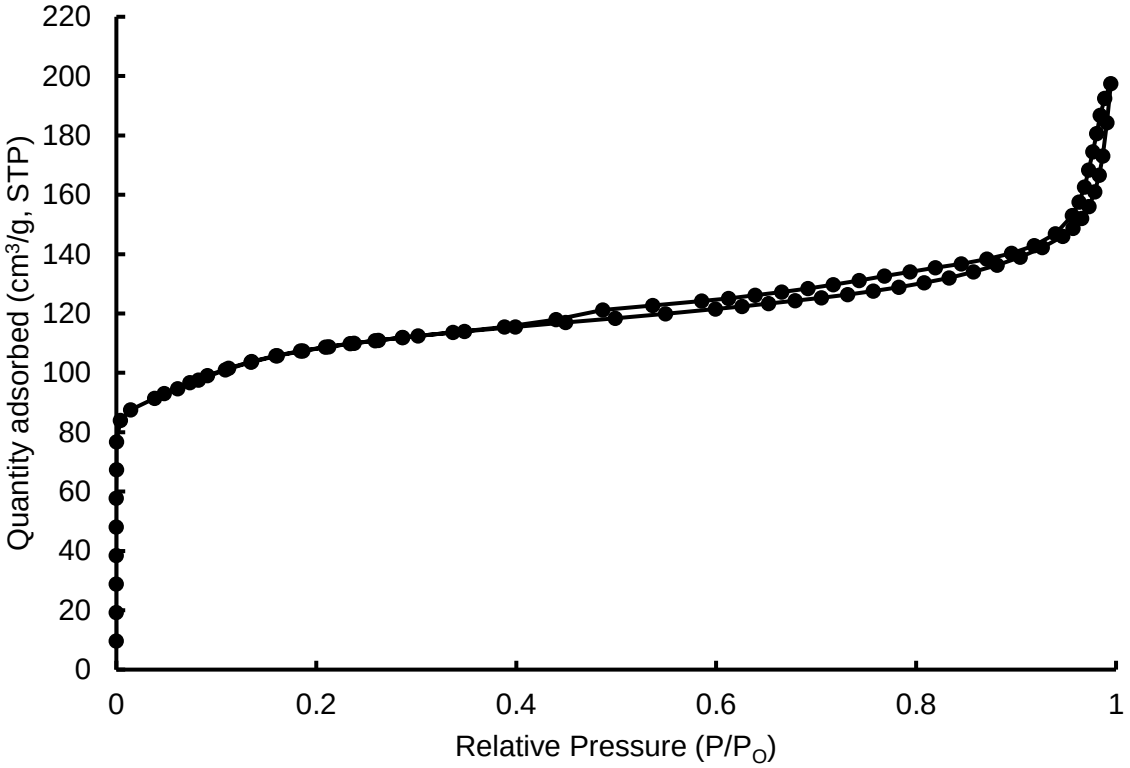

Fig 4B.3: Nitrogen sorption isotherm for ZSM-5 (36)

4. ZSM-5 (135)

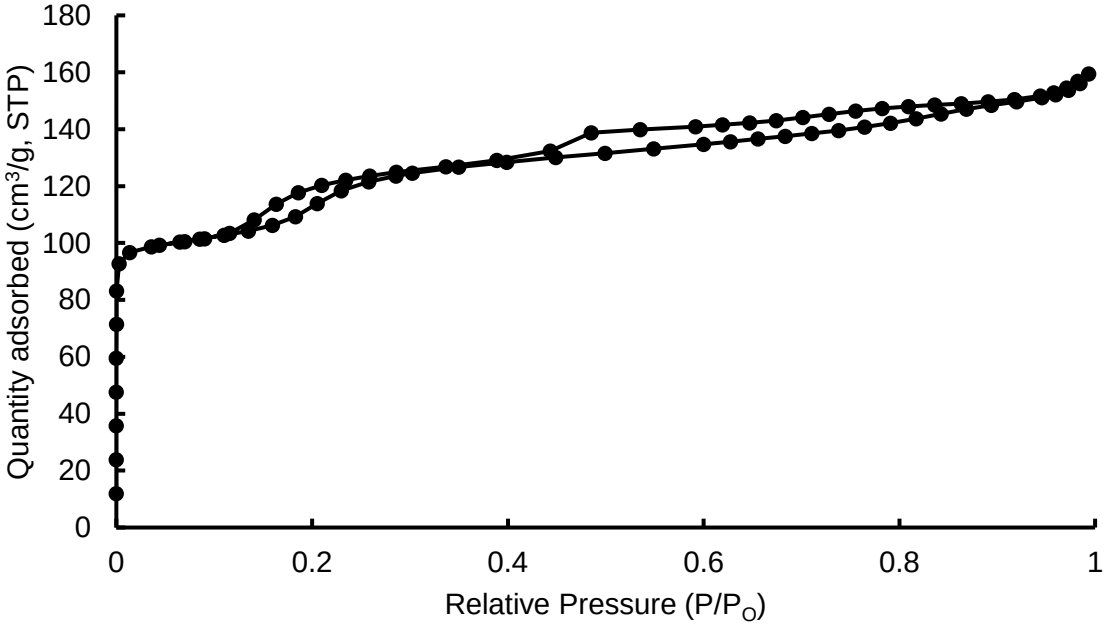

Fig 4B.4: Nitrogen sorption isotherm for ZSM-5 (135).

The various BET constants are given in chapters 4, 5 and 6

Chapter 5

5. A Mechanistic Investigation into the Induction Period of Dimethyl Ether Conversion to Olefins over ZSM-5 Catalysts

In the previous chapter, it was observed that in comparison to methanol, higher temperatures are required to desorb DME over ZSM-5 catalysts and that DME is the primary source of surface methoxy groups at temperatures relevant to methanol-to-olefins conversion. An excellent agreement was obtained between molecular adsorption on low temperature sites and dissociative adsorption on medium and high temperatures sites.

In this chapter, a study on the evolution of DME to primary olefins was conducted by combining kinetic data obtained from a temporal analysis of products (TAP) reactor and infrared spectroscopy. The TAP reactor is conventionally used for conducting pulse experiments. A novel methodology was developed in the TAP using step response experiments. Several variants were conducted: single-step, multi-step and consecutive-step response experiments to probe the induction period of the conversion of the key oxygenate (DME) to primary olefins over ZSM-5 catalysts.

5.1. Introduction

Fuels and chemicals are increasingly produced from non-conventional carbon feedstock due to rising demand, a lack of secure energy resources and a need to reduce carbon footprint. Methanol can be obtained from renewable energy resources such as biomass and converted to olefins (MTO) over zeolite and zeo-type catalysts. Although the MTO process has been recently commercialised (1), the mechanism underlying the formation of the first C-C bond and primary olefin(s) remains elusive.

The MTO process begins with the equilibration of methanol over fresh ZSM-5 zeolite catalysts (2, 3). Methanol and its equilibration products i.e. dimethyl ether (DME) and water compete initially for active sites. The first C-C bond is then formed from these initial species as the zeolite is transformed from its fresh state to its working state (4-6). The period leading up to the establishment of working state conditions is governed by the induction period and subsequent transition-regime. Under its working state, steady-state conditions are established and it is accepted that a “hydrocarbon pool” mechanism, consisting of an aromatic and an olefin cycle, regulates product distribution (7-9). The mechanism or pathway through which methanol and/or DME lead to the first C-C bond and primary olefin(s) during the induction period is currently debated (4, 5, 7-14).

Primary olefins are formed either through the direct (12, 15-17) or indirect mechanism (7-9, 18) over ZSM-5 catalysts. Many intermediates have been identified for both mechanisms. Alkyl-substituted cyclopentenyl carbenium ions are a persistent intermediate closely associated with indirect primary olefin formation pathway (19, 20). In particular, cyclopentadiene has been observed over SAPO-34 zeotype catalysts (21). Conversely, Novakova et al. (22), Liu et al. (14) and Chang et al. (23) provided evidence for dimethoxymethane (DMM) as a dominant intermediate in the pathway forming primary olefins directly. On silicalite, Liu et al. (14) observed the formation of carbon monoxide, hydrogen, methane and formaldehyde from methanol.

Haw and co-workers studied the induction period over zeolite and zeo-type catalysts in a pulse-quench catalytic reactor using ^{13}C MAS NMR spectroscopy (4-6, 19, 24, 25). They observed that: (a) the active site during MTO conversion is a composite of well-defined organic species and one or more inorganic acid sites, which can activate methanol and hold methyl cation equivalents (24) and (b) impurities such as ethanol and acetone control the induction period (5, 6, 25). Qi et al. (26) studied the induction period under continuous flow at low temperatures (245 – 280 °C) and 1 bar. They showed (26) that the formation of hydrocarbon pool species is rate limiting in their proposed three-stage induction period of methanol conversion.

Co-feeding methanol with olefin precursors i.e. ethanol, propanol, hexan-1-ol and cyclohexanol (27) or aromatics i.e. benzene, toluene, p-xylene and naphthalene (26, 28)

reduces the induction period. These earlier experiments suggested regulation by olefin and aromatic cycles respectively. A high zeolite acid site density increases the rate of formation of zeolite occluded species and their autocatalytic effect (29). Lee et al. (30) showed that catalysts with larger crystals and smaller external surface area exhibit a longer induction period due to a smaller number of accessible channels. The response of the induction period to impurities and olefin and aromatic precursors is similar to a crystal nucleation process where seeding agents alter the rate of agglomeration and duration of crystal formation (31-33).

Several pulses were injected and the catalyst was studied as it changed, intermittently, from its fresh to working state during experiments conducted by Haw and co-workers (4, 5). Alternatively, the evolution of products from the zeolite as it changes from its fresh to working state can be studied using step response experiments. The step response method bridges the intermittent data obtained during pulse experiments and steady-state data obtained over a fully working catalyst. This methodology is particularly relevant as methanol adsorbs easily onto the zeolite catalyst using pulses (34).

Temkin (35) distinguished two types of relaxation onto steady-state: (a) intrinsic relaxation, which is caused by the mechanism of the reaction itself, and (b) extrinsic relaxation, which is caused by modifications of the mechanism as a result of sub-surface chemistry. During the evolution from fresh to working state, intrinsic and extrinsic relaxation can be readily distinguished (35, 36). Kobayashi et al. (37-39) described various shapes and mechanisms underlying specie relaxation onto steady-state such as: (1) the S-shaped profile where effluents form with an induction period, (2) overshoot profile where effluents initially exceed steady-state values and, (3) monotonic profiles where effluents begin to form immediately and rise onto steady-state.

It was recently shown that higher temperatures are required to desorb DME in comparison to methanol from ZSM-5 catalysts (34). This has been further observed by Liu et al. (14) and Wei et al. (40) suggesting that DME remains on the zeolite for a longer period. Consequently, in this study, the roles of the direct and indirect mechanism towards primary olefin formation from DME using spectroscopically proven and dominant intermediates were investigated. DMM was chosen as the precursor of the direct mechanism and 1,5-hexadiene as a cylcopentadiene precursor for the indirect mechanism. Carbenium ion chemistry (41, 42) show how dienes accept protons to first form reactive carbenium ions. Cyclisation later occurs as the non-carbocationic unsaturated double bond attacks the postive cationic charge center closing the ring and resulting in alkylcyclopenta carbenium ions which form over ZSM-5 catalysts (43, 44). In this way, 1,5-hexadiene is justified as a precursor for cyclopentadiene. Furthermore, the influence of methanol decomposition products (carbon monoxide and hydrogen) on primary olefin formation is investigated.

5.2. Experimental

5.2.1. Materials

Fresh NH_4-ZSM-5 catalysts with Si/Al ratios of 11.5 and 25, referred to as ZSM-5 (11.5) and ZSM-5 (25) respectively, were purchased from Zeolyst International. The ammonium form of the zeolite was pressed, crushed, and sieved to obtain particle sizes in the range of 250 – 500 µm. Anhydrous DME (99.999%) and argon (99.999%) were purchased from CK Special Gases Ltd. Experiments were conducted in a transient reactor suited for the temporal analysis of products (TAP). The TAP consists of three chambers in series: (a) the reactor chamber, (b) the differential chamber and (c) detector chamber. Further details on the TAP reactor can be found in section S5.1 of the supplementary information.

The response of the quadrupole mass spectrometer (QMS), placed in the detector chamber, was calibrated by passing continuous streams of various gases (methanol, DME, propylene, etc.) in argon over an inert quartz bed with particle diameters between 355 – 500 µm. The QMS was operated either in a scan mode monitoring species up to an m/z ratio of 150 or in a multiple ion detection (MID) mode monitoring a maximum of 10 products simultaneously. The low base pressure (10^{-7} Pa) in the detector chamber allows for high detection sensitivity necessary for quantitative analysis. The inert quartz bed used for calibration had the same length as the catalyst bed. The time required to reach steady-state or to drop from steady-state was fastest over the inert quartz bed (see section S5.2 in supplementary information). The normalised step function of DME over the quartz bed in Fig. S5.2 was used to estimate a residence time of 45 s in the TAP reactor at 450 °C.

5.2.2. Characterisation

ZSM-5 (25) was used for the step response experiments whereas ZSM-5 (11.5) catalyst was used for transmission IR studies to increase loading of hydrocarbon species.

The ZSM-5 (25) catalyst has a crystal size of 0.10 ± 0.02 µm, an apparent (Rouquerol-adjusted) BET surface area (45) of 413 $m^2\ g^{-1}$, 428 µmol g^{-1} of Brønsted acid sites (BAS), 35 µmol g^{-1} of Lewis acid sites (LAS) and a BAS/LAS ratio of 12.2. NH_4-ZSM-5 (25) loses 4.2 wt% of its initial mass under dry air heating in a thermogravimetric analyser (TGA) at 5 °C min^{-1} up until 600 °C.

ZSM-5 (11.5) catalyst is highly crystalline and of roughly equal crystallite site as ZSM-5 (25). ZSM-5 (11.5) has an apparent BET surface area (45) of 403 $m^2\ g^{-1}$,1120 µmol g^{-1} of BAS, 30 µmol g^{-1} of LAS and a BAS/LAS ratio of 38. NH_4-ZSM-5 (11.5) loses 10 wt% of its initial mass under dry air heating in the TGA at 5 °C min^{-1} up until 600 °C.

Further characterisation details (XRD, SEM images, TGA) can be found in section S5.3 of the supplementary information.

5.2.3. Transient study

5.2.3.1. Methodology

10 mg of NH_4-ZSM-5 (25) catalyst was initially decomposed in the TAP reactor chamber by heating it at 10 °C min^{-1} up to 450 °C, holding for 30 min before bringing the sample to a reaction temperature between 300 and 450 °C. Background signal intensities were obtained. The catalyst was then subjected to a steady flow of argon at 10^{-8} mol s^{-1}. Afterwards, the flow was instantaneously switched to a feed of 5 vol% DME in argon (step-up) at a flow rate of 4.4 × 10^{-8} mol s^{-1}. During steady-state, the inlet DME feed was then switched to a flow of argon (stopped-flow). Thus, a single step response cycle consists of three phases: step-up, steady-state and stopped-flow. Two further series of step response experiments were performed at 300 °C with different feeds: (a) 5vol% DME, 0.33 vol% CO (balance argon) and (b) 5 vol% DME, 0.33 vol% hydrogen (balance argon).

The experiments were initially conducted in order of decreasing temperature such that a catalyst history effect occurs with a DME feed. However, at lower temperatures (300 and 330 °C), experiments were repeated over fresh catalysts and temperature programmed desorption was carried out in-between such that such catalyst history effect was eliminated. The experiments with DME/CO and DME/H_2 feed were carried out over fresh catalysts with temperature programmed desorption in-between such that they are comparable to step response cycles of the DME only feed at 300 °C.

5.2.3.2. Step response study

First, the full range of gaseous species was analysed when the ZSM-5 (25) catalyst reached its working state at the reaction temperature. Next, single and multi-step response cycles of 5 vol% DME (balance argon) were introduced separately over ZSM-5 (25) catalysts while the effluent was monitored with QMS.

Flow rates of the inert feed were similar to step response feed and were 10^{-8} mol s^{-1}, with an inlet pressure below 1000 Pa (46). The active catalyst bed length was short (2 mm) compared to the overall bed length of 25 mm (consisting of quartz wool/quartz beads/catalyst bed/quartz beads/quartz wool). This thin-zone configuration removes concentration gradients along the bed while achieving high conversions (47). The level of non-uniformity in a thin-zone TAP reactor is lower than 20% for conversions up to 75% and only becomes significant for conversions above 80% (48) when pulses are used. In our study, for the first time, we subjected the thin-zone packing configuration to convective flow in the TAP reactor.

Throughout all step response experiments, the temperature and the pressure were constant and the experiments were repeated to check for reproducibility. The raw data (QMS

ion currents) were corrected for background levels and fragmentation contributions for the different molecules and sensitivity factors (see S5.4 in the supplementary information).

Estimation of the induction times and autocatalytic rates are described using methods stated in section 5.3. Steady-state DME conversion was calculated using equation 5.1 below:

$$X_{DME} = \frac{2\dot{n}_{DME,i} - (\dot{n}_{MeOH,e} + 2\dot{n}_{DME,e})}{2\dot{n}_{DME,i}} \quad (5.1)$$

where X_{DME} is the conversion of DME, $\dot{n}_{DME,i}$ is the molar feed flowrate of DME, $\dot{n}_{MeOH,e}$ is the effluent molar flowrate of methanol and $\dot{n}_{DME,e}$ is the effluent molar flowrate of DME.

5.2.4. In-situ zeolite characterisation

Temperature programmed desorption (TPD) was carried out in two instances. Firstly, TPD was carried out after step response experiments by supplying argon at similar flow rates to the DME feed for 20 min to remove weakly adsorbed species from the ZSM-5 (25) catalyst and subjecting the zeolite to a linear temperature ramp at 15 °C min^{-1}. This TPD profile is referred to TPD-SR. Analysis of the TPD-SR profiles for estimation of maximum temperatures of desorption and activation energies of desorption was carried out using the microkinetic model described in chapter 4 (34). Secondly, TPD was conducted for DMM or 1,5-hexadiene over fresh ZSM-5 (25) catalysts. The ZSM-5 catalyst was saturated with the specie, purged with argon and subjected to a linear temperature ramp at 15 °C min^{-1}. These TPD profiles are referred to as TPD-IND.

Test TPD experiments were conducted on some samples after they were subjected to step response cycles. No major detectable species were observed (within the detection capabilities of the QMS under MID mode) below the step response temperatures.

5.2.5. Ex-situ zeolite characterisation

5.2.5.1. Sample preparation

Fresh NH_4-ZSM-5 (11.5) catalysts were decomposed under vacuum conditions at 15 °C min^{-1} up to 450 °C and held for 30 min and brought down to 370 °C. A step response of 5 vol% DME was passed over ZSM-5 (11.5) catalysts. A first series of experiments involved a minimum of two cycles of a step response of 5 vol% DME followed by cooling in argon. This sample is called sample A. Sample B was obtained after 10 min of introducing a step response of 5 vol% DME over ZSM-5 (11.5). It was observed that at 10 min, with *ca.* 150 mg of ZSM-5 catalyst at 370 °C, the zeolite was effectively in its induction period (See Fig. S5.5 in supplementary information). Sample C was obtained after decomposing the ammonium form of the zeolite in the TAP reactor. Sample D was the initial ammonium form of the ZSM-5 (11.5)

catalyst. These extracted samples were characterised by FTIR spectroscopy as described in section 5.2.5.2 below.

5.2.5.2. FTIR study

FTIR studies were carried out in the following instances: (1) over samples A, B, C and D described in section 5.2.5.1 activated at temperatures between 250 and 450 °C; (2) pyridine adsorbed on sample D and (3) DMM or 1,5-hexadiene adsorbed on sample D.

Prior to the separate pyridine, DMM or 1,5-hexadiene FTIR studies, the ZSM-5 catalyst was pressed into self-supporting discs (~9-12 mg, 13 mm in diameter) and pre-treated in an *in-situ* IR cell at 450 °C under vacuum (10^{-3} Pa) for 5 h. The adsorption experiments with different probe molecules were monitored by Thermo Nicolet iS10 FTIR spectrometer equipped with a deuterated triglycine sulfate detector at a spectral resolution of 4 cm^{-1} collecting 64 scans. An excess of probe molecules (pyridine, 1,5-hexadiene and DMM) was admitted by injection of 2.0 µL liquid into the IR cell. Physisorbed molecules were subsequently removed by evacuation at the adsorption temperature. Adsorption of 1,5-hexadiene and DMM were performed at room temperature while pyridine (Acros Organics, 99.5%) was adsorbed at 150 °C. Desorption profiles were obtained by evacuating the sample at increasing temperatures in 50 °C steps for pyridine and 100 °C steps for DMM and 1,5-hexadiene. The obtained spectra were analysed (including integration, subtraction and determination of peak positions) using the OMNIC 9 software. All the spectra presented in this work were normalised to 10 mg sample mass.

5.3. Results

As the QMS used in the TAP reactor is limited to monitoring 10 gaseous species simultaneously in the MID mode, it was important to establish the full range of gaseous species using the scan mode. No substantial gaseous products greater than an m/z ratio of 46 was observed as shown in Fig. S5.6 in the supplementary information. Butene, monitored at an m/z of 56 (49, 50) was minute and hardly distinguishable from the background signal at 300 °C.

5.3.1. Step response study

Dewaele et al. (49) conducted the first TAP reactor studies during MTO conversion and observed formaldehyde and methane to be primary products formed at low conversions and temperature. In their work, a step response was generated by pulsing at high frequencies.

This work has focused on obtaining a step response by using the continuous flow panel of the TAP reactor under close to vacuum conditions.

In this study, major species such as methanol, DME, water, ethylene and propylene were focused on. Blank experiments were carried out with 5 vol% DME over quartz wool/quartz beads/quartz wool system to ascertain that no reaction was obtained with the inert bed (see Fig. S5.2). The scan mode of the QMS (Fig. S5.6 in supplementary information) was used to obtain the full spectrum of products over the working catalyst. At 300 °C, products observed at m/z ratio of 46 and higher were minute. Moreover, low pressures at which the TAP study was conducted allow for conditions under which light olefin production is separated from their oligomerisation to higher olefins (49, 51). These three reasons give confidence that the major gaseous products can be limited to methanol, DME, water, ethylene and propylene.

Fig. 5.1 shows the results of the step response experiment with 5 vol% DME at 300 °C. Ethylene effluent is negligible while propylene effluent exhibits an S-shaped profile. A 43.5 min induction period in the steady-state flow of propylene effluent is observed in the first cycle. In the first cycle, methanol effluent displays a slight overshoot while water effluent displays a significant overshoot. DME effluent rises in two stages: first rapidly and then slowly onto its steady-state value. Water has a non-negligible induction period signifying that it is formed during the reaction and not desorbed from the reactor walls. The m/z ratio of 18 (see Table S5.4) used to identify water has no contribution from any other hydrocarbons in our analysis in accordance with the previous TAP study of Dewaele et al (49). Thermogravimetric analysis (TGA) of the NH_4-ZSM-5 (25) catalyst shows that it loses 4.2% of its initial mass at 600 °C. About 4% of its initial mass is lost at 450 °C indicating little loss of zeolite mass due to drying or decomposition of the zeolite above 450 °C. The low selectivity to ethylene at low temperatures has been observed previously by Dewaele et al. (49).

After steady molar flowrates of all effluent species were achieved at 300 °C, the catalyst was purged by a flow of argon for 20 min (i.e. after 80 min time on stream in Fig. 5.1). Subsequently, a second step response cycle of 5 vol% DME was passed over the ZSM-5 catalyst at *ca.* 100 min. The initial induction time of propylene effluent observed in the first step response cycle was eliminated on subsequent step response cycles. The steady flow of propylene effluent, which follows an S-shaped profile, shows that no deactivation of the catalyst had occurred over the timescale of this experiment at 300 °C. Also, there is no overshoot in the water effluent on subsequent step response cycles. The DME effluent rises immediately in the second and subsequent cycles in comparison to its slower pace in the first cycle. Similar behaviour is observed at 330 °C (Fig. 5.2)

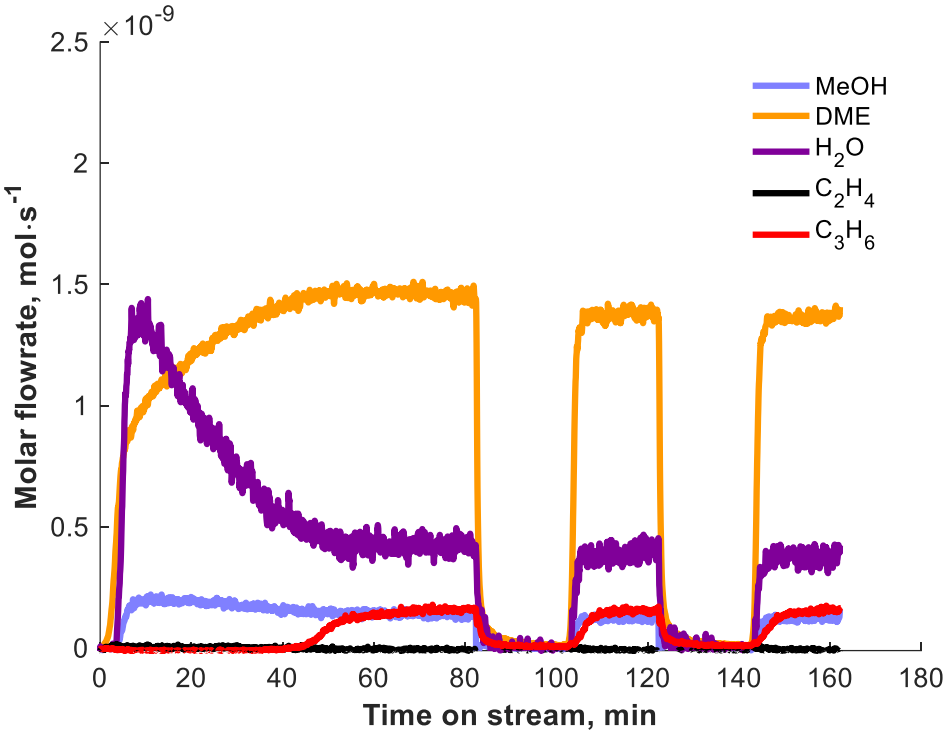

Fig. 5.1: Step response of 5 vol% DME at 300 °C over 10 mg of ZSM-5 (25) catalysts. Total molar flow rate (5 vol% DME, balance Ar) at STP = 4.4×10^{-8} mol s^{-1}. Steady-state conversion is 34.8%

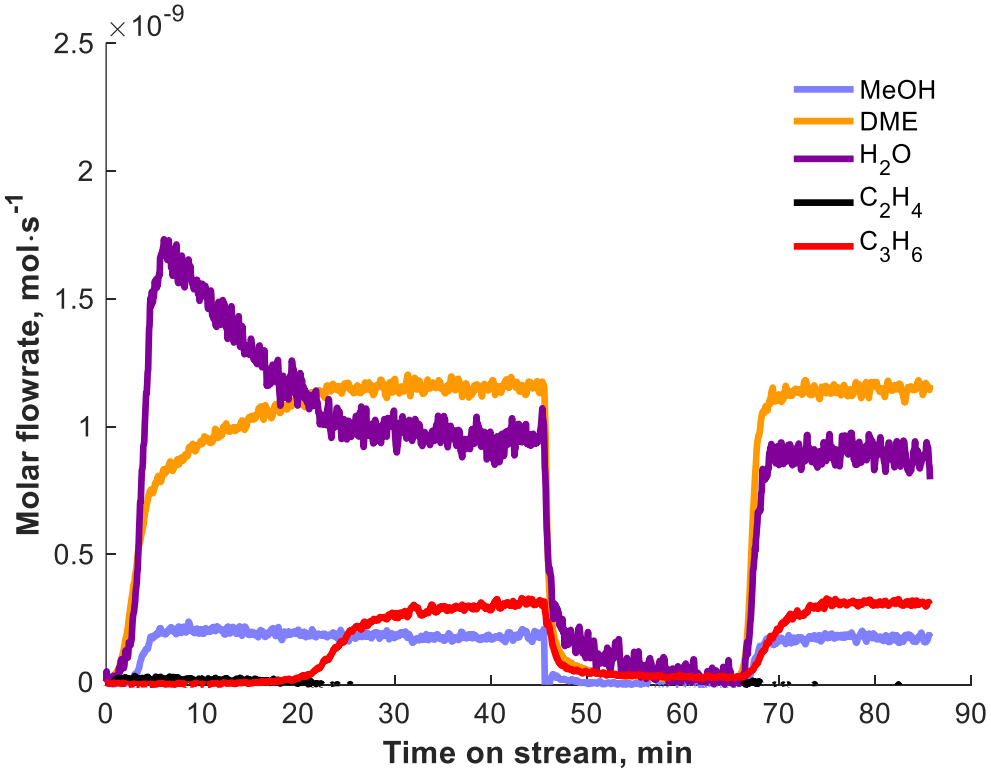

Fig. 5.2: Step response of 5 vol% DME at 330 °C over 10 mg ZSM-5 (25) catalysts. Total molar flow rate at STP (5 vol% DME, balance Ar) = 4.4×10^{-8} mol s^{-1}. Steady-state conversion is 45.9%

At low temperatures (300, 330 °C), both methanol and water effluents display an overshoot profile with propylene effluent being the dominant olefin and exhibiting an S-shaped profile (Fig. 1 and Fig. 5.2). However, at 450 °C, methanol and water effluents both portray a monotonic profile while both ethylene and propylene are observed and exhibit S-shaped profiles (Fig. 5.3). The ethylene and propylene S-shaped effluent profiles suggest they form through a common intermediate (49). The drop in induction time of propylene profiles with temperature can be observed in Fig. 5.4.

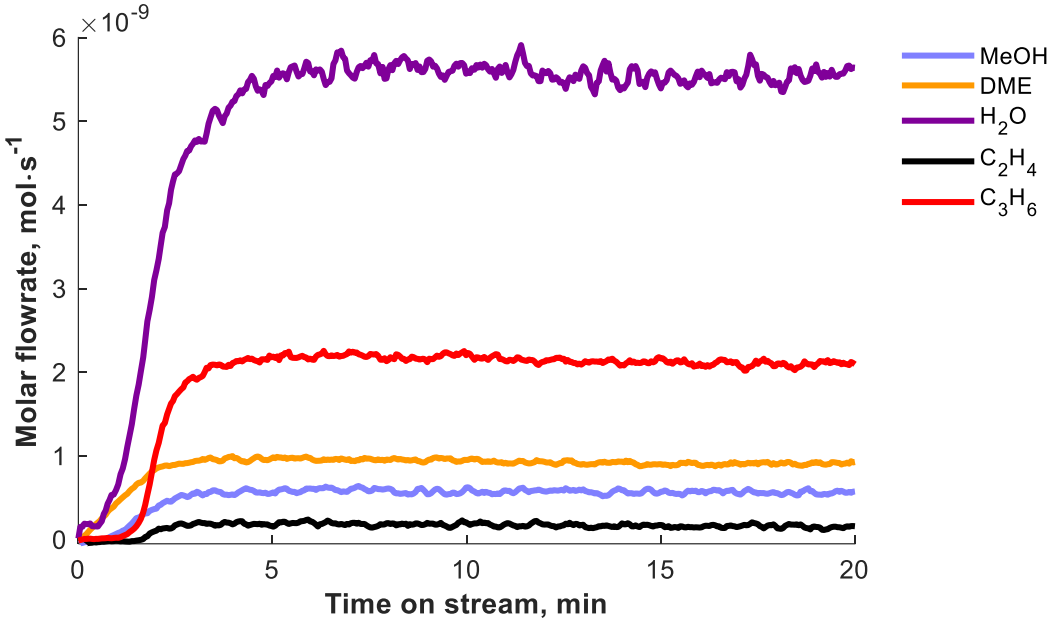

Fig. 5.3: Step response of 5 vol% DME at 450 °C over 10 mg ZSM-5 (25) catalysts. Total molar flow rate at STP (5 vol% DME, balance Ar) = 4.4×10^{-8} mol s^{-1}. Steady-state conversion is 57.9%

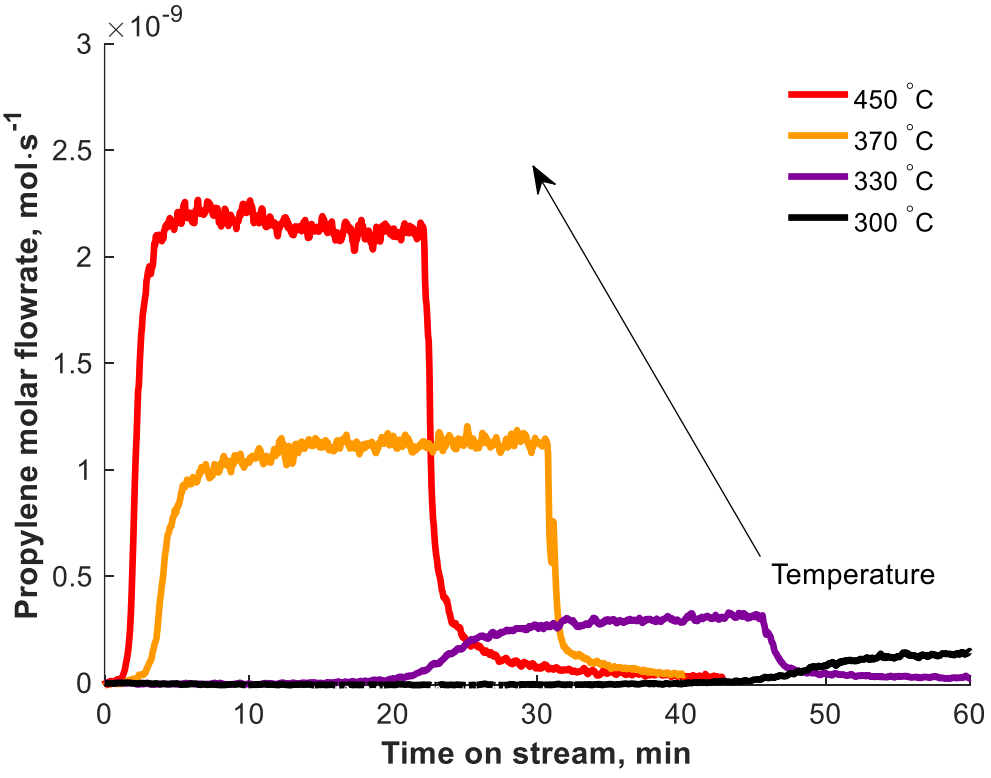

Fig. 5.4: Propylene effluent formation during step response of 5 vol% DME (balance Ar) at temperatures between 300 and 450 °C over ZSM-5 (25) catalysts. Total molar flow rate at STP (5 vol% DME, balance Ar) = 4.4×10^{-8} mol s^{-1}. *There is an added catalyst history effect for step response cycles at 370 and 450 °C.

To obtain phenomenological descriptions, the induction times of propylene formation was estimated by fitting its profile with a logistic (sigmoidal) function (52) using equations 5.2 and 5.3 while methanol and water were both fitted to a BiHill function (equation 5.4) and the DME profile was fitted to a Hill function (equation 5.5). The logistic (sigmoidal), BiHill and Hill functions have been used to describe the nucleation, growth and binding of new species (52, 53).

$$I(t) = \frac{I_{max}}{1 + e^{-k(t-t_m)}} \tag{5.2}$$

$$t_{ind} = t_m - \frac{2}{k} \tag{5.3}$$

$$I(t) = \frac{I_{max}}{\left[1+\left(\frac{K_a}{t}\right)^{H_a}\right]\left[1+\left(\frac{t}{K_i}\right)^{H_i}\right]} \tag{5.4}$$

$$I(t) = \frac{I_{max}}{\left[1+\left(\frac{k_m}{t}\right)^{n}\right]} \tag{5.5}$$

where *I(t)* is the intensity at time *t*, I_{max} is the maximum intensity at the plateau phase of the S-shaped profile, t_m is the inflection time at which the growth rate reaches its maximum and *k* is the apparent rate constant for the growth phase. The overshoot effluent profiles of methanol (slight) and water (strong) can be described by: (1) constants that describes the period required to reach maximum overshoot value (H_a) or fall from the overshoot value (H_i) and (2) constants that describe the rate at which it reaches the overshoot value (k_a) and fall from the overshoot value (k_i). The various functions (sigmoidal (logistic), BiHill and Hill) were fitted to the experimental data using the Origin 2018b 64bit program.

The parameters from the phenomenological description can also be used to assess the relative contributions of carbon monoxide or hydrogen to the induction period during dimethyl ether conversion to olefins (Fig. 5.5). The quantification analysis described in S5.4 is not amenable to step response cycles where more than one active feed is involved. Nonetheless, normalised curves of the step response cycles in Fig. 5.5 were subjected to phenomenological descriptions as described in equations 5.2 – 5.5.

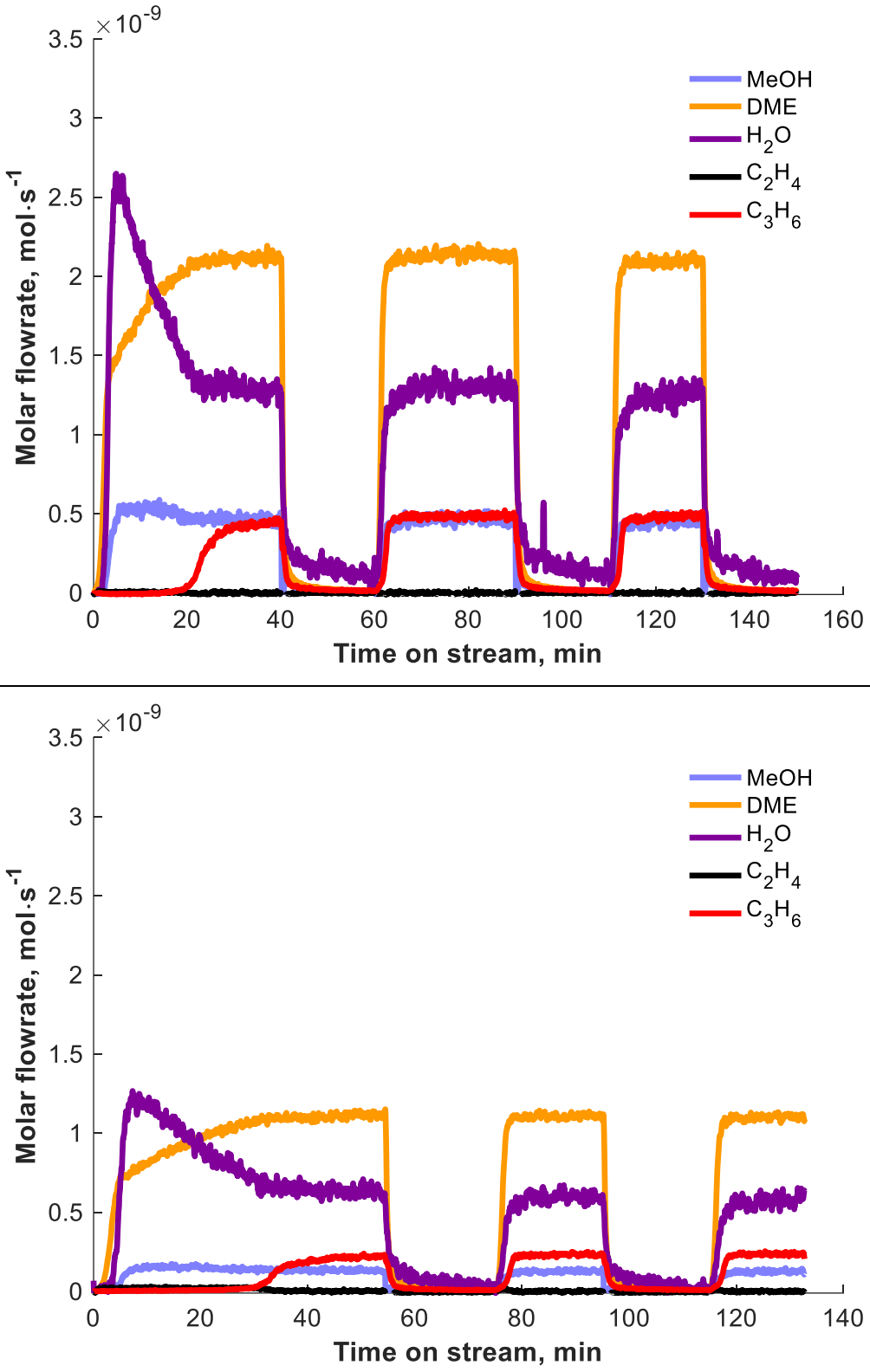

Fig. 5.5: Above - Step response of 5 vol% DME/0.33 vol% carbon monoxide (balance argon) and below - 5vol% DME/0.33 vol% hydrogen (balance argon) at 300 °C over 10mg ZSM-5 (25) catalysts. Total molar flow rate at STP (5 vol% DME, balance Ar) = 4.4×10^{-8} mol s^{-1}.

The S-shaped profile of propylene effluent can be described by an induction time, growth constant and the steady-state effluent flowrate. At 300 °C with a DME feed, a 43.5 min

induction time was observed before steady-state effluent flow of propylene is observed over ZSM-5 (25) catalysts. On addition of carbon monoxide or hydrogen, this induction time is reduced by *ca*. 54% and 34% respectively. The growth rate of the transition-regime is increased with carbon monoxide (79%) and hydrogen (24%) as shown in table 5.1.

While the S-shaped profile of propylene can be separated into three stages as stated above, the conversion of DME offers more resolution and can be separated into five stages (Fig. S5.7). Each of these stages represent regions where the rate of change of the molar flowrate with time on stream (TOS) exhibits a major different gradient. The five stages of the DME effluent all follow an S-shaped curve typical of autocatalytic reactions (54, 55). The initial four phases (a, b, c and d) of the profiles of DME all accumulate into the induction phase (ai) of the S-shaped propylene profile (Fig. S5.7) establishing a relationship. Thus, the S-shaped of the propylene profile maintains its integrated induction stage (ai), growth stage (bi) and plateau stage (ci).

Tables 5.1 – 5.3 give phenomenological constants describing propylene, water, methanol and DME profiles.

Table 5.1: Induction times and growth rates of the S-shaped propylene profile at 300 °C over ZSM-5 (25) catalysts

	Propylene profile		
	DME	DME/CO	DME/H2
k (min^{-1})	0.34	0.61	0.42
t_{ind} (min)	43.5	19.9	28.6

Table 5.2: Phenomenological constants describing water and methanol profiles at 300 °C over ZSM-5 (25) catalysts

	Water profile			**Methanol profile**		
	DME	DME/CO	DME/H2	DME	DME/CO	DME/H2
k_a	4.53	3.25	4.65	4.86	3.66	5.10
k_i	15.0	11.6	13.9	41.9	14.77	28.8
H_a	5.57	7.07	6.92	4.62	5.37	5.89
H_i	0.94	0.89	0.74	0.56	0.27	0.23

Table 5.3: Phenomenological constants describing DME profile at 300 °C over ZSM-5 (25) catalysts

	DME profile		
	DME	DME/CO	DME/H2
k_m	5.63	3.24	4.71
n	1.12	1.50	1.26

5.3.2. Nature of occluded species using TPD of ZSM-5 (25)

TPD of the ZSM-5 (25) catalyst was conducted after being subjected to multiple step response cycles at 300 °C (Fig. 5.1). At the end of the third step response cycle (stopped-flow), the ZSM-5 catalyst was heated from 300 to 470 °C at 15 °C min^{-1} (Fig. 5.6). The response was calculated as $R = \frac{I_i - I_{bl}}{I_{Ar}}$, normalised response was then calculated as $R_N = \frac{R}{R_{Max}}$, where I_i is the ion current intensity at a specified m/z ratio, I_{bl} is the background intensity, I_{Ar} is the ion current intensity for argon and R_{max} is the maximum response value.

Fig. 5.6 shows that species are occluded in the porous ZSM-5 catalyst during step response experiments. The heating rate at 15 °C min^{-1} gives an adequate temperature resolution while maintaining a high signal to noise ratio. Careful examination of Fig. 5.6 shows two groups of occluded species: (a) m/z ratio of 29, 31, 41 and 45 and (b) m/z ratio of 16, 18 and 91. These two groups can be distinguished based on their maximum temperatures and activation energies of desorption. Using m/z ratio of 41 as a proxy for the first group and m/z ratio of 91 for the second group, activation energies of desorption of 100 kJ mol^{-1} and 115 kJ mol^{-1} are obtained for maximum temperatures of desorption of 400 °C and 460 °C, respectively using simulations from a microkinetic model described in chapter 4 (34). These two groups could be representative of major components of the olefin and the aromatic cycle.

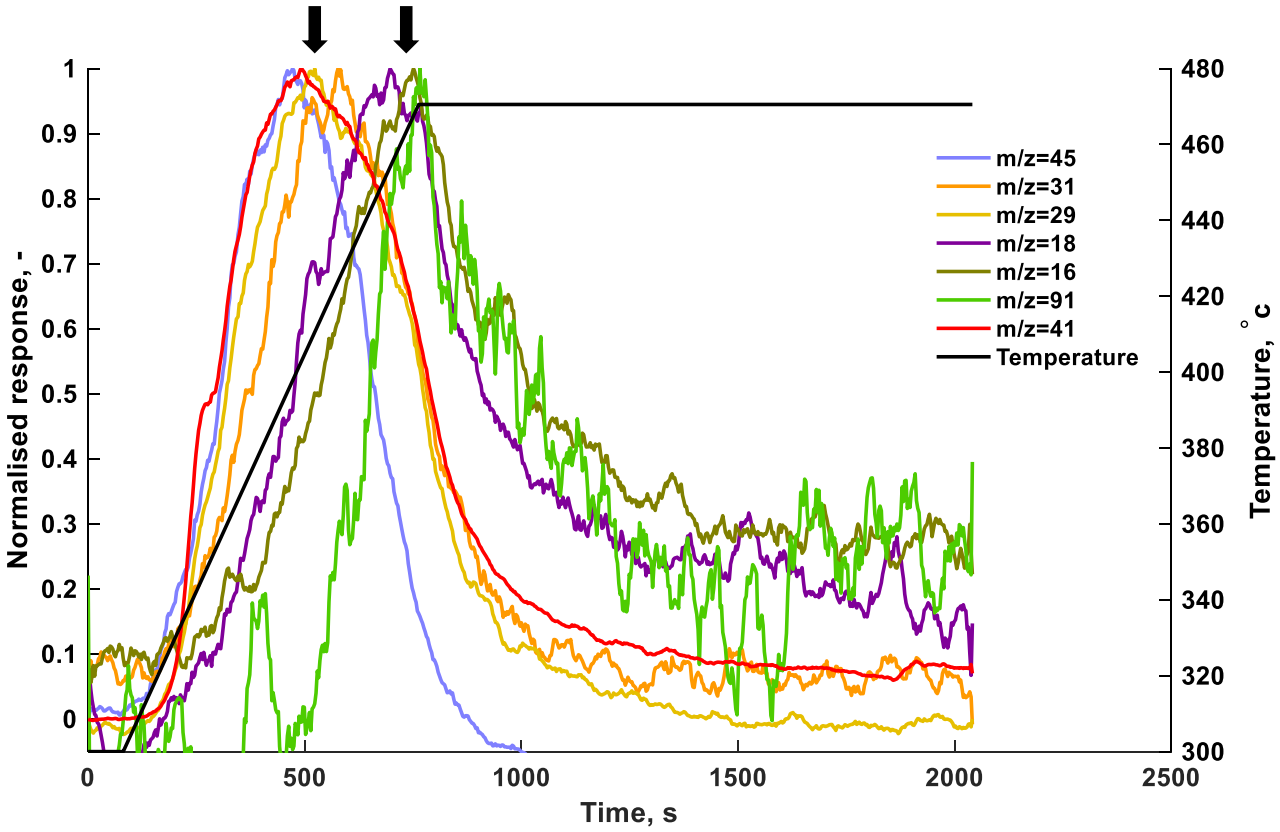

Fig. 5.6: TPD of the working ZSM-5 (25) catalyst from 300 °C to 470 °C at 15 °C min^{-1} after a step response of 5 vol% DME at 300 °C.

The mass, carbon, hydrogen and oxygen balances show an accumulation of 17.8, 22.5, 18.5 and 10.4% respectively (See section S5.9) at 300 °C, based on 5 key species. Although Fig. S5.6 shows that no species heavier than m/z = 46 is present in the gas phase, the TPD profiles in Fig. 5.6 show that heavier products up until m/z = 91 are occluded in the hydrocarbon-occluded catalyst highlighting product selectivity. The TPD profile of the hydrocarbon-occluded ZSM-5 catalyst was then compared to the individual TPD profiles of DMM and 1,5-hexadiene on fresh ZSM-5.

5.3.3. TPD-IND over ZSM-5 (25) catalysts: DMM and 1,5-hexadiene

Desorption profiles for DMM and 1,5-hexadiene were obtained over ZSM-5 (25) catalysts. DMM shows reactive decomposition under vacuum at 15 °C min^{-1} (Fig. S5.8a) while 1,5-hexadiene undergoes desorption at low temperatures (< 200 °C) and at higher temperatures between 250 and 450 °C (Fig. S5.8b). The desorption profiles for DMM and 1,5-hexadiene show that they either exist on the surface of the catalyst (1,5-hexadiene) or products of their dissociation (in the case of DMM) are present on the surface of the catalyst at the step response temperatures.

5.3.4. FTIR study of ZSM-5 (11.5) catalysts

FTIR experiments were carried out over ZSM-5 (11.5) catalyst with increased hydrocarbon loading. Fig. S5.10 gives IR of the ZSM-5 (11.5) catalyst and the pyridine IR study. FTIR spectrum of sample D which is the ammonium form of ZSM-5 (11.5) shows two major peaks (Fig. S5.10a): (1) 3744 cm^{-1} with a shoulder at 3735 cm^{-1} which are attributed to external and internal silanol groups (Si-OH), respectively and (2) 3610 cm^{-1} which is assigned to acidic bridging Si-OH-Al groups (56). The interaction and full accessibility of pyridine with sample D results in the complete disappearance of the band at 3610 cm^{-1} corresponding to bridging Si-OH-Al groups and a decrease in intensity of the band assigned to Si-OH groups. In the range of 1400 – 1700 cm^{-1} (Fig. S5.10b), chemisorbed pyridine is revealed with the two pyridinium ion bands at 1546 cm^{-1} and 1637 cm^{-1} (57), two bands assigned to pyridine coordinated to Lewis acid sites at 1455 cm^{-1} and 1622 cm^{-1} (56, 58) and the superposition of signals of Lewis and Brønsted acid sites at 1490 cm^{-1} (57).

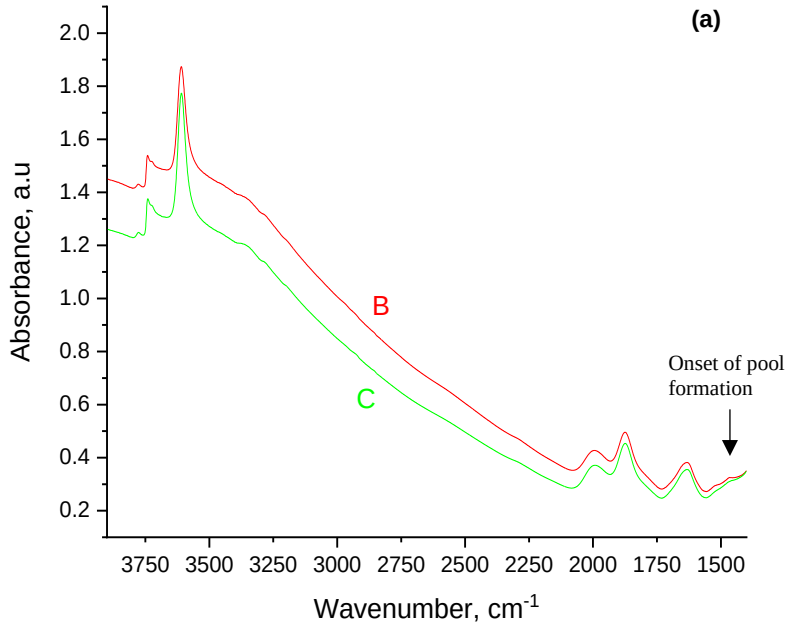
(a)
Absorbance, a.u
2.0
1.8
1.6
1.4
1.2
1.0
0.8
0.6
0.4
0.2
B
C
Onset of pool
formation
3750 3500 3250 3000 2750 2500 2250 2000 1750 1500
Wavenumber, cm-1

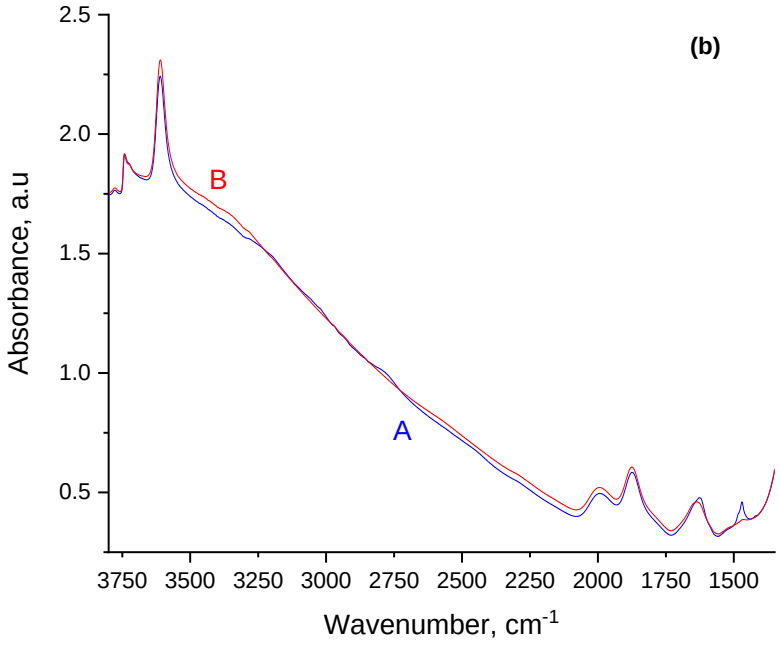
(b)
Absorbance, a.u
2.5
2.0
1.5
1.0
0.5
B
A
3750 3500 3250 3000 2750 2500 2250 2000 1750 1500
Wavenumber, cm-1

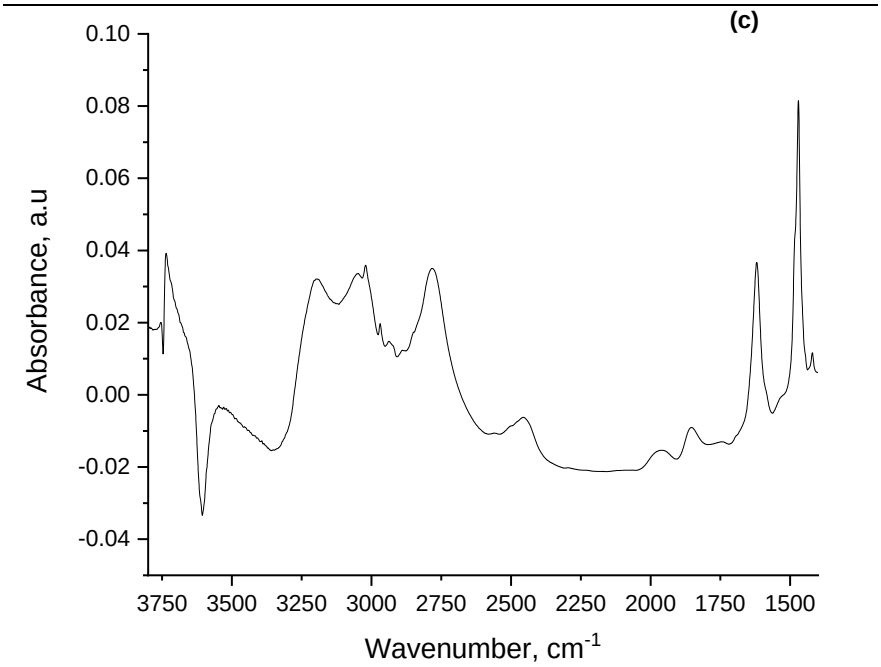

Fig. 5.7: **(a)** Infrared spectra of sample B and C activated at 300 °C. Sample C is the TAP-decomposed ZSM-5 zeolite while sample B is sample C subjected to 10 min of a step response cycle of 5 vol% DME at 370 °C, **(b)** Infrared spectra of sample A and B activated at 350 °C; **(c)** Difference spectrum of sample A activated at 350 °C minus sample B activated at 350 °C. Sample A is sample C subjected to multiple step response cycles of 5 vol% DME at 370 °C while sample B is sample C subjected to 10 min of a step response cycle of 5 vol% DME at 370 °C.

Fig. 5.7a shows that at very short time on stream, only the 1470 cm^{-1} can be readily distinguished. This corresponds to the beginning of the induction period and could be associated with the formation of the first C-C bond. Fig. 5.7b compares spectrum of samples A and B activated at 350 °C. The difference spectrum (Fig. 5.7c) shows the growth of major adsorbed species at 1483 and 1470 cm^{-1}. A decrease in intensity of bridging Si-OH-Al groups is observed. The band at 1620 cm^{-1} is due to OH deformation vibrations probably due to methanol (59). The appearance of a 1470 cm^{-1} band with a 1480 cm^{-1} shoulder has been previously attributed to alkenyl carbenium ion adsorption over ZSM-5 catalysts which could be attributed to the adsorption of methanol, propylene or butadiene (60). These bands are all persistent up until 450 °C as shown in Fig. S10c and are in accordance with the desorption profiles shown in Fig. 5.6. The 2900 and 2440 cm^{-1} bands refer to antisymmetric and symmetric stretching OH vibrations of protonated methanol molecules (59). As shown in ref. (34) and section 5.3.5, methanol desorbs at lower temperatures and propylene desorbs at temperatures lower than 350 °C (61). Thus, the adsorbed specie could be a diene as its conversion is also followed by the formation of alkenyl cations on ZSM-5 catalysts (60). The difference spectrum of sample A and B activated at 350 °C corresponds to the difference between the start of the induction period and a fully established working catalyst. The data suggest that dienes could be prominent in this region.

TPD-IND shows that components of dissociated dienes and DMM could be involved in the induction period (Fig. S5.8). Literature provides evidence for both compounds as intermediates during the induction period (13, 14, 22, 23). Further investigations on the IR spectrum of DMM and hexadiene were carried out separately.

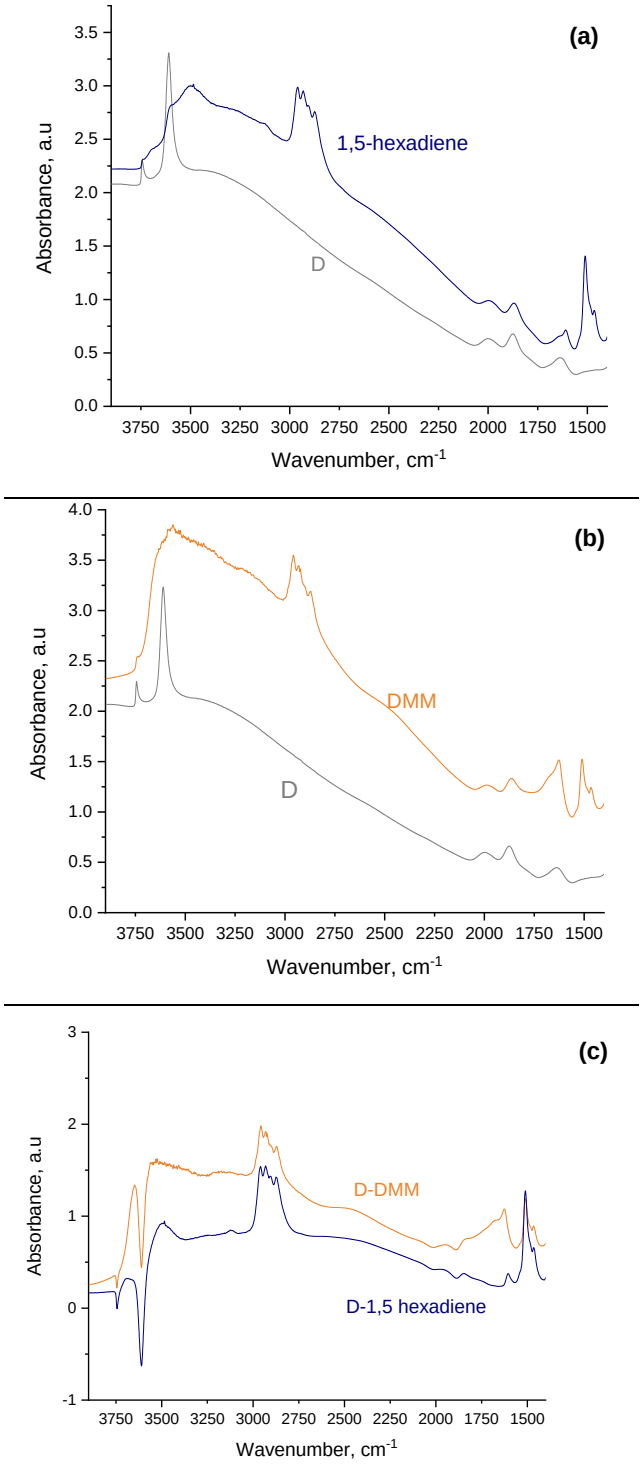

Fig. 5.8: (a) Infrared spectra of sample D after activating at 450 °C before and after adsorption of 1,5-hexadiene at 370 °C; **(b)** Infrared spectra of sample D after activating at 450 °C and sample D adsorbed with DMM at 370 °C; **(c)** Difference spectra between sample D adsorbed with 1,5-hexadiene and pure sample D at 370 °C and between sample D adsorbed with DMM and pure sample D at 370 °C. Sample D is the ammonium-form of ZSM-5 (11.5).

Fig. 5.8 shows the infrared spectra of sample D after heating at 450 °C and sample D with adsorbed 1,5-hexadiene (Fig. 5.4a) and DMM (Fig. 5.4b). A comparison of Fig. 5.8c to Fig. 5.7c shows that the IR spectrum are comparable in the region of persistent occluded species in the ZSM-5 (1470 – 1490 cm^{-1}) as the zeolite transitions through the induction period to its working state.

5.3.5. Reactive seeding in the TAP reactor over ZSM-5 (11.5) catalysts

Further experiments were carried out to investigate the effect of 1,5-hexadiene and DMM on a step response of DME in the TAP reactor. Reactive seeding in the TAP reactor was implemented by conducting two step response cycles with different feeds (consecutive step response): the first step-up/steady-flow cycle using the precursor (DMM or 1,5-hexadiene) and the second step response cycle using 5 vol% DME at 300 °C.

As a baseline study, 5 vol% DME over 10 mg of fresh ZSM-5 (11.5) gave an induction period of 20 min at 300 °C in a single step response cycle. To compare DMM to 1,5-hexadiene, equimolar carbon input of the precursor was used. A step response of 2.5 vol% of 1,5-hexadiene was carried out on the reactor for 5, 15 and 90 min giving molar carbon input of 2.1, 6.53 and 39.2 µmol respectively followed by a step response of 5 vol% DME over the ZSM-5 (11.5) catalyst. Also, a step response of 5 vol% of DMM was carried out for 5 min giving a molar carbon input of 1.9 µmol followed by a step response of 5 vol% DME over ZSM-5 (11.5). Thus, DMM can be compared to 1,5-hexadiene after having seeded both precursors for 5 min each, while the effect of increasing molar carbon input can be observed with 1,5-hexadiene.

The molar flowrate of propylene effluent, on seeding with DMM for 5 min, show similar profile shape as with the single step response cycle of DME (Fig. 5.9a). On addition of 1,5-hexadiene, the propylene effluent molar flowrate shows a different relaxation behaviour (although still exhibiting its logistic characteristics) to the single step response cycle of DME. DME and water reach their steady-state concentrations fastest with DMM compared to 1,5-hexadiene (Figs. 5.9b and 5.9c). Fig. 5.9b shows that increasing precursor seeding time changes the water profile gradually from an overshoot to a monotonic profile. At 300 °C, propylene is the major olefin formed (Figs. 5.1 and 5.9a). The S-shaped profile in Fig. 5.9a can be analysed with a logistic (sigmoidal) function, which is used to estimate phenomenological parameters (*vide infra*).

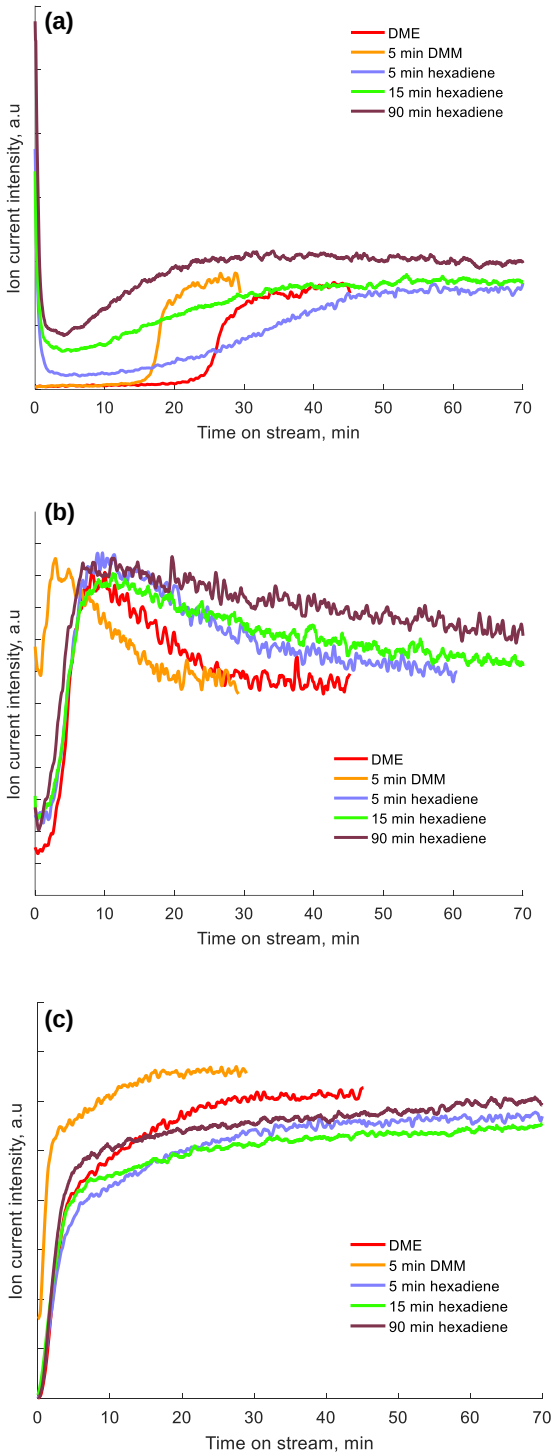

Fig. 5.9: Comparison of (a) induction times of propylene formation, (b) overshoot in water profiles and (c) time required for DME to reach steady-state after its introduction in argon only (-), after introduction of a first step response cycle of 2.5 vol% 1,5-hexadiene for 5 (-), 15 (-) and 90 (-) min followed by a step response of 5 vol% DME in argon, after introduction of a first step response cycle of 5 vol% DMM for 5 min followed by a step response of 5 vol% DME in argon (-) over ZSM-5. Water is formed during the initial induction of 5 vol% DMM for 5 min. Propylene is formed during the first step response of 2.5 vol% of 1,5-hexadiene. For brevity, only the effluents of the second step response cycle is shown.

5.4. Discussion

5.4.1. Step response study

The TAP reactor offers a low detection limit and an unperturbed measurement of signal intensities due to the direct placement of the measuring probe in the detection chamber. The decrease in the contribution of re-adsorption phenomena under vacuum conditions and the removal of extra-particle mass transfer demonstrates its immense benefit (34, 62, 63).

A slow build-up of a steady pool of intermediates and their reaction to propylene occur during the first step response cycle (Fig. 5.1). The reaction of the DME feed with the occluded pool of intermediates is initiated during subsequent step response cycles. Heavier species are formed in the pores of the zeolite compared to that observed in the gas phase (Fig. 5.6). Therefore, the first cycle must involve intrinsic and extrinsic relaxation (35) describing the innate mechanism and pore chemistry respectively while the second cycle involves intrinsic relaxation only. The data provides further evidence, in agreement with Haw and co-workers (24), that the reaction of DME on a working catalyst eliminates the induction period.

DME dissociates initially on acid sites and leads to the formation of surface methoxy species and methanol. Methanol further dissociates leading to surface methoxy species and water (12, 34, 64) or equilibrate leading to DME and water. Together, DME forms surface methoxy species, methanol and water. On further reaction, surface methoxy species are converted into hydrocarbons and regenerate the active site (16, 17, 65). The overshoot in Fig. 5.1, previously observed by Dewaele et al. (49), can be explained by two competing factors: (1) the generation of surface methoxy species, methanol and water release and (2) the consumption of these methoxy groups towards hydrocarbon formation. This behaviour has been explained before by Kobayashi et al. (37-39).

On the subsequent step cycles, the pool of intermediates is present and reacts with the DME feed such that no overshoots are observed and propylene forms faster. Reduction of the induction period in subsequent step cycles could also occur through further reactions such as hydrogen transfer between methanol and olefins (66-69) or between olefins (70, 71) and methylation (67, 69, 72-74) chemistries.

Overshoots in water and methanol profiles were observed as the DME feed reaches its steady-state flow. This overshoot profile is maintained on addition of carbon monoxide or hydrogen. A drop in k_a and k_i values of water and methanol profiles was obtained on the addition of carbon monoxide signifying a faster rise and fall respectively compared to the DME feed. The addition of hydrogen increases the k_a values of the water and methanol profiles signifying a slower rise onto the maximum overshoot point compared to the DME feed. k_i values of water and methanol profiles are reduced on addition of hydrogen to the DME feed.

H_a and H_i for the water profiles are higher and lower respectively on addition of carbon monoxide and hydrogen to the DME feed.

The period during which the overshoot profiles are observed by methanol and water effluent corresponds to the initial generation of surface intermediates followed by their conversion into secondary intermediates and hydrocarbons. DME rises rapidly followed by a slow rise onto steady-state. The initial rapid DME rise is observed on multiple step response cycles, while the slower rise is absent on the subsequent step response cycles. The absence of the slower rise in subsequent step response cycles signify that in the first step response cycle, the zeolite pores are being transformed from a fresh catalyst to a working catalyst. This transformation is absent on subsequent step response cycles. The earlier rapid DME rise is due to adsorption and very fast desorption rates associated with water, methanol and possible surface methoxy specie formation. Subsequently, during the slow DME rise, DME reacts with water, methanol, surface methoxy groups to generate secondary intermediates in the induction period with a possible decrease in desorption rates due to occlusion of hydrocarbons in the pores. Thus, the rise results in the generation of primary intermediates (water, methanol, surface methoxy groups) and the fall in overshoot results in the consumption of intermediates. Carbon monoxide results in the rapid generation and rapid consumption of surface intermediates during the conversion of dimethyl ether to olefins. However, while the addition of hydrogen results in the rapid generation of surface intermediates, their consumption is slow compared to a DME only feed.

The Hill function that describes DME profiles is the same as the BiHill function without its consuming components. Thus, only the rise of DME to steady-state effluent flow rate is described. The addition of carbon monoxide increases the rate at which DME reaches the steady-state value while hydrogen barely makes a difference. The period before steady-state values are reached are inversely proportional to n. As shown in the figure above, this period is similar on addition of carbon monoxide or hydrogen to the feed and lower than for a DME feed alone.

Multiple cycling gives similar effects in all three experiments (DME only, DME/CO and DME/H_2). The induction period in propylene formation is eliminated on the second and subsequent cycles. DME rises rapidly onto its steady-state values and no overshoots in methanol or water are observed.

5.4.2. TPD study

DMM decomposes on ZSM-5 catalysts to give formaldehyde, carbon monoxide and DME (14, 75). Propylene forms after DME and formaldehyde are fully desorbed (Fig. S5.8a). In comparison to the desorption of DME (34) and the low activation energies of desorption of CO (76), propylene could have been formed from: (a) an oligomer of formaldehyde or (b) an intermediate formed from the reaction of DME and formaldehyde leading to propylene.

Trioxane, an oligomer of formaldehyde, could form propylene. However, this would require ring breaking of C-O and forming of C-C in propylene and high activation barriers. Alternatively, in-situ generation of surface methoxy groups could occur during the induction period (16, 22, 77-82). These surface methoxy groups could react with DME to form methoxy methyl cation and other oxygenates (such as formaldehyde, DMM and dimethoxyethane) leading to propylene formation (40, 44, 83).

Fig. S5.8b shows the desorption profile of 1,5-hexadiene. The low temperature desorption profile is typical of molecular adsorption while the high temperature desorption profile indicates dissociative adsorption. The dissociative adsorption profile of 1,5-hexadiene indicates the presence of lighter products (43).

DMM and 1,5-hexadiene were further examined through FTIR and used as precursors in the TAP reactor.

5.4.3. FTIR study and seeding with precursors in the TAP reactor

Fig. 3c shows the IR spectrum of sample A minus sample B at 350 °C. This difference spectrum shows the change in adsorbed species as the zeolite transforms from the induction period to its working state. The hydrocarbon pool components can be obtained by the analysis of this spectrum. The IR spectrum of the hydrocarbon-occluded zeolite (Fig. 5.7c) within the 1400 – 1500 cm^{-1} region is comparable to the IR spectrum of adsorbed 1,5-hexadiene (Fig. 5.8a) or DMM (Fig. 5.8b) on a fresh zeolite. This indicates that either 1,5-hexadiene or DMM forms propylene in some similar steps with DME. As a result, no differentiation can be made based on FTIR alone.

Fig. 5.9 shows the effect of adding precursors to the ZSM-5 catalyst before feeding DME. Fig. 5.9 shows that precursors react with components of the active pool altering the dynamics of their generation and transformation. This is seen in Fig. 5.9b as the seeding time of 1,5-hexadiene is increased from 5 min to 90 min and the overshoot leads to a monotonic profile. The propylene effluent maintains an S-shaped profile irrespective of added precursors. A detailed analysis of the S-shaped profile of propylene with and without precursors was carried out using equations 5.2 and 5.3.

Table 5.4: Induction times and growth rate constants over ZSM-5 (11.5) catalysts

Precursor	Seeding time of precursor (min)	Molar carbon input of precursor (µmol)	t_{ind} (min)	k (min^{-1})
None	-	-	23.2	0.63
DMM	5	1.90	15.9	1.02
1,5-hexadiene	5	2.10	14.8	0.15
1,5-hexadiene	15	6.53	4.28	0.18
1,5-hexadiene	90	39.2	1.07	0.26

As a baseline study, 5 vol% DME over 10 mg of fresh ZSM-5 (11.5) catalysts gives an induction period and growth rate of 23 min and 0.63 min^{-1} at 300 °C respectively in a single step response cycle. This is half the induction period obtained and twice the growth rate of the transition regime of the hydrocarbon pool over 10 mg of ZSM-5 (25) at 300 °C suggesting a relationship between the number of active sites, induction period and the rate at which the hydrocarbon pool is established at constant molar flowrate in accordance with Qi et al. (29). The induction time reduces by 31 and 36% with roughly equimolar carbon input of dimethoxymethane and 1,5-hexadiene respectively (table 5.4). However, while DMM increases the growth rate of the transition-regime of hydrocarbon pool formation, 1,5-hexadiene attenuates it. The growth rate increases further with increasing seeding time of 1,5-hexadiene while the induction period drops by 73% after 90 min.

5.4.4. Reaction scheme for propylene formation

Following the S-shaped propylene profile described by the logistic (sigmoidal) function, the reaction scheme is envisioned in terms of a nucleus (dimethoxyethane), formed during the induction stage, which undergoes autocatalysis leading to propylene formation.

Stage	Scheme	Refs.
Induction	**i1**: $CH_3OCH_3 + HZ \rightleftharpoons CH_3 \cdot Z + CH_3OH$ **i2**: $CH_3OH + HZ \rightleftharpoons CH_3 \cdot Z + H_2O$ **i3**: $CH_3OH + CH_3 \cdot Z \rightleftharpoons CH_3OCH_3 + HZ$	(34, 64)
	i4: $CH_3 \cdot Z + CH_3OH \rightarrow CH_2O \cdot HZ + CH_4$ **i5**: $CH_3OH \rightarrow CO + 2H_2$	(11, 14, 49)
	i6: $CH_2O \cdot HZ + 2CH_3OH \rightleftharpoons CH_3OCH_2OCH_3 + H_2O \cdot HZ$	(84, 85)
	i7: $CH_3OCH_2OCH_3 \cdot HZ \rightarrow CH_2O \cdot HZ + CH_3OCH_3$ **i8**: $CH_3OCH_2OCH_3 \cdot HZ + CO \rightarrow CH_3OCH_2COOCH_3 \cdot HZ$ **i9**: $CH_3OCH_2COOCH_3 \cdot HZ + 2H_2 \rightarrow CH_3OCH_2CH_2OH \cdot HZ + CH_3OH$ **i10**: $CH_3OCH_2CH_2OH \cdot HZ + H_2O \rightarrow HOCH_2CH_2OH \cdot HZ + CH_3OH$ **i11**: $CH_3OCH_2CH_2OH \cdot HZ + CH_3OH \rightarrow CH_3OCH_2CH_2OCH_3 \cdot HZ + H_2O$ **i12**: $OHCH_2CH_2OH \cdot HZ + CH_3OCH_3 \rightarrow CH_3OCH_2CH_2OCH_3 \cdot HZ + H_2O$	(14, 75, 86-88)
Growth	**g1**: $CH_3OCH_2CH_2OCH_3 + CH_3 \cdot Z \rightarrow CH_2CHOCH_3 + CH_3OCH_3 + HZ$ **g2**: $CH_2CHOCH_3 + CH_3 \cdot Z \rightarrow CH_3CHCHOCH_3 + HZ$ **g3**: $CH_3CHCHOCH_3 + CH_3 \cdot Z \rightarrow CH_3OCH_2 \cdot Z + CH_2CHCH_3$	(83)

Scheme 5.1: Proposed pathway towards propylene formation from DME. *HZ is a Brønsted acid site. For brevity, the adsorption and desorption of all species except methanol and DME were omitted.

DME dissociation leading to methanol and surface methoxy species, further methanol dissociation leading to adsorbed surface methoxy species and water release as well as the equilibration reaction (steps i1-i3) readily occur on feeding DME over ZSM-5 catalysts (3, 64).

Methane and formaldehyde have been observed during methanol transformation over ZSM-5 catalysts at low temperatures and conversions (26, 49). Even on silicalite, Liu et al. (14) observed the formation of carbon monoxide, hydrogen, methane and formaldehyde from methanol. Steps i4-i5 represent the formation of these products.

Dimethoxymethane is formed from formaldehyde and methanol in step i6 through a series of sub-steps including carbonyl protonation, nucleophilic attack by the alcohol and water release (84, 85).

Dimethoxymethane decomposes on ZSM-5 to give formaldehyde, carbon monoxide and DME (Fig. S8a). This has been observed by Fu et al. (75) and Liu et al. (14). Studies with DMM should indicate the added reactions of carbon monoxide and formaldehyde to DME.

Steps i7-i10 show chemistries that involve carbon monoxide, hydrogen, DMM and water leading to methyl methoxy acetate, 2-methoxy ethanol and ethylene glycol formation respectively. Seeding with DMM (Fig. 5.9a) or co-feeding DME with carbon monoxide or hydrogen (table 5.1) reduces the induction period. Steps i11 and i12 describe observations on multi-step response cycles. Once the necessary intermediates are formed (surface methoxy species, DMM etc), re-introducing a DME or methanol feed reduces the induction period. Thus, the induction period of propylene formation is reduced because increasing the concentrations of carbon monoxide, hydrogen, DMM, DME or methanol decreases the time required to form the envisaged nucleus (dimethoxyethane).

Fan and co-workers (83) provided DFT evidence for every step (g1-g3) in the growth phase leading to propylene formation from dimethoxyethane. Adding DMM as a precursor would increase the amount of dimethoxyethane formed which would further increase the growth stage of propylene formation. Dimethoxyethane could also lead to ethylene formation (83). According to the reaction scheme, DMM could lead independently to propylene formation without any added DME. This was observed during the reactive decomposition of DMM as shown in Fig. S5.8a.

The S-shaped propylene profile showing logistic (sigmoidal) behaviour occurs because there is a build-up of methoxy species in the induction stage followed by a depletion of methoxy species in the growth stage. DMM hastens the growth stage probably because it increases the rate of depletion of these methoxy species during the growth stage and the converse occurs for 1,5-hexadiene. Hexadiene breaks down to give propylene over ZSM-5 catalysts (Fig. S5.8b) in the first step response cycle and the already formed propylene could react to form higher olefin homologues over ZSM-5 catalysts such that the growth rate of propylene as observed in Fig. 5.9a is reduced. Furthermore, Kobayashi (37) showed that the S-shaped profile is due to the presence of stable intermediates. These intermediates could include methyl methoxy acetate, 2-methoxy ethanol, ethylene glycol, dimethoxymethane and dimethoxyethane.

While TPD and FTIR could not distinguish the relevant precursor, reactive seeding in the TAP reactor gives proof that DMM is the dominant intermediate during olefin formation from propylene. The dual-cycle can be initiated through the olefin cycle once propylene is formed at low temperatures. Thus, the proposed mechanism activated under transient conditions could precede the dual-cycle model operating under steady-state conditions.

Future work would investigate the synergetic effects of Lewis acid sites and Brønsted acid sites for initial C-C bond and primary olefin formation during MTO conversion and the use of NMR to determine key intermediates.

5.5. Conclusions

The induction period of the conversion of dimethyl ether to primary olefins over ZSM-5 catalysts has been studied in a temporal analysis of products reactor at 300 °C. Propylene was observed as the primary olefin. A 44 min induction period is observed in the first step response cycle and is eliminated on the second and subsequent step response cycles.

FTIR analysis of the hydrocarbon-occluded ZSM-5 catalyst obtained after step response shows a similar spectrum (1400 – 1500 cm^{-1}) as pre-adsorbed dimethoxymethane or 1,5-hexadiene on a fresh ZSM-5 catalyst indicating that they both could be reactive precursors. An equal reduction in induction time of propylene formation was obtained on equimolar addition of 1,5-hexadiene or dimethoxymethane. However, while dimethoxymethane accelerates the formation of propylene, 1,5-hexadiene attenuates its growth.

As propylene displays an S-shaped profile similar to the logistic (sigmoidal) behaviour observed with crystal nucleation, these results were explained by a reaction mechanism where the addition of precursors such as dimethoxymethane, carbon monoxide and hydrogen reduce the induction period because they decrease the time required to form an envisioned nucleus (dimethoxyethane). These precursors also accelerate the growth rate of propylene formation because they increase the rate of reaction of dimethoxyethane to give propylene. On this basis, the direct mechanism is the most probable route towards primary olefin fromation.

5.6. Notes

All data supporting this study is provided as supplementary information accompanying this chapter.

5.7. References

1. Tian P, Wei Y, Ye M, Liu Z. Methanol to olefins (MTO): From fundamentals to commercialization. ACS Catalysis. 2015;5(3):1922-38.
2. Svelle S, Kolboe S, Swang O, Olsbye U. Methylation of Alkenes and Methylbenzenes by Dimethyl Ether or Methanol on Acidic Zeolites. The Journal of Physical Chemistry B. 2005;109(26):12874-8.
3. Svelle S, Visur M, Olsbye U, Saepurahman, Bjørgen M. Mechanistic aspects of the zeolite catalyzed methylation of alkenes and aromatics with methanol: A review. Top Catal. 2011;54(13-15):897-906.
4. Goguen PW, Xu T, Barich DH, Skloss TW, Song W, Wang Z, et al. Pulse-quench catalytic reactor studies reveal a carbon-pool mechanism in methanol-to-gasoline chemistry on zeolite HZSM-5. J Am Chem Soc. 1998;120(11):2650-1.
5. Song W, Marcus DM, Fu H, Ehresmann JO, Haw JF. An oft-studied reaction that may never have been: Direct catalytic conversion of methanol or dimethyl ether to hydrocarbons on the solid acids HZSM-5 or HSAPO-34. J Am Chem Soc. 2002;124(15):3844-5.
6. Haw JF, Song W, Marcus DM, Nicholas JB. The Mechanism of Methanol to Hydrocarbon Catalysis. Acc Chem Res. 2003;36:317-26.

7. Dahl IM, Kolboe S. On the reaction mechanism for propene formation in the MTO reaction over SAPO-34. Catal Lett. 1993;20(3-4):329-36.
8. Dahl IM, Kolboe S. On the Reaction Mechanism for Hydrocarbon Formation from Methanol over SAPO-34. I. Isotopic Labeling Studies of the Co-Reaction of Ethene and Methanol. J Catal. 1994;149(2):458-64.
9. Dahl IM, Kolboe S. On the reaction mechanism for hydrocarbon formation from methanol over SAPO-34: 2. Isotopic labeling studies of the Co-reaction of propene and methanol. J Catal. 1996;161(1):304-9.
10. Lesthaeghe D, Van Speybroeck V, Marin GB, Waroquier M. Understanding the failure of direct C-C coupling in the zeolite-catalyzed methanol-to-olefin process. Angewandte Chemie - International Edition. 2006;45(11):1714-9.
11. Lesthaeghe D, Van Speybroeck V, Marin GB, Waroquier M. The rise and fall of direct mechanisms in methanol-to-olefin catalysis: An overview of theoretical contributions. Ind Eng Chem Res. 2007;46(26):8832-8.
12. Yamazaki H, Shima H, Imai H, Yokoi T, Tatsumi T, Kondo JN. Direct production of propene from methoxy species and dimethyl ether over H-ZSM-5. Journal of Physical Chemistry C. 2012;116(45):24091-7.
13. Chowdhury AD, Houben K, Whiting GT, Mokhtar M, Asiri AM, Al-Thabaiti SA, et al. Initial Carbon–Carbon Bond Formation during the Early Stages of the Methanol-to-Olefin Process Proven by Zeolite-Trapped Acetate and Methyl Acetate. Angewandte Chemie - International Edition. 2016;55(51):15840-5.
14. Liu Y, Müller S, Berger D, Jelic J, Reuter K, Tonigold M, et al. Formation Mechanism of the First Carbon-Carbon Bond and the First Olefin in the Methanol Conversion into Hydrocarbons. Angewandte Chemie - International Edition. 2016;55(19):5723-6.
15. Yamazaki H, Shima H, Imai H, Yokoi T, Tatsumi T, Kondo JN. Evidence for a "carbene-like" intermediate during the reaction of methoxy species with light alkenes on H-ZSM-5. Angewandte Chemie - International Edition. 2011;50(8):1853-6.
16. Wang W, Buchholz A, Seiler M, Hunger M. Evidence for an Initiation of the Methanol-to-Olefin Process by Reactive Surface Methoxy Groups on Acidic Zeolite Catalysts. J Am Chem Soc. 2003;125(49):15260-7.
17. Wang W, Seiler M, Hunger M. Role of surface methoxy species in the conversion of methanol to dimethyl ether on acidic zeolites investigated by in situ stopped-flow MAS NMR spectroscopy. J Phys Chem B. 2001;105(50):12553-8.
18. Svelle S, Joensen F, Nerlov J, Olsbye U, Lillerud KP, Kolboe S, et al. Conversion of methanol into hydrocarbons over zeolite H-ZSM-5: Ethene formation is mechanistically separated from the formation of higher alkenes. J Am Chem Soc. 2006;128(46):14770-1.
19. Haw JF, Nicholas JB, Song W, Deng F, Wang Z, Xu T, et al. Roles for cyclopentenyl cations in the synthesis of hydrocarbons from methanol on zeolite catalyst HZSM-5. J Am Chem Soc. 2000;122(19):4763-75.
20. Wulfers MJ, Jentoft FC. The role of cyclopentadienium ions in methanol-to-hydrocarbons chemistry. ACS Catalysis. 2014;4:3521-32.
21. Dai W, Wang C, Dyballa M, Wu G, Guan N, Li L, et al. Understanding the Early Stages of the Methanol-to-Olefin Conversion on H-SAPO-34. ACS Catalysis. 2015;5(1):317-26.
22. Nováková J, Kubelková L, Dolejšek Z. Primary reaction steps in the methanol-to-olefin transformation on zeolites. J Catal. 1987;108(1):208-13.
23. Chang CD, Silvestri AJ. The conversion of methanol and other O-compounds to hydrocarbons over zeolite catalysts. J Catal. 1977;47(2):249-59.
24. Song W, Haw JF, Nicholas JB, Heneghan CS. Methylbenzenes are the organic reaction centers for methanol-to-olefin catalysis on HSAPO-34. J Am Chem Soc. 2000;122(43):10726-7.
25. Song W, Nicholas JB, Haw JF. A persistent carbenium ion on the methanol-to-olefin catalyst HSAPO-34: Acetone shows the way. J Phys Chem B. 2001;105(19):4317-23.

26. Qi L, Wei Y, Xu L, Liu Z. Reaction Behaviors and Kinetics during Induction Period of Methanol Conversion on HZSM-5 Zeolite. ACS Catalysis. 2015;5(7):3973-82.
27. Langner BE. Reactions of methanol on zeolites with different pore structures. Applied Catalysis. 1982;2(4):289-302.
28. Qi L, Li J, Wei Y, Xu L, Liu Z. Role of naphthalene during the induction period of methanol conversion on HZSM-5 zeolite. Catalysis Science and Technology. 2016;6(11):3737-44.
29. Qi L, Li J, Wei Y, He Y, Xu L, Liu Z. Influence of acid site density on the three-staged MTH induction reaction over HZSM-5 zeolite. RSC Advances. 2016;6(57):52284-91.
30. Lee KY, Chae HJ, Jeong SY, Seo G. Effect of crystallite size of SAPO-34 catalysts on their induction period and deactivation in methanol-to-olefin reactions. Applied Catalysis A: General. 2009;369(1-2):60-6.
31. Nielsen L, Khurana R, Coats A, Frokjaer S, Brange J, Vyas S, et al. Effect of environmental factors on the kinetics of insulin fibril formation: Elucidation of the molecular mechanism. Biochemistry. 2001;40(20):6036-46.
32. Arosio P, Knowles TPJ, Linse S. On the lag phase in amyloid fibril formation. PCCP. 2015;17(12):7606-18.
33. Shoffner SK, Schnell S. Estimation of the lag time in a subsequent monomer addition model for fibril elongation. PCCP. 2016;18(31):21259-68.
34. Omojola T, Cherkasov N, McNab AI, Lukyanov DB, Anderson JA, Rebrov EV, et al. Mechanistic Insights into the Desorption of Methanol and Dimethyl Ether Over ZSM-5 Catalysts. Catal Lett. 2018;148(1):474-88.
35. Temkin MI. Relaxation rate of a 2-stage catalytic reaction. Kinet Catal. 1976;17(5):1095 - 9.
36. Shapatina EN, Kuchaev VL, Temkin MI. Relaxation of rate of ammonia synthesis. Kinet Catal. 1985;26(3):575-82.
37. Kobayashi M. Characterization of transient response curves in heterogeneous catalysis—I Classification of the curves. Chem Eng Sci. 1982;37(3):393-401.
38. Kobayashi M. Characterization of transient response curves in heterogeneous catalysis - 2. Estimation of the reaction mechanism in the oxidation of ethylene over a silver catalyst from the mode of the transient response curves. Chem Eng Sci. 1982;37(3):403-9.
39. Kobayashi M, Maeda Y, Takahashi N. Discrimination of rival kinetic models in heterogeneous catalysis by the dynamic behaviour of products. Journal of Chemical Technology and Biotechnology, Chemical Technology. 1983;33 A(4):219-26.
40. Wei Z, Chen YY, Li J, Guo W, Wang S, Dong M, et al. Stability and Reactivity of Intermediates of Methanol Related Reactions and C-C Bond Formation over H-ZSM-5 Acidic Catalyst: A Computational Analysis. Journal of Physical Chemistry C. 2016;120(11):6075-87.
41. Giannetto G, Monque R, Galiasso R. Transformation of LPG into Aromatic Hydrocarbons and Hydrogen over Zeolite Catalysts. Catalysis Reviews. 1994;36(2):271-304.
42. Naccache C. Dehydrocyclization of Alkanes Over Zeolite-Supported Metal Catalysts: Monofunctional or Bifunctional Route AU - MÉRIAUDEAU, PAUL. Catalysis Reviews. 1997;39(1-2):5-48.
43. Joshi YV, Bhan A, Thomson KT. DFT-Based Reaction Pathway Analysis of Hexadiene Cyclization via Carbenium Ion Intermediates: Mechanistic Study of Light Alkane Aromatization Catalysis. The Journal of Physical Chemistry B. 2004;108(3):971-80.
44. Olsbye U, Svelle S, Lillerud KP, Wei ZH, Chen YY, Li JF, et al. The formation and degradation of active species during methanol conversion over protonated zeotype catalysts. Chem Soc Rev. 2015;44(20):7155-76.
45. Rouquerol J, Llewellyn P, Rouquerol F. Is the BET equation application to microporous adsorbents? In: Llewellyn P, Rodriquez-Reinoso F, Rouquerol J, Seaton N, editors. Stud Surf Sci Catal. 160: Elsevier; 2007. p. 49-56.

46. Hinrischen O, van Veen AC, Zanthoff HW, Muhler M. TAP Reactor Studies. In: Haw JF, editor. In-Situ Spectroscopy in Heterogeneous Catalysis. WeinHeim: Wiley-VCH; 2002.
47. Shekhtman SO, Yablonsky GS, Chen S, Gleaves JT. Thin-zone TAP-reactor - theory and application. Chem Eng Sci. 1999;54(20):4371-8.
48. Gleaves JT, Yablonsky G, Zheng X, Fushimi R, Mills PL. Temporal analysis of products (TAP)—Recent advances in technology for kinetic analysis of multi-component catalysts. J Mol Catal A: Chem. 2010;315(2):108-34.
49. Dewaele O, Geers VL, Froment GF, Marin GB. The conversion of methanol to olefins: A transient kinetic study. Chem Eng Sci. 1999;54(20):4385-95.
50. Stein SE. Mass Spectra. In: Linstrom PJ, Mallard WG, editors. NIST Chemistry WebBook, NIST Standard Reference Database Number 69: National Institute of Standards and Technology, Gaithersburg MD, 20899.
51. Chang CD, Lang WH, Smith RL. The conversion of methanol and other O-compounds to hydrocarbons over zeolite catalysts. II. Pressure effects. J Catal. 1979;56(2):169-73.
52. Verhulst PF. Recherches mathématiques sur la loi d'accroissement de la population. Nouveaux mémoires de l'Académie Royale des Sciences et Belles-Lettres de Bruxelles. 1845;18:14-54.
53. Hill AV. The possible effects of the aggregation of the molecules of haemoglobin on its dissociation curves. The Journal of Physiology. 1910;40(suppl):i-vii.
54. Hwang A, Kumar M, Rimer JD, Bhan A. Implications of methanol disproportionation on catalyst lifetime for methanol-to-olefins conversion by HSSZ-13. J Catal. 2017;346:154-60.
55. Dai W, Dyballa M, Wu G, Li L, Guan N, Hunger M. Intermediates and dominating reaction mechanism during the early period of the methanol-to-olefin conversion on SAPO-41. Journal of Physical Chemistry C. 2015;119(5):2637-45.
56. Freitas C, Barrow NS, Zholobenko V. Accessibility and Location of Acid Sites in Zeolites as Probed by Fourier Transform Infrared Spectroscopy and Magic Angle Spinning Nuclear Magnetic Resonance. Johnson Matthey Technology Review. 2018;62(3):279-90.
57. Castellà-Ventura M, Akacem Y, Kassab E. Vibrational analysis of pyridine adsorption on the brønsted acid sites of zeolites based on density functional cluster calculations. Journal of Physical Chemistry C. 2008;112(48):19045-54.
58. Kassab E, Castellà-Ventura M. Theoretical study of pyridine and 4,4′-bipyridine adsorption on the Lewis acid sites of alumina surfaces based on ab initio and density functional cluster calculations. J Phys Chem B. 2005;109(28):13716-28.
59. Mirth G, Lercher JA, Anderson MW, Klinowski J. Adsorption complexes of methanol on zeolite ZSM-5. J Chem Soc, Faraday Trans. 1990;86(17):3039-44.
60. Demidov AV, Davydov AA. Spectroscopic evidence for the formation of carbenium ions on H-ZSM-5 zeolites. Mater Chem Phys. 1994;39(1):13-20.
61. Kondo JN, Nishioka D, Yamazaki H, Kubota J, Domen K, Tatsumi T. Activation Energies for the Reaction of Ethoxy Species to Ethene over Zeolites. Journal of Physical Chemistry C. 2010;114.
62. Kanervo JM, Kouva S, Kanervo KJ, Kolvenbach R, Jentys A, Lercher JA. Prerequisites for kinetic modeling of TPD data of porous catalysts-Exemplified by toluene/H-ZSM-5 system. Chem Eng Sci. 2015;137:807-15.
63. Redhead PA. Thermal desorption of gases. Vacuum. 1962;12(4):203-11.
64. Park TY, Froment GF. Kinetic modeling of the methanol to olefins process. 1. Model formulation. Ind Eng Chem Res. 2001;40(20):4172-86.
65. Wang W, Hunger M. Reactivity of surface alkoxy species on acidic zeolite catalysts. Acc Chem Res. 2008;41(8):895-904.
66. Müller S, Liu Y, Kirchberger FM, Tonigold M, Sanchez-Sanchez M, Lercher JA. Hydrogen Transfer Pathways during Zeolite Catalyzed Methanol Conversion to Hydrocarbons. J Am Chem Soc. 2016;138(49):15994-6003.

67. Martinez-Espin JS, De Wispelaere K, Janssens TVW, Svelle S, Lillerud KP, Beato P, et al. Hydrogen Transfer versus Methylation: On the Genesis of Aromatics Formation in the Methanol-To-Hydrocarbons Reaction over H-ZSM-5. ACS Catalysis. 2017(7):5773-80.
68. Comas-Vives A, Valla M, Copéret C, Sautet P. Cooperativity between al sites promotes hydrogen transfer and carbon-carbon bond formation upon dimethyl ether activation on alumina. ACS Central Science. 2015;1(6):313-9.
69. Martinez-Espin JS, De Wispelaere K, Westgård Erichsen M, Svelle S, Janssens TVW, Van Speybroeck V, et al. Benzene co-reaction with methanol and dimethyl ether over zeolite and zeotype catalysts: Evidence of parallel reaction paths to toluene and diphenylmethane. J Catal. 2017;349:136-48.
70. Lukyanov DB, Gnep NS, Guisnet MR. Kinetic modeling of ethene and propene aromatization over HZSM-5 and GaHZSM-5. Ind Eng Chem Res. 1994;33(2):223-34.
71. Lukyanov DB. Application of a kinetic model for investigation of aromatization reactions of light paraffins and olefins over HZSM-5. Stud Surf Sci Catal. 1997;105 B:1301-8.
72. Hill IM, Hashimi SA, Bhan A. Kinetics and mechanism of olefin methylation reactions on zeolites. J Catal. 2012;285(1):115-23.
73. Svelle S, Rønning PO, Kolboe S. Kinetic studies of zeolite-catalyzed methylation reactions: 1. Coreaction of [12C]ethene and [13C]methanol. J Catal. 2004;224(1):115-23.
74. Svelle S, Rønning PO, Olsbye U, Kolboe S. Kinetic studies of zeolite-catalyzed methylation reactions. Part 2. Co-reaction of [12C]propene or [12C]n-butene and [13C]methanol. J Catal. 2005;234(2):385-400.
75. Fu Y, Zhu H, Shen J. Thermal decomposition of dimethoxymethane and dimethyl carbonate catalyzed by solid acids and bases. Thermochim Acta. 2005;434(1-2):88-92.
76. Szanyi J, Paffett MT. The adsorption of carbon monoxide on H-ZSM-5 and hydrothermally treated H-ZSM-5. Microporous Mater. 1996;7(4):201-18.
77. Forester TR, Howe RF. In situ FTIR studies of methanol and dimethyl ether in ZSM-5. J Am Chem Soc. 1987;109(17):5076-82.
78. Forester TR, Wong ST, Howe RF. In situ Fourier transofrm I.R observation of methylating species in ZSM-5. J Chem Soc, Chem Commun. 1986(21):1611-3.
79. Ono Y, Mori T. Mechanism of methanol conversion into hydrocarbons over ZSM-5 zeolite. Journal of the Chemical Society, Faraday Transactions 1: Physical Chemistry in Condensed Phases. 1981;77(9):2209-21.
80. Nováková J, Kubelková L, Habersberger K, Dolejšek Z. Catalytic activity of dealuminated Y and HZSM-5 zeolites measured by the temperature-programmed desorption of small amounts of preadsorbed methanol and by the low-pressure flow reaction of methanol. Journal of the Chemical Society, Faraday Transactions 1: Physical Chemistry in Condensed Phases. 1984;80(6):1457-65.
81. Kubelková L, Nováková J, Nedomová K. Reactivity of surface species on zeolites in methanol conversion. J Catal. 1990;124(2):441-50.
82. Wang W, Jiang Y, Hunger M. Mechanistic investigations of the methanol-to-olefin (MTO) process on acidic zeolite catalysts by in situ solid-state NMR spectroscopy. Catal Today. 2006;113(1–2):102-14.
83. Li J, Wei Z, Chen Y, Jing B, He Y, Dong M, et al. A route to form initial hydrocarbon pool species in methanol conversion to olefins over zeolites. J Catal. 2014;317(0):277-83.
84. Carey FA, Sundberg RJ. Addition, Condensation and Substitution Reactions of Carbonyl Compounds. Advanced Organic Chemistry: Part A: Structure and Mechanisms. Boston, MA: Springer US; 2007. p. 629-711.
85. Vollhardt K, Peter C, Schore NE. Organic Chemistry: Structure and Function. New York: W.H. Freeman and Company; 2007.

86. Celik FE, Kim T-J, Bell AT. Effect of zeolite framework type and Si/Al ratio on dimethoxymethane carbonylation. J Catal. 2010;270(1):185-95.
87. Celik FE, Kim T, Mlinar AN, Bell AT. An investigation into the mechanism and kinetics of dimethoxymethane carbonylation over FAU and MFI zeolites. J Catal. 2010;274(2):150-62.
88. Yu W, Lu F, Huang Q, Lu R, Chen S, Xu J. Selective synthesis of dimethoxyethane via directly catalytic etherification of crude ethylene glycol. Green Chemistry. 2017;19(14):3327-33.

S5. Supplementary information

A Mechanistic Investigation into the Induction Period of Dimethyl Ether Conversion to Olefins over ZSM-5 Catalysts

S5.1 TAP reactor

The TAP reactor consists of three chambers connected in series: the reactor chamber, the differential chamber, and the detector chamber. The reactor chamber contains a fixed-bed reactor, 6 mm O.D. (4 mm I.D.) and 40 mm long. The reactor chamber has a cone-shaped inset for uniform radial distribution. The differential chamber acts as a cryogenic trap to eliminate scattered molecules reaching the detector chamber where the quadrupole mass spectrometer is housed. The differential chamber works as a molecular beam. Gases are introduced either through two continuous feed valves or two pulse valves into the reactor inlet. The pressure at the exit of the reactor chamber is maintained at 10^{-5} Pa while the pressure at the end of the differential chamber is 10^{-6} Pa and QMS is 10^{-7} Pa. Further detailed description of the TAP reactor used in this work can be found in ref. (1). A baking procedure was carried before and in-between experiments to remove residual water or organics in the TAP reactor.

S5.2 Blank experiments

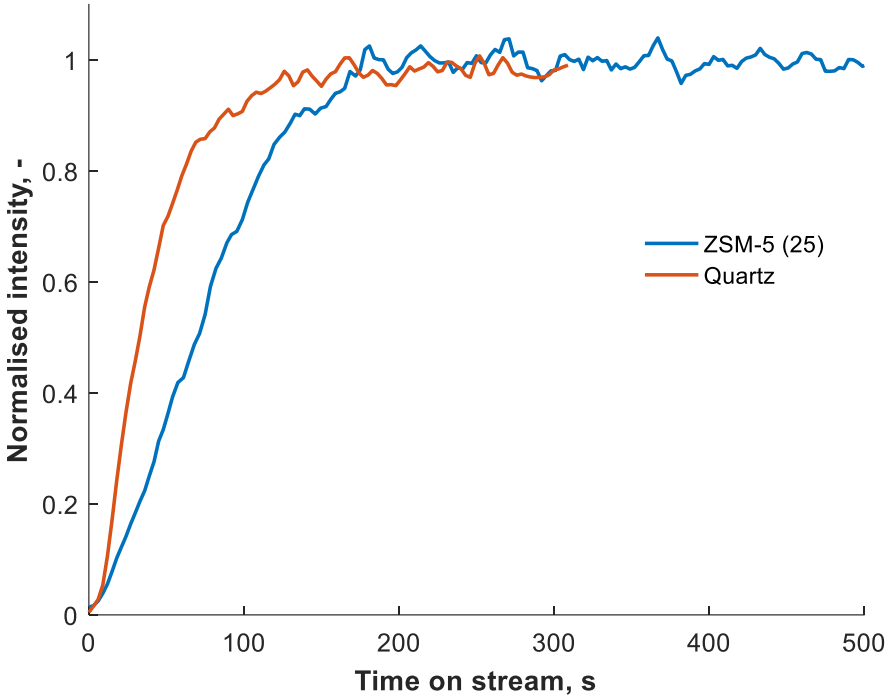

Fig. S5.2: A normalised step response of 5 vol% DME (balance argon) over ZSM-5 (25) and over an inert quartz bed, both at 450 °C.

S5.3 Characterisation

The zeolite samples were studied by X-ray diffraction (XRD) with a Bruker D5005 diffractometer using Cu K_α radiation equipped with standard Bragg-Brentano geometry and a diffracted beam graphite monochromator. The morphology was characterized using a Carl Zeiss sigma series Field Emission Scanning Electron Microscope (FE-SEM) at an accelerated voltage of 20 kV. The crystal size distribution was obtained from an image analysis software. Nitrogen physisorption studies were carried out on a Micromeritics 2020 unit. The samples were degassed by heating to 400 °C under vacuum (10^{-6} mbar) for 12 h prior to measurements. Fig. S3.1 below gives the XRD patterns of ZSM-5 (11.5) and ZSM-5 (25) used in this study.

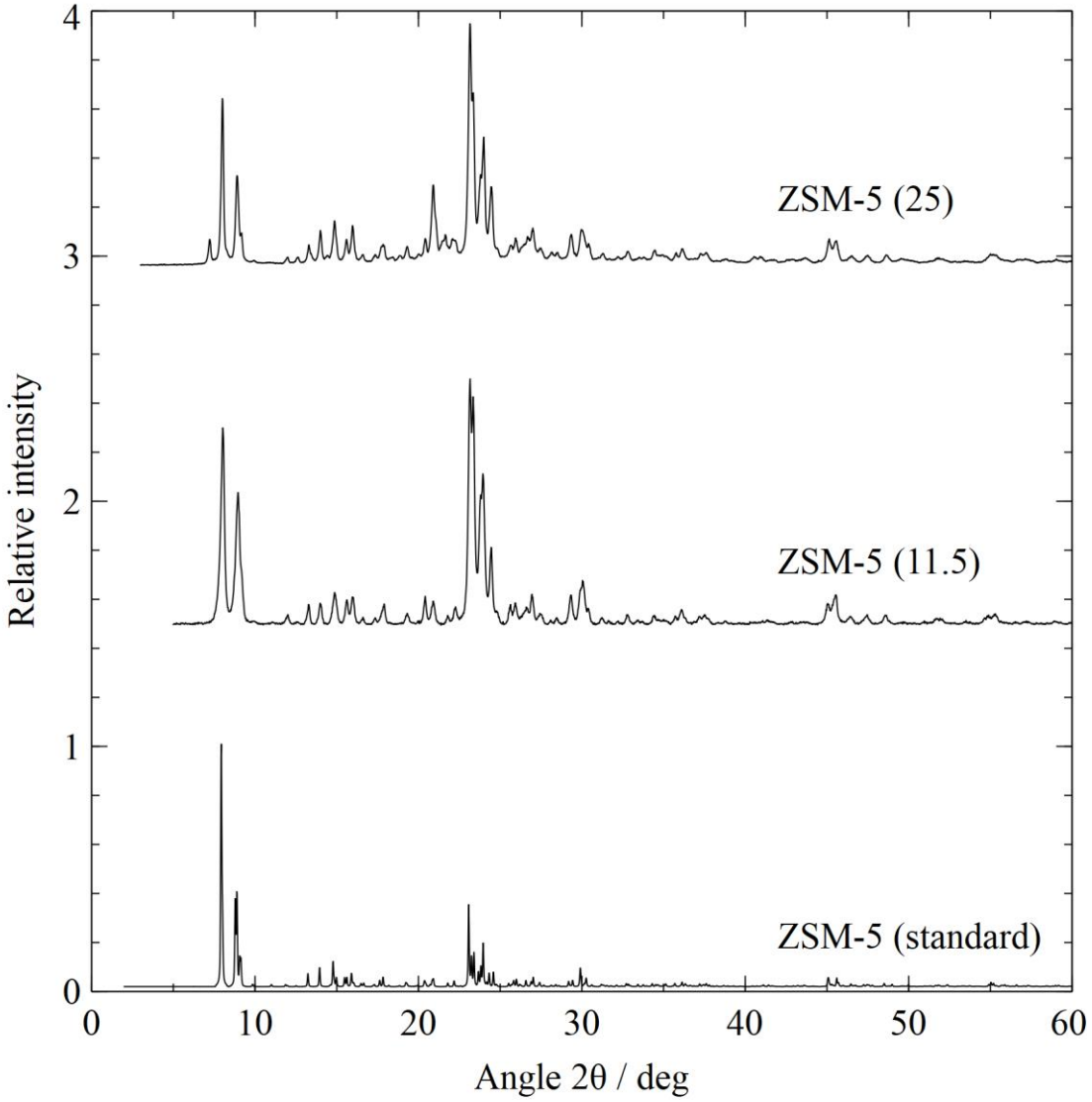

Fig. S5.3.1: XRD patterns of ZSM-5 (11.5), ZSM-5 (25) and a reference highly crystalline ZSM-5 sample (standard) obtained from the database of the International Zeolite Association (2).

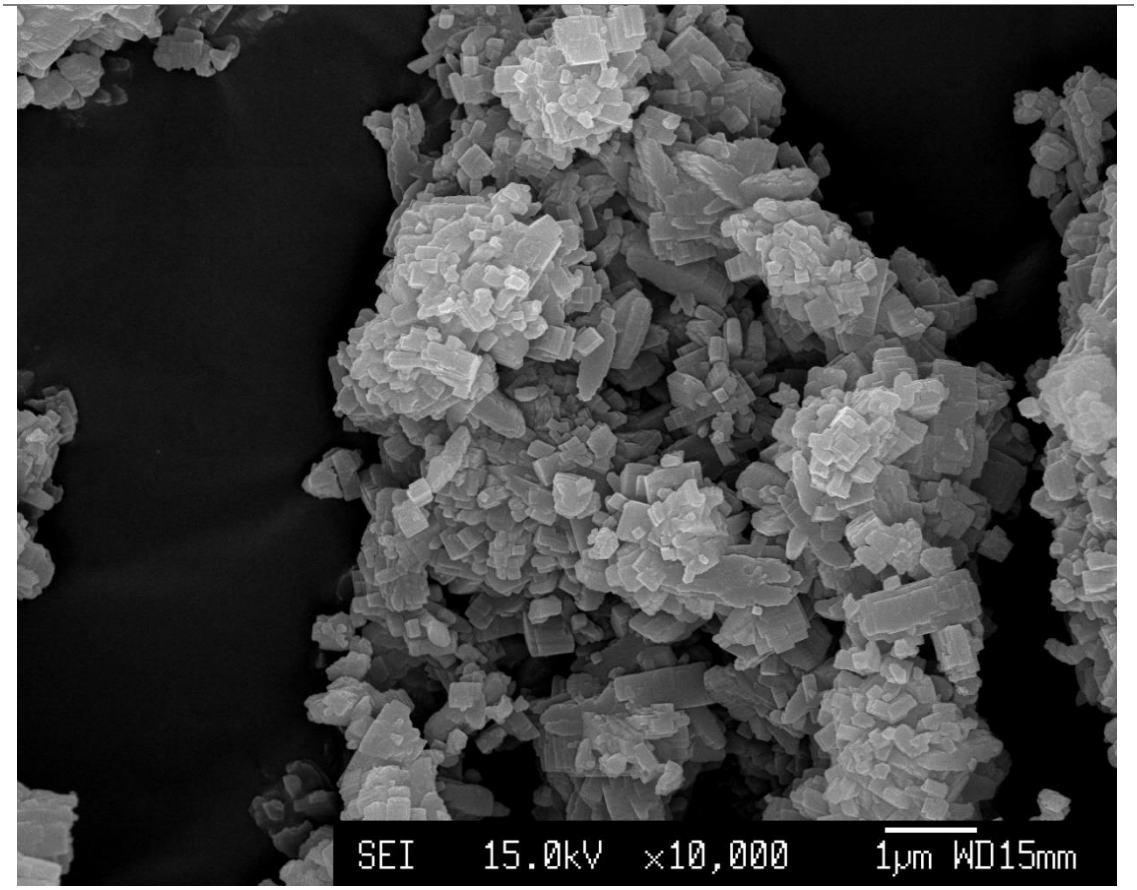

(a) ZSM-5 (11.5)

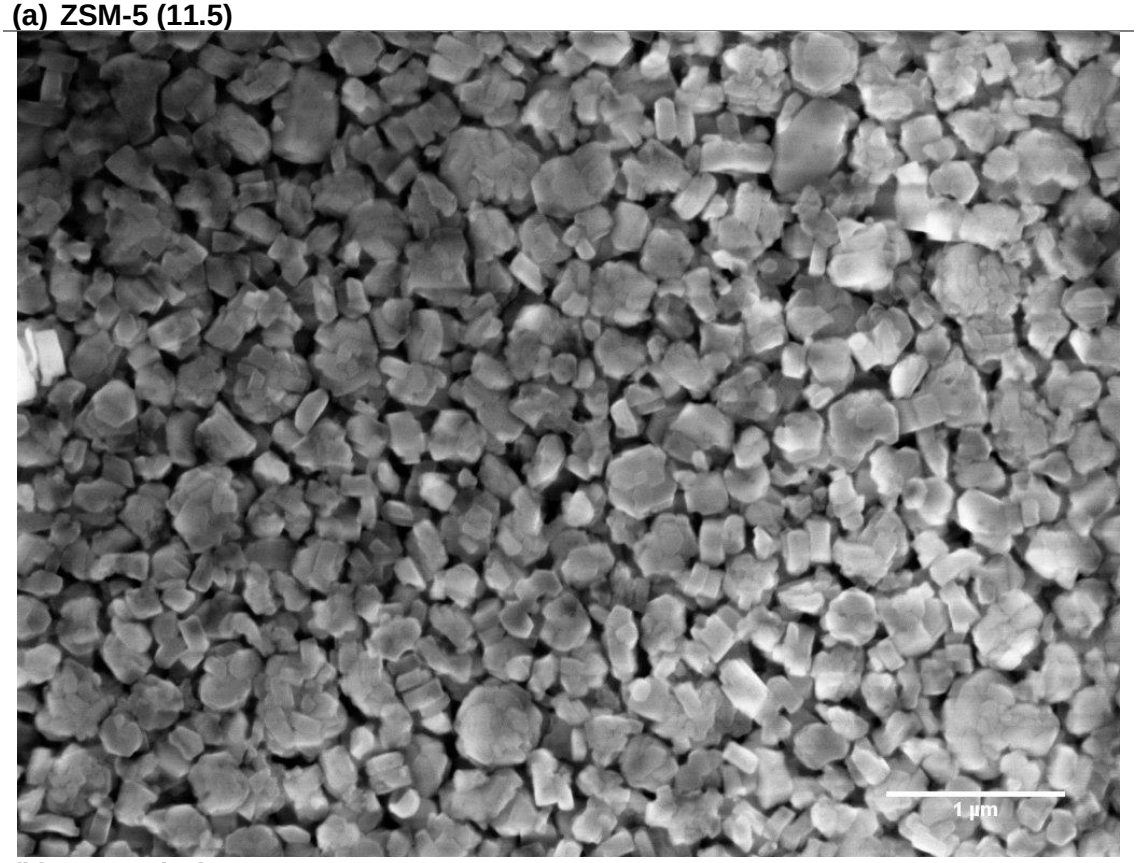

(b) ZSM-5 (25)

Fig. S5.3.2: SEM images of the zeolite particles

Thermogravimetric analysis (TGA) of the ZSM-5 (25) or ZSM-5 (11.5) catalyst powder was carried out in a Setsys Evolution TGA 16/18 instrument (SETARAM). Before each experiment, 12 mg of sample was placed into an alumina crucible held in a TGA chamber that was purged with air at 20 °C at 200 mL min^{-1} for 8 min. All gas flow rates refer to normal temperature and pressure. The experiments were performed under air flowing at 20 mL min^{-1} at a heating rate of 5 °C min^{-1} to the temperature of 600 °C.

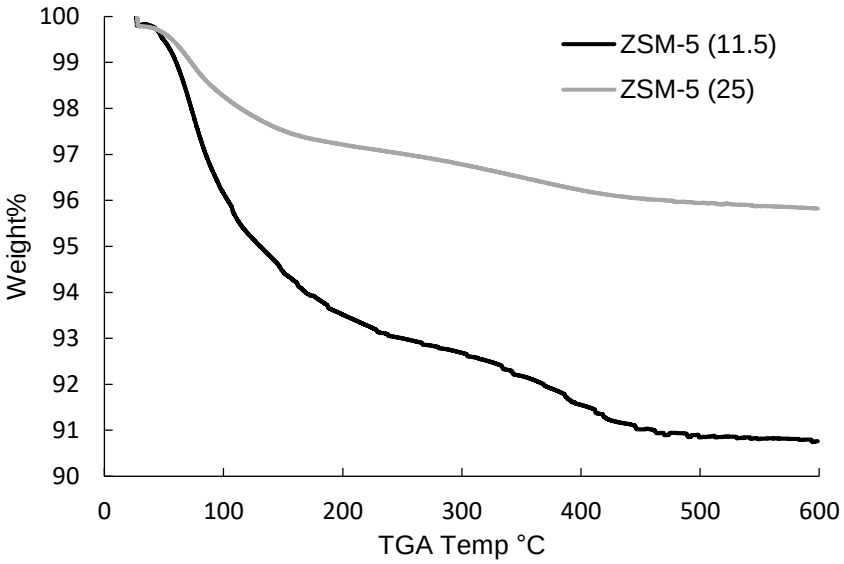

Fig. S5.3.3: TGA of ZSM-5 catalysts of Si/Al ratios of 11.5 and 25.

S5.4 Quantification

To ascertain what to quantify, the full gaseous product release during the step response cycles was obtained (see Fig. S6 below). The quantification methodology has been used before (3) and was performed in the following sequence: (1) Ion fragmentation patterns determined from calibration experiments done over a quartz bed of equal bed length and diameter to the ZSM-5 bed were obtained. Calibration experiments were conducted by passing each specie listed in Table S4 as well as argon through an inert bed consisting of quartz wool/quartz beads/quartz wool. The major m/e value was obtained in accordance with the NIST chemical database. Argon was used as internal standard for quantification, (2) Ion current intensities were taken relative to the inert standard, (3) Molar flow rates were obtained from the molar flow rate of the inert standard, the sensitivity coefficients, and the relative ion current intensities. A recursive deconvolution methodology was used: throughout all calculations, ion current intensities were taken relative to that of the chosen inert standard at the chosen m/e value:

$$I^{*}_{a(i),m(j)} = \frac{I_{a(i),m(j)}}{I_{S,m(S)}}$$

where $I_{a(i),m(j)}$ is the ion current intensity of specie i and m/z ratio of j. $I_{s,m(s)}$ is the ion current intensity of argon at m/z=40. Next, the sensitivity coefficient was calculated from calibration experiments where the partial pressures, respective mole fractions or molar flows are known:

$$Sens_{a(i),m(j)} = I^{*}_{a(i),m(j)} \cdot \frac{n_S}{n_{a(i)}} = \frac{I_{a(i),m(j)}}{I_{S,m(S)}} \cdot \frac{n_S}{n_{a(i)}}$$

where n_s is the molar flow rate of argon and $n_{a(i)}$ is the molar flow rate of specie i. $Sens_{a(i),m(j)}$ is the sensitivity coefficient of specie i at m/z ratio of j. To exploit an analysis by the mass spectrometer, the equation defining the sensitivity coefficient is rearranged, yielding an expression for the partial pressure, mole fraction or flow of the probe molecule as a function of the respective partial pressure, molar fraction, or flow of the inert standard.

$$n_{a(i)} = I^{*}_{a(i),m(j)} \cdot \frac{n_S}{Sens_{a(i),m(j)}} = \frac{I_{a(i),m(j)}}{I_{S,m(S)}} \cdot \frac{n_S}{Sens_{a(i),m(j)}}$$

A (recursive) deconvolution (unfolding of the different compound contributions to the ion current intensity at a given m/e value) can be accomplished if the ion current intensity of interfering compounds is known at other m/e values without overlap.

$$I^{*}_{a(i),m(j)} = I^{*}_{common,m(j)} - \frac{Sens_{a(l),m(j)}}{Sens_{a(l),m(n)}} \cdot I^{*}_{a(l),m(n)} = \frac{I_{common,m(j)}}{I_{S,m(S)}} - \frac{Sens_{a(l),m(j)}}{Sens_{a(l),m(n)}} \cdot \frac{I_{a(l),m(n)}}{I_{S,m(S)}}$$

where $I^{*}_{common,m(j)}$ is the overall contribution of specie i at m/z ratio of j. $Sens_{a(l),m(j)}$ is the sensitivity coefficient of an overlapping fragment at m/z ratio of j. $Sens_{a(l),m(n)}$ is the sensitivity coefficient of an overlapping fragment at its own non-interfering m/z ratio of n. $I_{a(l),m(n)}$ is the ion current intensity of an overlapping fragment at its own non-interfering m/z ratio of n. Ar was monitored at m/e = 40, CH_3OH at m/e = 31, DME at m/e = 45, H_2O at m/e = 18, CO at m/e = 28, CO_2 at m/e = 44, H_2 at m/e = 2, CH_4 at m/e = 16, C_2H_4 at m/e = 27 and C_3H_6 at m/e = 41.

Subsequent deconvolution allowed for the subtraction of minor fragments from main species. The original data was subjected to noise reduction (a smoothing function (moving average of 5) to the curves to smoothen out irregularities due to noise in the signal) before presentation in the manuscript. Deconvolution manipulations could be detrimental to signal/noise ratios (1) in which case CO, H_2 and butene are not displayed due to their negligible quantities.

Table S5.4 below gives an overview of the major gaseous components and most interfering components that were detected in this study.

Table S5.4: Species present in the effluent, m/e values for measurement and the most important interfering components

Specie	m/e value	Interfering components
CH_3OH	31	DME
DME	45	
H_2O	18	
CO	28	CH_3OH, DME, C_3H_6
H_2	2	CH_4, C_2H_4, C_3H_6
CH_4	16	CH_3OH, DME, CO, C_3H_6
C_2H_4	27	C_3H_6
C_3H_6	41	

Accurate quantification of species formed and consumed during the formation of primary olefins would require determination of all species formed under TAP conditions along with a recursive deconvolution to remove their influence. Instrumental limitations occur with a QMS as it can monitor only 10 species at once. As a heuristic, the work of Chang et al. (4) and Dewaele et al. (5) has been used to limit the possible chemistries involved under low pressure conditions.

S5.5 Sample identification for FTIR study

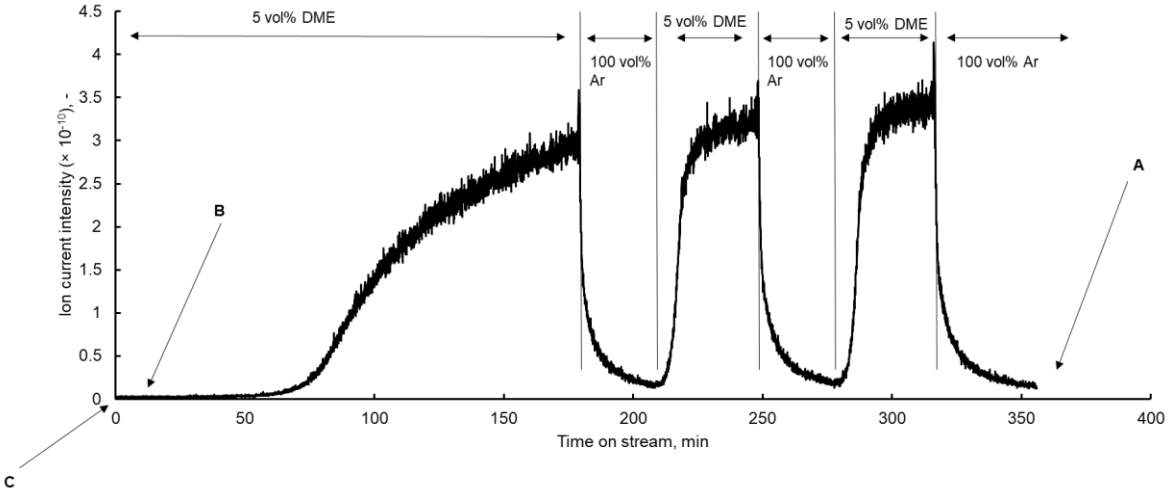

Fig. S5.5: Step response of 5 vol% DME over 157 mg of ZSM-5 (11.5) showing various stages of sample extraction for FTIR studies.

S5.6 Full spectrum of species

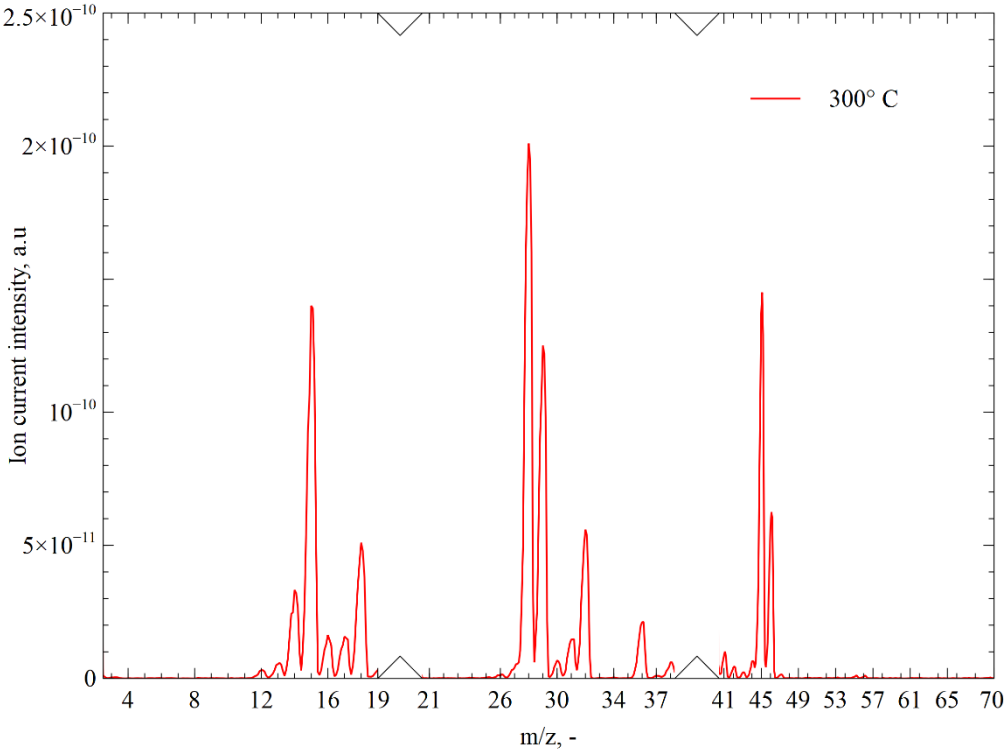

Fig. S5.6: Full spectrum of gaseous species formed after a step response of 5 vol% DME over ZSM-5 (25) catalysts at 300 °C. No products larger than m/z = 56 were observed in distinguishable quantities

S5.7 Profile relationships between DME and propylene effluent

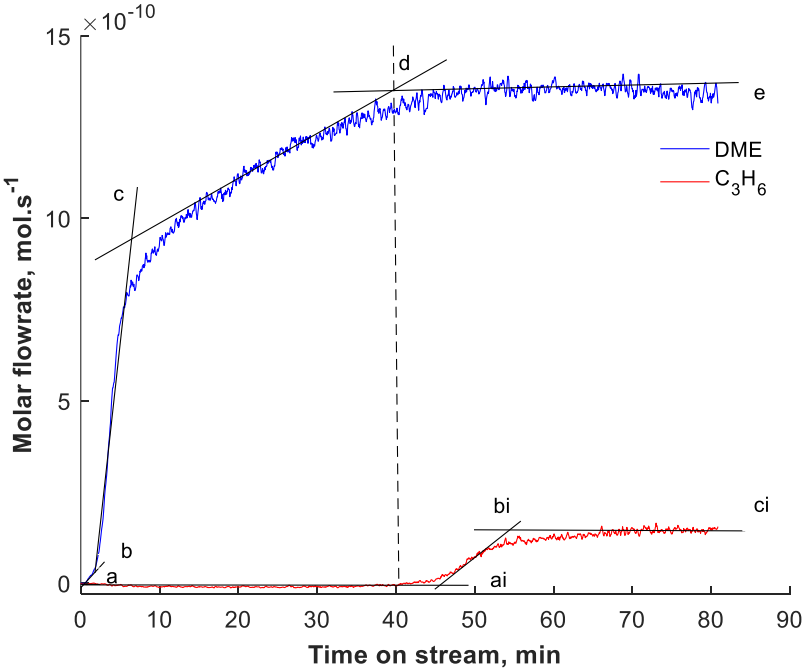

Fig. S5.7: Effluent profiles of DME and propylene following a step response of 5 vol% DME over ZSM-5 (25) at 300 °C. Total molar flow rate (5 vol% DME, balance Ar) at STP = 4.4 × 10^{-8} mol s^{-1}.

S5.8 TPD-IND of dimethoxymethane and 1,5-hexadiene

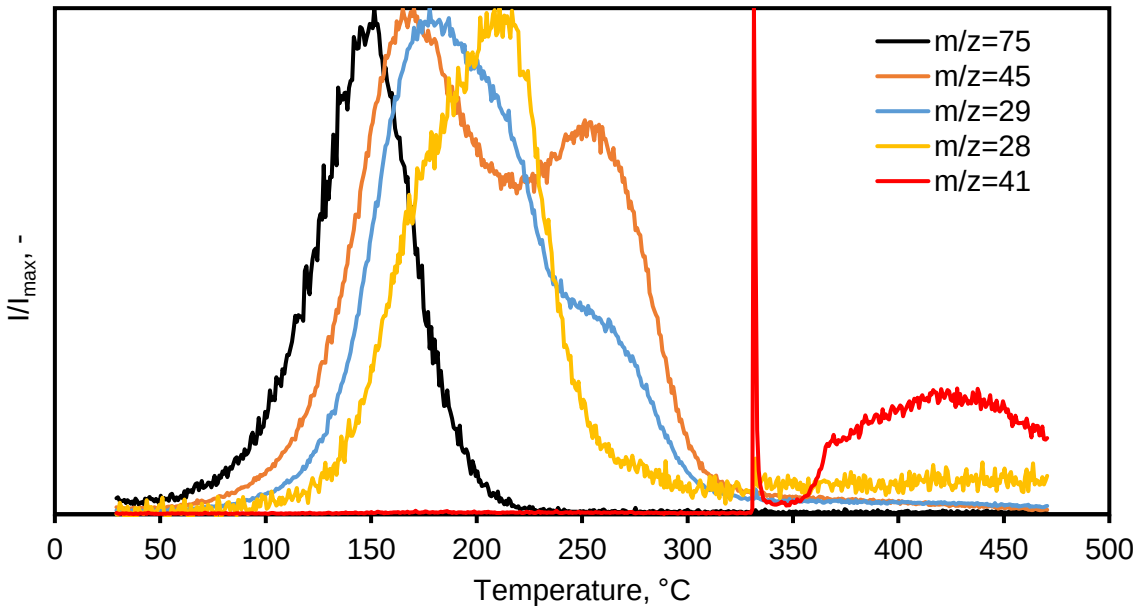

Fig. S5.8a: TPD of DMM (m/z=75) and its decomposition products (DME, m/z=45; formaldehyde, m/z=29; carbon monoxide, m/z=28 and propylene, m/z=41) over ZSM-5 at 15 °C min^{-1} up to 470 °C.

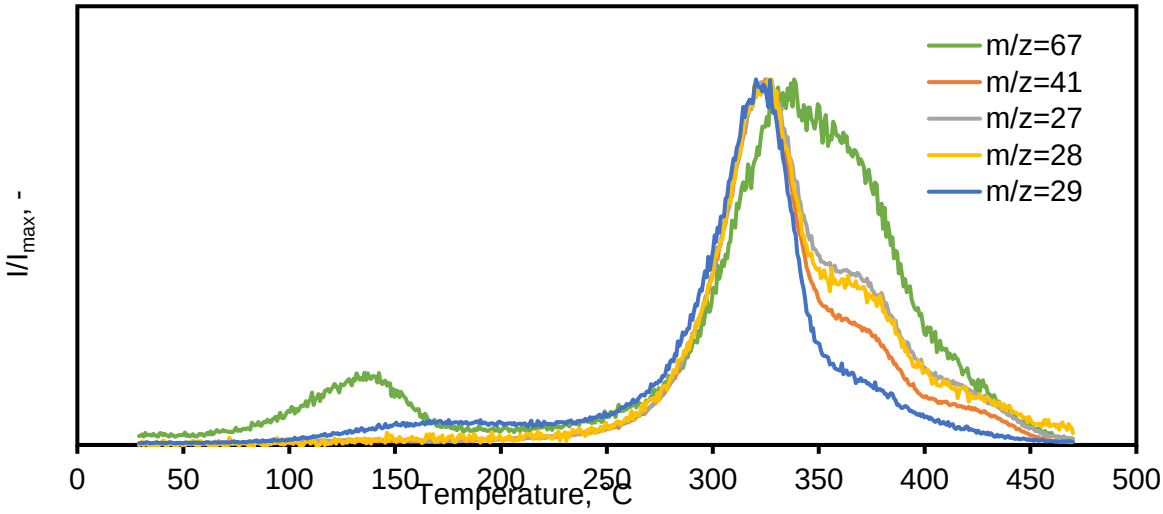

Fig. S5.8b: TPD of 1,5-hexadiene over ZSM-5 at 15 °C min^{-1} up to 470 °C showing temperatures of desorption.

S5.9 Mass and atom balances

Carbon accumulation was calculated as:

$2n_{DME,i} - 2n_{DME,e} - n_{MeOH,e} - 2n_{C2H4,e} - 3n_{C3H6,e}$

Hydrogen accumulation was calculated as:

$6n_{DME,i} - 6n_{DME,e} - 4n_{MeOH,e} - 4n_{C2H4,e} - 6n_{C3H6,e} - 2n_{H2O,e}$

Oxygen accumulation was calculated as:

$n_{DME,i} - n_{DME,e} - n_{MeOH,e} - n_{H2O,e}$

Mass accumulation was calculated as:

$46n_{DME,i} - 46n_{DME,e} - 32n_{MeOH,e} - 28n_{C2H4,e} - 42n_{C3H6,e} - 18n_{H2O,e}$

where $n_{j,i}$ is the steady-state feed molar flow rate of specie j and $n_{j,e}$ is the steady-state effluent molar flow rate of specie j.

S5.10 FTIR study

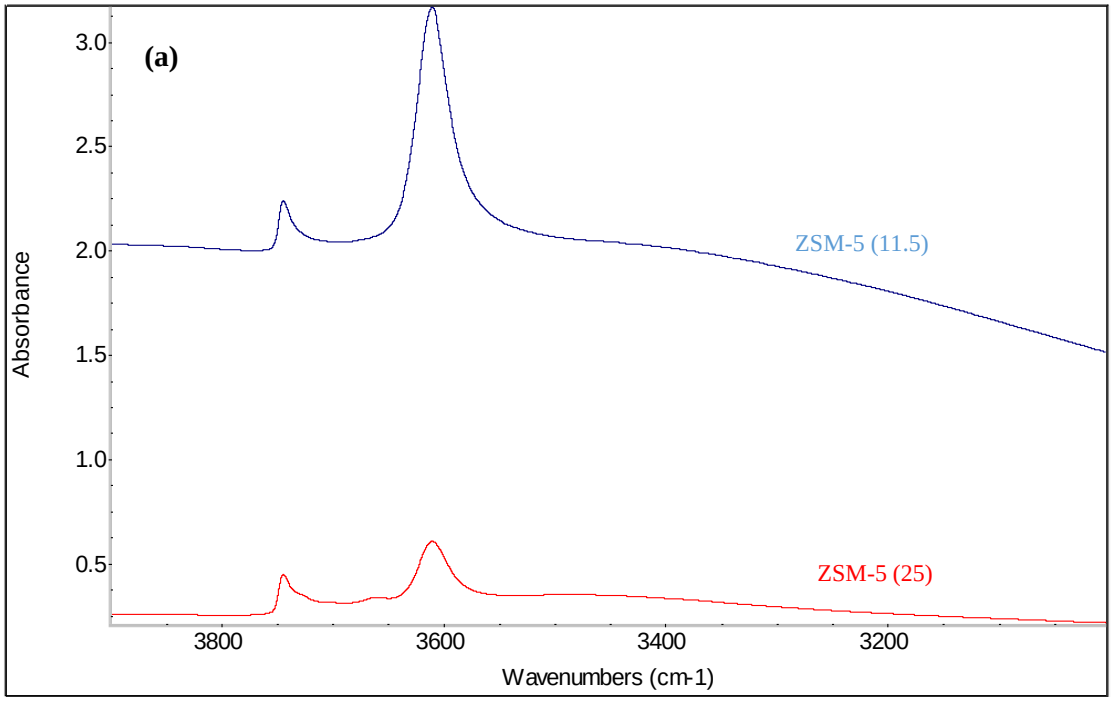

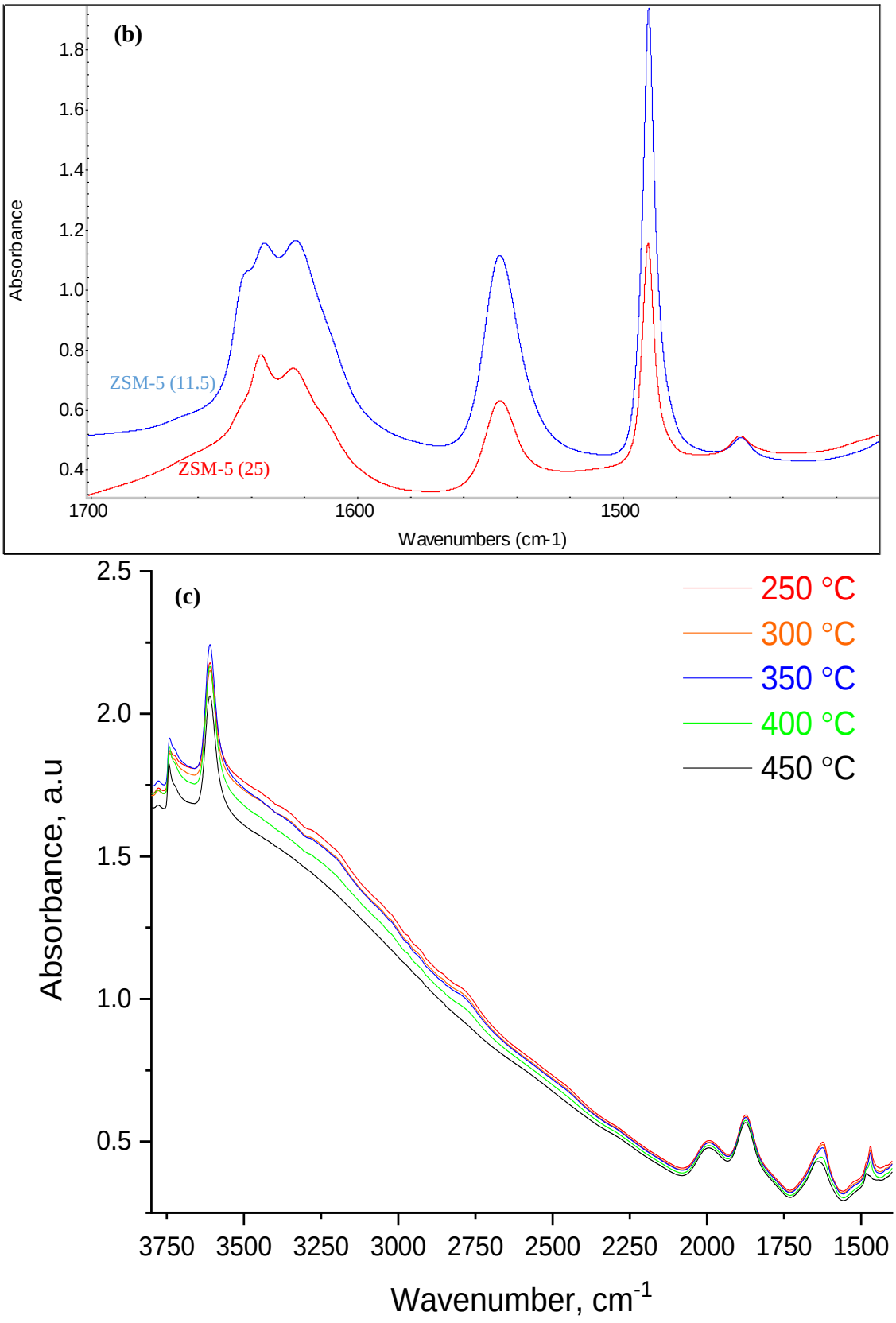

Fig. S5.10: (a) Infrared spectrum of the hydroxyl region of ZSM-5 (11.5) and ZSM-5 (25), activated at 450 °C; **(b)** infrared spectra of the pyridine region following pyridine adsorption on ZSM-5 (11.5) and ZSM-5 (25); **(c)** Spectra of sample A up until 450 °C

S5.11 References

1. Gleaves JT, Ebner JR, Kuechler TC. Temporal Analysis of Products (TAP) — A Unique Catalyst Evaluation System with Submillisecond Time Resolution. Catalysis Reviews. 1988;30(1):49-116.
2. Baerlocher C, McCusker LB. Database of Zeolite Structures http://www.iza-structure.org/databases/ [cited 2017 01/08/2017].
3. Gubanova EL. Experimental study and mathematical modeling of catalytic partial oxidation of methane to synthesis gas over monolith catalyst at short contact times [PhD Thesis]: Institut de Recherche sur la Catalyse et l'Environment de Lyon, IRCELYON; 2008.
4. Chang CD, Lang WH, Smith RL. The conversion of methanol and other O-compounds to hydrocarbons over zeolite catalysts. II. Pressure effects. J Catal. 1979;56(2):169-73.
5. Dewaele O, Geers VL, Froment GF, Marin GB. The conversion of methanol to olefins: A transient kinetic study. Chem Eng Sci. 1999;54(20):4385-95.

Chapter 6

6. Transient Kinetic Studies and Microkinetic Modelling of Primary Olefin Formation from Dimethyl Ether over ZSM-5 Catalysts

In the previous chapter, it was observed that propylene is the primary olefin formed from DME over ZSM-5 catalysts at 300 °C. An induction period during which a pool of intermediates form precedes propylene formation from DME. This induction period is eliminated if the pool of intermediates is already present as shown in subsequent step response cycles. Adding dimethoxymethane as a precursor to the ZSM-5 catalyst substantially reduces the induction period and increases the growth rate of propylene formation. Also, addition of carbon monoxide and hydrogen separately reduces the induction period and increases the growth rate of propylene formation showing that they could be key intermediates in propylene formation. The propylene effluent follows an S-shaped profile mirroring crystal nucleation kinetics. Consequently, a mechanism was proposed where all precursors examined (dimethoxymethane, carbon monoxide and hydrogen) are involved in the transformation of dimethyl ether in the formation of a nucleus (dimethoxyethane) which breaks down to form propylene. This mechanism agrees largely with recent proposals from DFT calculations from Fan and co-workers (Journal of Catalysis. 2014. 317. 277-283).

This declaration concerns the article entitled:									
Transient kinetic studies and microkinetic modelling of primary olefin formation from dimethyl ether over ZSM-5 catalysts									
Publication status (tick one)									
draft manuscript		**Submitted**		**In review**		**Accepted**		**Published**	✓
Publication details (reference)	Toyin Omojola, Dmitry B. Lukyanov, Andre C. van Veen. Transient kinetic studies and microkinetic modelling of primary olefin formation from dimethyl ether over ZSM-5 catalysts. 2019. *International Journal of Chemical Kinetics*. 51. 7. 528 – 537.								
Candidate's contribution to the paper (detailed, and also given as a percentage).	The candidate predominantly executed the… Formulation of ideas: Oluwatoyin Omojola (100 %) Design of methodology: Oluwatoyin Omojola (100 %) Experimental and simulation work: Oluwatoyin Omojola (100 %) Presentation of data in journal format: Oluwatoyin Omojola collated all data, conducted all data analysis and wrote the paper with supervision from Dmitry B. Lukyanov and Andre C. van Veen. Oluwatoyin Omojola (80 %)								
Statement from Candidate	This paper reports on original research I conducted during the period of my Higher Degree by Research candidature.								
Signed						**Date**	08/02/2019		

Abstract

The formation of primary olefins from dimethyl ether (DME) was studied over ZSM-5 catalysts at 300 °C using a novel step response methodology in a temporal analysis of products (TAP) reactor. For the first time, the TAP reactor framework was used to conduct single and multiple step response cycles of DME (balance argon) over a shallow bed with the continuous flow panel. Propylene is the major primary olefin and portrays an S-shaped profile with a preceding induction period when it is not observed in the gas phase. Methanol and water portray overshoot profiles due to their different rates of generation and consumption. DME effluent shows a rapid rise half-way to its steady state value leading to a slow rise thereafter because of its high desorption rates followed by subsequent reactions involving DME in further steps during the induction period. To analyse the experimental data quantitatively, nine reaction schemes were compared and kinetic parameters were obtained by solving a transient plug flow reactor model with coupled dispersion, convection, adsorption, desorption, and reaction steps. The methoxymethyl pathway involving dimethoxyethane and methyl propenyl ether gives the closest match to experimental data in agreement with recent DFT studies. Gaseous dispersion coefficients of *ca.* 10^{-9} m^2 s^{-1} were obtained in the TAP reactor. The novel experimental data validated against the transient kinetic model suggest that after the formation of initial species, the bottleneck in propylene formation is the transformation of the initial C-C bond i.e. dimethoxyethane formed initially from DME and methoxymethyl groups. DME adsorption on ZSM-5 catalyst generates surface methoxy groups which further react with the feed to give methoxymethyl groups. These methoxymethyl groups are regenerated through a series of reactions involving intermediates such as dimethoxymethane and methyl propenyl ether before propylene formation.

Keywords: induction period; hydrocarbon pool; dimethyl ether (DME); temporal analysis of products (TAP) reactor; ZSM-5 zeolite; transient kinetics; MTO; microkinetic model; step response; methanol

6.1. Introduction

An increasing demand in added-value chemicals and their security as well as incentives to reduce the carbon footprint needed for their generation and utilisation make the conversion of methanol to hydrocarbons (MTH) a viable chemical process. Non-conventional feedstock (such as biomass or organic process waste) and highly abundant resources (such as coal) are used to produce methanol *via* gasification and syngas liquefaction, and can later be transformed to fuels and chemicals over zeolite catalysts (1).

The production of hydrocarbons from methanol under steady-state conditions is regulated by a well-established “hydrocarbon pool” mechanism also known as the dual-cycle consisting of an olefin and aromatic cycle over ZSM-5 catalysts (2-6). The propagation of both cycles over the ZSM-5 catalyst is tunable depending on process conditions (7). Methanol conversion can be tuned towards light olefin production (MTO) at relatively high temperatures and low pressures (8-10).

Methanol undergoes a rapid equilibration process over ZSM-5 catalysts leading to the formation of dimethyl ether (DME) and water (11). There exists a long-standing debate on the evolution of the key oxygenate i.e. methanol and/or DME into the steady-state hydrocarbon pool. The debate centres on: (a) the role of methanol and/or DME, (b) the primary olefin(s) formed and (c) the exact mechanism leading from the key oxygenate to the primary olefin(s).

Various direct mechanisms have been proposed for the conversion of methanol/DME to primary olefins (12). These direct mechanisms are known by their intermediates and include oxonium ylide (13, 14), carbene (15), methane-formaldehyde (16, 17), carbon monoxide (18-20), methoxymethyl (21, 22) and surface methoxy groups (23-26). Using density functional theory (DFT) calculations, Lesthaeghe et al. (27-29) refuted some direct mechanisms based on high activation energy barriers and highly unstable intermediates. Conversely, primary olefins were proposed to form indirectly from impurities (acetone, ethanol) in the methanol feed (30, 31). Hunger and co-workers (23, 24, 32) later observed that the quantity of impurities proposed is insufficient for olefin formation.

Recently, there has been a surge in the evidence for the direct mechanisms leading to primary olefin formation (18, 19, 21, 22). Li et al. (22) gave evidence, using DFT calculations for the formation of propylene from methanol through methoxymethyl cations. In this pathway, 1,2-dimethoxyethane or 2-methoxyethanol were proposed as key intermediates propagating the direct formation of propylene. Wei et al. (21) compared formation pathways involving methane-formaldehyde and methoxymethyl cations for initial C-C bond formation from methanol. They obtained that the most favourable methane-formaldehyde pathway involved the formation of 1,2-ethanediol as the primary C-C bond. Nonetheless, the methoxymethyl pathway was more kinetically and thermodynamically favourable. Liu et al. (18), Chowdhury et al. (19, 20) and Plessow and Studt (33, 34) provided spectroscopic and theoretical evidence

for a carbon monoxide mechanism. The formation of the first C-C bond (surface acetate group) was shown to involve a low activation barrier of 80 kJ mol^{-1}.

Although theoretical calculations have shown the feasibility of the direct pathway involving methoxymethyl cations for the direct formation of ethylene and propylene from methanol, there are no kinetic studies to experimentally validate these proposals. Moreover, there is no kinetic model developed on a microscale level to describe and predict the formation of primary olefins from oxygenates particularly in the induction period.

Recently, we observed that higher temperatures are required to desorb DME in comparison to methanol providing evidence that DME stays longer on the catalysts (35) and is the key oxygenate. This was also evidenced by Liu et al. (18) and Wei et al. (21). In this paper, we investigate the induction period during the formation of primary olefins from DME at 300 °C by conducting novel step response experiments in a temporal analysis of products (TAP) reactor. Nine reaction schemes obtained from literature (18-22) were compared and used as a basis for a microkinetic model. The experimental data was simulated to extract kinetic parameters that describe the formation of primary olefins from DME over fresh ZSM-5 catalysts.

6.2. Materials and methods

6.2.1. Experimental

The ammonium form of the fresh ZSM-5 catalyst with a Si/Al ratio of 25, purchased from Zeolyst International, has a crystallite size of 0.10 ± 0.02 µm and an average particle size of 30 µm (35). The ZSM-5 catalysts were pressed, crushed, and sieved to obtain pellet sizes in the range of 250 – 500 µm. Anhydrous DME (99.999%) and argon (99.999%) were purchased from CK special gases Ltd. Experiments were conducted in a transient reactor suited for the temporal analysis of products under close to vacuum conditions. The TAP has three chambers in series: (a) the reactor chamber, (b) the differential chamber and (c) detector chamber. The reactor chamber contains a fixed-bed reactor, 6 mm O.D. (4 mm I.D.) and 40 mm long and has a cone-shaped inset for uniform radial distribution. The differential chamber acts as a cryogenic trap to eliminate scattered molecules reaching the detector chamber where the quadrupole mass spectrometer (QMS) is housed. The differential chamber works as a molecular beam. Gases were introduced through two continuous feeding valves into the reactor inlet. The pressure at the exit of the reactor chamber is maintained at 10^{-5} Pa while the pressure at the end of the differential chamber is 10^{-6} Pa and QMS is 10^{-7} Pa. The response of the QMS, placed in the detector chamber, was calibrated by passing continuous streams of various gases (methanol, DME, ethylene, propylene, etc.) in argon over an inert quartz bed with particle diameters between 355 – 500 µm. The QMS was operated in a multiple ion

detection (MID) mode monitoring a maximum of 10 products simultaneously. The low base pressure (10^{-7} Pa) in the detector chamber allows for high detection sensitivity necessary for quantitative analysis. The inert quartz bed used for calibration had the same length as the catalyst bed. The time required to reach steady state or to drop from steady state was fastest over the inert quartz bed.

10 mg of NH_4-ZSM-5 catalyst was initially decomposed in the TAP reactor chamber by heating it at 10 °C min^{-1} up to 450 °C, holding for 30 min before bringing the sample to 300 °C. Background signal intensities were obtained. The catalyst was then subjected to a steady flow of argon at 10^{-8} mol s^{-1}. Afterwards, the flow was instantaneously switched to a feed of 5 vol% DME in argon (step-up) at a flow rate of *ca*. 4.40 × 10^{-8} mol s^{-1}. At steady state, the inlet DME feed was instantaneously switched to a steady flow of argon (stopped-flow). Thus, a single step response cycle consists of three phases: step-up, steady-flow and stopped-flow. During the step response cycle, the effluent was monitored with the QMS. Single and multiple step response cycles were carried out.

Flow rates of the inert feed were similar to step response feed and were about 10^{-8} mol s^{-1}, with an inlet pressure of less than 1000 Pa (36). The active catalyst bed length was short (2 mm) compared to the overall bed length of 25 mm (consisting of quartz wool/quartz beads/active catalyst bed/quartz beads/quartz wool).

A novel methodology was developed as described above where ZSM-5 catalysts packed in a shallow bed were subjected to step response of probe molecules under continuous flow. Here, the rate is proportional to the difference of inlet and outlet concentrations. As conversions increase when the TAP reactor is operated as a convective flow device, the level of non-uniformity increases. The extent of the non-uniformity is circumvented in our experiments due to the use of a shallow bed. The above methodology is different from the conventional diffusional flow TAP reactor where the rate is proportional to the difference of inlet and outlet gradient of concentrations (37). Our novel methodology was developed in the TAP reactor to alleviate intricacies associated with the MTH reaction. Olsbye et al. (38) highlighted, in their review, the complexities associated with separating active species and deactivating species during MTO reaction during atmospheric studies. Herein, we show that on multiple step response cycles, deactivation is negligible under TAP conditions. As the pressures used were lower than 1000 Pa, external mass transfer to the particle is negligible due to low gas densities which allow for the absence of a stagnant film around the particle in the TAP reactor. They are suppressed due to negligible intramolecular collisions under vacuum conditions (39). In a previous contribution (35), we also showed that the rates of methanol and DME adsorption and desorption are limiting compared to intra-particle mass transport contributions. Below (section 4), we show that these rates compete with the rate of transformation of intermediates during the conversion of DME to primary olefins.

Throughout all step response experiments, the temperature and the pressure were constant. The raw data (QMS ion currents) were corrected for background levels and fragmentation contributions for the different molecules and sensitivity factors according to section S6.1 of supplementary information.

6.2.2. Modelling

To obtain estimates of the kinetic parameters, the reactor performance was simulated. The outlet concentrations of methanol, DME, water, ethylene and propylene were estimated using the measured inlet conditions of DME and argon in a step function as boundary conditions. Rate parameters were estimated by comparing experiment to model. A one-zone plug flow reactor model was applied. Ideal plug flow is assumed initially due to high gas velocities of the feed expanding to vacuum in the reactor. For a simple reversible adsorption, equations 6.1 and 6.2 are tenable (37).

$$Gas: \varepsilon_b \frac{\partial C_{i,g}}{\partial t} = -u \frac{\partial C_{i,g}}{\partial z} - \Gamma_t S_v (1-\varepsilon_b)(k_a c_i - k_d \theta_{iZ}) \quad (6.1)$$

where k_a is the adsorption coefficient (m^3 mol^{-1} s^{-1}), c_i is the concentration of gas phase component, i (mol m^{-3}), ε_b is bed porosity; u is the superficial velocity, m s^{-1}; z is the bed length, m; t is time, s; Γ_t is the concentration of active sites per unit surface area of catalyst (mol m_{cat}^{-2}) and S_v is the catalyst surface area per unit volume (m_{cat}^{-1}). Model properties are given in table 6.1.

$$Surface: \frac{\partial \theta_i}{\partial t} = k_a c_i - k_d \theta_{iZ} \quad (6.2)$$

where k_d is the desorption rate coefficient (s^{-1}) and θ_i is the fractional surface coverage of the adsorbed specie.

Initial condition: t = 0, $C_{i,g} = 0$, $\theta_i = 0$.

Boundary condition: (at t>0, z=0), C_j (0, t) = f(t), j = DME, Ar

The reactor model was solved in MATLAB (version R2016b) using the upwind scheme for solving the hyperbolic 1st order partial differential equation. Backward differencing was applied to the convection term in the PDE. To ensure numerical stability, the Courant-Friedrichs-Lewy (CFL) condition (40) was satisfied:

$$CFL = \left| a \frac{\Delta t}{\Delta z} \right| \leq 1 \quad (6.3)$$

where $a = u/\varepsilon_b$.

Thereafter, the influence of dispersion was simulated by solving a modification of equation 6.1 for a non-ideal PFR:

$$\varepsilon_b \frac{\partial C_{i,g}}{\partial t} = D_{i,e} \frac{\partial^2 C_{i,g}}{\partial z^2} - u \frac{\partial C_{i,g}}{\partial z} - \Gamma_t S_v (1-\varepsilon_b)(k_a c_i - k_d \theta_{iZ}) \quad (6.4)$$

where $D_{i,e}$ is the dispersion coefficient. The broader term dispersion coefficient is used although diffusion may be the main contributor here. Such differentiation cannot be extracted from our experimental data.

The Danckwerts boundary conditions (41) were applied to solving equation 6.4 for DME and argon:

$$C_{i,0} = C_i(0^+) - \frac{D_i}{u}\frac{dC_i(0^+)}{dz} \tag{6.5}$$

$$\frac{dC_i(1^-)}{dz} = 0 \tag{6.6}$$

The sum of square error (SSE) between experiment and model was obtained according to (42, 43):

$$SSE = \sum_{n=1}^{N_c}\sum_{m=1}^{N_d} w_{n,m}\left(Y_{n,m}^{obs} - Y_{n,m}^{cal}\right)^2 \rightarrow min \tag{6.7}$$

where:

n	component number;
m	observation number;
N_c	total number of components;
N_d	total number of observations;
$w_{n,m}$	weighting factor of the m-th observation of component n.
Y^{obs}	experimental data
Y^{cal}	model data

In equation 6.7., the weighting factors were calculated as (44):

$$w_{n,m} = \frac{1}{\sum_{m=1}^{x_{exp}} Y_{n,m}} \tag{6.8}$$

where x_{exp} is the total number of experimental points. The expression allows that the minority species in the reaction medium have a higher weighting factor. Future work would consider alternative weighting factors for optimisation.

Table 6.1: Catalyst and reactor properties used in the kinetic model

Parameter	Value	Unit
Active bed length	2	mm
Overall bed length	25	mm
Si/Al ratio	25	-
Brønsted acid site density	356	μmol g^{-1}
BET surface area	413	m^2 g^{-1}
Γ_t	0.862	μmol m_{cat}^{-2}
ε_b	0.5	-
S_v	2.0×10^5	m_{cat}^{-1}
Velocity, u	0.25	mm s^{-1}

* Brønsted acid site density and BET surface area are obtained from a previous communication (35)

Furthermore, to assess the sensitivity coefficients, the initial rate constants of each elementary step was multiplied by perturbation factors while other rate constants were kept constant. The relative changes in the sum of square error between the experimental and model were obtained with or without the perturbation factor. Subsequently, the sensitivity coefficient was obtained according to:

$$K_s = \frac{\ln(Y_p/Y_o)}{\ln(F)} \tag{6.9}$$

where Y_p and Y_o are the SSE values with or without the perturbation factor and F is the perturbation factor.

The initial parameter estimates were improved greatly by reducing the sum of squares error between model and experiment. Parameter optimisation through the minimisation of the sum of square error using an “fminsearch” function was implemented in MATLAB. The “fminsearch” function uses a Nelder-Mead simplex algorithm as described by Lagarias et al. (45). Nine reaction schemes involving methoxymethyl groups, methane-formaldehyde and carbon monoxide intermediates were compared.

6.3. Results

Firstly, it was important to establish the full range of gaseous species obtained at steady-state. As shown in Fig. 6.1, no substantial gaseous products greater than an m/z ratio of 56 was observed.

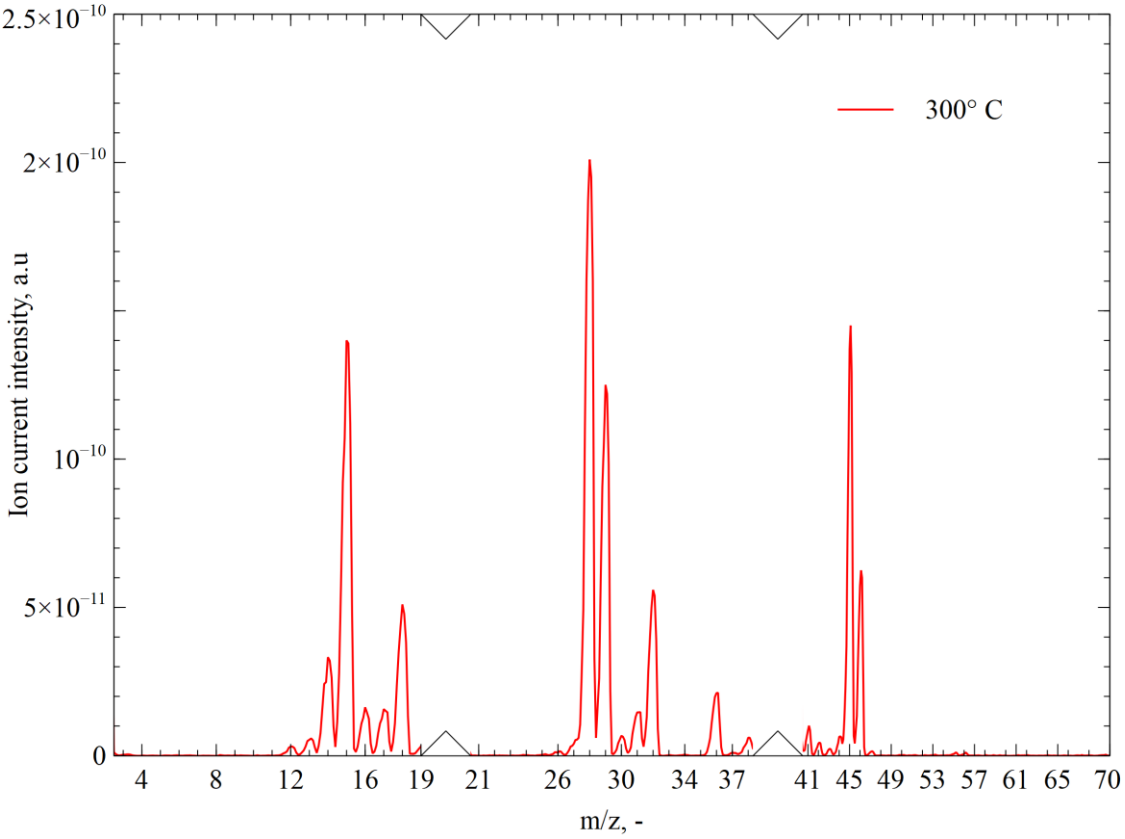

Fig. 6.1: Full spectrum of gaseous species at steady-state formed after a step response of 5 vol% DME (balance argon) over ZSM-5 (25) catalysts at 300 °C. Argon signals at m/z=20 and 40 have been removed for better clarity.

Propylene (m/z= 41) is the major olefin produced at 300 °C over ZSM-5 catalysts (Figs 6.1 & 6.2). The formation of propylene follows an S-shaped profile with a 44-min induction period. The S-shaped propylene profile is caused mainly by the formation of a series of stable intermediates (46, 47) during the induction period leading to the hydrocarbon pool chemistry at steady-state.

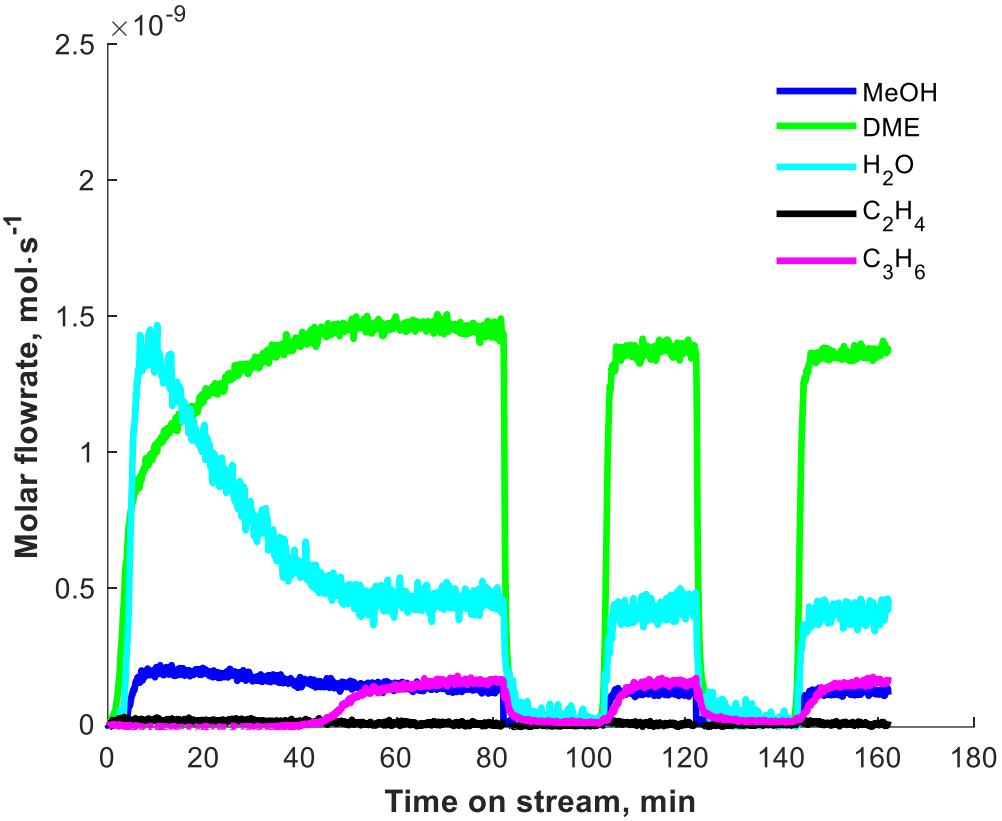

Fig. 6.2: Step response of 5 vol% DME at 300 °C over 10 mg of ZSM-5 (25) catalysts. Total molar flow rate (5 vol% DME, balance Ar) at STP = 4.4×10^{-8} mol s^{-1}. Steady state conversion is 34.8%

During the induction period of propylene formation, water is generated and released into the gas phase and consumed until steady-state effluent values are reached resulting in a stark overshoot profile. Methanol effluent mirrors this overshoot behaviour although its features are much subtler. DME effluent rises in two stages: rapidly at the beginning and then slowly until it reaches steady state. All effluent species attain steady-state at the same time. Steady-state conversion of DME into hydrocarbons is 34.8%.

After steady molar flowrates of all effluent species were achieved at 300 °C, the catalyst was purged by a flow of argon for 20 min (i.e. after 80 min time on stream in Fig. 6.2). Subsequently, a second step response cycle of 5 vol% DME was passed over the ZSM-5 catalyst at *ca.* 100 min. As shown in Fig. 6.2, the initial induction time of propylene effluent observed in the first step response cycle was eliminated. The steady flow of propylene effluent, which follows an S-shaped profile, shows that no deactivation of the catalyst had occurred over the timescale of this experiment at 300 °C. Also, there is no overshoot in the water effluent on subsequent step response cycles. The DME effluent rises immediately in the second and subsequent cycles in comparison to its slower pace in the first cycle.

Nine reaction schemes were compared to explain the induction period observed. These nine reaction schemes are based on the methane-formaldehyde, methoxymethyl and carbon monoxide pathways. Three routes were analysed for the methane-formaldehyde pathway

leading to ethanol (P1), 1,2-ethanediol (P2) and 2-methoxyethanol (P3) as the initial C-C bond (21). Two further routes were analysed that involved the formation of carbon monoxide without Brønsted acid sites (P4) according to the work of Liu et al. (18) or with Brønsted acid sites (P5) according to the work of Plessow and Studt (33) and Anderson and Klinowski (48). Three conventional routes resulting in the formation of the initial C-C bond from the reaction of methoxymethyl groups with methane, methanol and DME leading to ethyl methyl ether (P6), 2-methoxyethanol (P7) and dimethoxyethane (P8) respectively were analysed. A further route was analysed according to the work of Hoang et al. (49) that involves the conversion of dimethoxyethane to methyl propenyl ether which subsequently breaks down to propanal. Propanal forms dimers and trimers and leads to trimethylbenzene, thus initiating the aromatic cycle before ethylene and propylene formation *via* the aromatic dealkylation chemistry (P9). All reaction mechanisms are given in section S6.2 of the supplementary information. Finally, the effect of dispersion on the P8 route was analysed.

The experimental data was modelled initially using an ideal plug flow reactor model with the various reaction schemes described (table 6.2). Initial estimates were obtained by comparing experimental data to each model. Parameter optimization was then carried out alongside sensitivity analysis as described in section 6.2 above. The influence of dispersion was then modelled, although the relative proportions between kinetic parameters stayed constant as observed without dispersion.

Table 6.2: Comparison of different pathways for primary olefin formation from dimethyl ether

Code	Pathway	Initial C-C bond	SSE (× 10^{-11})
P1	Methane-formaldehyde	Ethanol	2.76
P2		1,2-ethanediol	2.74
P3		2-methoxyethanol	3.21
P4	Carbon monoxide	Surface acetate$^{\wedge}$	7.00
P5		Surface acetate^{+}	11.9
P6	Methoxymethyl	Ethyl methyl ether	2.41
P7		2-methoxyethanol	2.34
P8		Dimethoxyethane$^{\&}$	2.27
P9		Dimethoxyethane$^{\#}$	5.83

^ - carbon monoxide forms in the gas phase
+ - carbon monoxide forms in the presence of Brønsted acid sites
& - pathway involving secondary oxygenates (dimethoxyethane) leading to primary olefins
# - pathway involving secondary oxygenates and an aromatic cycle leading to primary olefins

* Reaction schemes for P1-P7 and P9 are given in section S6.2 of the supplementary information. Optimised parameters from P2 and P5 are given in section S6.2 in comparison with P8 given below.

6.4. Discussion

The debate on the formation of primary olefins is focused on advancing understanding on the mechanism through which the key oxygenate transforms during the induction period. This contribution is focused on the chemical kinetics of DME transformation to primary olefin(s) at low pressures in the TAP reactor at 300 °C. A focus on the chemical kinetics would help elucidate the major bottlenecks involved in primary olefin formation from DME. Ultimately, this study fits within the larger framework of quantitatively describing the evolution of the hydrocarbon pool that subsequently regulates product distribution over zeolite and zeotype catalysts at steady-state.

The methane-formaldehyde (16, 17, 29), carbon monoxide (18-20, 33, 34, 48, 50) and methoxymethyl (21, 22) pathways are competing pathways for the direct formation of primary olefins. The first route (P1) following methane and formaldehyde intermediates lead to the formation of ethanol as the initial C-C bond. Ethanol decomposes over ZSM-5 catalysts leading to ethylene as the primary olefin. Ethylene is then methylated by surface methoxy groups to propylene which is observed. This route has been previously suggested to be unfavourable due to the very slow reaction rates for the conversion of methane and formaldehyde to ethanol (29). Yamazaki et al. (51) further showed that the methylation of ethylene to produce propylene occurs at a far slower rate compared to the reaction of DME

with surface methoxy groups. Low reaction rates leading to the formation of ethanol as well as negligible rates of the formation of propylene from ethylene and surface methoxy groups lead to the unfavorability of this reaction pathway.

The route leading to the formation of 1,2-ethanediol (P2) is the most favourable methane-formaldehyde pathway following DFT studies (21). The lowest SSE is observed in this route compared to other routes involving methane-formaldehyde intermediates. Double methylation of 1,2-ethanediol leads to the formation of dimethoxyethane which leads to ethylene and propylene formation on decomposition on the ZSM-5 catalysts. A lower agreement is observed for the generation of 2-methoxyethanol (P3) as the initial C-C bond compared to 1,2-ethanediol (P2) from the methane-formaldehyde pathway. This is due to the faster rate of formation of the first C-C bond from the reaction of methanol with adsorbed formaldehyde. The rate of formation of 1,2-ethanediol exceeds 2-methoxyethanol formation by a factor of 5.

Carbon monoxide in pathways P4 and P5 involving surface acetate groups have the effect of reducing the induction time required to form propylene. Carbon monoxide functions as a co-catalyst (33, 34) as the predicted induction time is a factor of 10 times lower than the observed induction period leading to a high sum of squares error (SSE). The relative mismatch could be due to its negligible contribution at low pressures.

Methoxymethyl pathways are the most thermodynamically and kinetically favourable (21) and as a result have the better agreement amongst the three pathways to experimental data. The route involving dimethoxyethane (P8) shows the best agreement to experimental data given its low SSE and relatively high induction time prediction (Fig. 6.3). The reaction scheme is given below as:

$$CH_3OCH_3 + HZ \rightleftharpoons CH_3 \cdot Z + CH_3OH \quad (P8.1)$$

$$CH_3OH + HZ \rightleftharpoons CH_3 \cdot Z + H_2O \quad (P8.2)$$

$$H_2O + HZ \rightleftharpoons H_2O \cdot HZ \quad (P8.3)$$

$$CH_3 \cdot Z + CH_3OH \rightleftharpoons CH_3OCH_3 \cdot HZ \quad (P8.4)$$

$$CH_3 \cdot Z + CH_3OCH_3 \rightarrow CH_3OCH_2 \cdot Z + CH_4 \quad (P8.5)$$

$$CH_3OCH_2 \cdot Z + CH_3OCH_3 \rightarrow CH_3OCH_2CH_2OCH_3 \cdot HZ \quad (P8.6)$$

$$CH_3OCH_2CH_2OCH_3 \cdot HZ \rightarrow CH_3CHCHOCH_3 \cdot HZ + H_2O \quad (P8.7)$$

$$CH_3CHCHOCH_3 + HZ \rightleftharpoons CH_3CHCHOCH_3 \cdot HZ \quad (P8.8)$$

$$CH_3CHCHOCH_3 + CH_3 \cdot Z \rightarrow C_3H_6 + CH_3OCH_2 \cdot Z \quad (P8.9)$$

In this scheme, steps P8.if and P8.ib refer to the forward and backward reaction of P8.i respectively. A comparison of experimental data and simulations using initial estimated parameters is given in Fig. S6.3_P8 (see section S6.3 of the supplementary information).

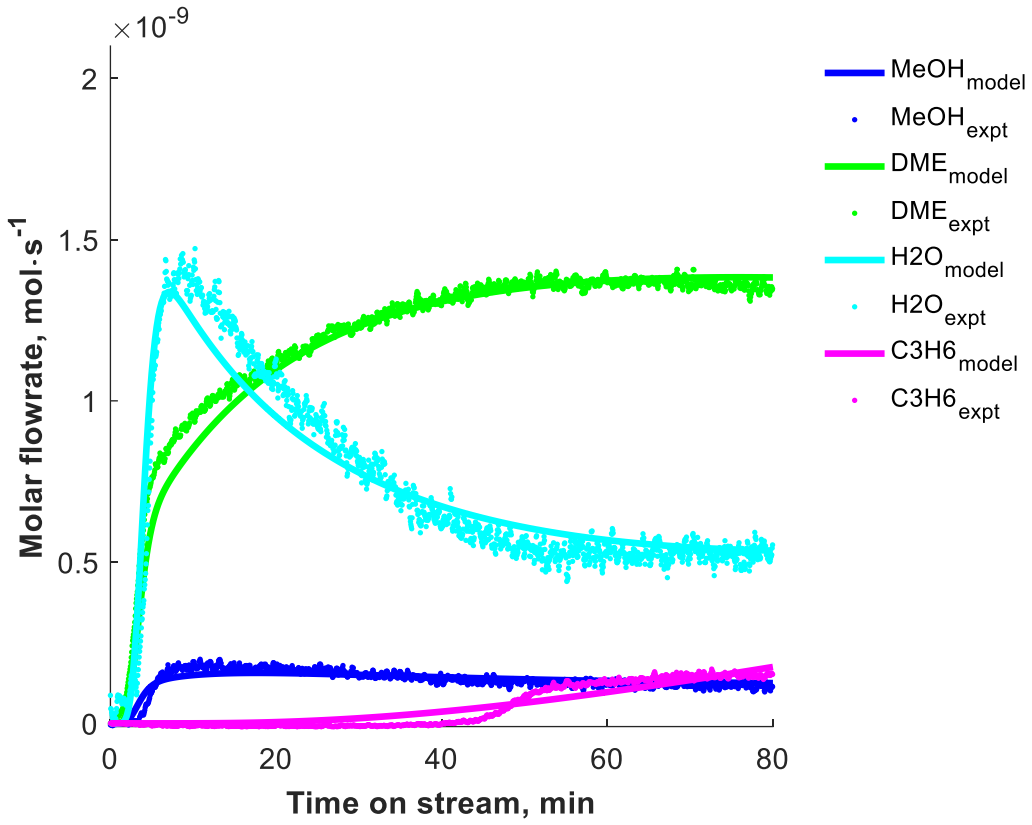

Fig. 6.3: Step response of DME over ZSM-5 catalysts at 300 °C using optimised parameters

The dissociative adsorption, and desorption of DME, methanol and water as well as the reaction of surface methoxy groups and methanol govern their initial release into the gas phase and the early concentrations of methoxy groups on the catalyst surface. The desorption of DME is much faster than its adsorption and the desorption of methanol is faster than its adsorption. DME desorption is faster than methanol desorption under reactive conditions (table 6.3). Gaseous DME reacts with surface methoxy groups and methoxy methyl groups in reaction steps P8.5 and P8.6 to produce methoxymethyl groups and dimethoxyethane respectively. The higher reverse dissociation rate of gaseous DME (step P8.1) on the active site is necessary to supply its gaseous form needed for reactions later (steps P8.5 and P8.6) during the induction period. In Fig. 6.3, DME effluent reaches steady state slowly following an initial rapid rise. The initial rapid rise is due to a fast-backward rate constant in step P8.1 leading to large releases of DME into the gas phase. The slower rate of rise following afterwards is due to the reactions involving DME in steps P8.5 and P8.6 later during the induction period. Alternatively, it could be due to DME saturation on the active sites ZSM-5 catalyst if molecular adsorption is considered. A better fit has been obtained with dissociative adsorption, however.

Table 6.3: Parameters for the conversion of DME to propylene over ZSM-5 catalysts in a TAP reactor*

Parameters	Initial estimates	Optimised values	Unit
k_{1f}	0.00045	0.000421	$Pa^{-1}\ s^{-1}$
k_{1b}	5.2	4.27	$Pa^{-1}\ s^{-1}$
k_{2f}	0.00182	0.00253	$Pa^{-1}\ s^{-1}$
k_{2b}	0.1010	0.468	$Pa^{-1}\ s^{-1}$
k_{3f}	0.0003	0.000142	$Pa^{-1}\ s^{-1}$
k_{3b}	50	152	s^{-1}
k_{4f}	0.00028	7.85e-8	$Pa^{-1}\ s^{-1}$
k_{4b}	1.7	0.215	s^{-1}
k_{5f}	0.02	0.028	$Pa^{-1}\ s^{-1}$
k_{6f}	0.5	0.469	$Pa^{-1}\ s^{-1}$
k_{7f}	0.129	0.0973	s^{-1}
k_{8f}	0.00375	0.00878	$Pa^{-1}\ s^{-1}$
k_{8b}	812.5	1.24	s^{-1}
k_{9f}	125	10.5	$Pa^{-1}\ s^{-1}$

*kif and kib refer to forward and backward rate constant of reaction step P8.i.

Surface methoxy groups are generated early in the induction period and consumed later leading to the formation of intermediates and propylene. Slow generation of surface methoxy groups occurs given the dissociation rates of DME and methanol in reaction steps P8.1f and P8.2f respectively. Surface methoxy groups are also slowly consumed leading to the formation of adsorbed DME (step P8.4f) and generation of methoxymethyl groups (step P8.5f). However, they are rapidly consumed in step P8.9f leading to the formation of propylene.

Water effluent portrays an overshoot profile with time on stream. The water effluent is controlled by its molecular adsorption and desorption (step P8.3) and the dissociative adsorption and desorption of methanol (step P8.2) and the formation of methyl propenyl ether from dimethoxyethane (step P8.7). Methanol adsorption and desorption leads to little concentrations of water in the gas phase (step P8.2). Once formed, water remains mostly in the gas phase (step P8.3). Step P8.7f shows a large reaction rate constant for water formation from dimethoxyethane. Although water is rapidly produced in step P8.7f and rapidly desorbed in step P8.3b, it reacts rapidly with surface methoxy groups to give methanol in step P8.2b. Thus, the overshoot in water effluent is due to the competing dynamics governing its formation and consumption during the induction period.

Gaseous methanol effluent is affected by the early reactions (steps P8.1, P8.2 and P8.4). Desorption rates greater than adsorption rates in steps P8.1 and P8.2 lead to a slow release of methanol in the gas phase. In step P8.4f, methanol is slowly consumed, although the rate of reaction is slower than its nominal formation rate in steps P8.1f and P8.2b. Thus, small concentrations of methanol are generated in steps P8.1 and P8.2, which are slowly consumed in step P8.4 during the induction period. The difference between the rates of methanol formation and consumption is responsible for its slight overshoot depicted in Fig. 6.3.

Methanol overshoot effectively mirrors water overshoot except that its features are subtler. This is probably due to reaction step P8.2. connecting methanol, water and surface methoxy groups.

Propylene is formed very rapidly (step P8.9f) from the initial species (methanol, DME, water, surface methoxy groups, methoxymethyl groups), in comparison to previous steps, through a series of intermediates (dimethoxyethane and methyl propenyl ether). Both intermediates are readily available in the pores of the ZSM-5 catalyst and in the gas phase due to high desorption rates respectively. After the formation of initial species (methanol, DME, water, surface methoxy groups and methoxymethyl groups), the bottleneck in propylene formation which is also a very important step according to the sensitivity analysis (Fig. 6.4) is the transformation of dimethoxyethane (step P8.7) formed initially from DME and methoxymethyl groups (step P8.6).

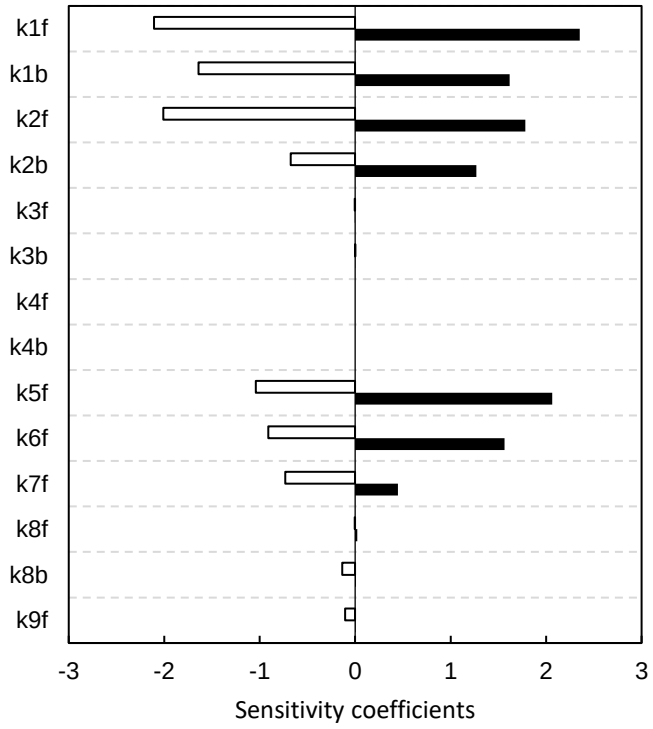

Fig. 6.4: Sensitivity analysis for elementary steps involved in the formation of propylene from DME over ZSM-5 catalysts at 300 °C

Kobayashi (46, 47) observed that an S-shaped profile observed during the induction period is due to the slow transformation of several stable intermediates. Hoang et al. (49) proposed reaction pathways that looked at the formation of dimers and trimers of aldehydes leading to aromatics formation which consequently dealkylate to give primary olefins. We modelled this pathway (P9) allowing for the formation of secondary oxygenates and aromatics before primary olefin formation. We observed that to obtain the detected propylene selectivity, the transformation rates between secondary oxygenates and aromatics must be rapid. The

high rates of transformation, however lead to lower induction times. The induction times are accurately predicted only at low rates of dimer and trimer transformation but leading to lower propylene selectivities than those observed. Based on the pathway giving the lowest sum of squares error, the dimethoxymethane route of the methoxymethyl pathway, as suggested by Fan and co-workers (21, 22) gives the closest agreement to experimental data.

The inclusion of the steady-state hydrocarbon pool chemistry along with the induction period chemistry (as investigated in this paper) would lead to a full description of the S-shaped propylene profile observed. It is beyond the scope here to investigate the effect of the hydrocarbon pool chemistry on the S-shaped propylene profile and indeed there are already collections of review articles (7, 12) on this topic. As soon as the primary olefin is formed in the induction period, olefin methylation, oligomerisation and cracking, and hydrogen transfer and cyclisation as well as aromatic methylation and dealkylation chemistries regulate steady-state conversion of initial oxygenates (methanol, DME) to hydrocarbons. Nonetheless, in this article, we have provided mechanistic insights on the challenges of the chemistries occurring only during the induction period.

Yablonsky et al. (52) proposed a reactive mixing index analysis (REMI) function for diagnostics of the hydrodynamic regime during ideal and non-ideal flow of pulse inputs into the TAP reactor. The REMI criterion for the characterization of the mixing quality in a catalytic reactor which, initially at steady-state, is perturbed by small pulses of a chemical reactant. CSTR, ideal PFR and non-ideal PFR were considered. In our analysis, step response has been carried out using the continuous feeding valves of the TAP reactor over a shallow bed hence representing the non-ideal PFR as convection and dispersion effects were considered. The effects of dispersion were modelled using equation 6.4 and dispersion coefficients were of the order of *ca.* 10^{-9} m^2 s^{-1}. The trend observed in rate constants without dispersion effects were the same as those when dispersion was included in the model.

6.5. Conclusions

The formation of primary olefins from dimethyl ether (DME) has been studied over ZSM-5 catalyst using a novel step response methodology in a temporal analysis of products (TAP) reactor. Propylene is the major olefin formed at 300 °C and portrays an S-shaped profile. Overshoot profiles are depicted by methanol and water with time on stream. DME effluent reaches its steady state flowrate in two phases: rapidly up until half its steady-state value and then slowly. The results were explained using a transient kinetic model that considers dispersion, convection, adsorption, desorption and reaction for step response cycles applied to ZSM-5 catalysts in a shallow bed packing configuration. Nine reaction schemes were tested using recent density functional theory studies. The methoxymethyl pathway involving dimethoxyethane as the first C-C bond gives the closest agreement to experiment. After the

formation of primary products (methanol, water, surface methoxy groups, methoxymethyl groups and methane) from DME, the transformation of the first C-C bond (reaction of methoxymethyl group with DME to give dimethoxyethane) represents the major bottleneck in propylene formation over ZSM-5 catalysts.

6.6. Acknowledgements

Financial support from the Petroleum Technology Development Fund of Nigeria (PTDF/ED/PHD/OO/766/15) and from the European Commission in the scope of the 7th Framework program BIOGO project (grant number: 604296) https://www.biogo.eu/ is acknowledged. T. Omojola is grateful for fruitful discussions with Dr Waleed Ali (Department of Mathematics, University of Bath).

6.7. Notes

Kinetic code and supplementary information supporting this study can be found in the appendix.

6.8. References

1. Tian P, Wei Y, Ye M, Liu Z. Methanol to olefins (MTO): From fundamentals to commercialization. ACS Catalysis. 2015;5(3):1922-38.
2. Dahl IM, Kolboe S. On the reaction mechanism for propene formation in the MTO reaction over SAPO-34. Catal Lett. 1993;20(3-4):329-36.
3. Dahl IM, Kolboe S. On the Reaction Mechanism for Hydrocarbon Formation from Methanol over SAPO-34. I. Isotopic Labeling Studies of the Co-Reaction of Ethene and Methanol. J Catal. 1994;149(2):458-64.
4. Dahl IM, Kolboe S. On the reaction mechanism for hydrocarbon formation from methanol over SAPO-34: 2. Isotopic labeling studies of the Co-reaction of propene and methanol. J Catal. 1996;161(1):304-9.
5. Olsbye U, Bjørgen M, Svelle S, Lillerud KP, Kolboe S. Mechanistic insight into the methanol-to-hydrocarbons reaction. International Conference on Gas-Fuel 05. 2005;106(1-4):108-11.
6. Bjørgen M, Svelle S, Joensen F, Nerlov J, Kolboe S, Bonino F, Palumbo L, Bordiga S, Olsbye U. Conversion of methanol to hydrocarbons over zeolite H-ZSM-5: On the origin of the olefinic species. J Catal. 2007;249(2):195-207.
7. Ilias S, Bhan A. Mechanism of the catalytic conversion of methanol to hydrocarbons. ACS Catalysis. 2013;3:18-31.
8. Vora BV, Marker TL, Barger PT, Nilsen HR, Kvisle S, Fuglerud T. Economic route for natural gas conversion to ethylene and propylene. In: Pontes Md, Espinoza RL, Nicolaides CP, Scholtz JH, Scurrell MS, editors. Stud Surf Sci Catal. Volume 107: Elsevier; 1997. 87-98.
9. Koempel H, Liebner W. Lurgi's Methanol To Propylene (MTP®) Report on a successful commercialisation. Stud Surf Sci Catal2007. p. 261-7.
10. Chang CD, Lang WH, Smith RL. The conversion of methanol and other O-compounds to hydrocarbons over zeolite catalysts. II. Pressure effects. J Catal. 1979;56(2):169-73.

11. Svelle S, Kolboe S, Swang O, Olsbye U. Methylation of Alkenes and Methylbenzenes by Dimethyl Ether or Methanol on Acidic Zeolites. The Journal of Physical Chemistry B. 2005;109(26):12874-8.
12. Stöcker M. Methanol-to-hydrocarbons: Catalytic materials and their behavior. Microporous Mesoporous Mater. 1999;29(1-2):3-48.
13. Mole T, Whiteside JA. Conversion of methanol to ethylene over ZSM-5 zeolite in the presence of deuterated water. J Catal. 1982;75(2):284-90.
14. Mole T. Conversion of methanol to ethylene over ZSM-5 zeolite: A reexamination of the oxonium-ylide hypothesis, using 13carbon- and deuterium-labeled feeds. J Catal. 1983;84(2):423-34.
15. Dass DV, Martin RW, Odell AL, Quinn GW. A Re-Examination of Evidence for Carbene (CH2:) As An Intermediate in the Conversion of Methanol to Gasoline. The Effect of Added Propane. In: Bibby DM, Chang CD, Howe RF, Yurchak S, editors. Stud Surf Sci Catal. 36: Elsevier; 1988. 177-81.
16. Nováková J, Kubelková L, Habersberger K, Dolejšek Z. Catalytic activity of dealuminated Y and HZSM-5 zeolites measured by the temperature-programmed desorption of small amounts of preadsorbed methanol and by the low-pressure flow reaction of methanol. Journal of the Chemical Society, Faraday Transactions 1: Physical Chemistry in Condensed Phases. 1984;80(6):1457-65.
17. Dewaele O, Geers VL, Froment GF, Marin GB. The conversion of methanol to olefins: A transient kinetic study. Chem Eng Sci. 1999;54(20):4385-95.
18. Liu Y, Müller S, Berger D, Jelic J, Reuter K, Tonigold M, Sanchez-Sanchez M, Lercher JA. Formation Mechanism of the First Carbon-Carbon Bond and the First Olefin in the Methanol Conversion into Hydrocarbons. Angewandte Chemie - International Edition. 2016;55(19):5723-6.
19. Chowdhury AD, Houben K, Whiting GT, Mokhtar M, Asiri AM, Al-Thabaiti SA, Basahel SN, Baldus M, Weckhuysen BM. Initial Carbon–Carbon Bond Formation during the Early Stages of the Methanol-to-Olefin Process Proven by Zeolite-Trapped Acetate and Methyl Acetate. Angewandte Chemie - International Edition. 2016;55(51):15840-5.
20. Chowdhury AD, Paioni AL, Houben K, Whiting GT, Baldus M, Weckhuysen BM. Bridging the Gap between the Direct and Hydrocarbon Pool Mechanisms of the Methanol-to-Hydrocarbons Process. Angewandte Chemie - International Edition. 2018.
21. Wei Z, Chen YY, Li J, Guo W, Wang S, Dong M, Qin Z, Wang J, Jiao H, Fan W. Stability and Reactivity of Intermediates of Methanol Related Reactions and C-C Bond Formation over H-ZSM-5 Acidic Catalyst: A Computational Analysis. Journal of Physical Chemistry C. 2016;120(11):6075-87.
22. Li J, Wei Z, Chen Y, Jing B, He Y, Dong M, Jiao H, Li X, Qin Z, Wang J, Fan W. A route to form initial hydrocarbon pool species in methanol conversion to olefins over zeolites. J Catal. 2014;317(0):277-83.
23. Wang W, Buchholz A, Seiler M, Hunger M. Evidence for an Initiation of the Methanol-to-Olefin Process by Reactive Surface Methoxy Groups on Acidic Zeolite Catalysts. J Am Chem Soc. 2003;125(49):15260-7.
24. Jiang Y, Wang W, Marthala VRR, Huang J, Sulikowski B, Hunger M. Effect of organic impurities on the hydrocarbon formation via the decomposition of surface methoxy groups on acidic zeolite catalysts. J Catal. 2006;238(1):21-7.
25. Jiang Y, Wang W, Reddy Marthala VR, Huang J, Sulikowski B, Hunger M. Response to comments on the paper: "Effect of organic impurities on the hydrocarbon formation via the decomposition of surface methoxy groups on acidic zeolite catalysts" by Y. Jiang, W. Wang, V.R.R. Marthala, J. Huang, B. Sulikowski, M. Hunger. J Catal. 2006;244(1):134-6.
26. Ono Y, Mori T. Mechanism of methanol conversion into hydrocarbons over ZSM-5 zeolite. Journal of the Chemical Society, Faraday Transactions 1: Physical Chemistry in Condensed Phases. 1981;77(9):2209-21.

27. Lesthaeghe D, Van Speybroeck V, Marin GB, Waroquier M. Understanding the failure of direct C-C coupling in the zeolite-catalyzed methanol-to-olefin process. Angewandte Chemie - International Edition. 2006;45(11):1714-9.
28. Lesthaeghe D, Van Speybroeck V, Marin GB, Waroquier M. What role do oxonium ions and oxonium ylides play in the ZSM-5 catalysed methanol-to-olefin process? Chem Phys Lett. 2006;417(4-6):309-15.
29. Lesthaeghe D, Van Speybroeck V, Marin GB, Waroquier M. The rise and fall of direct mechanisms in methanol-to-olefin catalysis: An overview of theoretical contributions. Ind Eng Chem Res. 2007;46(26):8832-8.
30. Goguen PW, Xu T, Barich DH, Skloss TW, Song W, Wang Z, Nicholas JB, Haw JF. Pulse-quench catalytic reactor studies reveal a carbon-pool mechanism in methanol-to-gasoline chemistry on zeolite HZSM-5. J Am Chem Soc. 1998;120(11):2650-1.
31. Song W, Marcus DM, Fu H, Ehresmann JO, Haw JF. An oft-studied reaction that may never have been: Direct catalytic conversion of methanol or dimethyl ether to hydrocarbons on the solid acids HZSM-5 or HSAPO-34. J Am Chem Soc. 2002;124(15):3844-5.
32. Wang W, Seiler M, Hunger M. Role of surface methoxy species in the conversion of methanol to dimethyl ether on acidic zeolites investigated by in situ stopped-flow MAS NMR spectroscopy. J Phys Chem B. 2001;105(50):12553-8.
33. Plessow PN, Studt F. Unraveling the Mechanism of the Initiation Reaction of the Methanol to Olefins Process Using ab Initio and DFT Calculations. ACS Catalysis. 2017;7(11):7987-94.
34. Plessow PN, Studt F. Theoretical Insights into the Effect of the Framework on the Initiation Mechanism of the MTO Process. Catal Lett. 2018;148(4):1246-53.
35. Omojola T, Cherkasov N, McNab AI, Lukyanov DB, Anderson JA, Rebrov EV, van Veen AC. Mechanistic Insights into the Desorption of Methanol and Dimethyl Ether Over ZSM-5 Catalysts. Catal Lett. 2018;148(1):474-88.
36. Hinrischen O, van Veen AC, Zanthoff HW, Muhler M. TAP Reactor Studies. In: Haw JF, editor. In-Situ Spectroscopy in Heterogeneous Catalysis. WeinHeim: Wiley-VCH; 2002.
37. Marin GB, Yablonsky GS. Kinetics of Chemical Reactions: Decoding Complexity Weinheim, Germany: WILEY-VCH; 2011. 1-428.
38. Olsbye U, Svelle S, Lillerud KP, Wei ZH, Chen YY, Li JF, Wang JG, Fan WB. The formation and degradation of active species during methanol conversion over protonated zeotype catalysts. Chem Soc Rev. 2015;44(20):7155-76.
39. Van Veen AC, Zanthoff HW, Hinrichsen O, Muhler M. Fixed-bed microreactor for transient kinetic experiments with strongly adsorbing gases under high vacuum conditions. Journal of Vacuum Science and Technology, Part A: Vacuum, Surfaces and Films. 2001;19(2):651-5.
40. Courant R, Friedrichs K, Lewy H. Über die partiellen Differenzengleichungen der mathematischen Physik. Mathematische Annalen. 1928;100(1):32-74.
41. Danckwerts PV. Continuous flow systems: Distribution of residence times. Chem Eng Sci. 1953;2(1):1-13.
42. Van Der Linde SC, Nijhuis TA, Dekker FHM, Kapteijn F, Moulijn JA. Mathematical treatment of transient kinetic data: Combination of parameter estimation with solving the related partial differential equations. Applied Catalysis A: General. 1997;151(1):27-57.
43. Rasmuson A, Andersson B, Olsson L, Andersson R. Mathematical Modeling in Chemical Engineering USA: Cambridge University Press; 2014.
44. Gayubo AG, Alonso A, Valle B, Aguayo AT, Bilbao J. Kinetic Model for the Transformation of Bioethanol into Olefins over a HZSM-5 Zeolite Treated with Alkali. Industrial & Engineering Chemistry Research. 2010;49(21):10836-44.
45. Lagarias JC, Reeds JA, Wright MH, Wright PE. Convergence properties of the Nelder-Mead simplex method in low dimensions. SIAM Journal on Optimization. 1998;9(1):112-47.

46. Kobayashi M. Characterization of transient response curves in heterogeneous catalysis—I Classification of the curves. Chem Eng Sci. 1982;37(3):393-401.
47. Kobayashi M. Characterization of transient response curves in heterogeneous catalysis - 2. Estimation of the reaction mechanism in the oxidation of ethylene over a silver catalyst from the mode of the transient response curves. Chem Eng Sci. 1982;37(3):403-9.
48. Anderson MW, Klinowski J. Solid-state NMR studies of the shape-selective catalytic conversion of methanol into gasoline on zeolite ZSM-5. J Am Chem Soc. 1990;112(1):10-6.
49. Hoang TQ, Zhu X, Sooknoi T, Resasco DE, Mallinson RG. A comparison of the reactivities of propanal and propylene on HZSM-5. J Catal. 2010(271).
50. Jackson JE, Bertsch FM, Bertsch FM. Conversion of Methanol to Gasoline: A New Mechanism for Formation of the First Carbon-Carbon Bond. J Am Chem Soc. 1990;112(25):9085-92.
51. Yamazaki H, Shima H, Imai H, Yokoi T, Tatsumi T, Kondo JN. Direct production of propene from methoxy species and dimethyl ether over H-ZSM-5. Journal of Physical Chemistry C. 2012;116(45):24091-7.
52. Yablonsky GS, Constales D, Marin GB. A new approach to diagnostics of ideal and non-ideal flow patterns: I. The concept of reactive-mixing index (REMI) analysis. Chem Eng Sci. 2009;64(23):4875-83.

S6. Supplementary information

Transient Kinetic Studies and Microkinetic Modelling of Primary Olefin Formation from Dimethyl Ether over ZSM-5 Catalysts

S6.1. Quantification

To ascertain what to quantify, the full gaseous product release at steady-state was monitored. This quantification method has been used before (1). The quantification was performed in the following sequence: (1) Ion fragmentation patterns determined from calibration experiments done over a quartz bed of equal bed length and diameter to the ZSM-5 bed were obtained. Calibration experiments were conducted by passing each specie listed in Table S1 as well as argon through an inert bed consisting of quartz wool/quartz beads/quartz wool. The major m/e value was obtained in accordance with the NIST chemical database. Argon was used as internal standard for quantification, (2) Ion current intensities were taken relative to the inert standard, (3) Molar flow rates were obtained from the molar flow rate of the inert standard, the sensitivity coefficients, and the relative ion current intensities. A recursive deconvolution methodology was used: throughout all calculations, ion current intensities were taken relative to that of the chosen inert standard at the chosen m/e value:

$$I^{*}_{a(i),m(j)} = \frac{I_{a(i),m(j)}}{I_{S,m(S)}}$$

where $I_{a(i),m(j)}$ is the ion current intensity of specie i and m/z ratio of j. $I_{s,m(s)}$ is the ion current intensity of argon at m/z=40. Next, the sensitivity coefficient was calculated from calibration experiments where the partial pressures, respective mole fractions or molar flows are known:

$$Sens_{a(i),m(j)} = I^{*}_{a(i),m(j)} \cdot \frac{n_S}{n_{a(i)}} = \frac{I_{a(i),m(j)}}{I_{S,m(S)}} \cdot \frac{n_S}{n_{a(i)}}$$

where n_s is the molar flow rate of argon and $n_{a(i)}$ is the molar flow rate of specie i. $Sens_{a(i),m(j)}$ is the sensitivity coefficient of specie i at m/z ratio of j. To exploit an analysis by the mass spectrometer, the equation defining the sensitivity coefficient is rearranged, yielding an expression for the partial pressure, mole fraction or flow of the probe molecule as a function of the respective partial pressure, molar fraction or flow of the inert standard.

$$n_{a(i)} = I^{*}_{a(i),m(j)} \cdot \frac{n_S}{Sens_{a(i),m(j)}} = \frac{I_{a(i),m(j)}}{I_{S,m(S)}} \cdot \frac{n_S}{Sens_{a(i),m(j)}}$$

A (recursive) deconvolution (unfolding of the different compound contributions to the ion current intensity at a given m/e value) can be accomplished if the ion current intensity of interfering compounds is known at other m/e values without overlap.

$$I^{*}_{a(i),m(j)} = I^{*}_{common,m(j)} - \frac{Sens_{a(l),m(j)}}{Sens_{a(l),m(n)}} \cdot I^{*}_{a(l),m(n)} = \frac{I_{common,m(j)}}{I_{S,m(S)}} - \frac{Sens_{a(l),m(j)}}{Sens_{a(l),m(n)}} \cdot \frac{I_{a(l),m(n)}}{I_{S,m(S)}}$$

where $I^{*}_{common,m(j)}$ is the overall contribution of specie i at m/z ratio of j. $Sens_{a(l),m(j)}$ is the sensitivity coefficient of an overlapping fragment at m/z ratio of j. $Sens_{a(l),m(n)}$ is the sensitivity coefficient of an overlapping fragment at its own non-interfering m/z ratio of n. $I_{a(l),m(n)}$ is the ion current intensity of an overlapping fragment at its own non-interfering m/z ratio of n. Ar was monitored at m/e = 40, CH_3OH at m/e = 31, DME at m/e = 45, H_2O at m/e = 18, C_2H_4 at m/e = 27 and C_3H_6 at m/e = 41.

Subsequent deconvolution allowed for the subtraction of minor fragments from main species. The original data was subjected to noise reduction (a smoothing function (moving average of 5) to the curves to smoothen out irregularities due to noise in the signal) before presentation in the manuscript.

Table S6.1 below gives an overview of the major gaseous components and most interfering components that were detected in this study.

Table S6.1
Species present in the effluent, m/e values for measurement and the most important interfering components

Specie	m/e value	Interfering components
CH_3OH	31	DME
DME	45	
H_2O	18	
C_2H_4	27	C_3H_6
C_3H_6	41	

S6.2. Reaction schemes

Scheme P1

$CH_3OCH_3 + HZ \rightleftharpoons CH_3 \cdot Z + CH_3OH$
$CH_3OH + HZ \rightleftharpoons CH_3 \cdot Z + H_2O$
$H_2O + HZ \rightleftharpoons H_2O \cdot HZ$
$CH_3 \cdot Z + CH_3OH \rightleftharpoons CH_3OCH_3 \cdot HZ$
$CH_3 \cdot Z + CH_3O\mathrm{H} \rightarrow CH_4 + CH_2O \cdot \mathrm{H}Z$
$CH_4 + CH_2O \cdot \mathrm{H}Z \rightarrow CH_3CH_2OH \cdot HZ$
$CH_3CH_2OH \cdot HZ \rightleftharpoons CH_3CH_2 \cdot Z + H_2O$
$CH_3CH_2 \cdot Z \rightleftharpoons C_2H_4 + HZ$
$C_2H_4 + CH_3 \cdot Z \rightarrow C_3H_6 + HZ$

Scheme P2

$CH_3OCH_3 + HZ \rightleftharpoons CH_3 \cdot Z + CH_3OH$
$CH_3OH + HZ \rightleftharpoons CH_3 \cdot Z + H_2O$
$H_2O + HZ \rightleftharpoons H_2O \cdot HZ$
$CH_3 \cdot Z + CH_3OH \rightleftharpoons CH_3OCH_3 \cdot HZ$
$CH_3 \cdot Z + CH_3\mathrm{OH} \rightarrow CH_4 + CH_2O \cdot \mathrm{HZ}$
$CH_3\mathrm{OH} + CH_2O \cdot \mathrm{HZ} \rightarrow HOCH_2CH_2OH \cdot HZ$
$HOCH_2CH_2OH \cdot HZ + CH_3OCH_3 \rightarrow CH_3OCH_2CH_2OCH_3 \cdot HZ + H_2O$
$CH_3OCH_2CH_2OCH_3 \cdot HZ \rightarrow CH_3CHCHOCH_3 \cdot HZ + H_2O$
$CH_3CHCHOCH_3 + HZ \rightleftharpoons CH_3CHCHOCH_3 \cdot HZ$
$CH_3CHCHOCH_3 \cdot HZ + CH_3 \cdot Z \rightarrow C_3H_6 + CH_3OCH_2 \cdot Z$

Parameters	Optimised values	Unit
k_{1f}	0.000396	$Pa^{-1}\ s^{-1}$
k_{1b}	3.62257	$Pa^{-1}\ s^{-1}$
k_{2f}	0.002832	$Pa^{-1}\ s^{-1}$
k_{2b}	0.683886	$Pa^{-1}\ s^{-1}$
k_{3f}	0.0003	$Pa^{-1}\ s^{-1}$
k_{3b}	45.86694	s^{-1}
k_{4f}	0.000277	$Pa^{-1}\ s^{-1}$
k_{4b}	1.70000	s^{-1}
k_{5f}	0.441306	$Pa^{-1}\ s^{-1}$
k_{6f}	19.5715	$Pa^{-1}\ s^{-1}$
k_{7f}	1.821271	$Pa^{-1}\ s^{-1}$
k_{8f}	0.156231	s^{-1}
k_{9f}	0.093926	$Pa^{-1}\ s^{-1}$
k_{9b}	0.550363	s^{-1}
k_{10f}	18.81861	$Pa^{-1}\ s^{-1}$

Scheme P3

$$CH_3OCH_3 + HZ \rightleftharpoons CH_3 \cdot Z + CH_3OH$$
$$CH_3OH + HZ \rightleftharpoons CH_3 \cdot Z + H_2O$$
$$H_2O + HZ \rightleftharpoons H_2O \cdot HZ$$
$$CH_3 \cdot Z + CH_3OH \rightleftharpoons CH_3OCH_3 \cdot HZ$$
$$CH_3 \cdot Z + CH_3O\mathrm{H} \rightarrow CH_4 + CH_2O \cdot \mathrm{H}Z$$
$$CH_3\mathrm{O}CH_3 + CH_2O \cdot \mathrm{H}Z \rightarrow CH_3OCH_2CH_2OH \cdot HZ$$
$$HOCH_2CH_2OH \cdot HZ + CH_3OH \rightarrow CH_3OCH_2CH_2OCH_3 \cdot HZ + H_2O$$
$$CH_3OCH_2CH_2OCH_3 \cdot HZ \rightarrow CH_3CHCHOCH_3 \cdot HZ + H_2O$$
$$CH_3CHCHOCH_3 + HZ \rightleftharpoons CH_3CHCHOCH_3 \cdot HZ$$
$$CH_3CHCHOCH_3 \cdot HZ + CH_3 \cdot Z \rightarrow C_3H_6 + CH_3OCH_2 \cdot Z$$

Scheme P4

$CH_3OCH_3 + HZ \rightleftharpoons CH_3 \cdot Z + CH_3OH$
$CH_3OH + HZ \rightleftharpoons CH_3 \cdot Z + H_2O$
$H_2O + HZ \rightleftharpoons H_2O \cdot HZ$
$CH_3 \cdot Z + CH_3OH \rightleftharpoons CH_3OCH_3 \cdot HZ$
$CH_3OH \rightarrow CO + 2H_2$
$CH_3 \cdot Z + CO \rightarrow CH_3CO \cdot Z$
$CH_3CO \cdot Z + CH_3OH \rightarrow CH_3COOCH_3 \cdot HZ$
$CH_3COOCH_3 \cdot HZ \rightleftharpoons CH_3COOCH_3 + HZ$
$CH_3CO \cdot Z + H_2O \rightarrow CH_3COOH \cdot HZ$
$CH_3COOH \cdot HZ \rightleftharpoons CH_3COOH + HZ$
$CH_3COOCH_3 + H_2O \rightleftharpoons CH_3COOH + CH_3OH$
$CH_3COOH + HZ \rightleftharpoons CH_2CO \cdot HZ + H_2O$
$CH_2CO \cdot HZ + CH_3OH \rightarrow CH_3 \cdot Z + CH_2CO + H_2O$
$CH_3 \cdot Z + CH_2CO \rightarrow (CH_3)CHCO \cdot HZ$
$(CH_3)CHCO \cdot HZ \rightarrow CO + C_2H_4 + HZ$
$(CH_3)CHCO \cdot HZ + CH_3OH \rightarrow (CH_3)_2CHCO \cdot HZ + H_2O$
$(CH_3)_2CHCO \cdot HZ \rightarrow CO + C_3H_6 + HZ$

Parameters	Optimised values	Unit
k_{1f}	0.000362	$Pa^{-1}\ s^{-1}$
k_{1b}	2.692328	$Pa^{-1}\ s^{-1}$
k_{2f}	0.002165	$Pa^{-1}\ s^{-1}$
k_{2b}	0.383114	$Pa^{-1}\ s^{-1}$
k_{3f}	0.000387	$Pa^{-1}\ s^{-1}$
k_{3b}	71.05336	s^{-1}
k_{4f}	2.35e-04	$Pa^{-1}\ s^{-1}$
k_{4b}	1.70000	s^{-1}
k_{5f}	8.25e-06	s^{-1}
k_{6f}	204.3048	$Pa^{-1}\ s^{-1}$
k_{7f}	0.000741	$Pa^{-1}\ s^{-1}$
k_{8f}	0.180464	s^{-1}
k_{8b}	0.0625	$Pa^{-1}\ s^{-1}$
k_{9f}	216.2476	$Pa^{-1}\ s^{-1}$
k_{10f}	424.9608	s^{-1}
k_{10b}	0.000271	$Pa^{-1}\ s^{-1}$
k_{11f}	3.829351	$Pa^{-2}\ s^{-1}$
k_{11b}	0.002495	$Pa^{-2}\ s^{-1}$
k_{12f}	1.180564	$Pa^{-1}\ s^{-1}$
k_{12b}	0.001038	$Pa^{-1}\ s^{-1}$
k_{13f}	515.7614	$Pa^{-1}\ s^{-1}$
k_{14f}	447.3874	$Pa^{-1}\ s^{-1}$
k_{15f}	0.002131	s^{-1}
k_{16f}	114.306	$Pa^{-1}\ s^{-1}$
k_{17f}	240.4066	s^{-1}

Scheme P5

$CH_3OCH_3 + HZ \rightleftharpoons CH_3 \cdot Z + CH_3OH$
$CH_3OH + HZ \rightleftharpoons CH_3 \cdot Z + H_2O$
$H_2O + HZ \rightleftharpoons H_2O \cdot HZ$
$CH_3 \cdot Z + CH_3OH \rightleftharpoons CH_3OCH_3 \cdot HZ$
$CH_3OH + HZ \rightleftharpoons CH_3OH \cdot HZ$
$CH_3OH \cdot HZ \rightarrow CH_2O \cdot HZ + H_2$
$2CH_2O \cdot HZ \rightarrow CH_3OH \cdot HZ + HCOOH \cdot HZ$
$HCOOH \cdot HZ \rightarrow H_2O \cdot HZ + CO$
$CH_3 \cdot Z + CO \rightarrow CH_3CO \cdot Z$
$CH_3CO \cdot Z + CH_3OH \rightarrow CH_3COOCH_3 \cdot HZ$
$CH_3COOCH_3 \cdot HZ \rightleftharpoons CH_3COOCH_3 + HZ$
$CH_3CO \cdot Z + H_2O \rightarrow CH_3COOH \cdot HZ$
$CH_3COOH \cdot HZ \rightleftharpoons CH_3COOH + HZ$
$CH_3COOCH_3 + H_2O \rightleftharpoons CH_3COOH + CH_3OH$
$CH_3COOH + HZ \rightleftharpoons CH_2CO \cdot HZ + H_2O$
$CH_2CO \cdot HZ + CH_3OH \rightarrow CH_3 \cdot Z + CH_2CO + H_2O$
$CH_3 \cdot Z + CH_2CO \rightarrow (CH_3)CHCO \cdot HZ$
$(CH_3)CHCO \cdot HZ \rightarrow CO + C_2H_4 + HZ$
$(CH_3)CHCO \cdot HZ + CH_3OH \rightarrow (CH_3)_2CHCO \cdot HZ + H_2O$
$(CH_3)_2CHCO \cdot HZ \rightarrow CO + C_3H_6 + HZ$

Scheme P6

$CH_3OCH_3 + HZ \rightleftharpoons CH_3 \cdot Z + CH_3OH$
$CH_3OH + HZ \rightleftharpoons CH_3 \cdot Z + H_2O$
$H_2O + HZ \rightleftharpoons H_2O \cdot HZ$
$CH_3 \cdot Z + CH_3OH \rightleftharpoons CH_3OCH_3 \cdot HZ$
$CH_3 \cdot Z + CH_3OCH_3 \rightarrow CH_3OCH_2 \cdot Z + CH_4$
$CH_3OCH_2 \cdot Z + CH_4 \rightarrow CH_3OCH_2CH_3 \cdot HZ$
$CH_3OCH_2CH_3 \cdot HZ \rightleftharpoons C_2H_4 + CH_3OH + HZ$
$C_2H_4 + CH_3 \cdot Z \rightarrow C_3H_6 + HZ$

Scheme P7

$CH_3OCH_3 + HZ \rightleftharpoons CH_3 \cdot Z + CH_3OH$
$CH_3OH + HZ \rightleftharpoons CH_3 \cdot Z + H_2O$
$H_2O + HZ \rightleftharpoons H_2O \cdot HZ$
$CH_3 \cdot Z + CH_3OH \rightleftharpoons CH_3OCH_3 \cdot HZ$
$CH_3 \cdot Z + CH_3OCH_3 \rightarrow CH_3OCH_2 \cdot Z + CH_4$
$CH_3OCH_2 \cdot Z + CH_3OH \rightarrow CH_3OCH_2CH_2OH \cdot HZ$
$CH_3OCH_2CH_2OH \cdot HZ \rightleftharpoons CH_3OCHCH_2 + H_2O \cdot HZ$
$CH_3OCHCH_2 + CH_3 \cdot Z \rightleftharpoons CH_3CHCHOCH_3 + HZ$
$CH_3CHCHOCH_3 + CH_3 \cdot Z \rightarrow C_3H_6 + CH_3OCH_2 \cdot Z$

Scheme P9

$CH_3OCH_3 + HZ \rightleftharpoons CH_3 \cdot Z + CH_3OH$
$CH_3OH + HZ \rightleftharpoons CH_3 \cdot Z + H_2O$
$H_2O + HZ \rightleftharpoons H_2O \cdot HZ$
$CH_3 \cdot Z + CH_3OH \rightleftharpoons CH_3OCH_3 \cdot HZ$
$CH_3 \cdot Z + CH_3OCH_3 \rightarrow CH_3OCH_2 \cdot Z + CH_4$
$CH_3OCH_2 \cdot Z + CH_3OCH_3 \rightarrow CH_3OCH_2CH_2OCH_3 \cdot HZ$
$CH_3OCH_2CH_2OCH_3 \cdot HZ \rightarrow CH_3CHCHOCH_3 \cdot HZ + H_2O$
$CH_3CHCHOCH_3 \cdot HZ \rightleftharpoons CH_3CHCHOH + CH_3 \cdot Z$
$CH_3CHCHOH + HZ \rightarrow CH_3CHCHOH \cdot HZ$
$CH_3CHCHOH \cdot HZ \rightleftharpoons CH_3CH_2CHO \cdot HZ$
$CH_3CHCHOH + CH_3CH_2CHO \cdot HZ \rightarrow CH_3CH_2CHC(CH_3)CHO \cdot HZ + H_2O$
$CH_3CHCHOH + CH_3CH_2CHC(CH_3)CHO \cdot HZ \rightarrow CH_3CH_2CHC(CH_3)CHC(CH_3)CHO \cdot HZ + H_2O$
$CH_3CH_2CHC(CH_3)CHC(CH_3)CHO \cdot HZ \rightleftharpoons CH_3CHCHC(CH_3)CHC(CH_3)CHOH \cdot HZ$
$CH_3CHCHC(CH_3)CHC(CH_3)CHOH \cdot HZ \rightarrow C_9H_{12} \cdot HZ + H_2O$
$C_9H_{12} \cdot HZ \rightarrow C_6H_6 \cdot HZ + C_3H_6$

S6.3. Comparison of experimental data with simulations of the P8 reaction scheme using initial estimated parameters

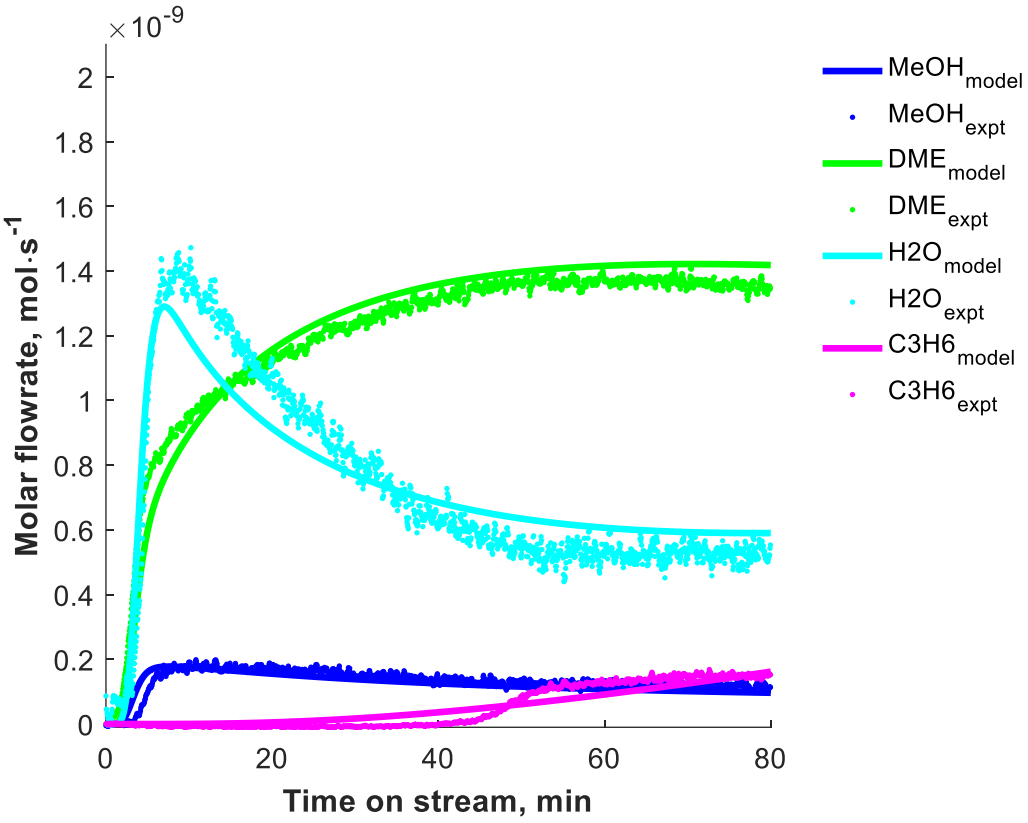

Fig. S6.3_P8: Step response of DME over ZSM-5 (Si/Al=25) catalyst at 300 °C using initial estimated parameters

S6.4. References

1. Gubanova EL. Experimental study and mathematical modeling of catalytic partial oxidation of methane to synthesis gas over monolith catalyst at short contact times [PhD Thesis]: Institut de Recherche sur la Catalyse et l'Environment de Lyon, IRCELYON; 2008.

Chapter 7

7. Experimental and Kinetic Modelling Studies of Methanol Conversion to Hydrocarbons over Zeolite Catalysts

This chapter focuses on MTH conversion over ZSM-5 (Si/Al =34) catalysts at 370 °C and 1 bar in a fixed bed reactor by combining experimental data and kinetic modelling results. The rational was to quantitatively describe the steady-state conversion of methanol to hydrocarbons and investigate the mechanisms that regulate product distribution over ZSM-5 catalysts. Propylene is the major olefin formed at 300 °C. Ethylene and propylene are observed at higher temperatures (see chapter 5). A transient kinetic model was used to investigate the induction period at 300 °C where only propylene is the major olefin produced (chapter 6). Having shown that they are produced directly from the methanol feed, a lumped kinetic model is used in this chapter to explain their direct formation at steady-state.

Abstract

A lumped kinetic model has been used to describe the conversion of methanol to hydrocarbons (MTH) over ZSM-5 catalysts at 370 °C and at conversions between 0.3 to 90%. The reduced lumped kinetic model, based on the law of mass action, contains 98 rate constants, 32 adsorption equilibrium constants and 98 reaction steps to describe the transformation of 33 components involved in its implicit chemistries. These chemistries include methanol equilibration, olefin formation, olefin methylation with methanol and DME, olefin oligomerisation, olefin cracking, hydrogen transfer and cyclisation, aromatic methylation, aromatic dealkylation (cracking), paraffin cracking and paraffin alkylation. The model shows that the direct formation of olefins can describe the formation of olefins at low contact times. The rate of ethylene formation is, however, 5 times slower than propylene formation. For the first time, olefin methylation with DME has been shown to be 3.5 times faster than its methylation with methanol and aromatic methylation with DME has been shown to be 2.5 times faster than its methylation with methanol. These results validate DME as the major methylating specie involved in surface reactions during MTH conversion and propylene as the major olefin. Of the chemistries involved, the methanol equilibration, direct olefin formation, olefin methylation, oligomerisation and cracking chemistries are the slowest steps involved in MTH conversion. The olefin cycle which consists of these chemistries control the rate of MTH conversion over ZSM-5 catalysts at 370 °C.

7.1. Introduction

The need to generate fuels and chemicals sustainably has fuelled interest in the conversion of methanol to hydrocarbons (MTH). Since its initial discovery in 1977 (1), a significant amount of qualitative information has been generated concerning the mechanistic aspects of the reaction (2-4). It has been shown that during the steady state MTH conversion over zeolite catalysts, a “hydrocarbon pool” mechanism regulates product distribution (5, 6). Over ZSM-5 catalysts, the hydrocarbon pool manifests itself through an aromatic cycle and an alkene cycle working in tandem. In the aromatic cycle, aromatics are methylated by oxygenates and dealkylate to give olefins. The olefin cycle involves methylating primary olefins to higher homologues that subsequently crack (5). Hydrogen transfer and cyclisation chemistries link the alkene to the aromatic cycle (2). The propagation of the alkene and aromatic cycles are tunable over the ZSM-5 catalysts depending on process conditions (2).

As stated in Chapter 2, several models have been constructed using lumped (7-10) or single event micro-kinetic (11-13) methodologies to obtain quantitative information on the kinetics of MTH conversion. For a short description here, Chen and Reagan (7) used a four-lump model in establishing the autocatalytic nature between oxygenates and olefins over ZSM-5. Schoenfelder and co-workers (8) used a seven-lump model in describing the methanol-to-hydrocarbons reaction over ZSM-5, while Bos and co-workers (9) used a model system of 12 reactions involving 6 lumps and coke. Aguayo and co-workers (14) used a seven-lump model to obtain the maximum yields of olefins at high temperatures (400 – 550 °C) during methanol-to-olefin conversion over ZSM-5 catalysts of Si/Al = 30.

Using the Single Event MicroKinetic (SEMK) methodology, Froment and co-workers (12, 13) obtained modelling results that show that a direct ylide mechanism and a carbenium mechanism can describe steady state generation of hydrocarbons from methanol over ZSM-5 catalysts with a Si/Al = 200 at temperatures between 360 – 480 °C and space time between 0.1 – 7 g_{cat} h mol^{-1} (0.36 – 25.2 kg_{cat} s mol^{-1}) . Conversely, Marin and co-workers (11) showed that steady-state MTH conversion can be obtained from the indirect hydrocarbon pool (via an aromatic cycle). They used the SEMK methodology over ZSM-5 with a Si/Al = 200 and temperatures between 370 – 480 °C and at space times between 0.5 and 6.5 kg_{cat} s mol^{-1}.

The fundamental challenge during the steady-state conversion of methanol to hydrocarbons over zeolite catalysts lie in identifying a single descriptor that quantitatively and statistically describes the product distribution observed. The key motivation stems from advances made with the Fischer-Tropsch process which was studied and understood as being dominated by surface polymerisation processes. The Fischer-Tropsch process is investigated in terms of essentially one kinetic parameter, α, the chain-growth probability factor. Advances in MTH chemistry could be sought in a similar way. The principal methodology lies in describing each major chemistry in the MTH process by a single kinetic parameter and then

explaining overall MTH product distribution by an overarching parameter consisting of these individual parameters. In a first step, this chapter aims to investigate the chemistries that control product distribution at steady-state. This contribution aims to describe MTH conversion over ZSM-5 catalysts of Si/Al = 34 at 370 °C and 1 bar and at space times between 0.0134 – 0.334 kg_{cat} s mol^{-1}. A reduced lumped kinetic model applying the law of mass action was used. Parameters were estimated for the MTH process using an ideal plug flow reactor.

7.2. Experimental

7.2.1. Methodology

Steady state experiments were conducted by Dr Dmitry Lukyanov. Experimental details are given as follows:

The ammonium form of a ZSM-5 catalyst with Si/Al ratio of 34 was used. The zeolite powder was pressed into disks, crushed and sieved to obtain size fractions between 0.25 - 0.5 mm, which were subsequently used in catalytic experiments. The zeolite pellets were housed between two quartz wool plugs in a quartz cylindrical reactor of 4.5 mm. Prior to catalytic experiments, the catalyst was calcined with a heating rate of 1 °C min^{-1} in a flow of nitrogen to 500 °C and maintained at this temperature for 4 h.

All reactions were carried out at 1 bar in a continuous flow micro reactor at 370 °C. Steady-state conditions were established after 7 min time-on-stream (TOS). The contact time was varied under steady-state conditions by changing the mass of catalyst charged at a constant feed of 25 wt% methanol (balance nitrogen) to obtain different levels of conversion. The reaction mixture was analysed by an online gas chromatograph equipped with a flame ionisation detector (GC-FID). The initial conditions were restored at the end of each experimental run to verify the absence of deactivation. The experimental data was then subjected to further kinetic modelling studies by the author.

7.3. Kinetic model development and methodology

7.3.1. Components of the kinetic model

MTH conversion is a complex multistage and multicomponent reaction. At 100% conversion, hydrocarbons with carbon number up to 10 appear in the product mixture. A final kinetic model involving 33 components which includes methane, formaldehyde, hydrogen, carbon monoxide, C2 – C10 olefins and paraffins, methanol, DME, water, dimethoxymethane, dimethoxyethane, C6 – C10 aromatics and nitrogen was constructed. Due to the intricate complexity of this reaction, isomers of the same carbon number and functional group were lumped into a single component. Such a lumping methodology has been shown to accurately

describe a subset of reactions for the design and development of industrial processes over ZSM-5 catalysts (15, 16).

7.3.2. Reaction and Adsorption steps

The reaction scheme and rate equations for the full kinetic model involving 33 species including nitrogen with 32 adsorption equilibrium constants, 17 reaction equilibrium constants and 230 rate constants are given in the supplementary information on this chapter. Units for rate constants are given either in mol g^{-1} s^{-1} bar^{-1} for reactions between one gaseous molecule and an adsorbed molecule or one gaseous molecule alone, mol g^{-1} s^{-1} for reactions involving one or two adsorbed molecules.

7.3.3. Rates of transformation

Rate equations were written according to the law of mass action. For instance, the rate equations for olefin methylation by methanol is as follows:

$$r_i = k_i P_{C_nH_{2n}}[CH_3OH.HZ] = k_i K_j P_{C_nH_{2n}} P_{CH_3OH}.[HZ] \quad (7.1)$$

where r_i is the rate of the ith step, k_i is the rate constant for the ith methylation step and K_j is the adsorption equilibrium constant of the adsorbed species, j. $P_{C_nH_{2n}}$ is the partial pressure of an olefin.

With specification of all components from 1 to 230 of the reaction steps from 1 to 33, the kinetic model of a set of 33 coupled ordinary differential equations (ODE) describing the rates of transformation of 33 components in 230 reaction steps is given as:

$$R_i = \sum_{j=1}^{33} \nu_{i,j} r_j \qquad (1 \leq i \leq 230) \quad (7.2)$$

where R_i is the rate of transformation of the component i (mol g^{-1} s^{-1}), $\nu_{i,j}$ is the stoichiometric coefficient of the component i in the reaction step j and r_j is the rate of the reaction step j.

For steady-state kinetic modelling, the plug flow reactor model was used as shown below:

$$\frac{dy_i}{d\tau} = R_i MW_i \qquad (1 \leq i \leq 230) \quad (7.3)$$

where y_i is the mass fraction of the component i in the reaction mixture (-), τ is the contact time (s) and MW_i is the molecular weight of the component i (g/mol). Contact time is defined as the ratio between catalyst weight (W) and mass flow rate of the feed (m), i.e. $\tau\ (g_{cat} g_{feed}^{-1} s) = W/m$. For the numerical integration of the system of differential equations, a stiff ode solver (ode15s) was used in MATLAB (version R2017b).

The ratio of the diameter of the reactor to the diameter of the catalyst particle was large enough to minimize channelling effects. Axial dispersion effects have been assumed to be

minimal in view of the catalyst particle size and configuration of the fixed bed. The ratio of bed length to diameter of the packed bed was greater than 50 in line with recommendations for isothermal packed bed reactors (17). Molar expansion is also assumed negligible.

The equations for the rate of transformation describing the kinetic model are given in the supplementary information accompanying this chapter.

7.3.4. Parameter Estimation: Non-linear Least Squares Method

An inverse kinetic problem is the identification of the type of kinetic model and its parameters. There is no universal method for solving inverse kinetic problems. Usually, the solution is often obtained by solving iteratively a series of direct kinetic problems. A direct kinetic problem involves calculating reaction rates on the basis of a known kinetic model with known kinetic parameters (18).

The non-linear least squares method involves minimizing the sum of squares of residuals (SSR). This is given by (19, 20):

$$SSR = \sum_{n=1}^{N_c} \sum_{m=1}^{N_d} w_{n,m}\left(Y_{n,m}^{obs} - Y_{n,m}^{cal}\right)^2 \rightarrow min \qquad (7.4)$$

where:

n	component number;
m	observation number;
N_c	total number of components;
N_d	total number of observations;
$w_{n,m}$	weighting factor of the m-th observation of component n.
Y^{obs}	experimental yield data
Y^{cal}	model yield data

The weighting factor will be taken as 1 as it is assumed that all data have the same significance since only yields were measured. The least square method (21, 22) is based on the following assumptions for the error (ε) of the observations (23):

1) The mean of ε is zero;
2) The probability distribution of ε is normal;
3) The variance of the probability distribution of ε is constant; and
4) The errors of any two observations are independent.

7.4. Estimation of kinetic parameters

7.4.1. Adsorption constants

The adsorption constant of methanol was obtained following the Langmuir adsorption isotherm:

$$HZ_i = \frac{K_i P_i}{1 + K_i P_i} \tag{7.5}$$

where K_i is the adsorption constant of the ith specie and P_i is the partial pressure of the ith gaseous specie and HZ_i is the fractional coverage of the ith specie. In the work of Svelle et al. (24) on the co-reaction of methanol with ethylene, the rates increased by 20% with an increase in the partial pressure of methanol from 20 mbar to 100 mbar. The increase in rates indicates that methanol coverage must have increased. Applying Langmuir adsorption isotherm for a 20% increase in coverage from 20 mbar to 100 mbar gave an adsorption constant of 190 bar^{-1}.

Similarly, the adsorption constant for DME can be obtained following the work of Hill et al. (25) on the co-reaction of benzene, toluene and xylene with DME over H-MFI catalysts. An adsorption constant of 250 bar^{-1} allowed for a 0.77% change in coverage from 290 mbar to 670 mbar in agreement with the results of Hill et al. (25).

The adsorption constant of olefins, paraffins and aromatics were obtained as 1.53 bar^{-1}, 0.01 bar^{-1} and 7.81 bar^{-1} following the work of Lukyanov and co-workers (26). A decrease in rates of methanol conversion by 10% is observed when methanol is co-fed with water (27). This was attributed to the preferential adsorption of water molecules. It was then assumed that the adsorption constant was 10% less than methanol.

From the following model with 33 species including nitrogen, the following adsorption equilibrium constants were used.

Table 7.1: Adsorption equilibrium constants

Adsorption constant	Value (bar^{-1})	Source
Methanol	190	(24, 28)
DME	250	(25)
Water	209	(27)
Hydrogen	0.01	(26)
Carbon monoxide	0.0033	(29)
Olefins	0.4 - 1.53	(26) and regression analysis
Paraffins	0.01	(26)
Formaldehyde	400	(30)
Dimethoxymethane, Dimethoxyethane	250	Assumed to be the same as DME
Aromatics	7.81	(26)

7.4.2. Equilibrium constants

Thermodynamic calculations for oligomerisation-cracking reaction used to constrain the parameters to be estimated. Firstly, the enthalpy, entropy and molar heat capacity changes were calculated at standard conditions (298 K and 1 bar). The enthalpies and entropies were calculated at 370 °C and 1 bar which allowed for the estimation of the Gibbs free energy.

At standard temperature and pressure, the enthalpy of the reaction is given by:

$$\Delta H_r^\theta = \sum_{products} \upsilon \Delta H_f^\theta - \sum_{reactants} \upsilon \Delta H_f^\theta \quad (7.6)$$

Entropy of reaction is given by:

$$\Delta S_r^\theta = \sum_{products} \upsilon \Delta S_f^\theta - \sum_{reactants} \upsilon \Delta S_f^\theta \quad (7.7)$$

Molar heat capacity is given by:

$$\Delta C_p^\theta = \sum_{products} \upsilon C_p^\theta - \sum_{reactants} \upsilon C_p^\theta \quad (7.8)$$

where ΔH_f^θ is the enthalpy of formation at standard temperature and pressure, υ is the stoichiometric coefficient, ΔS_f^θ is the entropy of formation at standard temperature and pressure, C_p^θ is the heat capacity at standard temperature and pressure. The enthalpies and entropies of reaction can be calculated at T equals 370 °C for the conversion of methanol to gasoline through the following reactions:

$$\Delta H_r^T = \Delta H_r^\theta + \int_{298}^{T} \Delta C_p dT \quad (7.9)$$

$$\Delta S_r^T = \Delta S_r^\theta + \int_{298}^{T} \frac{\Delta C_p}{T} dT \quad (7.10)$$

Consequently, the Gibb's free energy (ΔG_r^T) and the reaction equilibrium constant (K) can be determined for each reaction as:

$$\Delta G_r^T = \Delta H_r^T - T \cdot \Delta S_r^T \quad (7.11)$$

$$K = e^{-\frac{\Delta G_r^T}{RT}} \quad (7.12)$$

Thermodynamic data was obtained from Yaws' Handbook of Thermodynamic Properties for Hydrocarbons and Chemicals (31). The oligomerisation-cracking equilibrium constants were obtained as:

Table 7.2: Reaction equilibrium constants

	Enthalpies of formation (J mol^{-1})	**Entropy of Formation (J/mol K)**	**Molar heat Capacity (J/mol K)**		
Ethene	**52500**	**-53.6443**	**43.924**		
Propene	**19700**	**-142.55**	**64.994**		
Butene					
1-butene	-500	-273.80	88.41		
Trans-2-butene	-11000	-249.20	90.38		
Cis-2-butene	-7400	-244.51	82.16		
	-6300	**-255.84**	**86.98**		
Pentene					
1-pentene	-21300	-355.07	113.11		
Trans-2-pentene	-31100	-388.76	111.84		
Cis-2-pentene	-26300	-334.73	105.52		
2-methyl-2-butene	-40800	-343.45	108.97		
2-methyl-1-butene	-34900	-342.45	114.47		
3-methyl-1-butene	-27600	-347.48	121.51		
	-30333	**-351.99**	**112.57**		
Hexene					
1-hexene	-42000	-434.68	135.67		
cis-2-hexene	-50300	-433	130.09		
trans-2-hexene	-53300	-434.68	136.29		
cis-3-hexene	-47300	-441.72	129.65		
trans-3-hexene	-52300	-441.39	137.99		
2,3-dimethyl-1-butene	-61500	-445.75	145.83		
3,3-dimethyl-1-butene	-60400	-476.61	131.44		
2,3-dimethyl-2-butene	-70000	-453.8	127.33		
2-ethyl-1-butene	-56000	-441.39	137.44		
	-54789	**-444.78**	**134.64**		
Heptene					
1-heptene	**-62800**	**-529.6**	**159.43**		
Octene					
1-Octene	**-83600**	**-626.53**	**183.84**		
Nonene					
1-Nonene	**-104000**	**-723.8**	**206.59**		
Decene					
1-Decene	**-124690**	**-820.12**	**233.1**		
Reactions at 298 K					
Reactants				**Product**	
ethene-ethene	-111300	-148.55	-0.86	C4	
propene-ethene	-102533	-155.80	3.65	C5	

butene-ethene	-100989	-135.30	3.73	C6	
propene-propene	-94189	-159.68	4.65	C6	
pentene-ethene	-84967	-123.97	2.94	C7	
butene-propene	-76200	-131.21	7.45	C7	
hexene-ethene	-81311	-128.11	5.28	C8	
pentene-propene	-72967	-131.99	6.28	C8	
butene-butene	-71000	-114.86	9.87	C8	
heptene-ethene	-93700	-140.56	3.24	C9	
hexene-propene	-68911	-136.47	6.96	C9	
pentene-butene	-67367	-115.97	7.04	C9	
octene-ethene	-93590	-139.95	5.34	C10	
heptene-propene	-81590	-147.97	8.68	C10	
hexene-butene	-63601	-119.50	11.48	C10	
pentene-pentene	-64023	-116.14	7.96	C10	
Reactions at 643 K					
Reactants				**Product**	**Equilibrium constants**
ethene-ethene	-111598	-149	-15655	C4	18.7
propene-ethene	-101273	-153	-2903	C5	1.72
butene-ethene	-99703	-132	-14549	C6	15.2
propene-propene	-92585	-156	7790	C6	0.232
pentene-ethene	-83954	-122	-5696	C7	2.90
butene-propene	-73629	-125	7056	C7	0.267
hexene-ethene	-79490	-124	272	C8	0.950
pentene-propene	-70801	-127	10965	C8	0.129
butene-butene	-67595	-107	1377	C8	0.773
heptene-ethene	-92584	-138	-3806	C9	2.04
hexene-propene	-66510	-131	17799	C9	0.0358
pentene-butene	-64939	-111	6152	C9	0.316
octene-ethene	-91749	-136	-4403	C10	2.28
heptene-propene	-78597	-141	12258	C10	0.101
hexene-butene	-59641	-111	11523	C10	0.116
pentene-pentene	-61277	-110	9465	C10	0.170

The relative oligomerisation rates between the various oligomerisation-cracking equations were obtained directly from previous work by Lukyanov and co-workers (26) further constraining the amount of parameters to be directly estimated.

7.5. Modelling methodology

The estimation of parameters was carried out in a stepwise manner. The equilibrium constant for the methanol dehydration step was obtained following the correlation given with temperature by Aguayo and co-workers (14, 32).

$$K_p = exp\left[-9.76 + \frac{3200}{T} + 1.07 \cdot logT - 0.66 \times 10^{-3} \cdot T + 0.49 \times 10^{-7} \cdot T^2 + \frac{6500}{T^2}\right] \quad (7.13)$$

The model was initialised with the equilibration of methanol to DME and water at very low contact times. The model was made to fit experimental data by varying the rate constant of the forward reaction of one adsorbed methanol molecule and one gaseous molecule. Subsequent backward rate constant was calculated from the equilibrium constant of the methanol dehydration reaction. This was to ensure thermodynamic consistency and reduce the number of parameters obtained by regression. Next, the rate constants for the direct formation of ethylene from DME and propylene from methanol and DME were estimated. Thereafter, methylation of olefins was next initialised at relatively higher contact times before subsequent oligomerisation/cracking equilibration reactions. The rates of oligomerisation were fixed using previous work by Lukyanov and co-workers (26) and thermodynamic consistency was ensured using equilibrium constants to fix the rate of cracking reactions. Thereafter, the rate constants for hydrogen transfer and cyclisation of C6 – C10 olefins were obtained and aromatic methylation and dealkylation constants were estimated. The rate of methylation of olefins and aromatics with methanol were separated from methylation with DME in agreement with previous work by Olsbye and co-workers (33).

7.6. Results and discussion

7.6.1. Rate analysis

The conversion profile with contact time, τ was fitted using a logistic function (Fig. 1):

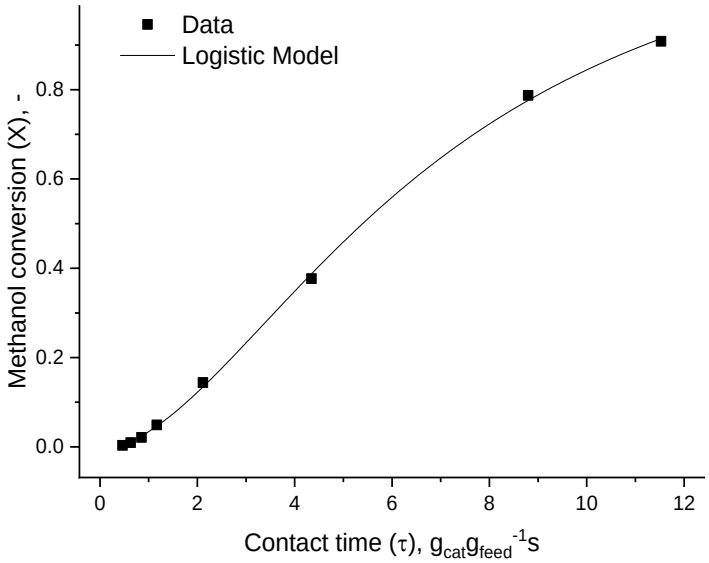

Fig. 7.1: The conversion of methanol with contact time over ZSM-5 catalysts (Si/Al = 34) at 370 °C

The S-shaped profile of methanol conversion with contact time signifies that the reaction is autocatalytic (34). After 7 min TOS, steady-state conditions are established before experimental studies were conducted. The minimum contact time required for the initiation of the reaction represents the concentration of accumulated reactive species necessary to initiate the jump in conversions. This concentration is determined by temperature, zeolite Si/Al ratio and the length of the induction period as shown in chapters 5 and 6.

Differential analysis of integral reactors was then employed to obtain rates (34). Here,

$$r = \frac{dX_A}{d(W/F_{AO})} = \frac{dX_A}{d(\tau)} \tag{7.14}$$

7.6.2. Estimation of transport effects

The various criteria (34, 35) for checking for the absence of internal mass transfer (Weisz-Prater), external mass transfer (Carberry number), internal and external heat transfer (Prater numbers) are evaluated mostly for conditions where the order of the reaction is known. For autocatalytic reactions consisting of many chemistries such as those involved in MTH conversion, the order of reaction varies with contact time. For instance, at low contact times, the effect of transport artefacts on primary olefin formation can be evaluated where these chemistries are exclusive to this region. With increasing contact times and conversion, various

chemistries can be evaluated: olefin methylation with methanol or DME, olefin oligomerisation and cracking, hydrogen transfer and cyclisation, aromatic methylation and dealkylation and paraffin cracking and dealkylation. For each specific chemistry, the order of reaction must be evaluation with contact time or conversion. Thereafter, the effect of transport on each chemistry can be evaluated using the various criteria described above.

Nonetheless, an assumption of first order reaction can be made such that transport effects can be predicted. The various criteria have been given in equations 3.14 – 3.17 in chapter 3. Firstly, rates obtained in equation 7.14 are given in $g_{feed}g_{cat}^{-1}s^{-1}$ and are converted to $mol_{feed}m_{cat}^{3}s^{-1}$ using the molecular weight of the feed mixture (29.02 g_{feed} mol_{feed}^{-1}), density of the solid catalyst (2.2×10^{6} g_{cat} m_{cat}^{-3}) and assumed particle porosity (0.5). Secondly, the concentration of species were obtained after converting the respective weight fractions to mole fractions for use in the ideal gas equation at GC-FID conditions (T_{FID} = 453 K). The concentrations in the reactor ($T_{reactor}$ = 643 K) is then estimated thereafter. Weisz number is estimated according to equation 3.16, the Carberry number is estimated according to 3.14, internal Prater number according to 3.17 and external Prater number according to equation 3.15. Catalyst and reaction parameters are given in table 7.3 and the ensuing transport parameters estimated at the pellet level are given in table 7.4.

Table 7.3: Catalyst and reaction parameters used for transport effect estimation at 370 °C

Parameter	**Value**	**Unit**
Average pellet diameter	375	µm
Porosity	0.5	-
Constriction factor	0.5	-
Tortuosity	3	-
Gaseous diffusivity	6.195×10^{-6}	$m^2\ s^{-1}$
Effective diffusivity	5.163×10^{-6}	$m^2\ s^{-1}$
Specific external surface area	16000	$m^2\ m^{-3}$
Si/Al ratio	34	-
Sherwood number (Sh)	2 (assumed)	-
Mass transfer coefficient	0.0275	$m\ s^{-1}$
Nusselt number (Nu)	2 (assumed)	-
Heat transfer coefficient	2167.89	$W\ m^{-2}\ K^{-1}$
Effective thermal conductivity	0.4065	$W\ m^{-1}\ K^{-1}$
Activation Energy, E_a*	153	$kJ\ mol^{-1}$
Heat of reaction, $(-\Delta H_r)$^	44.73	$J\ mol^{-1}$

* Obtained from Qi et al. (36) assuming the kinetics of the first carbon-carbon bond is rate-limiting
^ Obtained from Chang and Silvestri (1)

Table 7.4: Transport (Weisz, Carberry, Internal and External Prater numbers) parameters at 370 °C

Contact time, Tau, $g_{cat}g_{feed}^{-1}s$	Conversion, -	Weisz, -	Carberry number, -	Internal Prater ($\times 10^{-5}$), -	External Prater ($\times 10^{-3}$), -
0.463	0.0034	0.27	0.80	2.90	1.29
0.632	0.0095	0.34	1.01	3.65	1.62
0.855	0.021	0.41	1.24	4.53	2.01
1.166	0.0491	0.51	1.54	5.57	2.47
2.116	0.1441	0.70	2.10	7.63	3.38
4.345	0.3766	0.76	2.27	8.12	3.60
8.798	0.7873	0.42	1.25	4.52	2.00
11.528	0.9083	0.27	0.81	2.95	1.31

For intrinsic kinetic parameters, the Weisz, Carberry, internal and external Prater parameters, assuming first order kinetics, should be lower than 0.15, 0.05, 0.1, and 0.05 respectively. Table 7.4 shows that the data supplied were obtained under internal and external mass transport limitations at the pellet scale.

A more descriptive model can be obtained using a combination of the Maxwell-Stefan equations (where molecular diffusion persists) or the dusty gas model (where molecular and Knudsen diffusion are predominant) along with the equation of continuity for multi-component mixtures, bootstrap conditions linking the various stoichiometry and boundary equations. This model would result in coupled ordinary differential equations at steady-state describing the transport and reaction of species across the porous zeolite and its boundary layer.

7.6.3. Comparing model with experiment

Figure 7.2 shows the results of comparing experiment to model leading to parameter estimates. A very good agreement is obtained for methanol, DME, water, olefins, aromatics and paraffins. At low contact times, paraffins and aromatics are generally underestimated. This is probably due to higher measurement errors associated with acquiring data at such very small paraffin and aromatic mass fractions. Nonetheless, the model reproduces the trend observed at such low mass fractions.

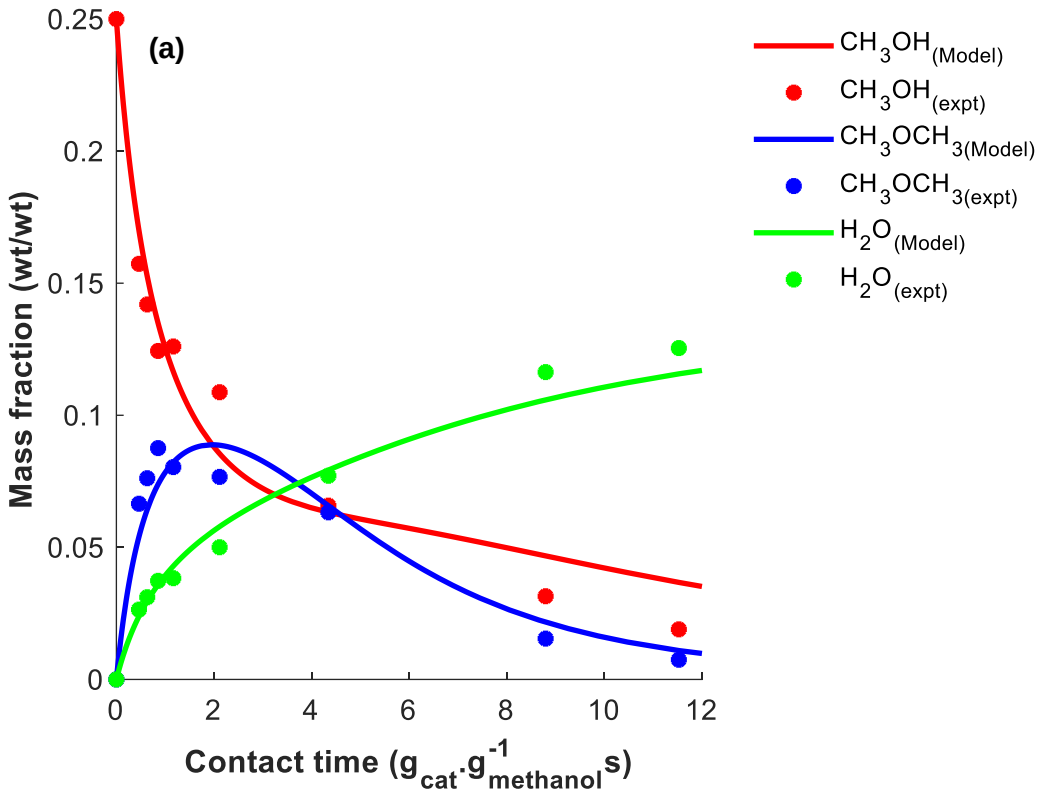
(a)
Mass fraction (wt/wt)
Contact time (g_cat.g^-1_methanol s)
CH3OH(Model)
CH3OH(expt)
CH3OCH3(Model)
CH3OCH3(expt)
H2O(Model)
H2O(expt)

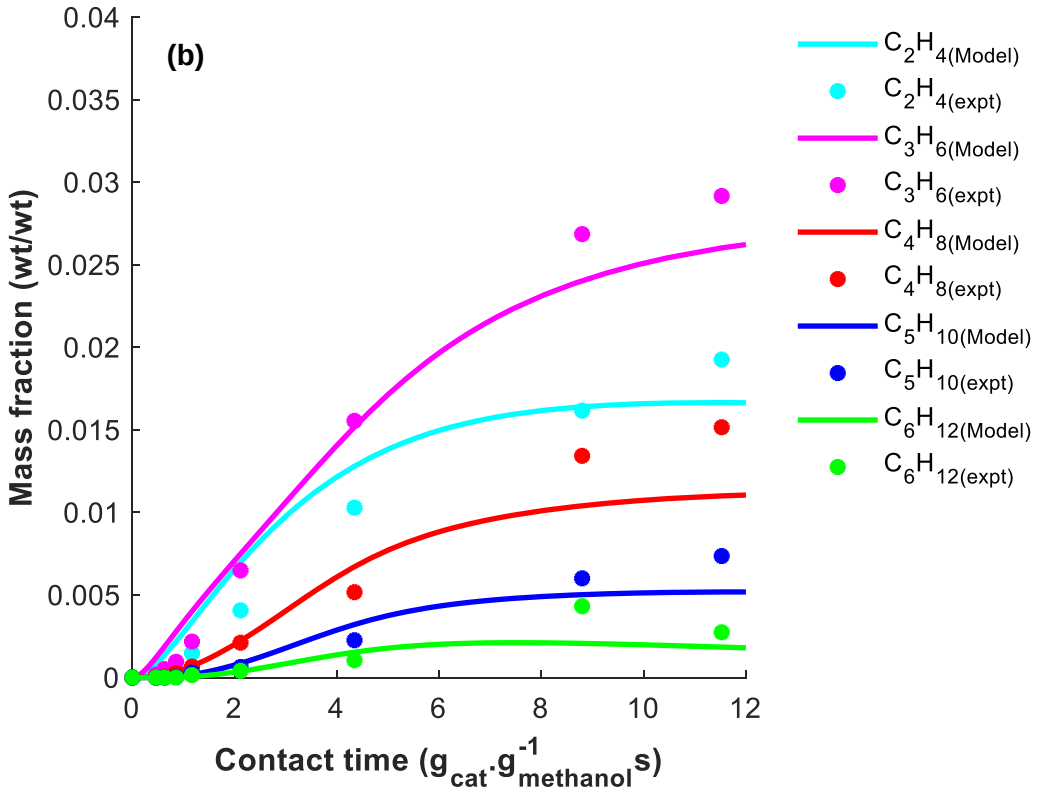
(b)
Mass fraction (wt/wt)
Contact time (g_cat.g^-1_methanol s)
C2H4(Model)
C2H4(expt)
C3H6(Model)
C3H6(expt)
C4H8(Model)
C4H8(expt)
C5H10(Model)
C5H10(expt)
C6H12(Model)
C6H12(expt)

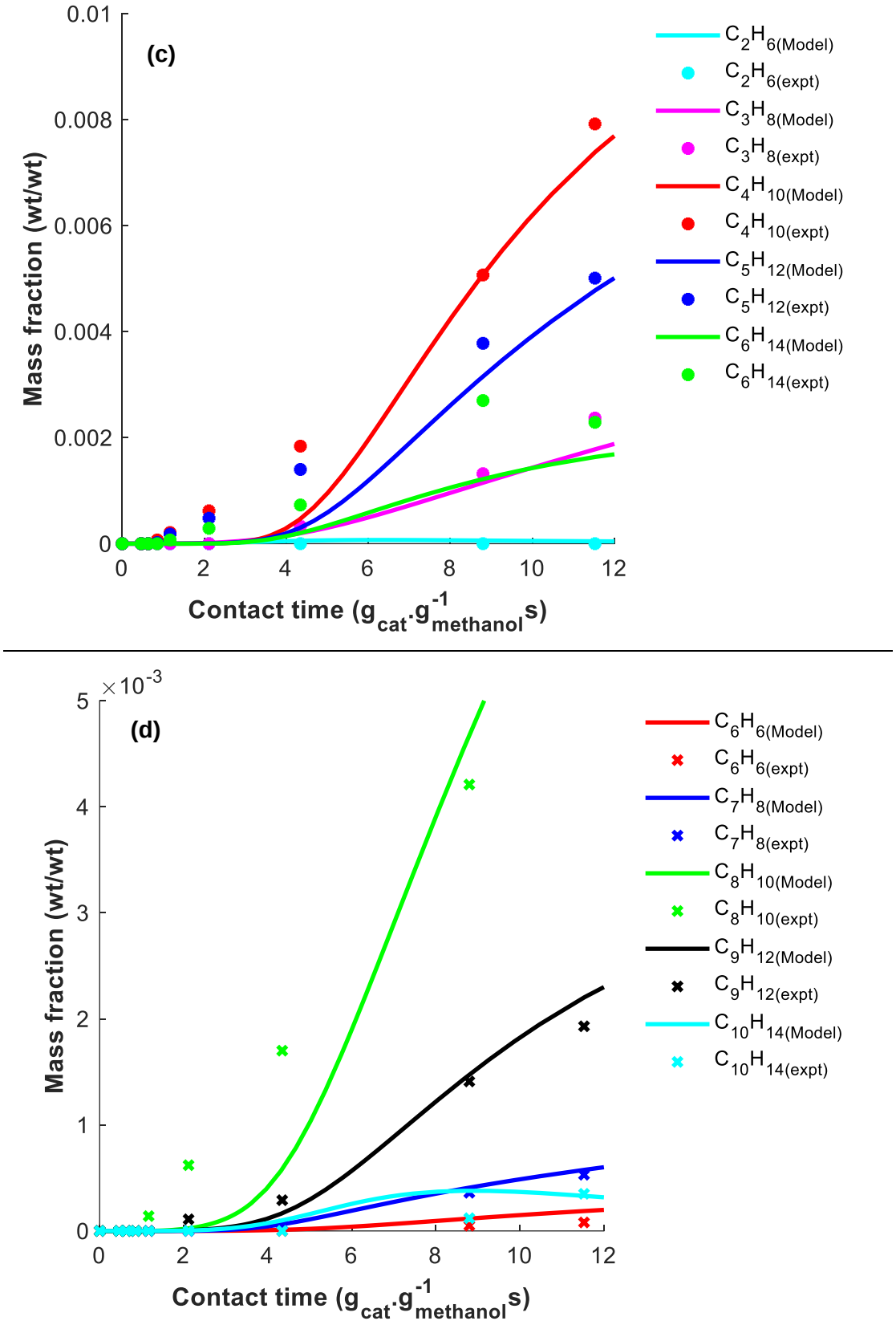

Fig. 7.2: Graphs showing initial comparisons of models to experiments for (a) initial equilibration products, (b) C2 – C6 olefins, (c) C2 – C6 paraffins and (d) C6 – C10 aromatics.

7.6.3.1. Equilibration reaction

The equilibration reaction is given as:

$CH_3OH \cdot HZ + CH_3OH \rightleftharpoons CH_3OCH_3 \cdot HZ + H_2O$

The rate of formation of DME and water was estimated, and then thermodynamic considerations as described in section 7.5 were used to estimate the equilibration rate constants. The rate of the backward reaction i.e. the formation of methanol from DME and water was then obtained from the forward reaction and the constraining effect from thermodynamic considerations. A forward rate constant of 0.0185 mol g^{-1} s^{-1} bar^{-1} and a backward rate constant of 0.0032 mol g^{-1} s^{-1} bar^{-1} were obtained.

7.6.3.2. Olefin formation

Olefin formation was described *via* the direct route:

$CH_3OCH_3 \cdot HZ + CH_3OH \rightarrow C_3H_6 \cdot HZ + 2H_2O$

$CH_3OCH_3 \cdot HZ \rightarrow C_2H_4 \cdot HZ + H_2O$

Here, the direct transformation of DME to ethylene was described and the co-reaction of DME and methanol was described to obtain propylene. The direct formation of propylene from methanol and DME was 5.5 times faster than the direct formation of ethylene from DME.

7.6.3.3. Olefin methylation

Olefin methylation by methanol or DME go according to:

$CH_3OH \cdot HZ + C_nH_{2n} \longrightarrow C_{n+1}H_{2n+2} \cdot HZ + H_2O \qquad 2 \leq n \leq 10$

$CH_3OCH_3 \cdot HZ + C_nH_{2n} \longrightarrow C_{n+1}H_{2n+2} \cdot HZ + CH_3OH \qquad 2 \leq n \leq 10$

The methylation of olefins by methanol was distinguished from olefin methylation by DME. Firstly, the ratios of the methylation of olefins (C2:C3:C4:C5:C6) with methanol was 1:2:4:9:15. The rate of olefin methylation with DME was higher than methanol by a factor of 3.5. For C6 – C10 olefins, the rate of methylation stayed constant and was higher than the methylation of ethylene by a factor of 15. The rates of methylation of ethylene was observed to be higher than its direct formation by a factor of 10.

7.6.3.4. Olefin oligomerisation and cracking

Olefin oligomerisation and cracking reactions occur according to:

$C_nH_{2n} \cdot HZ + C_mH_{2m} \rightleftharpoons C_{n+m}H_{2n+2m} \cdot HZ$

$2 \leq n \leq 5, 2 \leq m \leq 5, \qquad n + m \leq 10, 2n + 2m \leq 20$

The olefin oligomerisation constants were described relative to the oligomerisation of two ethylene molecules. These relations between several oligomerisation constants were

obtained from previous work of Lukyanov and co-workers (26). The equilibrium constants relating the oligomerisation to cracking reaction rate constants were obtained following thermodynamic considerations. The cracking rate constants were obtained sequentially following the estimated oligomerisation constants and thermodynamic equilibrium constants. It was possible to describe the oligomerisation/cracking constants without the need for the oligomerisation of two butene molecules leading to octene, one pentene and butene molecule leading to nonene and two pentene molecules leading to decene. This led to a reduction of the general model by 6 rate constants. To fit the experiments to model, deviations from the equilibrium constant were observed for C6 – C10 olefins. This is probably due to the competing hydrogen transfer and cyclisation reactions and methylation reactions.

The slowest oligomerisation reaction of two ethylene molecules was higher than the direct formation of ethylene by a factor of 24. The rates of oligomerisation were observed to increase with chain length in accordance to the previous work of Lukyanov and co-workers (26). The rate of olefin cracking also increase with chain length in the ratio of 1:145975 from butene to decene cracking.

7.6.3.5. Hydrogen transfer and Cyclisation

Hydrogen transfer and cyclisation reactions occur according to:

$C_nH_{2n} \cdot HZ + 3C_mH_{2m} \longrightarrow ArC_qH_{2q+1} \cdot HZ + 3C_mH_{2m+2}$

$Ar = C_6H_5, 6 \leq n \leq 10, q = n - 6, 2 \leq m \leq 10$

C6 - C10 olefins are further converted to a range of C6 - C10 aromatics and paraffins following hydrogen transfer and cyclisation between two olefins. The rate of hydrogen transfer and cyclisation increased with chain length of the first olefin. For a specific olefin chain length, the rate of hydrogen transfer and cyclisation also increased with an increase in the chain length of the second olefin.

Hydrogen transfer and cyclisation rates between olefins were relatively fast. Hexene showed the lowest hydrogen transfer and cyclisation rates but was higher than ethylene methylation rates with methanol by a factor of 1820, ethylene oligomerisation rates by a factor 660 and the direct formation of ethylene by a factor of 16130.

It was observed that the hydrogen transfer and cyclisation between two olefins can not sufficiently describe the low contact time data observed for paraffins and aromatics. Recently, a newly discovered hydrogen transfer pathway between methanol and olefins leading to the formation of aromatics and paraffins has been shown to occur in concert between Brønsted and Lewis acid sites and faster than the pathway between two olefins (37). Although the chemistry was described in sufficient detail, the mechanism was not quantitatively evaluated.

It is envisaged that such fast chemistries would describe the formation of aromatics and paraffins at low contact times.

7.6.3.6. Aromatic methylation

Aromatic methylation occurs through the following reactions:

$CH_3OH \cdot HZ + ArC_nH_{2n+1} \longrightarrow ArC_{n+1}H_{2(n+1)+1} \cdot HZ + H_2O \quad 0 \leq n \leq 4;\ Ar = C_6H_5,$

$CH_3OCH_3 \cdot HZ + ArC_nH_{2n+1} \longrightarrow ArC_{n+1}H_{2(n+1)+1} \cdot HZ + CH_3OH \quad 0 \leq n \leq 4$

Aromatic methylation by methanol was distinguished from methylation by DME. Firstly, the ratios of the methylation of aromatics (C6:C7:C8:C9) with methanol was 10:10:1:2 to produce xylene as the major aromatic during the conversion of methanol to hydrocarbons at 370 °C. Aromatic methylation with DME was higher than methanol by a factor of 2.5. Aromatic methylation rates with methanol were higher than ethylene formation rates by a factor of 260.

7.6.3.7. Aromatic dealkylation

The aromatic dealkylation chemistry goes mainly according to:

$ArC_nH_{2n+1}HZ \longrightarrow Ar\ H \cdot HZ + C_nH_{2n}$

$2 \leq n \leq 4, Ar = C_6H_5$

Cracking of aromatics (C8 – C10) increased with carbon chain length. For tetramethylbenzene, cracking into benzene and butene was faster than toluene and propylene which was subsequently faster than xylene and ethylene. The ratio of cracking rates of xylene, trimethylbenzene and tetramethylbenzene all leading to ethylene and the corresponding aromatics (benzene, toluene and xylene respectively) was 1:10:200. Xylene dealkylation (cracking) rates were in the same magnitude as ethylene formation rates.

7.6.3.8. Paraffin cracking

Only cracking of ethane to ethylene and hydrogen was dominant at the reaction temperature considered.

$C_2H_6 \cdot HZ \longrightarrow C_2H_4 \cdot HZ + H_2$

Thus, 44 rate constants describing the transformation of C3 – C10 paraffins were redundant in the model. The rate of ethane cracking was faster than direct ethylene formation by six orders of magnitude.

7.6.3.9. Paraffin alkylation

The major paraffin alkylation reaction occurred according to:

$C_nH_{2n+2} + C_mH_{2m} \cdot HZ \longrightarrow C_nH_{2n} \cdot HZ + C_mH_{2m+2}$

$n = 2, 3 \leq m \leq 10$

It was also observed that the alkylation of C3 – C10 paraffins by olefins were negligible during MTH reaction at 370 °C. This led to a redundancy of 64 constants. The alkylation of ethane with olefins were an order of magnitude smaller than ethane cracking and five orders of magnitude faster than direct ethylene formation.

7.6.4. Parameter estimation

The reduction in oligomerisation/cracking constants by 6 parameters, paraffin cracking constants by 44 parameters and paraffin alkylation constants by 64 parameters, a focus on the direct pathways (reduction of 5 parameters) and removal of decomposition products due to lack of experimental data (reduction of 2 parameters) led to a much-reduced model of 114 parameters to describe MTH conversion at 370 °C. Of these, 16 parameters were constrained to thermodynamic considerations and controlled by equilibrium constants. Thus, MTH conversion at 370 °C can be controlled by 98 parameters. This reduced model is one third the initial size of the general model used initially to describe MTH conversion

The initial parameter estimation conducted manually gives good fit to data requiring few parameters such as the distribution of methanol, DME and water and the formation of aromatics. The distribution of methanol, DME and water are controlled by the initial equilibration reaction parameters, olefin methylation and aromatic methylation totalling 28 parameters. This number is reduced to 16 parameters given that the methylation with DME of olefins or aromatics was obtained by multiplying their methylation values with methanol with 3.5 and 2.5 respectively. The distribution of aromatics on the other hand are controlled by methylation, cracking and hydrogen transfer reactions totalling 59 parameters. This number is reduced to 55 given that a DME factor of 2.5 was multiplied to methanol methylation of C6 – C10 aromatics. Olefins and paraffins are controlled by methylation, hydrogen transfer, paraffin cracking and alkylation reactions which constitute a significant proportion of the total number of parameters.

Of the 11 chemistries described above, hydrogen transfer and cyclisation, aromatic methylation and dealkylation rates of higher aromatics, paraffin cracking and alkylation rates were predominantly very fast steps. They occur at a rate several orders of magnitude higher than much slower steps such as the equilibration step, the direct formation of ethylene and propylene and olefin methylation steps (Table 7.5). These observations lead to the conclusion that the olefin cycle controls product distribution of the conversion of methanol to hydrocarbons over ZSM-5 catalysts at 370 °C.

Table 7.5: Estimated parameters used to describe MTH conversion at 370 °C

Constants	Value	Rate equation
k1f	0.0185	$CH_3OH \cdot HZ + CH_3OH \rightarrow CH_3OCH_3 \cdot HZ + H_2O$
k1b	0.003224	$CH_3OCH_3 \cdot HZ + H_2O \rightarrow CH_3OH \cdot HZ + CH_3OH$
k4d	0.0034	$CH_3OCH_3 \cdot HZ + CH_3OH \rightarrow C_3H_6 \cdot HZ + 2H_2O$
k5d	0.00062	$CH_3OCH_3 \cdot HZ \rightarrow C_2H_4 \cdot HZ + H_2O$
k8	0.0055	$C_2H_4 + CH_3OH \cdot HZ \rightarrow C_3H_6 \cdot HZ + H_2O$
k9	0.0086	$C_3H_6 + CH_3OH \cdot HZ \longrightarrow C_4H_8 \cdot HZ + H_2O$
k10	0.0241	$C_4H_8 + CH_3OH \cdot HZ \longrightarrow C_5H_{10} \cdot HZ + H_2O$
k11	0.0483	$C_5H_{10} + CH_3OH \cdot HZ \longrightarrow C_6H_{12} \cdot HZ + H_2O$
k12	0.0828	$C_6H_{12} + CH_3OH \cdot HZ \longrightarrow C_7H_{14} \cdot HZ + H_2O$
k13	0.0825	$C_7H_{14} + CH_3OH \cdot HZ \longrightarrow C_8H_{16} \cdot HZ + H_2O$
k14	0.0825	$C_8H_{16} + CH_3OH \cdot HZ \longrightarrow C_9H_{18} \cdot HZ + H_2O$
k15	0.0825	$C_9H_{18} + CH_3OH \cdot HZ \longrightarrow C_{10}H_{20} \cdot HZ + H_2$
k16	0.01925	$C_2H_4 + CH_3OCH_3 \cdot HZ \rightarrow C_3H_6 + CH_3OH \cdot HZ$
k17	0.0301	$C_3H_6 + CH_3OCH_3 \cdot HZ \rightarrow C_4H_8 + CH_3OH \cdot HZ$
k18	0.08435	$C_4H_8 + CH_3OCH_3 \cdot HZ \rightarrow C_5H_{10} + CH_3OH \cdot HZ$
k19	0.16905	$C_5H_{10} + CH_3OCH_3 \cdot HZ \rightarrow C_6H_{12} + CH_3OH \cdot HZ$
k20	0.2898	$C_6H_{12} + CH_3OCH_3 \cdot HZ \rightarrow C_7H_{14} + CH_3OH \cdot HZ$
k21	0.28875	$C_7H_{14} + CH_3OCH_3 \cdot HZ \rightarrow C_8H_{16} + CH_3OH \cdot HZ$
k22	0.28875	$C_8H_{16} + CH_3OCH_3 \cdot HZ \rightarrow C_9H_{18} + CH_3OH \cdot HZ$
k23	0.28875	$C_9H_{18} + CH_3OCH_3 \cdot HZ \rightarrow C_{10}H_{20} + CH_3OH \cdot HZ$
k24f	0.015	$C_2H_4 \cdot HZ + C_2H_4 \rightarrow C_4H_8 \cdot HZ$
k24b	0.000802	$C_4H_8 \cdot HZ \rightarrow C_2H_4 \cdot HZ + C_2H_4$
k25f	0.255	$C_3H_6 \cdot HZ + C_2H_4 \rightarrow C_5H_{10} \cdot HZ$
k25b	0.148161	$C_5H_{10} \cdot HZ \rightarrow C_3H_6 \cdot HZ + C_2H_4$
k26f	0.495	$C_4H_8 \cdot HZ + C_2H_4 \rightarrow C_6H_{12} \cdot HZ$
k26b	0.032559	$C_6H_{12} \cdot HZ \rightarrow C_4H_8 \cdot HZ + C_2H_4$
k27f	0.54	$C_3H_6 \cdot HZ + C_3H_6 \rightarrow C_6H_{12} \cdot HZ$
k27b	1.08	$C_6H_{12} \cdot HZ \rightarrow C_3H_6 \cdot HZ + C_3H_6$
k28f	0.495	$C_5H_{10} \cdot HZ + C_2H_4 \rightarrow C_7H_{14} \cdot HZ$
k28b	1.43654	$C_7H_{14} \cdot HZ \rightarrow C_5H_{10} \cdot HZ + C_2H_4$
k29f	2.385	$C_4H_8 \cdot HZ + C_3H_6 \rightarrow C_7H_{14} \cdot HZ$
k29b	89.25898	$C_7H_{14} \cdot HZ \rightarrow C_4H_8 \cdot HZ + C_3H_6$
k30f	3.465	$C_6H_{12} \cdot HZ + C_2H_4 \rightarrow C_8H_{16} \cdot HZ$

k30b	36.4545	$C_8H_{16} \cdot HZ \rightarrow C_6H_{12} \cdot HZ + C_2H_4$
k31f	3.465	$C_5H_{10} \cdot HZ + C_3H_6 \rightarrow C_8H_{16} \cdot HZ$
k31b	26.94401	$C_8H_{16} \cdot HZ \rightarrow \ C_5H_{10} \cdot HZ + C_3H_6$
k33f	3.465	$C_7H_{14} \cdot HZ + C_2H_4 \rightarrow C_9H_{18} \cdot HZ$
k33b	2.31	$C_9H_{18} \cdot HZ \rightarrow \ C_7H_{14} \cdot HZ + C_2H_4$
k34f	3.465	$C_6H_{12} \cdot HZ + C_3H_6 \rightarrow C_9H_{18} \cdot HZ$
k34b	96.78771	$C_9H_{18} \cdot HZ \rightarrow C_6H_{12} \cdot HZ + C_3H_6$
k36f	3.465	$C_8H_{16} \cdot HZ + C_2H_4 \rightarrow C_{10}H_{20} \cdot HZ$
k36b	1.520671	$C_{10}H_{20} \cdot HZ \rightarrow C_8H_{16} \cdot HZ + C_2H_4$
k37f	3.465	$C_7H_{14} \cdot HZ + C_3H_6 \rightarrow C_{10}H_{20} \cdot HZ$
k37b	34.30693	$C_{10}H_{20} \cdot HZ \ \ C_7 \rightarrow H_{14} \cdot HZ + C_3H_6$
k38f	13.86	$C_6H_{12} \cdot HZ + C_4H_8 \rightarrow C_{10}H_{20} \cdot HZ$
k38b	119.6891	$C_{10}H_{20} \cdot HZ \rightarrow \ C_6H_{12} \cdot HZ + C_4H_8$
k40	0.16	$C_6H_6 + CH_3OH \cdot HZ \rightarrow C_7H_8 \cdot HZ + H_2O$
k41	0.17	$C_7H_8 + CH_3OH \cdot HZ \rightarrow C_8H_{10} \cdot HZ + H_2O$
k42	0.011	$C_8H_{10} + CH_3OH \cdot HZ \rightarrow C_9H_{12} \cdot HZ + H_2O$
k43	0.031	$C_9H_{12} + CH_3OH \cdot HZ \rightarrow C_{10}H_{14} \cdot HZ + H_2O$
k44	1.4	$C_6H_6 + CH_3OCH_3 \cdot HZ \rightarrow C_7H_8 + CH_3OH \cdot HZ$
k45	1.4875	$C_7H_8 + CH_3OCH_3 \cdot HZ \rightarrow C_8H_{10} + CH_3OH \cdot HZ$
k46	0.09625	$C_8H_{10} + CH_3OCH_3 \cdot HZ \rightarrow C_9H_{12} + CH_3OH \cdot HZ$
k47	0.27125	$C_9H_{12} + CH_3OCH_3 \cdot HZ \rightarrow C_{10}H_{14} + CH_3OH \cdot HZ$
k48	0.0005	$C_8H_{10} \cdot HZ \ \rightarrow C_6H_6 \cdot HZ + C_2H_4$
k6	0.003	$C_9H_{12} \cdot HZ \rightarrow \ C_6H_6 \cdot HZ + C_3H_6$
k7	0.006	$C_9H_{12} \cdot HZ \rightarrow C_7H_8.HZ + C_2H_4$
k49	0.1	$C_{10}H_{14} \cdot HZ \rightarrow C_8H_{10} \cdot HZ + C_2H_4$
k50	0.2	$C_{10}H_{14} \cdot HZ \rightarrow C_7H_8 \cdot HZ + C_3H_6$
k51	0.4	$C_{10}H_{14} \cdot HZ \rightarrow C_6H_6 \cdot HZ + C_4H_8$
k52	10	$C_6H_{12} \cdot HZ + 3C_2H_4 \longrightarrow \ C_6H_6 \cdot HZ + 3C_2H_6$
k53	100	$C_6H_{12} \cdot HZ + 3C_3H_6 \longrightarrow \ C_6H_6 \cdot HZ + 3C_3H_8$
k54	100	$C_6H_{12} \cdot HZ + 3C_4H_8 \longrightarrow \ C_6H_6 \cdot HZ + 3C_4H_{10}$
k55	100	$C_6H_{12} \cdot HZ + 3C_5H_{10} \longrightarrow \ C_6H_6 \cdot HZ + 3C_5H_{12}$
k56	100	$C_6H_{12} \cdot HZ + 3C_6H_{12} \longrightarrow \ C_6H_6 \cdot HZ + 3C_6H_{14}$
k57	100	$C_6H_{12} \cdot HZ + 3C_7H_{14} \longrightarrow \ C_6H_6 \cdot HZ + 3C_7H_{16}$
k58	100	$C_6H_{12} \cdot HZ + 3C_8H_{16} \longrightarrow \ C_6H_6 \cdot HZ + 3C_8H_{18}$
k59	100	$C_6H_{12} \cdot HZ + 3C_9H_{18} \longrightarrow \ C_6H_6 \cdot HZ + 3C_9H_{20}$

k60	100	$C_6H_{12} \cdot HZ + 3C_{10}H_{20} \longrightarrow C_6H_6 \cdot HZ + 3C_{10}H_{22}$
k61	750000	$C_7H_{14} \cdot HZ + 3C_2H_4 \longrightarrow C_7H_8 \cdot HZ + 3C_2H_6$
k62	1200000	$C_7H_{14} \cdot HZ + 3C_3H_6 \longrightarrow C_7H_8 \cdot HZ + 3C_3H_8$
k63	2.2e08	$C_7H_{14} \cdot HZ + 3C_4H_8 \longrightarrow C_7H_8 \cdot HZ + 3C_4H_{10}$
k64	1.2e09	$C_7H_{14} \cdot HZ + 3C_5H_{10} \longrightarrow C_7H_8 \cdot HZ + 3C_5H_{12}$
k65	6.2e08	$C_7H_{14} \cdot HZ + 3C_6H_{12} \longrightarrow C_7H_8 \cdot HZ + 3C_6H_{14}$
k66	2.2e08	$C_7H_{14} \cdot HZ + 3C_7H_{14} \longrightarrow C_7H_8 \cdot HZ + 3C_7H_{16}$
k67	2.2e08	$C_7H_{14} \cdot HZ + 3C_8H_{16} \longrightarrow C_7H_8 \cdot HZ + 3C_8H_{18}$
k68	2.2e08	$C_7H_{14} \cdot HZ + 3C_9H_{18} \longrightarrow C_7H_8 \cdot HZ + 3C_9H_{20}$
k69	2.2e08	$C_7H_{14} \cdot HZ + 3C_{10}H_{20} \longrightarrow C_7H_8 \cdot HZ + 3C_{10}H_{22}$
k70	9.6e08	$C_8H_{16} \cdot HZ + 3C_2H_4 \longrightarrow C_8H_{10} \cdot HZ + 3C_2H_6$
k71	1.6e09	$C_8H_{16} \cdot HZ + 3C_3H_6 \longrightarrow C_8H_{10} \cdot HZ + 3C_3H_8$
k72	9.6e09	$C_8H_{16} \cdot HZ + 3C_4H_8 \longrightarrow C_8H_{10} \cdot HZ + 3C_4H_{10}$
k73	1.6e11	$C_8H_{16} \cdot HZ + 3C_5H_{10} \longrightarrow C_8H_{10} \cdot HZ + 3C_5H_{12}$
k74	1.6e13	$C_8H_{16} \cdot HZ + 3C_6H_{12} \longrightarrow C_8H_{10} \cdot HZ + 3C_6H_{14}$
k75	1.6e13	$C_8H_{16} \cdot HZ + 3C_7H_{14} \longrightarrow C_8H_{10} \cdot HZ + 3C_7H_{16}$
k76	1.6e13	$C_8H_{16} \cdot HZ + 3C_8H_{16} \longrightarrow C_8H_{10} \cdot HZ + 3C_8H_{18}$
k77	1.6e13	$C_8H_{16} \cdot HZ + 3C_9H_{18} \longrightarrow C_8H_{10} \cdot HZ + 3C_9H_{20}$
k78	1.6e13	$C_8H_{16} \cdot HZ + 3C_{10}H_{20} \longrightarrow C_8H_{10} \cdot HZ + 3C_{10}H_{22}$
k79	9.6e08	$C_9H_{18} \cdot HZ + 3C_2H_4 \longrightarrow C_9H_{12} \cdot HZ + 3C_2H_6$
k80	9.6e14	$C_9H_{18} \cdot HZ + 3C_3H_6 \longrightarrow C_9H_{12} \cdot HZ + 3C_3H_8$
k81	9.60e15	$C_9H_{18} \cdot HZ + 3C_4H_8 \longrightarrow C_9H_{12} \cdot HZ + 3C_4H_{10}$
k82	7.20e19	$C_9H_{18} \cdot HZ + 3C_5H_{10} \longrightarrow C_9H_{12} \cdot HZ + 3C_5H_{12}$
k83	9.60e19	$C_9H_{18} \cdot HZ + 3C_6H_{12} \longrightarrow C_9H_{12} \cdot HZ + 3C_6H_{14}$
k84	9.60e19	$C_9H_{18} \cdot HZ + 3C_7H_{14} \longrightarrow C_9H_{12} \cdot HZ + 3C_7H_{16}$
k85	9.60e19	$C_9H_{18} \cdot HZ + 3C_8H_{16} \longrightarrow C_9H_{12} \cdot HZ + 3C_8H_{18}$
k86	9.60e19	$C_9H_{18} \cdot HZ + 3C_9H_{18} \longrightarrow C_9H_{12} \cdot HZ + 3C_9H_{20}$
k87	9.60e19	$C_9H_{18} \cdot HZ + 3C_{10}H_{20} \longrightarrow C_9H_{12} \cdot HZ + 3C_{10}H_{22}$
k88	9.6e09	$C_{10}H_{20} \cdot HZ + 3C_2H_4 \longrightarrow C_{10}H_{14} \cdot HZ + 3C_2H_6$
k89	9.6e09	$C_{10}H_{20} \cdot HZ + 3C_3H_6 \longrightarrow C_{10}H_{14} \cdot HZ + 3C_3H_8$
k90	9.6e09	$C_{10}H_{20} \cdot HZ + 3C_4H_8 \longrightarrow C_{10}H_{14} \cdot HZ + 3C_4H_{10}$
k91	9.6e12	$C_{10}H_{20} \cdot HZ + 3C_5H_{10} \longrightarrow C_{10}H_{14} \cdot HZ + 3C_5H_{12}$
k92	9.6e13	$C_{10}H_{20} \cdot HZ + 3C_6H_{12} \longrightarrow C_{10}H_{14} \cdot HZ + 3C_6H_{14}$
k93	9.6e13	$C_{10}H_{20} \cdot HZ + 3C_7H_{14} \longrightarrow C_{10}H_{14} \cdot HZ + 3C_7H_{16}$
k94	9.6e13	$C_{10}H_{20} \cdot HZ + 3C_8H_{16} \longrightarrow C_{10}H_{14} \cdot HZ + 3C_8H_{18}$

k95	9.6e13	$C_{10}H_{20} \cdot HZ + 3C_9H_{18} \longrightarrow C_{10}H_{14} \cdot HZ + 3C_9H_{20}$
k96	9.6e13	$C_{10}H_{20} \cdot HZ + 3C_{10}H_{20} \longrightarrow C_{10}H_{14} \cdot HZ + 3C_{10}H_{22}$
k97	600	$C_2H_6 \cdot HZ \longrightarrow C_2H_4 \cdot HZ + H_2$
k142	10	$C_2H_6 + C_3H_6 \cdot HZ \longrightarrow C_2H_4 \cdot HZ + C_3H_8$
k143	10	$C_2H_6 + C_4H_8 \cdot HZ \longrightarrow C_2H_4 \cdot HZ + C_4H_{10}$
k144	10	$C_2H_6 + C_5H_{10} \cdot HZ \longrightarrow C_2H_4 \cdot HZ + C_5H_{12}$
k145	10	$C_2H_6 + C_6H_{12} \cdot HZ \longrightarrow C_2H_4 \cdot HZ + C_6H_{14}$
k146	10	$C_2H_6 + C_7H_{14} \cdot HZ \longrightarrow C_2H_4 \cdot HZ + C_7H_{16}$
k147	10	$C_2H_6 + C_8H_{16} \cdot HZ \longrightarrow C_2H_4 \cdot HZ + C_8H_{18}$
k148	10	$C_2H_6 + C_9H_{18} \cdot HZ \longrightarrow C_2H_4 \cdot HZ + C_9H_{20}$
k149	10	$C_2H_6 + C_{10}H_{20} \cdot HZ \longrightarrow C_2H_4 \cdot HZ + C_{10}H_{22}$

7.6.5. Parameter optimisation

The reduction of the general model to 98 parameters could be tested by an optimisation routine to further reduce the sum of squares error. A preliminary model tested in MATLAB (2016b) consisting of up to C6 products with only 42 parameters showed that only a local minimum can be reached despite expensive computational costs (time and resource) involved. The initial estimates were only marginally reduced.

In the present model with 98 parameters, the estimated apparent rate constants were used as the final parameters. Clearly, there are still many parameters to be fitted. Further work could be carried out to reduce the number of parameters by lumping functional groups into oxygenates (methanol and DME), water, olefins, paraffins and aromatics. Although this would imply a loss in mechanistic information, it could reduce the number of reactions involved to which a parameter optimisation routine could be applied.

7.7. Conclusion

MTH conversion over ZSM-5 catalysts with a Si/Al ratio of 34 has been studied in a fixed bed reactor at 370 °C and 1 bar. The model describes the experimental data. Propylene formation occurs ca. 5 times faster than ethylene formation. The chemistries involved in the olefin cycle namely olefin methylation with methanol and DME and olefin oligomerisation and cracking were several orders of magnitude slower than the hydrogen transfer and cyclisation steps and aromatic methylation and dealkylation. This leads to the conclusion that the olefin cycle controls product distribution as soon as the initial olefins are formed. The rate of olefin methylation with DME was 3.5 times faster than with methanol and aromatic methylation with DME was 2.5 times faster than with methanol validating the conclusion held in chapter 4 that DME is the main surface oxygenate involved in methylation reactions.

7.8. Notes

All data supporting this study is provided as supplementary information accompanying this paper. Kinetic code supporting this study can be found in the appendix.

7.9. References

1. Chang CD, Silvestri AJ. The conversion of methanol and other O-compounds to hydrocarbons over zeolite catalysts. J Catal. 1977;47(2):249-59.
2. Ilias S, Bhan A. Mechanism of the catalytic conversion of methanol to hydrocarbons. ACS Catalysis. 2013;3:18-31.
3. Sun X, Mueller S, Liu Y, Shi H, Haller GL, Sanchez-Sanchez M, Van Veen AC, Lercher JA. On reaction pathways in the conversion of methanol to hydrocarbons on HZSM-5. J Catal. 2014;317:185-97.
4. Sun X, Mueller S, Shi H, Haller GL, Sanchez-Sanchez M, Van Veen AC, Lercher JA. On the impact of co-feeding aromatics and olefins for the methanol-to-olefins reaction on HZSM-5. J Catal. 2014;314:21-31.
5. Bjørgen M, Svelle S, Joensen F, Nerlov J, Kolboe S, Bonino F, Palumbo L, Bordiga S, Olsbye U. Conversion of methanol to hydrocarbons over zeolite H-ZSM-5: On the origin of the olefinic species. J Catal. 2007;249(2):195-207.
6. Bjørgen M, Joensen F, Lillerud KP, Olsbye U, Svelle S. The mechanisms of ethene and propene formation from methanol over high silica H-ZSM-5 and H-beta. Catal Today. 2009;142(1-2):90-7.
7. Chen NY, Reagan WJ. Evidence of autocatalysis in methanol to hydrocarbon reactions over zeolite catalysts. J Catal. 1979;59(1):123-9.
8. Schoenfelder H, Hinderer J, Werther J, Keil FJ. Methanol to olefins-prediction of the performance of a circulating fluidized-bed reactor on the basis of kinetic experiments in a fixed-bed reactor. Chem Eng Sci. 1994;49(24):5377-90.
9. Bos ANR, Tromp PJJ, Akse HN. Conversion of methanol to lower olefins. Kinetic modeling, reactor simulation, and selection. Ind Eng Chem Res. 1995;34(11):3808-16.
10. Gayubo AG, Aguayo AT, Sánchez Del Campo AE, Tarrío AM, Bilbao J. Kinetic modeling of methanol transformation into olefins on a SAPO-34 catalyst. Ind Eng Chem Res. 2000;39(2):292-300.
11. Kumar P, Thybaut JW, Svelle S, Olsbye U, Marin GB. Single-event microkinetics for methanol to olefins on H-ZSM-5. Ind Eng Chem Res. 2013;52(4):1491-507.
12. Park TY, Froment GF. Kinetic modeling of the methanol to olefins process. 1. Model formulation. Ind Eng Chem Res. 2001;40(20):4172-86.
13. Park TY, Froment GF. Kinetic modeling of the methanol to olefins process. 2. Experimental results, model discrimination, and parameter estimation. Ind Eng Chem Res. 2001;40(20):4187-96.
14. Aguayo AT, Mier D, Gayubo AG, Gamero M, Bilbao J. Kinetics of methanol transformation into hydrocarbons on a HZSM-5 zeolite catalyst at high temperature (400-550 °c). Ind Eng Chem Res. 2010;49(24):12371-8.
15. Lukyanov DB, Gnep NS, Guisnet MR. Kinetic modeling of ethene and propene aromatization over HZSM-5 and GaHZSM-5. Ind Eng Chem Res. 1994;33(2):223-34.
16. Quann RJ, Kerambeck FJ. Olefin oligomerization kinetics over ZSM-5 Chemical Reactions in Complex Mixtures; The Mobil Workshop, van Nostrand Reinhold, New York 1991. p. 143-62.
17. Davis ME, Davis RJ. Fundamentals of Chemical Reaction Engineering New York: McGraw-Hill; 2003. 368.
18. Marin GB, Yablonsky GS. Kinetics of Chemical Reactions: Decoding Complexity Weinheim, Germany: WILEY-VCH; 2011. 1-428.

19. Van Der Linde SC, Nijhuis TA, Dekker FHM, Kapteijn F, Moulijn JA. Mathematical treatment of transient kinetic data: Combination of parameter estimation with solving the related partial differential equations. Applied Catalysis A: General. 1997;151(1):27-57.
20. Rasmuson A, Andersson B, Olsson L, Andersson R. Mathematical Modeling in Chemical Engineering USA: Cambridge University Press; 2014.
21. Froment GF, Hosten LH. Catalysis Science and Technology. Berlin: Srpinger-Verlag; 1989.
22. Press HP, Teukolsky SA, Vetterling WT, Flannery BP. Numerical Recipes in Fortran. Cambridge Cambridge University Press; 1992.
23. Mendenhall W, Sincich T. Statistics for the Engineering and the Sciences. Englewood Cliffs: Prentics-Hall; 1995.
24. Svelle S, Rønning PO, Kolboe S. Kinetic studies of zeolite-catalyzed methylation reactions: 1. Coreaction of [12C]ethene and [13C]methanol. J Catal. 2004;224(1):115-23.
25. Hill I, Hill A, Malek A, Bhan. Kinetics and Mechanism of Benzene, Toluene, and Xylene Methylation over H-MFI. ACS catalysis. 2013;3(9):1992-2001.
26. Nguyen LH, Vazhnova T, Kolaczkowski ST, Lukyanov DB. Combined experimental and kinetic modelling studies of the pathways of propane and n-butane aromatization over H-ZSM-5 catalyst. Chem Eng Sci. 2006;61(17):5881-94.
27. Möller KP, Böhringer W, Schnitzler AE, Van Steen E, O'Connor CT. The use of a jet loop reactor to study the effect of crystal size and the co-feeding of olefins and water on the conversion of methanol over HZSM-5. Microporous Mesoporous Mater. 1999;29(1-2):127-44.
28. Svelle S, Rønning PO, Olsbye U, Kolboe S. Kinetic studies of zeolite-catalyzed methylation reactions. Part 2. Co-reaction of [12C]propene or [12C]n-butene and [13C]methanol. J Catal. 2005;234(2):385-400.
29. Heymans N, Alban B, Moreau S, De Weireld G. Experimental and theoretical study of the adsorption of pure molecules and binary systems containing methane, carbon monoxide, carbon dioxide and nitrogen. Application to the syngas generation. Chem Eng Sci. 2011;66(17):3850-8.
30. Wei Z, Chen YY, Li J, Guo W, Wang S, Dong M, Qin Z, Wang J, Jiao H, Fan W. Stability and Reactivity of Intermediates of Methanol Related Reactions and C-C Bond Formation over H-ZSM-5 Acidic Catalyst: A Computational Analysis. Journal of Physical Chemistry C. 2016;120(11):6075-87.
31. Yaws CL. Yaws' Handbook of Thermodynamic Properties for Hydrocarbons and Chemicals. Knovel.
32. Pérez-Uriarte P, Ateka A, Aguayo AT, Gayubo AG, Bilbao J. Kinetic model for the reaction of DME to olefins over a HZSM-5 zeolite catalyst. Chem Eng J. 2016;302:801-10.
33. Svelle S, Visur M, Olsbye U, Saepurahman, Bjørgen M. Mechanistic aspects of the zeolite catalyzed methylation of alkenes and aromatics with methanol: A review. Top Catal. 2011;54(13-15):897-906.
34. Levenspiel O. Chemical Reaction Engineering. 3rd ed: John Wiley & Sons 1999. 668.
35. Pérez-Ramírez J, Berger RJ, Mul G, Kapteijn F, Moulijn JA. Six-flow reactor technology a review on fast catalyst screening and kinetic studies. Catal Today. 2000;60(1):93-109.
36. Qi L, Wei Y, Xu L, Liu Z. Reaction Behaviors and Kinetics during Induction Period of Methanol Conversion on HZSM-5 Zeolite. ACS Catalysis. 2015;5(7):3973-82.
37. Müller S, Liu Y, Kirchberger FM, Tonigold M, Sanchez-Sanchez M, Lercher JA. Hydrogen Transfer Pathways during Zeolite Catalyzed Methanol Conversion to Hydrocarbons. J Am Chem Soc. 2016;138(49):15994-6003.

S7. Supplementary information

Experimental and kinetic modelling studies of methanol conversion to hydrocarbons over zeolite catalysts

Reaction scheme for MTH transformation

The reaction scheme described below involves 33 species including nitrogen.

A. Adsorption and desorption constants

$CH_3OH + HZ \rightleftharpoons CH_3OH \cdot HZ$; $[CH_3OH \cdot HZ] = K_1 P_{CH_3OH}[HZ]$
$CH_3OCH_3 + HZ \rightleftharpoons CH_3OCH_3 \cdot HZ$; $[CH_3OCH_3 \cdot HZ] = K_2 P_{CH_3OCH_3}[HZ]$
$H_2O + HZ \rightleftharpoons H_2O \cdot HZ$; $[H_2O \cdot HZ] = K_3 P_{H_2O}[HZ]$

Products of methanol and DME decomposition

$CH_4 + HZ \rightleftharpoons CH_4 \cdot HZ$; $[CH_4 \cdot HZ] = K_4 P_{CH_4}[HZ]$
$H_2 + HZ \rightleftharpoons H_2 \cdot HZ$; $[H_2 \cdot HZ] = K_5 P_{H_2}[HZ]$
$CO + HZ \rightleftharpoons CO \cdot HZ$; $[CO \cdot HZ] = K_6 P_{CO}[HZ]$
$CH_2O + HZ \rightleftharpoons CH_2O \cdot HZ$; $[CH_2O \cdot HZ] = K_7 P_{CH_2O}[HZ]$

Olefins

$C_2H_4 + HZ \rightleftharpoons C_2H_4 \cdot HZ$; $[C_2H_4 \cdot HZ] = K_8 P_{C_2H_4}[HZ]$
$C_3H_6 + HZ \rightleftharpoons C_3H_6 \cdot HZ$; $[C_3H_6 \cdot HZ] = K_9 P_{C_3H_6}[HZ]$
$C_4H_8 + HZ \rightleftharpoons C_4H_8 \cdot HZ$; $[C_4H_8 \cdot HZ] = K_{10} P_{C_4H_8}[HZ]$
$C_5H_{10} + HZ \rightleftharpoons C_5H_{10} \cdot HZ$; $[C_5H_{10} \cdot HZ] = K_{11} P_{C_5H_{10}}[HZ]$
$C_6H_{12} + HZ \rightleftharpoons C_6H_{12} \cdot HZ$; $[C_6H_{12} \cdot HZ] = K_{12} P_{C_6H_{12}}[HZ]$
$C_7H_{14} + HZ \rightleftharpoons C_7H_{14} \cdot HZ$; $[C_7H_{14} \cdot HZ] = K_{13} P_{C_7H_{14}}[HZ]$
$C_8H_{16} + HZ \rightleftharpoons C_8H_{16} \cdot HZ$; $[C_8H_{16} \cdot HZ] = K_{14} P_{C_8H_{16}}[HZ]$
$C_9H_{18} + HZ \rightleftharpoons C_9H_{18} \cdot HZ$; $[C_9H_{18} \cdot HZ] = K_{15} P_{C_9H_{18}}[HZ]$
$C_{10}H_{20} + HZ \rightleftharpoons C_{10}H_{20} \cdot HZ$; $[C_{10}H_{20} \cdot HZ] = K_{16} P_{C_{10}H_{20}}[HZ]$

Paraffins

$C_2H_6 + HZ \rightleftharpoons C_2H_6 \cdot HZ$; $[C_2H_6 \cdot HZ] = K_{17} P_{C_2H_6}[HZ]$
$C_3H_8 + HZ \rightleftharpoons C_3H_8 \cdot HZ$; $[C_3H_8 \cdot HZ] = K_{18} P_{C_3H_8}[HZ]$
$C_4H_{10} + HZ \rightleftharpoons C_4H_{10} \cdot HZ$; $[C_4H_{10} \cdot HZ] = K_{19} P_{C_4H_{10}}[HZ]$
$C_5H_{12} + HZ \rightleftharpoons C_5H_{12} \cdot HZ$; $[C_5H_{12} \cdot HZ] = K_{20} P_{C_5H_{12}}[HZ]$
$C_6H_{14} + HZ \rightleftharpoons C_6H_{14} \cdot HZ$; $[C_6H_{14} \cdot HZ] = K_{21} P_{C_6H_{14}}[HZ]$
$C_7H_{16} + HZ \rightleftharpoons C_7H_{16} \cdot HZ$; $[C_7H_{16} \cdot HZ] = K_{22} P_{C_7H_{16}}[HZ]$
$C_8H_{18} + HZ \rightleftharpoons C_8H_{18} \cdot HZ$; $[C_8H_{18} \cdot HZ] = K_{23} P_{C_8H_{18}}[HZ]$
$C_9H_{20} + HZ \rightleftharpoons C_9H_{20} \cdot HZ$; $[C_9H_{20} \cdot HZ] = K_{24} P_{C_9H_{20}}[HZ]$
$C_{10}H_{22} + HZ \rightleftharpoons C_{10}H_{22} \cdot HZ$; $[C_{10}H_{22} \cdot HZ] = K_{25} P_{C_{10}H_{22}}[HZ]$

Intermediates

$C_3H_8O_2 + HZ \rightleftharpoons C_3H_8O_2 \cdot HZ$; $[C_3H_8O_2 \cdot HZ] = K_{26} P_{C_3H_8O_2}[HZ]$
$C_4H_{10}O_2 + HZ \rightleftharpoons C_4H_{10}O_2 \cdot HZ$; $[C_4H_{10}O_2 \cdot HZ] = K_{27} P_{C_4H_{10}O_2}[HZ]$

Aromatics

$C_6H_6 + HZ \rightleftharpoons C_6H_6 \cdot HZ;$ $\quad [C_6H_6 \cdot HZ] = K_{28}P_{C_6H_6}[HZ]$

$C_7H_8 + HZ \rightleftharpoons C_7H_8 \cdot HZ;$ $\quad [C_7H_8 \cdot HZ] = K_{29}P_{C_7H_8}[HZ]$

$C_8H_{10} + HZ \rightleftharpoons C_8H_{10} \cdot HZ;$ $\quad [C_8H_{10} \cdot HZ] = K_{30}P_{C_8H_{10}}[HZ]$

$C_9H_{12} + HZ \rightleftharpoons C_9H_{12} \cdot HZ;$ $\quad [C_9H_{12} \cdot HZ] = K_{31}P_{C_9H_{12}}[HZ]$

$C_{10}H_{14} + HZ \rightleftharpoons C_{10}H_{14} \cdot HZ;$ $\quad [C_{10}H_{14} \cdot HZ] = K_{32}P_{C_{10}H_{14}}[HZ]$

Nitrogen is the carrier gas and does not adsorb on the surface of the ZSM-5 zeolite catalysts. Here, [HZ] represents an empty Brønsted acid site. It is assumed that basic and Lewis acid sites do not participate in the reaction.

Consequently,

$$\begin{aligned}[HZ] + [CH_3OH \cdot HZ] + [CH_3OCH_3 \cdot HZ] + [H_2O \cdot HZ] + [CH_4 \cdot HZ] + [H_2 \cdot HZ] + [CO \cdot HZ] \\ + [CH_2O \cdot HZ] + [C_2H_4 \cdot HZ] + [C_3H_6 \cdot HZ] + [C_4H_8 \cdot HZ] + [C_5H_{10} \cdot HZ] \\ + [C_6H_{12} \cdot HZ] + [C_7H_{14} \cdot HZ] + [C_8H_{16} \cdot HZ] + [C_9H_{18} \cdot HZ] + [C_{10}H_{20} \cdot HZ] \\ + [C_2H_6 \cdot HZ] + [C_3H_8 \cdot HZ] + [C_4H_{10} \cdot HZ] + [C_5H_{12} \cdot HZ] + [C_6H_{14} \cdot HZ] \\ + [C_3H_8O_2 \cdot HZ] + [C_4H_{10}O_2 \cdot HZ] + [C_7H_{16} \cdot HZ] + [C_8H_{18} \cdot HZ] + [C_9H_{20} \cdot HZ] \\ + [C_{10}H_{22} \cdot HZ] + [C_6H_6 \cdot HZ] + [C_7H_8 \cdot HZ] + [C_8H_{10} \cdot HZ] + [C_9H_{12} \cdot HZ] \\ + [C_{10}H_{14} \cdot HZ] = 1\end{aligned}$$

$$[HZ] = \frac{1}{(1 + K_1P_{CH_3OH} + K_2P_{CH_3OCH_3} + K_3P_{H_2O} + K_4P_{CH_4} + K_5P_{H_2} + K_6P_{CO} + K_7P_{CH_2O}}$$
$$+ \frac{1}{K_8P_{C_2H_4} + K_9P_{C_3H_6} + K_{10}P_{C_4H_8} + K_{11}P_{C_5H_{10}} + K_{12}P_{C_6H_{12}}}$$
$$+ \frac{1}{K_{13}P_{C_7H_{14}} + K_{14}P_{C_8H_{16}} + K_{15}P_{C_9H_{18}} + K_{16}P_{C_{10}H_{20}}}$$
$$+ \frac{1}{K_{17}P_{C_2H_6} + K_{18}P_{C_3H_8} + K_{19}P_{C_4H_{10}} + K_{20}P_{C_5H_{12}} + K_{21}P_{C_6H_{14}}}$$
$$+ \frac{1}{K_{22}P_{C_7H_{16}} + K_{23}P_{C_8H_{18}} + K_{24}P_{C_9H_{20}} + K_{25}P_{C_{10}H_{22}}}$$
$$+ \frac{1}{K_{26}P_{C_3H_8O_2} + K_{27}P_{C_4H_{10}O_2}}$$
$$+ \frac{1}{K_{28}P_{C_6H_6} + K_{29}P_{C_7H_8} + K_{30}P_{C_8H_{10}} + K_{31}P_{C_9H_{12}} + K_{32}P_{C_{10}H_{14}})}$$

$P_i = x_iP_{avg};\ P_{avg} = 1\ bar$

P_{avg} is the inlet pressure through the reactor.

$$[HZ] = \frac{1}{(1 + K_1x_{CH_3OH} + K_2x_{CH_3OCH_3} + K_3x_{H_2O} + K_4x_{CH_4} + K_5x_{H_2} + K_6x_{CO} + K_7x_{CH_2O}}$$
$$+ \frac{1}{K_8x_{C_2H_4} + K_9x_{C_3H_6} + K_{10}x_{C_4H_8} + K_{11}x_{C_5H_{10}} + K_{12}x_{C_6H_{12}}}$$
$$+ \frac{1}{K_{13}x_{C_7H_{14}} + K_{14}x_{C_8H_{16}} + K_{15}x_{C_9H_{18}} + K_{16}x_{C_{10}H_{20}}}$$
$$+ \frac{1}{K_{17}x_{C_2H_6} + K_{18}x_{C_3H_8} + K_{19}x_{C_4H_{10}} + K_{20}x_{C_5H_{12}} + K_{21}x_{C_6H_{14}}}$$
$$+ \frac{1}{K_{22}x_{C_7H_{16}} + K_{23}x_{C_8H_{18}} + K_{24}x_{C_9H_{20}} + K_{25}x_{C_{10}H_{22}}}$$

$$+\frac{1}{K_{26}x_{C_3H_8O_2}+K_{27}x_{C_4H_{10}O_2}}$$
$$+\frac{1}{K_{28}x_{C_6H_6}+K_{29}x_{C_7H_8}+K_{30}x_{C_8H_{10}}+K_{31}x_{C_9H_{12}}+K_{32}x_{C_{10}H_{14}})}$$

B. Reactions

The following reaction scheme is valid for the whole range of conversions. In the following reaction scheme below, r_{if}, r_{ib} represents the rate of the forward reaction and the rate of the reverse reaction of step i

1. Equilibration of methanol, DME and water

r_{1f}, r_{1b}; $CH_3OH \cdot HZ + CH_3OH \rightleftharpoons CH_3OCH_3 \cdot HZ + H_2O$

2. Decomposition of methanol

r_2; $CH_3OH \longrightarrow CO + 2H_2$

3. Decomposition of DME

r_3; $CH_3OCH_3 \rightarrow CH_2O + CH_4$

4. Indirect formation of ethylene and propylene

Through the oxygenate pool

r_{ox1}; $CH_3OCH_3 + CH_3OCH_3 \cdot HZ \rightarrow C_3H_8O_2.HZ + CH_4$
r_{ox2}; $C_3H_8O_2 \cdot HZ + CH_3OCH_3 \rightarrow C_4H_{10}O_2 \cdot HZ + CH_3OH$
r_{ox3}; $C_3H_8O_2 \cdot HZ + CH_3OH \rightarrow C_4H_{10}O_2 \cdot HZ + H_2O$

r_{4id}; $C_4H_{10}O_2 \cdot HZ \rightarrow C_3H_6 \cdot HZ + H_2O + CH_2O$
r_{5id}; $C_4H_{10}O_2 \cdot HZ \rightarrow C_2H_4 \cdot HZ + H_2 + 2CH_2O$

Direct formation of propylene and ethylene

r_{4d}; $CH_3OCH_3 \cdot HZ + CH_3OH \rightarrow C_3H_6 \cdot HZ + 2H_2O$
r_{5d}; $CH_3OCH_3 \cdot HZ \rightarrow C_2H_4 \cdot HZ + H_2O$

5. Olefin methylation with methanol

r_8; $C_2H_4 + CH_3OH \cdot HZ \rightarrow C_3H_6 \cdot HZ + H_2O$
r_9; $C_3H_6 + CH_3OH \cdot HZ \longrightarrow C_4H_8 \cdot HZ + H_2O$
r_{10}; $C_4H_8 + CH_3OH \cdot HZ \longrightarrow C_5H_{10} \cdot HZ + H_2O$
r_{11}; $C_5H_{10} + CH_3OH \cdot HZ \longrightarrow C_6H_{12} \cdot HZ + H_2O$
r_{12}; $C_6H_{12} + CH_3OH \cdot HZ \longrightarrow C_7H_{14} \cdot HZ + H_2O$
r_{13}; $C_7H_{14} + CH_3OH \cdot HZ \longrightarrow C_8H_{16} \cdot HZ + H_2O$
r_{14}; $C_8H_{16} + CH_3OH \cdot HZ \longrightarrow C_9H_{18} \cdot HZ + H_2O$
r_{15}; $C_9H_{18} + CH_3OH \cdot HZ \longrightarrow C_{10}H_{20} \cdot HZ + H_2O$

6. Olefin methylation with DME

r_{16}; $C_2H_4 + CH_3OCH_3 \cdot HZ \rightarrow C_3H_6 + CH_3OH \cdot HZ$
r_{17}; $C_3H_6 + CH_3OCH_3 \cdot HZ \rightarrow C_4H_8 + CH_3OH \cdot HZ$
r_{18}; $C_4H_8 + CH_3OCH_3 \cdot HZ \rightarrow C_5H_{10} + CH_3OH \cdot HZ$
r_{19}; $C_5H_{10} + CH_3OCH_3 \cdot HZ \rightarrow C_6H_{12} + CH_3OH \cdot HZ$
r_{20}; $C_6H_{12} + CH_3OCH_3 \cdot HZ \rightarrow C_7H_{14} + CH_3OH \cdot HZ$
r_{21}; $C_7H_{14} + CH_3OCH_3 \cdot HZ \rightarrow C_8H_{16} + CH_3OH \cdot HZ$
r_{22}; $C_8H_{16} + CH_3OCH_3 \cdot HZ \rightarrow C_9H_{18} + CH_3OH \cdot HZ$

$r_{23};\ C_9H_{18} + CH_3OCH_3 \cdot HZ \rightarrow\ C_{10}H_{20} +\ CH_3OH \cdot HZ$

7. Oligomerisation and cracking of heavier olefins

$r_{24f}, r_{24b};\ \ C_2H_4 \cdot HZ + C_2H_4 \rightleftharpoons C_4H_8 \cdot HZ$
$r_{25f}, r_{25b};\ \ C_3H_6 \cdot HZ + C_2H_4 \rightleftharpoons C_5H_{10} \cdot HZ$
$r_{26f}, r_{26b};\ \ C_4H_8 \cdot HZ + C_2H_4 \rightleftharpoons C_6H_{12} \cdot HZ$
$r_{27f}, r_{27b};\ \ C_3H_6 \cdot HZ + C_3H_6 \rightleftharpoons C_6H_{12} \cdot HZ$
$r_{28f}, r_{28b};\ \ C_5H_{10} \cdot HZ + C_2H_4 \rightleftharpoons C_7H_{14} \cdot HZ$
$r_{29f}, r_{29b};\ \ C_4H_8 \cdot HZ + C_3H_6 \rightleftharpoons C_7H_{14} \cdot HZ$
$r_{30f}, r_{30b};\ \ C_6H_{12} \cdot HZ + C_2H_4 \rightleftharpoons C_8H_{16} \cdot HZ$
$r_{31f}, r_{31b};\ \ C_5H_{10} \cdot HZ + C_3H_6 \rightleftharpoons C_8H_{16} \cdot HZ$
$r_{32f}, r_{32b};\ \ C_4H_8 \cdot HZ + C_4H_8 \rightleftharpoons C_8H_{16} \cdot HZ$

$r_{33f}, r_{33b};\ \ C_7H_{14} \cdot HZ + C_2H_4 \rightleftharpoons C_9H_{18} \cdot HZ$
$r_{34f}, r_{34b};\ \ C_6H_{12} \cdot HZ + C_3H_6 \rightleftharpoons C_9H_{18} \cdot HZ$
$r_{35f}, r_{35b};\ \ C_5H_{10} \cdot HZ + C_4H_8 \rightleftharpoons C_9H_{18} \cdot HZ$
$r_{36f}, r_{36b};\ \ C_8H_{16} \cdot HZ + C_2H_4 \rightleftharpoons C_{10}H_{20} \cdot HZ$
$r_{37f}, r_{37b};\ \ C_7H_{14} \cdot HZ + C_3H_6 \rightleftharpoons C_{10}H_{20} \cdot HZ$
$r_{38f}, r_{38b};\ \ C_6H_{12} \cdot HZ + C_4H_8 \rightleftharpoons C_{10}H_{20} \cdot HZ$
$r_{39f}, r_{39b};\ \ C_5H_{10} \cdot HZ + C_5H_{10} \rightleftharpoons C_{10}H_{20} \cdot HZ$

8. Aromatic methylation

$r_{40};\ C_6H_6 + CH_3OH \cdot HZ \rightarrow C_7H_8 \cdot HZ + H_2O$
$r_{41};\ C_7H_8 + CH_3OH \cdot HZ \rightarrow C_8H_{10} \cdot HZ + H_2O$
$r_{42};\ C_8H_{10} + CH_3OH \cdot HZ \rightarrow C_9H_{12} \cdot HZ + H_2O$
$r_{43};\ C_9H_{12} + CH_3OH \cdot HZ \rightarrow C_{10}H_{14} \cdot HZ + H_2O$

$r_{44};\ C_6H_6 + CH_3OCH_3 \cdot HZ \rightarrow C_7H_8 + CH_3OH \cdot HZ$
$r_{45};\ C_7H_8 + CH_3OCH_3 \cdot HZ \rightarrow C_8H_{10} + CH_3OH \cdot HZ$
$r_{46};\ C_8H_{10} + CH_3OCH_3 \cdot HZ \rightarrow C_9H_{12} + CH_3OH \cdot HZ$
$r_{47};\ C_9H_{12} + CH_3OCH_3 \cdot HZ \rightarrow C_{10}H_{14} + CH_3OH \cdot HZ$

9. Aromatic dealkylation

$r_{48};\ C_8H_{10} \cdot HZ\ \rightarrow C_6H_6 \cdot HZ + C_2H_4$

$r_6;\ C_9H_{12} \cdot HZ \rightarrow\ C_6H_6 \cdot HZ + C_3H_6$
$r_7;\ C_9H_{12} \cdot HZ \rightarrow C_7H_8.HZ + C_2H_4$

$r_{49};\ C_{10}H_{14} \cdot HZ \rightarrow C_8H_{10} \cdot HZ + C_2H_4$
$r_{50};\ C_{10}H_{14} \cdot HZ \rightarrow C_7H_8 \cdot HZ + C_3H_6$
$r_{51};\ C_{10}H_{14} \cdot HZ \rightarrow C_6H_6 \cdot HZ + C_4H_8$

10. Olefin aromatisation

$r_{52};\ C_6H_{12} \cdot HZ + 3C_2H_4 \longrightarrow\ C_6H_6 \cdot HZ + 3C_2H_6$
$r_{53};\ C_6H_{12} \cdot HZ + 3C_3H_6 \longrightarrow\ C_6H_6 \cdot HZ + 3C_3H_8$
$r_{54};\ C_6H_{12} \cdot HZ + 3C_4H_8 \longrightarrow\ C_6H_6 \cdot HZ + 3C_4H_{10}$
$r_{55};\ C_6H_{12} \cdot HZ + 3C_5H_{10} \longrightarrow\ C_6H_6 \cdot HZ + 3C_5H_{12}$
$r_{56};\ C_6H_{12} \cdot HZ + 3C_6H_{12} \longrightarrow\ C_6H_6 \cdot HZ + 3C_6H_{14}$
$r_{57};\ C_6H_{12} \cdot HZ + 3C_7H_{14} \longrightarrow\ C_6H_6 \cdot HZ + 3C_7H_{16}$
$r_{58};\ C_6H_{12} \cdot HZ + 3C_8H_{16} \longrightarrow\ C_6H_6 \cdot HZ + 3C_8H_{18}$
$r_{59};\ C_6H_{12} \cdot HZ + 3C_9H_{18} \longrightarrow\ C_6H_6 \cdot HZ + 3C_9H_{20}$
$r_{60};\ C_6H_{12} \cdot HZ + 3C_{10}H_{20} \longrightarrow\ C_6H_6 \cdot HZ + 3C_{10}H_{22}$

$r_{61};\ C_7H_{14} \cdot HZ + 3C_2H_4 \longrightarrow\ C_7H_8 \cdot HZ + 3C_2H_6$
$r_{62};\ C_7H_{14} \cdot HZ + 3C_3H_6 \longrightarrow\ C_7H_8 \cdot HZ + 3C_3H_8$
$r_{63};\ C_7H_{14} \cdot HZ + 3C_4H_8 \longrightarrow\ C_7H_8 \cdot HZ + 3C_4H_{10}$
$r_{64};\ C_7H_{14} \cdot HZ + 3C_5H_{10} \longrightarrow\ C_7H_8 \cdot HZ + 3C_5H_{12}$
$r_{65};\ C_7H_{14} \cdot HZ + 3C_6H_{12} \longrightarrow\ C_7H_8 \cdot HZ + 3C_6H_{14}$
$r_{66};\ C_7H_{14} \cdot HZ + 3C_7H_{14} \longrightarrow\ C_7H_8 \cdot HZ + 3C_7H_{16}$
$r_{67};\ C_7H_{14} \cdot HZ + 3C_8H_{16} \longrightarrow\ C_7H_8 \cdot HZ + 3C_8H_{18}$
$r_{68};\ C_7H_{14} \cdot HZ + 3C_9H_{18} \longrightarrow\ C_7H_8 \cdot HZ + 3C_9H_{20}$
$r_{69};\ C_7H_{14} \cdot HZ + 3C_{10}H_{20} \longrightarrow\ C_7H_8 \cdot HZ + 3C_{10}H_{22}$

$r_{70};\ C_8H_{16} \cdot HZ + 3C_2H_4 \longrightarrow\ C_8H_{10} \cdot HZ + 3C_2H_6$
$r_{71};\ C_8H_{16} \cdot HZ + 3C_3H_6 \longrightarrow\ C_8H_{10} \cdot HZ + 3C_3H_8$
$r_{72};\ C_8H_{16} \cdot HZ + 3C_4H_8 \longrightarrow\ C_8H_{10} \cdot HZ + 3C_4H_{10}$
$r_{73};\ C_8H_{16} \cdot HZ + 3C_5H_{10} \longrightarrow\ C_8H_{10} \cdot HZ + 3C_5H_{12}$
$r_{74};\ C_8H_{16} \cdot HZ + 3C_6H_{12} \longrightarrow\ C_8H_{10} \cdot HZ + 3C_6H_{14}$
$r_{75};\ C_8H_{16} \cdot HZ + 3C_7H_{14} \longrightarrow\ C_8H_{10} \cdot HZ + 3C_7H_{16}$
$r_{76};\ C_8H_{16} \cdot HZ + 3C_8H_{16} \longrightarrow\ C_8H_{10} \cdot HZ + 3C_8H_{18}$
$r_{77};\ C_8H_{16} \cdot HZ + 3C_9H_{18} \longrightarrow\ C_8H_{10} \cdot HZ + 3C_9H_{20}$
$r_{78};\ C_8H_{16} \cdot HZ + 3C_{10}H_{20} \longrightarrow\ C_8H_{10} \cdot HZ + 3C_{10}H_{22}$

$r_{79};\ C_9H_{18} \cdot HZ + 3C_2H_4 \longrightarrow\ C_9H_{12} \cdot HZ + 3C_2H_6$
$r_{80};\ C_9H_{18} \cdot HZ + 3C_3H_6 \longrightarrow\ C_9H_{12} \cdot HZ + 3C_3H_8$
$r_{81};\ C_9H_{18} \cdot HZ + 3C_4H_8 \longrightarrow\ C_9H_{12} \cdot HZ + 3C_4H_{10}$
$r_{82};\ C_9H_{18} \cdot HZ + 3C_5H_{10} \longrightarrow\ C_9H_{12} \cdot HZ + 3C_5H_{12}$
$r_{83};\ C_9H_{18} \cdot HZ + 3C_6H_{12} \longrightarrow\ C_9H_{12} \cdot HZ + 3C_6H_{14}$
$r_{84};\ C_9H_{18} \cdot HZ + 3C_7H_{14} \longrightarrow\ C_9H_{12} \cdot HZ + 3C_7H_{16}$
$r_{85};\ C_9H_{18} \cdot HZ + 3C_8H_{16} \longrightarrow\ C_9H_{12} \cdot HZ + 3C_8H_{18}$
$r_{86};\ C_9H_{18} \cdot HZ + 3C_9H_{18} \longrightarrow\ C_9H_{12} \cdot HZ + 3C_9H_{20}$
$r_{87};\ C_9H_{18} \cdot HZ + 3C_{10}H_{20} \longrightarrow\ C_9H_{12} \cdot HZ + 3C_{10}H_{22}$

$r_{88};\ C_{10}H_{20} \cdot HZ + 3C_2H_4 \longrightarrow\ C_{10}H_{14} \cdot HZ + 3C_2H_6$
$r_{89};\ C_{10}H_{20} \cdot HZ + 3C_3H_6 \longrightarrow\ C_{10}H_{14} \cdot HZ + 3C_3H_8$
$r_{90};\ C_{10}H_{20} \cdot HZ + 3C_4H_8 \longrightarrow\ C_{10}H_{14} \cdot HZ + 3C_4H_{10}$
$r_{91};\ C_{10}H_{20} \cdot HZ + 3C_5H_{10} \longrightarrow\ C_{10}H_{14} \cdot HZ + 3C_5H_{12}$
$r_{92};\ C_{10}H_{20} \cdot HZ + 3C_6H_{12} \longrightarrow\ C_{10}H_{14} \cdot HZ + 3C_6H_{14}$
$r_{93};\ C_{10}H_{20} \cdot HZ + 3C_7H_{14} \longrightarrow\ C_{10}H_{14} \cdot HZ + 3C_7H_{16}$
$r_{94};\ C_{10}H_{20} \cdot HZ + 3C_8H_{16} \longrightarrow\ C_{10}H_{14} \cdot HZ + 3C_8H_{18}$
$r_{95};\ C_{10}H_{20} \cdot HZ + 3C_9H_{18} \longrightarrow\ C_{10}H_{14} \cdot HZ + 3C_9H_{20}$
$r_{96};\ C_{10}H_{20} \cdot HZ + 3C_{10}H_{20} \longrightarrow\ C_{10}H_{14} \cdot HZ + 3C_{10}H_{22}$

11. Paraffin cracking

$r_{97};\ C_2H_6 \cdot HZ \longrightarrow C_2H_4 \cdot HZ + H_2$

$r_{98};\ C_3H_8 \cdot HZ \longrightarrow C_2H_4 \cdot HZ + CH_4$
$r_{99};\ C_3H_8 \cdot HZ \longrightarrow C_3H_6 \cdot HZ + H_2$

$r_{100};\ C_4H_{10} \cdot HZ\ \longrightarrow C_2H_4 \cdot HZ + C_2H_6$
$r_{101};\ C_4H_{10} \cdot HZ \longrightarrow C_3H_6 \cdot HZ + CH_4$
$r_{102};\ C_4H_{10} \cdot HZ \longrightarrow C_4H_8 \cdot HZ + H_2$

$r_{103};\ C_5H_{12} \cdot HZ\ \longrightarrow C_2H_4 \cdot HZ + C_3H_8$
$r_{104};\ C_5H_{12} \cdot HZ\ \longrightarrow C_3H_6 \cdot HZ + C_2H_6$
$r_{105};\ C_5H_{12} \cdot HZ \longrightarrow C_4H_8 \cdot HZ + CH_4$
$r_{106};\ C_5H_{12} \cdot HZ \longrightarrow C_5H_{10} \cdot HZ + H_2$

$r_{107};\ C_6H_{14} \cdot HZ \longrightarrow C_2H_4 \cdot HZ + C_4H_{10}$
$r_{108};\ C_6H_{14} \cdot HZ \longrightarrow C_3H_6 \cdot HZ + C_3H_8$
$r_{109};\ C_6H_{14} \cdot HZ \longrightarrow C_4H_8 \cdot HZ + C_2H_6$
$r_{110};\ C_6H_{14} \cdot HZ \longrightarrow C_5H_{10} \cdot HZ + CH_4$
$r_{111};\ C_6H_{14} \cdot HZ \longrightarrow C_6H_{12} \cdot HZ + H_2$

$r_{112};\ C_7H_{16} \cdot HZ \longrightarrow C_2H_4 \cdot HZ + C_5H_{12}$
$r_{113};\ C_7H_{16} \cdot HZ \longrightarrow C_3H_6 \cdot HZ + C_4H_{10}$
$r_{114};\ C_7H_{16} \cdot HZ \longrightarrow C_4H_8 \cdot HZ + C_3H_8$
$r_{115};\ C_7H_{16} \cdot HZ \longrightarrow C_5H_{10} \cdot HZ + C_2H_6$
$r_{116};\ C_7H_{16} \cdot HZ \longrightarrow C_6H_{12} \cdot HZ + CH_4$
$r_{117};\ C_7H_{16} \cdot HZ \longrightarrow C_7H_{14} \cdot HZ + H_2$

$r_{118};\ C_8H_{18} \cdot HZ \longrightarrow C_2H_4 \cdot HZ + C_6H_{14}$
$r_{119};\ C_8H_{18} \cdot HZ \longrightarrow C_3H_6 \cdot HZ + C_5H_{12}$
$r_{120};\ C_8H_{18} \cdot HZ \longrightarrow C_4H_8 \cdot HZ + C_4H_{10}$
$r_{121};\ C_8H_{18} \cdot HZ \longrightarrow C_5H_{10} \cdot HZ + C_3H_8$
$r_{122};\ C_8H_{18} \cdot HZ \longrightarrow C_6H_{12} \cdot HZ + C_2H_6$
$r_{123};\ C_8H_{18} \cdot HZ \longrightarrow C_7H_{14} \cdot HZ + CH_4$
$r_{124};\ C_8H_{18} \cdot HZ \longrightarrow C_8H_{16} \cdot HZ + H_2$

$r_{125};\ C_9H_{20} \cdot HZ \longrightarrow C_2H_4 \cdot HZ + C_7H_{16}$
$r_{126};\ C_9H_{20} \cdot HZ \longrightarrow C_3H_6 \cdot HZ + C_6H_{14}$
$r_{127};\ C_9H_{20} \cdot HZ \longrightarrow C_4H_8 \cdot HZ + C_5H_{12}$
$r_{128};\ C_9H_{20} \cdot HZ \longrightarrow C_5H_{10} \cdot HZ + C_4H_{10}$
$r_{129};\ C_9H_{20} \cdot HZ \longrightarrow C_6H_{12} \cdot HZ + C_3H_8$
$r_{130};\ C_9H_{20} \cdot HZ \longrightarrow C_7H_{14} \cdot HZ + C_2H_6$
$r_{131};\ C_9H_{20} \cdot HZ \longrightarrow C_8H_{16} \cdot HZ + CH_4$
$r_{132};\ C_9H_{20} \cdot HZ \longrightarrow C_9H_{18} \cdot HZ + H_2$

$r_{133};\ C_{10}H_{22} \cdot HZ \longrightarrow C_2H_4 \cdot HZ + C_8H_{18}$
$r_{134};\ C_{10}H_{22} \cdot HZ \longrightarrow C_3H_6 \cdot HZ + C_7H_{16}$
$r_{135};\ C_{10}H_{22} \cdot HZ \longrightarrow C_4H_8 \cdot HZ + C_6H_{14}$
$r_{136};\ C_{10}H_{22} \cdot HZ \longrightarrow C_5H_{10} \cdot HZ + C_5H_{12}$
$r_{137};\ C_{10}H_{22} \cdot HZ \longrightarrow C_6H_{12} \cdot HZ + C_4H_{10}$
$r_{138};\ C_{10}H_{22} \cdot HZ \longrightarrow C_7H_{14} \cdot HZ + C_3H_8$
$r_{139};\ C_{10}H_{22} \cdot HZ \longrightarrow C_8H_{16} \cdot HZ + C_2H_6$
$r_{140};\ C_{10}H_{22} \cdot HZ \longrightarrow C_9H_{18} \cdot HZ + CH_4$
$r_{141};\ C_{10}H_{22} \cdot HZ \longrightarrow C_{10}H_{20} \cdot HZ + H_2$

12. Hydrogen transfer (Paraffin Alkylation)

$r_{142};\ C_2H_6 + C_3H_6 \cdot HZ \longrightarrow C_2H_4 \cdot HZ + C_3H_8$
$r_{143};\ C_2H_6 + C_4H_8 \cdot HZ \longrightarrow C_2H_4 \cdot HZ + C_4H_{10}$
$r_{144};\ C_2H_6 + C_5H_{10} \cdot HZ \longrightarrow C_2H_4 \cdot HZ + C_5H_{12}$
$r_{145};\ C_2H_6 + C_6H_{12} \cdot HZ \longrightarrow C_2H_4 \cdot HZ + C_6H_{14}$
$r_{146};\ C_2H_6 + C_7H_{14} \cdot HZ \longrightarrow C_2H_4 \cdot HZ + C_7H_{16}$
$r_{147};\ C_2H_6 + C_8H_{16} \cdot HZ \longrightarrow C_2H_4 \cdot HZ + C_8H_{18}$
$r_{148};\ C_2H_6 + C_9H_{18} \cdot HZ \longrightarrow C_2H_4 \cdot HZ + C_9H_{20}$
$r_{149};\ C_2H_6 + C_{10}H_{20} \cdot HZ \longrightarrow C_2H_4 \cdot HZ + C_{10}H_{22}$

$r_{150};\ C_3H_8 + C_2H_4 \cdot HZ \longrightarrow C_3H_6 \cdot HZ + C_2H_6$
$r_{151};\ C_3H_8 + C_4H_8 \cdot HZ \longrightarrow C_3H_6 \cdot HZ + C_4H_{10}$
$r_{152};\ C_3H_8 + C_5H_{10} \cdot HZ \longrightarrow C_3H_6 \cdot HZ + C_5H_{12}$

$r_{153};\ C_3H_8 + C_6H_{12} \cdot HZ \longrightarrow C_3H_6 \cdot HZ + C_6H_{14}$
$r_{154};\ C_3H_8 + C_7H_{14} \cdot HZ \longrightarrow C_3H_6 \cdot HZ + C_7H_{16}$
$r_{155};\ C_3H_8 + C_8H_{16} \cdot HZ \longrightarrow C_3H_6 \cdot HZ + C_8H_{18}$
$r_{156};\ C_3H_8 + C_9H_{18} \cdot HZ \longrightarrow C_3H_6 \cdot HZ + C_9H_{20}$
$r_{157};\ C_3H_8 + C_{10}H_{20} \cdot HZ \longrightarrow C_3H_6 \cdot HZ + C_{10}H_{22}$

$r_{158};\ C_4H_{10} + C_2H_4 \cdot HZ \longrightarrow C_4H_8 \cdot HZ + C_2H_6$
$r_{159};\ C_4H_{10} + C_3H_6 \cdot HZ \longrightarrow C_4H_8 \cdot HZ + C_3H_8$
$r_{160};\ C_4H_{10} + C_5H_{10} \cdot HZ \longrightarrow C_4H_8 \cdot HZ + C_5H_{12}$
$r_{161};\ C_4H_{10} + C_6H_{12} \cdot HZ \longrightarrow C_4H_8 \cdot HZ + C_6H_{14}$
$r_{162};\ C_4H_{10} + C_7H_{14} \cdot HZ \longrightarrow C_4H_8 \cdot HZ + C_7H_{16}$
$r_{163};\ C_4H_{10} + C_8H_{16} \cdot HZ \longrightarrow C_4H_8 \cdot HZ + C_8H_{18}$
$r_{164};\ C_4H_{10} + C_9H_{18} \cdot HZ \longrightarrow C_4H_8 \cdot HZ + C_9H_{20}$
$r_{165};\ C_4H_{10} + C_{10}H_{20} \cdot HZ \longrightarrow C_4H_8 \cdot HZ + C_{10}H_{22}$

$r_{166};\ C_5H_{12} + C_2H_4 \cdot HZ \longrightarrow C_5H_{10} \cdot HZ + C_2H_6$
$r_{167};\ C_5H_{12} + C_3H_6 \cdot HZ \longrightarrow C_5H_{10} \cdot HZ + C_3H_8$
$r_{168};\ C_5H_{12} + C_4H_8 \cdot HZ \longrightarrow C_5H_{10} \cdot HZ + C_4H_{10}$
$r_{169};\ C_5H_{12} + C_6H_{12} \cdot HZ \longrightarrow C_5H_{10} \cdot HZ + C_6H_{14}$
$r_{170};\ C_5H_{12} + C_7H_{14} \cdot HZ \longrightarrow C_5H_{10} \cdot HZ + C_7H_{16}$
$r_{171};\ C_5H_{12} + C_8H_{16} \cdot HZ \longrightarrow C_5H_{10} \cdot HZ + C_8H_{18}$
$r_{172};\ C_5H_{12} + C_9H_{18} \cdot HZ \longrightarrow C_5H_{10} \cdot HZ + C_9H_{20}$
$r_{173};\ C_5H_{12} + C_{10}H_{20} \cdot HZ \longrightarrow C_5H_{10} \cdot HZ + C_{10}H_{22}$

$r_{174};\ C_6H_{14} + C_2H_4 \cdot HZ \longrightarrow C_6H_{12} \cdot HZ + C_2H_6$
$r_{175};\ C_6H_{14} + C_3H_6 \cdot HZ \longrightarrow C_6H_{12} \cdot HZ + C_3H_8$
$r_{176};\ C_6H_{14} + C_4H_8 \cdot HZ \longrightarrow C_6H_{12} \cdot HZ + C_4H_{10}$
$r_{177};\ C_6H_{14} + C_5H_{10} \cdot HZ \longrightarrow C_6H_{12} \cdot HZ + C_5H_{12}$
$r_{178};\ C_6H_{14} + C_7H_{14} \cdot HZ \longrightarrow C_6H_{12} \cdot HZ + C_7H_{16}$
$r_{179};\ C_6H_{14} + C_8H_{16} \cdot HZ \longrightarrow C_6H_{12} \cdot HZ + C_8H_{18}$
$r_{180};\ C_6H_{14} + C_9H_{18} \cdot HZ \longrightarrow C_6H_{12} \cdot HZ + C_9H_{20}$
$r_{181};\ C_6H_{14} + C_{10}H_{20} \cdot HZ \longrightarrow C_6H_{12} \cdot HZ + C_{10}H_{22}$

$r_{182};\ C_7H_{16} + C_2H_4 \cdot HZ \longrightarrow C_7H_{14} \cdot HZ + C_2H_6$
$r_{183};\ C_7H_{16} + C_3H_6 \cdot HZ \longrightarrow C_7H_{14} \cdot HZ + C_3H_8$
$r_{184};\ C_7H_{16} + C_4H_8 \cdot HZ \longrightarrow C_7H_{14} \cdot HZ + C_4H_{10}$
$r_{185};\ C_7H_{16} + C_5H_{10} \cdot HZ \longrightarrow C_7H_{14} \cdot HZ + C_5H_{12}$
$r_{186};\ C_7H_{16} + C_6H_{12} \cdot HZ \longrightarrow C_7H_{14} \cdot HZ + C_6H_{14}$
$r_{187};\ C_7H_{16} + C_8H_{16} \cdot HZ \longrightarrow C_7H_{14} \cdot HZ + C_8H_{18}$
$r_{188};\ C_7H_{16} + C_9H_{18} \cdot HZ \longrightarrow C_7H_{14} \cdot HZ + C_9H_{20}$
$r_{189};\ C_7H_{16} + C_{10}H_{20} \cdot HZ \longrightarrow C_7H_{14} \cdot HZ + C_{10}H_{22}$

$r_{190};\ C_8H_{18} + C_2H_4 \cdot HZ \longrightarrow C_8H_{16} \cdot HZ + C_2H_6$
$r_{191};\ C_8H_{18} + C_3H_6 \cdot HZ \longrightarrow C_8H_{16} \cdot HZ + C_3H_8$
$r_{192};\ C_8H_{18} + C_4H_8 \cdot HZ \longrightarrow C_8H_{16} \cdot HZ + C_4H_{10}$
$r_{193};\ C_8H_{18} + C_5H_{10} \cdot HZ \longrightarrow C_8H_{16} \cdot HZ + C_5H_{12}$
$r_{194};\ C_8H_{18} + C_6H_{12} \cdot HZ \longrightarrow C_8H_{16} \cdot HZ + C_6H_{14}$
$r_{195};\ C_8H_{18} + C_7H_{14} \cdot HZ \longrightarrow C_8H_{16} \cdot HZ + C_7H_{16}$
$r_{196};\ C_8H_{18} + C_9H_{18} \cdot HZ \longrightarrow C_8H_{16} \cdot HZ + C_9H_{20}$
$r_{197};\ C_8H_{18} + C_{10}H_{20} \cdot HZ \longrightarrow C_8H_{16} \cdot HZ + C_{10}H_{22}$

$r_{198};\ C_9H_{20} + C_2H_4 \cdot HZ \longrightarrow C_9H_{18} \cdot HZ + C_2H_6$
$r_{199};\ C_9H_{20} + C_3H_6 \cdot HZ \longrightarrow C_9H_{18} \cdot HZ + C_3H_8$
$r_{200};\ C_9H_{20} + C_4H_8 \cdot HZ \longrightarrow C_9H_{18} \cdot HZ + C_4H_{10}$

$r_{201};\ C_9H_{20} + C_5H_{10} \cdot HZ \longrightarrow C_9H_{18} \cdot HZ + C_5H_{12}$
$r_{202};\ C_9H_{20} + C_6H_{12} \cdot HZ \longrightarrow C_9H_{18} \cdot HZ + C_6H_{14}$
$r_{203};\ C_9H_{20} + C_7H_{14} \cdot HZ \longrightarrow C_9H_{18} \cdot HZ + C_7H_{16}$
$r_{204};\ C_9H_{20} + C_8H_{16} \cdot HZ \longrightarrow C_9H_{18} \cdot HZ + C_8H_{18}$
$r_{205};\ C_9H_{20} + C_{10}H_{20} \cdot HZ \longrightarrow C_9H_{18} \cdot HZ + C_{10}H_{22}$

$r_{206};\ C_{10}H_{22} + C_2H_4 \cdot HZ \longrightarrow C_{10}H_{20} \cdot HZ + C_2H_6$
$r_{207};\ C_{10}H_{22} + C_3H_6 \cdot HZ \longrightarrow C_{10}H_{20} \cdot HZ + C_3H_8$
$r_{208};\ C_{10}H_{22} + C_4H_8 \cdot HZ \longrightarrow C_{10}H_{20} \cdot HZ + C_4H_{10}$
$r_{209};\ C_{10}H_{22} + C_5H_{10} \cdot HZ \longrightarrow C_{10}H_{20} \cdot HZ + C_5H_{12}$
$r_{210};\ C_{10}H_{22} + C_6H_{12} \cdot HZ \longrightarrow C_{10}H_{20} \cdot HZ + C_6H_{14}$
$r_{211};\ C_{10}H_{22} + C_7H_{14} \cdot HZ \longrightarrow C_{10}H_{20} \cdot HZ + C_7H_{16}$
$r_{212};\ C_{10}H_{22} + C_8H_{16} \cdot HZ \longrightarrow C_{10}H_{20} \cdot HZ + C_8H_{18}$
$r_{213};\ C_{10}H_{22} + C_9H_{18} \cdot HZ \longrightarrow C_{10}H_{20} \cdot HZ + C_9H_{20}$

As shown above, the reaction scheme involves 33 species including nitrogen with 32 adsorption equilibrium constants, 17 reaction equilibrium constants and 230 rate constants.

C. Rate equations

Methanol, DME and water equilibration
$r_{1f} = k_{1f}[CH_3OH \cdot HZ]P_{CH_3OH} = k_{1f}K_1P_{CH_3OH}^2[HZ]$
$r_{1b} = k_{1b}[CH_3OCH_3 \cdot HZ]P_{H_2O} = k_{1b}K_2P_{CH_3OCH_3}P_{H_2O}[HZ]$

Methanol decomposition
$r_2 = k_2P_{CH_3OH}$

DME decomposition
$r_3 = k_3P_{CH_3OCH_3}$

Indirect formation of ethylene and propylene
$r_{ox1} = k_{ox1}P_{CH_3OCH_3}[CH_3OCH_3 \cdot HZ] = k_{ox1}K_2P_{CH_3OCH_3}P_{CH_3OH}[HZ]$
$r_{ox2} = k_{ox2}P_{CH_3OCH_3}[C_3H_8O_2 \cdot HZ] = k_{ox2}K_{26}P_{CH_3OCH_3}P_{C_3H_8O_2}[HZ]$
$r_{ox3} = k_{ox3}P_{CH_3OH}[C_3H_8O_2 \cdot HZ] = k_{ox3}K_{26}P_{CH_3OH}P_{C_3H_8O_2}[HZ]$

$r_{4id} = k_{4id}[C_4H_{10}O_2 \cdot HZ] = k_{4id}K_{27}P_{C_4H_{10}O_2}[HZ]$
$r_{5id} = k_{5id}[C_4H_{10}O_2 \cdot HZ] = k_{5id}K_{27}P_{C_4H_{10}O_2}[HZ]$

Direct formation of ethylene and propylene
$r_{4d} = k_{4d}P_{CH_3OH}[CH_3OCH_3 \cdot HZ] = k_{4d}K_2P_{CH_3OH}P_{CH_3OCH_3}[HZ]$
$r_{5d} = k_{5d}[CH_3OCH_3 \cdot HZ] = k_{5d}K_2P_{CH_3OCH_3}[HZ]$

Olefin methylation with methanol
$r_8 = k_8P_{C_2H_4}[CH_3OH \cdot HZ] = k_8K_1P_{C_2H_4}P_{CH_3OH}[HZ]$
$r_9 = k_9P_{C_3H_6}[CH_3OH \cdot HZ] = k_9K_1P_{C_3H_6}P_{CH_3OH}[HZ]$
$r_{10} = k_{10}P_{C_4H_8}[CH_3OH \cdot HZ] = k_{10}K_1P_{C_4H_8}P_{CH_3OH}[HZ]$
$r_{11} = k_{11}P_{C_5H_{10}}[CH_3OH \cdot HZ] = k_{11}K_1P_{C_5H_{10}}P_{CH_3OH}[HZ]$
$r_{12} = k_{12}P_{C_6H_{12}}[CH_3OH \cdot HZ] = k_{12}K_1P_{C_6H_{12}}P_{CH_3OH}[HZ]$
$r_{13} = k_{13}P_{C_7H_{14}}[CH_3OH \cdot HZ] = k_{13}K_1P_{C_7H_{14}}P_{CH_3OH}[HZ]$
$r_{14} = k_{14}P_{C_8H_{16}}[CH_3OH \cdot HZ] = k_{14}K_1P_{C_8H_{16}}P_{CH_3OH}[HZ]$

$$r_{15} = k_{15} P_{C_9H_{18}} [CH_3OH \cdot HZ] = k_{15} K_1 P_{C_9H_{18}} P_{CH_3OH} [HZ]$$

Olefin methylation with DME

$$r_{16} = k_{16} [CH_3OCH_3 \cdot HZ] P_{C_2H_4} = k_{16} K_2 P_{C_2H_4} P_{CH_3OCH_3} [HZ]$$
$$r_{17} = k_{17} [CH_3OCH_3 \cdot HZ] P_{C_3H_6} = k_{17} K_2 P_{C_3H_6} P_{CH_3OCH_3} [HZ]$$
$$r_{18} = k_{18} [CH_3OCH_3 \cdot HZ] P_{C_4H_8} = k_{18} K_2 P_{C_4H_8} P_{CH_3OCH_3} [HZ]$$
$$r_{19} = k_{19} [CH_3OCH_3 \cdot HZ] P_{C_5H_{10}} = k_{19} K_2 P_{C_5H_{10}} P_{CH_3OCH_3} [HZ]$$
$$r_{20} = k_{20} [CH_3OCH_3 \cdot HZ] P_{C_6H_{12}} = k_{20} K_2 P_{C_6H_{12}} P_{CH_3OCH_3} [HZ]$$
$$r_{21} = k_{21} [CH_3OCH_3 \cdot HZ] P_{C_7H_{14}} = k_{21} K_2 P_{C_7H_{14}} P_{CH_3OCH_3} [HZ]$$
$$r_{22} = k_{22} [CH_3OCH_3 \cdot HZ] P_{C_8H_{16}} = k_{22} K_2 P_{C_8H_{16}} P_{CH_3OCH_3} [HZ]$$
$$r_{23} = k_{23} [CH_3OCH_3 \cdot HZ] P_{C_9H_{18}} = k_{23} K_2 P_{C_9H_{18}} P_{CH_3OCH_3} [HZ]$$

Olefin oligomerisation and cracking

$$r_{24f} = k_{24f} [C_2H_4 \cdot HZ] P_{C_2H_4} = k_{24f} K_8 P_{C_2H_4}^2 [HZ];$$
$$r_{24b} = k_{24b} [C_4H_8 \cdot HZ] = k_{24b} K_{10} P_{C_4H_8} [HZ]$$

$$r_{25f} = k_{25f} [C_3H_6 \cdot HZ\,] P_{C_2H_4} = k_{25f} K_9 P_{C_3H_6} P_{C_2H_4} [HZ]$$
$$r_{25b} = k_{25b} [C_5H_{10} \cdot HZ] = k_{25b} K_{11} P_{C_5H_{10}} [HZ]$$

$$r_{26f} = k_{26f} [C_4H_8 \cdot HZ] P_{C_2H_4} = k_{26f} K_{10} P_{C_4H_8} P_{C_2H_4} [HZ]$$
$$r_{26b} = k_{26b} [C_6H_{12} \cdot HZ] = k_{26b} K_{12} P_{C_6H_{12}} [HZ]$$

$$r_{27f} = k_{27f} [C_3H_6 \cdot HZ\,] P_{C_3H_6} = k_{27f} K_9 P_{C_3H_6}^2 [HZ]$$
$$r_{27b} = k_{27b} [C_6H_{12} \cdot HZ] = k_{27b} K_{12} P_{C_6H_{12}} [HZ]$$

$$r_{28f} = k_{28f} [C_5H_{10} \cdot HZ] P_{C_2H_4} = k_{28f} K_{11} P_{C_5H_{10}} P_{C_2H_4} [HZ]$$
$$r_{28b} = k_{28b} [C_7H_{14} \cdot HZ] = k_{28b} K_{13} P_{C_7H_{14}} [HZ]$$

$$r_{29f} = k_{29f} [C_4H_8 \cdot HZ\,] P_{C_3H_6} = k_{29f} K_{10} P_{C_4H_8} P_{C_3H_6} [HZ]$$
$$r_{29b} = k_{29b} [C_7H_{14} \cdot HZ] = k_{29b} K_{13} P_{C_7H_{14}} [HZ]$$

$$r_{30f} = k_{30f} [C_6H_{12} \cdot HZ\,] P_{C_2H_4} = k_{30f} K_{12} P_{C_6H_{12}} P_{C_2H_4} [HZ]$$
$$r_{30b} = k_{30b} [C_8H_{16} \cdot HZ] = k_{30b} K_{14} P_{C_8H_{16}} [HZ]$$

$$r_{31f} = k_{31f} [C_5H_{10} \cdot HZ\,] P_{C_3H_6} = k_{31f} K_{11} P_{C_5H_{10}} P_{C_3H_6} [HZ]$$
$$r_{31b} = k_{31b} [C_8H_{16} \cdot HZ] = k_{31b} K_{14} P_{C_8H_{16}} [HZ]$$

$$r_{32f} = k_{32f} [C_4H_8 \cdot HZ\,] P_{C_4H_8} = k_{32f} K_{10} P_{C_4H_8}^2 [HZ]$$
$$r_{32b} = k_{32b} [C_8H_{16} \cdot HZ] = k_{32b} K_{14} P_{C_8H_{16}} [HZ]$$

$$r_{33f} = k_{33f} [C_7H_{14} \cdot HZ\,] P_{C_2H_4} = k_{33f} K_{13} P_{C_7H_{14}} P_{C_2H_4} [HZ]$$
$$r_{33b} = k_{33b} [C_9H_{18} \cdot HZ] = k_{33b} K_{15} P_{C_9H_{18}} [HZ]$$

$$r_{34f} = k_{34f} [C_6H_{12} \cdot HZ\,] P_{C_3H_6} = k_{34f} K_{12} P_{C_6H_{12}} P_{C_3H_6} [HZ]$$
$$r_{34b} = k_{34b} [C_9H_{18} \cdot HZ] = k_{34b} K_{15} P_{C_9H_{18}} [HZ]$$
$$r_{35f} = k_{35f} [C_5H_{10} \cdot HZ\,] P_{C_4H_8} = k_{35f} K_{11} P_{C_5H_{10}} P_{C_4H_8} [HZ]$$
$$r_{35b} = k_{35b} [C_9H_{18} \cdot HZ] = k_{35b} K_{15} P_{C_9H_{18}} [HZ]$$

$$r_{36f} = k_{36f} [C_8H_{16} \cdot HZ\,] P_{C_2H_4} = k_{36f} K_{14} P_{C_8H_{16}} P_{C_2H_4} [HZ]$$

$$r_{36b} = k_{36b}[C_{10}H_{20} \cdot HZ] = k_{36b}K_{16}P_{C_{10}H_{20}}[HZ]$$

$$r_{37f} = k_{37f}[C_7H_{14} \cdot HZ\ ]P_{C_3H_6} = k_{37f}K_{13}P_{C_7H_{14}}P_{C_3H_6}[HZ]$$
$$r_{37b} = k_{37b}[C_{10}H_{20} \cdot HZ] = k_{37b}K_{16}P_{C_{10}H_{20}}[HZ]$$

$$r_{38f} = k_{38f}[C_6H_{12} \cdot HZ\ ]P_{C_4H_8} = k_{38f}K_{12}P_{C_6H_{12}}P_{C_4H_8}[HZ]$$
$$r_{38b} = k_{38b}[C_{10}H_{20} \cdot HZ] = k_{38b}K_{16}P_{C_{10}H_{20}}[HZ]$$

$$r_{39f} = k_{39f}[C_5H_{10} \cdot HZ\ ]P_{C_5H_{10}} = k_{39f}K_{11}P^2_{C_5H_{10}}[HZ]$$
$$r_{39b} = k_{39b}[C_{10}H_{20} \cdot HZ] = k_{39b}K_{16}P_{C_{10}H_{20}}[HZ]$$

Aromatic methylation with methanol

$$r_{40} = k_{40}[CH_3OH \cdot HZ]P_{C_6H_6} = k_{40}K_1P_{C_6H_6}P_{CH_3OH}[HZ]$$
$$r_{41} = k_{41}[CH_3OH \cdot HZ]P_{C_7H_8} = k_{41}K_1P_{C_7H_8}P_{CH_3OH}[HZ]$$
$$r_{42} = k_{42}[CH_3OH \cdot HZ]P_{C_8H_{10}} = k_{42}K_1P_{C_8H_{10}}P_{CH_3OH}[HZ]$$
$$r_{43} = k_{43}[CH_3OH \cdot HZ]P_{C_9H_{12}} = k_{43}K_1P_{C_9H_{12}}P_{CH_3OH}[HZ]$$

Aromatic methylation with DME

$$r_{44} = k_{44}[CH_3OCH_3 \cdot HZ]P_{C_6H_6} = k_{44}K_2P_{C_6H_6}P_{CH_3OCH_3}[HZ]$$
$$r_{45} = k_{45}[CH_3OCH_3 \cdot HZ]P_{C_7H_8} = k_{45}K_2P_{C_7H_8}P_{CH_3OCH_3}[HZ]$$
$$r_{46} = k_{46}[CH_3OCH_3 \cdot HZ]P_{C_8H_{10}} = k_{46}K_2P_{C_8H_{10}}P_{CH_3OCH_3}[HZ]$$
$$r_{47} = k_{47}[CH_3OCH_3 \cdot HZ]P_{C_9H_{12}} = k_{47}K_2P_{C_9H_{12}}P_{CH_3OCH_3}[HZ]$$

Aromatic dealkylation

$$r_{48} = k_{48}[C_8H_{10} \cdot HZ] = k_{48}K_{30}P_{C_8H_{10}}[HZ]$$

$$r_6 = k_6[C_9H_{12} \cdot HZ] = k_6K_{31}P_{C_9H_{12}}[HZ]$$
$$r_7 = k_7[C_9H_{12} \cdot HZ] = k_7K_{31}P_{C_9H_{12}}[HZ]$$

$$r_{49} = k_{49}[C_{10}H_{14} \cdot HZ] = k_{49}K_{32}P_{C_{10}H_{14}}[HZ]$$
$$r_{50} = k_{50}[C_{10}H_{14} \cdot HZ] = k_{50}K_{32}P_{C_{10}H_{14}}[HZ]$$
$$r_{51} = k_{51}[C_{10}H_{14} \cdot HZ] = k_{51}K_{32}P_{C_{10}H_{14}}[HZ]$$

Olefin aromatisation

$$r_{52} = k_{52}[C_6H_{12} \cdot HZ]P_{C_2H_4} = k_{52}K_{12}P_{C_6H_{12}}P_{C_2H_4}[HZ]$$
$$r_{53} = k_{53}[C_6H_{12} \cdot HZ]P_{C_3H_6} = k_{53}K_{12}P_{C_6H_{12}}P_{C_3H_6}[HZ]$$
$$r_{54} = k_{54}[C_6H_{12} \cdot HZ]P_{C_4H_8} = k_{54}K_{12}P_{C_6H_{12}}P_{C_4H_8}[HZ]$$
$$r_{55} = k_{55}[C_6H_{12} \cdot HZ]P_{C_5H_{10}} = k_{55}K_{12}P_{C_6H_{12}}P_{C_5H_{10}}[HZ]$$
$$r_{56} = k_{56}[C_6H_{12} \cdot HZ]P_{C_6H_{12}} = k_{56}K_{12}P_{C_6H_{12}}P_{C_6H_{12}}[HZ]$$
$$r_{57} = k_{57}[C_6H_{12} \cdot HZ]P_{C_7H_{14}} = k_{57}K_{12}P_{C_6H_{12}}P_{C_7H_{14}}[HZ]$$
$$r_{58} = k_{58}[C_6H_{12} \cdot HZ]P_{C_8H_{16}} = k_{58}K_{12}P_{C_6H_{12}}P_{C_8H_{16}}[HZ]$$
$$r_{59} = k_{59}[C_6H_{12} \cdot HZ]P_{C_9H_{18}} = k_{59}K_{12}P_{C_6H_{12}}P_{C_9H_{18}}[HZ]$$
$$r_{60} = k_{60}[C_6H_{12} \cdot HZ]P_{C_{10}H_{20}} = k_{60}K_{12}P_{C_6H_{12}}P_{C_{10}H_{20}}[HZ]$$

$$r_{61} = k_{61}[C_7H_{14} \cdot HZ]P_{C_2H_4} = k_{61}K_{13}P_{C_7H_{14}}P_{C_2H_4}[HZ]$$
$$r_{62} = k_{62}[C_7H_{14} \cdot HZ]P_{C_3H_6} = k_{62}K_{13}P_{C_7H_{14}}P_{C_3H_6}[HZ]$$
$$r_{63} = k_{63}[C_7H_{14} \cdot HZ]P_{C_4H_8} = k_{63}K_{13}P_{C_7H_{14}}P_{C_4H_8}[HZ]$$
$$r_{64} = k_{64}[C_7H_{14} \cdot HZ]P_{C_5H_{10}} = k_{64}K_{13}P_{C_7H_{14}}P_{C_5H_{10}}[HZ]$$
$$r_{65} = k_{65}[C_7H_{14} \cdot HZ]P_{C_6H_{12}} = k_{65}K_{13}P_{C_7H_{14}}P_{C_6H_{12}}[HZ]$$
$$r_{66} = k_{66}[C_7H_{14} \cdot HZ]P_{C_7H_{14}} = k_{66}K_{13}P_{C_7H_{14}}P_{C_7H_{14}}[HZ]$$

$$r_{67} = k_{67}[C_7H_{14} \cdot HZ]P_{C_8H_{16}} = k_{67}K_{13}P_{C_7H_{14}}P_{C_8H_{16}}[HZ]$$
$$r_{68} = k_{68}[C_7H_{14} \cdot HZ]P_{C_9H_{18}} = k_{68}K_{13}P_{C_7H_{14}}P_{C_9H_{18}}[HZ]$$
$$r_{69} = k_{69}[C_7H_{14} \cdot HZ]P_{C_{10}H_{20}} = k_{69}K_{13}P_{C_7H_{14}}P_{C_{10}H_{20}}[HZ]$$

$$r_{70} = k_{70}[C_8H_{16} \cdot HZ]P_{C_2H_4} = k_{70}K_{14}P_{C_8H_{16}}P_{C_2H_4}[HZ]$$
$$r_{71} = k_{71}[C_8H_{16} \cdot HZ]P_{C_3H_6} = k_{71}K_{14}P_{C_8H_{16}}P_{C_3H_6}[HZ]$$
$$r_{72} = k_{72}[C_8H_{16} \cdot HZ]P_{C_4H_8} = k_{72}K_{14}P_{C_8H_{16}}P_{C_4H_8}[HZ]$$
$$r_{73} = k_{73}[C_8H_{16} \cdot HZ]P_{C_5H_{10}} = k_{73}K_{14}P_{C_8H_{16}}P_{C_5H_{10}}[HZ]$$
$$r_{74} = k_{74}[C_8H_{16} \cdot HZ]P_{C_6H_{12}} = k_{74}K_{14}P_{C_8H_{16}}P_{C_6H_{12}}[HZ]$$
$$r_{75} = k_{75}[C_8H_{16} \cdot HZ]P_{C_7H_{14}} = k_{75}K_{14}P_{C_8H_{16}}P_{C_7H_{14}}[HZ]$$
$$r_{76} = k_{76}[C_8H_{16} \cdot HZ]P_{C_8H_{16}} = k_{76}K_{14}P_{C_8H_{16}}P_{C_8H_{16}}[HZ]$$
$$r_{77} = k_{77}[C_8H_{16} \cdot HZ]P_{C_9H_{18}} = k_{77}K_{14}P_{C_8H_{16}}P_{C_9H_{18}}[HZ]$$
$$r_{78} = k_{78}[C_8H_{16} \cdot HZ]P_{C_{10}H_{20}} = k_{78}K_{14}P_{C_8H_{16}}P_{C_{10}H_{20}}[HZ]$$

$$r_{79} = k_{79}[C_9H_{18} \cdot HZ]P_{C_2H_4} = k_{79}K_{15}P_{C_9H_{18}}P_{C_2H_4}[HZ]$$
$$r_{80} = k_{80}[C_9H_{18} \cdot HZ]P_{C_3H_6} = k_{80}K_{15}P_{C_9H_{18}}P_{C_3H_6}[HZ]$$
$$r_{81} = k_{81}[C_9H_{18} \cdot HZ]P_{C_4H_8} = k_{81}K_{15}P_{C_9H_{18}}P_{C_4H_8}[HZ]$$
$$r_{82} = k_{82}[C_9H_{18} \cdot HZ]P_{C_5H_{10}} = k_{82}K_{15}P_{C_9H_{18}}P_{C_5H_{10}}[HZ]$$
$$r_{83} = k_{83}[C_9H_{18} \cdot HZ]P_{C_6H_{12}} = k_{83}K_{15}P_{C_9H_{18}}P_{C_6H_{12}}[HZ]$$
$$r_{84} = k_{84}[C_9H_{18} \cdot HZ]P_{C_7H_{14}} = k_{84}K_{15}P_{C_9H_{18}}P_{C_7H_{14}}[HZ]$$
$$r_{85} = k_{85}[C_9H_{18} \cdot HZ]P_{C_8H_{16}} = k_{85}K_{15}P_{C_9H_{18}}P_{C_8H_{16}}[HZ]$$
$$r_{86} = k_{86}[C_9H_{18} \cdot HZ]P_{C_9H_{18}} = k_{86}K_{15}P_{C_9H_{18}}P_{C_9H_{18}}[HZ]$$
$$r_{87} = k_{87}[C_9H_{18} \cdot HZ]P_{C_{10}H_{20}} = k_{87}K_{15}P_{C_9H_{18}}P_{C_{10}H_{20}}[HZ]$$

$$r_{88} = k_{88}[C_{10}H_{20} \cdot HZ]P_{C_2H_4} = k_{88}K_{16}P_{C_{10}H_{20}}P_{C_2H_4}[HZ]$$
$$r_{89} = k_{89}[C_{10}H_{20} \cdot HZ]P_{C_3H_6} = k_{89}K_{16}P_{C_{10}H_{20}}P_{C_3H_6}[HZ]$$
$$r_{90} = k_{90}[C_{10}H_{20} \cdot HZ]P_{C_4H_8} = k_{90}K_{16}P_{C_{10}H_{20}}P_{C_4H_8}[HZ]$$
$$r_{91} = k_{91}[C_{10}H_{20} \cdot HZ]P_{C_5H_{10}} = k_{91}K_{16}P_{C_{10}H_{20}}P_{C_5H_{10}}[HZ]$$
$$r_{92} = k_{92}[C_{10}H_{20} \cdot HZ]P_{C_6H_{12}} = k_{92}K_{16}P_{C_{10}H_{20}}P_{C_6H_{12}}[HZ]$$
$$r_{93} = k_{93}[C_{10}H_{20} \cdot HZ]P_{C_7H_{14}} = k_{93}K_{16}P_{C_{10}H_{20}}P_{C_7H_{14}}[HZ]$$
$$r_{94} = k_{94}[C_{10}H_{20} \cdot HZ]P_{C_8H_{16}} = k_{94}K_{16}P_{C_{10}H_{20}}P_{C_8H_{16}}[HZ]$$
$$r_{95} = k_{95}[C_{10}H_{20} \cdot HZ]P_{C_9H_{18}} = k_{95}K_{16}P_{C_{10}H_{20}}P_{C_9H_{18}}[HZ]$$
$$r_{96} = k_{96}[C_{10}H_{20} \cdot HZ]P_{C_{10}H_{20}} = k_{96}K_{16}P_{C_{10}H_{20}}P_{C_{10}H_{20}}[HZ]$$

Paraffin cracking

$$r_{97} = k_{97}K_{17}P_{C_2H_6}[HZ]$$

$$r_{98} = k_{98}K_{18}P_{C_3H_8}[HZ]$$
$$r_{99} = k_{99}K_{18}P_{C_3H_8}[HZ]$$

$$r_{100} = k_{100}K_{19}P_{C_4H_{10}}[HZ]$$
$$r_{101} = k_{101}K_{19}P_{C_4H_{10}}[HZ]$$
$$r_{102} = k_{102}K_{19}P_{C_4H_{10}}[HZ]$$

$$r_{103} = k_{103}K_{20}P_{C_5H_{12}}[HZ]$$
$$r_{104} = k_{104}K_{20}P_{C_5H_{12}}[HZ]$$
$$r_{105} = k_{105}K_{20}P_{C_5H_{12}}[HZ]$$
$$r_{106} = k_{106}K_{20}P_{C_5H_{12}}[HZ]$$
$$r_{107} = k_{107}K_{21}P_{C_6H_{14}}[HZ]$$

$$r_{108} = k_{108}K_{21}P_{C_6H_{14}}[HZ]$$
$$r_{109} = k_{109}K_{21}P_{C_6H_{14}}[HZ]$$
$$r_{110} = k_{110}K_{21}P_{C_6H_{14}}[HZ]$$
$$r_{111} = k_{111}K_{21}P_{C_6H_{14}}[HZ]$$

$$r_{112} = k_{112}K_{22}P_{C_7H_{16}}[HZ]$$
$$r_{113} = k_{113}K_{22}P_{C_7H_{16}}[HZ]$$
$$r_{114} = k_{114}K_{22}P_{C_7H_{16}}[HZ]$$
$$r_{115} = k_{115}K_{22}P_{C_7H_{16}}[HZ]$$
$$r_{116} = k_{116}K_{22}P_{C_7H_{16}}[HZ]$$
$$r_{117} = k_{117}K_{22}P_{C_7H_{16}}[HZ]$$

$$r_{118} = k_{118}K_{23}P_{C_8H_{18}}[HZ]$$
$$r_{119} = k_{119}K_{23}P_{C_8H_{18}}[HZ]$$
$$r_{120} = k_{120}K_{23}P_{C_8H_{18}}[HZ]$$
$$r_{121} = k_{121}K_{23}P_{C_8H_{18}}[HZ]$$
$$r_{122} = k_{122}K_{23}P_{C_8H_{18}}[HZ]$$
$$r_{123} = k_{123}K_{23}P_{C_8H_{18}}[HZ]$$
$$r_{124} = k_{124}K_{23}P_{C_8H_{18}}[HZ]$$

$$r_{125} = k_{125}K_{24}P_{C_9H_{20}}[HZ]$$
$$r_{126} = k_{126}K_{24}P_{C_9H_{20}}[HZ]$$
$$r_{127} = k_{127}K_{24}P_{C_9H_{20}}[HZ]$$
$$r_{128} = k_{128}K_{24}P_{C_9H_{20}}[HZ]$$
$$r_{129} = k_{129}K_{24}P_{C_9H_{20}}[HZ]$$
$$r_{130} = k_{130}K_{24}P_{C_9H_{20}}[HZ]$$
$$r_{131} = k_{131}K_{24}P_{C_9H_{20}}[HZ]$$
$$r_{132} = k_{132}K_{24}P_{C_9H_{20}}[HZ]$$

$$r_{133} = k_{133}K_{25}P_{C_{10}H_{22}}[HZ]$$
$$r_{134} = k_{134}K_{25}P_{C_{10}H_{22}}[HZ]$$
$$r_{135} = k_{135}K_{25}P_{C_{10}H_{22}}[HZ]$$
$$r_{136} = k_{136}K_{25}P_{C_{10}H_{22}}[HZ]$$
$$r_{137} = k_{137}K_{25}P_{C_{10}H_{22}}[HZ]$$
$$r_{138} = k_{138}K_{25}P_{C_{10}H_{22}}[HZ]$$
$$r_{139} = k_{139}K_{25}P_{C_{10}H_{22}}[HZ]$$
$$r_{140} = k_{140}K_{25}P_{C_{10}H_{22}}[HZ]$$
$$r_{141} = k_{141}K_{25}P_{C_{10}H_{22}}[HZ]$$

$$r_{142} = k_{142}K_9P_{C_2H_6}P_{C_3H_6}[HZ]$$
$$r_{143} = k_{143}K_{10}P_{C_2H_6}P_{C_4H_8}[HZ]$$
$$r_{144} = k_{144}K_{11}P_{C_2H_6}P_{C_5H_{10}}[HZ]$$
$$r_{145} = k_{145}K_{12}P_{C_2H_6}P_{C_6H_{12}}[HZ]$$
$$r_{146} = k_{146}K_{13}P_{C_2H_6}P_{C_7H_{14}}[HZ]$$
$$r_{147} = k_{147}K_{14}P_{C_2H_6}P_{C_8H_{16}}[HZ]$$
$$r_{148} = k_{148}K_{15}P_{C_2H_6}P_{C_9H_{18}}[HZ]$$
$$r_{149} = k_{149}K_{16}P_{C_2H_6}P_{C_{10}H_{20}}[HZ]$$

$$r_{150} = k_{150}K_8P_{C_3H_8}P_{C_2H_4}[HZ]$$
$$r_{151} = k_{151}K_{10}P_{C_3H_8}P_{C_4H_8}[HZ]$$
$$r_{152} = k_{152}K_{11}P_{C_3H_8}P_{C_5H_{10}}[HZ]$$
$$r_{153} = k_{153}K_{12}P_{C_3H_8}P_{C_6H_{12}}[HZ]$$
$$r_{154} = k_{154}K_{13}P_{C_3H_8}P_{C_7H_{14}}[HZ]$$
$$r_{155} = k_{155}K_{14}P_{C_3H_8}P_{C_8H_{16}}[HZ]$$
$$r_{156} = k_{156}K_{15}P_{C_3H_8}P_{C_9H_{18}}[HZ]$$
$$r_{157} = k_{157}K_{16}P_{C_3H_8}P_{C_{10}H_{20}}[HZ]$$

$$r_{158} = k_{158}K_8P_{C_4H_{10}}P_{C_2H_4}[HZ]$$
$$r_{159} = k_{159}K_9P_{C_4H_{10}}P_{C_3H_6}[HZ]$$
$$r_{160} = k_{160}K_{11}P_{C_4H_{10}}P_{C_5H_{10}}[HZ]$$
$$r_{161} = k_{161}K_{12}P_{C_4H_{10}}P_{C_6H_{12}}[HZ]$$
$$r_{162} = k_{162}K_{13}P_{C_4H_{10}}P_{C_7H_{14}}[HZ]$$
$$r_{163} = k_{163}K_{14}P_{C_4H_{10}}P_{C_8H_{16}}[HZ]$$
$$r_{164} = k_{164}K_{15}P_{C_4H_{10}}P_{C_9H_{18}}[HZ]$$
$$r_{165} = k_{165}K_{16}P_{C_4H_{10}}P_{C_{10}H_{20}}[HZ]$$

$$r_{166} = k_{166}K_8P_{C_5H_{12}}P_{C_2H_4}[HZ]$$
$$r_{167} = k_{167}K_9P_{C_5H_{12}}P_{C_3H_6}[HZ]$$
$$r_{168} = k_{168}K_{10}P_{C_5H_{12}}P_{C_4H_8}[HZ]$$
$$r_{169} = k_{169}K_{12}P_{C_5H_{12}}P_{C_6H_{12}}[HZ]$$
$$r_{170} = k_{170}K_{13}P_{C_5H_{12}}P_{C_7H_{14}}[HZ]$$
$$r_{171} = k_{171}K_{14}P_{C_5H_{12}}P_{C_8H_{16}}[HZ]$$
$$r_{172} = k_{172}K_{15}P_{C_5H_{12}}P_{C_9H_{18}}[HZ]$$
$$r_{173} = k_{173}K_{16}P_{C_5H_{12}}P_{C_{10}H_{20}}[HZ]$$

$$r_{174} = k_{174}K_8P_{C_6H_{14}}P_{C_2H_4}[HZ]$$
$$r_{175} = k_{175}K_9P_{C_6H_{14}}P_{C_3H_6}[HZ]$$
$$r_{176} = k_{176}K_{10}P_{C_6H_{14}}P_{C_4H_8}[HZ]$$
$$r_{177} = k_{177}K_{11}P_{C_6H_{14}}P_{C_5H_{10}}[HZ]$$
$$r_{178} = k_{178}K_{13}P_{C_6H_{14}}P_{C_7H_{14}}[HZ]$$
$$r_{179} = k_{179}K_{14}P_{C_6H_{14}}P_{C_8H_{16}}[HZ]$$
$$r_{180} = k_{180}K_{15}P_{C_6H_{14}}P_{C_9H_{18}}[HZ]$$
$$r_{181} = k_{181}K_{16}P_{C_6H_{14}}P_{C_{10}H_{20}}[HZ]$$

$$r_{182} = k_{182}K_8P_{C_7H_{16}}P_{C_2H_4}[HZ]$$
$$r_{183} = k_{183}K_9P_{C_7H_{16}}P_{C_3H_6}[HZ]$$
$$r_{184} = k_{184}K_{10}P_{C_7H_{16}}P_{C_4H_8}[HZ]$$
$$r_{185} = k_{185}K_{11}P_{C_7H_{16}}P_{C_5H_{10}}[HZ]$$
$$r_{186} = k_{186}K_{12}P_{C_7H_{16}}P_{C_6H_{12}}[HZ]$$
$$r_{187} = k_{187}K_{14}P_{C_7H_{16}}P_{C_8H_{16}}[HZ]$$
$$r_{188} = k_{188}K_{15}P_{C_7H_{16}}P_{C_9H_{18}}[HZ]$$
$$r_{189} = k_{189}K_{16}P_{C_7H_{16}}P_{C_{10}H_{20}}[HZ]$$

$$r_{190} = k_{190}K_8P_{C_8H_{18}}P_{C_2H_4}[HZ]$$
$$r_{191} = k_{191}K_9P_{C_8H_{18}}P_{C_3H_6}[HZ]$$
$$r_{192} = k_{192}K_{10}P_{C_8H_{18}}P_{C_4H_8}[HZ]$$
$$r_{193} = k_{193}K_{11}P_{C_8H_{18}}P_{C_5H_{10}}[HZ]$$

$$r_{194} = k_{194}K_{12}P_{C_8H_{18}}P_{C_6H_{12}}[HZ]$$
$$r_{195} = k_{195}K_{13}P_{C_8H_{18}}P_{C_7H_{14}}[HZ]$$
$$r_{196} = k_{196}K_{15}P_{C_8H_{18}}P_{C_9H_{18}}[HZ]$$
$$r_{197} = k_{197}K_{16}P_{C_8H_{18}}P_{C_{10}H_{20}}[HZ]$$

$$r_{198} = k_{198}K_8P_{C_9H_{20}}P_{C_2H_4}[HZ]$$
$$r_{199} = k_{199}K_9P_{C_9H_{20}}P_{C_3H_6}[HZ]$$
$$r_{200} = k_{200}K_{10}P_{C_9H_{20}}P_{C_4H_8}[HZ]$$
$$r_{201} = k_{201}K_{11}P_{C_9H_{20}}P_{C_5H_{10}}[HZ]$$
$$r_{202} = k_{202}K_{12}P_{C_9H_{20}}P_{C_6H_{12}}[HZ]$$
$$r_{203} = k_{203}K_{13}P_{C_9H_{20}}P_{C_7H_{14}}[HZ]$$
$$r_{204} = k_{204}K_{14}P_{C_9H_{20}}P_{C_8H_{16}}[HZ]$$
$$r_{205} = k_{205}K_{16}P_{C_9H_{20}}P_{C_{10}H_{20}}[HZ]$$

$$r_{206} = k_{206}K_8P_{C_{10}H_{22}}P_{C_2H_4}[HZ]$$
$$r_{207} = k_{207}K_9P_{C_{10}H_{22}}P_{C_3H_6}[HZ]$$
$$r_{208} = k_{208}K_{10}P_{C_{10}H_{22}}P_{C_4H_8}[HZ]$$
$$r_{209} = k_{209}K_{11}P_{C_{10}H_{22}}P_{C_5H_{10}}[HZ]$$
$$r_{210} = k_{210}K_{12}P_{C_{10}H_{22}}P_{C_6H_{12}}[HZ]$$
$$r_{211} = k_{211}K_{13}P_{C_{10}H_{22}}P_{C_7H_{14}}[HZ]$$
$$r_{212} = k_{212}K_{14}P_{C_{10}H_{22}}P_{C_8H_{16}}[HZ]$$
$$r_{213} = k_{213}K_{15}P_{C_{10}H_{22}}P_{C_9H_{18}}[HZ]$$

D. Rates of transformation

$$R_i = \sum_i^n \nu_{i,j} r_j$$

$$R_{CH_3OH} = -2r_{1f} + 2r_{1b} - r_2 + r_{ox2} - r_{ox3} - r_{4d} - r_8 - r_9 - r_{10} - r_{11} - r_{12} - r_{13} - r_{14} - r_{15} + r_{16} + r_{17} + r_{18} + r_{19} + r_{20} + r_{21} + r_{22} + r_{23} - r_{40} - r_{41} - r_{42} - r_{43} + r_{44} + r_{45} + r_{46} + r_{47}$$

$$R_{DME} = r_{1f} - r_{1b} - r_3 - 2r_{ox1} - r_{ox2} - r_{4d} - r_{5d} - r_{16} - r_{17} - r_{18} - r_{19} - r_{20} - r_{21} - r_{22} - r_{23} - r_{44} - r_{45} - r_{46} - r_{47}$$

$$R_{H_2O} = r_{1f} - r_{1b} + r_{ox3} + r_{4id} + 2r_{4d} + r_{5d} + r_8 + r_9 + r_{10} + r_{11} + r_{12} + r_{13} + r_{14} + r_{15} + r_{40} + r_{41} + r_{42} + r_{43}$$

$$R_{CH_4} = r_3 + r_{ox1} + r_{98} + r_{101} + r_{105} + r_{110} + r_{116} + r_{123} + r_{131} + r_{140}$$

$$R_{H_2} = 2r_2 + r_{5id} + r_{97} + r_{99} + r_{102} + r_{106} + r_{111} + r_{117} + r_{124} + r_{132} + r_{141}$$

$$R_{CO} = r_2$$

$$R_{CH_2O} = r_3 + r_{4id} + 2r_{5id}$$

$$R_{C_2H_4} = r_{5id} + r_{5d} + r_7 - r_8 - r_{16} - 2r_{24f} + 2r_{24b} - r_{25f} + r_{25b} - r_{26f} + r_{26b} - r_{28f} + r_{28b} - r_{30f} + r_{30b} - r_{33f} + r_{33b} - r_{36f} + r_{36b} + r_{48} + r_{49} - 3r_{52} - 3r_{61} - 3r_{70} - 3r_{79} - 3r_{88} + r_{97} + r_{98} + r_{100} + r_{103} + r_{107} + r_{112} + r_{118} + r_{125} + r_{133} + r_{142} + r_{143} + r_{144} + r_{145} + r_{146} + r_{147} + r_{148} + r_{149} - r_{150} - r_{158} - r_{166} - r_{174} - r_{182} - r_{190} - r_{198} - r_{206}$$

$$R_{C_3H_6} = r_{4id} + r_{4d} + r_6 + r_8 - r_9 + r_{16} - r_{17} - r_{25f} + r_{25b} - 2r_{27f} + 2r_{27b} - r_{29f} + r_{29b} - r_{31f} + r_{31b} - r_{34f} + r_{34b} - r_{37f} + r_{37b} + r_{50} - 3r_{53} - 3r_{62} - 3r_{71} - 3r_{80} - 3r_{89} + r_{99} + r_{101} + r_{104} + r_{108} + r_{113} + r_{119} + r_{126} + r_{134} - r_{142} + r_{150} + r_{151} + r_{152} + r_{153} + r_{154} + r_{155} + r_{156} + r_{157} - r_{159} - r_{167} - r_{175} - r_{183} - r_{191} - r_{199} - r_{207}$$

$$R_{C_4H_8} = r_9 - r_{10} + r_{17} - r_{18} + r_{24f} - r_{24b} - r_{26f} + r_{26b} - r_{29f} + r_{29b} - 2r_{32f} + 2r_{32b} - r_{35f} + r_{35b} - r_{38f} + r_{38b} + r_{51} - 3r_{54} - 3r_{63} - 3r_{72} - 3r_{81} - 3r_{90} + r_{102} + r_{105} + r_{109} + r_{114} + r_{120} + r_{127} + r_{135} - r_{143} - r_{151} - r_{168} - r_{176} - r_{184} - r_{192} - r_{200} - r_{208} + r_{158} + r_{159} + r_{160} + r_{161} + r_{162} + r_{163} + r_{164} + r_{165}$$

$$R_{C_5H_{10}} = r_{10} - r_{11} + r_{18} - r_{19} + r_{25f} - r_{25b} - r_{28f} + r_{28b} - r_{31f} + r_{31b} - r_{35f} + r_{35b} - 2r_{39f} + 2r_{39b} - 3r_{55} - 3r_{64} - 3r_{73} - 3r_{82} - 3r_{91} + r_{106} + r_{110} + r_{115} + r_{121} + r_{128} + r_{136} - r_{144} - r_{152} - r_{160} - r_{177} - r_{185} - r_{193} - r_{201} - r_{209} + r_{166} + r_{167} + r_{168} + r_{169} + r_{170} + r_{171} + r_{172} + r_{173}$$

$$R_{C_6H_{12}} = r_{11} - r_{12} + r_{19} - r_{20} + r_{26f} - r_{26b} + r_{27f} - r_{27b} - r_{30f} + r_{30b} - r_{34f} + r_{34b} - r_{38f} + r_{38b} - r_{52} - r_{53} - r_{54} - r_{55} - r_{56} - r_{57} - r_{58} - r_{59} - r_{60} - 3r_{56} - 3r_{65} - 3r_{74} - 3r_{83} - 3r_{92} + r_{111} + r_{116} + r_{122} + r_{129} + r_{137} - r_{145} - r_{153} - r_{161} - r_{169} - r_{186} - r_{194} - r_{202} - r_{210} + r_{174} + r_{175} + r_{176} + r_{177} + r_{178} + r_{179} + r_{180} + r_{181}$$

$$R_{C_7H_{14}} = r_{12} - r_{13} + r_{20} - r_{21} + r_{28f} - r_{28b} + r_{29f} - r_{29b} - r_{33f} + r_{33b} - r_{37f} + r_{37b} - 3r_{57} - r_{61} - r_{62} - r_{63} - r_{64} - r_{65} - r_{66} - 3r_{66} - r_{67} - r_{68} - r_{69} - 3r_{75} - 3r_{84} - 3r_{93} + r_{117} + r_{123} + r_{130} + r_{138} - r_{146} - r_{154} - r_{162} - r_{170} - r_{178} - r_{195} - r_{203} - r_{211} + r_{182} + r_{183} + r_{184} + r_{185} + r_{186} + r_{187} + r_{188} + r_{189}$$

$$R_{C_8H_{16}} = r_{13} - r_{14} + r_{21} - r_{22} + r_{30f} - r_{30b} + r_{31f} - r_{31b} + r_{32f} - r_{32b} - r_{36f} + r_{36b} - 3r_{58} - 3r_{67} - 3r_{76} - r_{70} - r_{71} - r_{72} - r_{73} - r_{74} - r_{75} - r_{76} - r_{77} - r_{78} - 3r_{85} - 3r_{94} + r_{124} + r_{131} + r_{139} - r_{147} - r_{155} - r_{163} - r_{171} - r_{179} - r_{187} + r_{190} + r_{191} + r_{192} + r_{193} + r_{194} + r_{195} + r_{196} + r_{197} - r_{204} - r_{212}$$

$$R_{C_9H_{18}} = r_{14} - r_{15} + r_{22} - r_{23} + r_{33f} - r_{33b} + r_{34f} - r_{34b} + r_{35f} - r_{35b} - 3r_{59} - 3r_{68} - 3r_{77} - r_{79} - r_{80} - r_{81} - r_{82} - r_{83} - r_{84} - r_{85} - r_{86} - r_{87} - 3r_{86} - 3r_{95} + r_{132} + r_{140} - r_{148} - r_{156} - r_{164} - r_{172} - r_{180} - r_{188} - r_{196} - r_{213} + r_{198} + r_{199} + r_{200} + r_{201} + r_{202} + r_{203} + r_{204} + r_{205}$$

$$R_{C_{10}H_{20}} = r_{15} + r_{23} + r_{36f} - r_{36b} + r_{37f} - r_{37b} + r_{38f} - r_{38b} + r_{39f} - r_{39b} - 3r_{60} - 3r_{69} - 3r_{78} - 3r_{87} - r_{88} - r_{89} - r_{90} - r_{91} - r_{92} - r_{93} - r_{94} - r_{95} - r_{96} - 3r_{96} + r_{141} - r_{149} - r_{157} - r_{165} - r_{173} - r_{181} - r_{189} - r_{197} - r_{205} + r_{206} + r_{207} + r_{208} + r_{209} + r_{210} + r_{211} + r_{212} + r_{213}$$

$$R_{C_2H_6} = 3r_{52} + 3r_{61} + 3r_{70} + 3r_{79} + 3r_{88} - r_{97} + r_{100} + r_{104} + r_{109} + r_{115} + r_{122} + r_{130} + r_{139} - r_{142} - r_{143} - r_{144} - r_{145} - r_{146} - r_{147} - r_{148} - r_{149} + r_{150} + r_{158} + r_{166} + r_{174} + r_{182} + r_{190} + r_{198} + r_{206}$$

$$R_{C_3H_8} = 3r_{53} + 3r_{62} + 3r_{71} + 3r_{80} + 3r_{89} - r_{98} - r_{99} + r_{103} + r_{108} + r_{114} + r_{121} + r_{129} + r_{138} - r_{150} - r_{151} - r_{152} - r_{153} - r_{154} - r_{155} - r_{156} - r_{157} + r_{142} + r_{159} + r_{167} + r_{175} + r_{183} + r_{191} + r_{199} + r_{207}$$

$$R_{C_4H_{10}} = 3r_{54} + 3r_{63} + 3r_{72} + 3r_{81} + 3r_{90} - r_{100} - r_{101} - r_{102} + r_{107} + r_{113} + r_{120} + r_{128} + r_{137} - r_{158} - r_{159} - r_{160} - r_{161} - r_{162} - r_{163} - r_{164} - r_{165} + r_{143} + r_{151} + r_{168} + r_{176} + r_{184} + r_{192} + r_{200} + r_{208}$$

$$R_{C_5H_{12}} = 3r_{55} + 3r_{64} + 3r_{73} + 3r_{82} + 3r_{91} - r_{103} - r_{104} - r_{105} - r_{106} + r_{112} + r_{119} + r_{127} + r_{136} - r_{166} - r_{167} - r_{168} - r_{169} - r_{170} - r_{171} - r_{172} - r_{173} + r_{144} + r_{152} + r_{160} + r_{177} + r_{185} + r_{193} + r_{201} + r_{209}$$

$$R_{C_6H_{14}} = 3r_{56} + 3r_{65} + 3r_{74} + 3r_{83} + 3r_{92} - r_{107} - r_{108} - r_{109} - r_{110} - r_{111} + r_{118} + r_{126} + r_{135} - r_{174} - r_{175} - r_{176} - r_{177} - r_{178} - r_{179} - r_{180} - r_{181} + r_{145} + r_{153} + r_{161} + r_{169} + r_{186} + r_{194} + r_{202} + r_{210}$$

$$R_{C_7H_{16}} = 3r_{57} + 3r_{66} + 3r_{75} + 3r_{84} + 3r_{93} - r_{112} - r_{113} - r_{114} - r_{115} - r_{116} - r_{117} + r_{125} + r_{134} - r_{182} - r_{183} - r_{184} - r_{185} - r_{186} - r_{187} - r_{188} - r_{189} + r_{146} + r_{154} + r_{162} + r_{170} + r_{178} + r_{195} + r_{203} + r_{211}$$

$$R_{C_8H_{18}} = 3r_{58} + 3r_{67} + 3r_{76} + 3r_{85} + 3r_{94} - r_{118} - r_{119} - r_{120} - r_{121} - r_{122} - r_{123} - r_{124} + r_{133} - r_{190} - r_{191} - r_{192} - r_{193} - r_{194} - r_{195} - r_{196} - r_{197} + r_{147} + r_{155} + r_{163} + r_{171} + r_{179} + r_{187} + r_{204} + r_{212}$$

$$R_{C_9H_{20}} = 3r_{59} + 3r_{68} + 3r_{77} + 3r_{86} + 3r_{95} - r_{125} - r_{126} - r_{127} - r_{128} - r_{129} - r_{130} - r_{131} - r_{132} - r_{198} - r_{199} - r_{200} - r_{201} - r_{202} - r_{203} - r_{204} - r_{205} + r_{148} + r_{156} + r_{164} + r_{172} + r_{180} + r_{188} + r_{196} + r_{213}$$

$$R_{C_{10}H_{22}} = 3r_{60} + 3r_{69} + 3r_{78} + 3r_{87} + 3r_{96} - r_{133} - r_{134} - r_{135} - r_{136} - r_{137} - r_{138} - r_{139} - r_{140} - r_{141} - r_{206} - r_{207} - r_{208} - r_{209} - r_{210} - r_{211} - r_{212} - r_{213} + r_{149} + r_{157} + r_{165} + r_{173} + r_{181} + r_{189} + r_{197} + r_{205}$$

$$R_{C3H8O2} = r_{ox1} - r_{ox2} - r_{ox3}$$

$$R_{C4H10O2} = r_{ox2} + r_{ox3} - r_{4id} - r_{5id}$$

$$R_{C_6H_6} = r_6 - r_{40} - r_{44} + r_{48} + r_{51} + r_{52} + r_{53} + r_{54} + r_{55} + r_{56} + r_{57} + r_{58} + r_{59} + r_{60}$$

$$R_{C_7H_8} = r_7 + r_{40} - r_{41} + r_{44} - r_{45} + r_{50} + r_{61} + r_{62} + r_{63} + r_{64} + r_{65} + r_{66} + r_{67} + r_{68} + r_{69}$$

$$R_{C_8H_{10}} = r_{41} - r_{42} + r_{45} - r_{46} - r_{48} + r_{49} + r_{70} + r_{71} + r_{72} + r_{73} + r_{74} + r_{75} + r_{76} + r_{77} + r_{78}$$

$$R_{C_9H_{12}} = r_{42} - r_{43} + r_{46} - r_{47} - r_6 - r_7 + r_{79} + r_{80} + r_{81} + r_{82} + r_{83} + r_{84} + r_{85} + r_{86} + r_{87}$$

$$R_{C_{10}H_{14}} = r_{43} + r_{47} - r_{49} - r_{50} - r_{51} + r_{88} + r_{89} + r_{90} + r_{91} + r_{92} + r_{93} + r_{94} + r_{95} + r_{96}$$

$$R_{N_2} = 0$$

Chapter 8

8. Zeolite Minilith: A Unique Structured Catalyst for the Methanol to Gasoline Process

In the previous chapter, methanol to hydrocarbons was studied over zeolite catalysts at 370 °C. However, zeolite catalysts are used in industry in their structured form for MTH conversion. The following published paper considers the industrial practice of the conversion of methanol to gasoline in fixed bed reactors. The conversion of methanol to gasoline is considered at 370 °C as olefins become predominant at higher temperatures. A comparison is made between a novel type of structured reactor called zeolite miniliths to zeolite powder for improved gasoline yield and pressure drop reduction.

This declaration concerns the article entitled:									
Zeolite minilith: A unique structured catalyst for the methanol to gasoline process									
Publication status (tick one)									
draft manuscript		**Submitted**		**In review**		**Accepted**		**Published**	✓
Publication details (reference)	Toyin Omojola, Nikolay Cherkasov, Evgeny V. Rebrov, Dmitry B. Lukyanov, Semali P. Perera. Zeolite minilith: A unique structured catalyst for the methanol to gasoline process. 2018. *Chemical Engineering and Processing: Process Intensification.* 131. 137 – 143.								
Candidate's contribution to the paper (detailed, and also given as a percentage).	The candidate predominantly executed the… Formulation of ideas: Oluwatoyin Omojola conceived the initial idea for this project (100 %) Design of methodology (65%): Oluwatoyin Omojola designed all the experiments in this project with supervision from Prof. Semali P. Perera. Experimental work (100 %): Oluwatoyin Omojola conducted all experiments for this project Presentation of data in journal format (80%): Oluwatoyin Omojola analysed all data which was further checked by Dmitry B. Lukyanov and Semali P. Perera. Oluwatoyin Omojola wrote the paper with supervision and suggestions from all co-authors								
Statement from Candidate	This paper reports on original research I conducted during the period of my Higher Degree by Research candidature.								
Signed						**Date**	08/02/2019		

The final published version is available via: https://doi.org/10.1016/j.cep.2018.07.016

Abstract

Structured microchannel H-ZSM-5 catalysts containing up to 80 wt% zeolite (balance bentonite) were fabricated by unit operations of paste preparation, extrusion, drying and firing. The structured catalysts, called miniliths due to their micrometre-range dimensions, were composed of parallel cylindrical channels with a wall thickness of 200 – 300 μm, density of 2.1 channels/mm^2 and a channel diameter of 300 μm. These miniliths were characterised by X-ray diffraction, scanning electron microscopy, energy dispersive X-ray analysis, nitrogen physisorption and thermogravimetric analysis. For the first time, these miniliths were tested for the conversion of methanol to gasoline at 370 °C, 3 bar and a weight hourly space velocity (WHSV) of up to 1170 h^{-1}. A gasoline product yield of 53% was obtained at a methanol conversion of 74% over the ZSM-5 miniliths. The pressure drop at the same conversion over a packed-bed reactor of equal ZSM-5 content was 2 orders of magnitude higher than that of the minilith. Reducing the amount of ZSM-5 catalyst in the packed bed to obtain similar inlet pressure as the ZSM-5 minilith gave the same product yield at a much higher conversion (81%) demonstrating the potential of these structured microchannel reactors.

Keywords: methanol-to-gasoline, methanol-to-olefin, ZSM-5, minilith, gasoline, methanol, structured reactor, micromonolith

8.1. Introduction

In heterogeneous catalysis, product selectivity is regulated by an interaction of mass and heat transport, kinetics and fluid dynamics. This interaction can be particularly pronounced in constrained environments such as zeolites. Zeolites, which generally possess a well-defined pore architecture and size (1), are synthesised in their powder form and used in their pelletised form in packed bed reactors. The major drawbacks to this approach are (i) high pressure drop, (ii) limited use of catalyst bed, (iii) flow maldistribution (e.g. channelling) and (iv) heat and mass-transport limitations (2, 3). The high pressure drop is circumvented by using larger pellets that increase the inter-particle channel dimensions. Large pellets, however, lead to intra-pellet mass transfer limitations. Flow maldistribution is minimised by ensuring a high ratio of the reactor diameter to catalyst particle diameter (4-6). The need for small particle sizes and low pressure drop can be decoupled using a structured reactor such as a monolith (3).

The conversion of methanol to gasoline (MTG) over a packed-bed of ZSM-5 catalysts is an exothermic (1.74 MJ $kg_{methanol}^{-1}$) reaction (7, 8) with an adiabatic temperature rise of 600 °C observed in industrial packed-bed processes (8). The temperature rise in the reactors is kept within acceptable limits by separating the overall MTG process into two stages: dehydration of methanol to dimethyl ether (DME), and conversion of this mixture to hydrocarbons (9). The temperature rise in the second stage may be further reduced by applying a large recycle of gas, but this approach increases the operating costs. High exothermicity of the MTG reaction at full conversion leads to the presence of hot spots along the catalyst bed which generate uneven concentration distribution and facilitate catalyst deactivation; both resulting in an uncontrollable product selectivity. Thus, industrially, there is a demand for catalysts that: (i) show slow deactivation and (ii) allow for quick heat transfer leading to further reduction in operating costs. There has also been a long standing scholarly debate on the formation of primary products from methanol either directly (10-18) or through a hydrocarbon pool mechanism (19-27). Studying the induction period or steady state MTG conversion at low contact times can allow for mechanistic investigations of primary product formation.

A reduced probability of hot spots is obtained due to high reproducibility of size and surface characteristics of individual monolithic passages that allow for equal flow, mass and heat transport conditions under adiabatic operation (2). Short-length monoliths are used to enhance mass and heat transfer as velocity, temperature and concentration profiles are still developing (2). It is well established that for simultaneously developing flow, the fluid velocity, velocity gradients, and temperature gradients near the wall in the entrance region will be higher than that attained with fully developed profiles. Consequently, the higher velocities convect more thermal energy in the flow direction, and heat transfer in the thermal entrance region is higher for the case of developing velocity profiles (28).

Zeolite-coated spheres (29), zeolite membranes (30), ceramic foams (31), β-SiC foams (32), wash-coated monoliths (33, 34) have been used to intensify the conversion of methanol to hydrocarbons (MTH). In all these systems, catalyst inventory remains an important obstacle. This challenge can be overcome by co-extrusion of the catalyst substrate and a binder (2). Hargreaves and Munnoch (35) showed that binders can affect catalytic processes by modifying coking characteristics, entrapping poisons, transferring chemical species to or from the active phase, modifying heat transfer and porosity characteristics and improving physical durability. Whiting et al. (36) used microspectroscopy to show aluminium migration in ZSM-5-containing alumina-bound extrudates, forming additional Brønsted acid sites. Fougerit et al. (37) attributed the increase in the stability of a dealuminated mordenite catalyst for methanol to olefin conversion to the trapping of coke precursors in the binder phase. Shihabi et al. (38) showed that an α-alumina monohydrate binder inclusion on a siliceous H-ZSM-5 catalyst significantly enhanced the conversion of methanol to hydrocarbons. This enhancement was attributed to the transfer of aluminium species from the binder to the zeolite phase.

In this contribution, a co-extruded structured catalyst with micrometre-range channels for MTG conversion was fabricated, characterised and tested. The structured catalysts, extruded into a cylindrical form, contained the ZSM-5 catalyst in the bulk and on the outer surface of the channels. The structured catalysts referred to as ZSM-5 miniliths have a potential industrial significance as they not only reduce the pressure drop (thereby reducing operating costs) but also maintain high catalyst loading. These advantages have been achieved with similar gasoline yields as those obtained under reported industrial conditions. Also, the dimensions of short microchannels allow for the accessibility of very low residence times (39) which could be relevant to solving the initial C-C bond conundrum in the absence of transport restrictions.

8.2. Materials and methods

8.2.1. Catalyst preparation

A commercial NH_4-ZSM-5 zeolite catalyst with a Si/Al ratio of 25 was purchased from Zeolyst International. The catalyst powder was sieved (0.5 mm mesh) to remove larger particles and mixed with 20 – 50 wt% sodium bentonite powder received from RS minerals Ltd. The total solid weight (ZSM-5 and bentonite) was 100 g. Distilled water was added to the zeolite-bentonite mixture. The optimum water weight was found to be in the range from 0.9 (sample D) to 1.2 (sample A) times the weight of the solid mixture. The resulting paste was homogenised in a high-shear mixer (Clatronic, 1000W) for 2 min. Since the water content varied with binder content, the ZSM-5/bentonite ratio was altered to study its influence on pore volume and surface area. The compositions studied are listed in Table 8.1. For sample A2, 10

g of carbon (activated carbon, Nuchar) was added to the solid mixture. Sample B can also be compared to B2 to investigate the effect of water content as they both contain equal ZSM-5 and bentonite content.

The wet homogenous paste was kneaded to remove trapped air and extruded manually through a cylindrical multi-pin die with a bench mounted press. The extrudates, which possess micrometre-range channels, are called miniliths. The term, minilith, has been used before to refer to structured hydrodemetalation catalysts (40, 41). The minilith were further dried in a cold room (5 °C) and were rolled around periodically to ensure homogenous drying in accordance with the method used by Lee et al. (42). The dried minilith extrudates were heated in a kiln (Rohde) at 5 °C min^{-1} up to 450 °C and held for 0.5 h. This temperature was chosen to preserve the mechanical strength of the minilith while maintaining the distribution of acid sites between Brønsted and Lewis acid sites (43).

Table 8.1: Composition of the ZSM-5 miniliths

Sample code	ZSM-5 (g)	Bentonite (g)	Carbon (g)	Water (g)
A	50	50	-	121
B	60	40	-	111
C	70	30	-	91
D	80	20	-	91
A2	50	50	10	137
B2	60	40	-	82

8.2.2. Catalyst characterisation

The minilith samples were ground and X-ray diffraction (XRD) studies were performed with a Bruker Advance D8 diffractometer using Cu $K_{\alpha 1}$ radiation equipped with standard Bragg-Brentano geometry. Nitrogen physisorption studies were carried out on the unground samples with a Micromeritics ASAP 2020 unit. The samples were degassed by heating to 300 °C under vacuum (10^{-6} mbar) for 8 h. After degassing, nitrogen was adsorbed at -196 °C at increasing partial pressures to determine the BET surface area and the pore volume. A Rouquerol-adjusted BET surface area (44) was then calculated. The morphology and elemental analysis were obtained using energy dispersive X-ray analysis of the zeolite minilith was studied using a JEOL (JSM-6480LV) scanning electron microscope equipped with an Oxford INCA X–act 10 mm^2 SDD X-ray detector.

Thermogravimetric analysis (TGA) of the ground miniliths as well as the original ZSM-5 catalyst and bentonite powder was carried out in a Setsys Evolution TGA 16/18 instrument

(SETARAM). Before each experiment, 12 mg of sample was placed into an alumina crucible held in a TGA chamber that was purged with air at 20 °C at 200 mL min^{-1} for 8 min. All gas flow rates refer to normal temperature and pressure. The experiments were performed under air flowing at 20 mL min^{-1} at a heating rate of 5 °C min^{-1} to the temperature of 600 °C.

8.2.3. ZSM-5 minilith catalytic tests

The ZSM-5 minilith (~ 3.9 mm O.D, 14 mm length) was placed between two quartz wool plugs and inserted in a cylindrical quartz tube (4 mm I.D, 6 mm O.D). The quartz tube was housed in a heater (see Fig. S8.1 in supplementary information). To obtain the H-form, the NH_4-ZSM-5 minilith was additionally calcined under oxygen flow at 450 °C for 30 min at a heating rate 5 °C min^{-1}. This additional calcination was conducted to ensure the same integrity of miniliths used in catalytic tests. Thereafter, the ZSM-5 minilith was purged with nitrogen at a flowrate of 10 mL min^{-1} while the reactor temperature was brought down to 370 °C. During the MTG reaction, nitrogen was passed at various flowrates through a vessel containing methanol which was immersed in a saturator at 4.2 °C. A back-pressure controller was used to maintain an inlet pressure of 3 bar. The reaction products were sampled through an online gas chromatography (Shimadzu GC 2010) equipped with a flame ionisation detector and an Equity-1 fused silica capillary column (90m × 0.53mm × 3.0µm).

The methanol conversion and yield were calculated on a carbon basis. The conversion was defined as the fraction of oxygenates consumed during the reaction (equation 8.1), where $C_{MeOH,in}$ is the inlet methanol mole concentration, $C_{oxy,out}$ is the sum of the outlet mole concentrations of methanol and twice the outlet mole concentrations of DME. C_i is the mole concentrations of species (ethylene, propylene etc)

$$X = \frac{C_{MeOH,in} - C_{oxy,out}}{C_{MeOH,in}} \times 100\%, \quad (8.1)$$

Dry yield towards hydrocarbons was calculated based on carbon number. For instance, for ethylene and propylene, it is given as:

$$Y_{ethene} = \frac{2 \cdot C_{C2H4}}{C_{MeOH,in}} \times 100\%, \quad (8.2)$$

$$Y_{propene} = \frac{3 \cdot C_{C3H6}}{C_{MeOH,in}} \times 100\%, \quad (8.3)$$

The product distribution (mass fraction, w_i) of species was evaluated as:

$$w_i = \frac{m_i}{\sum m_c + m_{H_2O} + m_{N_2}} \quad (8.4)$$

where m_i is the mass of specie, i, m_c is the total mass of hydrocarbons (aliphatics and aromatics), m_{H2O} is the water mass and m_{N2} is the mass of carrier gas, nitrogen. The calculation of mass and moles of species are given in a sample calculation in Table S8.1 in supplementary information.

A test experiment on the effect of the binder was conducted at 370 °C and the lowest flow rate of 54 mL min^{-1}. Additionally, stability measurements were conducted over a chosen minilith (Sample C) and compared to a zeolite/bentonite mixture of equal ZSM-5 weight at 3 bar and a flowrate of 54 mL min^{-1}.

8.3. Results and discussion

8.3.1. Catalyst characterisation

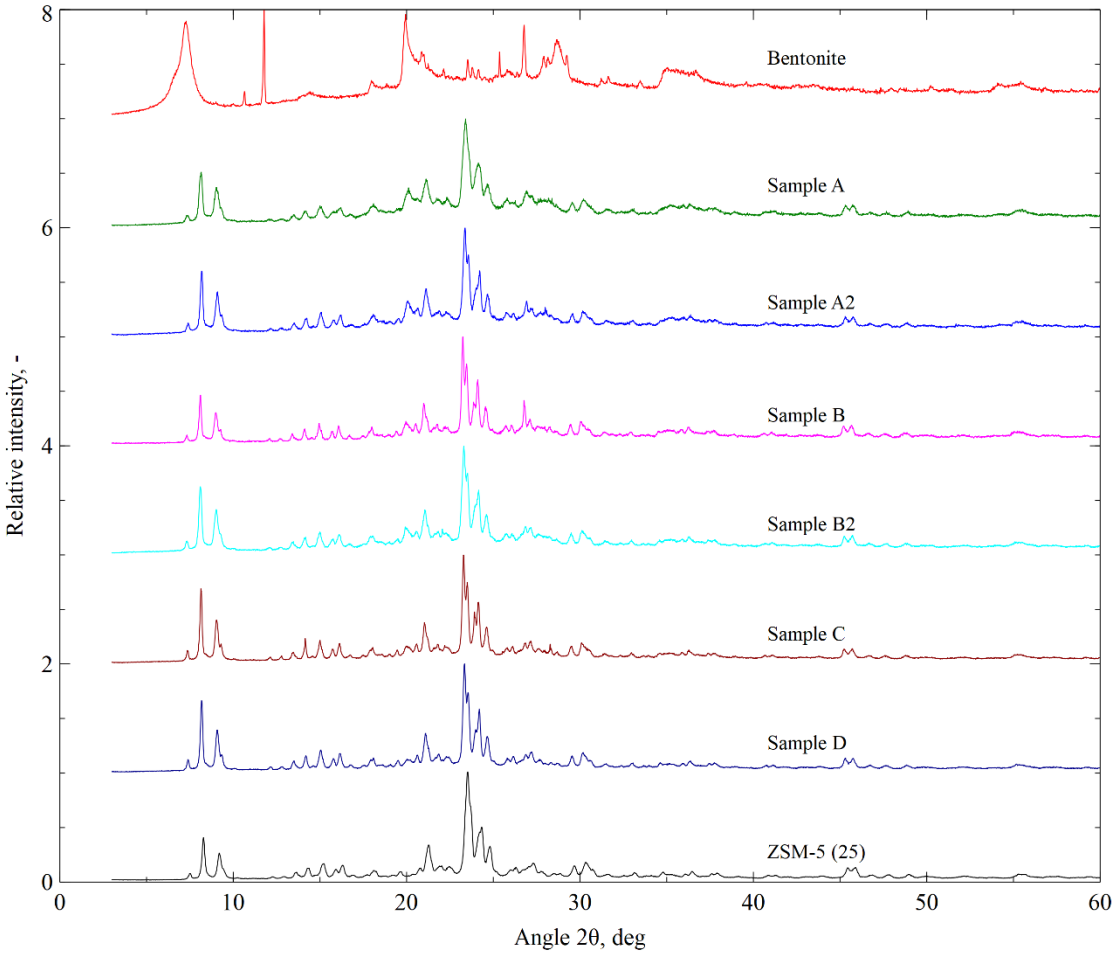

Fig. 8.1: Powder X-ray diffraction patterns of bentonite, ZSM-5 miniliths and ZSM-5 catalyst.

The XRD patterns of the miniliths composed of ZSM-5 and bentonite are presented in Fig. 8.1. All samples exhibit the MFI structure with major peaks located at *2θ* about 7.9° and 8.9° and the characteristic triplet at 23.5° (45, 46). ZSM-5 peaks did not shift on adding bentonite. Carbon as a pore template does not affect lattice crystallinity. This is because during firing the carbon is burnt-off to create mesoporosity. Carbon affects the porosity (as shown in Table 8.2) but not the crystallinity.

Table 8.2: Porosity data of the ZSM-5 miniliths

Sample code	ZSM-5 (g)	Bentonite (g)	Carbon (g)	Water (g)	BET$^{\Omega}$ surface area, m^2 g^{-1}	HK* micropore volume, cm^3 g^{-1}	Total pore volume, cm^3 g^{-1}	Si/Al ratio
A	50	50	-	121	293	0.114	0.175	7.6
B	60	40	-	111	273	0.109	0.183	9.4
C	70	30	-	91	323	0.129	0.235	11.7
D	80	20	-	91	353	0.142	0.238	14.6
A2	50	50	10	137	224	0.075	0.132	7.7
B2	60	40	-	82	279	0.111	0.193	10.2
ZSM-5	100	-	-	-	419	0.143	0.222	25$^{\Delta}$
Bentonite	-	100	-	-	48	0.013	0.048	1.5$^{\Delta}$

$^{\Omega}$Rouquerol-adjusted BET values. *HK:Horvath-Kawazoe. $^{\Delta}$Commercial values.

ZSM-5 and bentonite both have micropores (below 2 nm in diameter) and mesopores (2-50 nm in diameter). An increasing amount of bentonite added to a minilith generally reduces the BET surface area and micropore volume (Table 8.2). The addition of carbon to the ZSM-5/bentonite mixture to induce mesoporosity leads to a decrease in BET surface area and a decrease in micropore volume (comparing sample A to A2). This is probably due to the formation of larger pores in the minilith (see Fig. S8.2 in supplementary information). These macropores are formed during the burning-off of carbon during firing. Carbon agglomeration occurs during paste preparation leading to large pores on burning-off. The water content varied systematically with solid weight (ZSM-5 and bentonite). When solid weight content was kept constant (sample B vs B2), addition of more water to the paste made little impact on the minilith microporosity but a higher impact on total pore volume. The Si/Al ratios of the final miniliths increases as the ZSM-5 content increases.

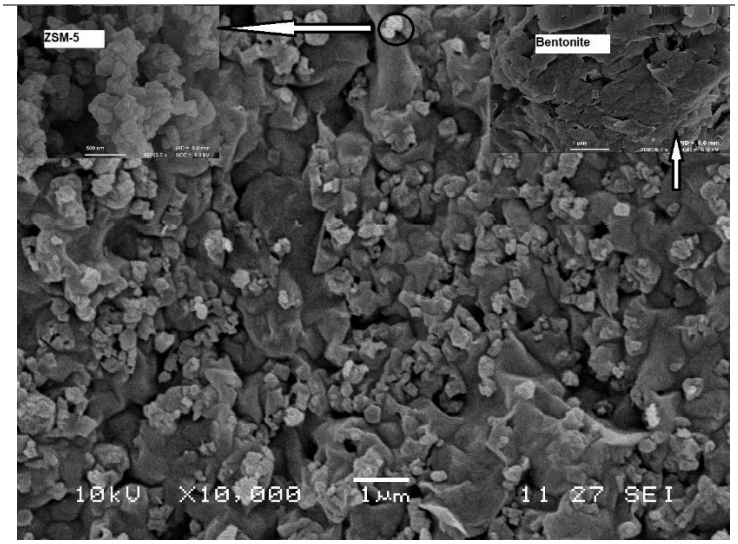

(a) A vertical cross-section of 50 wt% ZSM-5 (sample A) minilith showing an insert of the bentonite phase and ZSM-5 phase

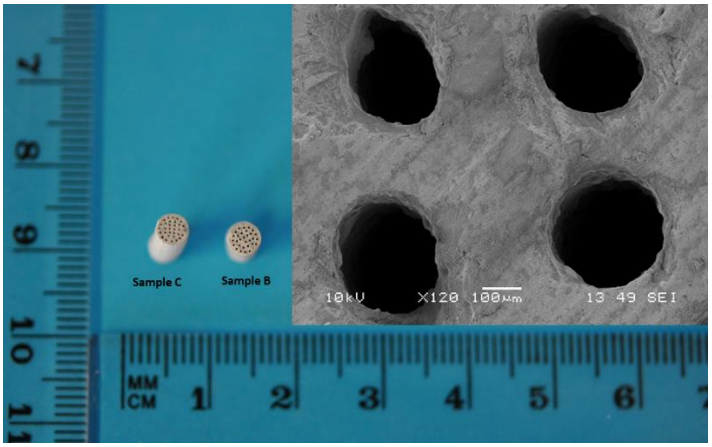

(b) Image of three minilith structures (L-R): 70 wt% (sample C) and 60 wt% ZSM-5 (sample B) with an inset of a horizontal cross-section of 70 wt% minilith (sample C)

Fig. 8.2: Scanning electron micrographs and images of the ZSM-5 miniliths

The scanning electron micrographs (Fig. 8.2) show that the ZSM-5 particles are dispersed on the bentonite structure. The ZSM-5 particles appear as tiny islands on the flat bentonite surface. Addition of carbon leads to large cavities in the ZSM-5 minilith (comparing sample A to A2). Before firing, the ZSM-5 minilith maintains a diameter of 4.4 mm. After firing, the channels shrink in accordance to the amount of bentonite present in the structure. For instance, visual inspection of the minilith diameters before and after firing show that a 13% shrinkage occurs with 70 wt% ZSM-5 (sample C).

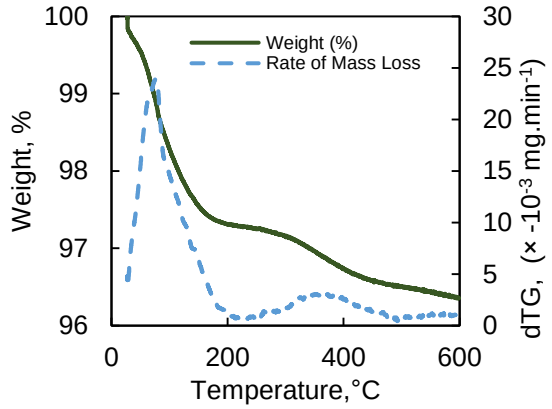

a. TGA of ZSM-5 used for ZSM-5 minilith preparation

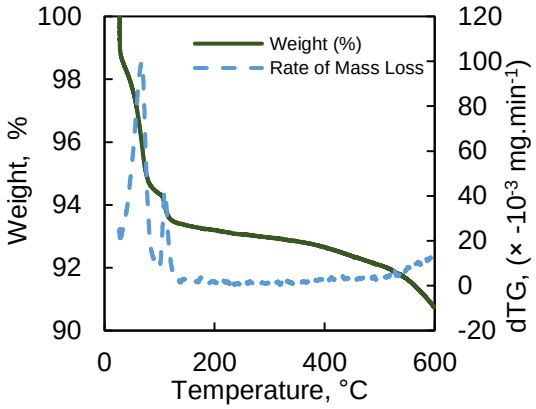

b. TGA of bentonite used for ZSM-5 minilith preparation

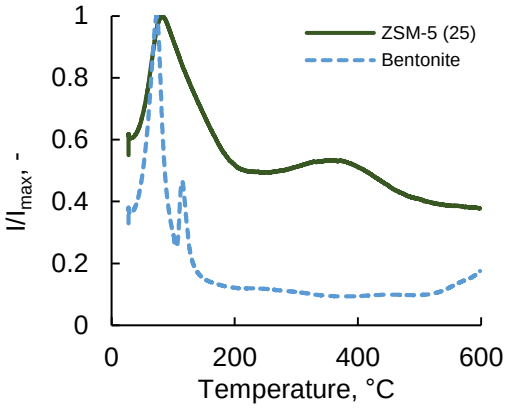

c. The release of H_2O at m/z=18 during TGA analysis

Fig. 8.3: TGA of weight loss (a, b) and (c) rate of H_2O release over ZSM-5 and bentonite.

Fig. 8.3a shows TGA curves for ZSM-5 where weight losses occur in two temperature ranges investigated: below 200°C and between 200 and 450 °C after which no weight changes are observed indicating that a stable zeolite is obtained. For bentonite, three weight loss temperature regions were obtained: below 100 °C, between 100 and 150 °C and at temperatures greater than 515 °C (Fig. 8.3b). The water profiles (Fig. 8.3c) are similar in shape to the rate of mass loss profiles (Figs. 8.3a and b) suggesting that water accounts for most of the sample loss. The bentonite weight loss below 150°C corresponds to the removal of adsorbed and interlayer water while the loss at temperatures above 515°C relates to the removal of water from bentonite (47). Therefore, prior to catalytic testing, the catalysts were fired at 450 °C to keep the chemical nature of the bentonite. This temperature is also enough to decompose the ammonium form of zeolite.

8.3.2. Catalytic tests

The characterisation studies show that it is possible to obtain miniliths with controlled ZSM-5 loading and porosity. All the miniliths maintained the extruded morphology with mechanical stability required for characterisation. Therefore, the MTG conversion could be performed with any minilith considering the catalyst loading, reactor dimensions and heat transfer. For a small-scale laboratory test, where heat transfer effects are less pronounced (*vide supra*), minilith C was selected to maintain a high ZSM-5 loading while keeping a reduced effect of the Si/Al ratio of bentonite on methanol to gasoline production. Although sample D had the highest ZSM-5 loading, sample C was more mechanically stable due to its higher bentonite content. A test experiment was carried out on the effect of bentonite on MTG conversion. A methanol conversion of only 0.9 % was obtained at 54 mL min^{-1}. This conversion is *ca.* 100 times lower compared to the conversion obtained under the same conditions over the minilith of similar bentonite content. Therefore, the effect of bentonite on MTG reaction over the minilith studied was negligible.

Fig. 8.4 shows the results of the catalytic test conducted over a minilith with 70 wt% ZSM-5 catalyst. As contact time increases, mass fractions of methanol decrease while DME rises until 5.3 $g_{cat}g_{feed}^{-1}s$ showing the activation of the methanol dehydration reaction. Consequently, the mass fraction of water rises. As contact time increases further, DME mass fraction decreases as it is involved in the chemistries of MTH chemistries such as olefin and aromatic methylation reactions (48).

The conversion of methanol to hydrocarbons is well established to be an autocatalytic reaction over ZSM-5 catalyst (49-51). The data on MTG reaction over the minilith show autocatalytic behaviour with a projected non-linear increase from zero contact times (Fig. 8.4). At low temperatures and high Si/Al ratios where kinetics control the rate of methanol conversion, Ono and co-workers (51) observed that the accumulation of reactive intermediates is responsible for the conversion jump as contact time is increased. This is due to the involvement of reactive species in methylation reactions. Also, rapid heat generation could be responsible for the conversion jump due to the increasing exothermicity of MTH conversion as contact time increases. The data (Fig. 8.4) shows that autocatalysis occurs over ZSM-5 miniliths but with the conversion jump occurring at much lower contact times. The binder acts as a heat sink by moderating temperature rise, heat generation and reaction conversion (35). Consequently, with a constant temperature across the short-length ZSM-5 minilith during MTG conversion (see section 8.1), the data suggests that a low concentration of autocatalysing species is necessary to initiate the conversion jump.

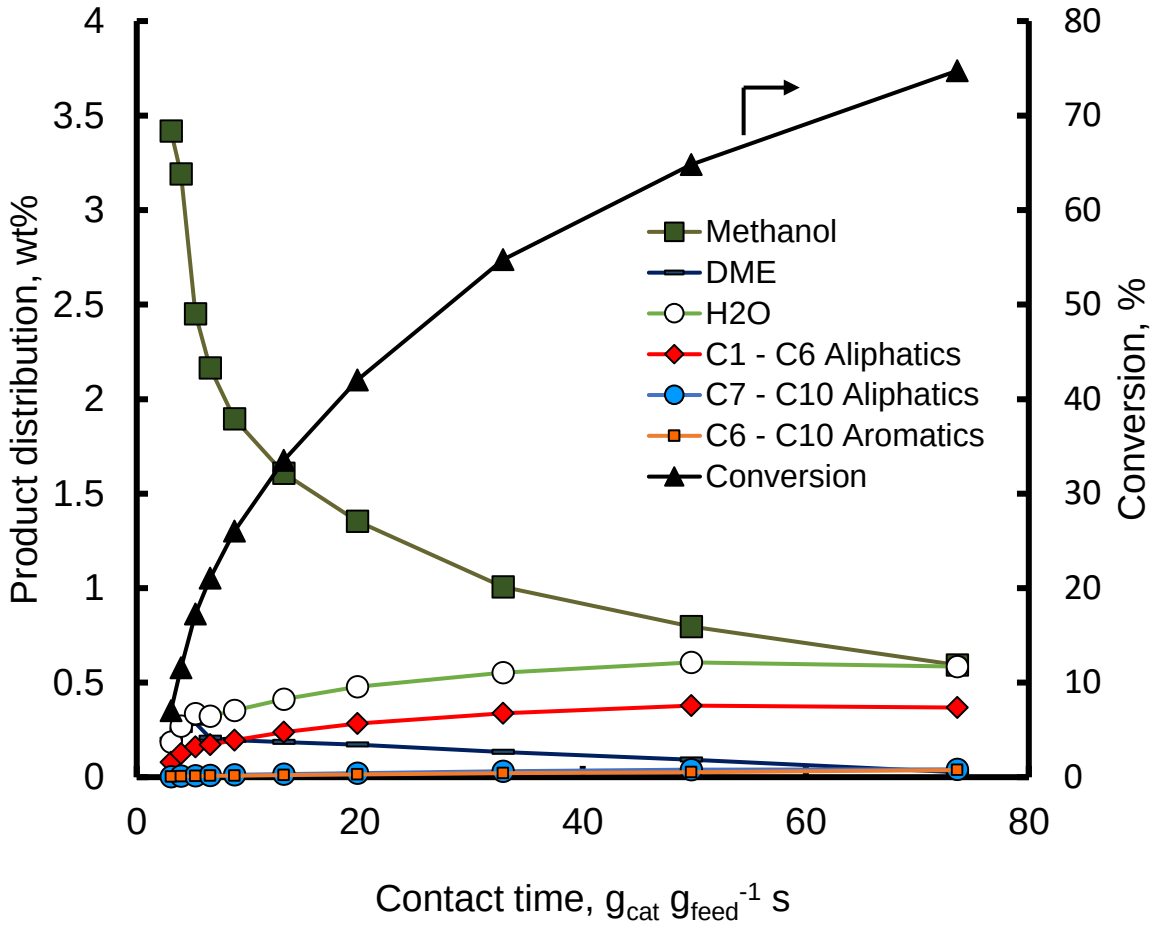

Fig. 8.4: Product distribution and conversion with contact time over ZSM-5 minilith (sample C) at 370 °C and an inlet pressure of 3 bar. Methanol, DME, C1-C6 aliphatics, C7 –C10 aliphatics and C6 – C10 aromatics were obtained experimentally. Water was calculated.

Fig. 8.4 also shows a rise in aliphatics and aromatics as contact time is increased. Recently, it was shown that DME is the main methylating agent present at conditions required for MTG conversion (52, 53). At high contact times, any DME produced from the equilibration reaction is fully consumed for aliphatic and aromatic production. During this period, the mass fraction of methanol falls until it reaches a plateau. Thus, DME acts as an intermediate between methanol and products (aliphatics and aromatics). DME concentration goes through a maximum because at first it is produced via the equilibration reaction (which is predominant at early contact times) and then converted into products (aliphatics and aromatics) during which it is also used as a methylating agent. The equilibration reaction leads to a continuous depletion of methanol while DME is increasingly consumed as contact time increases. This implies that the equilibrium product concentrations can be attained at high contact times.

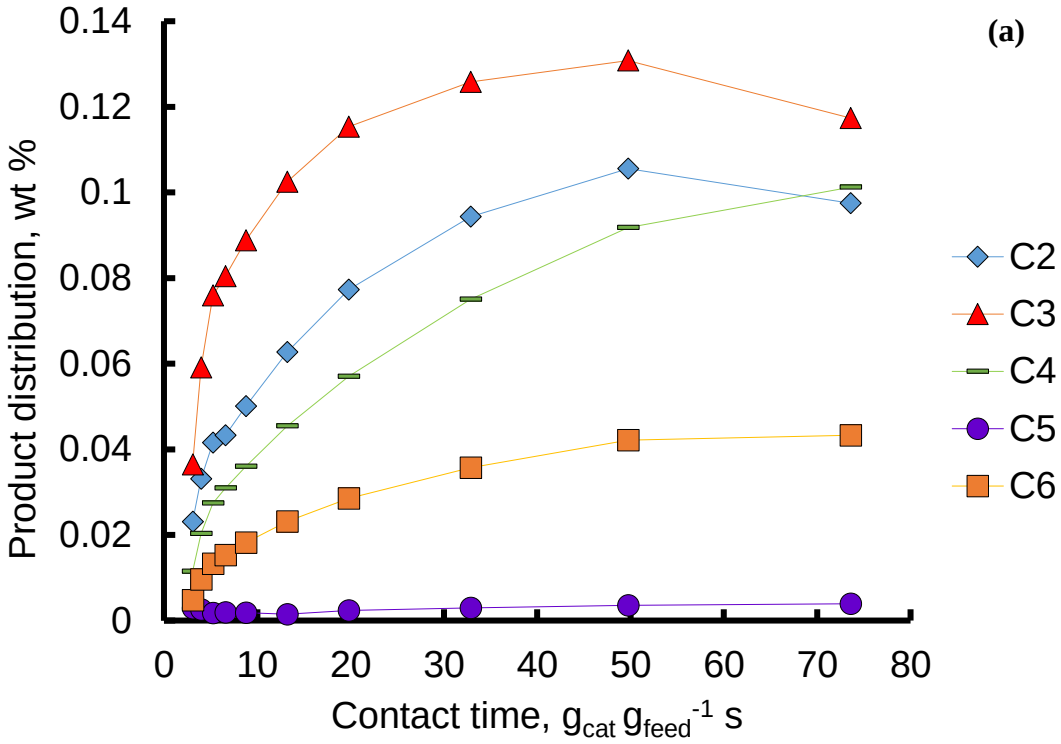
(a)
0.14
0.12
0.1
0.08
0.06
0.04
0.02
0
Product distribution, wt %
0
10
20
30
40
50
60
70
80
Contact time, $g_{cat}\,g_{feed}^{-1}$ s
C2
C3
C4
C5
C6

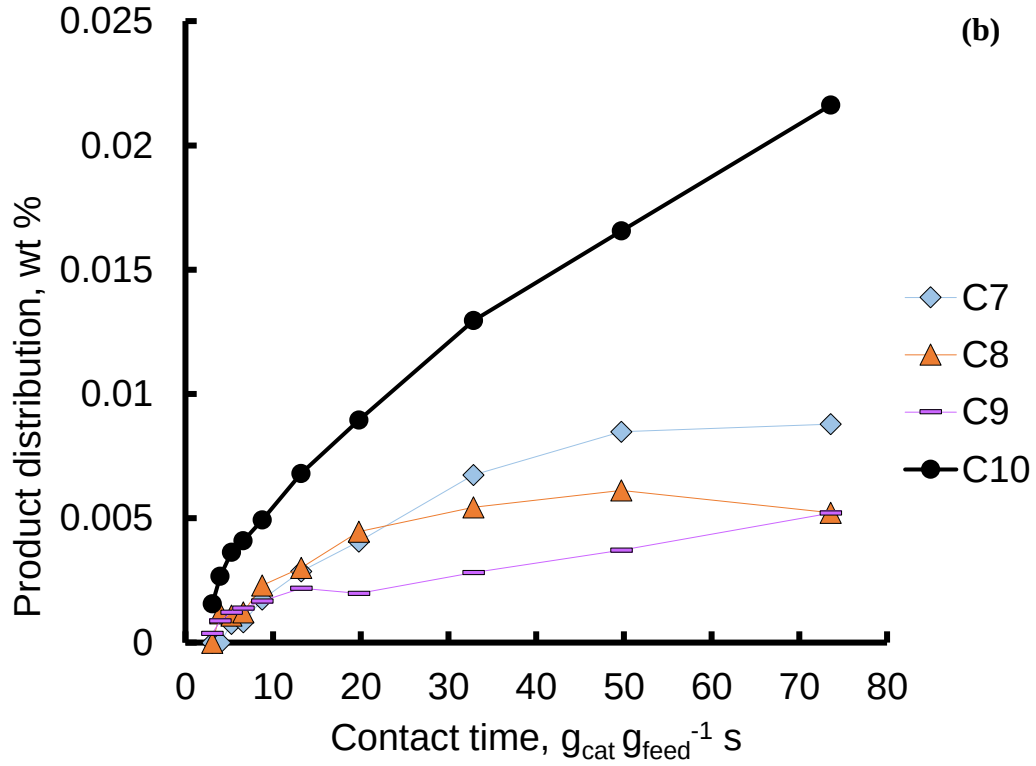
(b)
0.025
0.02
0.015
0.01
0.005
0
Product distribution, wt %
0
10
20
30
40
50
60
70
80
Contact time, $g_{cat}\,g_{feed}^{-1}$ s
C7
C8
C9
C10

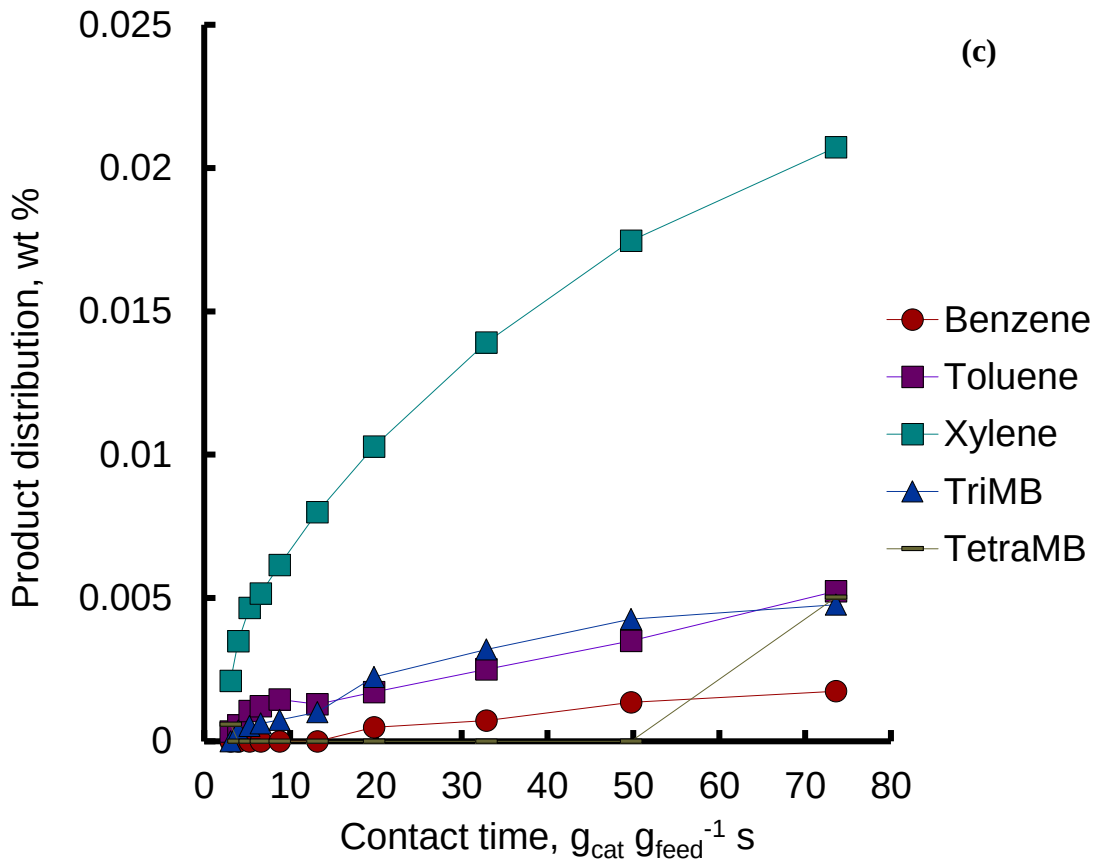

Fig. 8.5: (a) Aliphatic C2-C6, (b) aliphatic C7-C10 and (c) aromatics product distribution with contact time over ZSM-5 minilith (sample C) at 370 °C and 3 bar.

Fig. 8.5 shows how product distribution varies as contact time is increased. At the lowest contact time of 3.1g_{cat} g_{feed}^{-1} s, a diverse range of primary products are observed. As short miniliths would allow for both low residence times and efficient heat and mass transfer due to developing profiles in the channels, the varied product distribution at low contact times is likely due to an established hydrocarbon pool within the ZSM-5/bentonite pore wall (19-21). With comparisons made between the time taken for species to travel through the axial length of the minilith and the time required to diffuse radially to the surface of the channel, bulk of the minilith or to active sites on the zeolite crystal surface, the product distribution obtained at low contact times is subjected to intracrystalline diffusion limitations. The presence of active species in the hydrocarbon pool at low contact times corresponds with conversion profiles depicted in Fig. 8.4. As contact time increases, a range of aliphatics and aromatics are formed. The underlying mechanism involves a complex interaction of oligomerisation, methylation, hydrogen transfer and cracking chemistries which are responsible for the olefin product distribution (48, 54). Aliphatics are formed at lower contact times during MTG conversion. As the contact time increases, aromatics are formed via hydrogen transfer and cyclisation reactions between methanol and olefins (55) or between olefins (56). The presence of aromatics (hydrogen-poor) at short contact times imply that paraffins (hydrogen-rich) are additionally formed from olefins.

Initially, the proportion of olefins grow and at higher contact times, C2 and C3 hit a maximum and fall while C4 and C6 continue to grow. This could be due to (i) formation of C2 and C3 from primary oxygenates as well as their methylation and oligomerisation and (ii) C6 aromatisation. C6 aromatisation results in the formation of alkanes and aromatics. As contact time increases, aromatic methylation and dealkylation play an increasing role in MTG conversion and also regulate product distribution (48).

At highest conversions, the product distribution consists predominantly of C4 and C10 aliphatics and xylene aromatics which are in the gasoline boiling range and are expected from bare ZSM-5 catalysts (7). The product yield of C4 to C10 range of aliphatics and aromatics account for 53% of the dry product distribution at the highest conversions (73.6%) in this study. This is comparable with the gasoline yields obtained from bench-scale studies (57).

Pressure drop through the packed bed of ZSM-5 catalysts and one ZSM-5 minilith channel were calculated using the Ergun (58) and Hagen-Poiseuille (59, 60) equations respectively. At a weight hourly space velocity of 273 h^{-1}, the pressure drop through the packed bed of zeolite catalysts was 2 orders of magnitude higher than that through the zeolite minilith of equal ZSM-5 weight. This difference is representative of all flowrates. It was challenging to compare the performance of zeolite powders directly to miniliths of similar ZSM-5 active weight due to differences in pressure drop through the reactor. Nonetheless, Fig. S8.3 (see supplementary information) shows a comparison of conversions obtained over ZSM-5 powder and miniliths (sample C). Similar conversions are obtained over both systems (ZSM-5 powder and minilith) at 13.2 and 19.8 $g_{cat}\, g_{feed}^{-1}$ s albeit at a pressure drop of 2 orders of magnitude lower with ZSM-5 minilith. The difference in pressure drop is in accordance with literature (61-63). While the conversion data obtained over the miniliths were investigated under similar inlet pressures (3 bar), there was a variation in inlet pressure for the packed bed leading to an irregular conversion with contact time profile.

A long duration stability experiment comparing zeolite minilith to powder of equal ZSM-5 weight at 49 h^{-1} shows higher stability for the powder than the minilith (Fig. S4 in supplementary information). Consequently, higher conversions are obtained over the minilith up until 40 h beyond which the powders outperform the minilith in stability. As discussed above, packed beds show significant practical limitations associated with a higher pressure drop at high catalyst loading. Moreover, a higher minilith stability can be obtained by using a larger quantity of pore-former or different binders to prevent the slip wall condition obtained during extrusion.

Simulations conducted by Guo et al. (64), on comparing the conversion of methanol to propylene over a packed bed of ZSM-5 particles to an extruded monolith, show a higher reactor efficiency and propylene selectivity for monoliths. In this study, reducing the catalyst inventory to allow for equal inlet pressures of 3 bar gives the same gasoline yield (53%) at a

higher conversion of 80% over a packed bed of catalyst. This further highlights the high performing potential of ZSM-5 miniliths. Future work would elaborate on characterizing transport effects in miniliths during hydrocarbon transformations, getting an understanding on primary products formed at much lower contact times and minilith design optimisation to facilitate longer lifetime.

8.4. Conclusions

A novel form of a structured catalyst was prepared using a bentonite binder and ZSM-5 catalyst powder and then evaluated for the conversion of methanol to gasoline. The results of this study demonstrate that the conversion of methanol to gasoline can be performed with the ZSM-5 minilith reactor. The miniliths retain the crystal structure of the ZSM-5 catalyst and increase in Si/Al ratio, surface area and pore volume with an increase in zeolite content. The product distribution obtained over the ZSM-5 minilith reactor is in the gasoline range and similar to that obtained over ZSM-5 powder catalysts. The minilith achieves similar conversions at a pressure drop two orders of magnitude lower than with zeolite powder of equal ZSM-5 weight.

8.5. Notes

All data supporting this study is provided as supplementary information and the dataset (DOI: https://doi.org/10.15125/BATH-00524) accompanying this paper.

8.6. References

1. Wright PA. Microporous framework solids. Cambridge: RSC; 2008.
2. Cybulski A, Moulin J. Monoliths in Heterogeneous Catalysis. Catalysis Reviews. 1994;36(2):179-270.
3. Pangarkar K, Schildhauer TJ, Van Ommen JR, Nijenhuis J, Kapteijn F, Moulijn JA. Structured packings for multiphase catalytic reactors. Ind Eng Chem Res. 2008;47(10):3720-51.
4. Rase HF. Chemical Reactor Design for Process Plant, Vol. 1: Principles and Techniques. New York: Wiley; 1977.
5. Richardson JT. Principles of Catalyst Development. New York: Plenum Press; 1989.
6. Satterfield CN. Heterogeneous Catalysis in Practice. New York: McGraw-Hill; 1980.
7. Chang CD, Silvestri AJ. The conversion of methanol and other O-compounds to hydrocarbons over zeolite catalysts. J Catal. 1977;47(2):249-59.
8. Keil FJ. Methanol-to-hydrocarbons: process technology. Microporous Mesoporous Mater. 1999;29(1):49-66.
9. Blauwhoff PMM, Gosselink JW, Kieffer EP, Sie ST, Stork WHJ. Zeolites as Catalysts in Industrial Processes. In: Weitkamp J, Puppe L, editors. Catalysis and Zeolites: Fundamentals and Applications: Springer-Verlag; 1999. 437-538.
10. Stöcker M. Methanol-to-hydrocarbons: Catalytic materials and their behavior. Microporous Mesoporous Mater. 1999;29(1-2):3-48.

11. Hunter R, Hutchings GJ. Hydrocarbon formation from methylating agents over the zeolite catalyst H-ZSM-5 and its conjugate base: Evidence against the trimethyloxonium ion-ylide mechanism. J Chem Soc, Chem Commun. 1985(22):1643-5.
12. Hutchings GJ, Gottschalk F, Hall MVM, Hunter R. Hydrocarbon formation from methylating agents over the zeolite catalyst ZSM-5. Comments on the mechanism of carbon-carbon bond and methane formation. Journal of the Chemical Society, Faraday Transactios 1: Physical Chemistry in Condensed Phases. 1987;83(3):571-83.
13. Hunter R, Hutchings GJ. Hydrocarbon formation from methanol using WO3/Al 2O3 and zeolite H-ZSM-5 catalysts: Further evidence on the reaction mechanism. J Chem Soc, Chem Commun. 1987(5):377-9.
14. Hunter R, Hutchings GJ, Pickl W. Mechanistic studies on initial C-C bond formation in the zeolite ZSM-5 catalysed methanol conversion reaction: Evidence against a radical pathway. J Chem Soc, Chem Commun. 1987(11):843-4.
15. Wang W, Seiler M, Hunger M. Role of surface methoxy species in the conversion of methanol to dimethyl ether on acidic zeolites investigated by in situ stopped-flow MAS NMR spectroscopy. J Phys Chem B. 2001;105(50):12553-8.
16. Wang W, Buchholz A, Seiler M, Hunger M. Evidence for an Initiation of the Methanol-to-Olefin Process by Reactive Surface Methoxy Groups on Acidic Zeolite Catalysts. J Am Chem Soc. 2003;125(49):15260-7.
17. Yamazaki H, Shima H, Imai H, Yokoi T, Tatsumi T, Kondo JN. Direct production of propene from methoxy species and dimethyl ether over H-ZSM-5. Journal of Physical Chemistry C. 2012;116(45):24091-7.
18. Li J, Wei Z, Chen Y, Jing B, He Y, Dong M, Jiao H, Li X, Qin Z, Wang J, Fan W. A route to form initial hydrocarbon pool species in methanol conversion to olefins over zeolites. J Catal. 2014;317(0):277-83.
19. Bjørgen M, Svelle S, Joensen F, Nerlov J, Kolboe S, Bonino F, Palumbo L, Bordiga S, Olsbye U. Conversion of methanol to hydrocarbons over zeolite H-ZSM-5: On the origin of the olefinic species. J Catal. 2007;249(2):195-207.
20. Svelle S, Joensen F, Nerlov J, Olsbye U, Lillerud KP, Kolboe S, Bjørgen M. Conversion of methanol into hydrocarbons over zeolite H-ZSM-5: Ethene formation is mechanistically separated from the formation of higher alkenes. J Am Chem Soc. 2006;128(46):14770-1.
21. Bjørgen M, Joensen F, Lillerud KP, Olsbye U, Svelle S. The mechanisms of ethene and propene formation from methanol over high silica H-ZSM-5 and H-beta. Catal Today. 2009;142(1-2):90-7.
22. Dahl IM, Kolboe S. On the Reaction Mechanism for Hydrocarbon Formation from Methanol over SAPO-34. I. Isotopic Labeling Studies of the Co-Reaction of Ethene and Methanol. J Catal. 1994;149(2):458-64.
23. Dahl IM, Kolboe S. On the reaction mechanism for hydrocarbon formation from methanol over SAPO-34: 2. Isotopic labeling studies of the Co-reaction of propene and methanol. J Catal. 1996;161(1):304-9.
24. Wang C, Xu J, Qi G, Gong Y, Wang W, Gao P, Wang Q, Feng N, Liu X, Deng F. Methylbenzene hydrocarbon pool in methanol-to-olefins conversion over zeolite H-ZSM-5. J Catal. 2015;332:127-37.
25. Svelle S, Olsbye U, Joensen F, Bjørgen M. Conversion of methanol to alkenes over medium- and large-pore acidic zeolites: Steric manipulation of the reaction intermediates governs the ethene/propene product selectivity. Journal of Physical Chemistry C. 2007;111(49):17981-4.
26. Goguen PW, Xu T, Barich DH, Skloss TW, Song W, Wang Z, Nicholas JB, Haw JF. Pulse-quench catalytic reactor studies reveal a carbon-pool mechanism in methanol-to-gasoline chemistry on zeolite HZSM-5. J Am Chem Soc. 1998;120(11):2650-1.
27. Haw JF, Nicholas JB, Song W, Deng F, Wang Z, Xu T, Heneghan CS. Roles for cyclopentenyl cations in the synthesis of hydrocarbons from methanol on zeolite catalyst HZSM-5. J Am Chem Soc. 2000;122(19):4763-75.

28. Shah RK, London AL. Laminar Flow Forced Convection in Ducts. Irvine TF, Hartnett JP, editors: Academic Press, Inc; 1978.
29. Schulz H, Lau K, Claeys M. Kinetic regimes of zeolite deactivation and reanimation. Applied Catalysis A, General. 1995;132(1):29-40.
30. Masuda T, Asanuma T, Shouji M, Mukai SR, Kawase M, Hashimoto K. Methanol to olefins using ZSM-5 zeolite catalyst membrane reactor. Chem Eng Sci. 2003;58(3-6):649-56.
31. Patcas FC. The methanol-to-olefins conversion over zeolite-coated ceramic foams. J Catal. 2005;231:194-200.
32. Ivanova S, Louis B, Madani B, Tessonnier JP, Ledoux MJ, Pham-Huu C. ZSM-5 Coatings on β-SiC Monoliths: Possible New Structured Catalyst for the Methanol-to-Olefins Process. The Journal of Physical Chemistry C. 2007;111(11):4368-74.
33. Anita JE, Govind R. Conversion of Methanol to Gasoline-Range Hydrocarbons in a ZSM-5 Coated Monolithic Reactor. Industrial Engineering and Chemistry Research. 1995;34:140-7.
34. Patil MD, Lachman IM. Methanol Conversion on Ceramic Honeycombs Coated with Silicalite. In: Flank WH, editor. Perspectives in Molecular Sieve Science. Washington D.C: American Chemical Society; 1988. 492-9.
35. Hargreaves JSJ, Munnoch AL. A survey of the influence of binders in zeolite catalysis. Catalysis Science and Technology. 2013;3(5):1165-71.
36. Whiting GT, Meirer F, Mertens MM, Bons AJ, Weiss BM, Stevens PA, De Smit E, Weckhuysen BM. Binder effects in SiO_2- and Al_2O_3-bound zeolite ZSM-5-based extrudates as studied by microspectroscopy. ChemCatChem. 2015;7(8):1312-21.
37. Fougerit JM, Gnep NS, Guisnet M, Amigues P, Duplan JL, Hugues F. Effect of the binder on the properties of a mordenite catalyst for the selective conversion of methanol into light olefins. Stud Surf Sci Catal. 1994;84:1723-30.
38. Shihabi DS, Garwood WE, Chu P, Miale JN, Lago RM, Chu CTW, Chang CD. Aluminum insertion into high-silica zeolite frameworks. II. Binder activation of high-silica ZSM-5. J Catal. 1985;93(2):471-4.
39. Divins NJ, López E, Rodríguez Á, Vega D, Llorca J. Bio-ethanol steam reforming and autothermal reforming in 3-μm channels coated with RhPd/CeO2 for hydrogen generation. Chemical Engineering and Processing: Process Intensification. 2013;64:31-7.
40. Pereira CJ, Cheng WC, Beeckman JW, Suarez W. Performance of the minilith-a shaped hydrodemetallation catalyst. Applied Catalysis. 1988;42(1):47-60.
41. Pereira CJ, Beeckman JW. Modeling of hydrodemetalation catalysts. Industrial & Engineering Chemistry Research. 1989;28(4):422-7.
42. Lee LY, Perera SP, Crittenden BD, Kolaczkowski ST. Manufacture and characterisation of silicalite monoliths. Adsorpt Sci Technol. 2000;18(2):147-70.
43. Spivey JJ. Review: Dehydration catalysts for the methanol/dimethyl ether reaction. Chem Eng Commun. 1991;110(1):123-42.
44. Rouquerol J, Llewellyn P, Rouquerol F. Is the BET equation application to microporous adsorbents? In: Llewellyn P, Rodriquez-Reinoso F, Rouquerol J, Seaton N, editors. Stud Surf Sci Catal. 160: Elsevier; 2007. 49-56.
45. van Koningsveld HV, van Bekkm H, Jansen JC. On the Location and Disorder of the Tetrapropylammonium (TPA) Ion in Zeolite ZSM-5 with Improved Framework Accuracy. Acta Crystallography. 1987;B43(Part 2):127-32.
46. Olson DH, Kokotailo GT, Lawton SL, Meier WM. Crystal structure and structure-related properties of ZSM-5. J Phys Chem. 1981;85(15):2238-43.
47. Ayari F, Srasra E, Trabelsi-Ayadi M. Characterization of bentonitic clays and their use as adsorbent. Desalination. 2005;185(1):391-7.
48. Ilias S, Bhan A. Mechanism of the catalytic conversion of methanol to hydrocarbons. ACS Catalysis. 2013;3:18-31.
49. Chen NY, Reagan WJ. Evidence of autocatalysis in methanol to hydrocarbon reactions over zeolite catalysts. J Catal. 1979;59(1):123-9.

50. Ono Y, Mori T. Mechanism of methanol conversion into hydrocarbons over ZSM-5 zeolite. Journal of the Chemical Society, Faraday Transactions 1: Physical Chemistry in Condensed Phases. 1981;77(9):2209-21.
51. Ono Y, Imai E, Mori T. The Autocatalytic Nature of Methanol Conversion over ZSM-5 Zeolites. Z Phys Chem1979. p. 99.
52. Omojola T, Cherkasov N, McNab AI, Lukyanov DB, Anderson JA, Rebrov EV, van Veen AC. Mechanistic Insights into the Desorption of Methanol and Dimethyl Ether Over ZSM-5 Catalysts. Catal Lett. 2018;148(1):474-88.
53. Svelle S, Kolboe S, Swang O, Olsbye U. Methylation of Alkenes and Methylbenzenes by Dimethyl Ether or Methanol on Acidic Zeolites. The Journal of Physical Chemistry B. 2005;109(26):12874-8.
54. Pines H. Acid-Catalyzed Reactions The Chemistry of Catalytic Hydrocarbon Conversions. United Kingdom: Academic Press; 1981.
55. Müller S, Liu Y, Kirchberger FM, Tonigold M, Sanchez-Sanchez M, Lercher JA. Hydrogen Transfer Pathways during Zeolite Catalyzed Methanol Conversion to Hydrocarbons. J Am Chem Soc. 2016;138(49):15994-6003.
56. Lukyanov DB, Gnep NS, Guisnet MR. Kinetic modeling of ethene and propene aromatization over HZSM-5 and GaHZSM-5. Ind Eng Chem Res. 1994;33(2):223-34.
57. Tabak SA, Yurchak S. Conversion of methanol over ZSM-5 to fuels and chemicals. Catal Today. 1990;6(3):307-27.
58. Ergun S. Fluid flow through packed columns. Chem Eng Prog. 1952;48(2):89-94.
59. Hagen G. Ueber die Bewegung des Wassers in engen cylindrischen Röhren. Annalen der Physik. 1839;122(3):423-42.
60. Hagenbach E. Ueber die Bestimmung der Zähigkeit einer Flüssigkeit durch den Ausfluss aus Röhren. Annalen der Physik. 1860;185(3):385-426.
61. Lachman IM, McNally RN. Monolithic Honeycomb Supports for Catalysis. Chem Eng Prog. 1985;81(1):29-31.
62. Marín P, Hevia MAG, Ordóñez S, Díez FV. Combustion of methane lean mixtures in reverse flow reactors: Comparison between packed and structured catalyst beds. Catal Today. 2005;105(3-4):701-8.
63. Lei Z, Wen C, Zhang J, Chen B. Selective catalytic reduction for NO removal: Comparison of transfer and reaction performances among monolith catalysts. Ind Eng Chem Res. 2011;50(10):5942-51.
64. Guo W, Xiao W, Luo M. Comparison among monolithic and randomly packed reactors for the methanol-to-propylene process. Chem Eng J. 2012;207-208:734-45.

S8. Supplementary information

Zeolite Minilith: A Unique Structured Catalyst for the Methanol to Gasoline Process

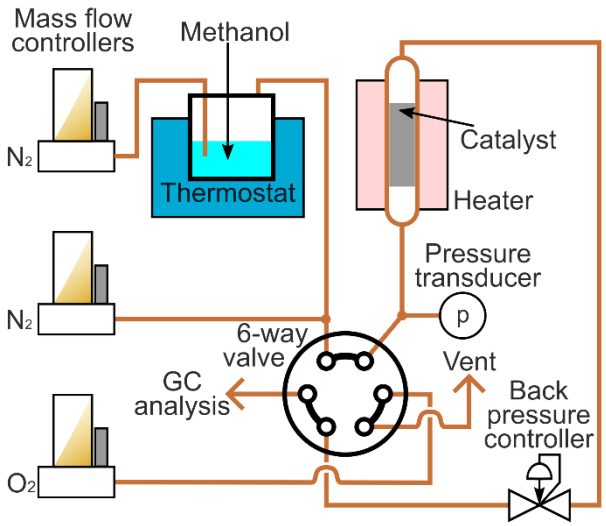

Fig. S8.1: Reactor set-up for minilith experiments

Table S8.1: **Sample calculation for mass and mol of species.** Mass and mole of species were calculated as follows: Firstly, concentrations (ppm) were converted to vol%. Thereafter, using the volume of the sampling loop (500 µL) and the density at the sampling temperature, the mass of each specie was calculated. Mass of H_2O was calculated by (M_{CH2} × (18/14) + M_{DME} × (18/46)), where M_{CH2} is the total mass of all hydrocarbons and M_{DME} is the outlet mass of DME. Nitrogen vol% was obtained from the balance of initial feed vol% of methanol. Mol% values were calculated from mass after considering the molecular weight of each specie (in this case, alkanes were used as a proxy for C1-C10 aliphatics). Since inlet methanol quantity was based on the total output carbon for the C1-C10 products, mass balance was checked through consistent inlet moles of methanol at all flowrates. For more information, please see the University of Bath Research Data Archive (DOI: https://doi.org/10.15125/BATH-00524)

Data was obtained at 54 mL min^{-1} over sample C (70 wt% ZSM-5, balance bentonite).

Specie	Concentration (ppm)	Dry Yield	Mass	Mole
Methanol	5882.5		6.67×10^{-6}	2.08×10^{-7}
DME	260.1		2.95×10^{-7}	6.41×10^{-9}
Benzene	17.3	0.41	1.96×10^{-8}	2.51×10^{-10}
Toluene	51.9	1.43	5.88×10^{-8}	6.39×10^{-10}
Xylene	205.4	6.48	2.33×10^{-7}	2.20×10^{-9}
Trimethylbenzene	47.2	1.68	5.35×10^{-8}	4.46×10^{-10}
Tetramethylbenzene	49.8	1.96	5.64×10^{-8}	4.21×10^{-10}
C1	50.8	0.20	5.76×10^{-8}	3.60×10^{-9}
C2	966.2	7.62	1.09×10^{-6}	3.65×10^{-8}
C3	1163.0	13.76	1.32×10^{-6}	3.00×10^{-8}
C4	1003.2	15.83	1.14×10^{-6}	1.96×10^{-8}
C5	38.9	0.77	4.41×10^{-8}	6.12×10^{-10}
C6	429.0	10.15	4.86×10^{-7}	5.65×10^{-9}
C7	87.1	2.40	9.87×10^{-8}	9.87×10^{-10}
C8	51.8	1.63	5.87×10^{-8}	5.15×10^{-10}
C9	51.6	1.83	5.85×10^{-8}	4.57×10^{-10}
C10	214.3	8.45	2.43×10^{-7}	1.71×10^{-9}
H_2O			6.57×10^{-6}	3.65×10^{-7}
Conversion	0.747			

Sample code	Zeolite Minilith
A	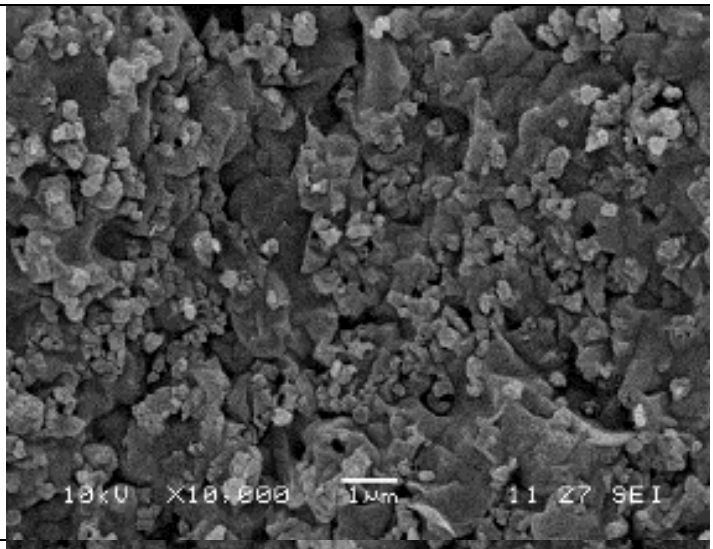
A2	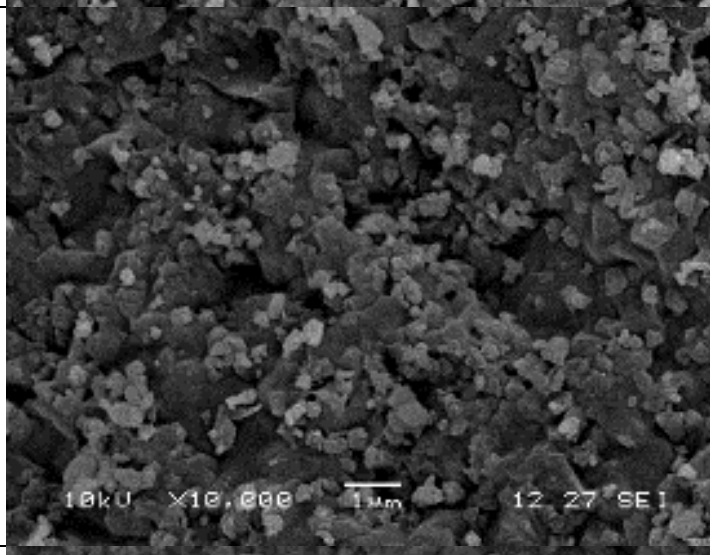
B	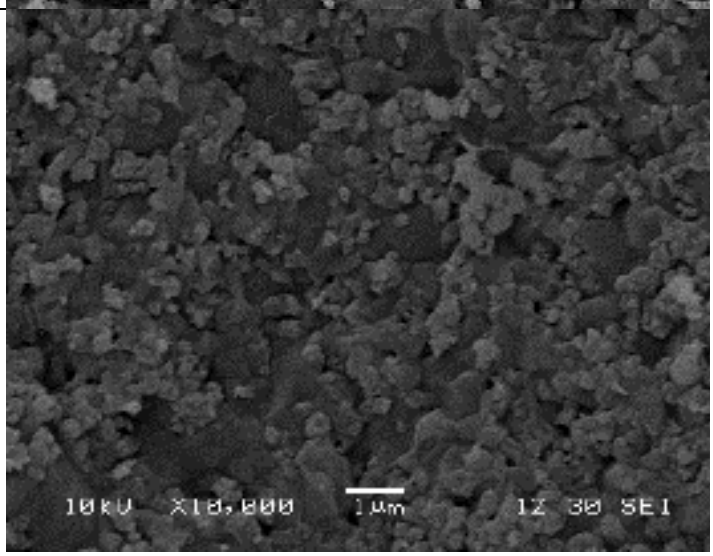

B2

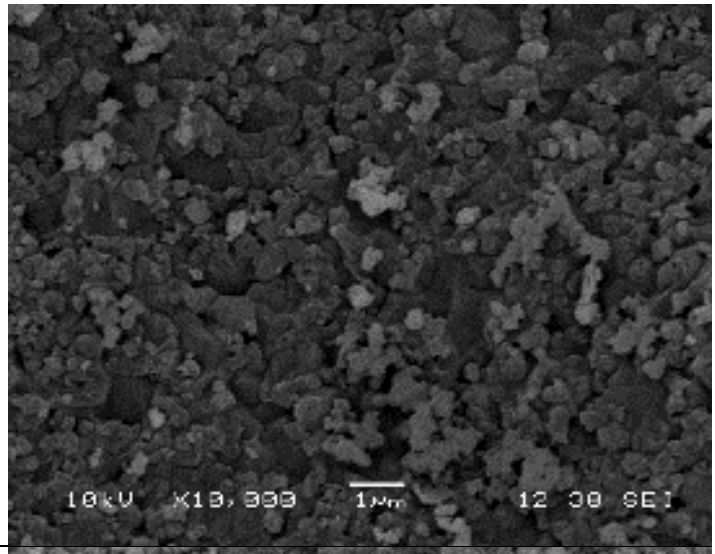

C

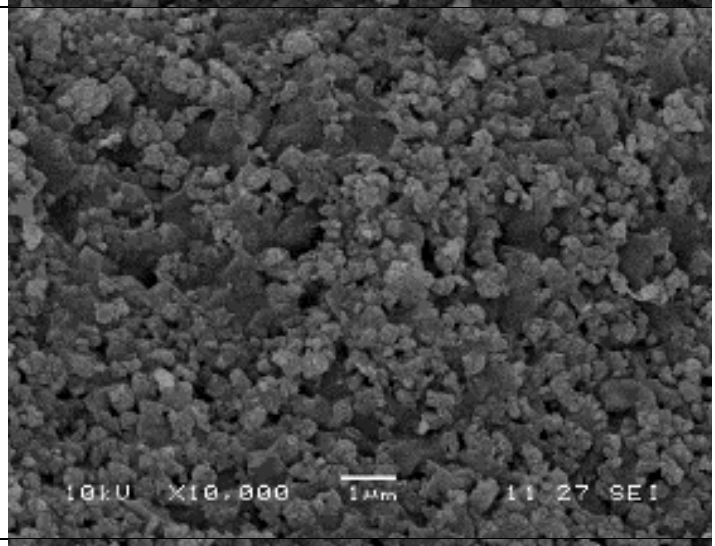

D

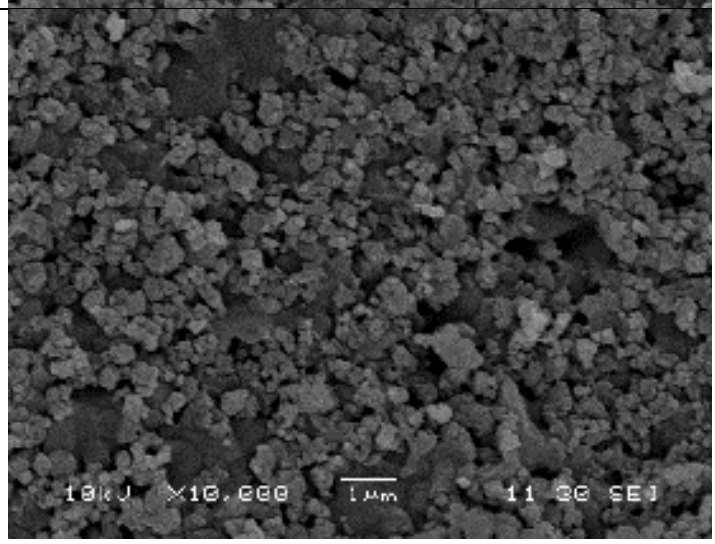

Fig. S8.2: Minilith channel SEMs.

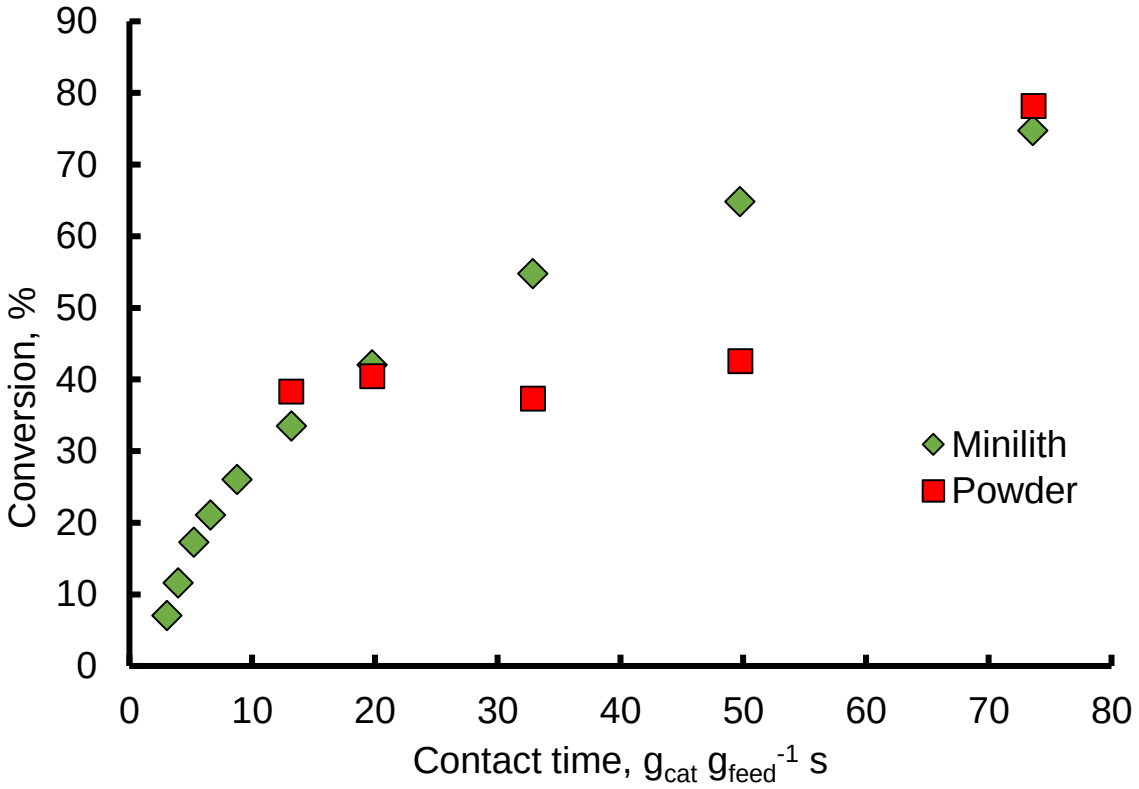

Fig. S8.3: Conversions through a packed bed and minilith (sample C) of equal ZSM-5 content with contact time at 370 °C.

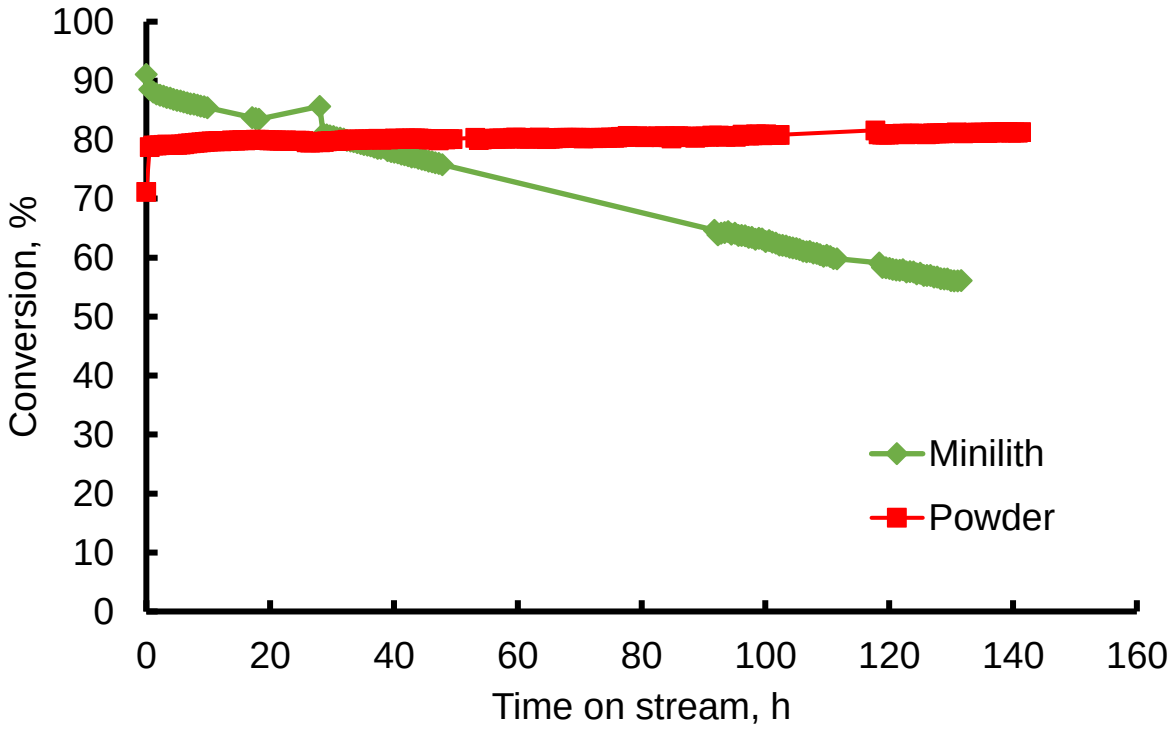

Fig. S8.4: Stability tests for ZSM-5 minilith and packed bed during the conversion of methanol to gasoline at 370 °C, 3 bar and a WHSV of 49 h^{-1}.

Chapter 9

9. Conclusions and future work

9.1. Conclusions

The conversion of methanol to hydrocarbons over ZSM-5 catalysts has been examined mainly through a kinetic point of view. Kinetic modelling has been used for detailed analysis, to obtain key mechanistic insights and added depth while vibrational spectroscopy (FTIR) has been used for added breadth and perspective.

The general aims, and purpose of this PhD thesis were:

1. To advance understanding of the induction period during which the first C-C bond and primary olefins are formed from methanol;
2. To quantitatively describe the mechanisms that regulate product distribution during MTH conversion at steady-state over ZSM-5 catalysts;
3. To develop a novel structured zeolite catalyst that can reduce pressure drop and optimise yield of products from methanol.

The fundamental challenges during the conversion of methanol to hydrocarbons over zeolite catalysts in the induction period can be grouped into three main themes: (a) identification of the key oxygenate (methanol or DME), (b) identification of the primary olefins (ethylene, propylene or ethylene and propylene) and (c) identification of the exact mechanism linking the key oxygenate to primary olefins.

In chapter 4, the desorption profiles of DME are compared to methanol over fresh and hydrocarbon-occluded ZSM-5 catalysts of different Si/Al ratios. Higher temperatures are necessary to desorb DME from ZSM-5 zeolite catalysts of Si/Al ratios of 25, 36 and 135. The desorption profiles were deconvoluted into two sites for ZSM-5 (135) and three sites for ZSM-5 (25) and (36) using the Redhead method. A transient plug flow reactor model with coupled convection, adsorption and desorption steps shows higher activation energies of desorption of DME compared to methanol over all ZSM-5 catalysts studied. Consideration of adsorption stoichiometry of ZSM-5 catalysts show that the total number of molecules adsorbed per active site of ZSM-5 (25) on the medium and high temperature sites equal the total number of molecules adsorbed per active site on the high temperature sites of ZSM-5 (135). A comparison of experiments with the plug flow reactor model shows that no re-adsorption occurs on the high temperature sites. Molecular adsorption on the low temperature sites and dissociative adsorption on the medium and high temperature sites give excellent agreement between experiment and model. No differences were observed, other than in site densities when extracting kinetic parameters for fresh and hydrocarbon-occluded catalysts at full coverage in the TAP reactor. The microkinetic model along with pyridine FTIR data suggest

that the medium temperature and high temperature sites are of a Brønsted acid nature while the low temperature site is of Lewis acid nature or exhibit hydrogen bonding with oxygenates.

In chapter 5, the induction period was studied as the fresh ZSM-5 catalyst was transformed to a working catalyst where product distribution is regulated by the hydrocarbon pool. The evolution of chemical species, specifically from the key oxygenate (DME) to primary olefins was observed using a novel step response methodology in a TAP reactor. In the first step response cycle, propylene is the major olefin formed at low temperatures (300 °C) with a DME feed in the TAP reactor. At higher temperatures, ethylene is also formed. The profile of primary olefins follows an S-shaped behaviour and is sensitive to addition of precursors (dimethoxymethane, carbon monoxide, hydrogen). In the literature, the induction period of primary olefin formation has been shown to be sensitive to olefin precursors, aromatics and impurities. To explain these results, a crystal nucleation kinetic scheme involving secondary oxygenates (dimethoxyethane) is proposed where propylene is formed through the direct mechanism from the DME feed. Over multiple step response cycles, propylene is still the primary olefin formed at low temperatures and the induction period of propylene formation is eliminated. In the first step response cycle, methanol and water portray overshoot profiles while DME rises rapidly up until half-way to its steady-state value followed by a slow rise. The overshoot profiles of methanol and water as well as the DME profiles all change to monotonic profiles on applying subsequent step response cycles. Hence, this work shows clearly that there is an induction period, during which precursors molecules are formed inside the zeolite pores. Thus, the first step response cycle involves intrinsic and extrinsic relaxation while the subsequent step response cycles involve intrinsic relaxation alone.

In chapter 6, the experiments reported in chapter 5 were described using a transient kinetic model that describes plug flow reactor behaviour with coupled convection, adsorption, desorption and reaction steps. The formation of the key olefin (propylene) from DME in the first step response cycle is modelled. For the first time, it is shown with clarity that the transformation of the first C-C bond is the key bottleneck (rate limiting step) in propylene formation from DME.

The dual-cycle consisting of an olefin cycle and an aromatic cycle regulating product distribution over ZSM-5 catalysts is tunable depending on process conditions. In chapter 7, the control of the product distribution by the olefin cycle is established over a ZSM-5 catalyst with Si/Al=34 at 370 °C. It was observed that the steady-state propylene formation rate exceeds direct ethylene formation by a factor of 5. Oligomerisation and cracking rates are higher than direct olefin formation by two orders of magnitude. Olefin methylation by methanol occurs by an order of magnitude faster than direct ethylene formation. Olefin methylation by DME is faster than with methanol by a factor of 3.2 and aromatic methylation by DME is faster than with methanol by a factor of 2.5. Faster methylation rates observed during steady-state

studies confirm initial transient studies in the TAP reactor that show that DME is the key oxygenate involved in surface reactions. Also, higher steady-state propylene formation rates validate the initial step response studies which show propylene to be the primary olefin formed. The relative rates of the chemistries of the olefin cycle (olefin methylation, oligomerisation and cracking) are much slower than the rates of hydrogen transfer and cyclisation steps as well as chemistries of the aromatic cycle (aromatic methylation and dealkylation). Consequently, through kinetic modelling, evidence is provided that the olefin cycle controls the autocatalytic rate of methanol conversion to hydrocarbons over ZSM-5 catalysts at 370 °C.

The fundamental challenge relating to the industrial MTH process centres around material and energy usage efficiency and operating cost reduction. In chapter 8, by using a binder with high thermal conductivity, zeolite microchannel reactors called miniliths produce higher gasoline yields at the same conversion as ZSM-5 powder albeit at a much lower pressure drop. They exhibit moderate stability which can be improved by the presence of a pore-former leading to increased diffusion across the structured catalyst.

The key philosophy developed in these chapters is that transient and steady-state kinetics can be described phenomenologically and mechanistically. The Redhead method was used in chapter 4 before mechanistic insights were obtained using the plug flow reactor model for the adsorption and desorption of methanol and DME over ZSM-5 catalysts. Profiles of DME; water and methanol; propylene and ethylene were described at first using the Hill, BiHill and logistic (sigmoidal) functions respectively in chapter 5 before a more detailed mechanistic description was obtained in chapter 6 using a transient kinetic model. The S-shaped curve of conversion with contact time during steady-state experiments in chapter 7 was first described using a logistic function. Further detailed kinetic modelling in chapter 7 gives mechanistic insights into chemistries governing product distribution underlying such phenomenological descriptions.

The TAP reactor has been used for kinetic investigations for over 40 years using conventional pulse experiments. For the first time, novel step response experiments (single step, multiple step and consecutive step) have been carried out within the TAP framework. Transient experiments led to an induction period of over 40 min during MTH conversion in a first step response cycle. The influence of hydrocarbon-occluded species in the zeolite pores as the induction period is eliminated on subsequent step response cycles after steady-state is established is shown clearly. Many precursors (such as formaldehyde, dimethoxymethane, dimethoxyethane, carbon monoxide, hydrogen, cyclopentadienes etc) have been investigated and shown to have an impact on MTH conversion. However, up until now, there has been no framework to synthesise these investigations. The consecutive step response experiments provide such a framework as the influence of precursors on the induction period and the rate of hydrocarbon pool establishment can be studied following the S-shaped profiles observed.

Furthermore, for TAP reactor was modelled as a non-ideal fixed bed reactor where the influence of dispersion and convection were evaluated. Dispersion coefficients of 10^{-9} m^2 s^{-1} were obtained for step response experiments in the TAP reactor.

For 40 years, the debate on the formation of the first C-C bond from methanol. Various direct mechanisms have been proposed including carbene, oxonium ylide, methane-formaldehyde, methoxymethyl, carbon monoxide, and indirect mechanisms. These mechanisms have always been investigated separately. The step response data obtained from the TAP reactor presented an opportunity for comparing various direct mechanism proposals on a microscopic modelling level. The methoxymethyl mechanism showed the closest agreement to experimental data. The transformation of the first C-C bond is rate-limiting during the induction period.

Kinetic modelling of steady-state data revealed that the olefin cycle controls product distribution. Transient experiments were conducted at different conditions to steady-state experiments and there is limiting evidence to suggest the key bottleneck of the overall MTH process circumpassing the induction period and steady-state. Nonetheless, the transient experiments buttress steady-state data by providing evidence for propylene formation at low temperatures and boosting ethylene formation with temperature. TAP data shows that these olefins are formed under negligible external mass and heat transfer, and internal heat transfer limitations. For the first time, a unique form of a ZSM-5 structured catalyst (minilith) is synthesised, fabricated and tested for MTG conversion. Further evaluation of the miniliths would facilitate reactor design.

The novel form of kinetic characterisation, elucidation of complex reaction mechanisms, validation of governing chemistries and novel forms of reactor design during this PhD work lead to advancement of the state of knowledge and art of MTH conversion.

9.2. Suggestions for future work

Transient experiments were carried out in a TAP reactor (chapters 4, 5 and 6) and the effluents were monitored with time on stream. During steady-state experiments (chapters 7 and 8), effluents were monitored with contact time. The transient experiments elucidated the chemical processes that occur during the evolution of fresh ZSM-5 catalysts to working ZSM-5 catalysts. Adsorption, desorption and reaction of species were studied as methanol undergoes transformation to primary olefin (propylene) and the hydrocarbon pool. Over ZSM-5 catalysts, the nature and concentration of this hydrocarbon pool is dependent on temperature, pressure, zeolite Si/Al ratio and precursors as shown by the results given in chapters 5 and 6.

Steady-state experiments, allowing for an investigation of the evolution of effluents with contact time, give information about the relative propagation of olefin and aromatic cycles of the hydrocarbon pool. At low contact times, only the olefin cycle is propagated such that gaseous olefins are released. With an increase in contact time, the additional aromatic cycle is propagated. It is shown that the olefin cycle is rate-controlling over ZSM-5 catalysts at all contact times studied.

Future work following this PhD project could include:

1. An attempt to bridge transient kinetic experiments with steady-state kinetic experiments. The effect of the duration of the induction period on the product distribution during steady state could be considered.
2. Further complementary studies on the formation of primary olefins: A technique called temperature programmed surface reaction could be used to elucidate the formation of primary olefins using temperature transients. Frequency factors and activation energies could be determined during the induction period. Also, a quasi-elastic neutron scattering technique could be used to probe mobility of methanol, DME, water and other species over ZSM-5 of different Si/Al ratios. *Operando* micro-infrared spectroscopy could be applied to the equilibration reaction of methanol to determine concentration profiles on a zeolite catalyst. These concentration profiles could be used to obtain effectiveness factors of the ZSM-5 catalyst. Such analysis involving continuity and Stefan-Maxwell equations would consider the adsorption, desorption, diffusion and reaction of species leading to the gaseous product release.
3. Methanol can be compared to DME, based on their equilibrium composition, for MTH conversion at specific regimes. The comparison would be based on regimes of intrinsic kinetic control, pore diffusion control or external mass transfer control.
4. Steady State Isotopic Kinetic Analysis could be applied to determine the exact source of secondary oxygenates (dimethoxymethane, dimethoxyethane). A

transient kinetic model using the reaction scheme derived in chapter 5 accounting for the influence of carbon monoxide, hydrogen, dimethoxymethane and water can be used to model the induction period. This can be compared to the rival reaction mechanism used to model the induction period in chapter 6.

5. Each chemistry of the MTH process could be studied for identification of a single parameter governing product distribution from that chemistry. This could later be combined into an overarching parameter that determines the product distribution during MTH conversion.
6. The miniliths could be characterised by determining mass transfer (Sherwood) and heat transfer (Nusselt) correlations during MTH conversion. This would facilitate reactor design for MTH conversion.
7. Hydrodynamics in the TAP reactor could also be studied. Regimes of axial and radial dispersion as well as laminar flow can be mapped with convection applied to thin-zone packing configuration under concentration transients.

These separate pieces of work would be considered by the author in further elucidation of MTH conversion over zeolite catalysts.

Appendix

A. Transient kinetic modelling code used in chapter 6

i. Obtaining initial estimates

```
%% using upwind scheme to solve PDE's arising from step response
experiments%%
%% using reaction scheme based on recent DFT evidence -
methoxymethyl mechanism - 3rd pathway%%

%Date created - 25/10/2017
%1. CH3OH+HZ<>CH3.Z+H2O
%2. CH3OCH3+HZ<>CH3.Z+CH3OH
%3. H2O+HZ<>H2O.HZ
%13. CH3.Z+CH3OH<>CH3OCH3.HZ

%4. CH4+HZ<>CH4.HZ
%5. CH2O+HZ<>CH2O.HZ
%6. H2+HZ<>H2.HZ
%7. C3H6+HZ<>C3H6.HZ
%8. CH3OCH3+HZ<>CH3OCH2.Z+H2
%9. CH3OCH2OCH3+HZ<>CH3OCH2OCH3.HZ
%10. CH3OCH2CH2OCH3+HZ<>CH3OCH2CH2OCH3.HZ

%11. CH3CHCHOCH3+HZ<>CH3CHCHOCH3.HZ

%12. CH2(OH)2+HZ<>CH2(OH)2.HZ
%14. CH3OH+HZ>CH2O.HZ+H2
%15. CH3OCH3+HZ>CH2O.HZ+CH4
%16. CH2O.HZ+H2O<>CH2(OH)2.HZ

%17. CH3.Z+CH3OCH3>CH3OCH2.Z+CH4
%18. CH3OCH2.Z+CH3OCH3>CH3OCH2CH2OCH3.HZ
%19. CH3OCH2CH2OCH3.HZ>CH3CHCHOCH3.HZ+H2O
%20. CH3CHCHOCH3+CH3.Z>C3H6+CH3OCH2.Z

%21. CH3OCH2OCH3.HZ+CH3OCH2.Z>CH3OCH2CH2OCH3.HZ+CH2O.HZ

close all; clear all
tic

%% parameters
% Rate constants corresponding to equations above
k1=0.00182;
k_1=0.1010;
k2=0.00045;
k_2=2.5;
k3=0.0003;
k_3=50;
k13=0.00028;
k_13=1.7;

k4=0;
k_4=0;
```

```
k5=0;
k_5=0;
k6=0;
k_6=0;
k7=0;
k_7=0;
k8=0;
k_8=0;
k9=0;
k_9=0;
k10=0;
k_10=0;
k11=0.00375;
k_11=812.5;
k12=0;
k_12=0;

k14=0;
k15=0;
k16=0;
k_16=0;
k17=0.010;
k18=1.0;
k19=0.12875;
k20=200;
k21=0;

%% experimental data
% Inlet feed

load('deconvolution_b_v3')

n_amu31_exp = R_amu31s;
n_amu45_exp = R_amu45s;
n_amu18_exp = R_amu18s;
n_amu40_exp = R_amu40s;
n_amu28_exp = R_amu28s;
n_amu91_exp = R_amu91s;
n_amu27_exp = R_amu27s;
n_amu41_exp = R_amu41s;

%% gas properties
meth_volume_fraction=0;
argon_volume_fraction=0.95;
dme_volume_fraction=0.05;

pres = 1000;     %total pressure in the fixed bed (Pa)
R = 8.314;       %Molar gas constant, J/mol/K
temp = 573; %input('what is the step response temperature in C?
')+273; %Temperature in Kelvin


%% reactor properties
bed_length = 2e-3;
reactor_diameter = 4e-3; %m
bed_area=(pi*reactor_diameter^2)/4; %m^2
```

```
bed_volume=bed_area*bed_length; %m^3


%% Catalyst properties
cat_density = 2200; %kg/m^3
bed_porosity = 0.5;
cat_diameter = 30e-6; %m

%Pyridine FTIR acid site density
sites_gram_25=356e-6; %mol/g
sites_gram_36=117e-6; %mol/g
sites_gram_135=78e-6; %mol/g

%BET surface area
BET_25=413; %m^2/g
BET_36=410; %m^2/g
BET_135=358; %m^2/g

% concentration of active sites per unit surface area of catalyst =
acid
% site density * BET surface area
conc_sites_gram_25=sites_gram_25/BET_25; %mol/m^2
conc_sites_gram_36=sites_gram_36/BET_36; %mol/m^2
conc_sites_gram_135=sites_gram_135/BET_135; %mol/m^2

%specific surface area of catalyst = 6/particle diameter
Sv=6/cat_diameter;

%% Define space and time domain

% For bed length of 2 mm, define space domain parameters
z0 = 0; %initial length of reactor
z1 = 2e-3; %bed length
J = 10; % number of strips
dz = (z1-z0)/J;
disp(['J = ', num2str(J)]);
disp(' ');
disp(['dz = ', num2str(dz)]);
disp(' ');
Z = dz*(0:J);
dv=bed_area*dz;

% For time equals time at last data point, define time domain
t0 = 0;  %initial time
time;
tf = time(end); %final time (min)
N = 4000000; %number of time steps
dt=tf/N; %time step size
disp(['dt = ', num2str(dt)]);
disp(' ');
disp(['N = ', num2str(N)]);
disp(' ');

% T = (dt*(0:N))';
Tt = (dt*(0:N))';
```

```
%% stability factor, (u/eb)*(dt/dz)
vel=0.00025;
SF = (vel/bed_porosity)*(dt/dz);
disp(['SF = ', num2str(SF)]);
disp(' ');

SF_X=dt/(bed_porosity*(dz^2));
cortn_factor=2e-4;
D_meth=1.03e-5*cortn_factor;
D_dme=8.56e-6*cortn_factor;
D_water=1.37e-5*cortn_factor;
D_methane=1.45e-5*cortn_factor;

D_formaldehyde=1.08e-5*cortn_factor;
D_hydrogen=4.10e-5*cortn_factor;
D_methylal=6.66e-6*cortn_factor;
D_dimethoxyethane=6.12e-6*cortn_factor;
D_methanediol=8.38e-6*cortn_factor;
D_alkene_ether=6.84e-6*cortn_factor;

D_propene=8.96e-6*cortn_factor;
D_Ar=9.18e-6*cortn_factor;

if SF < 1
    %% initialise solution space
    n_meth_model=zeros(N+1, J+1);
    n_dme_model=zeros(N+1, J+1);
    n_water_model=zeros(N+1, J+1);
    n_Ar_model=zeros(N+1, J+1);
    n_formaldehyde_model=zeros(N+1, J+1);
    n_methane_model=zeros(N+1, J+1);
    n_hydrogen_model=zeros(N+1, J+1);
    n_propene_model=zeros(N+1, J+1);
    n_methylal_model=zeros(N+1, J+1);
    n_dimethoxyethane_model=zeros(N+1, J+1);
    n_methanediol_model=zeros(N+1, J+1);
    n_alkene_ether_model=zeros(N+1,J+1);

    theta_sms_model=zeros(N+1, J+1);
    theta_methoxymethyl_model=zeros(N+1, J+1);
    theta_dme_model=zeros(N+1, J+1);
    theta_water_model=zeros(N+1, J+1);
    theta_Ar_model=zeros(N+1, J+1);
    theta_formaldehyde_model=zeros(N+1, J+1);
    theta_methane_model=zeros(N+1, J+1);
    theta_hydrogen_model=zeros(N+1, J+1);
    theta_propene_model=zeros(N+1, J+1);
    theta_methylal_model=zeros(N+1, J+1);
    theta_dimethoxyethane_model=zeros(N+1, J+1);
    theta_methanediol_model=zeros(N+1, J+1);
    theta_alkene_ether_model=zeros(N+1,J+1);
    theta_vacant_model=zeros(N+1, J+1);

    % insert initial conditions into solution matrix. At time = t0,
    % catalyst is empty and begins to fill up.
    theta_sms_model(1,1) = 0;
```

```
    theta_methoxymethyl_model(1,1) = 0;
    theta_dme_model(1,1) = 0;
    theta_water_model(1,1) = 0;
    theta_Ar_model(1,1) = 0;
    theta_formaldehyde_model(1,1) = 0;
    theta_methane_model(1,1) = 0;
    theta_hydrogen_model(1,1) = 0;
    theta_propene_model(1,1) = 0;
    theta_methylal_model(1,1) = 0;
    theta_dimethoxyethane_model(1,1) = 0;
    theta_methanediol_model(1,1) = 0;
    theta_alkene_ether_model(1,1) = 0;
    theta_vacant_model(1,1) = 1-theta_sms_model(1,1)-
theta_methoxymethyl_model(1,1)...
        -theta_dme_model(1,1)-theta_water_model(1,1)-
theta_Ar_model(1,1)...
        -theta_formaldehyde_model(1,1)-theta_methane_model(1,1)-
theta_hydrogen_model(1,1)...
        -theta_methylal_model(1,1)-theta_dimethoxyethane_model(1,1)-
theta_methanediol_model(1,1)...
        -theta_alkene_ether_model(1,1)-theta_propene_model(1,1);

    % n_dme_model(1,1) = n_DME;   %obtained from deconvolution file
    % n_Ar_model(1,1) = n_ar;     %obtained from deconvolution file
    n_meth_model(1,1) = 0;
    n_water_model(1,1) = 0;
    n_formaldehyde_model(1,1) = 0;
    n_methane_model(1,1) = 0;
    n_hydrogen_model(1,1) = 0;
    n_propene_model(1,1) = 0;
    n_methylal_model(1,1) = 0;
    n_dimethoxyethane_model(1,1) = 0;
    n_methanediol_model(1,1) = 0;
    n_alkene_ether_model(1,1) = 0;


    %% step function
    % insert boundary conditions into solution matrix. At z = 0, a
step
    % response of oxygenates is introduced.

    %% convection alone
    %     if Tt(1,1) >= t0 && Tt(1,1) <= t0+dt
    %         n_dme_model(:,1)=n_DME;
    %         n_Ar_model(:,1)=n_ar;
    %     elseif Tt(1,1) < t0
    %         n_dme_model(:,1)=0;
    %         n_Ar_model(:,1)=0;
    %     elseif Tt(1,1)> t0+dt
    %         n_dme_model(:,1)=n_DME;
    %         n_Ar_model(:,1)=n_ar;
    %     end
```

```
    %% convection and dispersion
    if Tt(1,1) >= t0 && Tt(1,1) <= t0+dt
        n_dme_model(:,1)=n_DME-((D_dme/(vel*dz))*(n_dme_model(:,2)-
n_dme_model(:,1)));
        n_Ar_model(:,1)=n_ar-((D_Ar/(vel*dz))*(n_Ar_model(:,2)-
n_Ar_model(:,1)));
    elseif Tt(1,1) < t0
        n_dme_model(:,1)=0;
        n_Ar_model(:,1)=0;
    elseif Tt(1,1)> t0+dt
        n_dme_model(:,1)=n_DME-((D_dme/(vel*dz))*(n_dme_model(:,2)-
n_dme_model(:,1)));
        n_Ar_model(:,1)=n_ar-((D_Ar/(vel*dz))*(n_Ar_model(:,2)-
n_Ar_model(:,1)));
    end


    theta_sms_model(:,1) = 0;
    theta_methoxymethyl_model(:,1) = 0;
    theta_dme_model(:,1) = 0;
    theta_water_model(:,1) = 0;
    theta_Ar_model(:,1) = 0;
    theta_formaldehyde_model(:,1) = 0;
    theta_methane_model(:,1) = 0;

    theta_hydrogen_model(:,1) = 0;

    theta_propene_model(:,1) = 0;
    theta_methylal_model(:,1) = 0;
    theta_dimethoxyethane_model(:,1) = 0;
    theta_methanediol_model(:,1) = 0;
    theta_alkene_ether_model(:,1) = 0;
    theta_vacant_model(:,1) = 1-theta_sms_model(:,1)-
theta_methoxymethyl_model(:,1)...
        -theta_dme_model(:,1)-theta_water_model(:,1)-
theta_Ar_model(:,1)...
        -theta_formaldehyde_model(:,1)-theta_methane_model(:,1)-
theta_hydrogen_model(:,1)...
        -theta_methylal_model(:,1)-theta_dimethoxyethane_model(:,1)-
theta_methanediol_model(:,1)...
        -theta_alkene_ether_model(:,1)-theta_propene_model(:,1);

    n_meth_model(:,1) = 0;
    n_water_model(:,1) = 0;
    n_formaldehyde_model(:,1) = 0;
    n_methane_model(:,1) = 0;
    n_hydrogen_model(:,1) = 0;
    n_propene_model(:,1) = 0;
    n_methylal_model(:,1) = 0;
    n_dimethoxyethane_model(:,1) = 0;
    n_methanediol_model(:,1) = 0;
    n_alkene_ether_model(:,1) = 0;


    for n=0:1:N-1
        for j=1:1:J-1
```

```
r1=k1*((n_meth_model(n+1,j+1)./dv)*R*temp*dt)*theta_vacant_model(n+1
,j+1);
            r_1=k_1*theta_sms_model(n+1,
j+1)*((n_water_model(n+1,j+1)./dv)*R*temp*dt);

r2=k2*((n_dme_model(n+1,j+1)./dv)*R*temp*dt)*theta_vacant_model(n+1,
j+1);
            r_2=k_2*theta_sms_model(n+1,
j+1)*((n_meth_model(n+1,j+1)./dv)*R*temp*dt);

r3=k3*((n_water_model(n+1,j+1)./dv)*R*temp*dt)*theta_vacant_model(n+
1,j+1);
            r_3=k_3*theta_water_model(n+1, j+1);

r4=k4*((n_methane_model(n+1,j+1)./dv)*R*temp*dt)*theta_vacant_model(
n+1,j+1);
            r_4=k_4*theta_methane_model(n+1, j+1);

r5=k5*((n_formaldehyde_model(n+1,j+1)./dv)*R*temp*dt)*theta_vacant_m
odel(n+1,j+1);
            r_5=k_5*theta_formaldehyde_model(n+1, j+1);

r6=k6*((n_hydrogen_model(n+1,j+1)./dv)*R*temp*dt)*theta_vacant_model
(n+1,j+1);
            r_6=k_6*theta_hydrogen_model(n+1, j+1);

r7=k7*((n_propene_model(n+1,j+1)./dv)*R*temp*dt)*theta_vacant_model(
n+1,j+1);
            r_7=k_7*theta_propene_model(n+1, j+1);

r8=k8*((n_dme_model(n+1,j+1)./dv)*R*temp*dt)*theta_vacant_model(n+1,
j+1);
            r_8=k_8*theta_methoxymethyl_model(n+1,
j+1)*((n_hydrogen_model(n+1,j+1)./dv)*R*temp*dt);

r9=k9*((n_methylal_model(n+1,j+1)./dv)*R*temp*dt)*theta_vacant_model
(n+1,j+1);
            r_9=k_9*theta_methylal_model(n+1, j+1);

r10=k10*((n_dimethoxyethane_model(n+1,j+1)./dv)*R*temp*dt)*theta_vac
ant_model(n+1,j+1);
            r_10=k_10*theta_dimethoxyethane_model(n+1, j+1);

r11=k11*((n_alkene_ether_model(n+1,j+1)./dv)*R*temp*dt)*theta_vacant
_model(n+1,j+1);
            r_11=k_11*theta_alkene_ether_model(n+1, j+1);

r12=k12*((n_methanediol_model(n+1,j+1)./dv)*R*temp*dt)*theta_vacant_
model(n+1,j+1);
            r_12=k_12*theta_methanediol_model(n+1, j+1);

r13=k13*((n_meth_model(n+1,j+1)./dv)*R*temp*dt)*theta_sms_model(n+1,
j+1);
            r_13=k_13*theta_dme_model(n+1,j+1);
```

```
r14=k14*((n_meth_model(n+1,j+1)./dv)*R*temp*dt)*theta_vacant_model(n
+1,j+1);

r15=k15*((n_dme_model(n+1,j+1)./dv)*R*temp*dt)*theta_vacant_model(n+
1,j+1);
            r16=k16*theta_formaldehyde_model(n+1,
j+1)*((n_water_model(n+1,j+1)./dv)*R*temp*dt);
            r_16=k_16*theta_methanediol_model(n+1, j+1);
            r17=k17*theta_sms_model(n+1,
j+1)*((n_dme_model(n+1,j+1)./dv)*R*temp*dt);
            r18=k18*theta_methoxymethyl_model(n+1,
j+1)*((n_dme_model(n+1,j+1)./dv)*R*temp*dt);
            r19=k19*theta_dimethoxyethane_model(n+1, j+1);
            r20=k20*theta_sms_model(n+1,
j+1)*((n_alkene_ether_model(n+1,j+1)./dv)*R*temp*dt);
            r21=k21*theta_methoxymethyl_model(n+1,
j+1)*theta_methylal_model(n+1,j+1);


            R_meth_g=-r1+r_1+r2-r_2-r13+r_13-r14;
            R_sms_ss=r1-r_1+r2-r_2-r13+r_13-r17-r20;
            R_dme_g=-r2+r_2-r8+r_8-r15-r17-r18;
            R_dme_ss=r13-r_13;
            R_water_g=r1-r_1-r3+r_3-r16+r_16+r19;
            R_water_ss=r3-r_3;
            R_propene_g=-r7+r_7+r20;
            R_propene_ss=r7-r_7;
            R_formaldehyde_g=-r5+r_5;
            R_formaldehyde_ss=r5-r_5+r14+r15-r16+r_16+r21;
            R_hydrogen_g=-r6+r_6+r8-r_8+r14;
            R_hydrogen_ss=r6-r_6;
            R_methane_g=-r4+r_4+r15+r17;
            R_methane_ss=r4-r_4;
            R_methoxymethyl_ss=r8-r_8+r17+r20-r21-r18;
            R_methanediol_g=-r12+r_12;
            R_methanediol_ss=r12-r_12+r16-r_16;
            R_methylal_g=-r9+r_9;
            R_methylal_ss=r9-r_9-r21;
            R_dimethoxyethane_g=-r10+r_10;
            R_dimethoxyethane_ss=r10-r_10+r18-r19+r21;
            R_alkene_ether_g=-r11+r_11-r20;
            R_alkene_ether_ss=r11-r_11+r19;

            R_Ar_g=0;
            R_Ar_ss=0;


n_meth_model(n+2,j+1)=n_meth_model(n+1,j+1)+((SF_X*D_meth)*(n_meth_m
odel(n+1,j+2)-
(2*n_meth_model(n+1,j+1))+n_meth_model(n+1,j)))+(SF*(n_meth_model(n+
1,j)-n_meth_model(n+1,j+1)))+((dv*Sv*conc_sites_gram_25*((1-
bed_porosity)/(bed_porosity)))*R_meth_g);

n_dme_model(n+2,j+1)=n_dme_model(n+1,j+1)+((SF_X*D_dme)*(n_dme_model
(n+1,j+2)-
```

```
(2*n_dme_model(n+1,j+1))+n_dme_model(n+1,j)))+(SF*(n_dme_model(n+1,j
)-n_dme_model(n+1,j+1)))+((dv*Sv*conc_sites_gram_25*((1-
bed_porosity)/(bed_porosity)))*R_dme_g);

n_water_model(n+2,j+1)=n_water_model(n+1,j+1)+((SF_X*D_water)*(n_wat
er_model(n+1,j+2)-
(2*n_water_model(n+1,j+1))+n_water_model(n+1,j)))+(SF*(n_water_model
(n+1,j)-n_water_model(n+1,j+1)))+((dv*Sv*conc_sites_gram_25*((1-
bed_porosity)/(bed_porosity)))*R_water_g);

n_formaldehyde_model(n+2,j+1)=n_formaldehyde_model(n+1,j+1)+((SF_X*D
_formaldehyde)*(n_formaldehyde_model(n+1,j+2)-
(2*n_formaldehyde_model(n+1,j+1))+n_formaldehyde_model(n+1,j)))+(SF*
(n_formaldehyde_model(n+1,j)-
n_formaldehyde_model(n+1,j+1)))+((dv*Sv*conc_sites_gram_25*((1-
bed_porosity)/(bed_porosity)))*R_formaldehyde_g);

n_methane_model(n+2,j+1)=n_methane_model(n+1,j+1)+((SF_X*D_methane)*
(n_methane_model(n+1,j+2)-
(2*n_methane_model(n+1,j+1))+n_methane_model(n+1,j)))+(SF*(n_methane
_model(n+1,j)-
n_methane_model(n+1,j+1)))+((dv*Sv*conc_sites_gram_25*((1-
bed_porosity)/(bed_porosity)))*R_methane_g);

n_hydrogen_model(n+2,j+1)=n_hydrogen_model(n+1,j+1)+((SF_X*D_hydroge
n)*(n_hydrogen_model(n+1,j+2)-
(2*n_hydrogen_model(n+1,j+1))+n_hydrogen_model(n+1,j)))+(SF*(n_hydro
gen_model(n+1,j)-
n_hydrogen_model(n+1,j+1)))+((dv*Sv*conc_sites_gram_25*((1-
bed_porosity)/(bed_porosity)))*R_hydrogen_g);

n_dimethoxyethane_model(n+2,j+1)=n_dimethoxyethane_model(n+1,j+1)+((
SF_X*D_dimethoxyethane)*(n_dimethoxyethane_model(n+1,j+2)-
(2*n_dimethoxyethane_model(n+1,j+1))+n_dimethoxyethane_model(n+1,j))
)+(SF*(n_dimethoxyethane_model(n+1,j)-
n_dimethoxyethane_model(n+1,j+1)))+((dv*Sv*conc_sites_gram_25*((1-
bed_porosity)/(bed_porosity)))*R_dimethoxyethane_g);

n_methanediol_model(n+2,j+1)=n_methanediol_model(n+1,j+1)+((SF_X*D_m
ethanediol)*(n_methanediol_model(n+1,j+2)-
(2*n_methanediol_model(n+1,j+1))+n_methanediol_model(n+1,j)))+(SF*(n
_methanediol_model(n+1,j)-
n_methanediol_model(n+1,j+1)))+((dv*Sv*conc_sites_gram_25*((1-
bed_porosity)/(bed_porosity)))*R_methanediol_g);

n_alkene_ether_model(n+2,j+1)=n_alkene_ether_model(n+1,j+1)+((SF_X*D
_alkene_ether)*(n_alkene_ether_model(n+1,j+2)-
(2*n_alkene_ether_model(n+1,j+1))+n_alkene_ether_model(n+1,j)))+(SF*
(n_alkene_ether_model(n+1,j)-
n_alkene_ether_model(n+1,j+1)))+((dv*Sv*conc_sites_gram_25*((1-
bed_porosity)/(bed_porosity)))*R_alkene_ether_g);

n_methylal_model(n+2,j+1)=n_methylal_model(n+1,j+1)+((SF_X*D_methyla
l)*(n_methylal_model(n+1,j+2)-
(2*n_methylal_model(n+1,j+1))+n_methylal_model(n+1,j)))+(SF*(n_methy
lal_model(n+1,j)-
```

```
n_methylal_model(n+1,j+1)))+((dv*Sv*conc_sites_gram_25*((1-
bed_porosity)/(bed_porosity)))*R_methylal_g);

n_propene_model(n+2,j+1)=n_propene_model(n+1,j+1)+((SF_X*D_propene)*
(n_propene_model(n+1,j+2)-
(2*n_propene_model(n+1,j+1))+n_propene_model(n+1,j)))+(SF*(n_propene
_model(n+1,j)-
n_propene_model(n+1,j+1)))+((dv*Sv*conc_sites_gram_25*((1-
bed_porosity)/(bed_porosity)))*R_propene_g);


n_Ar_model(n+2,j+1)=n_Ar_model(n+1,j+1)+((SF_X*D_Ar)*(n_Ar_model(n+1
,j+2)-
(2*n_Ar_model(n+1,j+1))+n_Ar_model(n+1,j)))+(SF*(n_Ar_model(n+1,j)-
n_Ar_model(n+1,j+1)))+((dv*Sv*conc_sites_gram_25*((1-
bed_porosity)/(bed_porosity)))*R_Ar_g);

            theta_sms_model(n+2,j+1)=theta_sms_model(n+1,
j+1)+(dt*R_sms_ss);

theta_dme_model(n+2,j+1)=theta_dme_model(n+1,j+1)+(dt*R_dme_ss);

theta_water_model(n+2,j+1)=theta_water_model(n+1,j+1)+(dt*R_water_ss
);

theta_formaldehyde_model(n+2,j+1)=theta_formaldehyde_model(n+1,j+1)+
(dt*R_formaldehyde_ss);

theta_methane_model(n+2,j+1)=theta_methane_model(n+1,j+1)+(dt*R_meth
ane_ss);

theta_hydrogen_model(n+2,j+1)=theta_hydrogen_model(n+1,j+1)+(dt*R_hy
drogen_ss);

theta_dimethoxyethane_model(n+2,j+1)=theta_dimethoxyethane_model(n+1
,j+1)+(dt*R_dimethoxyethane_ss);

theta_methanediol_model(n+2,j+1)=theta_methanediol_model(n+1,j+1)+(d
t*R_methanediol_ss);

theta_alkene_ether_model(n+2,j+1)=theta_alkene_ether_model(n+1,j+1)+
(dt*R_alkene_ether_ss);

theta_methylal_model(n+2,j+1)=theta_methylal_model(n+1,j+1)+(dt*R_me
thylal_ss);

theta_propene_model(n+2,j+1)=theta_propene_model(n+1,j+1)+(dt*R_prop
ene_ss);

theta_methoxymethyl_model(n+2,j+1)=theta_methoxymethyl_model(n+1,j+1
)+(dt*R_methoxymethyl_ss);

            theta_Ar_model(n+2,j+1)=theta_Ar_model(n+1,j+1)+(dt*0);

            theta_vacant_model(n+2,j+1) = 1-
theta_sms_model(n+2,j+1)-theta_dme_model(n+2,j+1)...
```

```
                -theta_water_model(n+2,j+1)-theta_Ar_model(n+2,j+1)-
theta_formaldehyde_model(n+2,j+1)...
                -theta_methane_model(n+2,j+1)-
theta_hydrogen_model(n+2,j+1)-
theta_dimethoxyethane_model(n+2,j+1)...
                -theta_methanediol_model(n+2,j+1)-
theta_alkene_ether_model(n+2,j+1)...
                -theta_methylal_model(n+2,j+1)-
theta_propene_model(n+2,j+1)-theta_methoxymethyl_model(n+2,j+1);
        end
    end
end

%% 2nd boundary condition
n_meth_model(:, J+1) = n_meth_model(:, J);
n_dme_model(:, J+1) = n_dme_model(:, J);
n_water_model(:, J+1) = n_water_model(:, J);
n_formaldehyde_model(:, J+1) = n_formaldehyde_model(:, J);
n_methane_model(:, J+1) = n_methane_model(:, J);
n_hydrogen_model(:, J+1) = n_hydrogen_model(:, J);
n_dimethoxyethane_model(:, J+1) = n_dimethoxyethane_model(:, J);
n_methanediol_model(:, J+1) = n_methanediol_model(:, J);
n_alkene_ether_model(:, J+1) = n_alkene_ether_model(:, J);
n_methylal_model(:, J+1) = n_methylal_model(:, J);
n_propene_model(:, J+1) = n_propene_model(:, J);
n_Ar_model(:, J+1) = n_Ar_model(:,J);

theta_sms_model(:, J+1) = theta_sms_model(:, J);
theta_dme_model(:, J+1) = theta_dme_model(:, J);
theta_water_model(:, J+1) = theta_water_model(:, J);
theta_formaldehyde_model(:, J+1) = theta_formaldehyde_model(:, J);
theta_methane_model(:, J+1) = theta_methane_model(:, J);
theta_hydrogen_model(:, J+1) = theta_hydrogen_model(:, J);
theta_dimethoxyethane_model(:, J+1) = theta_dimethoxyethane_model(:,
J);
theta_methanediol_model(:, J+1) = theta_methanediol_model(:, J);
theta_alkene_ether_model(:, J+1) = theta_alkene_ether_model(:, J);
theta_methylal_model(:, J+1) = theta_methylal_model(:, J);
theta_propene_model(:, J+1) = theta_propene_model(:, J);
theta_methoxymethyl_model(:, J+1) = theta_methoxymethyl_model(:, J);
theta_Ar_model(:, J+1) = theta_Ar_model(:, J);
theta_vacant_model(:, J+1) = theta_vacant_model(:, J);


%%
close all
figure
plot(Tt, n_meth_model(:,end), 'b-',time,n_amu31_exp,
'b.','LineWidth', 2.5)
hold on
plot(Tt, n_dme_model(:,end), 'g-',time,
n_amu45_exp,'g.','LineWidth', 2.5)
hold on
plot(Tt, n_water_model(:,end), 'c-', time, n_amu18_exp,'c.',
'LineWidth', 2.5)
hold on
```

```
plot(Tt, n_propene_model(:,end), 'm-', time, n_amu41_exp,'m.',
'LineWidth', 2.5)
ylim([-1e-11 2.1e-9]);
xlim([0 80]);
xlabel('Time on stream, min','Fontweight', 'Bold', 'FontSize', 11)
ylabel('Molar flowrate, mol\cdots^{-1}','Fontweight', 'Bold',
'FontSize', 11)
legend('MeOH_{model}','MeOH_{expt}', 'DME_{model}', 'DME_{expt}',
'H2O_{model}','H2O_{expt}','C3H6_{model}', 'C3H6_{expt}',
'location', 'bestoutside')

box off
legend boxoff
ax=gca;
ax.FontSize = 11;

figure
plot(Tt, theta_sms_model(:,end), 'b-', Tt, theta_dme_model(:,end),
'g-', Tt, theta_water_model(:,end), 'k-', Tt,
theta_alkene_ether_model(:,end), 'c-', Tt,
theta_methoxymethyl_model(:,end), 'm-', Tt,
theta_formaldehyde_model(:,end), 'r-')
legend('SMS', 'DME', 'H2O', 'Alkene-ether','Methoxymethyl',
'formaldehyde')
box off
legend boxoff
ax=gca;
ax.FontSize = 11;
toc;

%% objective function

time_location=find(time | ~time);
time_res=time(time_location);
time_res_v2=round(time_res*1000)/1000; %round to 3d.p
Tt_v2=round(Tt*1000)/1000;             %round to 3d.p

[~,index]=ismember(time_res_v2, Tt_v2); % what elements of
experimental time belongs to model time
n_meth_model_v2=n_meth_model(:,end);
n_dme_model_v2=n_dme_model(:,end);
n_water_model_v2=n_water_model(:,end);
n_propene_model_v2=n_propene_model(:,end);
y_model=[n_meth_model_v2(index), n_dme_model_v2(index),
n_water_model_v2(index), n_propene_model_v2(index)];
y_expt=[n_amu31_exp(time_location), n_amu45_exp(time_location),
n_amu18_exp(time_location), n_amu41_exp(time_location)];


%%
sse = (y_model - y_expt).^2;
obj = sum(sum(sse))


sse_meth = (1/sum(y_expt(:,1)))*sse(:,1);
sse_dme = (1/sum(y_expt(:,2)))*sse(:,2);
```

```
sse_water = (1/sum(y_expt(:,3)))*sse(:,3);
sse_propene = (1/sum(y_expt(:,4)))*sse(:,4);

sse_v2=[sse_meth, sse_dme, sse_water, sse_propene];
obj_v2 = sum(sum(sse_v2))


figure; plot(Tt, n_propene_model(:,end), 'm-', time,
n_amu41_exp,'m.', 'LineWidth', 2.5)
figure; plot(Tt, n_dme_model(:, end))
```

ii. Function file – optimisation routine

```
function obj_v2 = MOL21_obj_v3_appendix(k);
%% using upwind scheme to solve PDE's arising from step response
experiments%%
%% using reaction scheme based on recent DFT evidence%%
%Date created - 25/10/2017

%1. CH3OH+HZ<>CH3.Z+H2O
%2. CH3OCH3+HZ<>CH3.Z+CH3OH
%3. H2O+HZ<>H2O.HZ
%4. CH3.Z+CH3OH<>CH3OCH3.HZ
%5. CH3CHCHOCH3+HZ<>CH3CHCHOCH3.HZ
%6. CH3.Z+CH3OCH3>CH3OCH2.Z+CH4
%7. CH3OCH2.Z+CH3OCH3>CH3OCH2CH2OCH3.HZ
%8. CH3OCH2CH2OCH3.HZ>CH3CHCHOCH3.HZ+H2O
%9. CH3CHCHOCH3+CH3.Z>C3H6+CH3OCH2.Z


tic

k1=k(1);
k_1=k(2);
k2=k(3);
k_2=k(4);
k3=k(5);
k_3=k(6);
k4=k(7);
k_4=k(8);
k5=k(9);
k_5=k(10);
k6=k(11);
k7=k(12);
k8=k(13);
k9=k(14);

%% experimental data
% Inlet feed

load('deconvolution_b_v3')

n_amu31_exp = R_amu31s;
n_amu45_exp = R_amu45s;
n_amu18_exp = R_amu18s;
n_amu40_exp = R_amu40s;
n_amu28_exp = R_amu28s;
n_amu91_exp = R_amu91s;
n_amu27_exp = R_amu27s;
n_amu41_exp = R_amu41s;

%% gas properties
meth_volume_fraction=0;
argon_volume_fraction=0.95;
dme_volume_fraction=0.05;

pres = 1000;    %total pressure in the fixed bed (Pa)
```

```
R = 8.314;      %Molar gas constant, J/mol/K
temp = 573; %input('what is the step response temperature in C?
')+273; %Temperature in Kelvin


%% reactor properties
bed_length = 2e-3; %0.002 m
reactor_diameter = 4e-3; %m
bed_area=(pi*reactor_diameter^2)/4; %m^2
bed_volume=bed_area*bed_length; %m^3

%% Catalyst properties
cat_density = 2200; %kg/m^3
bed_porosity = 0.5;
cat_diameter = 30e-6; %m

%Pyridine FTIR acid site density
sites_gram_25=356e-6; %mol/g
sites_gram_36=117e-6; %mol/g
sites_gram_135=78e-6; %mol/g

%BET surface area
BET_25=413; %m^2/g
BET_36=410; %m^2/g
BET_135=358; %m^2/g

% concentration of active sites per unit surface area of catalyst =
acid
% site density * BET surface area
conc_sites_gram_25=sites_gram_25/BET_25; %mol/m^2
conc_sites_gram_36=sites_gram_36/BET_36; %mol/m^2
conc_sites_gram_135=sites_gram_135/BET_135; %mol/m^2

%specific surface area of catalyst = 6/particle diameter
Sv=6/cat_diameter;

%% Define space and time domain

% For bed length of 2 mm, define space domain parameters
z0 = 0; %initial length of reactor
z1 = 2e-3; %bed length
J = 10; % number of strips
dz = (z1-z0)/J;
% disp(['J = ', num2str(J)]);
% disp(' ');
% disp(['dz = ', num2str(dz)]);
% disp(' ');
Z = dz*(0:J);
dv=bed_area*dz;

% For time equals time at last data point, define time domain
t0 = 0;  %initial time
time;
tf = time(end); %final time (min)
N = 4000000; %number of time steps
dt=tf/N; %time step size
```

```
% disp(['dt = ', num2str(dt)]);
% disp(' ');
% disp(['N = ', num2str(N)]);
% disp(' ');

% T = (dt*(0:N))';
Tt = (dt*(0:N))';

%% stability factor, (u/eb)*(dt/dz)
vel=0.00025;
SF = (vel/bed_porosity)*(dt/dz);
% disp(['SF = ', num2str(SF)]);
% disp(' ');

SF_X=dt/(bed_porosity*(dz^2));
cortn_factor=2e-4;
D_meth=1.03e-5*cortn_factor;
D_dme=8.56e-6*cortn_factor;
D_water=1.37e-5*cortn_factor;
D_methane=1.45e-5*cortn_factor;
D_alkene_ether=6.84e-6*cortn_factor;
D_propene=8.96e-6*cortn_factor;
D_Ar=9.18e-6*cortn_factor;

if SF < 1
    %% initialise solution space
    n_meth_model=zeros(N+1, J+1);
    n_dme_model=zeros(N+1, J+1);
    n_water_model=zeros(N+1, J+1);
    n_Ar_model=zeros(N+1, J+1);
    n_methane_model=zeros(N+1, J+1);
    n_propene_model=zeros(N+1, J+1);
    n_alkene_ether_model=zeros(N+1,J+1);

    theta_sms_model=zeros(N+1, J+1);
    theta_methoxymethyl_model=zeros(N+1, J+1);
    theta_dme_model=zeros(N+1, J+1);
    theta_water_model=zeros(N+1, J+1);
    theta_Ar_model=zeros(N+1, J+1);


    theta_dimethoxyethane_model=zeros(N+1, J+1);

    theta_alkene_ether_model=zeros(N+1,J+1);
    theta_vacant_model=zeros(N+1, J+1);

    % insert initial conditions into solution matrix. At time = t0,
    % catalyst is empty and begins to fill up.
    theta_sms_model(1,1) = 0;
    theta_methoxymethyl_model(1,1) = 0;
    theta_dme_model(1,1) = 0;
    theta_water_model(1,1) = 0;
    theta_Ar_model(1,1) = 0;
    theta_dimethoxyethane_model(1,1) = 0;
    theta_alkene_ether_model(1,1) = 0;
```

```
    theta_vacant_model(1,1) = 1-theta_sms_model(1,1)-
theta_methoxymethyl_model(1,1)...
        -theta_dme_model(1,1)-theta_water_model(1,1)-
theta_Ar_model(1,1)...
        -theta_dimethoxyethane_model(1,1)...
        -theta_alkene_ether_model(1,1);

    % n_dme_model(1,1) = n_DME;    %obtained from deconvolution file
    % n_Ar_model(1,1) = n_ar;      %obtained from deconvolution file
    n_meth_model(1,1) = 0;
    n_water_model(1,1) = 0;
    n_methane_model(1,1) = 0;
    n_propene_model(1,1) = 0;
    n_alkene_ether_model(1,1) = 0;


    %% step function
    % insert boundary conditions into solution matrix. At z = 0, a
step
    % response of oxygenates is introduced.


    %% convection alone
    %     if Tt(1,1) >= t0 && Tt(1,1) <= t0+dt
    %         n_dme_model(:,1)=n_DME;
    %         n_Ar_model(:,1)=n_ar;
    %     elseif Tt(1,1) < t0
    %         n_dme_model(:,1)=0;
    %         n_Ar_model(:,1)=0;
    %     elseif Tt(1,1)> t0+dt
    %         n_dme_model(:,1)=n_DME;
    %         n_Ar_model(:,1)=n_ar;
    %     end

    %% convection and dispersion
    if Tt(1,1) >= t0 && Tt(1,1) <= t0+dt
        n_dme_model(:,1)=n_DME-((D_dme/(vel*dz))*(n_dme_model(:,2)-
n_dme_model(:,1)));
        n_Ar_model(:,1)=n_ar-((D_Ar/(vel*dz))*(n_Ar_model(:,2)-
n_Ar_model(:,1)));
    elseif Tt(1,1) < t0
        n_dme_model(:,1)=0;
        n_Ar_model(:,1)=0;
    elseif Tt(1,1)> t0+dt
        n_dme_model(:,1)=n_DME-((D_dme/(vel*dz))*(n_dme_model(:,2)-
n_dme_model(:,1)));
        n_Ar_model(:,1)=n_ar-((D_Ar/(vel*dz))*(n_Ar_model(:,2)-
n_Ar_model(:,1)));
    end



    theta_sms_model(:,1) = 0;
    theta_methoxymethyl_model(:,1) = 0;
    theta_dme_model(:,1) = 0;
    theta_water_model(:,1) = 0;
```

```
    theta_Ar_model(:,1) = 0;

    theta_dimethoxyethane_model(:,1) = 0;

    theta_alkene_ether_model(:,1) = 0;
    theta_vacant_model(:,1) = 1-theta_sms_model(:,1)-
theta_methoxymethyl_model(:,1)...
        -theta_dme_model(:,1)-theta_water_model(:,1)-
theta_Ar_model(:,1)...
        -theta_dimethoxyethane_model(:,1)...
        -theta_alkene_ether_model(:,1);

    n_meth_model(:,1) = 0;
    n_water_model(:,1) = 0;
    n_methane_model(:,1) = 0;
    n_propene_model(:,1) = 0;
    n_alkene_ether_model(:,1) = 0;


    for n=0:1:N-1
        for j=1:1:J-1


r1=k1*((n_meth_model(n+1,j+1)./dv)*R*temp*dt)*theta_vacant_model(n+1
,j+1);
            r_1=k_1*theta_sms_model(n+1,
j+1)*((n_water_model(n+1,j+1)./dv)*R*temp*dt);

r2=k2*((n_dme_model(n+1,j+1)./dv)*R*temp*dt)*theta_vacant_model(n+1,
j+1);
            r_2=k_2*theta_sms_model(n+1,
j+1)*((n_meth_model(n+1,j+1)./dv)*R*temp*dt);

r3=k3*((n_water_model(n+1,j+1)./dv)*R*temp*dt)*theta_vacant_model(n+
1,j+1);
            r_3=k_3*theta_water_model(n+1, j+1);

r4=k4*((n_meth_model(n+1,j+1)./dv)*R*temp*dt)*theta_sms_model(n+1,
j+1);
            r_4=k_4*theta_dme_model(n+1,j+1);

r5=k5*((n_alkene_ether_model(n+1,j+1)./dv)*R*temp*dt)*theta_vacant_m
odel(n+1,j+1);
            r_5=k_5*theta_alkene_ether_model(n+1, j+1);
            r6=k6*theta_sms_model(n+1,
j+1)*((n_dme_model(n+1,j+1)./dv)*R*temp*dt);
            r7=k7*theta_methoxymethyl_model(n+1,
j+1)*((n_dme_model(n+1,j+1)./dv)*R*temp*dt);
            r8=k8*theta_dimethoxyethane_model(n+1, j+1);
            r9=k9*theta_sms_model(n+1,
j+1)*((n_alkene_ether_model(n+1,j+1)./dv)*R*temp*dt);



            R_meth_g=-r1+r_1+r2-r_2-r4+r_4;
            R_sms_ss=r1-r_1+r2-r_2-r4+r_4-r6-r9;
```

```
R_dme_g=-r2+r_2-r6-r7;
R_dme_ss=r4-r_4;
R_water_g=r1-r_1-r3+r_3+r8;
R_water_ss=r3-r_3;
R_propene_g=r9;
R_methane_g=r6;
R_methoxymethyl_ss=r6+r9-r7;
R_dimethoxyethane_ss=r7-r8;
R_alkene_ether_g=-r5+r_5-r9;
R_alkene_ether_ss=r5-r_5+r8;

R_Ar_g=0;
R_Ar_ss=0;


n_meth_model(n+2,j+1)=n_meth_model(n+1,j+1)+((SF_X*D_meth)*(n_meth_m
odel(n+1,j+2)-
(2*n_meth_model(n+1,j+1))+n_meth_model(n+1,j)))+(SF*(n_meth_model(n+
1,j)-n_meth_model(n+1,j+1)))+((dv*Sv*conc_sites_gram_25*((1-
bed_porosity)/(bed_porosity)))*R_meth_g);

n_dme_model(n+2,j+1)=n_dme_model(n+1,j+1)+((SF_X*D_dme)*(n_dme_model
(n+1,j+2)-
(2*n_dme_model(n+1,j+1))+n_dme_model(n+1,j)))+(SF*(n_dme_model(n+1,j
)-n_dme_model(n+1,j+1)))+((dv*Sv*conc_sites_gram_25*((1-
bed_porosity)/(bed_porosity)))*R_dme_g);

n_water_model(n+2,j+1)=n_water_model(n+1,j+1)+((SF_X*D_water)*(n_wat
er_model(n+1,j+2)-
(2*n_water_model(n+1,j+1))+n_water_model(n+1,j)))+(SF*(n_water_model
(n+1,j)-n_water_model(n+1,j+1)))+((dv*Sv*conc_sites_gram_25*((1-
bed_porosity)/(bed_porosity)))*R_water_g);

n_methane_model(n+2,j+1)=n_methane_model(n+1,j+1)+((SF_X*D_methane)*
(n_methane_model(n+1,j+2)-
(2*n_methane_model(n+1,j+1))+n_methane_model(n+1,j)))+(SF*(n_methane
_model(n+1,j)-
n_methane_model(n+1,j+1)))+((dv*Sv*conc_sites_gram_25*((1-
bed_porosity)/(bed_porosity)))*R_methane_g);

n_alkene_ether_model(n+2,j+1)=n_alkene_ether_model(n+1,j+1)+((SF_X*D
_alkene_ether)*(n_alkene_ether_model(n+1,j+2)-
(2*n_alkene_ether_model(n+1,j+1))+n_alkene_ether_model(n+1,j)))+(SF*
(n_alkene_ether_model(n+1,j)-
n_alkene_ether_model(n+1,j+1)))+((dv*Sv*conc_sites_gram_25*((1-
bed_porosity)/(bed_porosity)))*R_alkene_ether_g);

n_propene_model(n+2,j+1)=n_propene_model(n+1,j+1)+((SF_X*D_propene)*
(n_propene_model(n+1,j+2)-
(2*n_propene_model(n+1,j+1))+n_propene_model(n+1,j)))+(SF*(n_propene
_model(n+1,j)-
n_propene_model(n+1,j+1)))+((dv*Sv*conc_sites_gram_25*((1-
bed_porosity)/(bed_porosity)))*R_propene_g);


n_Ar_model(n+2,j+1)=n_Ar_model(n+1,j+1)+((SF_X*D_Ar)*(n_Ar_model(n+1
```

```
,j+2)-
(2*n_Ar_model(n+1,j+1))+n_Ar_model(n+1,j)))+(SF*(n_Ar_model(n+1,j)-
n_Ar_model(n+1,j+1)))+((dv*Sv*conc_sites_gram_25*((1-
bed_porosity)/(bed_porosity)))*R_Ar_g);

            theta_sms_model(n+2,j+1)=theta_sms_model(n+1,
j+1)+(dt*R_sms_ss);

theta_dme_model(n+2,j+1)=theta_dme_model(n+1,j+1)+(dt*R_dme_ss);

theta_water_model(n+2,j+1)=theta_water_model(n+1,j+1)+(dt*R_water_ss
);

theta_dimethoxyethane_model(n+2,j+1)=theta_dimethoxyethane_model(n+1
,j+1)+(dt*R_dimethoxyethane_ss);

theta_alkene_ether_model(n+2,j+1)=theta_alkene_ether_model(n+1,j+1)+
(dt*R_alkene_ether_ss);

theta_methoxymethyl_model(n+2,j+1)=theta_methoxymethyl_model(n+1,j+1
)+(dt*R_methoxymethyl_ss);

            theta_Ar_model(n+2,j+1)=theta_Ar_model(n+1,j+1)+(dt*0);

            theta_vacant_model(n+2,j+1) = 1-
theta_sms_model(n+2,j+1)-theta_dme_model(n+2,j+1)...
                -theta_water_model(n+2,j+1)-
theta_Ar_model(n+2,j+1)...
                -theta_dimethoxyethane_model(n+2,j+1)...
                -theta_alkene_ether_model(n+2,j+1)...
                -theta_methoxymethyl_model(n+2,j+1);
        end
    end
end

%% 2nd boundary condition
n_meth_model(:, J+1) = n_meth_model(:, J);
n_dme_model(:, J+1) = n_dme_model(:, J);
n_water_model(:, J+1) = n_water_model(:, J);
n_methane_model(:, J+1) = n_methane_model(:, J);
n_alkene_ether_model(:, J+1) = n_alkene_ether_model(:, J);
n_propene_model(:, J+1) = n_propene_model(:, J);
n_Ar_model(:, J+1) = n_Ar_model(:,J);

theta_sms_model(:, J+1) = theta_sms_model(:, J);
theta_dme_model(:, J+1) = theta_dme_model(:, J);
theta_water_model(:, J+1) = theta_water_model(:, J);
theta_dimethoxyethane_model(:, J+1) = theta_dimethoxyethane_model(:,
J);
theta_alkene_ether_model(:, J+1) = theta_alkene_ether_model(:, J);
theta_methoxymethyl_model(:, J+1) = theta_methoxymethyl_model(:, J);
theta_Ar_model(:, J+1) = theta_Ar_model(:, J);
theta_vacant_model(:, J+1) = theta_vacant_model(:, J);


close all
```

```
figure
plot(Tt, n_meth_model(:,end), 'b-',time,n_amu31_exp,
'b.','LineWidth', 2.5)
hold on
plot(Tt, n_dme_model(:,end), 'g-',time,
n_amu45_exp,'g.','LineWidth', 2.5)
hold on
plot(Tt, n_water_model(:,end), 'c-', time, n_amu18_exp,'c.',
'LineWidth', 2.5)
hold on
plot(Tt, n_propene_model(:,end), 'm-', time, n_amu41_exp,'m.',
'LineWidth', 2.5)
ylim([-1e-11 2.5e-9]);
xlim([0 80]);
xlabel('Time on stream, min','Fontweight', 'Bold', 'FontSize', 11)
ylabel('Molar flowrate, mol\cdots^{-1}','Fontweight', 'Bold',
'FontSize', 11)
legend('MeOH_{model}','MeOH_{expt}', 'DME_{model}', 'DME_{expt}',
'H2O_{model}','H2O_{expt}','C3H6_{model}', 'C3H6_{expt}',
'location', 'bestoutside')

box off
legend boxoff
ax=gca;
ax.FontSize = 11;

figure
plot(Tt, theta_sms_model(:,end), 'b-', Tt, theta_dme_model(:,end),
'g-', Tt, theta_water_model(:,end), 'k-', Tt,
theta_alkene_ether_model(:,end), 'c-', Tt,
theta_methoxymethyl_model(:,end), 'm-')
legend('SMS', 'DME', 'H2O', 'methyl propenyl ether', 'Methyl methoxy
group')
box off
legend boxoff
ax=gca;
ax.FontSize = 11;


%% Objective  function

time_location=find(time | ~time);
time_res=time(time_location);
time_res_v2=round(time_res*1000)/1000; %round to 3d.p
Tt_v2=round(Tt*1000)/1000;             %round to 3d.p

[~,index]=ismember(time_res_v2, Tt_v2); % what elements of
experimental time belongs to model time
n_meth_model_v2=n_meth_model(:,end);
n_dme_model_v2=n_dme_model(:,end);
n_water_model_v2=n_water_model(:,end);
n_propene_model_v2=n_propene_model(:,end);
y_model=[n_meth_model_v2(index), n_dme_model_v2(index),
n_water_model_v2(index), n_propene_model_v2(index)];
y_expt=[n_amu31_exp(time_location), n_amu45_exp(time_location),
n_amu18_exp(time_location), n_amu41_exp(time_location)];
```

```
%%
sse = (y_model - y_expt).^2;
obj = sum(sum(sse))


sse_meth = (1/sum(y_expt(:,1)))*sse(:,1);
sse_dme = (1/sum(y_expt(:,2)))*sse(:,2);
sse_water = (1/sum(y_expt(:,3)))*sse(:,3);
sse_propene = (1/sum(y_expt(:,4)))*sse(:,4);

sse_v2=[sse_meth, sse_dme, sse_water, sse_propene];
obj_v2 = sum(sum(sse_v2))

toc;
```

iii. Script file – optimisation routine

```
%% using fminsearch

k0=[0.00182 0.1010 0.00045 2.5 0.0003 50 0.00028 1.7 0.00375 812.5
0.01 1.0 0.12875 200];
% options = optimset('PlotFcns',@optimplotfval);
k = fminsearch('MOL21_obj_v3_Appendix', k0);
disp(['fminsearch: k = ' num2str(k)]);
MOL21_obj_v3(k);
```

iv. Model data of the induction period experiments conducted in chapter 6

Table S4: Model data obtained from raw data (QMS ion currents) after which were corrected for background levels and fragmentation contributions for the different molecules and sensitivity factors according to section S1 of supplementary information.

time (s)	R_amu31s (mol/s)	R_amu45s (mol/s)	R_amu18s (mol/s)	R_amu27s (mol/s)	R_amu41s (mol/s)
0	-4.87E-12	1.08E-13	8.68E-11	-4.65E-12	5.41E-13
0.05	-4.06E-12	1.51E-13	4.57E-11	-2.17E-12	1.54E-13
0.100517	-4.84E-12	5.65E-13	4.36E-11	-1.01E-11	2.76E-13
0.150517	-5.50E-12	8.77E-13	3.36E-11	-1.10E-11	-5.65E-14
0.199467	-6.27E-12	1.71E-12	2.56E-11	-1.24E-11	-3.37E-13
0.250517	-7.06E-12	2.17E-12	1.55E-11	-1.38E-11	-7.93E-13
0.299467	-6.75E-12	3.65E-12	2.64E-11	-8.57E-12	-1.47E-12
0.35	-4.53E-12	5.77E-12	2.86E-11	-1.86E-12	-1.83E-12
0.4	-4.10E-12	7.41E-12	2.00E-11	-4.47E-13	-2.07E-12
0.45025	-2.52E-12	8.96E-12	2.69E-11	4.91E-12	-1.30E-12
0.499467	-1.72E-12	1.15E-11	2.82E-11	7.41E-12	-8.75E-13
0.55	-9.08E-13	1.31E-11	1.02E-11	7.29E-12	-6.40E-13
0.599733	-3.63E-12	1.38E-11	-4.04E-12	5.67E-12	4.99E-13
0.649467	-2.65E-12	1.58E-11	1.45E-11	7.85E-12	1.43E-12
0.70025	-3.27E-12	1.79E-11	3.40E-11	5.68E-12	1.18E-12
0.75	-2.74E-12	1.86E-11	4.58E-11	7.96E-12	8.79E-13
0.8	-3.03E-12	2.02E-11	6.80E-11	1.27E-11	1.03E-12
0.85	-1.98E-12	2.22E-11	8.24E-11	1.51E-11	6.12E-13
0.900517	-2.73E-13	2.19E-11	8.79E-11	1.67E-11	9.09E-14
0.95	8.08E-13	2.22E-11	7.75E-11	1.68E-11	1.26E-12
0.999733	1.50E-12	2.39E-11	8.24E-11	1.53E-11	1.52E-12
1.05025	3.13E-12	2.48E-11	7.12E-11	1.34E-11	1.60E-12
1.10025	3.14E-12	2.78E-11	8.56E-11	1.45E-11	1.72E-12
1.149733	7.04E-13	3.01E-11	7.05E-11	1.41E-11	2.32E-12
1.204683	1.71E-12	3.38E-11	7.63E-11	1.69E-11	1.80E-12
1.266917	3.40E-12	3.63E-11	8.01E-11	1.57E-11	2.50E-12
1.321867	2.30E-12	3.94E-11	7.64E-11	1.59E-11	1.86E-12
1.383333	2.04E-12	4.02E-11	6.05E-11	1.42E-11	1.55E-12
1.43775	2.79E-12	4.40E-11	7.78E-11	1.30E-11	9.83E-13
1.499733	1.18E-12	4.66E-11	6.49E-11	1.02E-11	8.70E-13
1.5539	3.48E-15	5.18E-11	6.69E-11	1.35E-11	-2.34E-13
1.616667	1.42E-12	5.81E-11	7.72E-11	1.34E-11	-6.07E-13
1.6716	1.48E-12	6.34E-11	7.69E-11	1.27E-11	-1.14E-13
1.7328	1.69E-12	6.97E-11	6.31E-11	1.35E-11	-8.05E-14
1.7875	2.31E-12	7.62E-11	6.91E-11	1.55E-11	-1.33E-12
1.850767	1.11E-12	8.26E-11	5.64E-11	1.58E-11	-1.48E-12

1.9052	2.74E-13	8.69E-11	6.66E-11	1.69E-11	-9.96E-13
1.966667	-3.24E-13	9.64E-11	6.73E-11	1.71E-11	-1.56E-12
2.02135	-8.18E-13	1.08E-10	7.04E-11	1.97E-11	-1.98E-12
2.083067	-2.58E-12	1.17E-10	7.11E-11	2.04E-11	-1.16E-12
2.133333	-3.59E-12	1.27E-10	6.59E-11	1.96E-11	-5.98E-13
2.1888	-4.77E-12	1.38E-10	6.49E-11	2.00E-11	6.75E-13
2.25	-3.22E-12	1.50E-10	7.44E-11	2.28E-11	5.51E-14
2.3052	-3.36E-12	1.58E-10	9.04E-11	1.93E-11	6.93E-13
2.367183	-4.97E-13	1.68E-10	1.03E-10	1.75E-11	-2.56E-13
2.416917	9.50E-13	1.77E-10	1.25E-10	2.04E-11	-2.02E-13
2.4664	1.75E-12	1.89E-10	1.38E-10	2.25E-11	-1.25E-12
2.516133	2.28E-12	2.04E-10	1.48E-10	2.06E-11	-1.97E-13
2.565883	6.40E-12	2.21E-10	1.44E-10	2.39E-11	-4.69E-13
2.620833	6.06E-12	2.40E-10	1.46E-10	2.37E-11	6.65E-13
2.68385	5.97E-12	2.57E-10	1.45E-10	2.00E-11	3.58E-13
2.733333	9.35E-12	2.67E-10	1.23E-10	1.68E-11	-5.29E-13
2.783583	8.85E-12	2.76E-10	1.08E-10	1.44E-11	-4.27E-13
2.8328	6.95E-12	2.88E-10	1.23E-10	1.52E-11	-1.11E-12
2.883583	7.92E-12	2.99E-10	1.42E-10	1.75E-11	-2.38E-12
2.938017	7.63E-12	3.14E-10	1.44E-10	2.06E-11	-3.33E-12
3.00025	5.67E-12	3.33E-10	1.34E-10	2.08E-11	-2.86E-12
3.05	7.10E-12	3.56E-10	1.27E-10	2.39E-11	-3.86E-12
3.1	4.07E-12	3.73E-10	1.12E-10	2.23E-11	-3.37E-12
3.15	4.20E-12	3.86E-10	8.85E-11	2.47E-11	-2.68E-12
3.200517	8.42E-12	3.98E-10	9.75E-11	2.51E-11	-1.60E-12
3.25	8.07E-12	4.08E-10	1.24E-10	2.45E-11	-1.22E-12
3.304417	6.90E-12	4.28E-10	1.49E-10	2.38E-11	-1.61E-12
3.366133	8.95E-12	4.43E-10	1.67E-10	2.76E-11	-2.39E-12
3.416133	7.48E-12	4.65E-10	1.87E-10	2.38E-11	-3.25E-12
3.470567	7.56E-12	4.88E-10	2.05E-10	2.06E-11	-4.29E-12
3.533067	1.87E-11	5.11E-10	2.23E-10	2.16E-11	-5.76E-12
3.583333	2.15E-11	5.25E-10	2.38E-10	2.29E-11	-5.91E-12
3.633067	2.49E-11	5.40E-10	2.55E-10	1.97E-11	-4.15E-12
3.68385	2.77E-11	5.40E-10	2.71E-10	1.96E-11	-3.60E-12
3.73385	3.25E-11	5.47E-10	2.96E-10	2.10E-11	-2.79E-12
3.783583	2.64E-11	5.54E-10	3.21E-10	2.19E-11	-2.63E-12
3.833067	2.72E-11	5.55E-10	3.24E-10	1.92E-11	-2.58E-12
3.883067	2.77E-11	5.68E-10	3.44E-10	2.08E-11	-4.40E-12
3.93255	2.86E-11	5.83E-10	3.60E-10	2.00E-11	-4.96E-12
3.983333	2.56E-11	5.98E-10	3.70E-10	2.15E-11	-4.80E-12
4.033333	2.80E-11	6.14E-10	3.81E-10	2.10E-11	-4.20E-12
4.09035	3.46E-11	6.31E-10	4.17E-10	2.07E-11	-4.63E-12
4.150767	4.09E-11	6.47E-10	4.30E-10	1.87E-11	-3.95E-12
4.200517	4.94E-11	6.61E-10	4.46E-10	2.14E-11	-3.39E-12
4.250767	5.39E-11	6.71E-10	4.65E-10	2.04E-11	-4.40E-12

4.30155	5.88E-11	6.82E-10	4.94E-10	1.82E-11	-3.71E-12
4.35025	5.95E-11	6.87E-10	5.26E-10	1.89E-11	-2.88E-12
4.404683	6.01E-11	6.86E-10	5.73E-10	1.76E-11	-3.57E-12
4.466667	5.97E-11	6.96E-10	6.15E-10	1.37E-11	-2.51E-12
4.520567	6.11E-11	7.11E-10	6.60E-10	1.39E-11	-2.95E-12
4.58385	6.42E-11	7.16E-10	6.75E-10	1.54E-11	-2.63E-12
4.633067	6.85E-11	7.21E-10	7.17E-10	1.70E-11	-2.31E-12
4.683333	7.45E-11	7.27E-10	7.56E-10	1.45E-11	-1.15E-12
4.7341	7.83E-11	7.33E-10	7.92E-10	1.69E-11	-2.77E-12
4.789583	8.63E-11	7.32E-10	8.13E-10	1.28E-11	-3.02E-12
4.850517	9.10E-11	7.40E-10	8.69E-10	1.40E-11	-4.22E-12
4.9052	9.34E-11	7.46E-10	8.93E-10	1.17E-11	-5.32E-12
4.967183	9.44E-11	7.55E-10	9.16E-10	1.52E-11	-7.39E-12
5.0164	9.98E-11	7.64E-10	9.39E-10	1.43E-11	-7.61E-12
5.067183	1.00E-10	7.64E-10	1.00E-09	1.72E-11	-6.73E-12
5.117183	1.07E-10	7.63E-10	1.03E-09	1.44E-11	-7.19E-12
5.167183	1.10E-10	7.62E-10	1.07E-09	1.63E-11	-6.55E-12
5.216917	1.13E-10	7.70E-10	1.08E-09	1.44E-11	-5.63E-12
5.266667	1.14E-10	7.70E-10	1.11E-09	1.56E-11	-6.14E-12
5.317433	1.18E-10	7.78E-10	1.10E-09	1.39E-11	-6.69E-12
5.3664	1.11E-10	7.86E-10	1.11E-09	1.28E-11	-6.84E-12
5.4216	1.13E-10	8.05E-10	1.11E-09	9.95E-12	-6.08E-12
5.483333	1.16E-10	8.00E-10	1.14E-09	1.42E-11	-6.30E-12
5.533583	1.19E-10	8.00E-10	1.14E-09	1.57E-11	-5.49E-12
5.5828	1.26E-10	7.96E-10	1.15E-09	1.80E-11	-4.53E-12
5.6341	1.31E-10	7.95E-10	1.18E-09	1.97E-11	-3.03E-12
5.683333	1.37E-10	7.94E-10	1.18E-09	2.30E-11	-4.39E-12
5.733583	1.41E-10	7.95E-10	1.19E-09	1.91E-11	-3.49E-12
5.783583	1.39E-10	8.08E-10	1.23E-09	1.46E-11	-3.68E-12
5.833333	1.38E-10	8.16E-10	1.24E-09	1.56E-11	-3.45E-12
5.883333	1.44E-10	8.23E-10	1.22E-09	1.61E-11	-3.34E-12
5.93385	1.45E-10	8.19E-10	1.25E-09	1.33E-11	-2.38E-12
5.983067	1.44E-10	8.38E-10	1.27E-09	1.27E-11	-3.08E-12
6.033583	1.50E-10	8.30E-10	1.27E-09	1.70E-11	-3.07E-12
6.083583	1.56E-10	8.24E-10	1.28E-09	1.38E-11	-4.09E-12
6.133583	1.51E-10	8.27E-10	1.28E-09	1.61E-11	-6.07E-12
6.18385	1.51E-10	8.33E-10	1.31E-09	1.73E-11	-6.72E-12
6.233583	1.55E-10	8.21E-10	1.31E-09	1.75E-11	-6.70E-12
6.283583	1.59E-10	8.22E-10	1.31E-09	1.45E-11	-7.61E-12
6.333333	1.51E-10	8.27E-10	1.30E-09	1.48E-11	-7.71E-12
6.38385	1.49E-10	8.17E-10	1.32E-09	1.26E-11	-7.51E-12
6.4328	1.50E-10	8.10E-10	1.31E-09	1.50E-11	-6.65E-12
6.483583	1.48E-10	8.09E-10	1.33E-09	1.67E-11	-5.89E-12
6.5375	1.40E-10	8.13E-10	1.35E-09	1.75E-11	-5.24E-12
6.60025	1.39E-10	8.21E-10	1.40E-09	1.75E-11	-5.35E-12

6.65025	1.47E-10	8.36E-10	1.44E-09	1.87E-11	-5.04E-12
6.700517	1.43E-10	8.51E-10	1.43E-09	1.58E-11	-6.70E-12
6.75025	1.48E-10	8.53E-10	1.40E-09	1.68E-11	-7.82E-12
6.799467	1.57E-10	8.51E-10	1.38E-09	1.68E-11	-7.26E-12
6.849467	1.65E-10	8.49E-10	1.37E-09	1.71E-11	-7.87E-12
6.900517	1.70E-10	8.46E-10	1.37E-09	1.90E-11	-7.75E-12
6.949467	1.82E-10	8.37E-10	1.36E-09	2.09E-11	-6.93E-12
7.004167	1.72E-10	8.41E-10	1.37E-09	1.80E-11	-6.48E-12
7.067183	1.65E-10	8.54E-10	1.37E-09	1.80E-11	-6.81E-12
7.117183	1.62E-10	8.63E-10	1.33E-09	1.89E-11	-6.29E-12
7.166667	1.54E-10	8.60E-10	1.31E-09	1.43E-11	-6.82E-12
7.217183	1.47E-10	8.66E-10	1.33E-09	1.52E-11	-7.01E-12
7.266133	1.56E-10	8.68E-10	1.33E-09	1.46E-11	-7.37E-12
7.3164	1.57E-10	8.63E-10	1.33E-09	1.37E-11	-8.10E-12
7.3664	1.57E-10	8.65E-10	1.34E-09	1.02E-11	-6.80E-12
7.416667	1.58E-10	8.76E-10	1.32E-09	1.11E-11	-6.89E-12
7.466667	1.63E-10	8.79E-10	1.34E-09	9.02E-12	-7.34E-12
7.516667	1.66E-10	8.80E-10	1.36E-09	1.37E-11	-8.20E-12
7.567183	1.73E-10	8.81E-10	1.36E-09	1.30E-11	-7.56E-12
7.617183	1.77E-10	8.72E-10	1.39E-09	1.26E-11	-8.54E-12
7.666667	1.79E-10	8.82E-10	1.40E-09	1.44E-11	-8.51E-12
7.7164	1.76E-10	8.77E-10	1.38E-09	1.53E-11	-8.66E-12
7.766917	1.71E-10	8.93E-10	1.35E-09	1.23E-11	-8.62E-12
7.817433	1.65E-10	9.02E-10	1.37E-09	1.27E-11	-8.09E-12
7.866917	1.61E-10	9.13E-10	1.33E-09	1.82E-11	-9.06E-12
7.916917	1.63E-10	8.97E-10	1.33E-09	1.61E-11	-8.84E-12
7.967433	1.64E-10	9.06E-10	1.33E-09	1.53E-11	-8.61E-12
8.017433	1.71E-10	8.93E-10	1.37E-09	1.55E-11	-7.58E-12
8.066917	1.79E-10	8.90E-10	1.38E-09	1.58E-11	-8.78E-12
8.1164	1.77E-10	8.87E-10	1.39E-09	1.30E-11	-8.19E-12
8.1664	1.85E-10	8.92E-10	1.37E-09	1.53E-11	-7.92E-12
8.216133	1.88E-10	8.93E-10	1.40E-09	1.78E-11	-7.22E-12
8.267433	1.79E-10	8.89E-10	1.38E-09	1.75E-11	-6.88E-12
8.322133	1.75E-10	8.93E-10	1.40E-09	1.87E-11	-6.85E-12
8.383583	1.78E-10	8.88E-10	1.41E-09	2.22E-11	-6.34E-12
8.4341	1.73E-10	8.90E-10	1.44E-09	1.99E-11	-5.93E-12
8.483333	1.71E-10	8.94E-10	1.42E-09	1.61E-11	-5.67E-12
8.533333	1.70E-10	9.13E-10	1.44E-09	1.73E-11	-5.79E-12
8.58385	1.70E-10	9.12E-10	1.45E-09	1.74E-11	-5.17E-12
8.63905	1.69E-10	9.22E-10	1.44E-09	1.47E-11	-5.62E-12
8.70025	1.64E-10	9.24E-10	1.44E-09	1.28E-11	-6.53E-12
8.75	1.68E-10	9.16E-10	1.46E-09	1.49E-11	-6.73E-12
8.8	1.75E-10	9.12E-10	1.43E-09	1.41E-11	-6.70E-12
8.85	1.69E-10	9.19E-10	1.40E-09	1.46E-11	-6.28E-12
8.90025	1.76E-10	9.16E-10	1.38E-09	1.42E-11	-5.80E-12

8.95	1.78E-10	9.23E-10	1.40E-09	1.72E-11	-5.19E-12
9	1.79E-10	9.30E-10	1.40E-09	1.51E-11	-4.57E-12
9.049733	1.76E-10	9.16E-10	1.41E-09	1.63E-11	-4.85E-12
9.100517	1.79E-10	9.09E-10	1.39E-09	1.63E-11	-5.42E-12
9.15025	1.74E-10	9.09E-10	1.39E-09	1.72E-11	-6.03E-12
9.201033	1.73E-10	9.07E-10	1.34E-09	1.65E-11	-7.23E-12
9.25	1.65E-10	9.15E-10	1.33E-09	1.71E-11	-7.87E-12
9.316917	1.67E-10	9.22E-10	1.34E-09	1.52E-11	-7.98E-12
9.367183	1.70E-10	9.24E-10	1.38E-09	1.48E-11	-8.55E-12
9.417183	1.71E-10	9.18E-10	1.39E-09	1.41E-11	-8.55E-12
9.4664	1.80E-10	9.22E-10	1.42E-09	1.73E-11	-8.38E-12
9.516917	1.80E-10	9.27E-10	1.39E-09	1.94E-11	-9.84E-12
9.5664	1.76E-10	9.32E-10	1.36E-09	1.97E-11	-9.78E-12
9.617183	1.71E-10	9.48E-10	1.31E-09	1.92E-11	-9.94E-12
9.666917	1.73E-10	9.56E-10	1.32E-09	2.14E-11	-9.26E-12
9.719	1.58E-10	9.52E-10	1.32E-09	1.86E-11	-7.97E-12
9.766917	1.57E-10	9.49E-10	1.33E-09	1.61E-11	-7.66E-12
9.8177	1.64E-10	9.49E-10	1.37E-09	1.81E-11	-8.52E-12
9.866667	1.75E-10	9.46E-10	1.39E-09	1.73E-11	-7.83E-12
9.917967	1.82E-10	9.62E-10	1.37E-09	1.59E-11	-8.37E-12
9.968217	1.91E-10	9.59E-10	1.36E-09	1.88E-11	-7.85E-12
10.01692	1.91E-10	9.52E-10	1.41E-09	2.16E-11	-7.54E-12
10.0664	1.90E-10	9.51E-10	1.40E-09	2.36E-11	-7.15E-12
10.11692	1.91E-10	9.40E-10	1.44E-09	2.54E-11	-7.18E-12
10.16743	1.81E-10	9.34E-10	1.43E-09	2.52E-11	-7.57E-12
10.21743	1.76E-10	9.36E-10	1.47E-09	2.11E-11	-8.41E-12
10.26667	1.79E-10	9.47E-10	1.41E-09	2.15E-11	-6.73E-12
10.31718	1.77E-10	9.56E-10	1.38E-09	2.14E-11	-6.73E-12
10.36667	1.69E-10	9.69E-10	1.34E-09	2.03E-11	-6.96E-12
10.41718	1.73E-10	9.56E-10	1.36E-09	1.93E-11	-6.41E-12
10.48358	1.72E-10	9.61E-10	1.33E-09	2.25E-11	-6.01E-12
10.53358	1.71E-10	9.63E-10	1.35E-09	2.27E-11	-7.30E-12
10.5841	1.71E-10	9.68E-10	1.38E-09	1.94E-11	-6.69E-12
10.6328	1.75E-10	9.65E-10	1.37E-09	1.90E-11	-5.78E-12
10.68437	1.79E-10	9.69E-10	1.37E-09	1.81E-11	-5.03E-12
10.73385	1.90E-10	9.66E-10	1.34E-09	1.43E-11	-6.16E-12
10.78358	1.95E-10	9.64E-10	1.37E-09	1.10E-11	-4.43E-12
10.83385	1.99E-10	9.66E-10	1.34E-09	9.61E-12	-4.57E-12
10.88385	1.92E-10	9.65E-10	1.33E-09	8.94E-12	-5.35E-12
10.93358	1.82E-10	9.81E-10	1.35E-09	8.65E-12	-6.99E-12
10.98385	1.81E-10	9.83E-10	1.35E-09	8.70E-12	-5.82E-12
11.03437	1.79E-10	9.86E-10	1.32E-09	1.16E-11	-7.33E-12
11.08358	1.74E-10	9.79E-10	1.33E-09	1.15E-11	-7.90E-12
11.1341	1.76E-10	9.76E-10	1.33E-09	1.32E-11	-7.19E-12
11.18385	1.80E-10	9.70E-10	1.30E-09	1.38E-11	-6.44E-12

11.23385	1.71E-10	9.79E-10	1.31E-09	1.27E-11	-6.68E-12
11.28333	1.71E-10	9.70E-10	1.31E-09	1.19E-11	-7.22E-12
11.33385	1.81E-10	9.68E-10	1.30E-09	1.16E-11	-6.94E-12
11.3841	1.78E-10	9.69E-10	1.29E-09	1.30E-11	-7.65E-12
11.4341	1.73E-10	9.71E-10	1.27E-09	1.31E-11	-7.35E-12
11.4841	1.65E-10	9.74E-10	1.28E-09	1.57E-11	-7.79E-12
11.5341	1.67E-10	9.88E-10	1.29E-09	1.36E-11	-7.88E-12
11.58358	1.64E-10	9.98E-10	1.27E-09	1.54E-11	-7.57E-12
11.63333	1.70E-10	1.01E-09	1.29E-09	1.38E-11	-8.62E-12
11.6828	1.78E-10	1.00E-09	1.30E-09	1.36E-11	-8.53E-12
11.73385	1.87E-10	1.01E-09	1.29E-09	1.24E-11	-9.43E-12
11.78437	1.86E-10	1.00E-09	1.28E-09	1.47E-11	-8.71E-12
11.83307	1.79E-10	9.95E-10	1.31E-09	1.44E-11	-8.30E-12
11.88307	1.79E-10	9.90E-10	1.33E-09	1.63E-11	-6.04E-12
11.93358	1.83E-10	9.99E-10	1.32E-09	1.64E-11	-6.85E-12
11.9828	1.84E-10	9.84E-10	1.33E-09	1.59E-11	-5.18E-12
12.03385	1.92E-10	9.84E-10	1.31E-09	1.60E-11	-5.23E-12
12.10025	1.91E-10	9.88E-10	1.31E-09	1.32E-11	-6.30E-12
12.15025	1.88E-10	1.01E-09	1.28E-09	1.42E-11	-7.24E-12
12.19973	1.80E-10	9.99E-10	1.27E-09	1.69E-11	-7.15E-12
12.25103	1.78E-10	1.01E-09	1.27E-09	1.90E-11	-8.31E-12
12.30025	1.69E-10	1.02E-09	1.28E-09	1.79E-11	-8.26E-12
12.35077	1.68E-10	1.02E-09	1.28E-09	1.99E-11	-8.40E-12
12.40025	1.69E-10	1.01E-09	1.28E-09	2.02E-11	-8.57E-12
12.45	1.75E-10	1.01E-09	1.32E-09	1.76E-11	-9.38E-12
12.5	1.74E-10	1.01E-09	1.32E-09	1.58E-11	-8.83E-12
12.55	1.70E-10	1.01E-09	1.34E-09	1.55E-11	-9.68E-12
12.60025	1.72E-10	1.01E-09	1.35E-09	1.42E-11	-9.57E-12
12.64922	1.79E-10	9.98E-10	1.37E-09	1.13E-11	-8.96E-12
12.70077	1.66E-10	1.00E-09	1.31E-09	9.16E-12	-7.63E-12
12.74973	1.67E-10	9.99E-10	1.28E-09	9.55E-12	-7.79E-12
12.80025	1.72E-10	1.01E-09	1.26E-09	1.11E-11	-7.45E-12
12.85	1.74E-10	1.01E-09	1.25E-09	1.55E-11	-7.21E-12
12.90077	1.73E-10	1.01E-09	1.25E-09	1.46E-11	-7.35E-12
12.95	1.79E-10	1.01E-09	1.31E-09	1.65E-11	-7.30E-12
13.00077	1.86E-10	1.02E-09	1.34E-09	1.57E-11	-7.26E-12
13.0664	1.93E-10	1.01E-09	1.37E-09	1.42E-11	-7.74E-12
13.11667	1.96E-10	1.01E-09	1.37E-09	1.18E-11	-7.29E-12
13.16692	1.97E-10	1.02E-09	1.34E-09	1.39E-11	-7.63E-12
13.2177	1.98E-10	1.03E-09	1.30E-09	1.59E-11	-6.89E-12
13.26692	1.94E-10	1.02E-09	1.27E-09	2.11E-11	-6.85E-12
13.31718	1.88E-10	1.02E-09	1.23E-09	1.98E-11	-6.41E-12
13.36667	1.86E-10	1.02E-09	1.19E-09	2.09E-11	-6.05E-12
13.41667	1.74E-10	1.02E-09	1.23E-09	1.81E-11	-6.21E-12
13.4664	1.73E-10	1.01E-09	1.24E-09	1.50E-11	-8.01E-12

13.5164	1.73E-10	1.02E-09	1.27E-09	1.35E-11	-7.65E-12
13.56667	1.74E-10	1.02E-09	1.26E-09	1.38E-11	-6.77E-12
13.6164	1.63E-10	1.01E-09	1.28E-09	1.03E-11	-6.71E-12
13.66743	1.70E-10	1.01E-09	1.27E-09	1.26E-11	-6.08E-12
13.71692	1.66E-10	1.02E-09	1.26E-09	1.15E-11	-4.28E-12
13.76667	1.66E-10	1.02E-09	1.22E-09	1.17E-11	-5.33E-12
13.81743	1.61E-10	1.03E-09	1.24E-09	1.05E-11	-5.33E-12
13.86692	1.64E-10	1.03E-09	1.27E-09	1.43E-11	-6.42E-12
13.91692	1.68E-10	1.03E-09	1.26E-09	1.14E-11	-6.69E-12
13.96692	1.68E-10	1.03E-09	1.26E-09	1.28E-11	-7.85E-12
14.01667	1.62E-10	1.04E-09	1.27E-09	7.18E-12	-7.45E-12
14.06667	1.66E-10	1.05E-09	1.24E-09	9.20E-12	-8.81E-12
14.11797	1.73E-10	1.05E-09	1.24E-09	5.92E-12	-8.21E-12
14.16692	1.66E-10	1.05E-09	1.24E-09	6.18E-12	-9.07E-12
14.21667	1.68E-10	1.03E-09	1.26E-09	9.77E-12	-9.57E-12
14.26667	1.70E-10	1.02E-09	1.26E-09	1.72E-11	-9.82E-12
14.3177	1.72E-10	1.02E-09	1.28E-09	1.54E-11	-9.45E-12
14.36692	1.78E-10	1.01E-09	1.24E-09	1.66E-11	-8.94E-12
14.41667	1.79E-10	1.01E-09	1.23E-09	2.01E-11	-9.53E-12
14.46718	1.78E-10	1.02E-09	1.22E-09	1.99E-11	-8.78E-12
14.53358	1.85E-10	1.04E-09	1.21E-09	1.72E-11	-7.69E-12
14.58567	1.78E-10	1.05E-09	1.22E-09	1.64E-11	-7.62E-12
14.6341	1.67E-10	1.06E-09	1.23E-09	1.62E-11	-8.81E-12
14.68358	1.64E-10	1.06E-09	1.26E-09	1.35E-11	-7.60E-12
14.73385	1.76E-10	1.07E-09	1.26E-09	1.12E-11	-7.76E-12
14.78358	1.76E-10	1.06E-09	1.24E-09	1.39E-11	-7.77E-12
14.83358	1.82E-10	1.04E-09	1.22E-09	1.88E-11	-7.92E-12
14.88307	1.84E-10	1.03E-09	1.25E-09	1.77E-11	-7.90E-12
14.93385	1.88E-10	1.04E-09	1.26E-09	1.59E-11	-7.98E-12
14.98437	1.80E-10	1.03E-09	1.23E-09	1.65E-11	-8.07E-12
15.03488	1.70E-10	1.04E-09	1.25E-09	1.00E-11	-9.10E-12
15.08463	1.66E-10	1.05E-09	1.25E-09	9.08E-12	-9.13E-12
15.13385	1.68E-10	1.05E-09	1.23E-09	8.87E-12	-8.72E-12
15.18385	1.70E-10	1.05E-09	1.22E-09	1.25E-11	-8.45E-12
15.23358	1.70E-10	1.06E-09	1.22E-09	1.02E-11	-8.40E-12
15.28333	1.72E-10	1.05E-09	1.19E-09	1.25E-11	-8.23E-12
15.3341	1.71E-10	1.05E-09	1.18E-09	9.83E-12	-6.99E-12
15.38488	1.74E-10	1.05E-09	1.17E-09	1.37E-11	-7.55E-12
15.43542	1.77E-10	1.06E-09	1.14E-09	1.23E-11	-7.23E-12
15.4841	1.74E-10	1.06E-09	1.14E-09	1.34E-11	-7.60E-12
15.53488	1.78E-10	1.08E-09	1.17E-09	1.09E-11	-8.33E-12
15.5841	1.87E-10	1.08E-09	1.17E-09	1.18E-11	-8.74E-12
15.63515	1.80E-10	1.08E-09	1.16E-09	7.95E-12	-8.34E-12
15.6841	1.75E-10	1.08E-09	1.18E-09	9.16E-12	-9.67E-12
15.73542	1.75E-10	1.07E-09	1.20E-09	1.29E-11	-9.97E-12

15.78437	1.75E-10	1.06E-09	1.19E-09	1.84E-11	-9.37E-12
15.83385	1.63E-10	1.06E-09	1.21E-09	1.77E-11	-1.02E-11
15.88333	1.69E-10	1.07E-09	1.20E-09	2.01E-11	-1.00E-11
15.93333	1.63E-10	1.06E-09	1.19E-09	1.78E-11	-9.86E-12
15.98488	1.66E-10	1.06E-09	1.17E-09	1.42E-11	-9.74E-12
16.0341	1.64E-10	1.06E-09	1.16E-09	1.18E-11	-9.70E-12
16.10103	1.71E-10	1.06E-09	1.15E-09	1.28E-11	-9.55E-12
16.15052	1.72E-10	1.07E-09	1.16E-09	1.35E-11	-9.36E-12
16.20052	1.71E-10	1.08E-09	1.17E-09	1.42E-11	-9.08E-12
16.25052	1.77E-10	1.07E-09	1.18E-09	1.79E-11	-7.95E-12
16.30103	1.79E-10	1.06E-09	1.16E-09	1.73E-11	-8.16E-12
16.35025	1.76E-10	1.06E-09	1.14E-09	1.84E-11	-9.14E-12
16.40103	1.73E-10	1.06E-09	1.15E-09	1.62E-11	-1.02E-11
16.45025	1.79E-10	1.06E-09	1.17E-09	1.51E-11	-9.54E-12
16.5	1.73E-10	1.06E-09	1.15E-09	1.48E-11	-1.10E-11
16.55077	1.71E-10	1.06E-09	1.15E-09	1.40E-11	-1.02E-11
16.60077	1.65E-10	1.06E-09	1.17E-09	1.59E-11	-8.30E-12
16.65	1.67E-10	1.05E-09	1.15E-09	1.85E-11	-7.20E-12
16.70103	1.73E-10	1.05E-09	1.11E-09	2.15E-11	-7.42E-12
16.75052	1.80E-10	1.06E-09	1.10E-09	2.15E-11	-6.89E-12
16.80025	1.73E-10	1.06E-09	1.13E-09	2.49E-11	-7.39E-12
16.85052	1.80E-10	1.06E-09	1.12E-09	2.16E-11	-9.01E-12
16.90025	1.72E-10	1.07E-09	1.13E-09	2.10E-11	-8.64E-12
16.95	1.67E-10	1.07E-09	1.13E-09	1.97E-11	-9.34E-12
17	1.59E-10	1.08E-09	1.16E-09	1.97E-11	-8.35E-12
17.04973	1.66E-10	1.08E-09	1.17E-09	1.59E-11	-8.16E-12
17.09973	1.66E-10	1.08E-09	1.18E-09	1.52E-11	-7.65E-12
17.15025	1.67E-10	1.08E-09	1.15E-09	1.27E-11	-8.63E-12
17.19947	1.66E-10	1.08E-09	1.15E-09	1.17E-11	-8.39E-12
17.25052	1.68E-10	1.08E-09	1.14E-09	1.11E-11	-8.75E-12
17.30025	1.67E-10	1.08E-09	1.11E-09	1.24E-11	-9.25E-12
17.34973	1.63E-10	1.09E-09	1.08E-09	1.19E-11	-8.96E-12
17.41692	1.69E-10	1.08E-09	1.08E-09	1.27E-11	-8.74E-12
17.46667	1.70E-10	1.08E-09	1.08E-09	1.38E-11	-8.71E-12
17.51718	1.74E-10	1.06E-09	1.08E-09	1.39E-11	-8.63E-12
17.56613	1.73E-10	1.07E-09	1.08E-09	1.28E-11	-8.14E-12
17.61692	1.71E-10	1.06E-09	1.11E-09	1.41E-11	-8.35E-12
17.66692	1.71E-10	1.06E-09	1.14E-09	1.53E-11	-8.97E-12
17.71667	1.73E-10	1.06E-09	1.12E-09	1.82E-11	-9.40E-12
17.76667	1.64E-10	1.08E-09	1.12E-09	1.50E-11	-1.03E-11
17.81718	1.73E-10	1.07E-09	1.13E-09	1.65E-11	-1.03E-11
17.86718	1.75E-10	1.08E-09	1.14E-09	1.55E-11	-1.04E-11
17.9177	1.71E-10	1.07E-09	1.09E-09	1.28E-11	-1.02E-11
17.96667	1.69E-10	1.09E-09	1.11E-09	7.91E-12	-1.01E-11
18.01613	1.78E-10	1.08E-09	1.12E-09	8.83E-12	-8.41E-12

18.06718	1.73E-10	1.08E-09	1.09E-09	6.31E-12	-8.69E-12
18.11692	1.79E-10	1.08E-09	1.08E-09	6.89E-12	-8.00E-12
18.16692	1.82E-10	1.08E-09	1.11E-09	6.47E-12	-7.35E-12
18.21692	1.84E-10	1.08E-09	1.11E-09	6.21E-12	-7.04E-12
18.26667	1.76E-10	1.09E-09	1.12E-09	6.72E-12	-7.53E-12
18.31613	1.74E-10	1.09E-09	1.11E-09	7.85E-12	-7.09E-12
18.36667	1.75E-10	1.09E-09	1.10E-09	9.76E-12	-6.78E-12
18.41718	1.81E-10	1.09E-09	1.07E-09	1.11E-11	-7.27E-12
18.46667	1.77E-10	1.09E-09	1.09E-09	1.25E-11	-7.89E-12
18.5164	1.83E-10	1.07E-09	1.08E-09	1.29E-11	-7.95E-12
18.56743	1.82E-10	1.08E-09	1.09E-09	1.53E-11	-9.32E-12
18.61692	1.75E-10	1.08E-09	1.09E-09	1.50E-11	-1.07E-11
18.66692	1.74E-10	1.08E-09	1.09E-09	1.28E-11	-1.10E-11
18.71692	1.84E-10	1.08E-09	1.07E-09	1.28E-11	-9.40E-12
18.76692	1.75E-10	1.09E-09	1.06E-09	1.36E-11	-9.73E-12
18.81667	1.72E-10	1.09E-09	1.08E-09	1.17E-11	-8.95E-12
18.86692	1.77E-10	1.10E-09	1.06E-09	1.19E-11	-8.05E-12
18.91692	1.75E-10	1.11E-09	1.07E-09	1.30E-11	-7.60E-12
18.96692	1.65E-10	1.11E-09	1.09E-09	1.50E-11	-9.48E-12
19.01692	1.71E-10	1.11E-09	1.07E-09	1.44E-11	-9.94E-12
19.06692	1.74E-10	1.12E-09	1.05E-09	1.42E-11	-8.79E-12
19.1164	1.74E-10	1.12E-09	1.06E-09	1.08E-11	-9.54E-12
19.16718	1.66E-10	1.11E-09	1.09E-09	1.29E-11	-9.22E-12
19.21718	1.69E-10	1.11E-09	1.07E-09	1.11E-11	-7.72E-12
19.26692	1.65E-10	1.11E-09	1.06E-09	8.27E-12	-8.58E-12
19.31667	1.70E-10	1.10E-09	1.06E-09	9.10E-12	-8.63E-12
19.36692	1.64E-10	1.11E-09	1.06E-09	1.22E-11	-8.21E-12
19.41718	1.68E-10	1.12E-09	1.05E-09	1.49E-11	-8.18E-12
19.46822	1.67E-10	1.13E-09	1.04E-09	1.50E-11	-8.65E-12
19.51692	1.73E-10	1.13E-09	1.04E-09	1.70E-11	-7.46E-12
19.56692	1.73E-10	1.13E-09	1.05E-09	1.69E-11	-7.95E-12
19.61743	1.83E-10	1.12E-09	1.04E-09	1.67E-11	-7.83E-12
19.66743	1.88E-10	1.12E-09	1.06E-09	1.41E-11	-7.60E-12
19.7164	1.88E-10	1.11E-09	1.07E-09	1.43E-11	-8.62E-12
19.76718	1.82E-10	1.10E-09	1.05E-09	1.52E-11	-8.77E-12
19.81692	1.79E-10	1.11E-09	1.11E-09	1.37E-11	-8.55E-12
19.86667	1.69E-10	1.12E-09	1.12E-09	1.23E-11	-8.24E-12
19.91667	1.68E-10	1.13E-09	1.11E-09	1.27E-11	-8.72E-12
19.96718	1.77E-10	1.12E-09	1.12E-09	1.20E-11	-7.15E-12
20.01743	1.81E-10	1.11E-09	1.13E-09	9.51E-12	-6.20E-12
20.06667	1.79E-10	1.12E-09	1.08E-09	1.13E-11	-5.50E-12
20.11667	1.84E-10	1.12E-09	1.07E-09	1.18E-11	-5.80E-12
20.16588	1.79E-10	1.13E-09	1.05E-09	1.31E-11	-4.87E-12
20.21692	1.68E-10	1.14E-09	1.01E-09	1.47E-11	-5.25E-12
20.26667	1.70E-10	1.15E-09	1.03E-09	1.68E-11	-4.74E-12

20.31692	1.77E-10	1.15E-09	1.04E-09	1.80E-11	-6.23E-12
20.36692	1.78E-10	1.14E-09	1.05E-09	1.71E-11	-5.88E-12
20.41667	1.76E-10	1.14E-09	1.04E-09	1.35E-11	-6.49E-12
20.4664	1.80E-10	1.14E-09	1.09E-09	1.15E-11	-6.58E-12
20.51718	1.77E-10	1.14E-09	1.08E-09	9.77E-12	-7.54E-12
20.56667	1.72E-10	1.14E-09	1.08E-09	1.01E-11	-7.60E-12
20.63358	1.68E-10	1.14E-09	1.08E-09	9.94E-12	-6.79E-12
20.69973	1.70E-10	1.13E-09	1.08E-09	9.95E-12	-6.55E-12
20.75103	1.70E-10	1.13E-09	1.04E-09	1.18E-11	-6.35E-12
20.80025	1.76E-10	1.13E-09	1.05E-09	1.41E-11	-6.63E-12
20.85025	1.70E-10	1.13E-09	1.02E-09	1.32E-11	-6.20E-12
20.9	1.71E-10	1.13E-09	1.04E-09	1.15E-11	-7.21E-12
20.95	1.71E-10	1.14E-09	1.02E-09	1.55E-11	-7.96E-12
21.00077	1.65E-10	1.13E-09	1.06E-09	1.26E-11	-8.69E-12
21.05	1.60E-10	1.13E-09	1.04E-09	9.51E-12	-9.26E-12
21.1	1.66E-10	1.14E-09	1.06E-09	9.28E-12	-9.44E-12
21.14973	1.62E-10	1.15E-09	1.02E-09	1.27E-11	-9.74E-12
21.19947	1.66E-10	1.14E-09	1.03E-09	1.00E-11	-9.29E-12
21.24973	1.75E-10	1.15E-09	9.85E-10	1.47E-11	-9.60E-12
21.29947	1.72E-10	1.15E-09	1.00E-09	1.63E-11	-9.51E-12
21.35	1.66E-10	1.15E-09	1.02E-09	1.56E-11	-8.61E-12
21.40052	1.70E-10	1.14E-09	1.04E-09	1.22E-11	-8.97E-12
21.45	1.68E-10	1.14E-09	1.03E-09	1.29E-11	-9.70E-12
21.50052	1.69E-10	1.15E-09	1.02E-09	1.44E-11	-9.19E-12
21.55	1.69E-10	1.16E-09	9.82E-10	1.41E-11	-9.08E-12
21.59973	1.72E-10	1.15E-09	9.48E-10	1.59E-11	-9.78E-12
21.65	1.67E-10	1.16E-09	9.42E-10	1.72E-11	-8.67E-12
21.7	1.61E-10	1.15E-09	9.34E-10	1.72E-11	-7.50E-12
21.75052	1.55E-10	1.15E-09	9.29E-10	1.19E-11	-8.06E-12
21.80025	1.61E-10	1.16E-09	9.40E-10	1.18E-11	-7.61E-12
21.85	1.68E-10	1.16E-09	9.79E-10	1.00E-11	-6.92E-12
21.90103	1.73E-10	1.15E-09	9.71E-10	1.24E-11	-7.75E-12
21.95025	1.79E-10	1.15E-09	1.01E-09	1.50E-11	-8.05E-12
22.00052	1.72E-10	1.15E-09	1.03E-09	1.79E-11	-8.05E-12
22.05025	1.70E-10	1.15E-09	1.02E-09	1.73E-11	-8.10E-12
22.1	1.63E-10	1.14E-09	1.00E-09	1.70E-11	-8.09E-12
22.14947	1.64E-10	1.15E-09	1.00E-09	1.63E-11	-7.80E-12
22.20077	1.60E-10	1.16E-09	9.73E-10	1.18E-11	-8.03E-12
22.25	1.65E-10	1.17E-09	9.52E-10	9.24E-12	-7.93E-12
22.30077	1.63E-10	1.16E-09	9.56E-10	1.03E-11	-9.12E-12
22.36667	1.65E-10	1.17E-09	9.70E-10	1.17E-11	-1.05E-11
22.41692	1.58E-10	1.15E-09	9.76E-10	1.04E-11	-1.09E-11
22.46743	1.63E-10	1.14E-09	9.91E-10	9.92E-12	-1.05E-11
22.51692	1.63E-10	1.13E-09	1.00E-09	9.77E-12	-1.02E-11
22.56692	1.67E-10	1.14E-09	1.02E-09	9.83E-12	-9.99E-12

22.6177	1.66E-10	1.14E-09	9.99E-10	1.05E-11	-9.68E-12
22.66743	1.66E-10	1.15E-09	9.95E-10	1.22E-11	-9.49E-12
22.7164	1.73E-10	1.14E-09	9.83E-10	1.27E-11	-1.05E-11
22.7664	1.71E-10	1.13E-09	9.70E-10	1.52E-11	-1.03E-11
22.81692	1.64E-10	1.13E-09	9.62E-10	1.60E-11	-9.60E-12
22.86667	1.55E-10	1.14E-09	9.65E-10	1.44E-11	-1.03E-11
22.91718	1.63E-10	1.14E-09	9.56E-10	1.19E-11	-9.22E-12
22.96692	1.53E-10	1.15E-09	9.52E-10	1.46E-11	-7.91E-12
23.01692	1.56E-10	1.14E-09	9.67E-10	1.26E-11	-6.78E-12
23.06692	1.60E-10	1.15E-09	9.67E-10	1.07E-11	-7.53E-12
23.11667	1.69E-10	1.15E-09	9.28E-10	1.13E-11	-6.02E-12
23.16692	1.70E-10	1.15E-09	9.15E-10	1.26E-11	-6.32E-12
23.2164	1.65E-10	1.15E-09	9.40E-10	1.33E-11	-7.98E-12
23.2664	1.61E-10	1.17E-09	9.44E-10	1.39E-11	-8.88E-12
23.31692	1.62E-10	1.16E-09	9.49E-10	1.45E-11	-8.28E-12
23.36667	1.60E-10	1.16E-09	9.73E-10	1.31E-11	-8.54E-12
23.4328	1.53E-10	1.17E-09	9.92E-10	1.62E-11	-9.42E-12
23.48437	1.61E-10	1.17E-09	9.85E-10	1.45E-11	-9.10E-12
23.5341	1.68E-10	1.17E-09	9.92E-10	1.36E-11	-9.11E-12
23.58358	1.69E-10	1.17E-09	9.97E-10	1.62E-11	-9.02E-12
23.65025	1.68E-10	1.16E-09	1.02E-09	1.51E-11	-8.29E-12
23.7	1.63E-10	1.17E-09	1.01E-09	1.41E-11	-8.23E-12
23.75025	1.66E-10	1.16E-09	9.99E-10	1.59E-11	-7.88E-12
23.8	1.65E-10	1.15E-09	9.56E-10	1.70E-11	-7.51E-12
23.85025	1.63E-10	1.15E-09	9.53E-10	1.41E-11	-8.56E-12
23.89947	1.64E-10	1.15E-09	9.28E-10	1.76E-11	-9.43E-12
23.95103	1.70E-10	1.14E-09	9.38E-10	1.46E-11	-9.28E-12
24.00077	1.66E-10	1.15E-09	9.68E-10	1.13E-11	-9.11E-12
24.06692	1.62E-10	1.14E-09	9.79E-10	1.39E-11	-7.85E-12
24.11692	1.56E-10	1.15E-09	9.47E-10	1.44E-11	-6.87E-12
24.16667	1.57E-10	1.15E-09	9.74E-10	1.23E-11	-7.59E-12
24.21667	1.58E-10	1.15E-09	9.79E-10	1.64E-11	-7.98E-12
24.2664	1.56E-10	1.16E-09	9.42E-10	1.59E-11	-7.42E-12
24.3164	1.57E-10	1.17E-09	9.71E-10	1.37E-11	-8.35E-12
24.3664	1.63E-10	1.19E-09	9.77E-10	1.28E-11	-8.61E-12
24.41667	1.61E-10	1.19E-09	9.39E-10	1.35E-11	-8.39E-12
24.46667	1.63E-10	1.19E-09	9.30E-10	9.86E-12	-8.50E-12
24.51718	1.68E-10	1.19E-09	9.28E-10	1.03E-11	-9.12E-12
24.56667	1.67E-10	1.19E-09	8.95E-10	7.73E-12	-9.91E-12
24.61692	1.69E-10	1.18E-09	9.31E-10	8.35E-12	-9.24E-12
24.6664	1.75E-10	1.18E-09	9.36E-10	8.78E-12	-9.76E-12
24.71718	1.75E-10	1.19E-09	9.34E-10	8.25E-12	-9.79E-12
24.7677	1.64E-10	1.19E-09	9.42E-10	9.47E-12	-1.01E-11
24.81692	1.63E-10	1.19E-09	9.57E-10	1.26E-11	-9.96E-12
24.86743	1.58E-10	1.19E-09	9.26E-10	1.51E-11	-1.05E-11

24.9177	1.54E-10	1.20E-09	9.50E-10	1.67E-11	-1.01E-11
24.96692	1.58E-10	1.20E-09	9.37E-10	1.78E-11	-9.82E-12
25.01692	1.66E-10	1.20E-09	9.20E-10	1.69E-11	-9.45E-12
25.06743	1.72E-10	1.20E-09	9.14E-10	1.74E-11	-9.80E-12
25.11667	1.69E-10	1.20E-09	9.25E-10	1.47E-11	-9.29E-12
25.1664	1.71E-10	1.20E-09	9.11E-10	1.36E-11	-8.87E-12
25.2164	1.78E-10	1.20E-09	9.25E-10	1.22E-11	-8.79E-12
25.26743	1.84E-10	1.20E-09	9.32E-10	1.46E-11	-8.37E-12
25.31743	1.82E-10	1.19E-09	9.27E-10	1.42E-11	-8.89E-12
25.36718	1.84E-10	1.19E-09	9.12E-10	1.68E-11	-9.60E-12
25.41692	1.80E-10	1.18E-09	9.04E-10	1.81E-11	-9.54E-12
25.46667	1.64E-10	1.19E-09	9.48E-10	1.79E-11	-9.94E-12
25.51667	1.68E-10	1.18E-09	9.68E-10	1.44E-11	-9.86E-12
25.56692	1.70E-10	1.20E-09	9.42E-10	1.62E-11	-8.80E-12
25.63307	1.67E-10	1.20E-09	9.65E-10	1.43E-11	-8.14E-12
25.68307	1.68E-10	1.20E-09	9.83E-10	1.45E-11	-7.25E-12
25.73385	1.68E-10	1.19E-09	9.56E-10	1.75E-11	-6.50E-12
25.78333	1.60E-10	1.21E-09	9.37E-10	2.10E-11	-7.44E-12
25.83358	1.63E-10	1.19E-09	9.92E-10	1.61E-11	-6.06E-12
25.88437	1.69E-10	1.19E-09	9.54E-10	1.62E-11	-5.89E-12
25.93307	1.68E-10	1.19E-09	9.25E-10	1.53E-11	-5.60E-12
25.98358	1.72E-10	1.20E-09	9.36E-10	1.59E-11	-5.04E-12
26.03333	1.67E-10	1.19E-09	9.22E-10	1.42E-11	-3.17E-12
26.08358	1.68E-10	1.19E-09	8.87E-10	1.79E-11	-3.86E-12
26.13385	1.62E-10	1.19E-09	9.08E-10	1.89E-11	-4.39E-12
26.20025	1.69E-10	1.21E-09	8.99E-10	1.58E-11	-5.81E-12
26.25	1.67E-10	1.22E-09	8.69E-10	1.61E-11	-7.61E-12
26.30025	1.75E-10	1.22E-09	8.86E-10	1.67E-11	-8.18E-12
26.3638	1.65E-10	1.23E-09	8.77E-10	1.36E-11	-7.18E-12
26.41978	1.70E-10	1.22E-09	8.67E-10	1.71E-11	-6.42E-12
26.46718	1.66E-10	1.22E-09	8.76E-10	1.85E-11	-7.16E-12
26.51822	1.66E-10	1.23E-09	8.75E-10	1.76E-11	-6.77E-12
26.56743	1.73E-10	1.22E-09	8.61E-10	2.02E-11	-7.41E-12
26.61667	1.66E-10	1.23E-09	8.70E-10	2.26E-11	-9.57E-12
26.66743	1.63E-10	1.23E-09	8.72E-10	1.82E-11	-1.05E-11
26.71743	1.58E-10	1.22E-09	8.78E-10	1.60E-11	-9.86E-12
26.76692	1.59E-10	1.22E-09	8.65E-10	1.41E-11	-9.89E-12
26.83307	1.42E-10	1.23E-09	8.61E-10	1.33E-11	-1.08E-11
26.88072	1.44E-10	1.22E-09	8.51E-10	1.04E-11	-1.01E-11
26.93307	1.51E-10	1.23E-09	8.57E-10	9.74E-12	-1.04E-11
26.98358	1.59E-10	1.22E-09	8.39E-10	1.26E-11	-1.02E-11
27.03358	1.59E-10	1.20E-09	8.41E-10	1.47E-11	-9.84E-12
27.08437	1.60E-10	1.20E-09	8.44E-10	1.31E-11	-8.86E-12
27.13333	1.64E-10	1.20E-09	8.63E-10	1.42E-11	-9.54E-12
27.18385	1.60E-10	1.21E-09	8.92E-10	1.68E-11	-9.24E-12

27.23358	1.63E-10	1.21E-09	9.07E-10	1.66E-11	-9.38E-12
27.28437	1.71E-10	1.23E-09	9.35E-10	1.33E-11	-9.26E-12
27.33385	1.68E-10	1.23E-09	9.31E-10	1.43E-11	-9.87E-12
27.38307	1.71E-10	1.22E-09	9.35E-10	1.37E-11	-1.02E-11
27.43385	1.68E-10	1.22E-09	9.01E-10	1.26E-11	-9.04E-12
27.48358	1.61E-10	1.24E-09	8.94E-10	1.28E-11	-9.17E-12
27.5341	1.50E-10	1.22E-09	8.44E-10	1.61E-11	-9.79E-12
27.58358	1.65E-10	1.21E-09	8.52E-10	1.63E-11	-9.20E-12
27.63307	1.60E-10	1.22E-09	8.31E-10	1.70E-11	-8.77E-12
27.68307	1.67E-10	1.22E-09	8.31E-10	1.85E-11	-8.16E-12
27.73307	1.66E-10	1.22E-09	8.14E-10	1.96E-11	-7.86E-12
27.78307	1.66E-10	1.22E-09	8.54E-10	2.11E-11	-6.52E-12
27.83358	1.56E-10	1.23E-09	8.58E-10	1.74E-11	-5.66E-12
27.88385	1.65E-10	1.22E-09	8.52E-10	1.91E-11	-5.69E-12
27.93307	1.68E-10	1.22E-09	8.58E-10	1.72E-11	-6.75E-12
27.98307	1.70E-10	1.23E-09	8.95E-10	1.53E-11	-6.25E-12
28.0341	1.73E-10	1.23E-09	8.60E-10	1.29E-11	-6.17E-12
28.08358	1.79E-10	1.22E-09	8.77E-10	1.53E-11	-6.96E-12
28.1341	1.66E-10	1.23E-09	9.18E-10	1.46E-11	-6.72E-12
28.18307	1.57E-10	1.23E-09	8.88E-10	1.55E-11	-8.04E-12
28.23358	1.55E-10	1.23E-09	8.78E-10	1.55E-11	-9.03E-12
28.28333	1.52E-10	1.23E-09	9.11E-10	1.36E-11	-9.21E-12
28.33385	1.51E-10	1.23E-09	8.93E-10	1.20E-11	-9.55E-12
28.38358	1.60E-10	1.23E-09	8.45E-10	1.19E-11	-9.94E-12
28.43358	1.54E-10	1.22E-09	8.47E-10	9.22E-12	-8.91E-12
28.48358	1.50E-10	1.23E-09	8.29E-10	8.70E-12	-7.96E-12
28.53307	1.52E-10	1.23E-09	8.08E-10	1.05E-11	-9.03E-12
28.58385	1.45E-10	1.23E-09	7.67E-10	1.16E-11	-6.30E-12
28.63307	1.43E-10	1.23E-09	7.75E-10	1.34E-11	-6.18E-12
28.68437	1.46E-10	1.24E-09	7.90E-10	1.70E-11	-6.45E-12
28.73358	1.51E-10	1.24E-09	7.90E-10	1.83E-11	-7.55E-12
28.78358	1.47E-10	1.21E-09	7.90E-10	1.64E-11	-6.38E-12
28.83358	1.53E-10	1.22E-09	8.36E-10	1.71E-11	-7.82E-12
28.8841	1.52E-10	1.22E-09	8.26E-10	1.22E-11	-7.77E-12
28.93307	1.52E-10	1.21E-09	8.30E-10	8.50E-12	-6.86E-12
28.98358	1.52E-10	1.20E-09	8.36E-10	6.66E-12	-5.93E-12
29.03385	1.61E-10	1.21E-09	8.44E-10	1.04E-11	-6.29E-12
29.08333	1.54E-10	1.21E-09	8.31E-10	1.05E-11	-6.54E-12
29.13307	1.60E-10	1.20E-09	8.51E-10	1.57E-11	-7.47E-12
29.18358	1.74E-10	1.21E-09	8.56E-10	2.04E-11	-8.20E-12
29.23333	1.70E-10	1.21E-09	8.53E-10	1.97E-11	-6.29E-12
29.28358	1.64E-10	1.21E-09	8.53E-10	1.71E-11	-6.33E-12
29.33333	1.72E-10	1.22E-09	8.41E-10	1.66E-11	-6.54E-12
29.38358	1.59E-10	1.22E-09	8.57E-10	1.49E-11	-5.13E-12
29.43358	1.56E-10	1.23E-09	8.50E-10	1.03E-11	-6.00E-12

29.48358	1.55E-10	1.24E-09	8.43E-10	1.21E-11	-8.41E-12
29.53333	1.56E-10	1.24E-09	8.43E-10	1.49E-11	-7.38E-12
29.58333	1.51E-10	1.23E-09	8.67E-10	1.80E-11	-6.54E-12
29.63307	1.54E-10	1.23E-09	8.48E-10	2.04E-11	-7.33E-12
29.6841	1.50E-10	1.23E-09	8.31E-10	2.12E-11	-6.94E-12
29.73358	1.53E-10	1.22E-09	8.44E-10	2.27E-11	-7.32E-12
29.78385	1.57E-10	1.23E-09	8.28E-10	2.01E-11	-7.60E-12
29.83307	1.52E-10	1.23E-09	8.13E-10	1.66E-11	-9.32E-12
29.88385	1.48E-10	1.24E-09	8.08E-10	1.30E-11	-8.35E-12
29.93333	1.46E-10	1.24E-09	7.99E-10	1.21E-11	-8.08E-12
29.9841	1.49E-10	1.24E-09	7.97E-10	1.11E-11	-7.15E-12
30.0341	1.41E-10	1.23E-09	8.11E-10	1.12E-11	-9.26E-12
30.08333	1.42E-10	1.24E-09	8.25E-10	1.36E-11	-8.98E-12
30.13358	1.49E-10	1.23E-09	8.02E-10	1.45E-11	-9.98E-12
30.18307	1.45E-10	1.23E-09	8.12E-10	1.38E-11	-8.56E-12
30.23358	1.44E-10	1.23E-09	7.81E-10	1.53E-11	-8.69E-12
30.28307	1.47E-10	1.23E-09	7.70E-10	1.77E-11	-7.62E-12
30.33307	1.46E-10	1.23E-09	7.46E-10	1.29E-11	-7.78E-12
30.38333	1.45E-10	1.23E-09	7.68E-10	1.36E-11	-8.04E-12
30.43358	1.48E-10	1.24E-09	7.69E-10	1.73E-11	-8.71E-12
30.48385	1.44E-10	1.25E-09	7.92E-10	1.39E-11	-8.79E-12
30.53358	1.44E-10	1.26E-09	8.18E-10	1.11E-11	-8.29E-12
30.58437	1.50E-10	1.26E-09	8.09E-10	1.43E-11	-8.99E-12
30.63307	1.45E-10	1.25E-09	7.98E-10	1.22E-11	-7.42E-12
30.6841	1.49E-10	1.25E-09	8.02E-10	8.95E-12	-8.58E-12
30.73307	1.56E-10	1.24E-09	7.95E-10	8.83E-12	-8.65E-12
30.78358	1.54E-10	1.24E-09	7.54E-10	9.51E-12	-8.14E-12
30.83358	1.56E-10	1.24E-09	7.50E-10	1.16E-11	-6.86E-12
30.88307	1.57E-10	1.24E-09	7.46E-10	1.05E-11	-7.00E-12
30.93333	1.53E-10	1.25E-09	7.27E-10	1.09E-11	-7.07E-12
30.98358	1.53E-10	1.24E-09	7.41E-10	1.49E-11	-6.84E-12
31.0328	1.46E-10	1.25E-09	7.47E-10	1.43E-11	-5.28E-12
31.08437	1.43E-10	1.25E-09	7.66E-10	1.28E-11	-5.10E-12
31.13307	1.43E-10	1.26E-09	7.95E-10	1.35E-11	-5.13E-12
31.18358	1.46E-10	1.26E-09	8.16E-10	1.49E-11	-4.24E-12
31.23385	1.45E-10	1.25E-09	7.82E-10	1.29E-11	-4.41E-12
31.28333	1.52E-10	1.24E-09	7.80E-10	1.18E-11	-6.18E-12
31.33385	1.52E-10	1.22E-09	7.74E-10	9.95E-12	-7.06E-12
31.3841	1.53E-10	1.22E-09	7.62E-10	1.09E-11	-7.26E-12
31.43333	1.46E-10	1.22E-09	7.69E-10	8.89E-12	-6.83E-12
31.48385	1.42E-10	1.23E-09	7.89E-10	1.02E-11	-7.62E-12
31.53385	1.50E-10	1.25E-09	8.04E-10	1.00E-11	-8.53E-12
31.58358	1.49E-10	1.26E-09	7.90E-10	9.54E-12	-7.72E-12
31.63333	1.56E-10	1.26E-09	7.71E-10	1.04E-11	-8.14E-12
31.68333	1.65E-10	1.25E-09	7.55E-10	1.26E-11	-8.60E-12

31.7328	1.65E-10	1.26E-09	7.70E-10	1.06E-11	-7.54E-12
31.78358	1.58E-10	1.24E-09	7.78E-10	1.43E-11	-7.19E-12
31.83385	1.53E-10	1.24E-09	8.03E-10	1.44E-11	-6.53E-12
31.88333	1.48E-10	1.24E-09	8.23E-10	1.45E-11	-6.78E-12
31.93385	1.41E-10	1.24E-09	8.38E-10	1.33E-11	-6.66E-12
31.98385	1.39E-10	1.24E-09	8.35E-10	1.36E-11	-6.65E-12
32.03333	1.40E-10	1.25E-09	8.27E-10	1.20E-11	-6.63E-12
32.08358	1.46E-10	1.24E-09	8.07E-10	1.44E-11	-8.99E-12
32.13333	1.46E-10	1.26E-09	8.23E-10	1.44E-11	-9.27E-12
32.1841	1.42E-10	1.27E-09	8.18E-10	1.43E-11	-1.01E-11
32.23333	1.49E-10	1.27E-09	8.23E-10	1.39E-11	-1.08E-11
32.28358	1.50E-10	1.27E-09	8.15E-10	1.16E-11	-9.73E-12
32.33385	1.47E-10	1.27E-09	8.16E-10	7.89E-12	-8.84E-12
32.38358	1.50E-10	1.25E-09	7.97E-10	5.31E-12	-8.07E-12
32.4328	1.51E-10	1.25E-09	7.88E-10	5.73E-12	-7.36E-12
32.4841	1.42E-10	1.24E-09	7.74E-10	5.25E-12	-6.91E-12
32.53333	1.45E-10	1.25E-09	7.56E-10	1.05E-11	-7.27E-12
32.58333	1.51E-10	1.25E-09	7.65E-10	1.28E-11	-7.46E-12
32.63358	1.52E-10	1.27E-09	7.61E-10	1.40E-11	-7.57E-12
32.68385	1.56E-10	1.26E-09	7.62E-10	1.25E-11	-6.75E-12
32.73333	1.58E-10	1.27E-09	7.94E-10	9.23E-12	-7.53E-12
32.78307	1.57E-10	1.27E-09	8.43E-10	3.80E-12	-8.27E-12
32.83333	1.53E-10	1.27E-09	8.19E-10	5.45E-12	-7.20E-12
32.8841	1.48E-10	1.26E-09	8.07E-10	5.26E-12	-7.38E-12
32.93307	1.48E-10	1.26E-09	8.13E-10	9.47E-12	-7.48E-12
32.98358	1.41E-10	1.27E-09	8.02E-10	1.09E-11	-6.79E-12
33.0341	1.43E-10	1.28E-09	8.04E-10	1.27E-11	-6.20E-12
33.0841	1.44E-10	1.28E-09	8.11E-10	1.16E-11	-6.76E-12
33.13307	1.41E-10	1.29E-09	8.05E-10	1.03E-11	-7.50E-12
33.18307	1.43E-10	1.27E-09	7.71E-10	8.56E-12	-7.93E-12
33.23463	1.56E-10	1.26E-09	7.40E-10	1.12E-11	-7.00E-12
33.28358	1.61E-10	1.26E-09	6.97E-10	1.13E-11	-7.62E-12
33.33358	1.58E-10	1.25E-09	6.99E-10	1.07E-11	-8.90E-12
33.38358	1.62E-10	1.24E-09	7.05E-10	1.41E-11	-7.18E-12
33.43307	1.61E-10	1.25E-09	7.21E-10	1.22E-11	-8.34E-12
33.4841	1.57E-10	1.27E-09	7.45E-10	1.29E-11	-9.70E-12
33.53307	1.51E-10	1.27E-09	7.50E-10	1.16E-11	-8.83E-12
33.58333	1.48E-10	1.28E-09	7.50E-10	1.09E-11	-6.78E-12
33.6328	1.47E-10	1.28E-09	7.48E-10	9.99E-12	-7.05E-12
33.68437	1.49E-10	1.29E-09	7.40E-10	1.03E-11	-6.46E-12
33.73358	1.42E-10	1.28E-09	7.27E-10	8.12E-12	-6.06E-12
33.78358	1.38E-10	1.27E-09	7.41E-10	9.53E-12	-6.06E-12
33.83333	1.39E-10	1.28E-09	7.37E-10	1.23E-11	-7.05E-12
33.88385	1.46E-10	1.28E-09	7.61E-10	1.21E-11	-7.45E-12
33.93463	1.45E-10	1.27E-09	7.58E-10	1.30E-11	-4.83E-12

33.98307	1.46E-10	1.28E-09	7.58E-10	1.35E-11	-5.38E-12
34.03307	1.47E-10	1.30E-09	7.32E-10	1.45E-11	-5.92E-12
34.08385	1.54E-10	1.30E-09	7.61E-10	1.24E-11	-6.02E-12
34.13358	1.51E-10	1.30E-09	7.37E-10	1.13E-11	-7.30E-12
34.18307	1.57E-10	1.28E-09	7.42E-10	1.08E-11	-9.58E-12
34.23307	1.64E-10	1.27E-09	7.46E-10	1.13E-11	-8.41E-12
34.28333	1.65E-10	1.27E-09	7.70E-10	1.11E-11	-8.36E-12
34.33333	1.61E-10	1.26E-09	7.34E-10	8.58E-12	-7.61E-12
34.38358	1.59E-10	1.26E-09	7.31E-10	9.94E-12	-7.07E-12
34.43307	1.51E-10	1.27E-09	7.33E-10	8.57E-12	-6.62E-12
34.48307	1.45E-10	1.27E-09	7.08E-10	8.67E-12	-7.07E-12
34.53358	1.49E-10	1.27E-09	6.83E-10	6.78E-12	-6.45E-12
34.58358	1.44E-10	1.30E-09	6.88E-10	8.61E-12	-6.20E-12
34.63358	1.42E-10	1.30E-09	6.82E-10	7.95E-12	-5.64E-12
34.68307	1.40E-10	1.30E-09	6.77E-10	8.75E-12	-5.89E-12
34.73307	1.44E-10	1.29E-09	6.90E-10	7.85E-12	-5.01E-12
34.78358	1.44E-10	1.29E-09	6.99E-10	1.03E-11	-5.62E-12
34.83307	1.47E-10	1.27E-09	7.13E-10	1.16E-11	-5.66E-12
34.88333	1.48E-10	1.26E-09	7.13E-10	1.15E-11	-5.67E-12
34.9328	1.61E-10	1.27E-09	7.00E-10	1.32E-11	-6.06E-12
34.98385	1.60E-10	1.26E-09	6.96E-10	1.54E-11	-7.20E-12
35.03307	1.60E-10	1.27E-09	6.81E-10	1.32E-11	-7.29E-12
35.08437	1.55E-10	1.28E-09	6.59E-10	9.92E-12	-7.65E-12
35.13488	1.55E-10	1.29E-09	6.78E-10	1.03E-11	-7.43E-12
35.18307	1.44E-10	1.28E-09	7.01E-10	8.36E-12	-6.22E-12
35.23358	1.41E-10	1.30E-09	6.77E-10	8.82E-12	-6.28E-12
35.28358	1.40E-10	1.30E-09	6.96E-10	7.15E-12	-5.62E-12
35.33385	1.40E-10	1.30E-09	7.06E-10	1.05E-11	-6.34E-12
35.38333	1.43E-10	1.29E-09	7.06E-10	1.19E-11	-6.85E-12
35.43255	1.42E-10	1.30E-09	6.96E-10	1.28E-11	-6.20E-12
35.48333	1.39E-10	1.30E-09	7.13E-10	1.10E-11	-5.22E-12
35.53358	1.35E-10	1.29E-09	7.17E-10	1.04E-11	-5.15E-12
35.58307	1.46E-10	1.29E-09	7.19E-10	9.66E-12	-4.82E-12
35.63385	1.38E-10	1.30E-09	7.23E-10	9.96E-12	-4.26E-12
35.68385	1.42E-10	1.29E-09	7.44E-10	9.08E-12	-4.32E-12
35.73358	1.47E-10	1.28E-09	7.08E-10	9.94E-12	-3.24E-12
35.78358	1.55E-10	1.28E-09	7.10E-10	1.18E-11	-2.94E-12
35.83333	1.49E-10	1.28E-09	7.21E-10	1.33E-11	-3.04E-12
35.88333	1.64E-10	1.28E-09	7.03E-10	1.05E-11	-2.80E-12
35.9341	1.60E-10	1.29E-09	7.01E-10	1.38E-11	-4.41E-12
35.98358	1.57E-10	1.29E-09	7.26E-10	1.19E-11	-4.97E-12
36.03385	1.48E-10	1.31E-09	6.93E-10	1.15E-11	-5.57E-12
36.08358	1.48E-10	1.31E-09	6.73E-10	8.97E-12	-4.59E-12
36.13358	1.43E-10	1.30E-09	6.71E-10	1.22E-11	-4.03E-12
36.18333	1.43E-10	1.29E-09	6.37E-10	7.88E-12	-3.14E-12

36.23333	1.39E-10	1.29E-09	6.26E-10	9.32E-12	-3.68E-12
36.28385	1.38E-10	1.29E-09	6.17E-10	1.20E-11	-3.09E-12
36.33385	1.36E-10	1.28E-09	6.10E-10	9.48E-12	-3.30E-12
36.38437	1.34E-10	1.29E-09	6.03E-10	7.76E-12	-3.83E-12
36.43358	1.42E-10	1.28E-09	6.37E-10	9.41E-12	-4.62E-12
36.48385	1.51E-10	1.27E-09	6.79E-10	7.83E-12	-4.09E-12
36.53333	1.49E-10	1.27E-09	7.15E-10	5.57E-12	-5.38E-12
36.58385	1.47E-10	1.27E-09	7.38E-10	1.04E-11	-4.87E-12
36.63437	1.49E-10	1.28E-09	7.33E-10	1.19E-11	-6.22E-12
36.68358	1.49E-10	1.28E-09	7.30E-10	1.36E-11	-6.01E-12
36.73333	1.43E-10	1.29E-09	7.04E-10	1.58E-11	-6.66E-12
36.78358	1.48E-10	1.29E-09	7.10E-10	1.56E-11	-5.57E-12
36.83307	1.48E-10	1.30E-09	6.80E-10	1.36E-11	-5.16E-12
36.88358	1.41E-10	1.31E-09	7.12E-10	1.23E-11	-4.05E-12
36.93385	1.39E-10	1.32E-09	6.92E-10	1.28E-11	-3.40E-12
36.98358	1.42E-10	1.33E-09	6.99E-10	1.10E-11	-2.25E-12
37.03437	1.39E-10	1.34E-09	6.60E-10	1.33E-11	-2.68E-12
37.0841	1.47E-10	1.33E-09	6.61E-10	1.16E-11	-2.70E-12
37.1341	1.47E-10	1.32E-09	6.48E-10	1.18E-11	-1.64E-12
37.18385	1.44E-10	1.33E-09	6.50E-10	9.86E-12	-7.83E-13
37.23385	1.43E-10	1.32E-09	6.23E-10	9.00E-12	-1.01E-12
37.2841	1.46E-10	1.32E-09	6.32E-10	5.56E-12	-1.30E-12
37.33333	1.39E-10	1.30E-09	6.32E-10	8.93E-12	-2.76E-12
37.38358	1.33E-10	1.31E-09	6.16E-10	7.29E-12	-2.82E-12
37.4328	1.36E-10	1.30E-09	5.91E-10	5.76E-12	-4.00E-12
37.48333	1.33E-10	1.31E-09	6.12E-10	6.50E-12	-5.49E-12
37.5341	1.35E-10	1.31E-09	6.15E-10	7.59E-12	-2.81E-12
37.58358	1.36E-10	1.31E-09	6.25E-10	7.45E-12	-1.25E-12
37.63333	1.40E-10	1.30E-09	6.56E-10	1.10E-11	-3.51E-12
37.68333	1.35E-10	1.29E-09	6.74E-10	1.48E-11	-4.53E-12
37.73333	1.46E-10	1.28E-09	6.53E-10	1.57E-11	-2.76E-12
37.78385	1.45E-10	1.28E-09	6.55E-10	1.59E-11	-4.64E-12
37.83333	1.43E-10	1.29E-09	6.74E-10	1.36E-11	-4.82E-12
37.88385	1.51E-10	1.29E-09	6.54E-10	1.07E-11	-2.58E-12
37.93358	1.51E-10	1.30E-09	6.48E-10	1.18E-11	-1.48E-12
37.98358	1.42E-10	1.31E-09	6.44E-10	1.26E-11	-3.29E-12
38.03437	1.40E-10	1.31E-09	6.39E-10	1.53E-11	-3.89E-12
38.08333	1.45E-10	1.31E-09	6.31E-10	1.96E-11	-4.65E-12
38.13385	1.40E-10	1.31E-09	6.10E-10	2.03E-11	-4.90E-12
38.18333	1.42E-10	1.31E-09	6.30E-10	1.49E-11	-4.78E-12
38.23333	1.40E-10	1.30E-09	6.41E-10	1.27E-11	-4.04E-12
38.28358	1.39E-10	1.29E-09	6.45E-10	1.16E-11	-4.90E-12
38.33333	1.42E-10	1.29E-09	6.29E-10	6.75E-12	-5.93E-12
38.3828	1.38E-10	1.28E-09	6.43E-10	4.42E-12	-7.36E-12
38.43358	1.40E-10	1.29E-09	6.46E-10	9.57E-12	-6.56E-12

38.48333	1.41E-10	1.29E-09	6.36E-10	1.10E-11	-5.51E-12
38.53358	1.38E-10	1.30E-09	6.48E-10	8.60E-12	-5.36E-12
38.58307	1.33E-10	1.31E-09	6.76E-10	8.56E-12	-2.06E-12
38.63385	1.33E-10	1.32E-09	6.74E-10	9.96E-12	-9.63E-13
38.68333	1.26E-10	1.32E-09	6.75E-10	7.41E-12	-2.59E-12
38.7341	1.27E-10	1.32E-09	7.00E-10	9.26E-12	-3.47E-12
38.78385	1.35E-10	1.30E-09	6.91E-10	1.07E-11	-3.00E-12
38.8341	1.29E-10	1.31E-09	6.65E-10	1.21E-11	-5.38E-12
38.8841	1.30E-10	1.31E-09	6.61E-10	1.05E-11	-5.19E-12
38.93333	1.31E-10	1.31E-09	6.72E-10	9.00E-12	-4.04E-12
38.98333	1.35E-10	1.33E-09	6.53E-10	9.52E-12	-3.93E-12
39.0341	1.34E-10	1.32E-09	6.41E-10	1.02E-11	-3.44E-12
39.0841	1.41E-10	1.31E-09	6.31E-10	1.03E-11	-3.20E-12
39.13307	1.41E-10	1.30E-09	6.54E-10	1.20E-11	-2.53E-12
39.18307	1.41E-10	1.30E-09	6.25E-10	1.30E-11	-3.10E-12
39.23358	1.36E-10	1.30E-09	6.20E-10	8.29E-12	-1.51E-12
39.28358	1.31E-10	1.31E-09	6.30E-10	7.79E-12	-1.45E-12
39.33307	1.24E-10	1.30E-09	6.47E-10	6.92E-12	-2.34E-12
39.38358	1.18E-10	1.31E-09	6.38E-10	5.30E-12	-3.49E-12
39.43333	1.21E-10	1.31E-09	6.23E-10	5.27E-12	-2.03E-12
39.48437	1.21E-10	1.30E-09	6.40E-10	7.82E-12	-5.04E-12
39.53385	1.20E-10	1.30E-09	6.55E-10	6.51E-12	-4.46E-12
39.58307	1.21E-10	1.30E-09	6.59E-10	7.42E-12	-4.22E-12
39.63307	1.29E-10	1.31E-09	6.51E-10	1.10E-11	-3.54E-12
39.68437	1.33E-10	1.30E-09	6.63E-10	1.20E-11	-5.65E-12
39.73437	1.39E-10	1.31E-09	6.56E-10	1.39E-11	-4.62E-12
39.78358	1.45E-10	1.31E-09	6.22E-10	1.42E-11	-4.78E-12
39.83333	1.50E-10	1.30E-09	6.12E-10	1.26E-11	-2.75E-12
39.88333	1.55E-10	1.30E-09	6.07E-10	1.15E-11	-3.75E-12
39.93307	1.49E-10	1.30E-09	6.03E-10	8.35E-12	-3.02E-12
39.98385	1.42E-10	1.30E-09	6.05E-10	5.66E-12	-5.19E-13
40.03333	1.35E-10	1.31E-09	6.15E-10	4.81E-12	-8.82E-13
40.08358	1.28E-10	1.32E-09	6.18E-10	7.13E-12	-2.04E-12
40.13307	1.22E-10	1.32E-09	6.11E-10	6.34E-12	6.12E-13
40.18385	1.20E-10	1.32E-09	6.31E-10	8.19E-12	1.18E-12
40.2341	1.21E-10	1.33E-09	6.31E-10	8.63E-12	-7.80E-13
40.2841	1.23E-10	1.34E-09	6.41E-10	8.87E-12	1.60E-13
40.33385	1.29E-10	1.34E-09	6.42E-10	8.88E-12	2.31E-13
40.38385	1.32E-10	1.35E-09	6.36E-10	9.69E-12	-1.47E-12
40.43385	1.34E-10	1.34E-09	6.32E-10	9.61E-12	-4.08E-13
40.48385	1.33E-10	1.34E-09	6.27E-10	9.52E-12	9.17E-13
40.53307	1.43E-10	1.33E-09	6.28E-10	1.11E-11	1.54E-12
40.58385	1.39E-10	1.34E-09	6.17E-10	1.02E-11	1.89E-12
40.6341	1.42E-10	1.33E-09	6.35E-10	1.13E-11	1.97E-12
40.68358	1.45E-10	1.33E-09	6.33E-10	1.38E-11	1.82E-12

40.73333	1.49E-10	1.32E-09	6.35E-10	1.57E-11	1.78E-12
40.78307	1.41E-10	1.33E-09	6.20E-10	1.37E-11	-2.65E-14
40.83333	1.45E-10	1.32E-09	6.37E-10	1.24E-11	1.39E-12
40.88358	1.38E-10	1.31E-09	6.37E-10	1.23E-11	3.07E-12
40.93307	1.43E-10	1.31E-09	6.45E-10	1.25E-11	3.17E-12
40.98385	1.45E-10	1.31E-09	6.40E-10	1.06E-11	1.91E-12
41.03437	1.36E-10	1.32E-09	7.28E-10	1.68E-11	2.90E-12
41.08437	1.41E-10	1.32E-09	7.12E-10	2.00E-11	8.69E-13
41.13333	1.40E-10	1.32E-09	6.96E-10	1.86E-11	1.71E-13
41.18333	1.41E-10	1.32E-09	6.94E-10	1.59E-11	1.54E-12
41.23333	1.34E-10	1.32E-09	7.02E-10	1.44E-11	2.11E-12
41.28385	1.45E-10	1.31E-09	6.04E-10	1.03E-11	1.54E-12
41.33333	1.36E-10	1.30E-09	5.96E-10	1.03E-11	2.48E-12
41.38358	1.38E-10	1.31E-09	6.13E-10	9.02E-12	1.77E-12
41.43385	1.34E-10	1.31E-09	6.11E-10	8.80E-12	5.19E-13
41.48358	1.40E-10	1.32E-09	6.24E-10	1.34E-11	-3.47E-13
41.53463	1.38E-10	1.32E-09	6.12E-10	1.19E-11	8.57E-13
41.58307	1.41E-10	1.33E-09	6.51E-10	1.04E-11	1.29E-12
41.63437	1.42E-10	1.33E-09	6.48E-10	1.45E-11	1.44E-12
41.68358	1.43E-10	1.33E-09	6.19E-10	1.56E-11	1.50E-12
41.73385	1.38E-10	1.34E-09	5.97E-10	1.26E-11	2.93E-12
41.78463	1.39E-10	1.34E-09	6.49E-10	1.29E-11	2.54E-12
41.83385	1.38E-10	1.34E-09	6.30E-10	1.07E-11	3.43E-12
41.88385	1.36E-10	1.33E-09	6.18E-10	6.72E-12	5.33E-12
41.93515	1.31E-10	1.33E-09	6.24E-10	5.66E-12	5.08E-12
41.98488	1.42E-10	1.32E-09	6.41E-10	8.11E-12	4.13E-12
42.03567	1.48E-10	1.31E-09	6.07E-10	6.61E-12	5.90E-12
42.08463	1.45E-10	1.33E-09	5.82E-10	9.66E-12	4.45E-12
42.13333	1.41E-10	1.34E-09	5.93E-10	1.10E-11	3.30E-12
42.18333	1.45E-10	1.34E-09	5.98E-10	9.39E-12	4.85E-12
42.23358	1.36E-10	1.36E-09	5.80E-10	6.74E-12	5.63E-12
42.28463	1.27E-10	1.36E-09	5.76E-10	8.21E-12	3.63E-12
42.33333	1.26E-10	1.34E-09	5.84E-10	7.02E-12	4.66E-12
42.3828	1.35E-10	1.33E-09	5.74E-10	4.22E-12	5.99E-12
42.43488	1.31E-10	1.32E-09	5.78E-10	5.57E-12	3.84E-12
42.48463	1.28E-10	1.31E-09	5.82E-10	5.72E-12	4.41E-12
42.53358	1.28E-10	1.33E-09	5.87E-10	4.67E-12	7.64E-12
42.58333	1.30E-10	1.34E-09	6.02E-10	3.10E-12	9.05E-12
42.63385	1.27E-10	1.33E-09	6.37E-10	7.09E-12	9.06E-12
42.68515	1.36E-10	1.34E-09	6.48E-10	5.38E-12	9.67E-12
42.73333	1.39E-10	1.35E-09	6.33E-10	4.44E-12	7.95E-12
42.78333	1.46E-10	1.35E-09	6.44E-10	6.30E-12	5.92E-12
42.83437	1.45E-10	1.35E-09	6.25E-10	5.76E-12	5.23E-12
42.88358	1.42E-10	1.36E-09	6.01E-10	5.48E-12	4.82E-12
42.9341	1.35E-10	1.36E-09	5.67E-10	1.11E-11	5.07E-12

42.98463	1.33E-10	1.35E-09	6.02E-10	1.09E-11	5.83E-12
43.03385	1.24E-10	1.34E-09	5.96E-10	1.03E-11	5.26E-12
43.08333	1.25E-10	1.33E-09	6.08E-10	1.15E-11	4.21E-12
43.13333	1.19E-10	1.31E-09	6.16E-10	1.04E-11	2.56E-12
43.18333	1.21E-10	1.30E-09	6.48E-10	7.19E-12	2.37E-12
43.23358	1.25E-10	1.30E-09	6.24E-10	6.98E-12	4.10E-12
43.28307	1.29E-10	1.31E-09	6.21E-10	5.70E-12	4.85E-12
43.33358	1.30E-10	1.30E-09	5.95E-10	8.45E-12	4.74E-12
43.38358	1.37E-10	1.31E-09	5.66E-10	7.45E-12	6.34E-12
43.43333	1.38E-10	1.31E-09	5.65E-10	7.48E-12	9.43E-12
43.48385	1.35E-10	1.31E-09	5.60E-10	8.40E-12	8.07E-12
43.5328	1.32E-10	1.31E-09	5.73E-10	1.46E-11	8.61E-12
43.58385	1.32E-10	1.31E-09	6.11E-10	1.34E-11	8.50E-12
43.63385	1.31E-10	1.33E-09	6.07E-10	1.39E-11	8.16E-12
43.68333	1.22E-10	1.34E-09	5.97E-10	1.58E-11	5.50E-12
43.73385	1.26E-10	1.35E-09	5.93E-10	1.98E-11	6.22E-12
43.78358	1.25E-10	1.35E-09	5.67E-10	1.78E-11	4.85E-12
43.83358	1.34E-10	1.35E-09	5.51E-10	2.16E-11	4.50E-12
43.88463	1.34E-10	1.35E-09	5.69E-10	2.22E-11	5.98E-12
43.93358	1.40E-10	1.35E-09	5.75E-10	1.78E-11	6.64E-12
43.9841	1.35E-10	1.35E-09	6.01E-10	1.49E-11	7.28E-12
44.03333	1.41E-10	1.35E-09	6.15E-10	1.20E-11	1.04E-11
44.08385	1.34E-10	1.35E-09	6.24E-10	9.45E-12	1.18E-11
44.13333	1.26E-10	1.35E-09	6.22E-10	6.24E-12	1.15E-11
44.18333	1.24E-10	1.35E-09	6.15E-10	9.35E-12	1.08E-11
44.23385	1.26E-10	1.35E-09	6.08E-10	8.31E-12	9.50E-12
44.28358	1.23E-10	1.34E-09	6.11E-10	9.09E-12	8.43E-12
44.33358	1.20E-10	1.36E-09	6.00E-10	7.71E-12	6.97E-12
44.38385	1.29E-10	1.36E-09	6.03E-10	9.83E-12	6.98E-12
44.4341	1.27E-10	1.36E-09	6.16E-10	6.98E-12	7.12E-12
44.48333	1.30E-10	1.36E-09	6.09E-10	8.77E-12	8.28E-12
44.53358	1.26E-10	1.35E-09	6.08E-10	9.56E-12	8.80E-12
44.58385	1.23E-10	1.34E-09	6.08E-10	9.19E-12	1.07E-11
44.6341	1.22E-10	1.35E-09	5.89E-10	8.33E-12	1.19E-11
44.68437	1.29E-10	1.36E-09	5.80E-10	1.16E-11	1.35E-11
44.73333	1.24E-10	1.36E-09	5.91E-10	8.80E-12	1.45E-11
44.78385	1.28E-10	1.35E-09	5.74E-10	6.65E-12	1.41E-11
44.83333	1.29E-10	1.35E-09	5.63E-10	7.69E-12	1.42E-11
44.88437	1.24E-10	1.35E-09	5.60E-10	7.10E-12	1.50E-11
44.93437	1.20E-10	1.35E-09	5.53E-10	6.78E-12	1.60E-11
44.98333	1.22E-10	1.34E-09	5.48E-10	6.65E-12	1.57E-11
45.03333	1.24E-10	1.35E-09	5.62E-10	7.51E-12	1.53E-11
45.08385	1.29E-10	1.35E-09	5.62E-10	4.72E-12	1.57E-11
45.13437	1.27E-10	1.35E-09	5.90E-10	9.52E-12	1.42E-11
45.18488	1.28E-10	1.35E-09	5.79E-10	7.82E-12	1.35E-11

45.23385	1.31E-10	1.34E-09	5.62E-10	8.85E-12	1.52E-11
45.2841	1.29E-10	1.33E-09	5.60E-10	9.46E-12	1.98E-11
45.33307	1.34E-10	1.33E-09	5.94E-10	1.37E-11	1.86E-11
45.38385	1.46E-10	1.33E-09	5.65E-10	6.73E-12	2.27E-11
45.43463	1.51E-10	1.33E-09	6.00E-10	6.01E-12	2.46E-11
45.48385	1.45E-10	1.34E-09	6.06E-10	4.43E-12	2.61E-11
45.5341	1.41E-10	1.36E-09	6.05E-10	3.95E-12	2.27E-11
45.58358	1.37E-10	1.36E-09	5.68E-10	-5.02E-13	2.52E-11
45.6341	1.32E-10	1.36E-09	5.88E-10	4.77E-12	2.23E-11
45.68333	1.28E-10	1.38E-09	5.71E-10	6.56E-12	2.24E-11
45.7341	1.34E-10	1.37E-09	5.96E-10	8.99E-12	2.05E-11
45.78437	1.36E-10	1.36E-09	6.05E-10	6.34E-12	2.38E-11
45.8341	1.32E-10	1.36E-09	6.12E-10	7.02E-12	2.52E-11
45.8841	1.25E-10	1.36E-09	6.04E-10	6.85E-12	2.60E-11
45.93358	1.23E-10	1.35E-09	5.97E-10	5.37E-12	2.53E-11
45.98358	1.18E-10	1.34E-09	5.77E-10	6.78E-12	2.57E-11
46.03385	1.19E-10	1.34E-09	5.52E-10	7.52E-12	2.34E-11
46.08385	1.26E-10	1.34E-09	5.43E-10	7.62E-12	2.27E-11
46.13333	1.36E-10	1.35E-09	5.46E-10	7.08E-12	2.25E-11
46.1841	1.41E-10	1.35E-09	5.45E-10	9.39E-12	2.63E-11
46.23333	1.50E-10	1.35E-09	5.47E-10	1.00E-11	2.61E-11
46.28437	1.51E-10	1.36E-09	5.51E-10	1.18E-11	2.61E-11
46.3341	1.48E-10	1.36E-09	5.56E-10	1.15E-11	2.81E-11
46.38358	1.44E-10	1.35E-09	5.49E-10	1.09E-11	2.92E-11
46.4341	1.43E-10	1.34E-09	5.42E-10	1.10E-11	2.78E-11
46.48358	1.35E-10	1.34E-09	5.29E-10	6.73E-12	3.32E-11
46.53358	1.28E-10	1.35E-09	5.25E-10	8.17E-12	3.29E-11
46.58385	1.26E-10	1.34E-09	5.53E-10	9.91E-12	3.22E-11
46.63333	1.29E-10	1.34E-09	5.72E-10	1.12E-11	3.24E-11
46.68333	1.26E-10	1.35E-09	5.86E-10	1.03E-11	3.19E-11
46.73437	1.34E-10	1.35E-09	6.00E-10	1.20E-11	2.89E-11
46.78358	1.39E-10	1.36E-09	6.21E-10	1.17E-11	2.96E-11
46.83358	1.35E-10	1.36E-09	6.00E-10	9.69E-12	2.90E-11
46.88358	1.30E-10	1.37E-09	6.15E-10	8.74E-12	2.85E-11
46.93358	1.26E-10	1.37E-09	5.94E-10	1.15E-11	2.93E-11
46.98358	1.16E-10	1.37E-09	5.71E-10	1.09E-11	3.07E-11
47.03358	1.17E-10	1.35E-09	5.67E-10	1.11E-11	3.36E-11
47.08358	1.23E-10	1.34E-09	5.55E-10	1.19E-11	3.38E-11
47.1341	1.25E-10	1.34E-09	5.41E-10	1.12E-11	3.78E-11
47.18333	1.29E-10	1.35E-09	5.50E-10	7.31E-12	4.02E-11
47.23358	1.27E-10	1.35E-09	5.65E-10	5.51E-12	4.17E-11
47.28437	1.28E-10	1.35E-09	5.50E-10	5.47E-12	3.98E-11
47.3341	1.28E-10	1.36E-09	5.57E-10	3.06E-12	4.22E-11
47.38333	1.26E-10	1.35E-09	5.51E-10	4.71E-12	4.07E-11
47.43333	1.23E-10	1.35E-09	5.57E-10	4.95E-12	3.93E-11

47.48358	1.30E-10	1.35E-09	5.55E-10	7.66E-12	3.79E-11
47.53437	1.24E-10	1.36E-09	5.61E-10	6.77E-12	4.05E-11
47.58385	1.21E-10	1.36E-09	5.56E-10	8.58E-12	4.12E-11
47.63358	1.28E-10	1.35E-09	5.73E-10	4.51E-12	4.47E-11
47.6841	1.33E-10	1.37E-09	5.75E-10	5.43E-12	4.81E-11
47.73385	1.25E-10	1.37E-09	5.85E-10	4.51E-12	4.86E-11
47.78437	1.28E-10	1.37E-09	5.86E-10	4.16E-12	5.11E-11
47.83358	1.30E-10	1.37E-09	5.87E-10	5.60E-12	5.00E-11
47.8841	1.24E-10	1.37E-09	5.68E-10	8.32E-12	4.61E-11
47.93358	1.20E-10	1.35E-09	5.58E-10	7.47E-12	4.50E-11
47.98333	1.21E-10	1.35E-09	5.40E-10	1.06E-11	4.73E-11
48.03333	1.17E-10	1.35E-09	5.42E-10	1.13E-11	4.59E-11
48.08333	1.14E-10	1.33E-09	5.54E-10	1.04E-11	4.90E-11
48.13385	1.08E-10	1.34E-09	5.48E-10	7.95E-12	5.25E-11
48.18385	1.05E-10	1.34E-09	5.84E-10	8.51E-12	5.35E-11
48.23463	1.13E-10	1.34E-09	6.04E-10	5.06E-12	5.37E-11
48.30025	1.11E-10	1.35E-09	6.07E-10	5.35E-12	5.38E-11
48.3565	1.13E-10	1.36E-09	5.93E-10	7.30E-12	5.28E-11
48.41692	1.23E-10	1.36E-09	5.85E-10	1.15E-11	5.34E-11
48.4677	1.35E-10	1.36E-09	5.42E-10	9.59E-12	5.75E-11
48.51797	1.27E-10	1.37E-09	5.20E-10	1.26E-11	5.78E-11
48.56797	1.35E-10	1.36E-09	5.17E-10	1.20E-11	6.40E-11
48.6177	1.39E-10	1.37E-09	5.30E-10	1.02E-11	6.90E-11
48.66743	1.37E-10	1.37E-09	5.35E-10	8.72E-12	6.87E-11
48.71743	1.29E-10	1.37E-09	5.38E-10	9.42E-12	6.71E-11
48.76692	1.37E-10	1.37E-09	5.48E-10	7.42E-12	7.03E-11
48.81822	1.31E-10	1.38E-09	5.33E-10	5.74E-12	7.20E-11
48.86797	1.32E-10	1.38E-09	5.28E-10	3.90E-12	7.07E-11
48.91667	1.34E-10	1.37E-09	5.16E-10	1.90E-12	7.16E-11
48.96718	1.37E-10	1.37E-09	5.20E-10	4.39E-12	6.88E-11
49.01667	1.35E-10	1.36E-09	5.11E-10	8.30E-12	6.90E-11
49.06718	1.36E-10	1.36E-09	5.37E-10	7.01E-12	6.68E-11
49.11692	1.28E-10	1.35E-09	5.22E-10	9.56E-12	7.00E-11
49.16692	1.23E-10	1.35E-09	5.37E-10	8.41E-12	7.15E-11
49.21743	1.23E-10	1.36E-09	5.30E-10	3.81E-12	7.44E-11
49.26692	1.23E-10	1.36E-09	5.62E-10	6.99E-13	7.16E-11
49.31718	1.25E-10	1.36E-09	5.52E-10	2.39E-12	7.21E-11
49.36718	1.33E-10	1.36E-09	5.49E-10	1.42E-12	6.84E-11
49.41718	1.33E-10	1.36E-09	5.50E-10	5.73E-12	6.89E-11
49.46718	1.27E-10	1.37E-09	5.51E-10	8.18E-12	7.24E-11
49.51743	1.23E-10	1.37E-09	5.47E-10	6.08E-12	7.43E-11
49.56718	1.21E-10	1.37E-09	5.53E-10	5.14E-12	7.34E-11
49.61797	1.19E-10	1.37E-09	5.59E-10	6.74E-12	7.54E-11
49.66667	1.25E-10	1.36E-09	5.68E-10	5.71E-12	7.32E-11
49.71692	1.25E-10	1.36E-09	5.78E-10	3.65E-12	7.34E-11

49.76743	1.34E-10	1.36E-09	5.71E-10	3.86E-12	7.37E-11
49.81667	1.35E-10	1.36E-09	5.54E-10	2.68E-12	8.00E-11
49.86718	1.36E-10	1.36E-09	5.43E-10	9.11E-13	7.99E-11
49.91743	1.32E-10	1.37E-09	5.19E-10	-2.10E-12	8.50E-11
49.96718	1.37E-10	1.36E-09	5.13E-10	-1.55E-12	8.14E-11
50.01692	1.30E-10	1.36E-09	5.26E-10	-2.97E-12	8.66E-11
50.06692	1.31E-10	1.36E-09	5.39E-10	7.65E-13	8.49E-11
50.11692	1.34E-10	1.35E-09	5.62E-10	7.79E-14	8.70E-11
50.16667	1.39E-10	1.35E-09	5.80E-10	7.32E-13	9.03E-11
50.21743	1.36E-10	1.36E-09	5.82E-10	1.87E-12	8.92E-11
50.2677	1.39E-10	1.36E-09	5.57E-10	6.93E-12	8.34E-11
50.3177	1.42E-10	1.36E-09	5.48E-10	4.84E-12	8.05E-11
50.36667	1.38E-10	1.37E-09	5.62E-10	5.71E-12	8.16E-11
50.41743	1.39E-10	1.37E-09	5.46E-10	7.50E-12	7.49E-11
50.46797	1.35E-10	1.38E-09	5.46E-10	1.04E-11	8.53E-11
50.51743	1.31E-10	1.38E-09	5.55E-10	6.89E-12	8.58E-11
50.56743	1.27E-10	1.38E-09	5.45E-10	1.05E-11	8.26E-11
50.61692	1.22E-10	1.38E-09	5.18E-10	1.09E-11	8.43E-11
50.66743	1.11E-10	1.39E-09	5.42E-10	1.57E-11	9.23E-11
50.71797	1.13E-10	1.38E-09	5.42E-10	1.15E-11	8.81E-11
50.76667	1.14E-10	1.39E-09	5.17E-10	1.19E-11	8.92E-11
50.81692	1.24E-10	1.37E-09	5.37E-10	8.28E-12	9.39E-11
50.86718	1.23E-10	1.36E-09	5.49E-10	8.16E-12	9.09E-11
50.9177	1.31E-10	1.35E-09	5.46E-10	-5.62E-13	9.10E-11
50.96743	1.34E-10	1.34E-09	5.37E-10	8.46E-14	9.39E-11
51.01797	1.39E-10	1.32E-09	5.51E-10	-2.71E-13	9.78E-11
51.06692	1.31E-10	1.34E-09	5.36E-10	-2.27E-13	9.53E-11
51.11718	1.35E-10	1.34E-09	5.34E-10	4.80E-13	9.58E-11
51.16667	1.32E-10	1.35E-09	4.96E-10	2.02E-12	9.45E-11
51.21667	1.30E-10	1.35E-09	5.05E-10	7.78E-13	9.69E-11
51.26718	1.30E-10	1.36E-09	5.29E-10	1.03E-12	9.68E-11
51.31718	1.28E-10	1.35E-09	5.46E-10	3.77E-12	9.87E-11
51.36692	1.28E-10	1.36E-09	5.36E-10	4.58E-13	1.00E-10
51.4177	1.26E-10	1.37E-09	5.78E-10	3.71E-12	9.94E-11
51.46692	1.25E-10	1.38E-09	5.82E-10	6.61E-12	9.54E-11
51.51692	1.19E-10	1.39E-09	5.44E-10	5.32E-12	9.72E-11
51.56692	1.23E-10	1.40E-09	5.24E-10	3.75E-12	9.69E-11
51.61667	1.27E-10	1.38E-09	5.21E-10	6.64E-12	9.60E-11
51.6664	1.20E-10	1.37E-09	5.10E-10	4.71E-12	9.49E-11
51.71667	1.27E-10	1.37E-09	5.21E-10	3.48E-12	9.64E-11
51.76718	1.25E-10	1.37E-09	5.23E-10	5.48E-12	9.61E-11
51.8164	1.24E-10	1.37E-09	5.34E-10	5.62E-12	9.49E-11
51.86667	1.22E-10	1.39E-09	5.40E-10	5.53E-12	9.79E-11
51.91743	1.27E-10	1.37E-09	5.55E-10	6.03E-12	9.72E-11
51.96667	1.23E-10	1.37E-09	5.25E-10	3.98E-12	9.97E-11

52.01718	1.25E-10	1.37E-09	5.26E-10	1.84E-12	9.92E-11
52.06743	1.26E-10	1.36E-09	5.26E-10	2.56E-12	1.03E-10
52.11743	1.17E-10	1.36E-09	5.03E-10	4.90E-12	1.04E-10
52.16848	1.19E-10	1.37E-09	4.76E-10	2.63E-12	1.04E-10
52.21718	1.18E-10	1.36E-09	5.12E-10	4.88E-12	1.02E-10
52.2664	1.23E-10	1.36E-09	5.38E-10	7.25E-12	1.03E-10
52.31743	1.31E-10	1.37E-09	5.59E-10	3.55E-12	1.03E-10
52.36718	1.33E-10	1.36E-09	5.79E-10	-1.33E-12	1.02E-10
52.41822	1.32E-10	1.37E-09	5.67E-10	7.54E-13	1.06E-10
52.46718	1.32E-10	1.38E-09	5.39E-10	-1.24E-12	1.07E-10
52.51692	1.28E-10	1.38E-09	5.03E-10	-4.15E-12	1.09E-10
52.56797	1.23E-10	1.37E-09	4.69E-10	-2.52E-12	1.11E-10
52.61718	1.30E-10	1.37E-09	4.77E-10	2.35E-13	1.09E-10
52.66743	1.31E-10	1.36E-09	4.87E-10	3.45E-12	1.03E-10
52.71743	1.31E-10	1.36E-09	4.93E-10	5.91E-12	1.01E-10
52.76848	1.30E-10	1.37E-09	4.91E-10	5.88E-12	1.04E-10
52.81692	1.27E-10	1.38E-09	5.14E-10	7.78E-12	1.03E-10
52.86822	1.24E-10	1.38E-09	4.87E-10	6.56E-12	1.06E-10
52.91718	1.24E-10	1.38E-09	5.01E-10	4.90E-12	1.10E-10
52.96848	1.24E-10	1.38E-09	4.77E-10	3.26E-12	1.08E-10
53.01743	1.24E-10	1.38E-09	5.07E-10	6.02E-12	1.02E-10
53.06692	1.19E-10	1.38E-09	5.08E-10	4.94E-12	1.05E-10
53.11692	1.21E-10	1.38E-09	5.30E-10	4.60E-12	1.08E-10
53.16718	1.23E-10	1.39E-09	5.17E-10	3.97E-12	1.06E-10
53.2177	1.24E-10	1.38E-09	5.49E-10	2.59E-12	1.09E-10
53.26692	1.26E-10	1.39E-09	5.32E-10	1.81E-12	1.09E-10
53.31667	1.29E-10	1.38E-09	5.37E-10	1.51E-12	1.09E-10
53.36743	1.26E-10	1.38E-09	5.24E-10	8.19E-14	1.15E-10
53.4164	1.25E-10	1.36E-09	5.34E-10	-9.92E-13	1.20E-10
53.46692	1.30E-10	1.36E-09	5.35E-10	-9.52E-14	1.23E-10
53.51692	1.26E-10	1.35E-09	5.60E-10	-1.37E-12	1.27E-10
53.56718	1.27E-10	1.35E-09	5.36E-10	9.04E-13	1.24E-10
53.61718	1.28E-10	1.36E-09	5.32E-10	1.45E-12	1.16E-10
53.66667	1.31E-10	1.36E-09	5.29E-10	3.27E-12	1.10E-10
53.7177	1.25E-10	1.38E-09	5.02E-10	3.30E-12	1.12E-10
53.76743	1.26E-10	1.39E-09	5.11E-10	2.89E-12	1.10E-10
53.81718	1.25E-10	1.40E-09	5.10E-10	9.25E-13	1.09E-10
53.86743	1.27E-10	1.40E-09	5.41E-10	3.02E-12	1.09E-10
53.91718	1.24E-10	1.39E-09	5.47E-10	7.43E-14	1.17E-10
53.96692	1.28E-10	1.37E-09	5.55E-10	3.34E-13	1.14E-10
54.01718	1.35E-10	1.35E-09	5.21E-10	5.54E-13	1.12E-10
54.06718	1.31E-10	1.35E-09	5.09E-10	-2.64E-12	1.14E-10
54.11743	1.24E-10	1.35E-09	4.87E-10	-3.23E-12	1.14E-10
54.16667	1.22E-10	1.36E-09	4.74E-10	-1.42E-12	1.11E-10
54.21692	1.23E-10	1.36E-09	4.88E-10	-1.89E-12	1.12E-10

54.26667	1.16E-10	1.37E-09	5.05E-10	7.31E-13	1.12E-10
54.31667	1.16E-10	1.36E-09	5.09E-10	3.00E-12	1.12E-10
54.3664	1.18E-10	1.36E-09	5.15E-10	4.27E-12	1.08E-10
54.41718	1.23E-10	1.37E-09	5.35E-10	3.54E-12	1.11E-10
54.46692	1.23E-10	1.36E-09	5.25E-10	7.20E-12	1.07E-10
54.51692	1.19E-10	1.36E-09	5.20E-10	7.79E-12	1.10E-10
54.56718	1.21E-10	1.37E-09	5.29E-10	7.81E-12	1.11E-10
54.61743	1.22E-10	1.36E-09	5.27E-10	5.84E-12	1.14E-10
54.66692	1.23E-10	1.35E-09	5.30E-10	4.46E-12	1.13E-10
54.71613	1.18E-10	1.35E-09	5.36E-10	3.79E-13	1.16E-10
54.76667	1.30E-10	1.35E-09	5.27E-10	-1.93E-12	1.13E-10
54.81718	1.35E-10	1.34E-09	5.57E-10	-1.83E-12	1.12E-10
54.86743	1.36E-10	1.34E-09	5.60E-10	-2.29E-12	1.16E-10
54.91718	1.33E-10	1.35E-09	5.23E-10	-2.89E-12	1.19E-10
54.96692	1.31E-10	1.36E-09	5.21E-10	-2.77E-12	1.24E-10
55.01692	1.25E-10	1.36E-09	5.13E-10	-4.51E-12	1.26E-10
55.06743	1.24E-10	1.38E-09	4.62E-10	-4.76E-12	1.32E-10
55.11667	1.21E-10	1.37E-09	4.40E-10	-3.12E-12	1.31E-10
55.16743	1.18E-10	1.37E-09	4.43E-10	-1.45E-12	1.28E-10
55.21667	1.24E-10	1.37E-09	4.57E-10	-1.68E-12	1.30E-10
55.26692	1.29E-10	1.37E-09	4.50E-10	-9.76E-13	1.32E-10
55.3177	1.27E-10	1.37E-09	4.81E-10	-4.58E-13	1.27E-10
55.36718	1.31E-10	1.37E-09	4.98E-10	-1.65E-12	1.24E-10
55.41692	1.33E-10	1.36E-09	5.19E-10	-3.19E-12	1.28E-10
55.46692	1.34E-10	1.35E-09	5.31E-10	8.23E-13	1.21E-10
55.51743	1.28E-10	1.36E-09	5.47E-10	1.55E-13	1.18E-10
55.56692	1.25E-10	1.36E-09	5.64E-10	-3.21E-12	1.20E-10
55.61692	1.24E-10	1.36E-09	5.75E-10	-2.11E-12	1.21E-10
55.66692	1.16E-10	1.36E-09	5.48E-10	-2.88E-12	1.19E-10
55.71718	1.09E-10	1.37E-09	5.33E-10	-4.25E-12	1.20E-10
55.76667	1.09E-10	1.36E-09	5.36E-10	-9.23E-13	1.19E-10
55.81692	1.09E-10	1.37E-09	5.02E-10	2.87E-12	1.18E-10
55.86822	1.10E-10	1.38E-09	5.20E-10	1.34E-12	1.17E-10
55.91692	1.23E-10	1.38E-09	5.33E-10	2.99E-12	1.19E-10
55.96667	1.28E-10	1.37E-09	5.29E-10	2.93E-12	1.15E-10
56.0177	1.35E-10	1.38E-09	5.44E-10	2.47E-12	1.12E-10
56.06743	1.34E-10	1.39E-09	5.62E-10	4.79E-12	1.11E-10
56.11797	1.38E-10	1.39E-09	5.67E-10	2.99E-12	1.15E-10
56.16718	1.32E-10	1.38E-09	5.63E-10	4.00E-12	1.09E-10
56.21797	1.33E-10	1.39E-09	5.57E-10	6.35E-12	1.13E-10
56.2677	1.23E-10	1.39E-09	5.26E-10	3.25E-12	1.19E-10
56.3177	1.26E-10	1.37E-09	5.33E-10	1.36E-12	1.21E-10
56.36667	1.23E-10	1.37E-09	5.14E-10	5.27E-12	1.20E-10
56.41743	1.20E-10	1.37E-09	5.19E-10	4.90E-12	1.24E-10
56.46718	1.23E-10	1.37E-09	5.17E-10	1.91E-12	1.21E-10

56.51743	1.26E-10	1.36E-09	5.45E-10	3.67E-12	1.19E-10
56.56718	1.19E-10	1.37E-09	5.35E-10	3.27E-12	1.21E-10
56.61797	1.20E-10	1.37E-09	5.56E-10	8.07E-13	1.20E-10
56.6677	1.22E-10	1.38E-09	5.66E-10	1.23E-12	1.17E-10
56.71743	1.20E-10	1.37E-09	5.78E-10	2.02E-12	1.18E-10
56.7677	1.22E-10	1.38E-09	5.57E-10	5.20E-12	1.13E-10
56.8164	1.26E-10	1.37E-09	5.63E-10	4.95E-12	1.15E-10
56.86692	1.27E-10	1.35E-09	5.43E-10	4.95E-12	1.20E-10
56.91692	1.22E-10	1.34E-09	5.51E-10	4.27E-12	1.18E-10
56.96743	1.11E-10	1.34E-09	5.51E-10	2.54E-12	1.20E-10
57.0177	1.09E-10	1.33E-09	5.64E-10	-1.34E-12	1.25E-10
57.06718	1.05E-10	1.34E-09	5.46E-10	-2.58E-12	1.26E-10
57.11692	1.00E-10	1.35E-09	5.25E-10	-3.51E-12	1.23E-10
57.1677	1.04E-10	1.35E-09	5.06E-10	-1.69E-12	1.23E-10
57.21692	1.12E-10	1.34E-09	5.11E-10	-2.85E-12	1.25E-10
57.26718	1.23E-10	1.33E-09	4.92E-10	-3.81E-12	1.23E-10
57.31692	1.32E-10	1.33E-09	4.88E-10	-3.14E-12	1.18E-10
57.36797	1.34E-10	1.34E-09	5.07E-10	7.51E-13	1.20E-10
57.41743	1.39E-10	1.35E-09	5.21E-10	3.21E-14	1.21E-10
57.46692	1.39E-10	1.37E-09	5.15E-10	6.97E-12	1.16E-10
57.51718	1.32E-10	1.37E-09	5.40E-10	8.22E-12	1.18E-10
57.5664	1.28E-10	1.37E-09	5.74E-10	7.65E-12	1.20E-10
57.6164	1.25E-10	1.36E-09	5.44E-10	5.05E-12	1.18E-10
57.6677	1.22E-10	1.36E-09	5.48E-10	4.02E-12	1.22E-10
57.71743	1.24E-10	1.35E-09	5.54E-10	-2.60E-12	1.24E-10
57.76743	1.30E-10	1.35E-09	5.25E-10	-4.66E-12	1.28E-10
57.81743	1.32E-10	1.36E-09	4.92E-10	-2.01E-12	1.29E-10
57.86667	1.37E-10	1.37E-09	5.15E-10	-2.90E-13	1.28E-10
57.91743	1.34E-10	1.37E-09	5.00E-10	9.63E-13	1.28E-10
57.96718	1.39E-10	1.37E-09	5.34E-10	4.72E-12	1.29E-10
58.01718	1.33E-10	1.38E-09	5.74E-10	7.11E-12	1.26E-10
58.06718	1.37E-10	1.38E-09	5.95E-10	5.07E-12	1.26E-10
58.11692	1.33E-10	1.37E-09	5.94E-10	4.17E-12	1.27E-10
58.16743	1.35E-10	1.37E-09	5.97E-10	2.16E-12	1.26E-10
58.21743	1.27E-10	1.37E-09	5.42E-10	3.57E-12	1.27E-10
58.26667	1.23E-10	1.38E-09	5.41E-10	8.49E-12	1.27E-10
58.31718	1.12E-10	1.37E-09	5.14E-10	9.23E-12	1.24E-10
58.3664	1.19E-10	1.37E-09	5.09E-10	1.20E-11	1.26E-10
58.41718	1.22E-10	1.37E-09	5.13E-10	1.39E-11	1.25E-10
58.46667	1.23E-10	1.36E-09	5.32E-10	9.79E-12	1.24E-10
58.51718	1.31E-10	1.36E-09	4.87E-10	4.95E-12	1.22E-10
58.5677	1.31E-10	1.36E-09	5.02E-10	6.85E-12	1.23E-10
58.6177	1.34E-10	1.36E-09	5.15E-10	1.69E-12	1.21E-10
58.66692	1.32E-10	1.36E-09	5.41E-10	7.93E-13	1.23E-10
58.71743	1.24E-10	1.36E-09	5.19E-10	-1.76E-12	1.26E-10

58.7677	1.15E-10	1.37E-09	5.58E-10	-1.23E-12	1.28E-10
58.81743	1.22E-10	1.37E-09	5.64E-10	-5.78E-12	1.29E-10
58.86667	1.13E-10	1.38E-09	5.62E-10	-4.57E-12	1.27E-10
58.91718	1.10E-10	1.37E-09	5.45E-10	-5.83E-12	1.29E-10
58.96718	1.16E-10	1.37E-09	5.51E-10	-8.14E-13	1.23E-10
59.0177	1.23E-10	1.36E-09	5.35E-10	-4.07E-12	1.30E-10
59.06718	1.16E-10	1.36E-09	5.36E-10	-2.55E-12	1.30E-10
59.11667	1.20E-10	1.36E-09	5.30E-10	-2.65E-12	1.33E-10
59.16718	1.21E-10	1.37E-09	5.07E-10	-1.59E-12	1.29E-10
59.21667	1.16E-10	1.37E-09	5.15E-10	-1.90E-12	1.34E-10
59.26743	1.12E-10	1.37E-09	5.16E-10	7.03E-13	1.26E-10
59.31743	1.11E-10	1.37E-09	4.90E-10	2.41E-13	1.27E-10
59.36692	1.07E-10	1.38E-09	4.75E-10	2.28E-12	1.24E-10
59.41743	1.16E-10	1.38E-09	4.66E-10	4.61E-12	1.26E-10
59.4677	1.20E-10	1.39E-09	4.92E-10	3.63E-12	1.28E-10
59.5177	1.26E-10	1.39E-09	4.84E-10	4.66E-12	1.32E-10
59.56718	1.30E-10	1.38E-09	5.02E-10	6.29E-12	1.30E-10
59.61667	1.35E-10	1.39E-09	5.25E-10	3.84E-12	1.35E-10
59.66718	1.27E-10	1.39E-09	5.56E-10	-4.11E-14	1.39E-10
59.7164	1.26E-10	1.40E-09	5.27E-10	1.21E-12	1.35E-10
59.76718	1.28E-10	1.40E-09	5.29E-10	4.52E-13	1.32E-10
59.81692	1.25E-10	1.40E-09	5.21E-10	1.06E-12	1.30E-10
59.8664	1.18E-10	1.39E-09	5.33E-10	2.85E-12	1.25E-10
59.91718	1.27E-10	1.38E-09	5.18E-10	4.26E-12	1.25E-10
59.96692	1.30E-10	1.37E-09	5.34E-10	2.45E-12	1.24E-10
60.01692	1.31E-10	1.37E-09	5.26E-10	7.02E-12	1.22E-10
60.06692	1.29E-10	1.37E-09	5.54E-10	5.60E-12	1.26E-10
60.11743	1.34E-10	1.37E-09	5.47E-10	7.36E-12	1.29E-10
60.16797	1.25E-10	1.37E-09	5.50E-10	7.18E-12	1.25E-10
60.21667	1.19E-10	1.37E-09	5.55E-10	8.09E-12	1.23E-10
60.26692	1.19E-10	1.37E-09	5.48E-10	3.10E-12	1.30E-10
60.31692	1.21E-10	1.37E-09	5.36E-10	5.07E-12	1.26E-10
60.36692	1.18E-10	1.37E-09	5.11E-10	7.83E-12	1.21E-10
60.41743	1.20E-10	1.36E-09	5.29E-10	6.62E-12	1.25E-10
60.46667	1.26E-10	1.37E-09	5.38E-10	3.05E-12	1.30E-10
60.51667	1.16E-10	1.36E-09	5.89E-10	4.66E-12	1.29E-10
60.56718	1.17E-10	1.36E-09	5.86E-10	1.32E-12	1.31E-10
60.61667	1.23E-10	1.36E-09	6.04E-10	-6.77E-12	1.37E-10
60.66718	1.17E-10	1.35E-09	5.99E-10	-5.68E-12	1.36E-10
60.71743	1.18E-10	1.36E-09	5.90E-10	-1.22E-12	1.32E-10
60.76692	1.24E-10	1.37E-09	5.40E-10	-7.12E-13	1.27E-10
60.81718	1.27E-10	1.37E-09	5.45E-10	3.51E-12	1.28E-10
60.86667	1.23E-10	1.37E-09	5.45E-10	7.19E-12	1.24E-10
60.91692	1.35E-10	1.37E-09	5.43E-10	1.05E-11	1.22E-10
60.96718	1.31E-10	1.36E-09	5.20E-10	1.17E-11	1.21E-10

61.01692	1.37E-10	1.36E-09	5.30E-10	9.97E-12	1.24E-10
61.06743	1.38E-10	1.37E-09	5.27E-10	6.33E-12	1.24E-10
61.11743	1.34E-10	1.37E-09	5.06E-10	7.47E-12	1.27E-10
61.1677	1.35E-10	1.36E-09	4.99E-10	4.09E-12	1.27E-10
61.21797	1.37E-10	1.37E-09	4.98E-10	-1.39E-12	1.30E-10
61.26718	1.30E-10	1.37E-09	5.05E-10	-3.23E-12	1.35E-10
61.3177	1.26E-10	1.36E-09	5.03E-10	-2.21E-12	1.36E-10
61.3677	1.27E-10	1.36E-09	5.14E-10	-3.14E-12	1.41E-10
61.41718	1.21E-10	1.37E-09	5.15E-10	-2.94E-12	1.43E-10
61.46743	1.17E-10	1.37E-09	5.28E-10	2.40E-12	1.39E-10
61.51718	1.16E-10	1.38E-09	5.25E-10	3.86E-12	1.35E-10
61.56692	1.15E-10	1.37E-09	5.28E-10	5.91E-12	1.32E-10
61.61692	1.12E-10	1.38E-09	5.35E-10	5.40E-12	1.27E-10
61.66692	1.16E-10	1.38E-09	5.29E-10	5.02E-12	1.25E-10
61.7177	1.20E-10	1.36E-09	5.33E-10	4.18E-12	1.29E-10
61.76718	1.21E-10	1.35E-09	5.59E-10	6.22E-12	1.30E-10
61.81692	1.24E-10	1.35E-09	5.54E-10	8.22E-12	1.26E-10
61.8677	1.29E-10	1.35E-09	5.44E-10	7.56E-12	1.31E-10
61.91667	1.23E-10	1.35E-09	5.55E-10	9.81E-12	1.29E-10
61.96692	1.28E-10	1.36E-09	5.26E-10	7.54E-12	1.29E-10
62.01667	1.29E-10	1.36E-09	5.30E-10	3.60E-12	1.30E-10
62.06718	1.29E-10	1.36E-09	5.24E-10	5.37E-13	1.32E-10
62.11718	1.35E-10	1.36E-09	5.13E-10	9.74E-13	1.29E-10
62.16718	1.30E-10	1.38E-09	4.98E-10	2.01E-12	1.29E-10
62.2164	1.18E-10	1.38E-09	5.00E-10	5.80E-13	1.31E-10
62.26692	1.20E-10	1.38E-09	4.84E-10	1.43E-12	1.33E-10
62.31692	1.25E-10	1.37E-09	4.98E-10	1.98E-12	1.32E-10
62.36692	1.16E-10	1.36E-09	5.24E-10	3.06E-12	1.30E-10
62.41718	1.17E-10	1.36E-09	5.02E-10	9.29E-13	1.29E-10
62.46667	1.19E-10	1.36E-09	5.17E-10	4.00E-12	1.27E-10
62.5177	1.17E-10	1.35E-09	5.12E-10	7.85E-12	1.26E-10
62.56692	1.12E-10	1.36E-09	5.04E-10	5.48E-12	1.30E-10
62.6177	1.18E-10	1.36E-09	5.04E-10	4.63E-12	1.32E-10
62.6677	1.20E-10	1.36E-09	5.17E-10	2.12E-12	1.38E-10
62.71692	1.24E-10	1.36E-09	5.27E-10	-2.09E-13	1.39E-10
62.76718	1.24E-10	1.37E-09	5.25E-10	-4.30E-12	1.37E-10
62.81718	1.26E-10	1.37E-09	5.24E-10	-1.00E-12	1.37E-10
62.86667	1.21E-10	1.38E-09	5.13E-10	-1.21E-12	1.38E-10
62.91743	1.22E-10	1.38E-09	5.05E-10	-9.49E-13	1.36E-10
62.96718	1.18E-10	1.37E-09	5.06E-10	3.86E-12	1.39E-10
63.01667	1.18E-10	1.37E-09	4.96E-10	5.87E-12	1.38E-10
63.06718	1.24E-10	1.37E-09	5.05E-10	6.05E-12	1.36E-10
63.11797	1.25E-10	1.37E-09	5.31E-10	4.39E-12	1.32E-10
63.1677	1.18E-10	1.36E-09	5.41E-10	3.30E-12	1.29E-10
63.21797	1.13E-10	1.37E-09	5.19E-10	3.68E-12	1.23E-10

63.2677	1.10E-10	1.39E-09	5.31E-10	1.40E-12	1.27E-10
63.31797	1.04E-10	1.39E-09	5.38E-10	4.29E-13	1.29E-10
63.36743	1.03E-10	1.38E-09	5.04E-10	3.23E-13	1.37E-10
63.41692	1.08E-10	1.39E-09	5.11E-10	5.99E-12	1.36E-10
63.46743	1.14E-10	1.38E-09	5.05E-10	1.05E-12	1.37E-10
63.51692	1.21E-10	1.37E-09	5.03E-10	1.24E-12	1.34E-10
63.569	1.16E-10	1.37E-09	4.93E-10	-3.25E-12	1.35E-10
63.6177	1.22E-10	1.37E-09	5.06E-10	-9.59E-13	1.28E-10
63.66743	1.23E-10	1.36E-09	5.30E-10	-9.76E-13	1.28E-10
63.71718	1.26E-10	1.36E-09	5.28E-10	-6.98E-13	1.31E-10
63.76743	1.24E-10	1.36E-09	5.20E-10	2.86E-12	1.32E-10
63.81848	1.27E-10	1.35E-09	5.25E-10	4.92E-12	1.31E-10
63.86718	1.20E-10	1.36E-09	5.21E-10	4.25E-12	1.33E-10
63.91743	1.21E-10	1.37E-09	4.93E-10	3.11E-12	1.35E-10
63.96718	1.25E-10	1.37E-09	5.17E-10	1.89E-12	1.35E-10
64.01743	1.29E-10	1.38E-09	5.20E-10	-3.14E-12	1.41E-10
64.06743	1.35E-10	1.38E-09	5.08E-10	-2.90E-12	1.42E-10
64.11718	1.35E-10	1.38E-09	5.16E-10	-4.46E-12	1.41E-10
64.1677	1.39E-10	1.37E-09	5.12E-10	-7.88E-12	1.39E-10
64.21743	1.30E-10	1.38E-09	5.24E-10	-7.07E-12	1.40E-10
64.2677	1.26E-10	1.38E-09	5.72E-10	-5.11E-12	1.37E-10
64.31718	1.20E-10	1.38E-09	5.88E-10	-5.11E-12	1.41E-10
64.36718	1.21E-10	1.37E-09	5.65E-10	-3.11E-12	1.37E-10
64.41848	1.17E-10	1.38E-09	5.75E-10	-3.68E-12	1.38E-10
64.46743	1.19E-10	1.37E-09	5.53E-10	-5.75E-12	1.37E-10
64.51797	1.13E-10	1.37E-09	5.18E-10	-3.80E-12	1.36E-10
64.56667	1.08E-10	1.37E-09	4.94E-10	-2.79E-12	1.32E-10
64.61667	1.12E-10	1.38E-09	5.24E-10	-3.37E-12	1.34E-10
64.66692	1.10E-10	1.37E-09	5.37E-10	-1.96E-12	1.36E-10
64.71667	1.13E-10	1.38E-09	5.35E-10	-4.51E-13	1.35E-10
64.76718	1.19E-10	1.37E-09	5.30E-10	1.07E-12	1.32E-10
64.81692	1.19E-10	1.37E-09	5.32E-10	6.64E-13	1.33E-10
64.86718	1.21E-10	1.37E-09	5.23E-10	-1.65E-12	1.38E-10
64.91692	1.24E-10	1.36E-09	5.18E-10	-4.44E-12	1.38E-10
64.96743	1.22E-10	1.36E-09	5.25E-10	-1.52E-12	1.36E-10
65.01667	1.17E-10	1.36E-09	5.10E-10	-4.18E-12	1.36E-10
65.06692	1.17E-10	1.36E-09	5.12E-10	-2.10E-12	1.34E-10
65.11667	1.09E-10	1.36E-09	4.91E-10	2.94E-13	1.32E-10
65.16822	1.07E-10	1.36E-09	4.89E-10	3.11E-12	1.29E-10
65.21667	1.08E-10	1.37E-09	4.91E-10	2.04E-12	1.32E-10
65.2677	1.12E-10	1.37E-09	4.96E-10	-6.17E-14	1.35E-10
65.3177	1.12E-10	1.36E-09	5.10E-10	-3.90E-12	1.37E-10
65.36692	1.15E-10	1.38E-09	5.33E-10	-3.67E-12	1.38E-10
65.41718	1.09E-10	1.38E-09	5.34E-10	-4.60E-12	1.43E-10
65.46743	1.08E-10	1.38E-09	5.22E-10	-3.23E-12	1.40E-10

65.51692	1.06E-10	1.37E-09	5.42E-10	-9.26E-13	1.45E-10
65.56667	1.10E-10	1.37E-09	5.51E-10	-1.47E-12	1.48E-10
65.61718	1.10E-10	1.37E-09	5.21E-10	7.44E-13	1.52E-10
65.66692	1.19E-10	1.36E-09	5.38E-10	1.34E-12	1.56E-10
65.71797	1.16E-10	1.37E-09	5.64E-10	-1.74E-12	1.60E-10
65.76718	1.22E-10	1.37E-09	5.69E-10	-4.93E-13	1.56E-10
65.81692	1.23E-10	1.38E-09	5.69E-10	1.71E-12	1.50E-10
65.86692	1.27E-10	1.38E-09	5.74E-10	-1.99E-12	1.43E-10
65.91743	1.26E-10	1.38E-09	5.54E-10	-1.37E-12	1.37E-10
65.96743	1.24E-10	1.37E-09	5.38E-10	-5.96E-13	1.33E-10
66.01667	1.26E-10	1.36E-09	5.38E-10	-2.45E-12	1.33E-10
66.06692	1.22E-10	1.36E-09	5.18E-10	-3.99E-12	1.39E-10
66.11692	1.17E-10	1.35E-09	5.40E-10	-5.08E-13	1.42E-10
66.16718	1.15E-10	1.36E-09	5.66E-10	-1.22E-12	1.40E-10
66.21743	1.17E-10	1.37E-09	5.80E-10	2.27E-13	1.40E-10
66.26692	1.17E-10	1.37E-09	5.77E-10	3.77E-12	1.38E-10
66.3177	1.22E-10	1.38E-09	5.68E-10	5.51E-12	1.38E-10
66.36692	1.28E-10	1.38E-09	5.62E-10	5.91E-12	1.32E-10
66.41718	1.32E-10	1.38E-09	5.33E-10	6.19E-12	1.36E-10
66.46743	1.37E-10	1.38E-09	5.19E-10	3.13E-12	1.40E-10
66.51743	1.38E-10	1.38E-09	4.92E-10	-1.85E-12	1.46E-10
66.56718	1.37E-10	1.38E-09	5.05E-10	5.73E-13	1.43E-10
66.61718	1.39E-10	1.38E-09	5.17E-10	-2.95E-12	1.47E-10
66.66743	1.30E-10	1.38E-09	5.19E-10	-2.25E-13	1.46E-10
66.71743	1.37E-10	1.38E-09	5.17E-10	3.46E-12	1.38E-10
66.76692	1.36E-10	1.37E-09	5.20E-10	4.20E-12	1.31E-10
66.81797	1.31E-10	1.37E-09	5.13E-10	3.00E-12	1.34E-10
66.86743	1.24E-10	1.37E-09	4.78E-10	4.36E-12	1.36E-10
66.91718	1.28E-10	1.37E-09	4.87E-10	6.83E-12	1.37E-10
66.96718	1.13E-10	1.37E-09	4.82E-10	3.19E-12	1.42E-10
67.01718	1.12E-10	1.36E-09	5.16E-10	3.26E-13	1.48E-10
67.06718	1.14E-10	1.37E-09	5.01E-10	-2.19E-12	1.50E-10
67.11692	1.12E-10	1.35E-09	5.23E-10	-3.23E-12	1.50E-10
67.16718	1.11E-10	1.36E-09	5.10E-10	-5.36E-12	1.50E-10
67.2177	1.16E-10	1.36E-09	5.08E-10	-4.37E-12	1.48E-10
67.26743	1.13E-10	1.37E-09	4.52E-10	-1.77E-12	1.42E-10
67.31718	1.16E-10	1.37E-09	4.82E-10	-9.45E-13	1.41E-10
67.36797	1.22E-10	1.38E-09	4.95E-10	-1.26E-12	1.41E-10
67.41952	1.23E-10	1.38E-09	4.91E-10	-3.13E-12	1.39E-10
67.4677	1.31E-10	1.37E-09	5.09E-10	-1.92E-12	1.44E-10
67.51718	1.36E-10	1.36E-09	5.41E-10	-2.05E-12	1.46E-10
67.56743	1.37E-10	1.35E-09	5.50E-10	2.75E-12	1.40E-10
67.61743	1.32E-10	1.34E-09	5.31E-10	7.17E-12	1.35E-10
67.66692	1.29E-10	1.34E-09	5.33E-10	9.11E-12	1.36E-10
67.7177	1.17E-10	1.34E-09	5.26E-10	8.49E-12	1.35E-10

67.76743	1.14E-10	1.36E-09	5.22E-10	9.27E-12	1.38E-10
67.81743	1.18E-10	1.36E-09	5.09E-10	4.90E-12	1.40E-10
67.86743	1.18E-10	1.37E-09	5.01E-10	1.39E-12	1.48E-10
67.91692	1.18E-10	1.38E-09	5.07E-10	2.36E-13	1.52E-10
67.96692	1.22E-10	1.38E-09	5.26E-10	8.32E-13	1.47E-10
68.0177	1.21E-10	1.39E-09	5.31E-10	2.77E-12	1.44E-10
68.06718	1.13E-10	1.39E-09	5.30E-10	2.70E-12	1.44E-10
68.11692	1.13E-10	1.38E-09	5.48E-10	5.34E-12	1.34E-10
68.16822	1.14E-10	1.36E-09	5.38E-10	1.68E-12	1.39E-10
68.21718	1.16E-10	1.37E-09	5.41E-10	2.94E-12	1.46E-10
68.26667	1.12E-10	1.38E-09	5.47E-10	2.08E-12	1.45E-10
68.31692	1.13E-10	1.39E-09	5.37E-10	1.32E-12	1.47E-10
68.3664	1.12E-10	1.40E-09	5.35E-10	-4.56E-12	1.58E-10
68.41743	1.15E-10	1.41E-09	5.54E-10	-1.59E-12	1.51E-10
68.46718	1.13E-10	1.41E-09	5.40E-10	-4.69E-13	1.48E-10
68.51692	1.17E-10	1.39E-09	5.33E-10	-1.12E-12	1.51E-10
68.56692	1.17E-10	1.39E-09	5.51E-10	2.62E-12	1.46E-10
68.61743	1.22E-10	1.38E-09	5.51E-10	7.29E-12	1.36E-10
68.6664	1.28E-10	1.37E-09	5.31E-10	7.61E-12	1.34E-10
68.71667	1.27E-10	1.36E-09	5.24E-10	2.03E-12	1.37E-10
68.76718	1.28E-10	1.36E-09	5.16E-10	3.91E-12	1.39E-10
68.81718	1.34E-10	1.36E-09	5.24E-10	-6.44E-13	1.49E-10
68.86718	1.36E-10	1.38E-09	5.15E-10	-3.96E-12	1.53E-10
68.91718	1.32E-10	1.37E-09	5.22E-10	-4.88E-12	1.57E-10
68.96692	1.40E-10	1.36E-09	5.32E-10	-8.77E-13	1.52E-10
69.01692	1.43E-10	1.35E-09	5.30E-10	-3.49E-12	1.48E-10
69.06718	1.36E-10	1.35E-09	5.00E-10	2.33E-12	1.37E-10
69.11692	1.24E-10	1.34E-09	5.11E-10	5.19E-12	1.41E-10
69.16667	1.25E-10	1.35E-09	5.19E-10	5.95E-12	1.40E-10
69.21718	1.19E-10	1.37E-09	5.31E-10	3.60E-12	1.40E-10
69.2677	1.15E-10	1.38E-09	5.38E-10	5.50E-12	1.42E-10
69.31692	1.15E-10	1.39E-09	5.62E-10	6.61E-12	1.46E-10
69.36667	1.26E-10	1.39E-09	5.68E-10	6.14E-12	1.48E-10
69.41667	1.27E-10	1.39E-09	5.71E-10	5.28E-12	1.52E-10
69.46692	1.22E-10	1.38E-09	5.67E-10	7.11E-12	1.54E-10
69.51692	1.22E-10	1.37E-09	5.67E-10	3.87E-12	1.55E-10
69.56743	1.27E-10	1.37E-09	5.78E-10	-2.21E-12	1.56E-10
69.61718	1.17E-10	1.37E-09	5.44E-10	-4.49E-13	1.54E-10
69.66743	1.14E-10	1.36E-09	5.38E-10	-5.99E-13	1.53E-10
69.71667	1.19E-10	1.36E-09	5.05E-10	1.10E-12	1.53E-10
69.76718	1.20E-10	1.35E-09	5.28E-10	3.24E-12	1.48E-10
69.8177	1.16E-10	1.34E-09	4.94E-10	4.03E-12	1.52E-10
69.86743	1.20E-10	1.35E-09	5.14E-10	1.82E-12	1.49E-10
69.91692	1.20E-10	1.35E-09	5.15E-10	4.61E-12	1.43E-10
69.96743	1.16E-10	1.34E-09	5.35E-10	2.27E-12	1.41E-10

70.0164	1.15E-10	1.35E-09	5.10E-10	1.92E-12	1.42E-10
70.06797	1.15E-10	1.36E-09	5.25E-10	1.00E-12	1.40E-10
70.11667	1.18E-10	1.35E-09	5.44E-10	9.08E-13	1.44E-10
70.1664	1.15E-10	1.35E-09	5.44E-10	8.83E-13	1.49E-10
70.21718	1.21E-10	1.36E-09	5.61E-10	3.05E-12	1.51E-10
70.26692	1.19E-10	1.38E-09	5.60E-10	3.26E-12	1.50E-10
70.31718	1.19E-10	1.38E-09	5.84E-10	4.20E-12	1.44E-10
70.36692	1.16E-10	1.41E-09	5.89E-10	4.69E-12	1.39E-10
70.41692	1.22E-10	1.41E-09	5.78E-10	2.77E-12	1.34E-10
70.46718	1.16E-10	1.41E-09	5.66E-10	-1.09E-13	1.32E-10
70.51718	1.13E-10	1.38E-09	5.65E-10	4.72E-12	1.32E-10
70.56667	1.12E-10	1.37E-09	5.52E-10	5.44E-12	1.37E-10
70.61718	1.11E-10	1.36E-09	5.33E-10	7.65E-12	1.40E-10
70.66718	1.04E-10	1.35E-09	5.35E-10	4.52E-12	1.48E-10
70.71718	1.07E-10	1.35E-09	5.41E-10	4.67E-12	1.50E-10
70.76797	1.15E-10	1.36E-09	5.51E-10	1.97E-12	1.52E-10
70.81667	1.17E-10	1.37E-09	5.42E-10	3.41E-12	1.48E-10
70.86667	1.15E-10	1.37E-09	5.55E-10	4.06E-13	1.48E-10
70.91692	1.18E-10	1.37E-09	5.77E-10	7.59E-12	1.47E-10
70.96743	1.22E-10	1.36E-09	5.49E-10	5.70E-12	1.52E-10
71.01692	1.21E-10	1.37E-09	5.25E-10	4.18E-12	1.53E-10
71.06718	1.12E-10	1.36E-09	5.29E-10	8.44E-13	1.61E-10
71.11718	1.10E-10	1.37E-09	5.13E-10	1.01E-12	1.60E-10
71.16718	1.09E-10	1.37E-09	4.98E-10	-1.60E-12	1.59E-10
71.21743	1.09E-10	1.37E-09	5.29E-10	-1.27E-12	1.56E-10
71.26718	1.08E-10	1.36E-09	5.58E-10	-2.02E-12	1.56E-10
71.31797	1.14E-10	1.36E-09	5.37E-10	-2.58E-12	1.54E-10
71.36718	1.24E-10	1.36E-09	5.28E-10	-2.71E-12	1.55E-10
71.41667	1.28E-10	1.36E-09	5.24E-10	-3.62E-12	1.49E-10
71.46743	1.22E-10	1.36E-09	5.18E-10	1.77E-12	1.49E-10
71.51743	1.10E-10	1.37E-09	5.23E-10	1.74E-12	1.52E-10
71.56718	1.12E-10	1.37E-09	5.33E-10	1.87E-12	1.55E-10
71.61743	1.00E-10	1.37E-09	5.46E-10	4.14E-13	1.53E-10
71.66743	1.02E-10	1.37E-09	5.33E-10	-2.48E-12	1.60E-10
71.71743	1.08E-10	1.37E-09	5.37E-10	-4.34E-12	1.58E-10
71.76667	1.14E-10	1.37E-09	4.99E-10	-5.67E-12	1.55E-10
71.81667	1.15E-10	1.36E-09	4.99E-10	-7.45E-12	1.49E-10
71.86667	1.25E-10	1.36E-09	4.99E-10	-3.75E-12	1.46E-10
71.91692	1.22E-10	1.35E-09	5.36E-10	-2.10E-12	1.41E-10
71.96667	1.19E-10	1.37E-09	5.11E-10	-1.15E-12	1.42E-10
72.01718	1.22E-10	1.36E-09	5.59E-10	1.73E-12	1.42E-10
72.06667	1.24E-10	1.36E-09	5.56E-10	5.14E-12	1.37E-10
72.11667	1.19E-10	1.37E-09	5.66E-10	2.09E-12	1.43E-10
72.16667	1.20E-10	1.37E-09	5.49E-10	1.29E-12	1.46E-10
72.21667	1.15E-10	1.36E-09	5.41E-10	2.04E-13	1.44E-10

72.26718	1.14E-10	1.35E-09	5.13E-10	-1.44E-13	1.42E-10
72.31718	1.09E-10	1.36E-09	5.27E-10	-1.30E-12	1.49E-10
72.36743	1.09E-10	1.35E-09	5.31E-10	2.92E-12	1.41E-10
72.41692	1.03E-10	1.36E-09	5.35E-10	5.57E-12	1.45E-10
72.46692	1.13E-10	1.36E-09	5.21E-10	6.54E-12	1.48E-10
72.5177	1.15E-10	1.37E-09	5.31E-10	5.07E-12	1.56E-10
72.56692	1.22E-10	1.37E-09	5.30E-10	4.50E-12	1.59E-10
72.61743	1.24E-10	1.37E-09	5.14E-10	-3.89E-12	1.68E-10
72.66797	1.29E-10	1.36E-09	5.04E-10	-5.48E-12	1.60E-10
72.71797	1.21E-10	1.37E-09	5.18E-10	-5.49E-12	1.62E-10
72.76875	1.22E-10	1.36E-09	5.17E-10	-5.11E-12	1.58E-10
72.8177	1.19E-10	1.36E-09	4.92E-10	-3.35E-12	1.50E-10
72.86875	1.23E-10	1.37E-09	4.80E-10	3.87E-12	1.42E-10
72.91797	1.25E-10	1.35E-09	4.58E-10	1.95E-12	1.46E-10
72.9677	1.23E-10	1.34E-09	4.88E-10	-1.85E-12	1.47E-10
73.01718	1.19E-10	1.36E-09	4.86E-10	-1.28E-12	1.42E-10
73.06692	1.12E-10	1.37E-09	5.17E-10	-3.16E-12	1.44E-10
73.11667	1.06E-10	1.38E-09	5.10E-10	-5.01E-12	1.47E-10
73.16692	1.12E-10	1.38E-09	5.29E-10	3.11E-13	1.47E-10
73.21718	1.23E-10	1.38E-09	5.08E-10	1.91E-12	1.45E-10
73.26743	1.30E-10	1.35E-09	5.19E-10	9.79E-13	1.50E-10
73.31692	1.30E-10	1.35E-09	5.03E-10	3.78E-12	1.48E-10
73.3677	1.27E-10	1.34E-09	5.28E-10	7.25E-12	1.51E-10
73.41667	1.16E-10	1.35E-09	5.40E-10	5.46E-12	1.47E-10
73.46743	1.10E-10	1.35E-09	5.33E-10	4.93E-12	1.45E-10
73.51718	1.03E-10	1.36E-09	5.43E-10	9.01E-12	1.45E-10
73.56718	1.07E-10	1.35E-09	5.45E-10	9.08E-12	1.43E-10
73.61667	1.11E-10	1.35E-09	5.30E-10	4.61E-12	1.40E-10
73.66667	1.15E-10	1.36E-09	5.36E-10	2.88E-12	1.40E-10
73.7164	1.21E-10	1.35E-09	5.28E-10	6.57E-12	1.42E-10
73.7677	1.29E-10	1.34E-09	5.07E-10	2.63E-12	1.41E-10
73.8177	1.29E-10	1.34E-09	5.10E-10	3.13E-13	1.46E-10
73.86718	1.34E-10	1.35E-09	5.42E-10	-2.46E-12	1.52E-10
73.91718	1.33E-10	1.34E-09	5.04E-10	-3.56E-12	1.52E-10
73.9677	1.28E-10	1.36E-09	5.22E-10	-6.05E-12	1.48E-10
74.01692	1.21E-10	1.36E-09	5.23E-10	-6.21E-12	1.52E-10
74.06718	1.21E-10	1.35E-09	5.31E-10	-5.97E-12	1.52E-10
74.11718	1.13E-10	1.35E-09	5.13E-10	-4.39E-12	1.49E-10
74.16667	1.15E-10	1.34E-09	5.48E-10	-6.71E-12	1.52E-10
74.21718	1.11E-10	1.34E-09	5.66E-10	-8.83E-12	1.58E-10
74.26718	1.14E-10	1.34E-09	5.44E-10	-8.12E-12	1.54E-10
74.31718	1.17E-10	1.36E-09	5.24E-10	-7.99E-12	1.53E-10
74.3677	1.17E-10	1.36E-09	5.35E-10	-3.91E-12	1.49E-10
74.41743	1.12E-10	1.37E-09	5.13E-10	-1.37E-12	1.49E-10
74.46743	1.20E-10	1.37E-09	4.96E-10	1.06E-12	1.43E-10

74.5177	1.17E-10	1.37E-09	5.22E-10	2.23E-12	1.41E-10
74.5677	1.15E-10	1.36E-09	5.49E-10	3.19E-12	1.38E-10
74.61667	1.15E-10	1.36E-09	5.18E-10	2.43E-12	1.40E-10
74.66718	1.23E-10	1.36E-09	5.39E-10	3.03E-12	1.38E-10
74.71718	1.18E-10	1.36E-09	5.38E-10	3.42E-12	1.43E-10
74.76692	1.17E-10	1.36E-09	5.43E-10	1.20E-12	1.45E-10
74.81743	1.17E-10	1.36E-09	5.25E-10	1.23E-12	1.51E-10
74.86743	1.24E-10	1.36E-09	5.49E-10	7.60E-13	1.50E-10
74.91667	1.12E-10	1.35E-09	5.36E-10	-2.03E-12	1.54E-10
74.96743	1.14E-10	1.35E-09	5.35E-10	-5.06E-12	1.53E-10
75.01692	1.13E-10	1.34E-09	5.22E-10	-5.17E-12	1.56E-10
75.06718	1.14E-10	1.35E-09	5.18E-10	-6.47E-12	1.53E-10
75.11743	1.14E-10	1.35E-09	5.20E-10	-7.86E-12	1.51E-10
75.16743	1.22E-10	1.35E-09	5.17E-10	-4.24E-12	1.52E-10
75.21692	1.21E-10	1.36E-09	5.39E-10	-3.22E-12	1.53E-10
75.26667	1.23E-10	1.35E-09	5.26E-10	-1.41E-12	1.54E-10
75.31692	1.20E-10	1.35E-09	5.17E-10	2.95E-12	1.55E-10
75.36797	1.16E-10	1.36E-09	5.07E-10	2.55E-12	1.62E-10
75.4177	1.14E-10	1.36E-09	5.01E-10	3.51E-12	1.62E-10
75.46743	1.19E-10	1.37E-09	4.77E-10	5.03E-12	1.59E-10
75.51743	1.15E-10	1.37E-09	4.86E-10	3.85E-12	1.55E-10
75.56822	1.19E-10	1.37E-09	5.03E-10	7.90E-13	1.54E-10
75.6177	1.19E-10	1.37E-09	5.11E-10	6.47E-12	1.51E-10
75.66848	1.22E-10	1.37E-09	5.08E-10	6.67E-12	1.47E-10
75.71743	1.12E-10	1.36E-09	5.26E-10	6.12E-12	1.51E-10
75.76743	1.16E-10	1.37E-09	5.34E-10	9.55E-12	1.50E-10
75.81718	1.08E-10	1.37E-09	5.37E-10	8.49E-12	1.49E-10
75.86718	1.13E-10	1.37E-09	5.51E-10	3.40E-12	1.41E-10
75.91718	1.19E-10	1.38E-09	5.60E-10	-7.46E-13	1.44E-10
75.96692	1.33E-10	1.36E-09	5.39E-10	-2.85E-12	1.42E-10
76.01692	1.37E-10	1.35E-09	5.28E-10	-2.41E-12	1.42E-10
76.0677	1.43E-10	1.35E-09	4.92E-10	-2.02E-13	1.43E-10
76.1164	1.37E-10	1.36E-09	4.80E-10	-1.09E-12	1.53E-10
76.16692	1.26E-10	1.35E-09	4.74E-10	4.10E-12	1.50E-10
76.21743	1.24E-10	1.35E-09	4.74E-10	4.60E-12	1.49E-10
76.26743	1.18E-10	1.36E-09	4.88E-10	3.97E-12	1.51E-10
76.31667	1.17E-10	1.36E-09	5.42E-10	2.32E-12	1.47E-10
76.36718	1.27E-10	1.36E-09	5.36E-10	2.57E-12	1.44E-10
76.41718	1.31E-10	1.36E-09	5.29E-10	-9.44E-13	1.49E-10
76.46718	1.27E-10	1.37E-09	5.26E-10	8.38E-13	1.52E-10
76.51718	1.32E-10	1.35E-09	5.00E-10	-1.68E-12	1.51E-10
76.56692	1.34E-10	1.34E-09	4.87E-10	-2.61E-12	1.55E-10
76.6177	1.24E-10	1.35E-09	4.77E-10	-1.00E-12	1.53E-10
76.66667	1.20E-10	1.35E-09	4.81E-10	3.23E-12	1.51E-10
76.71692	1.17E-10	1.36E-09	4.92E-10	2.38E-13	1.47E-10

76.76667	1.10E-10	1.37E-09	5.30E-10	3.54E-13	1.51E-10
76.81692	1.14E-10	1.37E-09	5.23E-10	1.99E-12	1.50E-10
76.86743	1.22E-10	1.36E-09	5.43E-10	1.97E-12	1.49E-10
76.91848	1.23E-10	1.36E-09	5.64E-10	-3.29E-12	1.51E-10
76.96743	1.25E-10	1.36E-09	5.58E-10	-2.07E-13	1.50E-10
77.0177	1.31E-10	1.36E-09	5.17E-10	1.09E-12	1.43E-10
77.06692	1.29E-10	1.34E-09	5.23E-10	-7.11E-14	1.40E-10
77.1177	1.18E-10	1.33E-09	4.94E-10	-3.06E-12	1.46E-10
77.16667	1.22E-10	1.31E-09	4.72E-10	1.69E-12	1.45E-10
77.21743	1.15E-10	1.31E-09	4.89E-10	8.43E-13	1.47E-10
77.26667	1.10E-10	1.31E-09	5.17E-10	-4.27E-13	1.52E-10
77.31718	1.15E-10	1.32E-09	5.09E-10	-1.58E-13	1.57E-10
77.36718	1.18E-10	1.33E-09	5.40E-10	1.53E-12	1.51E-10
77.41718	1.13E-10	1.33E-09	5.47E-10	-2.56E-12	1.50E-10
77.46718	1.12E-10	1.34E-09	5.32E-10	-3.50E-13	1.48E-10
77.51667	1.10E-10	1.36E-09	5.19E-10	-1.04E-12	1.46E-10
77.5677	1.00E-10	1.35E-09	5.08E-10	-2.12E-12	1.43E-10
77.61718	9.87E-11	1.36E-09	5.00E-10	-2.25E-12	1.42E-10
77.66848	9.80E-11	1.36E-09	5.20E-10	-2.07E-12	1.49E-10
77.71743	1.02E-10	1.35E-09	5.25E-10	-6.90E-12	1.50E-10
77.76692	1.05E-10	1.34E-09	5.52E-10	-8.18E-12	1.52E-10
77.8177	1.01E-10	1.36E-09	5.92E-10	-5.99E-12	1.53E-10
77.86692	1.02E-10	1.37E-09	5.77E-10	-3.83E-12	1.51E-10
77.91692	1.06E-10	1.36E-09	5.79E-10	-3.30E-12	1.44E-10
77.96692	1.05E-10	1.37E-09	5.70E-10	-7.04E-13	1.43E-10
78.01692	1.04E-10	1.37E-09	5.38E-10	-1.65E-12	1.49E-10
78.06667	1.08E-10	1.36E-09	5.11E-10	1.58E-12	1.47E-10
78.11692	1.12E-10	1.34E-09	5.21E-10	8.07E-13	1.45E-10
78.16797	1.19E-10	1.34E-09	5.07E-10	4.04E-12	1.45E-10
78.21743	1.17E-10	1.34E-09	5.27E-10	3.85E-12	1.43E-10
78.26692	1.22E-10	1.33E-09	5.45E-10	4.69E-12	1.40E-10
78.31718	1.26E-10	1.33E-09	5.24E-10	-1.72E-12	1.46E-10
78.3677	1.22E-10	1.33E-09	5.18E-10	-4.03E-12	1.47E-10
78.41743	1.17E-10	1.34E-09	5.18E-10	-7.60E-12	1.51E-10
78.46692	1.22E-10	1.33E-09	5.10E-10	-6.95E-12	1.50E-10
78.51692	1.17E-10	1.34E-09	5.14E-10	-6.14E-12	1.49E-10
78.56743	1.15E-10	1.34E-09	5.51E-10	1.25E-12	1.45E-10
78.61718	1.15E-10	1.35E-09	5.70E-10	1.68E-12	1.51E-10
78.6677	1.15E-10	1.36E-09	5.65E-10	1.54E-12	1.46E-10
78.71743	1.20E-10	1.37E-09	5.56E-10	3.21E-12	1.46E-10
78.76743	1.30E-10	1.38E-09	5.59E-10	1.86E-12	1.45E-10
78.81718	1.21E-10	1.38E-09	5.51E-10	-2.44E-12	1.41E-10
78.86692	1.20E-10	1.38E-09	5.41E-10	-7.67E-13	1.36E-10
78.9177	1.16E-10	1.38E-09	5.59E-10	2.27E-13	1.41E-10
78.96718	1.01E-10	1.38E-09	5.65E-10	4.52E-13	1.41E-10

79.01692	9.74E-11	1.36E-09	5.44E-10	3.63E-12	1.41E-10
79.0677	1.03E-10	1.36E-09	5.39E-10	3.59E-12	1.44E-10
79.11692	1.04E-10	1.36E-09	5.50E-10	6.51E-12	1.47E-10
79.16667	1.12E-10	1.34E-09	5.32E-10	5.08E-12	1.46E-10
79.21692	1.28E-10	1.34E-09	5.22E-10	1.46E-12	1.50E-10
79.26692	1.23E-10	1.33E-09	5.34E-10	1.14E-13	1.52E-10
79.31692	1.24E-10	1.34E-09	5.22E-10	-1.84E-12	1.56E-10
79.36692	1.23E-10	1.34E-09	5.10E-10	-4.19E-12	1.53E-10
79.4177	1.21E-10	1.35E-09	5.18E-10	-4.59E-12	1.53E-10
79.46667	1.14E-10	1.34E-09	5.12E-10	-2.26E-12	1.56E-10
79.51718	1.11E-10	1.35E-09	5.05E-10	-1.01E-12	1.52E-10
79.56692	1.09E-10	1.34E-09	5.03E-10	5.68E-13	1.49E-10
79.61718	1.09E-10	1.33E-09	5.01E-10	3.80E-12	1.51E-10
79.66692	1.03E-10	1.34E-09	5.03E-10	3.63E-12	1.54E-10
79.71743	1.01E-10	1.35E-09	5.10E-10	2.16E-12	1.49E-10
79.76743	1.09E-10	1.34E-09	5.20E-10	2.29E-12	1.53E-10
79.81692	1.10E-10	1.35E-09	5.18E-10	9.49E-13	1.55E-10
79.86797	1.13E-10	1.35E-09	5.23E-10	-4.43E-12	1.55E-10
79.91718	1.15E-10	1.34E-09	5.43E-10	-1.43E-12	1.53E-10
79.96667	1.13E-10	1.35E-09	5.53E-10	-1.30E-12	1.52E-10
80.0177	1.09E-10	1.35E-09	5.52E-10	-4.95E-12	1.55E-10
80.06718	1.16E-10	1.36E-09	5.54E-10	-6.44E-12	1.56E-10
80.1177	1.24E-10	1.37E-09	5.58E-10	-4.37E-12	1.53E-10
80.16718	1.38E-10	1.38E-09	5.40E-10	-2.75E-12	1.53E-10
80.21743	1.34E-10	1.38E-09	5.39E-10	-4.84E-12	1.52E-10
80.26743	1.32E-10	1.38E-09	5.49E-10	-1.07E-13	1.51E-10
80.31692	1.23E-10	1.37E-09	5.54E-10	2.38E-12	1.51E-10
80.36718	1.13E-10	1.36E-09	5.30E-10	1.42E-12	1.53E-10
80.41667	9.89E-11	1.34E-09	5.14E-10	-1.49E-12	1.54E-10
80.46743	1.08E-10	1.33E-09	5.00E-10	-9.45E-13	1.59E-10
80.51718	1.13E-10	1.33E-09	4.95E-10	-1.21E-12	1.55E-10
80.56692	1.17E-10	1.33E-09	5.05E-10	3.55E-12	1.50E-10
80.61797	1.22E-10	1.34E-09	5.16E-10	3.72E-12	1.51E-10
80.6677	1.23E-10	1.35E-09	5.43E-10	3.69E-12	1.47E-10
80.71667	1.23E-10	1.35E-09	5.55E-10	3.97E-12	1.46E-10
80.76692	1.30E-10	1.36E-09	5.60E-10	8.90E-13	1.50E-10
80.81797	1.32E-10	1.35E-09	5.68E-10	-6.40E-12	1.56E-10
80.86743	1.28E-10	1.34E-09	5.71E-10	-5.09E-12	1.51E-10
80.91797	1.32E-10	1.34E-09	5.63E-10	-4.95E-12	1.52E-10
80.96718	1.30E-10	1.34E-09	5.50E-10	-3.62E-12	1.48E-10
81.01667	1.17E-10	1.34E-09	5.31E-10	-1.51E-12	1.46E-10
81.06692	1.10E-10	1.35E-09	5.10E-10	-9.29E-13	1.47E-10
81.11718	1.14E-10	1.33E-09	5.12E-10	-6.35E-13	1.48E-10
81.16718	1.10E-10	1.33E-09	5.01E-10	-3.32E-12	1.50E-10
81.21692	1.11E-10	1.33E-09	5.27E-10	-3.37E-12	1.54E-10

81.26667	1.15E-10	1.32E-09	5.42E-10	-7.92E-12	1.54E-10
81.3177	1.20E-10	1.32E-09	5.43E-10	-7.49E-12	1.50E-10
81.36718	1.20E-10	1.33E-09	5.37E-10	-7.17E-12	1.50E-10
81.4177	1.17E-10	1.34E-09	5.29E-10	-5.10E-12	1.52E-10
81.46718	1.19E-10	1.36E-09	5.24E-10	-5.49E-12	1.50E-10
81.51743	1.18E-10	1.37E-09	4.97E-10	-2.57E-12	1.46E-10
81.56692	1.19E-10	1.39E-09	4.91E-10	-2.28E-12	1.49E-10
81.61692	1.16E-10	1.39E-09	4.85E-10	-6.52E-12	1.53E-10
81.66718	1.17E-10	1.38E-09	4.98E-10	-8.39E-12	1.55E-10
81.71692	1.19E-10	1.37E-09	4.84E-10	-6.83E-12	1.57E-10
81.76718	1.23E-10	1.35E-09	5.01E-10	-4.46E-12	1.56E-10
81.81692	1.13E-10	1.34E-09	4.97E-10	-6.83E-13	1.51E-10
81.86822	1.18E-10	1.32E-09	4.92E-10	7.25E-12	1.45E-10
81.91692	8.23E-11	1.33E-09	4.61E-10	1.22E-11	1.41E-10

References

1. Gubanova EL. Experimental study and mathematical modeling of catalytic partial oxidation of methane to synthesis gas over monolith catalyst at short contact times [PhD Thesis]: Institut de Recherche sur la Catalyse et l'Environment de Lyon, IRCELYON; 2008.

B. Steady-state kinetic modelling code used in chapter 7

i. Function file

```
function ydot = MTHmodel9(Tau, mf)

global k1fValue
global k1bValue

global k2Value
global k3Value

global kox1Value
global kox2Value
global kox3Value

global k4idValue
global k5idValue

global k6Value
global k7Value

global k4dValue
global k5dValue

global k8Value
global k9Value
global k10Value
global k11Value
global k12Value
global k13Value
global k14Value
global k15Value
global k16Value

global k17Value
global k18Value
global k19Value
global k20Value
global k21Value
global k22Value
global k23Value

global k24fValue
global k24bValue
global k25fValue
global k25bValue
global k26fValue
global k26bValue
global k27fValue
global k27bValue
global k28fValue
global k28bValue
global k29fValue
global k29bValue
global k30fValue
global k30bValue
global k31fValue
global k31bValue
global k32fValue
```

```
global k32bValue
global k33fValue
global k33bValue
global k34fValue
global k34bValue
global k35fValue
global k35bValue
global k36fValue
global k36bValue
global k37fValue
global k37bValue
global k38fValue
global k38bValue
global k39fValue
global k39bValue

global k40Value
global k41Value
global k42Value
global k43Value
global k44Value
global k45Value

global k46Value
global k47Value
global k48Value
global k49Value
global k50Value
global k51Value

global k52Value
global k53Value
global k54Value
global k55Value
global k56Value

global k57Value
global k58Value
global k59Value
global k60Value
global k61Value
global k62Value
global k63Value
global k64Value
global k65Value

global k66Value
global k67Value
global k68Value
global k69Value
global k70Value
global k71Value
global k72Value
global k73Value
global k74Value

global k75Value
global k76Value
global k77Value
global k78Value
global k79Value
```

```
global k80Value
global k81Value
global k82Value
global k83Value

global k84Value
global k85Value
global k86Value
global k87Value
global k88Value
global k89Value
global k90Value
global k91Value
global k92Value

global k93Value
global k94Value
global k95Value
global k96Value
global k97Value
global k98Value
global k99Value
global k100Value
global k101Value

global k102Value
global k103Value
global k104Value
global k105Value
global k106Value
global k107Value
global k108Value
global k109Value
global k110Value
global k111Value
global k112Value
global k113Value
global k114Value
global k115Value
global k116Value
global k117Value
global k118Value
global k119Value
global k120Value
global k121Value
global k122Value
global k123Value
global k124Value
global k125Value
global k126Value
global k127Value
global k128Value
global k129Value
global k130Value
global k131Value
global k132Value
global k133Value
global k134Value
global k135Value
global k136Value
global k137Value
```

```
global k138Value
global k139Value
global k140Value
global k141Value
global k142Value
global k143Value
global k144Value
global k145Value
global k146Value

global k147Value
global k148Value
global k149Value
global k150Value
global k151Value
global k152Value
global k153Value
global k154Value
global k155Value
global k156Value
global k157Value
global k158Value
global k159Value
global k160Value
global k161Value
global k162Value
global k163Value
global k164Value
global k165Value
global k166Value
global k167Value
global k168Value
global k169Value
global k170Value
global k171Value
global k172Value
global k173Value
global k174Value
global k175Value
global k176Value
global k177Value
global k178Value
global k179Value
global k180Value
global k181Value
global k182Value
global k183Value
global k184Value
global k185Value
global k186Value
global k187Value
global k188Value
global k189Value
global k190Value
global k191Value
global k192Value
global k193Value
global k194Value
global k195Value
global k196Value
global k197Value
global k198Value
```

```
global k199Value
global k200Value
global k201Value
global k202Value
global k203Value
global k204Value
global k205Value
global k206Value
global k207Value
global k208Value
global k209Value
global k210Value
global k211Value
global k212Value
global k213Value


%constants
P_Tot = 1; %(bar)
N_tot =
(mf(1)/32)+(mf(2)/46)+(mf(3)/18)+(mf(4)/16)+(mf(5)/2)+(mf(6)/28)+(mf(7)/30)
+(mf(8)/28)+(mf(9)/42)+(mf(10)/56)+(mf(11)/70)+(mf(12)/84)+(mf(13)/98)+(mf(
14)/112)+(mf(15)/126)+(mf(16)/140)+(mf(17)/30)+(mf(18)/44)+(mf(19)/58)+(mf(
20)/72)+(mf(21)/86)+(mf(22)/100)+(mf(23)/114)+(mf(24)/128)+(mf(25)/142)+(mf
(26)/76)+(mf(27)/90)+(mf(28)/78)+(mf(29)/92)+(mf(30)/106)+(mf(31)/120)+(mf(
32)/134)+(mf(33)/28);

%%Adsorption constants
%Oxygenates (1/bar)
K1 = 190;
K2 = 250;
K3 = 209;

%Methane, Hydrogen, CO and CH2O (1/bar)
K4 = 0.005;
K5 = 0.01;
K6 = (1/3)*K4;
K7 = 400;

%Alkenes (1/bar)
K8 = 1.5;
K9 = 1.3;
K10 = 0.7;
K11 = 0.3;
K12 = 1.00;
K13 = 1.53;
K14 = 1.53;
K15 = 1.53;
K16 = 1.53;

%Alkanes (1/bar)
K17 = K4;
K18 = K4;
K19 = K4;
K20 = K4;
K21 = K4;
K22 = K4;
K23 = K4;
K24 = K4;
K25 = K4;
```

```
%intermediates
K26 = K2; % same as DME
K27 = K2;

%Aromatics
K28=7.81;
K29=7.81;
K30=4;
K31=7.81;
K32=7.81;

%Mole fraction (mf) definitions
x_CH3OH = (mf(1)/32)/N_tot;
x_CH3OCH3 = (mf(2)/46)/N_tot;
x_H2O = (mf(3)/18)/N_tot;

x_CH4=(mf(4)/16)/N_tot;
x_H2=(mf(5)/2)/N_tot;
x_CO=(mf(6)/28)/N_tot;
x_CH2O=(mf(7)/30)/N_tot;

x_C2H4 = (mf(8)/28)/N_tot;
x_C3H6 = (mf(9)/42)/N_tot;
x_C4H8 = (mf(10)/56)/N_tot;
x_C5H10 = (mf(11)/70)/N_tot;
x_C6H12 = (mf(12)/84)/N_tot;
x_C7H14 = (mf(13)/98)/N_tot;
x_C8H16 = (mf(14)/112)/N_tot;
x_C9H18 = (mf(15)/126)/N_tot;
x_C10H20 = (mf(16)/140)/N_tot;

x_C2H6 = (mf(17)/30)/N_tot;
x_C3H8 = (mf(18)/44)/N_tot;
x_C4H10 = (mf(19)/58)/N_tot;
x_C5H12 = (mf(20)/72)/N_tot;
x_C6H14 = (mf(21)/86)/N_tot;
x_C7H16 = (mf(22)/100)/N_tot;
x_C8H18 = (mf(23)/114)/N_tot;
x_C9H20 = (mf(24)/128)/N_tot;
x_C10H22 = (mf(25)/142)/N_tot;

x_C3H8O2 = (mf(26)/76)/N_tot;
x_C4H10O2 = (mf(27)/90)/N_tot;

x_C6H6 = (mf(28)/78)/N_tot;
x_C7H8 = (mf(29)/92)/N_tot;
x_C8H10 = (mf(30)/106)/N_tot;
x_C9H12 = (mf(31)/120)/N_tot;
x_C10H14 = (mf(32)/134)/N_tot;

x_N2 = (mf(33)/28)/N_tot;

HZ=1/(1+(K1*x_CH3OH*P_Tot)+(K2*x_CH3OCH3*P_Tot)+(K3*x_H2O*P_Tot)+(K4*x_CH4*
P_Tot)+(K5*x_H2*P_Tot)+(K6*x_CO*P_Tot)+(K7*x_CH2O*P_Tot)+...

(K8*x_C2H4*P_Tot)+(K9*x_C3H6*P_Tot)+(K10*x_C4H8*P_Tot)+(K11*x_C5H10*P_Tot)+
(K12*x_C6H12*P_Tot)+(K13*x_C7H14*P_Tot)+(K14*x_C8H16*P_Tot)+(K15*x_C9H18*P_
Tot)+(K16*x_C10H20*P_Tot)+...
```

```
(K17*x_C2H6*P_Tot)+(K18*x_C3H8*P_Tot)+(K19*x_C4H10*P_Tot)+(K20*x_C5H12*P_To
t)+(K21*x_C6H14*P_Tot)+(K22*x_C7H16*P_Tot)+(K23*x_C8H18*P_Tot)+(K24*x_C9H20
*P_Tot)+(K25*x_C10H22*P_Tot)+...
    (K26*x_C3H8O2*P_Tot)+(K27*x_C4H10O2*P_Tot)+...

(K28*x_C6H6*P_Tot)+(K29*x_C7H8*P_Tot)+(K30*x_C8H10*P_Tot)+(K31*x_C9H12*P_To
t)+(K32*x_C10H14*P_Tot));


k1f = k1fValue;
k1b = k1bValue;

k2 = k2Value;
k3 = k3Value;

kox1 = kox1Value;
kox2 = kox2Value;
kox3 = kox3Value;

k4id = k4idValue;
k5id = k5idValue;

k4d = k4dValue;
k5d = k5dValue;

k6 = k6Value;
k7 = k7Value;

k8 = k8Value;
k9 = k9Value;
k10 = k10Value;
k11 = k11Value;
k12 = k12Value;
k13 = k13Value;
k14 = k14Value;
k15 = k15Value;

k16 = k16Value;
k17 = k17Value;
k18 = k18Value;
k19 = k19Value;
k20 = k20Value;
k21 = k21Value;
k22 = k22Value;
k23 = k23Value;

k24f = k24fValue;
k24b = k24bValue;
k25f = k25fValue;
k25b = k25bValue;
k26f = k26fValue;
k26b = k26bValue;
k27f = k27fValue;
k27b = k27bValue;
k28f = k28fValue;
k28b = k28bValue;
k29f = k29fValue;
k29b = k29bValue;
k30f = k30fValue;
```

```
k30b = k30bValue;
k31f = k31fValue;
k31b = k31bValue;
k32f = k32fValue;
k32b = k32bValue;
k33f = k33fValue;
k33b = k33bValue;
k34f = k34fValue;
k34b = k34bValue;
k35f = k35fValue;
k35b = k35bValue;
k36f = k36fValue;
k36b = k36bValue;
k37f = k37fValue;
k37b = k37bValue;
k38f = k38fValue;
k38b = k38bValue;
k39f = k39fValue;
k39b = k39bValue;

k40 = k40Value;
k41 = k41Value;
k42 = k42Value;
k43 = k43Value;
k44 = k44Value;
k45 = k45Value;

k46 = k46Value;
k47 = k47Value;
k48 = k48Value;
k49 = k49Value;
k50 = k50Value;
k51 = k51Value;

k52 = k52Value;
k53 = k53Value;
k54 = k54Value;
k55 = k55Value;
k56 = k56Value;


k57 = k57Value;
k58 = k58Value;
k59 = k59Value;
k60 = k60Value;
k61 = k61Value;
k62 = k62Value;
k63 = k63Value;
k64 = k64Value;
k65 = k65Value;

k66 = k66Value;
k67 = k67Value;
k68 = k68Value;
k69 = k69Value;
k70 = k70Value;
k71 = k71Value;
k72 = k72Value;
k73 = k73Value;
k74 = k74Value;
```

```
k75 = k75Value;
k76 = k76Value;
k77 = k77Value;
k78 = k78Value;
k79 = k79Value;
k80 = k80Value;
k81 = k81Value;
k82 = k82Value;
k83 = k83Value;

k84 = k84Value;
k85 = k85Value;
k86 = k86Value;
k87 = k87Value;
k88 = k88Value;
k89 = k89Value;
k90 = k90Value;
k91 = k91Value;
k92 = k92Value;

k93 = k93Value;
k94 = k94Value;
k95 = k95Value;
k96 = k96Value;
k97 = k97Value;
k98 = k98Value;
k99 = k99Value;
k100 = k100Value;
k101 = k101Value;

k102 = k102Value;
k103 = k103Value;
k104 = k104Value;
k105 = k105Value;
k106 = k106Value;
k107 = k107Value;
k108 = k108Value;
k109 = k109Value;
k110 = k110Value;
k111 = k111Value;
k112 = k112Value;
k113 = k113Value;
k114 = k114Value;
k115 = k115Value;
k116 = k116Value;
k117 = k117Value;
k118 = k118Value;
k119 = k119Value;
k120 = k120Value;
k121 = k121Value;
k122 = k122Value;
k123 = k123Value;
k124 = k124Value;
k125 = k125Value;
k126 = k126Value;
k127 = k127Value;
k128 = k128Value;
k129 = k129Value;
k130 = k130Value;
k131 = k131Value;
```

```
k132 = k132Value;
k133 = k133Value;
k134 = k134Value;
k135 = k135Value;
k136 = k136Value;
k137 = k137Value;
k138 = k138Value;
k139 = k139Value;
k140 = k140Value;
k141 = k141Value;
k142 = k142Value;
k143 = k143Value;
k144 = k144Value;
k145 = k145Value;
k146 = k146Value;
k147 = k147Value;
k148 = k148Value;
k149 = k149Value;
k150 = k150Value;
k151 = k151Value;
k152 = k152Value;
k153 = k153Value;
k154 = k154Value;
k155 = k155Value;
k156 = k156Value;
k157 = k157Value;
k158 = k158Value;
k159 = k159Value;
k160 = k160Value;
k161 = k161Value;
k162 = k162Value;
k163 = k163Value;
k164 = k164Value;
k165 = k165Value;
k166 = k166Value;
k167 = k167Value;
k168 = k168Value;
k169 = k169Value;
k170 = k170Value;
k171 = k171Value;
k172 = k172Value;
k173 = k173Value;
k174 = k174Value;
k175 = k175Value;
k176 = k176Value;
k177 = k177Value;
k178 = k178Value;
k179 = k179Value;
k180 = k180Value;
k181 = k181Value;
k182 = k182Value;
k183 = k183Value;
k184 = k184Value;
k185 = k185Value;
k186 = k186Value;
k187 = k187Value;
k188 = k188Value;
k189 = k189Value;
k190 = k190Value;
k191 = k191Value;
k192 = k192Value;
k193 = k193Value;
```

```
k194 = k194Value;
k195 = k195Value;
k196 = k196Value;
k197 = k197Value;
k198 = k198Value;
k199 = k199Value;
k200 = k200Value;
k201 = k201Value;
k202 = k202Value;
k203 = k203Value;
k204 = k204Value;
k205 = k205Value;
k206 = k206Value;
k207 = k207Value;
k208 = k208Value;
k209 = k209Value;
k210 = k210Value;
k211 = k211Value;
k212 = k212Value;
k213 = k213Value;


%% rate equations
r1f=k1f*K1*(x_CH3OH^2)*(P_Tot^2)*HZ;
r1b=k1b*K2*x_CH3OCH3*x_H2O*(P_Tot^2)*HZ;

%Methanol decomposition
r2=k2*x_CH3OH*P_Tot;

%DME decomposition
r3=k3*(x_CH3OCH3)*P_Tot;

%Indirect formation of ethene and propene

rox1=kox1*K2*x_CH3OCH3*x_CH3OH*(P_Tot^2)*HZ;
rox2=kox2*K26*x_CH3OCH3*x_C3H8O2*(P_Tot^2)*HZ;
rox3=kox3*K26*x_CH3OH*x_C3H8O2*(P_Tot^2)*HZ;

r4id=k4id*K27*x_C4H10O2*P_Tot*HZ;
r5id=k5id*K27*x_C4H10O2*P_Tot*HZ;

r6=k6*K31*x_C9H12*P_Tot*HZ;
r7=k7*K31*x_C9H12*P_Tot*HZ;

%Direct formation of ethene and propene
r4d = k4d*K2*x_CH3OH*x_CH3OCH3*(P_Tot^2)*HZ;
r5d = k5d*K2*x_CH3OCH3*P_Tot*HZ;

%Olefin methylation with MeOH
r8=k8*K1*x_C2H4*x_CH3OH*(P_Tot^2)*HZ;
r9=k9*K1*x_C3H6*x_CH3OH*(P_Tot^2)*HZ;
r10=k10*K1*x_C4H8*x_CH3OH*(P_Tot^2)*HZ;
r11=k11*K1*x_C5H10*x_CH3OH*(P_Tot^2)*HZ;
r12=k12*K1*x_C6H12*x_CH3OH*(P_Tot^2)*HZ;
r13=k13*K1*x_C7H14*x_CH3OH*(P_Tot^2)*HZ;
r14=k14*K1*x_C8H16*x_CH3OH*(P_Tot^2)*HZ;
r15=k15*K1*x_C9H18*x_CH3OH*(P_Tot^2)*HZ;

%Olefin methylation with DME
r16=k16*K2*x_C2H4*x_CH3OCH3*(P_Tot^2)*HZ;
```

```
r17=k17*K2*x_C3H6*x_CH3OCH3*(P_Tot^2)*HZ;
r18=k18*K2*x_C4H8*x_CH3OCH3*(P_Tot^2)*HZ;
r19=k19*K2*x_C5H10*x_CH3OCH3*(P_Tot^2)*HZ;
r20=k20*K2*x_C6H12*x_CH3OCH3*(P_Tot^2)*HZ;
r21=k21*K2*x_C7H14*x_CH3OCH3*(P_Tot^2)*HZ;
r22=k22*K2*x_C8H16*x_CH3OCH3*(P_Tot^2)*HZ;
r23=k23*K2*x_C9H18*x_CH3OCH3*(P_Tot^2)*HZ;

%oligomerisation/cracking reactions
r24f=k24f*K8*(x_C2H4^2)*(P_Tot^2)*HZ;
r24b=k24b*K10*(x_C4H8)*(P_Tot)*HZ;
r25f=k25f*K9*x_C2H4*x_C3H6*(P_Tot^2)*HZ;
r25b=k25b*K11*x_C5H10*P_Tot*HZ;
r26f=k26f*K10*x_C2H4*x_C4H8*(P_Tot^2)*HZ;
r26b=k26b*K12*x_C6H12*P_Tot*HZ;
r27f=k27f*K9*(x_C3H6^2)*(P_Tot^2)*HZ;
r27b=k27b*K12*x_C6H12*P_Tot*HZ;
r28f=k28f*K11*x_C5H10*x_C2H4*(P_Tot^2)*HZ;
r28b=k28b*K13*x_C7H14*P_Tot*HZ;
r29f=k29f*K10*x_C4H8*x_C3H6*(P_Tot^2)*HZ;
r29b=k29b*K13*x_C7H14*P_Tot*HZ;
r30f=k30f*K12*x_C6H12*x_C2H4*(P_Tot^2)*HZ;
r30b=k30b*K14*x_C8H16*P_Tot*HZ;
r31f=k31f*K11*x_C5H10*x_C3H6*(P_Tot^2)*HZ;
r31b=k31b*K14*x_C8H16*P_Tot*HZ;
r32f=k32f*K10*x_C4H8*x_C4H8*(P_Tot^2)*HZ;
r32b=k32b*K14*x_C8H16*P_Tot*HZ;
r33f=k33f*K13*x_C7H14*x_C2H4*(P_Tot^2)*HZ;
r33b=k33b*K15*x_C9H18*P_Tot*HZ;
r34f=k34f*K12*x_C6H12*x_C3H6*(P_Tot^2)*HZ;
r34b=k34b*K15*x_C9H18*P_Tot*HZ;
r35f=k35f*K11*x_C5H10*x_C4H8*(P_Tot^2)*HZ;
r35b=k35b*K15*x_C9H18*P_Tot*HZ;
r36f=k36f*K14*x_C8H16*x_C2H4*(P_Tot^2)*HZ;
r36b=k36b*K16*x_C10H20*P_Tot*HZ;
r37f=k37f*K13*x_C7H14*x_C3H6*(P_Tot^2)*HZ;
r37b=k37b*K16*x_C10H20*P_Tot*HZ;
r38f=k38f*K12*x_C6H12*x_C4H8*(P_Tot^2)*HZ;
r38b=k38b*K16*x_C10H20*P_Tot*HZ;
r39f=k39f*K11*x_C5H10*x_C5H10*(P_Tot^2)*HZ;
r39b=k39b*K16*x_C10H20*P_Tot*HZ;

%Aromatic methylation with methanol
r40=k40*K1*x_C6H6*x_CH3OH*(P_Tot^2)*HZ;
r41=k41*K1*x_C7H8*x_CH3OH*(P_Tot^2)*HZ;
r42=k42*K1*x_C8H10*x_CH3OH*(P_Tot^2)*HZ;
r43=k43*K1*x_C9H12*x_CH3OH*(P_Tot^2)*HZ;

%Aromatic methylation with DME
r44=k44*K2*x_C6H6*x_CH3OCH3*(P_Tot^2)*HZ;
r45=k45*K2*x_C7H8*x_CH3OCH3*(P_Tot^2)*HZ;
r46=k46*K2*x_C8H10*x_CH3OCH3*(P_Tot^2)*HZ;
r47=k47*K2*x_C9H12*x_CH3OCH3*(P_Tot^2)*HZ;

%Aromatic dealkylation
r48=k48*K30*x_C8H10*P_Tot*HZ;
r49=k49*K32*x_C10H14*P_Tot*HZ;
r50=k50*K32*x_C10H14*P_Tot*HZ;
r51=k51*K32*x_C10H14*P_Tot*HZ;

%Olefin aromatization
```

```
r52=k52*K12*x_C6H12*(x_C2H4^3)*(P_Tot^4)*HZ;
r53=k53*K12*x_C6H12*(x_C3H6^3)*(P_Tot^4)*HZ;
r54=k54*K12*x_C6H12*(x_C4H8^3)*(P_Tot^4)*HZ;
r55=k55*K12*x_C6H12*(x_C5H10^3)*(P_Tot^4)*HZ;
r56=k56*K12*x_C6H12*(x_C6H12^3)*(P_Tot^4)*HZ;
r57=k57*K12*x_C6H12*(x_C7H14^3)*(P_Tot^4)*HZ;
r58=k58*K12*x_C6H12*(x_C8H16^3)*(P_Tot^4)*HZ;
r59=k59*K12*x_C6H12*(x_C9H18^3)*(P_Tot^4)*HZ;
r60=k60*K12*x_C6H12*(x_C10H20^3)*(P_Tot^4)*HZ;

r61=k61*K13*x_C7H14*(x_C2H4^3)*(P_Tot^4)*HZ;
r62=k62*K13*x_C7H14*(x_C3H6^3)*(P_Tot^4)*HZ;
r63=k63*K13*x_C7H14*(x_C4H8^3)*(P_Tot^4)*HZ;
r64=k64*K13*x_C7H14*(x_C5H10^3)*(P_Tot^4)*HZ;
r65=k65*K13*x_C7H14*(x_C6H12^3)*(P_Tot^4)*HZ;
r66=k66*K13*x_C7H14*(x_C7H14^3)*(P_Tot^4)*HZ;
r67=k67*K13*x_C7H14*(x_C8H16^3)*(P_Tot^4)*HZ;
r68=k68*K13*x_C7H14*(x_C9H18^3)*(P_Tot^4)*HZ;
r69=k69*K13*x_C7H14*(x_C10H20^3)*(P_Tot^4)*HZ;

r70=k70*K14*x_C8H16*(x_C2H4^3)*(P_Tot^4)*HZ;
r71=k71*K14*x_C8H16*(x_C3H6^3)*(P_Tot^4)*HZ;
r72=k72*K14*x_C8H16*(x_C4H8^3)*(P_Tot^4)*HZ;
r73=k73*K14*x_C8H16*(x_C5H10^3)*(P_Tot^4)*HZ;
r74=k74*K14*x_C8H16*(x_C6H12^3)*(P_Tot^4)*HZ;
r75=k75*K14*x_C8H16*(x_C7H14^3)*(P_Tot^4)*HZ;
r76=k76*K14*x_C8H16*(x_C8H16^3)*(P_Tot^4)*HZ;
r77=k77*K14*x_C8H16*(x_C9H18^3)*(P_Tot^4)*HZ;
r78=k78*K14*x_C8H16*(x_C10H20^3)*(P_Tot^4)*HZ;

r79=k79*K15*x_C9H18*(x_C2H4^3)*(P_Tot^4)*HZ;
r80=k80*K15*x_C9H18*(x_C3H6^3)*(P_Tot^4)*HZ;
r81=k81*K15*x_C9H18*(x_C4H8^3)*(P_Tot^4)*HZ;
r82=k82*K15*x_C9H18*(x_C5H10^3)*(P_Tot^4)*HZ;
r83=k83*K15*x_C9H18*(x_C6H12^3)*(P_Tot^4)*HZ;
r84=k84*K15*x_C9H18*(x_C7H14^3)*(P_Tot^4)*HZ;
r85=k85*K15*x_C9H18*(x_C8H16^3)*(P_Tot^4)*HZ;
r86=k86*K15*x_C9H18*(x_C9H18^3)*(P_Tot^4)*HZ;
r87=k87*K15*x_C9H18*(x_C10H20^3)*(P_Tot^4)*HZ;

r88=k88*K16*x_C10H20*(x_C2H4^3)*(P_Tot^4)*HZ;
r89=k89*K16*x_C10H20*(x_C3H6^3)*(P_Tot^4)*HZ;
r90=k90*K16*x_C10H20*(x_C4H8^3)*(P_Tot^4)*HZ;
r91=k91*K16*x_C10H20*(x_C5H10^3)*(P_Tot^4)*HZ;
r92=k92*K16*x_C10H20*(x_C6H12^3)*(P_Tot^4)*HZ;
r93=k93*K16*x_C10H20*(x_C7H14^3)*(P_Tot^4)*HZ;
r94=k94*K16*x_C10H20*(x_C8H16^3)*(P_Tot^4)*HZ;
r95=k95*K16*x_C10H20*(x_C9H18^3)*(P_Tot^4)*HZ;
r96=k96*K16*x_C10H20*(x_C10H20^3)*(P_Tot^4)*HZ;

r97=k97*K17*x_C2H6*P_Tot*HZ;
r98=k98*K18*x_C3H8*P_Tot*HZ;
r99=k99*K18*x_C3H8*P_Tot*HZ;
r100=k100*K19*x_C4H10*P_Tot*HZ;
r101=k101*K19*x_C4H10*P_Tot*HZ;
r102=k102*K19*x_C4H10*P_Tot*HZ;
r103=k103*K20*x_C5H12*P_Tot*HZ;
r104=k104*K20*x_C5H12*P_Tot*HZ;
r105=k105*K20*x_C5H12*P_Tot*HZ;
r106=k106*K20*x_C5H12*P_Tot*HZ;
r107=k107*K21*x_C6H14*P_Tot*HZ;
```

```
r108=k108*K21*x_C6H14*P_Tot*HZ;
r109=k109*K21*x_C6H14*P_Tot*HZ;
r110=k110*K21*x_C6H14*P_Tot*HZ;
r111=k111*K21*x_C6H14*P_Tot*HZ;
r112=k112*K22*x_C7H16*P_Tot*HZ;
r113=k113*K22*x_C7H16*P_Tot*HZ;
r114=k114*K22*x_C7H16*P_Tot*HZ;
r115=k115*K22*x_C7H16*P_Tot*HZ;
r116=k116*K22*x_C7H16*P_Tot*HZ;
r117=k117*K22*x_C7H16*P_Tot*HZ;
r118=k118*K23*x_C8H18*P_Tot*HZ;
r119=k119*K23*x_C8H18*P_Tot*HZ;
r120=k120*K23*x_C8H18*P_Tot*HZ;
r121=k121*K23*x_C8H18*P_Tot*HZ;
r122=k122*K23*x_C8H18*P_Tot*HZ;
r123=k123*K23*x_C8H18*P_Tot*HZ;
r124=k124*K23*x_C8H18*P_Tot*HZ;
r125=k125*K24*x_C9H20*P_Tot*HZ;
r126=k126*K24*x_C9H20*P_Tot*HZ;
r127=k127*K24*x_C9H20*P_Tot*HZ;
r128=k128*K24*x_C9H20*P_Tot*HZ;
r129=k129*K24*x_C9H20*P_Tot*HZ;
r130=k130*K24*x_C9H20*P_Tot*HZ;
r131=k131*K24*x_C9H20*P_Tot*HZ;
r132=k132*K24*x_C9H20*P_Tot*HZ;
r133=k133*K25*x_C10H22*P_Tot*HZ;
r134=k134*K25*x_C10H22*P_Tot*HZ;
r135=k135*K25*x_C10H22*P_Tot*HZ;
r136=k136*K25*x_C10H22*P_Tot*HZ;
r137=k137*K25*x_C10H22*P_Tot*HZ;
r138=k138*K25*x_C10H22*P_Tot*HZ;
r139=k139*K25*x_C10H22*P_Tot*HZ;
r140=k140*K25*x_C10H22*P_Tot*HZ;
r141=k141*K25*x_C10H22*P_Tot*HZ;

r142=k142*K9*x_C2H6*x_C3H6*(P_Tot^2)*HZ;
r143=k143*K10*x_C2H6*x_C4H8*(P_Tot^2)*HZ;
r144=k144*K11*x_C2H6*x_C5H10*(P_Tot^2)*HZ;
r145=k145*K12*x_C2H6*x_C6H12*(P_Tot^2)*HZ;
r146=k146*K13*x_C2H6*x_C7H14*(P_Tot^2)*HZ;
r147=k147*K14*x_C2H6*x_C8H16*(P_Tot^2)*HZ;
r148=k148*K15*x_C2H6*x_C9H18*(P_Tot^2)*HZ;
r149=k149*K16*x_C2H6*x_C10H20*(P_Tot^2)*HZ;

r150=k150*K8*x_C2H4*x_C3H8*(P_Tot^2)*HZ;
r151=k151*K10*x_C4H8*x_C3H8*(P_Tot^2)*HZ;
r152=k152*K11*x_C5H10*x_C3H8*(P_Tot^2)*HZ;
r153=k153*K12*x_C6H12*x_C3H8*(P_Tot^2)*HZ;
r154=k154*K13*x_C7H14*x_C3H8*(P_Tot^2)*HZ;
r155=k155*K14*x_C8H16*x_C3H8*(P_Tot^2)*HZ;
r156=k156*K15*x_C9H18*x_C3H8*(P_Tot^2)*HZ;
r157=k157*K16*x_C10H20*x_C3H8*(P_Tot^2)*HZ;

r158=k158*K8*x_C2H4*x_C4H10*(P_Tot^2)*HZ;
r159=k159*K9*x_C3H6*x_C4H10*(P_Tot^2)*HZ;
r160=k160*K11*x_C5H10*x_C4H10*(P_Tot^2)*HZ;
r161=k161*K12*x_C6H12*x_C4H10*(P_Tot^2)*HZ;
r162=k162*K13*x_C7H14*x_C4H10*(P_Tot^2)*HZ;
r163=k163*K14*x_C8H16*x_C4H10*(P_Tot^2)*HZ;
r164=k164*K15*x_C9H18*x_C4H10*(P_Tot^2)*HZ;
r165=k165*K16*x_C10H20*x_C4H10*(P_Tot^2)*HZ;
```

```
r166=k166*K8*x_C2H4*x_C5H12*(P_Tot^2)*HZ;
r167=k167*K9*x_C3H6*x_C5H12*(P_Tot^2)*HZ;
r168=k168*K10*x_C4H8*x_C5H12*(P_Tot^2)*HZ;
r169=k169*K12*x_C6H12*x_C5H12*(P_Tot^2)*HZ;
r170=k170*K13*x_C7H14*x_C5H12*(P_Tot^2)*HZ;
r171=k171*K14*x_C8H16*x_C5H12*(P_Tot^2)*HZ;
r172=k172*K15*x_C9H18*x_C5H12*(P_Tot^2)*HZ;
r173=k173*K16*x_C10H20*x_C5H12*(P_Tot^2)*HZ;

r174=k174*K8*x_C2H4*x_C6H14*(P_Tot^2)*HZ;
r175=k175*K9*x_C3H6*x_C6H14*(P_Tot^2)*HZ;
r176=k176*K10*x_C4H8*x_C6H14*(P_Tot^2)*HZ;
r177=k177*K11*x_C5H10*x_C6H14*(P_Tot^2)*HZ;
r178=k178*K13*x_C7H14*x_C6H14*(P_Tot^2)*HZ;
r179=k179*K14*x_C8H16*x_C6H14*(P_Tot^2)*HZ;
r180=k180*K15*x_C9H18*x_C6H14*(P_Tot^2)*HZ;
r181=k181*K16*x_C10H20*x_C6H14*(P_Tot^2)*HZ;

r182=k182*K8*x_C2H4*x_C7H16*(P_Tot^2)*HZ;
r183=k183*K9*x_C3H6*x_C7H16*(P_Tot^2)*HZ;
r184=k184*K10*x_C4H8*x_C7H16*(P_Tot^2)*HZ;
r185=k185*K11*x_C5H10*x_C7H16*(P_Tot^2)*HZ;
r186=k186*K12*x_C6H12*x_C7H16*(P_Tot^2)*HZ;
r187=k187*K14*x_C8H16*x_C7H16*(P_Tot^2)*HZ;
r188=k188*K15*x_C9H18*x_C7H16*(P_Tot^2)*HZ;
r189=k189*K16*x_C10H20*x_C7H16*(P_Tot^2)*HZ;

r190=k190*K8*x_C2H4*x_C8H18*(P_Tot^2)*HZ;
r191=k191*K9*x_C3H6*x_C8H18*(P_Tot^2)*HZ;
r192=k192*K10*x_C4H8*x_C8H18*(P_Tot^2)*HZ;
r193=k193*K11*x_C5H10*x_C8H18*(P_Tot^2)*HZ;
r194=k194*K12*x_C6H12*x_C8H18*(P_Tot^2)*HZ;
r195=k195*K13*x_C7H14*x_C8H18*(P_Tot^2)*HZ;
r196=k196*K15*x_C9H18*x_C8H18*(P_Tot^2)*HZ;
r197=k197*K16*x_C10H20*x_C8H18*(P_Tot^2)*HZ;

r198=k198*K8*x_C2H4*x_C9H20*(P_Tot^2)*HZ;
r199=k199*K9*x_C3H6*x_C9H20*(P_Tot^2)*HZ;
r200=k200*K10*x_C4H8*x_C9H20*(P_Tot^2)*HZ;
r201=k201*K11*x_C5H10*x_C9H20*(P_Tot^2)*HZ;
r202=k202*K12*x_C6H12*x_C9H20*(P_Tot^2)*HZ;
r203=k203*K13*x_C7H14*x_C9H20*(P_Tot^2)*HZ;
r204=k204*K14*x_C8H16*x_C9H20*(P_Tot^2)*HZ;
r205=k205*K16*x_C10H20*x_C9H20*(P_Tot^2)*HZ;

r206=k206*K8*x_C2H4*x_C10H22*(P_Tot^2)*HZ;
r207=k207*K9*x_C3H6*x_C10H22*(P_Tot^2)*HZ;
r208=k208*K10*x_C4H8*x_C10H22*(P_Tot^2)*HZ;
r209=k209*K11*x_C5H10*x_C10H22*(P_Tot^2)*HZ;
r210=k210*K12*x_C6H12*x_C10H22*(P_Tot^2)*HZ;
r211=k211*K13*x_C7H14*x_C10H22*(P_Tot^2)*HZ;
r212=k212*K14*x_C8H16*x_C10H22*(P_Tot^2)*HZ;
r213=k213*K15*x_C9H18*x_C10H22*(P_Tot^2)*HZ;


%% Differential equations

ydot=zeros(33,1);
```

```
ydot(1)=32*((-2*r1f)+(2*r1b)-r2+rox2-rox3-r4d-r8-r9-r10-r11-r12-r13-r14-
r15+r16+r17+r18+r19+r20+r21+r22+r23-r40-r41-r42-r43+r44+r45+r46+r47);
ydot(2)=46*(r1f-r1b-r3-(2*rox1)-rox2-r4d-r5d-r16-r17-r18-r19-r20-r21-r22-
r23-r44-r45-r46-r47);
ydot(3)=18*(r1f-
r1b+rox3+r4id+(2*r4d)+r5d+r8+r9+r10+r11+r12+r13+r14+r15+r40+r41+r42+r43);

ydot(4)=16*(r3+rox1+r98+r101+r105+r110+r116+r123+r131+r140);
ydot(5)=2*((2*r2)+r5id+r97+r99+r102+r106+r111+r117+r124+r132+r141);
ydot(6)=28*r2;
ydot(7)=30*(r3+r4id+(2*r5id));

ydot(8)=28*(r5id+r5d+r7-r8-r16-(2*r24f)+(2*r24b)-r25f+r25b-r26f+r26b-
r28f+r28b-r30f+r30b-r33f+r33b-r36f+r36b+r48+r49-(3*r52)-(3*r61)-(3*r70)-
(3*r79)-
(3*r88)+r97+r98+r100+r103+r107+r112+r118+r125+r133+r142+r143+r144+r145+r146
+r147+r148+r149-r150-r158-r166-r174-r182-r190-r198-r206);
ydot(9)=42*(r4id+r4d+r6+r8-r9+r16-r17-r25f+r25b-(2*r27f)+(2*r27b)-
r29f+r29b-r31f+r31b-r34f+r34b-r37f+r37b+r50-(3*r53)-(3*r62)-(3*r71)-
(3*r80)-(3*r89)+r99+r101+r104+r108+r113+r119+r126+r134-
r142+r150+r151+r152+r153+r154+r155+r156+r157-r159-r167-r175-r183-r191-r199-
r207);
ydot(10)=56*(r9-r10+r17-r18+r24f-r24b-r26f+r26b-r29f+r29b-
(2*r32f)+(2*r32b)-r35f+r35b-r38f+r38b+r51-(3*r54)-(3*r63)-(3*r72)-(3*r81)-
(3*r90)+r102+r105+r109+r114+r120+r127+r135-r143-r151-r168-r176-r184-r192-
r200-r208+r158+r159+r160+r161+r162+r163+r164+r165);
ydot(11)=70*(r10-r11+r18-r19+r25f-r25b-r28f+r28b-r31f+r31b-r35f+r35b-
(2*r39f)+(2*r39b)-(3*r55)-(3*r64)-(3*r73)-(3*r82)-
(3*r91)+r106+r110+r115+r121+r128+r136-r144-r152-r160-r177-r185-r193-r201-
r209+r166+r167+r168+r169+r170+r171+r172+r173);
ydot(12)=84*(r11-r12+r19-r20+r26f-r26b+r27f-r27b-r30f+r30b-r34f+r34b-
r38f+r38b-r52-r53-r54-r55-r56-r58-r59-r60-(3*r56)-(3*r65)-(3*r74)-(3*r83)-
(3*r92)+r111+r116+r122+r129+r137-r145-r153-r161-r169-r186-r194-r202-
r210+r174+r175+r176+r177+r178+r179+r180+r181);
ydot(13)=98*(r12-r13+r20-r21+r28f-r28b+r29f-r29b-r33f+r33b-r37f+r37b-
(3*r57)-(3*r66)-(3*r75)-(3*r84)-(3*r93)-r61-r62-r63-r64-r65-r66-r67-r68-
r69+r117+r123+r130+r138-r146-r154-r162-r170-r178-r195-r203-
r211+r182+r183+r184+r185+r186+r187+r188+r189);
ydot(14)=112*(r13-r14+r21-r22+r30f-r30b+r31f-r31b+r32f-r32b-r36f+r36b-
(3*r58)-(3*r67)-(3*r76)-(3*r85)-(3*r94)+r124+r131+r139-r147-r155-r163-r171-
r179-r187+r190+r191+r192+r193+r194+r195+r196+r197-r204-r212-r70-r71-r72-
r73-r74-r75-r76-r77-r78);
ydot(15)=126*(r14-r15+r22-r23+r33f-r33b+r34f-r34b+r35f-r35b-(3*r59)-
(3*r68)-(3*r77)-(3*r86)-(3*r95)+r132+r140-r148-r156-r164-r172-r180-r188-
r196-r213+r198+r199+r200+r201+r202+r203+r204+r205-r79-r80-r81-r82-r83-r84-
r85-r86-r87);
ydot(16)=140*(r15+r23+r36f-r36b+r37f-r37b+r38f-r38b+r39f-r39b-(3*r60)-
(3*r69)-(3*r78)-(3*r87)-(3*r96)+r141-r149-r157-r165-r173-r181-r189-r197-
r205+r206+r207+r208+r209+r210+r211+r212+r213-r88-r89-r90-r91-r92-r93-r94-
r95-r96);

ydot(17)=30*((3*r52)+(3*r61)+(3*r70)+(3*r79)+(3*r88)-
r97+r100+r104+r109+r115+r122+r130+r139-r142-r143-r144-r145-r146-r147-r148-
r149+r150+r158+r166+r174+r182+r190+r198+r206);
ydot(18)=44*((3*r53)+(3*r62)+(3*r71)+(3*r80)+(3*r89)-r98-
r99+r103+r108+r114+r121+r129+r138-r150-r151-r152-r153-r154-r155-r156-
r157+r142+r159+r167+r175+r183+r191+r199+r207);
ydot(19)=58*((3*r54)+(3*r63)+(3*r72)+(3*r81)+(3*r90)-r100-r101-
r102+r107+r113+r120+r128+r137-r158-r159-r160-r161-r162-r163-r164-
r165+r143+r151+r168+r176+r184+r192+r200+r208);
```

```
ydot(20)=72*((3*r55)+(3*r64)+(3*r73)+(3*r82)+(3*r91)-r103-r104-r105-
r106+r112+r119+r127+r136-r166-r167-r168-r169-r170-r171-r172-
r173+r144+r152+r160+r177+r185+r193+r201+r209);
ydot(21)=86*((3*r56)+(3*r65)+(3*r74)+(3*r83)+(3*r92)-r107-r108-r109-r110-
r111+r118+r126+r135-r174-r175-r176-r177-r178-r179-r180-
r181+r145+r153+r161+r169+r186+r194+r202+r210);
ydot(22)=100*((3*r57)+(3*r66)+(3*r75)+(3*r84)+(3*r93)-r112-r113-r114-r115-
r116-r117+r125+r134-r182-r183-r184-r185-r186-r187-r188-
r189+r146+r154+r162+r170+r178+r195+r203+r211);
ydot(23)=114*((3*r58)+(3*r67)+(3*r76)+(3*r85)+(3*r94)-r118-r119-r120-r121-
r122-r123-r124+r133-r190-r191-r192-r193-r194-r195-r196-
r197+r147+r155+r163+r171+r179+r187+r204+r212);
ydot(24)=128*((3*r59)+(3*r68)+(3*r77)+(3*r86)+(3*r95)-r125-r126-r127-r128-
r129-r130-r131-r132-r198-r199-r200-r201-r202-r203-r204-
r205+r148+r156+r164+r172+r180+r188+r196+r213);
ydot(25)=142*((3*r60)+(3*r69)+(3*r78)+(3*r87)+(3*r96)-r133-r134-r135-r136-
r137-r138-r139-r140-r141-r206-r207-r208-r209-r210-r211-r212-
r213+r149+r157+r165+r173+r181+r189+r197+r205);

ydot(26)=76*(rox1-rox2-rox3);
ydot(27)=90*(rox2+rox3-r4id-r5id);

ydot(28)=78*(r6-r40-r44+r48+r51+r52+r53+r54+r55+r56+r57+r58+r59+r60);
ydot(29)=92*(r7+r40-r41+r44-r45+r50+r61+r62+r63+r64+r65+r66+r67+r68+r69);
ydot(30)=106*(r41-r42+r45-r46-r48+r49+r70+r71+r72+r73+r74+r75+r76+r77+r78);
ydot(31)=120*(r42-r43+r46-r47-r6-r7+r79+r80+r81+r82+r83+r84+r85+r86+r87);
ydot(32)=134*(r43+r47-r49-r50-r51+r88+r89+r90+r91+r92+r93+r94+r95+r96);

ydot(33)=28*(0);
end
```

ii. Script file

```
tic;
clear all; close all; clc

%mf = mass fraction, Tau = contact time

global k1fValue
global k1bValue

global k2Value
global k3Value

global kox1Value
global kox2Value
global kox3Value

global k4idValue
global k5idValue

global k4dValue
global k5dValue

global k6Value
global k7Value

global k8Value
global k9Value
global k10Value
```

```
global k11Value
global k12Value
global k13Value
global k14Value
global k15Value
global k16Value

global k17Value
global k18Value
global k19Value
global k20Value
global k21Value
global k22Value
global k23Value

global k24fValue
global k24bValue
global k25fValue
global k25bValue
global k26fValue
global k26bValue
global k27fValue
global k27bValue
global k28fValue
global k28bValue
global k29fValue
global k29bValue
global k30fValue
global k30bValue
global k31fValue
global k31bValue
global k32fValue
global k32bValue
global k33fValue
global k33bValue
global k34fValue
global k34bValue
global k35fValue
global k35bValue
global k36fValue
global k36bValue
global k37fValue
global k37bValue
global k38fValue
global k38bValue
global k39fValue
global k39bValue

global k40Value
global k41Value
global k42Value
global k43Value
global k44Value
global k45Value

global k46Value
global k47Value
global k48Value
global k49Value
global k50Value
global k51Value
```

```
global k52Value
global k53Value
global k54Value
global k55Value
global k56Value

global k57Value
global k58Value
global k59Value
global k60Value
global k61Value
global k62Value
global k63Value
global k64Value
global k65Value

global k66Value
global k67Value
global k68Value
global k69Value
global k70Value
global k71Value
global k72Value
global k73Value
global k74Value

global k75Value
global k76Value
global k77Value
global k78Value
global k79Value
global k80Value
global k81Value
global k82Value
global k83Value

global k84Value
global k85Value
global k86Value
global k87Value
global k88Value
global k89Value
global k90Value
global k91Value
global k92Value

global k93Value
global k94Value
global k95Value
global k96Value
global k97Value
global k98Value
global k99Value
global k100Value
global k101Value

global k102Value
global k103Value
global k104Value
```

```
global k105Value
global k106Value
global k107Value
global k108Value
global k109Value
global k110Value
global k111Value
global k112Value
global k113Value
global k114Value
global k115Value
global k116Value
global k117Value
global k118Value
global k119Value
global k120Value
global k121Value
global k122Value
global k123Value
global k124Value
global k125Value
global k126Value
global k127Value
global k128Value
global k129Value
global k130Value
global k131Value
global k132Value
global k133Value
global k134Value
global k135Value
global k136Value
global k137Value
global k138Value
global k139Value
global k140Value
global k141Value
global k142Value
global k143Value
global k144Value
global k145Value
global k146Value
global k147Value

global k148Value
global k149Value
global k150Value
global k151Value
global k152Value
global k153Value
global k154Value
global k155Value
global k156Value
global k157Value
global k158Value
global k159Value
global k160Value
global k161Value
global k162Value
global k163Value
global k164Value
global k165Value
```

```
global k166Value
global k167Value
global k168Value
global k169Value
global k170Value
global k171Value
global k172Value
global k173Value
global k174Value
global k175Value
global k176Value
global k177Value
global k178Value
global k179Value
global k180Value
global k181Value
global k182Value
global k183Value
global k184Value
global k185Value
global k186Value
global k187Value
global k188Value
global k189Value
global k190Value
global k191Value
global k192Value
global k193Value
global k194Value
global k195Value
global k196Value
global k197Value
global k198Value
global k199Value
global k200Value
global k201Value
global k202Value
global k203Value
global k204Value
global k205Value
global k206Value
global k207Value
global k208Value
global k209Value
global k210Value
global k211Value
global k212Value
global k213Value

tau_initial = 0; tau_final = 20;


T = 370+273;
K_p=exp(-9.76+(3200/T)+(1.07*log(T))-(0.66e-3*T)+(0.49e-
7*(T^2))+(6500/(T^2)));

k1fValues = 0.0185;
k1bValues = k1fValues/K_p;

k2Values = 0;
k3Values = 0;
```

```
kox1Values = 0;
kox2Values = 0;
kox3Values = 0;

k4idValues = 0;
k5idValues = 0;

k5dValues = 6.2e-4;
k4dValues = 0.0034;

k40Values = 0.16;
k41Values = 0.17;
k42Values = 0.011;
k43Values = 0.031;

DMEfactor = 3.5;
DMEfactor_aromatic = DMEfactor*2.5;

k44Values = k40Values*DMEfactor_aromatic;
k45Values = k41Values*DMEfactor_aromatic;
k46Values = k42Values*DMEfactor_aromatic;
k47Values = k43Values*DMEfactor_aromatic;

k48Values = 0.0005;
k6Values = 0.003;
k7Values = 0.006;
k49Values = 0.1;
k50Values = 0.2;
k51Values = 0.4;

k8Values = 0.0055;
k9Values = 0.0086;
k10Values = 0.0241;
k11Values = 0.0483;
k12Values = 0.0828;
k13Values = k8Values*15;
k14Values = k8Values*15;
k15Values = k8Values*15;

k16Values = k8Values*DMEfactor;
k17Values = k9Values*DMEfactor;
k18Values = k10Values*DMEfactor;
k19Values = k11Values*DMEfactor;
k20Values = k12Values*DMEfactor;
k21Values = k13Values*DMEfactor;
k22Values = k14Values*DMEfactor;
k23Values = k15Values*DMEfactor;

k24fValues = 0.015;
k24bValues = k24fValues/18.696;
k25fValues = k24fValues*17;
k25bValues = k25fValues/1.7211;
k26fValues = k24fValues*33;
k26bValues = k26fValues/15.203;
k27fValues = k24fValues*36;
k27bValues = k27fValues/0.5;
k28fValues = k24fValues*33;
k28bValues = k28fValues*2.9021;
k29fValues = k24fValues*159;
```

```
k29bValues = k29fValues/0.02672;
k30fValues = k24fValues*231;
k30bValues = k30fValues/0.09505;
k31fValues = k24fValues*231;
k31bValues = k31fValues/0.1286;
k32fValues = 0;
k32bValues = k32fValues/0.7729;

k33fValues = k24fValues*231;
k33bValues = k33fValues/1.5;
k34fValues = k24fValues*231;
k34bValues = k34fValues/0.0358;
k35fValues = 0;
k35bValues = k35fValues/0.3164;
k36fValues = k24fValues*231;
k36bValues = k36fValues/2.2786;
k37fValues = k24fValues*231;
k37bValues = k37fValues/0.101;
k38fValues = k24fValues*924;
k38bValues = k38fValues/0.1158;
k39fValues = 0;
k39bValues = k39fValues/0.1703;

k52Values = 10;
k53Values = 100;
k54Values = k53Values;
k55Values = k53Values;
k56Values = k53Values;
k57Values = k53Values;
k58Values = k53Values;
k59Values = k53Values;
k60Values = k53Values;

k61Values = 7.5e5;
k62Values = 1.2e6;
k63Values = 2.2e8;
k64Values = 1.2e9;
k65Values = 6.2e8;
k66Values = k63Values;
k67Values = k63Values;
k68Values = k63Values;
k69Values = k63Values;

k70Values = 9.6e8;
k71Values = 1.6e9;
k72Values = 9.6e9;
k73Values = 1.6e11;
k74Values = 1.6e13;
k75Values = k74Values;
k76Values = k74Values;
k77Values = k74Values;
k78Values = k74Values;

k79Values = 9.6e8;
k80Values = 9.6e14;
k81Values = 9.6e15;
k82Values = 7.2e19;
k83Values = 9.6e19;
k84Values = 9.6e19;
k85Values = 9.6e19;
k86Values = 9.6e19;
```

```
k87Values = 9.6e19;

k88Values = 9.6e9;
k89Values = k88Values;
k90Values = k88Values;
k91Values = 9.6e12;
k92Values = 9.6e13;
k93Values = k92Values;
k94Values = k92Values;
k95Values = k92Values;
k96Values = k92Values;

k97Values = 600;

k98Values = 0;
k99Values = k98Values;

k100Values = 0;
k101Values = 0;
k102Values = 0;

k103Values = 0;
k104Values = 0;
k105Values = 0;
k106Values = 0;

k107Values = 0;
k108Values = 0;
k109Values = 0;
k110Values = k109Values;
k111Values = k109Values;

k112Values = 0;
k113Values = k112Values;
k114Values = k112Values;
k115Values = k112Values;
k116Values = k112Values;
k117Values = k112Values;

k118Values = 0;
k119Values = k118Values;
k120Values = k118Values;
k121Values = k118Values;
k122Values = k118Values;
k123Values = k118Values;
k124Values = k118Values;

k125Values = 0;
k126Values = k125Values;
k127Values = k125Values;
k128Values = k125Values;
k129Values = k125Values;
k130Values = k125Values;
k131Values = k125Values;
k132Values = k125Values;

k133Values = 0;
k134Values = k133Values;
k135Values = k133Values;
k136Values = k133Values;
```

```
k137Values = k133Values;
k138Values = k133Values;
k139Values = k133Values;
k140Values = k133Values;
k141Values = k133Values;

k142Values = 10;
k143Values = k142Values;
k144Values = k142Values;
k145Values = k142Values;
k146Values = k142Values;
k147Values = k142Values;
k148Values = k142Values;
k149Values = k142Values;

k150Values = 0;
k151Values = k150Values;
k152Values = k150Values;
k153Values = k150Values;
k154Values = k150Values;
k155Values = k150Values;
k156Values = k150Values;
k157Values = k150Values;

k158Values = 0;
k159Values = 0;
k160Values = 0;
k161Values = 0;
k162Values = 0;
k163Values = 0;
k164Values = 0;
k165Values = 0;

k166Values = 0;
k167Values = 0;
k168Values = 0;
k169Values = 0;
k170Values = 0;
k171Values = 0;
k172Values = 0;
k173Values = 0;

k174Values = 0;
k175Values = 0;
k176Values = 0;
k177Values = 0;
k178Values = 0;
k179Values = 0;
k180Values = 0;
k181Values = 0;

k182Values = 0;
k183Values = 0;
k184Values = 0;
k185Values = 0;
k186Values = 0;
k187Values = 0;
k188Values = 0;
k189Values = 0;
```

```
k190Values = 0;
k191Values = 0;
k192Values = 0;
k193Values = 0;
k194Values = 0;
k195Values = 0;
k196Values = 0;
k197Values = 0;

k198Values = 0;
k199Values = 0;
k200Values = 0;
k201Values = 0;
k202Values = 0;
k203Values = 0;
k204Values = 0;
k205Values = 0;

k206Values = 0;
k207Values = 0;
k208Values = 0;
k209Values = 0;
k210Values = 0;
k211Values = 0;
k212Values = 0;
k213Values = 0;


k1fValue = k1fValues;
k1bValue = k1bValues;

k2Value=k2Values;
k3Value=k3Values;

kox1Value=kox1Values;
kox2Value=kox2Values;
kox3Value=kox3Values;

k4idValue=k4idValues;
k5idValue=k5idValues;


k4dValue=k4dValues;
k5dValue=k5dValues;

k6Value=k6Values;
k7Value=k7Values;

k8Value=k8Values;
k9Value=k9Values;
k10Value=k10Values;
k11Value=k11Values;
k12Value=k12Values;
k13Value=k13Values;
k14Value=k14Values;
k15Value=k15Values;

k16Value=k16Values;
k17Value=k17Values;
```

```
k18Value=k18Values;
k19Value=k19Values;
k20Value=k20Values;
k21Value=k21Values;
k22Value=k22Values;
k23Value=k23Values;

k24fValue=k24fValues;
k24bValue=k24bValues;
k25fValue=k25fValues;
k25bValue=k25bValues;
k26fValue=k26fValues;
k26bValue=k26bValues;
k27fValue=k27fValues;
k27bValue=k27bValues;
k28fValue=k28fValues;
k28bValue=k28bValues;
k29fValue=k29fValues;
k29bValue=k29bValues;
k30fValue=k30fValues;
k30bValue=k30bValues;
k31fValue=k31fValues;
k31bValue=k31bValues;
k32fValue=k32fValues;
k32bValue=k32bValues;
k33fValue=k33fValues;
k33bValue=k33bValues;
k34fValue=k34fValues;
k34bValue=k34bValues;
k35fValue=k35fValues;
k35bValue=k35bValues;
k36fValue=k36fValues;
k36bValue=k36bValues;
k37fValue=k37fValues;
k37bValue=k37bValues;
k38fValue=k38fValues;
k38bValue=k38bValues;
k39fValue=k39fValues;
k39bValue=k39bValues;

k40Value=k40Values;
k41Value=k41Values;
k42Value=k42Values;
k43Value=k43Values;
k44Value=k44Values;
k45Value=k45Values;
k46Value=k46Values;
k47Value=k47Values;

k48Value=k48Values;
k49Value=k49Values;
k50Value=k50Values;
k51Value=k51Values;

k52Value=k52Values;
k53Value=k53Values;
k54Value=k54Values;
k55Value=k55Values;
k56Value=k56Values;

k57Value=k57Values;
```

```
k58Value=k58Values;
k59Value=k59Values;
k60Value=k60Values;
k61Value=k61Values;
k62Value=k62Values;
k63Value=k63Values;
k64Value=k64Values;
k65Value=k65Values;

k66Value=k66Values;
k67Value=k67Values;
k68Value=k68Values;
k69Value=k69Values;
k70Value=k70Values;
k71Value=k71Values;
k72Value=k72Values;
k73Value=k73Values;
k74Value=k74Values;

k75Value=k75Values;
k76Value=k76Values;
k77Value=k77Values;
k78Value=k78Values;
k79Value=k79Values;
k80Value=k80Values;
k81Value=k81Values;
k82Value=k82Values;
k83Value=k83Values;

k84Value=k84Values;
k85Value=k85Values;
k86Value=k86Values;
k87Value=k87Values;
k88Value=k88Values;
k89Value=k89Values;
k90Value=k90Values;
k91Value=k91Values;
k92Value=k92Values;

k93Value=k93Values;
k94Value=k94Values;
k95Value=k95Values;
k96Value=k96Values;
k97Value=k97Values;
k98Value=k98Values;
k99Value=k99Values;
k100Value=k100Values;
k101Value=k101Values;


k102Value=k102Values;
k103Value=k103Values;
k104Value=k104Values;
k105Value=k105Values;
k106Value=k106Values;
k107Value=k107Values;
k108Value=k108Values;
k109Value=k109Values;
k110Value=k110Values;
k111Value=k111Values;
k112Value=k112Values;
```

```
k113Value=k113Values;
k114Value=k114Values;
k115Value=k115Values;
k116Value=k116Values;
k117Value=k117Values;
k118Value=k118Values;
k119Value=k119Values;
k120Value=k120Values;
k121Value=k121Values;
k122Value=k122Values;
k123Value=k123Values;
k124Value=k124Values;
k125Value=k125Values;
k126Value=k126Values;
k127Value=k127Values;
k128Value=k128Values;
k129Value=k129Values;
k130Value=k130Values;
k131Value=k131Values;
k132Value=k132Values;
k133Value=k133Values;
k134Value=k134Values;
k135Value=k135Values;
k136Value=k136Values;
k137Value=k137Values;
k138Value=k138Values;
k139Value=k139Values;
k140Value=k140Values;
k141Value=k141Values;
k142Value=k142Values;
k143Value=k143Values;
k144Value=k144Values;
k145Value=k145Values;
k146Value=k146Values;
k147Value=k147Values;
k148Value=k148Values;
k149Value=k149Values;
k150Value=k150Values;
k151Value=k151Values;
k152Value=k152Values;
k153Value=k153Values;
k154Value=k154Values;
k155Value=k155Values;
k156Value=k156Values;
k157Value=k157Values;
k158Value=k158Values;
k159Value=k159Values;
k160Value=k160Values;
k161Value=k161Values;
k162Value=k162Values;
k163Value=k163Values;
k164Value=k164Values;
k165Value=k165Values;
k166Value=k166Values;
k167Value=k167Values;
k168Value=k168Values;
k169Value=k169Values;
k170Value=k170Values;
k171Value=k171Values;
k172Value=k172Values;
k173Value=k173Values;
k174Value=k174Values;
```

```
k175Value=k175Values;
k176Value=k176Values;
k177Value=k177Values;
k178Value=k178Values;
k179Value=k179Values;
k180Value=k180Values;
k181Value=k181Values;
k182Value=k182Values;
k183Value=k183Values;
k184Value=k184Values;
k185Value=k185Values;
k186Value=k186Values;
k187Value=k187Values;
k188Value=k188Values;
k189Value=k189Values;
k190Value=k190Values;
k191Value=k191Values;
k192Value=k192Values;
k193Value=k193Values;
k194Value=k194Values;
k195Value=k195Values;
k196Value=k196Values;
k197Value=k197Values;
k198Value=k198Values;
k199Value=k199Values;
k200Value=k200Values;
k201Value=k201Values;
k202Value=k202Values;
k203Value=k203Values;
k204Value=k204Values;
k205Value=k205Values;
k206Value=k206Values;
k207Value=k207Values;
k208Value=k208Values;
k209Value=k209Values;
k210Value=k210Values;
k211Value=k211Values;
k212Value=k212Values;
k213Value=k213Values;



mfo =
[0.25;0;0;0
```

```
C3H8O2_expt=data(1:9,29);C4H10O2_expt=data(1:9,29);
N2_expt=data(1:9,5);

figure
title('Oxygenates and H2O');
plot(Tau(:,1),mf(:,1),'r-
',Tau_expt(:,1),MeOH_expt(:,1),'r*',Tau(:,1),mf(:,2),'b-
',Tau_expt(:,1),DME_expt(:,1),'b*',Tau(:,1),mf(:,3),'g-
',Tau_expt(:,1),H2O_expt(:,1),'g*', 'Linewidth',2)
legend('CH_{3}OH_{(Model)}','CH_{3}OH_{(expt)}','CH_{3}OCH_{3}_{(Model)}','
CH_{3}OCH_{3}_{(expt)}','H_{2}O_{(Model)}','H_{2}O_{(expt)}','Location',
'bestoutside','Orientation','vertical')
xlabel('Contact time (g_{cat}.g_{methanol}^{-1}s)', 'Fontweight', 'Bold'),
ylabel('Mass fraction (wt/wt)', 'Fontweight', 'Bold');
ylim([0 0.25]);xlim([0 12]);
box off
grid off
legend boxoff
ax=gca;
ax.FontSize = 11;

figure
title('Olefins: C2-C6');
plot(Tau(:,1),mf(:,8),'c-
',Tau_expt(:,1),C2H4_expt(:,1),'c*',Tau(:,1),mf(:,9),'m-
',Tau_expt(:,1),C3H6_expt(:,1),'m*',Tau(:,1),mf(:,10),'r-
',Tau_expt(:,1),C4H8_expt(:,1),'r*',Tau(:,1),mf(:,11),'b-
',Tau_expt(:,1),C5H10_expt(:,1),'b*',Tau(:,1),mf(:,12),'g-
',Tau_expt(:,1),C6H12_expt(:,1),'g*','Linewidth',2)
legend('C_{2}H_{4}_{(Model)}','C_{2}H_{4}_{(expt)}','C_{3}H_{6}_{(Model)}',
'C_{3}H_{6}_{(expt)}','C_{4}H_{8}_{(Model)}','C_{4}H_{8}_{(expt)}','C_{5}H_
{10}_{(Model)}','C_{5}H_{10}_{(expt)}','C_{6}H_{12}_{(Model)}','C_{6}H_{12}
_{(expt)}','Location', 'bestoutside','Orientation','vertical');
xlabel('Contact time (g_{cat}.g_{methanol}^{-1}s)', 'Fontweight', 'Bold'),
ylabel('Mass fraction (wt/wt)', 'Fontweight', 'Bold');
ylim([0 0.040]); xlim([0 12]);
box off
grid off
legend boxoff
ax=gca;
ax.FontSize = 11;

figure
title('Paraffin: C2-C6')
plot(Tau(:,1), mf(:,17),'c-',Tau_expt(:,1),C2H6_expt(:,1),'c*',Tau(:,1),
mf(:,18),'m-',Tau_expt(:,1),C3H8_expt(:,1), 'm*',Tau(:,1),mf(:,19), 'r-
',Tau_expt(:,1), C4H10_expt(:,1), 'r*', Tau(:,1),mf(:,20),'b-',
Tau_expt(:,1), C5H12_expt(:,1), 'b*', Tau(:,1), mf(:,21),'g-
',Tau_expt(:,1), C6H14_expt(:,1), 'g*','Linewidth',2)
legend('C_{2}H_{6}_{(Model)}','C_{2}H_{6}_{(expt)}','C_{3}H_{8}_{(Model)}',
'C_{3}H_{8}_{(expt)}','C_{4}H_{10}_{(Model)}','C_{4}H_{10}_{(expt)}','C_{5}
H_{12}_{(Model)}','C_{5}H_{12}_{(expt)}','C_{6}H_{14}_{(Model)}','C_{6}H_{1
4}_{(expt)}','Location', 'bestoutside','Orientation','vertical');
xlabel('Contact time (g_{cat}.g_{methanol}^{-1}s)', 'Fontweight', 'Bold'),
ylabel('Mass fraction (wt/wt)', 'Fontweight', 'Bold');
grid off
box off
ylim([0 0.01]);xlim([0 12]);
legend boxoff
ax=gca;
ax.FontSize = 11;
```

```
figure
title('Aromatics')
plot(Tau(:,1),mf(:,28),'r-
',Tau_expt(:,1),C6H6_expt(:,1),'rx',Tau(:,1),mf(:,29),'b-
',Tau_expt(:,1),C7H8_expt(:,1),'bx',Tau(:,1),mf(:,30),'g-
',Tau_expt(:,1),C8H10_expt(:,1),'gx',Tau(:,1),mf(:,31),'k-
',Tau_expt(:,1),C9H12_expt(:,1),'kx', Tau(:,1),mf(:,32),'c-
',Tau_expt(:,1),C10H14_expt(:,1),'cx', 'Linewidth',2)
legend('C_{6}H_{6}_{(Model)}','C_{6}H_{6}_{(expt)}',
'C_{7}H_{8}_{(Model)}','C_{7}H_{8}_{(expt)}',
'C_{8}H_{10}_{(Model)}','C_{8}H_{10}_{(expt)}','C_{9}H_{12}_{(Model)}','C_{
9}H_{12}_{(expt)}','C_{10}H_{14}_{(Model)}','C_{10}H_{14}_{(expt)}','Locati
on', 'bestoutside','Orientation','vertical')
xlabel('Contact time (g_{cat}.g_{methanol}^{-1}s)', 'Fontweight', 'Bold'),
ylabel('Mass fraction (wt/wt)', 'Fontweight', 'Bold');
grid off

ylim([0 0.005]);xlim([0 12]);
box off
legend boxoff
ax=gca;
ax.FontSize = 11;

toc;
```